

Modelling neoclassical tearing modes in tokamak plasmas

Aleksandra Valerievna Dudkovskaia

Doctor of Philosophy

University of York

Physics

August 2019

Abstract

Understanding the physics of the neoclassical tearing mode (NTM) onset and its stabilisation is one of the key issues in providing successful operation of future power plants. The latter, in turn, requires a well developed predictive theory of the tearing mode threshold in order to specify and optimise control schemes.

A new drift kinetic theory is presented to calculate the plasma response to the NTM magnetic island. Small magnetic islands compared to the tokamak minor radius are assumed but island widths, w , comparable to the ion banana orbit width, ρ_{bi} , are treated accurately, retaining finite orbit width effects. To provide dimensionality reduction, streamlines, S , are derived that can be interpreted as a generalised radial coordinate. Adopting a low collisionality plasma, the distribution function is found to be constant on contours of constant S when collisions are neglected. Proceeding to next order, and introducing collisions, the dependence of the particle distribution on S and pitch angle, λ , is determined. S contours reproduce the magnetic island geometry but have a radial shift of a few poloidal gyro-radii, ρ_{ϑ} . This radial shift is found only for passing particles and is in opposite directions for $V_{\parallel} \gtrless 0$, V_{\parallel} is the parallel component of velocity. The distribution function being flattened across these S islands rather than the magnetic island restores the pressure gradient across a magnetic island of width $w \lesssim \rho_{\vartheta i}$, which provides a physics basis for the NTM threshold by suppressing the NTM drive. Collisions cannot be treated perturbatively near the trapped-passing boundary in pitch angle, and thus here a thin collisional boundary layer is identified. This layer matches the passing and trapped solutions outside the layer and being the dominant source of dissipation provides the island propagation frequency.

The solution provides a threshold island width, w_c (below which magnetic islands are healed), which arises from the passing particle dynamics, and the relevant parameter is the ion poloidal gyro-radius, $\rho_{\vartheta i}$: $w_c = 3\rho_{\vartheta i}$.

Contents

Abstract

List of Figures	i
List of Tables	ix
Acknowledgements	x
Declaration of Authorship	xi
1 Introduction	1
1.1 World energy problem	1
1.2 Nuclear Fusion	3
1.3 Ignition criteria	4
1.4 Physics of plasmas	6
1.5 Plasma description	9
1.6 Tokamak concept	17
1.7 Overview	20
2 Neoclassical tearing modes	22
2.1 Magnetic topology and NTM dispersion relation	29
2.2 Ion response	32
2.3 Electron response	37
2.4 Drift magnetic islands	37
2.5 Plasma quasi-neutrality and electrostatic potential	45
2.6 Summary	48
3 Boundary layer solution in the vicinity of the trapped-passing boundary	53
3.1 Dissipative layer solution	55
3.2 Summary	63
4 Solution technique and the RDK-NTM results	64
4.1 Numerical algorithm	64
4.2 The ion/electron distribution function and its density and flow moments	69
4.3 Contributions to the modified Rutherford equation	83
4.4 Polarisation contribution and island propagation frequency	88
4.4.1 The polarisation current contribution with the model $\propto \sqrt{S}$ diffusion	90
4.4.2 The polarisation current contribution based on the full RDK-NTM solution	93
4.5 Summary	96
5 Stability analysis of secondary modes, driven by a phase space island	98
5.1 Specification of the problem	99
5.2 Primary equilibrium	104
5.2.1 Self-consistency	109
5.3 Stability analysis. Secondary modes	111

5.3.1	Filtered solution	111
5.3.2	Full solution of the Vlasov/Fokker-Planck – Poisson system	113
5.4	Summary	121
6	Summary and Conclusions	123
6.1	Future work	128
	Appendix	130
A	Formation of magnetic islands	130
B	Magnetic island perturbation	134
C	Switching from poloidal flux function, ψ, to toroidal canonical momentum, p_φ	136
D	Derivation of the drift magnetic island kinetic equation	137
D.1	Some useful identities	137
D.2	Derivation of the NTM orbit averaged drift kinetic equation	138
D.3	Perturbative treatment	155
D.4	Orbit averaging	156
D.5	The $\langle R^2 (\mathbf{B}_1 \cdot \nabla p_\varphi) \rangle_{\vartheta}^{p_\varphi}$ term	158
D.6	Normalisation	159
D.6.1	Ion-ion and electron-electron/ion collision operator	161
D.6.2	Orbit averaged drift kinetic equation in normalised form	163
D.7	\mathcal{S} island formalism.	
D.7.1	Drift kinetic equation in \mathcal{S} space	163
D.7.1	Direct switch from ψ to \mathcal{S}	172
E	Numerical scheme	174
E.1	B coefficients	174
E.2	Boundary conditions in λ and \mathcal{S} space	180
E.3	First and second order derivatives	181
E.4	C coefficients	183
E.5	A coefficients	184
E.6	In terms of P, Q and R	185
E.6.1	Left boundary (passing branch)	188
E.6.2	Right boundary (trapped branch)	193
E.6.3	Matching at the trapped-passing boundary	198
E.7	Block diagram	200
F	Figures not included in the main part	204
G	Stability analysis of secondary modes, driven by a phase space island: appendix	207
G.1	Resonant and non-resonant forms of the secondary mode dispersion relation	207
	Abbreviations	210
	References	211

List of Figures

- | | | |
|-----|---|----|
| 1.1 | Time evolution of the total world population [1] (left) and the corresponding energy consumption in Mtoe, million tonnes of oil equivalent [2] (right). The probabilistic population up to 2100 based on "high" (upper95 and upper80) and "low" (lower95 and lower80) UN projections is indicated by thin/thick dashed and dotted blue curves, respectively. The "medium" projection is indicated by blue circle markers. Inset: zoom in a region from 1971 to 2015. | 1 |
| 1.2 | Time evolution of the atmospheric concentration of carbon dioxide, CO_2 , in parts per million, ppm [3] (left) and its emission in billion tonnes (Gt) per year [4] (right). A time interval from 1751 to 2015 is covered. | 2 |
| 1.3 | Cross section of main MCF fusion reactions. E is energy in keV. | 3 |
| 1.4 | Sketch of a conventional tokamak (source: [27]). A set of the toroidal field coils, the inner/outer set of the poloidal field coils, the vacuum vessel region are indicated. The toroidal and poloidal magnetic field components form the total, helical magnetic field. | 17 |
| 1.5 | Sketch of a conventional tokamak (source: [30]). The origin of the $\mathbf{E} \times \mathbf{B}$ drift in tokamak plasmas is demonstrated. | 18 |
| 1.6 | A schematic representation of the conventional tokamak circular poloidal cross section. r and R are the minor and major radii of the tokamak ($r = a$ at the plasma edge and $R = R_0$ at the magnetic axis). $\Delta = \Delta(r)$ denotes the Shafranov shift of the magnetic flux surfaces in the direction of the low magnetic field side. ϑ is the poloidal angle. | 19 |
| 2.1 | Formation of magnetic islands in large aspect ratio circular cross section tokamak geometry. Poloidal cross section in the absence of NTM activity (left); in the presence of NTM magnetic islands (right). O and X denote the magnetic island O- and X-points, respectively. Green arrow is in the poloidal direction (figure courtesy of H. Wilson). | 22 |
| 2.2 | A ring of toroidal plasma in slab geometry in the absence of NTM activity. $\{x, y, z\}$ correspond to $\{r, \vartheta, \varphi\}$ with r being the radial coordinate, ϑ the poloidal angle and φ the toroidal angle, respectively (figure courtesy of H. Wilson). . . | 23 |
| 2.3 | Same as Fig.2.2 but in the presence of NTM magnetic islands. The O-point at the centre of the island and the X-point at the separatrix are indicated. The red curve indicates the magnetic island separatrix, i.e. the last closed magnetic flux surface of the island (note: a similar structure can be seen in the poloidal cross section of a tokamak with double-null divertor). Here poloidal/toroidal mode numbers are $m = 2/n = 1$, respectively (figure courtesy of H. Wilson). | 23 |
| 2.4 | The Globus-M shot 26148 (saturated plasma current, $I_\varphi = 200\text{kA}$, $B_\varphi = 0.4\text{T}$). Time traces of the plasma current, chord-averaged density, nl, magnetic field perturbation obtained by the Mirnov coil system and poloidal beta reconstructed by EFIT. Arrows indicate the beginning of the NTM activity (at plasma beta $\beta_\vartheta \approx 0.25$). | 24 |

- 2.5 Confinement loss due to the tearing mode occurrence. Dashed curve indicates the radial plasma pressure profile in the absence of the magnetic island. Solid curve corresponds to the pressure profile in the presence of the NTM. The pressure flattening inside the island results in its reduction in a core. If plasma temperature is constant, the bootstrap current density is $\propto \varepsilon^{1/2} B_{\vartheta}^{-1} \nabla_r p$ and hence has a hole inside the island (figure courtesy of H. Wilson). 24
- 2.6 Projections of passing and trapped particle trajectories shown in a tokamak poloidal cross section (figure courtesy of K. Imada). 36
- 2.7 Contours of constant S in the (x, ξ) plane in the absence of the electrostatic potential, $\hat{\Phi} = 0$, for $w \gg \rho_{\vartheta i}$ (left) and $w \gtrsim \rho_{\vartheta i}$ (right). $\lambda = 0.84$, $\varepsilon = 0.1$, $V = V_{Ti}$, $\sigma = +1$, $\hat{L}_q = 1$. White dashed line indicates the position of the magnetic island separatrix, $\Omega = 1$. The S island separatrix is at $\hat{w}/4\hat{L}_q$ (black dashed line). 40
- 2.8 Leading order ion distribution function $g_i^{(0,0)}$ vs. pitch angle, λ , at $\hat{p}_{\varphi} = 1.83$, $\xi = 0$. $w = 0.02r_s$, $\rho_{\vartheta i} = 1.0 \cdot 10^{-3}r_s$, ion collisionality $\nu_i^* = 10^{-4}$, $\varepsilon = 0.1$, $\hat{L}_q = 1$. $g_i^{(0,0)}$ is normalised to $n_0/(\pi^{3/2}V_{Ti}^3)$. Inset: a full solution of Eq.2.36 in a collisional layer around λ_c . $\sqrt{\nu^*}$ represents the width of the layer with $\nu^* = \nu_{ii}/\varepsilon\omega$. The trapped branch solution is σ -independent due to the summation over σ in Eq.2.24. 42
- 2.9 Sketch of the ion distribution function vs. \hat{p}_{φ} at $\lambda = 0.89$, $\xi = 0$ for $w \gg \rho_{\vartheta i}$ (left) and $w \gtrsim \rho_{\vartheta i}$ (right). $g_i^{(0)}$ is normalised to $n_0/(\pi^{3/2}V_{Ti}^3)$. $\varepsilon = 0.1$, $\hat{L}_q = 1$. Ion density/temperature length scales, $L_{n0}/L_{Ti} = 1$. $\bar{p}_{\varphi}(\sigma) = \hat{\omega}_D(\sigma)\hat{\rho}_{\vartheta i}\hat{L}_q/\hat{w}$. Dashed lines indicate the $\sigma = \pm 1$ passing ion distribution function, $g_i^{(0),\sigma}$, while solid line represents $\frac{1}{2} \sum_{\sigma} g_i^{(0),\sigma}$. The $\sigma = \pm 1$ drift islands are centered around $\bar{p}_{\varphi}(\sigma = \pm 1)$. The magnetic island is located between them; $\hat{p}_{\varphi} = \pm 1$ corresponds to the separatrix of the magnetic island. 43
- 2.10 Sum of the $\sigma = \pm 1$ leading order ion distribution functions plotted against $y = \sqrt{S - S_{\min}}$ at $\lambda = 0.89$, $\xi = 0$ for $w \gg \rho_{\vartheta i}$ (left) and $w \gtrsim \rho_{\vartheta i}$ (right). $g_i^{(0)}$ is normalised to $n_0/(\pi^{3/2}V_{Ti}^3)$. $\varepsilon = 0.1$, $\hat{L}_q = 1$. $L_n \equiv L_{n0}/(1 + \hat{\omega}_E)$ with $L_{n0} = 1$ being the density gradient length scale, $\hat{\omega}_E \equiv m\Phi'_{eqm}/q_s\omega_{dia,e} = 0$. $\eta_i \equiv L_n/L_{Ti} = 1$. L_{Tj} is the ion/electron temperature gradient length scale. Dashed line represents the analytic limit far from the island in the absence of Φ . 44
- 2.11 Radial density profile across the magnetic island O-point ($\xi = 0$) for different $\rho_{\vartheta i}$. $w = 0.02r_s$, $\varepsilon = 0.1$, $\hat{L}_q = 1$, ion collisionality $\nu_i^* = 10^{-3}$. Dashed line indicates the equilibrium density profile, $\propto L_n^{-1}\hat{w}\hat{\psi}$, $\hat{\omega}_E = 0$. Here n_{eqm} is the equilibrium density, i.e. in the absence of the magnetic island. 45
- 2.12 Radial derivative of the electrostatic potential, $\partial\hat{\Phi}/\partial\hat{\psi}$, across the magnetic island O-point ($\xi = 0$) for different $\rho_{\vartheta i}$ (notations are the same as used in Fig.2.11). $w = 0.02r_s$, $\varepsilon = 0.1$, $\hat{L}_q = 1$, ion collisionality $\nu_i^* = 10^{-3}$. The equilibrium density profile $\propto L_n^{-1}\hat{w}\hat{\psi}$, $\hat{\omega}_E = 0$. $\partial_{\hat{\psi}}\hat{\Phi}|_{\hat{\psi} \rightarrow \pm\infty} = 0$ 46
- 2.13 Contours of constant $\partial\hat{\Phi}/\partial\hat{\psi}$ in the (x, ξ) plane for a different ion poloidal Larmor radius value. $\varepsilon = 0.1$, $\hat{L}_q = 1$, $w = 0.02r_s$, ion collisionality $\nu_i^* = 10^{-3}$. The equilibrium density profile $\propto L_n^{-1}\hat{w}\hat{\psi}$, $\hat{\omega}_E = 0$. $\partial_{\hat{\psi}}\hat{\Phi}|_{\hat{\psi} \rightarrow \pm\infty} = 0$ 47

2.14	Contours of constant S in the (\hat{p}_φ, ξ) plane in the presence of the self-consistent electrostatic potential. $\lambda = 0.84$ ($\lambda_c = 0.91$), $\varepsilon = 0.1$, $V = V_{Ti}$, $\sigma = -1$, $\hat{L}_q = 1$, $w = 0.02r_s$, $\rho_{\vartheta i} = 1.0 \cdot 10^{-3}r_s$, ion collisionality $\nu_i^* = 10^{-3}$. Grey contour lines represent contours of constant S in the absence of the potential for the same input parameters.	50
2.15	Contours of constant S in the (\hat{p}_φ, ξ) plane in the presence of the self-consistent electrostatic potential. $\lambda = 0.84$ ($\lambda_c = 0.91$), $\varepsilon = 0.1$, $V = V_{Ti}$, $\sigma = -1$, $\hat{L}_q = 1$, $w = 0.02r_s$, $\rho_{\vartheta i} = 2.0 \cdot 10^{-3}r_s$, ion collisionality $\nu_i^* = 10^{-3}$. Grey contour lines represent contours of constant S in the absence of the potential for the same input parameters.	50
2.16	Same as Figs.2.14,2.15 except for the ion poloidal Larmor radius value, $\rho_{\vartheta i} = 5.0 \cdot 10^{-3}r_s$	50
2.17	Same as Figs.2.14,2.15 except for the ion poloidal Larmor radius value, $\rho_{\vartheta i} = 7.0 \cdot 10^{-3}r_s$	50
2.18	Same as Figs.2.14,2.15 except for the ion poloidal Larmor radius value, $\rho_{\vartheta i} = 8.0 \cdot 10^{-3}r_s$	50
2.19	Same as Figs.2.14,2.15 except for $\lambda = 0.98$, $\sigma = \sigma_t$, $\rho_{\vartheta i} = 1.0 \cdot 10^{-3}r_s$	50
2.20	Same as Figs.2.14,2.15 except for $\lambda = 0.98$, $\sigma = \sigma_t$, $\rho_{\vartheta i} = 2.0 \cdot 10^{-3}r_s$	51
2.21	Same as Figs.2.14,2.15 except for $\lambda = 0.98$, $\sigma = \sigma_t$, $\rho_{\vartheta i} = 5.0 \cdot 10^{-3}r_s$	51
2.22	Same as Figs.2.14,2.15 except for $\lambda = 0.98$, $\sigma = \sigma_t$, $\rho_{\vartheta i} = 7.0 \cdot 10^{-3}r_s$	51
2.23	Same as Figs.2.14,2.15 except for $\lambda = 0.98$, $\sigma = \sigma_t$, $\rho_{\vartheta i} = 8.0 \cdot 10^{-3}r_s$	51
2.24	Same as Figs.2.14,2.15 except for $\lambda = \lambda_{fin}$, $\sigma = \sigma_t$, $\rho_{\vartheta i} = 1.0 \cdot 10^{-3}r_s$	51
2.25	Same as Figs.2.14,2.15 except for $\lambda = \lambda_{fin}$, $\sigma = \sigma_t$, $\rho_{\vartheta i} = 2.0 \cdot 10^{-3}r_s$	51
2.26	Same as Figs.2.14,2.15 except for $\lambda = \lambda_{fin}$, $\sigma = \sigma_t$, $\rho_{\vartheta i} = 5.0 \cdot 10^{-3}r_s$	52
2.27	Same as Figs.2.14,2.15 except for $\lambda = \lambda_{fin}$, $\sigma = \sigma_t$, $\rho_{\vartheta i} = 7.0 \cdot 10^{-3}r_s$	52
2.28	Same as Figs.2.14,2.15 except for $\lambda = \lambda_{fin}$, $\sigma = \sigma_t$, $\rho_{\vartheta i} = 8.0 \cdot 10^{-3}r_s$	52
3.1	$g_j^{(0)}$ vs. λ at $\hat{p}_\varphi = -4.5$, $\xi = 0$, $V = V_{Ti}$. $w = 0.02r_s$, $\rho_{\vartheta i} = 1.0 \cdot 10^{-3}r_s$, ion collisionality $\hat{\nu}_i = 10^{-4}$, $\varepsilon = 0.1$, $\hat{L}_q = 1$. $g_i^{(0)}$ is normalised to $n_0/(\pi^{3/2}V_{Ti}^3)$. Red line indicates the trapped-passing boundary.	60
3.2	$g_j^{(0)}$ vs. λ at $\hat{p}_\varphi = 4.5$, $\xi = 0$, $V = V_{Ti}$. $w = 0.02r_s$, $\rho_{\vartheta i} = 1.0 \cdot 10^{-3}r_s$, ion collisionality $\hat{\nu}_i = 10^{-4}$, $\varepsilon = 0.1$, $\hat{L}_q = 1$. $g_i^{(0)}$ is normalised to $n_0/(\pi^{3/2}V_{Ti}^3)$. Red line indicates the trapped-passing boundary.	60
3.3	Same as Figs.3.1,3.2 except for $\hat{p}_\varphi = -2.52$	60
3.4	Same as Figs.3.1,3.2 except for $\hat{p}_\varphi = 2.52$	60
3.5	Same as Figs.3.1,3.2 except for $\hat{p}_\varphi = -1.26$	60
3.6	Same as Figs.3.1,3.2 except for $\hat{p}_\varphi = 1.26$	60
3.7	Same as Figs.3.1,3.2 except for $\hat{p}_\varphi = -1.08$	61
3.8	Same as Figs.3.1,3.2 except for $\hat{p}_\varphi = 1.08$	61
3.9	Same as Figs.3.1,3.2 except for $\hat{p}_\varphi = -0.36$	61
3.10	Same as Figs.3.1,3.2 except for $\hat{p}_\varphi = 0.36$	61
3.11	Same as Figs.3.1,3.2 except for $\rho_{\vartheta i} = 8.0 \cdot 10^{-3}r_s$	61
3.12	Same as Figs.3.1,3.2 except for $\rho_{\vartheta i} = 8.0 \cdot 10^{-3}r_s$	61
3.13	Same as Figs.3.1,3.2 except for $\hat{p}_\varphi = -2.52$, $\rho_{\vartheta i} = 8.0 \cdot 10^{-3}r_s$	61
3.14	Same as Figs.3.1,3.2 except for $\hat{p}_\varphi = 2.52$, $\rho_{\vartheta i} = 8.0 \cdot 10^{-3}r_s$	61
3.15	Same as Figs.3.1,3.2 except for $\hat{p}_\varphi = -1.26$, $\rho_{\vartheta i} = 8.0 \cdot 10^{-3}r_s$	62
3.16	Same as Figs.3.1,3.2 except for $\hat{p}_\varphi = 1.26$, $\rho_{\vartheta i} = 8.0 \cdot 10^{-3}r_s$	62
3.17	Same as Figs.3.1,3.2 except for $\hat{p}_\varphi = -1.08$, $\rho_{\vartheta i} = 8.0 \cdot 10^{-3}r_s$	62

- 3.18 Same as Figs.3.1,3.2 except for $\hat{p}_\varphi = 1.08$, $\rho_{\vartheta i} = 8.0 \cdot 10^{-3} r_s$ 62
- 3.19 Same as Figs.3.1,3.2 except for $\hat{p}_\varphi = -0.36$, $\rho_{\vartheta i} = 8.0 \cdot 10^{-3} r_s$ 62
- 3.20 Same as Figs.3.1,3.2 except for $\hat{p}_\varphi = 0.36$, $\rho_{\vartheta i} = 8.0 \cdot 10^{-3} r_s$ 62
- 4.1 A schematic representation of the solution technique.² 66
- 4.2 A schematic block diagram of the RDK-NTM solver.³ 67
- 4.3 The leading order ion distribution function plotted against y . Dashed curves correspond to $g_i^{(0,0)}$, i.e. the Reduced drift kinetic NTM solver: finds a solution of the reduced orbit-averaged drift kinetic equation to leading order in Δ , i.e. Eq.2.35 in the dissipative layer and Eq.2.40 outside the layer. The electrostatic potential is calculated self-consistently from the plasma quasi-neutrality condition. RDK-NTM has been developed in this dissertation. Its numerical scheme and numerical algorithm can be found in Sec.4 and Appendix E. (RDK-NTM) solution. Markers indicate the solution of Eq.2.35 [73, 74, 93], which is a function of p_φ , ξ and λ and keeps collisions to leading order for a full range of λ variation (to be referred to as the Drift kinetic NTM solver: finds a solution of the orbit-averaged drift kinetic equation to leading order in Δ , i.e. Eq.2.35 for a full range of the pitch angle variation. The electrostatic potential is calculated self-consistently from the plasma quasi-neutrality condition. DK-NTM with model analytic electrons has been developed in [73, 93, 74]. Its numerical scheme and numerical algorithm can be found in [74]. DK-NTM that treats electrons similar to RDK-NTM is under development by K. Imada. (DK-NTM) solution). $\nu_i^* = 10^{-2}$, $\rho_{\vartheta i}/w = 0.05$, $w/r_s = 0.02$. The distribution function is normalised to $n_0/(\pi^{3/2}V_{Ti}^3)$.⁴ 69
- 4.4 The DK-NTM leading order ion distribution function, $g_i^{(0)}$, plotted against y at different λ . (a),(b): zoom in the vicinity of the S island separatrix, $y = 0.1$, denoted by the grey vertical line. The green ($\sigma = -1$) and yellow ($\sigma = +1$) markers denote the DK-NTM solution. The red ($\sigma = -1$) and blue ($\sigma = +1$) dashed curves correspond to the RDK-NTM solution, $g_i^{(0,0)}$. The grey dashed line is the equilibrium in the absence of the island. (c)-(e) outside and (f)-(h) inside the dissipative layer (zoom in the vicinity of the drift island is shown in Fig.F.2). (h) is at the trapped-passing boundary. $\sigma_{p_\varphi} > / < 0$ in the upper/lower half-plane. $g_i^{(0,0)}$ is normalised to $n_0/(\pi^{3/2}V_{Ti}^3)$. $w = 0.02r_s$, $\rho_{\vartheta i} = 1.0 \cdot 10^{-3}r_s$, $\nu_i^* = 10^{-2}$, $\varepsilon = 0.1$, $\hat{L}_q = 1$. $L_{n0} = 1$, $\hat{\omega}_E = 0$. (c)-(h): markers are as in Figs.4.3a,4.3b. 71
- 4.5 The leading order ion distribution function, $g_i^{(0,0)}$, and its y derivative, $\partial g_i^{(0,0)}/\partial y|_{\xi,\lambda}$, localised to the vicinity of the magnetic island of width $w = 0.02r_s$ at the deeply passing end, $\lambda = 0$, (a) and (c), and at $\lambda = \lambda_p$, (b) and (d) (blue and red dashed curves/x-markers, $\sigma_{p_\varphi} > / < 0$ is the upper/lower half-plane). $g_i^{(0,0)}$ is normalised to $n_0/(\pi^{3/2}V_{Ti}^3)$. $\rho_{\vartheta i} = 1.0 \cdot 10^{-3}r_s$, $\nu_i^* = 10^{-2}$, $\varepsilon = 0.1$, $\hat{L}_q = 1$. $L_{n0} = 1$, $\hat{\omega}_E = 0$. The dashed grey line corresponds to an analytic limit far from the magnetic island, i.e. equilibrium gradient denoted by *eqm*. The solid grey line indicates the location of the S island separatrix. DK-NTM results are presented across the S island O-point. Pink and purple $H96$ curves represent an analytic solution, $h(\Omega)$, [53] rewritten in terms of y (a),(b) and differentiated with respect to y (c),(d) for $\sigma = \pm 1$, respectively. $h(\Omega)$ is valid in the limit of large w and small $\rho_{\vartheta i}$ outside the magnetic island separatrix. The light blue and orange curves/green diamond markers indicate the RDK-NTM solution with the model S diffusion with $\sqrt{S}/\sqrt{S+\cos\xi}$ taken for the weight function for $\sigma = \pm 1$. 72

- 4.6 Sum of the $\sigma = \pm 1$ leading order ion distribution functions plotted against p_φ at fixed λ . $g_i^{(0,0)}$ is normalised to $n_0/(\pi^{3/2}V_{Ti}^3)$. $w = 0.02r_s$, $\rho_{\vartheta i} = 1.0 \cdot 10^{-3}r_s$, $\nu_i^* = 10^{-2}$, $\varepsilon = 0.1$, $\hat{L}_q = 1$. $L_{n0} = 1$, $\hat{\omega}_E = 0$. The red dashed line represents the analytic limit far from the magnetic island in the absence of the electrostatic potential. DK-NTM denotes the solution of Eq.2.35 [73, 74, 93]. However, in contrast to [73, 74, 93], DK-NTM (provisional) adds numerical electrons to the model similar to the RDK-NTM solver. 73
- 4.7 Same as Fig.4.6 except for $\nu_i^* = 10^{-3}$ 74
- 4.8 Same as Fig.4.7 except for $\rho_{\vartheta i} = 7.0 \cdot 10^{-3}r_s$, corresponding to $\rho_{\vartheta i}/w = 0.35$ 75
- 4.9 (right-to-left) The leading order ion distribution function vs. \hat{p}_φ , $g_i^\sigma = g_i^\sigma(\hat{p}_\varphi)$ at fixed λ at the 0th iteration in Φ . Its density moment, $(1/2) \sum_\sigma g_i^\sigma$, against \hat{p}_φ . Dashed red line corresponds to equilibrium in the absence of the magnetic island. Its flow moment, $(1/2) \sum_\sigma \sigma g_i^\sigma$, against \hat{p}_φ . $g_i^{red} \equiv g_i^\sigma - \mathcal{C}\hat{p}_\varphi$ against λ at fixed \hat{p}_φ . The λ dependence is presented at $\rho_{\vartheta i} = 7.0 \cdot 10^{-3}r_s$. The vertical red line indicates the trapped-passing boundary, $\lambda_c \approx 0.909$. $w = 0.02r_s$, $\varepsilon = 0.1$, $\hat{L}_q = 1$, $L_{n0} = 1$, $\hat{\omega}_E = 0$, $\eta_i = 1$ and $\hat{\nu}_i = 10^{-4}$ 78
- 4.10 Same as Fig.4.9 but for the electron plasma component. $\hat{\nu}_i = 10^{-4}$ unless otherwise stated. 79
- 4.11 Same as Fig.2.11 except for the ion collisionality $\nu_i^* = 10^{-4}$ 80
- 4.12 The ion flow moment, $\sum_\sigma \sigma g_i^\sigma$, plotted against p_φ at $\lambda = 0.0873$, $\xi = 0$ for $w = 0.02r_s$, $\rho_{\vartheta i} = 1.0 \cdot 10^{-3}r_s$ (left) and $w = 0.02r_s$, $\rho_{\vartheta i} = 7.0 \cdot 10^{-3}r_s$ (right), $\varepsilon = 0.1$, $\hat{L}_q = 1$, $L_{n0} = 1$, $\hat{\omega}_E = 0$, $\eta_i = 1$ and $\hat{\nu}_i = 10^{-4}$. The grey lines in Fig.4.12a correspond to $p_\varphi = w$, which is close to the magnetic island separatrix for small $\rho_{\vartheta i}/w$. The red dashed line in Figs.4.12a,4.12b corresponds to the equilibrium gradient, i.e. in the absence of the NTM island. 81
- 4.13 The sum of the bootstrap and curvature contributions to the modified Rutherford equation normalised to poloidal beta, $(\Delta_{bs} + \Delta_{cur})/\beta_\vartheta$, vs. w/r_s for different values of the ion poloidal Larmor radius, $\rho_{\vartheta i}$. The dashed line is the analytic result for the bootstrap current contribution, valid in the limit of large magnetic island widths. Here w_c defined as a solution of $\Delta_{bs} + \Delta_{cur} = 0$ represents a magnetic island threshold, also called a critical magnetic island half-width. Inset: w_c vs. $\rho_{\vartheta i}$. $\varepsilon = 0.1$, $\hat{L}_q = 1$, ion collisionality $\nu_i^* = 10^{-4}$. The equilibrium density and temperature gradients are $L_n^{-1} = 1$ with $\hat{\omega}_E = 0$, $L_{Tj}^{-1} = 1$ 83
- 4.14 A sum of the bootstrap and curvature contributions, $\Delta_{bs} + \Delta_{cur}$, plotted against $w/\rho_{\vartheta i}$ for different $\rho_{\vartheta i}$ at the end of the 0th iteration in Φ (left) and with self-consistent electrostatic potential Φ (right) (green: electrons, blue: ions, red: total; markers denote the corresponding value of $\rho_{\vartheta i}$). $\varepsilon = 0.1$, $\hat{L}_q = 1$, $\hat{\nu}_i = 10^{-4}$. The equilibrium density and temperature gradients are $L_n^{-1} = 1$, $L_{Tj}^{-1} = 1$. The ion/electron distribution function has been calculated with the model $\propto \sqrt{S}$ diffusion. 84
- 4.15 Same as Fig.4.14b but based on the full RDK-NTM solution. 85
- 4.16 The sum of the bootstrap and curvature contributions, $\Delta_{bs} + \Delta_{cur}$, (filled markers, extremum in the upper half-plane) and the polarisation contribution, Δ_{pol} , (un-filled markers, extremum in the lower half-plane) against w/r_s for different $\rho_{\vartheta,i}$ with self-consistent Φ . The dashed black line $\propto 1/w$ and the dashed grey line $\propto 1/w^3$ indicate the limit of large magnetic island width. $\varepsilon = 0.1$, $\hat{L}_q = 1$, ion collisionality $\nu_i^* = 10^{-3}$. The equilibrium density and temperature gradients are $L_n^{-1} = 1$, $L_{Tj}^{-1} = 1$ 87

- 4.17 The full critical magnetic island width, w_c , defined as a solution of $\Delta_{neo}(w) = 0$ as a function of the ion poloidal Larmor radius, $\rho_{\vartheta i}$. The red dashed line is the best fit line that provides the approximation. w_c and $\rho_{\vartheta i}$ are normalised to the radius of the rational surface, r_s . $\varepsilon = 0.1$, $\hat{L}_q = 1$, ion collisionality $\nu_i^* = 10^{-4}$. The equilibrium density and temperature gradients are $L_n^{-1} = 1$ with $\hat{\omega}_E = 0$, $L_{Tj}^{-1} = 1$ 87
- 4.18 (left) The integrated through the island sine component of $\partial\mathcal{L}/\partial A_{\parallel}$ plotted against ω_E with the self-consistent electrostatic potential. (right) $\partial\mathcal{L}/\partial\Phi$, integrated through the island region, plotted against ω_E for the model potential, $\hat{\Phi} = \hat{\omega}_E L_{n0}^{-1} \hat{w} \hat{\psi}$ (circle red markers). The Lagrangian density, \mathcal{L} , is given by Eq.2.8. Solutions of $[\partial\mathcal{L}/\partial A_{\parallel}]^s(\omega) = 0$ and $[\partial\mathcal{L}/\partial\Phi](\omega) = 0$ match at $\omega_E = -0.93\omega_{dia,e}$. Ion collisionality $\nu_i^* = 10^{-4}$, $\varepsilon = 0.1$, $\hat{L}_q = 1$. The equilibrium density and temperature gradients are $L_{n0}^{-1} = 1$, $L_{Tj}^{-1} = 1$ 88
- 4.19 (a) The cosine component of the ϑ -averaged parallel current density perturbation integrated over ξ at fixed Ω , $\langle \bar{J}_{\parallel} \cos \xi \rangle_{\xi}^{\Omega}$, plotted against Ω for different $\rho_{\vartheta i}$. The in-phase component of the ion (b)/electron (c) parallel flow averaged over ϑ and over ξ at fixed Ω plotted against Ω for different $\rho_{\vartheta i}$. (d) Zoom of (a) outside the magnetic island separatrix, i.e. $\Omega \geq 1$. (e) $\langle \bar{J}_{\parallel} \cos \xi \rangle_{\xi}^{\Omega}$ for different $\hat{\nu}_i$. (f) $\langle \bar{J}_{\parallel} \cos \xi \rangle_{\xi}^{\Omega}$ for different w 91
- 4.20 (a) The cosine component of the ϑ -averaged parallel current density perturbation integrated over ξ at fixed Ω , $\langle \bar{J}_{\parallel} \cos \xi \rangle_{\xi}^{\Omega}$, plotted against Ω for different $\rho_{\vartheta i}$. The in-phase component of the ion (b)/electron (c) parallel flow averaged over ϑ and over ξ at fixed Ω plotted against Ω for different $\rho_{\vartheta i}$. (d) Same as (a) except for $\hat{\nu}_i = 10^{-3}$. (f) $\langle \bar{J}_{\parallel} \cos \xi \rangle_{\xi}^{\Omega}$ at small and large $\rho_{\vartheta i}$ 94
- 4.21 The polarisation contribution to the evolution of the magnetic island vs. ω_E (note: region of $\Delta_{pol} < 0$ is stable). The ω_E dependence in the island rest frame provides the ω_0 dependence in the reference frame, where the radial electric field is zero far from the island. Inset: zoom in a region $\Delta_{pol}(\omega_E) = 0$. Red curves indicate a parabolic approximation. The ω_E^2 behaviour is predicted in the analytic limit of large w . Ion collisionality $\nu_i^* = 10^{-4}$, $\varepsilon = 0.1$, $\hat{L}_q = 1$, $L_{n0}^{-1} = -0.1$. $0 \leq \omega_E \leq \omega_{dia,e}$ corresponds to a region of coupling to electron drift waves. For these parameters: $\omega_0/\omega_{dia,e} \in \{\dots, -1.04, -0.93, 0, 0.92, \dots\}$ 95
- 5.1 Sketch of the bump-on-tail distribution function. The local maximum is localised around V_b 99
- 5.2 A phase space island near the resonant surface, $\mathbf{n} \cdot \mathbf{\Omega}(\mathbf{J}) = 0$ [96]. 101
- 5.3 Sketch of H_0 against ξ at $p = 0$ [96]. ξ varies from $-\pi$ to π outside the phase space island and between the bounce points, $\xi_{b1,2}$, given by $H_0 = -\omega_b^2 \cos \xi_{b1,2}$, inside the island region. 101
- 5.4 The EP distribution function $\hat{f}_{0,j}$ plotted against \hat{p} across the island O-point, i.e. $\xi = 0$, for arbitrary \hat{D}_p and $\hat{\nu}_{f,p}$. The solution, $\hat{f}_{0,j}$, is localised to the island vicinity, which allows the initial equilibrium distribution function to be Taylor expanded around the resonant surface. The dashed lines indicate the position of the phase space island separatrix, $\hat{H}_0 = \hat{\omega}_b^2$. Hats indicate the normalisation that has been chosen as in [95].⁵ 105

- 5.5 (top) The leading order EP distribution function vs. $y = \sqrt{\hat{H}_0 + \hat{\omega}_b^2}$ for two branches of the stream, $\sigma_p = \pm 1$ for (a) a case of pure diffusion, (b) when velocity diffusion and drag are comparable and (c) when the drag term is dominant. The dotted line represents the trapped-passing boundary, $y_b = \sqrt{2}\hat{\omega}_b$. $y \geq y_b$ and $0 \leq y < y_b$ correspond to the passing and trapped regions, respectively. The trapped particle solution is σ_p -independent and hence both σ_p branches match in the trapped region. (bottom) Contours of constant $\hat{f}_{0,j}^{(0)}$ in the (\hat{p}, ξ) plane, which reproduce the phase space island structure; $\hat{\omega}_b = 1$. Hats indicate the normalisation that has been chosen as in [95].⁶⁹ 107
- 5.6 The ξ -averaged EP distribution function, $\langle f_{0,j} \rangle_\xi$, vs. p for arbitrary D_p and $\nu_{f,p}$, $\omega_b = 0.1\omega_{pe}$. $f_{0,j}$ is normalised to $n_{eqm}k_0/\omega_{pe}$, n_{eqm} is the equilibrium density. Thick lines indicate the solution of Eq.(14), which is localised to the island vicinity. Thin lines indicate the COBBLES distribution function. Diffusion and friction rates in velocity space are $\nu_{d,V} = 0.01\omega_{pe}$ and $\nu_{f,V} = 0$ (blue curves), $\nu_{d,V} = 0.01\omega_{pe}$ and $\nu_{f,V} = 0.0216\omega_{pe}$ (red curves). In p space, these correspond to diffusion $D_p = \nu_{d,V}^3(k_0/k_1)^2 = 1.6 \cdot 10^{-5}\omega_{pe}^3$ and drag $\nu_{f,p} = \nu_{f,V}^2(k_0/k_1) = 0/4.0 \cdot 10^{-4}\omega_{pe}^2$, respectively. $\nu_{f,V}/\nu_{d,V} = 2.16$ 108
- 5.7 Same as Fig.5.6 except for the bounce frequency value, $\omega_b = 0.07\omega_{pe}$ 108
- 5.8 Same as Fig.5.6 except for the bounce frequency value, $\omega_b = 0.05\omega_{pe}$ 108
- 5.9 The normalised secondary mode growth/decay rate as a function of l in a pure diffusion case (diamond markers) and in the presence of drag (circle markers). Solid lines represent the best fit line for each case. The bounce frequency at the deeply trapped end is $\omega_b/\omega_{p,e} = 0.1$. The D_p and $\nu_{f,p}$ values and normalisation correspond to Figs.5.6-5.8, i.e. $D_p = 1.6 \cdot 10^{-5}\omega_{pe}^3$, $\nu_{f,p} = 4.0 \cdot 10^{-4}\omega_{pe}^2/0$. The regions of negative γ are stable. 119
- 5.10 The normalised secondary mode growth/decay rate as a function of the bounce frequency of the deeply trapped particles, ω_b , in the presence of slowing down, $\nu_{f,p}$ (solid lines represent the best fit line for each case). The p space diffusion is kept fixed, $D_p = 1.6 \cdot 10^{-5}\omega_{pe}^3$. The primary/secondary wave number ratio, $l = 1.25$. The D_p and $\nu_{f,p}$ normalisation correspond to Figs.5.6-5.8. In each case arrows indicate roots of $\gamma = \gamma(\omega_b)$. The first root, $\omega_{b,c}$, denotes a critical island half-width, below which the secondary mode stability is achieved. The second root, $\omega_{b,s}$ corresponds to the saturation level, above which the secondary mode is stable. The regions of negative γ are stable. 120
- 5.11 The secondary mode growth/decay rate vs. ω_b in a pure diffusion case, $D_p = 1.6 \cdot 10^{-5}\omega_{pe}^3$ (D_p value and normalisation correspond to Figs.5.6-5.8). The primary/secondary mode number ratio, $k_0/k = 4/5$. An analytic solution (square and diamond markers) is calculated based on Eqs.5.51,5.52/Eq.5.53. Solid lines indicate the COBBLES growth/decay rates. The regions of negative γ are stable. 121
- A.1 A ring of toroidal plasma in the presence of the NTM magnetic islands. . . . 130
- E.1 Block diagram 202
- F.1 The neoclassical MRE contributions to the island time evolution for different $\rho_{\vartheta i}$. 204
- F.2 Zoom of Fig.4.4(c)-(h) in the vicinity of the S island, $\sigma = \pm 1$, $\sigma_{p\varphi} = +1$. The ξ dependence of $g_i^{(0)}$ for each σ is weak outside the dissipative layer, (c)-(e), and becomes significant close to the trapped-passing boundary, (f)-(h). 205

- F.3 Orbit-averaged parallel current density perturbation plotted against Ω in the vicinity of the magnetic island separatrix for small $\rho_{\vartheta i}/w = 0.05$ (a) and large $\rho_{\vartheta i}/w = 0.33$ (c). (b)/(d) Zoom of (a)/(c) far from the magnetic island, respectively. Blue curves indicate an analytic limit far from the magnetic island obtained in [53]. Here the maximum value of ψ is $2.9w$, i.e. 1.45 island widths. 206

List of Tables

4.1	Area under the $\langle \bar{J}_{\parallel} \cos \xi \rangle_{\xi}^{\Omega}$ curve inside, $-1 \leq \Omega \leq 1$, and outside the magnetic island, $\Omega \geq 1$ for a different right limit, i.e. maximum value of ψ/w . $\hat{\psi} = 2.9$ corresponds to 1.45 island widths, and $\hat{\psi} = 10$ corresponds to 5 island widths. $w = 0.02r_s$, $\hat{\nu}_i = 10^{-4}$, $\varepsilon = 0.1$, $\hat{L}_q = 1$, $\eta_i = 1$. The presented data corresponds to Fig.4.19, (a).	92
4.2	Same as Table 4.1, except for $\hat{\nu}_i = 10^{-3}$	93

Acknowledgements

Firstly, I would like to thank my scientific advisor, Howard Wilson. I would also like to thank David Dickinson and Peter Hill for many useful discussions and a lot of good advice that helped improve the RDK-NTM performance. I would like to thank Jacek Dobaczewski, Ben Dudson and Koki Imada for helpful conversations regarding the work presented here.

I would also like to thank Xavier Garbet and Maxime Lesur for their support with the island stability project. I am grateful to Jeff Candy for helping improve the island stability paper and his helpful advice.

Finally, I thank my mum and dad for their support. I would also like to thank Alisa, in particular for her help with implementing some of my drawings.

Declaration of Authorship

I, Aleksandra Dudkovskaia, declare that this dissertation titled "Modelling Neoclassical Tearing Modes in Tokamak Plasmas" and the work presented in it are my own. I confirm that

- This work was done wholly or mainly while in candidature for a research degree at this University.
- Where I have consulted the published work of others, this is always clearly attributed.
- Where I have quoted from the work of others, the source is always given. With the exception of such quotations, this dissertation is entirely my own work.
- I have acknowledged all main sources of help.

The work and results described in this dissertation have previously been published or presented at conferences. The neoclassical tearing mode threshold results have been presented at the following conferences:

- A reduced drift magnetic island theory of neoclassical tearing modes for low collisionality plasmas, 45th EPS conference on Plasma Physics, Prague, Czech Republic, 2018 (poster);
- Drift kinetic description of neoclassical tearing modes, 46th EPS conference on Plasma Physics, Milan, Italy, 2019 (talk);
- Drift kinetic effects on the neoclassical tearing mode threshold, 46th EPS conference on Plasma Physics, Milan, Italy, 2019 (co-author, poster presented by K. Imada)

and partially appears in the following publications:

- K. Imada, H.R. Wilson, J.W. Connor, A.V. Dudkovskaia and P. Hill *Phys. Rev. Lett.* **121** (2018) 175001;
- K. Imada, H. R. Wilson, J. W. Connor, A. V. Dudkovskaia and P. Hill *J. Phys.: Conf. Ser.* 1125 (2018) 012013;
- K. Imada, H.R. Wilson, J.W. Connor A.V. Dudkovskaia and P. Hill *Nucl. Fusion* **59** (2019) 046016.

The paper that fully accounts for the results presented in Chapter IV including calculations of the neoclassical tearing mode threshold island width and the polarisation current contribution to the island evolution is in preparation:

- A.V. Dudkovskaia, J.W. Connor, D. Dickinson, K. Imada, P. Hill and H.R. Wilson, in preparation (2019).

The work and results discussed in Chapter V have been presented at

- Island stability in phase space, Festival de Théorie, Aix-en-Provence, France, 2017 (talk);
- Searching for the secondary instabilities in magnetically confined plasmas, Theory of Fusion Plasmas workshop, Varenna, Italy, 2018 (poster);

and published in

-
- A. V. Dudkovskaia, X. Garbet, M. Lesur, H. R. Wilson *J. Phys.: Conf. Ser.* 1125 (2018) 012009;
 - A. V. Dudkovskaia, X. Garbet, M. Lesur, H. R. Wilson *Nucl. Fusion* **59** (2019) 086010.

Chapter I

1 Introduction

1.1 World energy problem

The world population and its growth rate determine energy consumption. According to the recent United Nations (UN) estimates (as of May 2019), the current world population is over 7.7 billion people [1] and is still growing (see Fig.1.1). In the best case scenario, it will start decreasing by 2075. The "high" UN scenario predicts that the population of 10 billion people will be exceeded by 2050 and will continue growing. This, in turn, results in a rapid increase in the demand of energy and the necessity of its production.

Currently, fossil fuels solve the problem of the energy demand. Petroleum, coal and natural gas (up to 85% in total) form the primary world sources of energy. However, they are limited and products of their burning have a significant impact on the atmosphere leading to climate changes. In Fig.1.2 we show the global average long-term concentration of CO_2 in the atmosphere [3] and global annual fossil fuel CO_2 emissions according to the Carbon Dioxide Information Analysis Center (CDIAC) [4]. The CO_2 emissions have increased rapidly over the past century. The global emission of carbon dioxide had been reported to be saturated from

2014 to 2017. However, the recent report provided by the Global Carbon Project stated a 2.7% emission growth in 2018 [5]. The amount of carbon dioxide in the atmosphere has

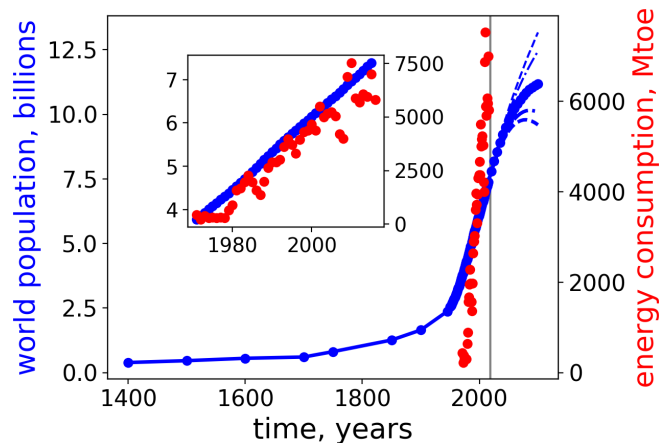


Figure 1.1: Time evolution of the total world population [1] (left) and the corresponding energy consumption in Mtoe, million tonnes of oil equivalent [2] (right). The probabilistic population up to 2100 based on "high" (upper95 and upper80) and "low" (lower95 and lower80) UN projections is indicated by thin/thick dashed and dotted blue curves, respectively. The "medium" projection is indicated by blue circle markers. Inset: zoom in a region from 1971 to 2015.

grown significantly since 1700s, which correlates directly with its emission and explained by the global industrialisation that began in 17th-18th centuries. The atmospheric carbon residence time is around five years but is much greater in the ocean. Carbon Capture and Storage (CCS) might be able to reduce the future emitted carbon dioxide but cannot decrease its current amount, which is 411 ppm as of 2019 according to the latest measurement [6] (300 ppm level has never been exceeded till the last century).

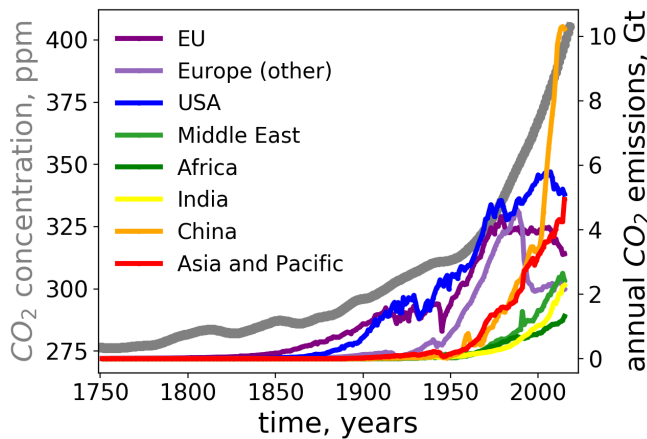


Figure 1.2: Time evolution of the atmospheric concentration of carbon dioxide, CO_2 , in parts per million, ppm [3] (left) and its emission in billion tonnes (Gt) per year [4] (right). A time interval from 1751 to 2015 is covered.

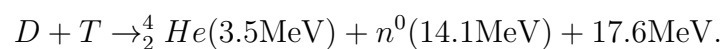
resources, nuclear fission and nuclear fusion. The main concern about renewable energy is its strong time dependence, which requires energy to be stored and thus results in additional costs and technical challenges. Fission waste is highly radioactive with long life-times but its amount is relatively low. Leaving the safety problem beyond the scope of this discussion, we have to highlight that the lifetime of the uranium isotope reserves with the current types of reactors is around 70-80 years, i.e. comparable to that of fossil fuels. The latter, fusion energy, is less understood and developed and represents the focus of this study.

On the other hand, taking into account the current production rates, we have known resources of coal, oil and natural gas for 114, 51 and 53 years, respectively. Although these numbers are provisional and depend on the economical situation and on the consumption rate, they still provide the perspective picture. An energy transition is unavoidable. There is a small number of alternative, non-fossil energy sources that potentially can provide long-term energy production:

energy generated from renewable

1.2 Nuclear Fusion

The Sun is the main energy source in our solar system. It releases 384.6 yotta watts or around 4.26 million metric tons each second according to mass-energy equivalence Einstein's formula. There are two main concepts to bring fusion to Earth: magnetic confinement fusion (MCF) in tokamaks and stellarators (or reversed field pinches) and laser or beam induced inertial confinement fusion (ICF). Here we focus on MCF in tokamak devices. The current goal is to achieve controlled fusion through the DT fusion reaction:



The corresponding mass defect can be calculated as $\Delta m = m_D + m_T - (m_{{}^4_2\text{He}} + m_{n^0})$ and gives $3.1 \cdot 10^{-29}\text{kg}$ of mass loss per reaction, or the energy release of $\Delta E = \Delta mc^2 = 17.6\text{MeV}$, i.e. 3.5MeV per nucleon is released in this reaction. In contrast, at the high atomic mass end of the curve of binding energy

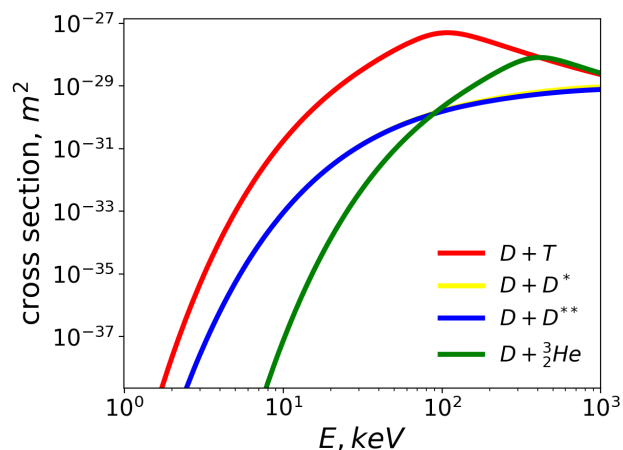
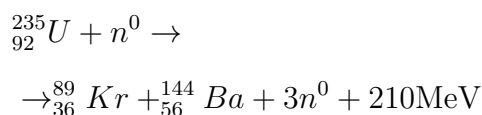
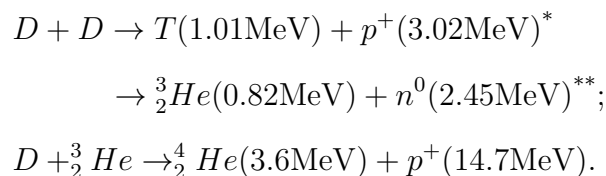


Figure 1.3: Cross section of main MCF fusion reactions. E is energy in keV.



produces 0.9MeV per nucleon. Other popular fusion reactions are



In Fig.1.3 we compare their cross sections. The DD and D³He cross sections are relatively lower than that of DT. The reaction reactivity plotted as a function of temperature is 1-2 orders of magnitude larger for the DT reaction than DD and D³He in an interval from 1

to 100keV and has a maximum. This, in turn, provides an optimum temperature. The reaction cross section is one of the reasons why the DT fusion reaction is considered as the most preferable nowadays. Fusion in this form has potentially inexhaustible resources. Deuterium produced by nature is abundant in the ocean. Tritium is radioactive with a half-life of around 12.3 years. Thus, tritium is rare and has to be produced. ${}^6_3\text{Li} + n^0$, ${}^7_3\text{Li} + n^0$, ${}^{10}_5\text{B} + n^0$ have tritium in their products. The following reaction is to be tested on ITER



in a breeder blanket for testing tritium production (lithium-6 is 7.5% of natural lithium, the rest 92.5% is lithium-7). We have to note here that while ITER will be valuable for testing tritium breeding blankets, its operation will not rely on tritium production. The alpha particle generated by the DT reaction carries about 1/5 of total fusion energy. It is charged and therefore is able to interact with fuel ions. Neutrons carry about 4/5 of the produced fusion energy and being uncharged tend to escape the fuel. To collect the neutrons, capture their energy and breed tritium, the blanket modules are placed around the plasma in front of the vacuum vessel inner wall. They therefore provide a shield for the wall from the fusion generated highly energetic neutrons and in-vessel heat loads. Inside the blanket modules, the neutrons are to be slowed down and their energy is to be gathered by a coolant (e.g. water or helium coolants) in the form of heat [7]. The blankets contain ${}^6_3\text{Li}$ to breed tritium that is then to be used in the DT reaction providing the self-sustaining mechanism. This breeding blanket concept is to be tested on ITER and is then to be applied to DEMO.

1.3 Ignition criteria

The power balance can be written as $P_{in} = P_L + dW/dt$. Here P_{in} is the heating power, P_L is the power that leaks out of the plasma and W is the thermal energy of the plasma. P_{in} has two components: external heating, P_H , and the heating provided by the fusion produced alpha particles, P_α . External heating sources such as neutral beam injection (NBI), ion and electron cyclotron heating (ICRH and ECRH) are required to achieve

plasma temperatures necessary to start fusion. Defining the energy confinement time, τ_E , as W/P_L , we write in steady state: $P_H = [3nT/\tau_E - n^2 \langle \sigma V \rangle \mathcal{E}_\alpha/4] \mathcal{V}$, where n and T are the plasma density and temperature, \mathcal{E}_α is energy of alpha particles, $\langle \sigma V \rangle$ is the reaction reactivity and \mathcal{V} is the characteristic volume of the system. $P_H > 0$ defines a burning plasma, while $P_H < 0$ provides the ignition condition:

$$nT\tau_E > \frac{12T^2}{\langle \sigma V \rangle \mathcal{E}_\alpha}, \quad (1.1)$$

also known as the Lawson criteria [8]. One can also introduce the fusion gain factor, Q , as the ratio of the fusion power output to the power necessary to keep the plasma in steady state, i.e. external heating power. $Q = \infty$ corresponds to ignition. The burning plasma regime starts at $Q = 5$. The ITER goal in its inductive regime is $Q \gtrsim 10$. We have to stress here that for future power plants, the actual "engineering" Q factor is much lower as it takes into account the fact that fusion energy extracted from the reactor has to be converted into electricity and the heating systems are not 100% efficient. Eq.1.1 implies a pure plasma in the absence of any impurities. Considering the Lawson parameter, $n\tau_E$, as a function of temperature, we find that it has a minimum around 25keV and thus ignition is easier to achieve at this temperature. This is to be used in ICF. In MCF including the temperature dependence, we obtain a good fit for $10\text{keV} < T < 20\text{keV}$: $\langle \sigma V \rangle = 1.1 \cdot 10^{-24} T^2 \text{m}^3 \text{s}^{-1}$. Thus, for the hydrogen (DT) plasma, Eq.1.1 gives $3 \cdot 10^{21} \text{m}^{-3} \text{keVs}$. The left hand side of Eq.1.1 is called the fusion triple product. The Lawson criteria of the form Eq.1.1 is usually applied to magnetically confined plasmas. ICF usually operates with $n\tau_E$ or ρr_p , where ρ is the mass density and r_p is the radius of fuel pellet. Estimating the energy confinement time as r_p/V_{Ti} with V_{Ti} being the ion thermal velocity, we write $\rho r_p > 0.6 \text{kgm}^{-2}$ for the ignition requirement. So the aim of ICF is to achieve the maximum density within a finite, very short period of time, while MCF tends to reach the maximum energy confinement time keeping the density low. In ICF the inertia plays a key role keeping the fuel together. In MCF the plasma is held by the magnetic fields. The latter is the subject of this study.

1.4 Physics of plasmas

Not every ionised gas can be treated as a plasma. A plasma is quasi-neutral, i.e. ion and electron densities are nearly equal. However, the charge imbalance is still sufficient for the electromagnetic effects to play a role. To estimate the charge difference, we write Poisson's equation

$$\Delta\Phi = -\frac{e}{\varepsilon_0} (Z_i n_i - n_e), \quad (1.2)$$

where Φ is the electrostatic potential, $n_{i/e}$ is the ion/electron density and eZ_i is the ion charge. Estimating the electrostatic potential as $\sim T_e/e$ (T_e is the electron temperature) and the left hand side of Eq.1.2 through $\Delta\Phi \sim \Phi/L^2$ with L being the characteristic length of the considered system, we obtain:

$$\frac{|n_i - n_e|}{n_e} \sim \frac{r_D^2}{L^2} \ll 1$$

with $r_D = \sqrt{\varepsilon_0 T_e / n_e e^2}$ being the Debye radius. $Z_i = 1$ has been assumed here. L can be understood as $|\nabla_r \ln n|^{-1}$, the density gradient length scale. Quasi-neutrality holds only outside the Debye sphere, i.e. a sphere of radius r_D . Hence, to behave as a plasma, an ionised gas must satisfy the requirement: $L \gg r_D$. The second characteristic feature of plasma is its collective behaviour. The number of particles in the Debye sphere is $N_D = (4\pi/3)n_e r_D^3 \gg 1$. N_D is also called the plasma parameter. In plasma, collisions between charged and neutral particles must not be dominant and can be considered as being infrequent. Charged particles can be neutralised colliding with neutrals due to the charge exchange process. Charged particles have to remain charged within a period $\sim \Omega^{-1}$ for a gas to be defined as a plasma in addition to the conditions described above (Ω here is a characteristic frequency of plasma oscillations). This requirement reads as $\tau\Omega \gg 1$ with τ being the time between charged particle and neutral collisions. Therefore, the plasma should be dense enough and its temperature is high enough so that only a relatively few numbers of neutrals could exist.

Let us start with a brief discussion of motions of each individual particle and then consider the effects of collective motion. Each charged particle in the magnetic field experiences

the Lorentz force in accordance with

$$m_j \frac{d\mathbf{V}_j}{dt} = eZ_j [\mathbf{V}_j \times \mathbf{B}] + eZ_j \mathbf{E}, \quad (1.3)$$

where eZ_j and m_j are the particle charge and mass, respectively. \mathbf{E} is the electric field, \mathbf{B} is the magnetic field and \mathbf{V}_j is the velocity of the particle. j is used to label particle species. In the absence of the electric field, the particle experiences a magnetic force that is orthogonal to \mathbf{B} and thus it gyrates around the magnetic field line. The particle trajectory becomes helical provided the component of velocity parallel to the magnetic field, V_{\parallel} , is non-zero. The radius of this circular motion is called the Larmor radius and is defined as $\rho_{cj} = V_{\perp}/\omega_{cj}$. $\omega_{cj} = eZ_j B/m_j$ is the corresponding cyclotron frequency of a species j . The component of velocity perpendicular to the magnetic field lines, V_{\perp} , being estimated through the thermal velocity of a species, provides $\rho_{cj} \sim m_j V_{Tj}/eZ_j B$. Defining the guiding centre as the point or line around which a charged particle gyrates, we note that this line follows the \mathbf{B} field line provided the magnetic field is homogeneous and its field lines are straight. The particle drift effects force the guiding centre to drift away from a certain field line. Replacing $eZ_j \mathbf{E}$ in Eq.1.3 with \mathbf{F} , where \mathbf{F} is a constant homogeneous force, allows one to define individual particle drifts. The parallel component of \mathbf{F} simply accelerates the charge along the field line, while its perpendicular components, \mathbf{F}_{\perp} , provide a constant drift velocity,

$$\mathbf{V}_{\perp} = \frac{\mathbf{F}_{\perp} \times \mathbf{B}}{eZ_j B^2}. \quad (1.4)$$

If the force is associated with the electric field, then Eq.1.4 gives the expression for the $\mathbf{E} \times \mathbf{B}$ drift, $\mathbf{V}_E = [\mathbf{E} \times \mathbf{B}]/B^2$, that is independent of particle properties and thus does not generate a current. Taking into account the fact that the magnetic field lines are not straight, we have to introduce the centrifugal force in Eq.1.4. Therefore, we derive $\mathbf{V}_{cur} = (m_j V_{\parallel}^2/eZ_j B^2) [\mathbf{R}_c \times \mathbf{B}]/R_c^2$ for the so called curvature drift. R_c is the radius of curvature of the particle trajectory along the field lines. The magnetic field has a spatial dependence, i.e. is not homogeneous, in most cases, and then the gyrating particle has to experience a varying magnetic field. This provides the ∇B drift with $\mathbf{V}_{\nabla B} = (\rho_{cj} V_{\perp}/2) [\mathbf{B} \times \nabla B]/B^2$. In a tokamak, $\nabla B/B = -\nabla R/R$ and hence the above expressions for the curvature and ∇B drifts can be combined to give $\mathbf{V}_b = (m_j/eZ_j B)(V_{\parallel}^2 + V_{\perp}^2/2) [\mathbf{B} \times \nabla B]/B^2$ for

the total magnetic drift. It has no mass dependence⁶ but being charge dependent it provides a current. The electric field can vary in time, which results in the polarisation drift. Its velocity is given by $\mathbf{V}_{pol} = (m_j/eZ_jB^2)\partial\mathbf{E}/\partial t$. It is charge dependent, and the corresponding current is known as the polarisation current.

All the above drifts are associated with motion of each individual charged particle in the electro-magnetic field. However, charges also move relative to each other. According to Poisson's equation, this can modify the applied electric field due to changes in charge density. In addition, this can modify the magnetic field in accordance with - Ampère's law as moving charged particles generate a current. Treating plasma as a fluid (more detailed information can be found in the following section), we can derive drifts related to the particle collective motion. The force balance equation reads

$$n_j m_j \frac{d\mathbf{u}_j}{dt} \equiv n_j m_j \left[\frac{\partial \mathbf{u}_j}{\partial t} + (\mathbf{u}_j \cdot \nabla) \mathbf{u}_j \right] = -\nabla p_j - \nabla \cdot \Pi_j + n_j e Z_j [\mathbf{E} + \mathbf{u}_j \times \mathbf{B}] \quad (1.5)$$

(to be derived in Sec.1.5). The left hand side is the ion/electron inertia (the latter is usually neglected as $m_e \ll m_i$). The first term on the right hand side of Eq.1.5 is the ion/electron pressure gradient, the second term represents the divergence of the viscosity tensor. \mathbf{u}_j is the ion/electron flow velocity. Crossing both sides of Eq.1.5 with \mathbf{B} , we obtain

$$\mathbf{u}_{\perp j} = \frac{\mathbf{E} \times \mathbf{B}}{B^2} + \frac{m_j}{eZ_j B^2} \left[\mathbf{B} \times \frac{d\mathbf{u}_j}{dt} \right] + \frac{\mathbf{B} \times \nabla p_j}{n_j e Z_j B^2} + \frac{\mathbf{B} \times \nabla \cdot \Pi_j}{n_j e Z_j B^2}.$$

The first term on the right is the $\mathbf{E} \times \mathbf{B}$ drift introduced above. The second term corresponds to the inertial drift. We note that if acceleration results from a change in the electric field, the inertial drift is called the polarisation drift. The third term provides the diamagnetic drift, while the fourth term gives the viscosity drift. Both of them are in opposite directions for electrons and ions and thus provide a current perpendicular to the magnetic field. The diamagnetic and viscosity drifts cannot be introduced from the picture of each individual particle. They result from the plasma collective behaviour being associated with the ion/electron density/temperature gradient or the viscosity gradient.

Having defined plasma and its main drifts, we have to introduce two main approaches

⁶if $V_{\perp} \sim V_{\parallel} \sim V_{Tj}$ provided the electron and ion temperatures are comparable.

used for its description. This is the subject of the forthcoming section.

1.5 Plasma description

In the previous section, we have considered the dynamics of a single charged particle in the electro-magnetic field. However, to describe a multi-particle system such as plasma or gas, we have to take into account that the particle motions and the electric and magnetic fields are coupled. Hence, the problem becomes self-consistent: the particle trajectories must be calculated self-consistently with the fields and vice versa. One would need to solve a set of coupled equations of motion to determine the interaction between charged particles and add Maxwell's equations to keep the solution consistent with the electro-magnetic field. These calculations might be possible but computationally are very expensive. Moreover, the convergence of such a solution is not guaranteed. In a typical tokamak plasma, the number of particles is around $10^{19} - 10^{20}$ per cubic meter. The inertial plasma is even more dense. To simplify the problem, a statistical approach is implemented.

In a gas or plasma, particles are determined by position and velocity at a certain moment of time, i.e. $\{t, \mathbf{r}, \mathbf{V}\}$. We define the particle distribution function as the density in 6D phase space:

$$dn_j = f_j(\mathbf{r}, \mathbf{V}) d\mathbf{V}. \quad (1.6)$$

The total density is then to be introduced as the particle distribution function integrated over velocity space, $n_j(t, \mathbf{r}) = \int f_j(t, \mathbf{r}, \mathbf{V}) d\mathbf{V}$, and represents its 0th moment. j here can be used not only to label electrons and ions, but also different quantum states of atoms and molecules (the latter is usually applied to a gas). The particle distribution function, f_j , satisfies the following 6D *continuity* equation:

$$\frac{\partial f_j}{\partial t} + \sum_{i=1}^3 \frac{\partial}{\partial r_i} (f_j V_i) + \sum_{i=1}^3 \frac{\partial}{\partial V_i} (f_j \dot{V}_i) = C_j \quad (1.7)$$

(dot here denotes the derivative with respect to time). The right hand side represents the collision operator for species j . \dot{V}_i is the acceleration connected with external forces. In a plasma this is associated with the Lorentz force in accordance with Eq.1.3. Therefore,

Eq.1.7 reduces to

$$\frac{df_j}{dt} \equiv \frac{\partial f_j}{\partial t} + \mathbf{V} \cdot \nabla_{\mathbf{r}} f_j + \frac{eZ_j}{m_j} [\mathbf{E} + \mathbf{V} \times \mathbf{B}] \cdot \nabla_{\mathbf{V}} f_j = C_j. \quad (1.8)$$

Here $\nabla_{\mathbf{r}/\mathbf{V}} f_j$ denotes the gradient of the distribution function in \mathbf{r}/\mathbf{V} space. Eq.1.8 is a kinetic equation (or the Boltzmann equation) in its general form. If its right hand side is zero, then it is known as the Vlasov equation. It can be written for any generalised coordinate, q_i , and momentum, p_i , in accordance with the Hamiltonian formalism. When collisions are taken into account, the particle distribution function is no longer constant along the phase space trajectory. The collision operator is to be understood as

$$C_j = \sum_k C_{jk}(f_j, f_k),$$

where j and k denote the colliding particle species. The Boltzmann collision integral is given by

$$C_{jk}(f_j, f_k) = \int_{\mathbf{V}_k} \int_{\Omega} (f'_j f'_k - f_j f_k) \frac{d\sigma}{d\Omega} |\mathbf{V}_j - \mathbf{V}_k| d\Omega d\mathbf{V}_k, \quad (1.9)$$

where $f'_j = f_j(\mathbf{V}'_j)$ and $f'_k = f_k(\mathbf{V}'_k)$. $V_{j,k}$ and $V'_{j,k}$ denote velocities before and after the collision, respectively. $d\sigma$ is the differential size of the corresponding cross section, $d\Omega$ is the solid angle element [9, 10]. Thus, the Boltzmann equation becomes an integro-differential equation that includes all colliding particle distribution functions. To solve it in its general form is much of the challenge. The great complication comes from the collision integral. However, in a number of problems it can be simplified or replaced with a model form. Indeed, the Boltzmann collision integral is not convenient to describe the Coulomb collisions that are governed by small angle scattering events [9, 11]. Instead, the Landau collision integral is employed:

$$C_{jk}(f_j, f_k) = -\frac{2\pi \ln \Lambda (Z_j Z_k e^2)^2}{m_j} \frac{\partial}{\partial V_\alpha} \int \mathcal{U}_{\alpha\beta} \left(\frac{f_j}{m_k} \frac{\partial f'_k}{\partial V'_\beta} - \frac{f'_k}{m_j} \frac{\partial f_j}{\partial V_\beta} \right) d\mathbf{V}', \quad (1.10)$$

where the tensor $\mathcal{U}_{\alpha\beta}$ is defined as $\mathcal{U}_{\alpha\beta} = \delta_{\alpha\beta}/u^r - u^r_\alpha u^r_\beta / (u^r)^3$ with $\mathbf{u}^r = \mathbf{V}_j - \mathbf{V}_k$, $u^r = |\mathbf{u}^r|$. $\ln \Lambda$ is the Coulomb logarithm and $\delta_{\alpha\beta}$ denotes the Kronecker delta. The Landau collision integral can be further simplified. For example, assuming a small fraction of heavy particles in a plasma, $n_j \ll n_k$, we write $\partial f'_k / \partial V'_\beta = -(m_k/T_k) V'_\beta f'_k$, where the background has

been assumed to be Maxwellian. Therefore, Eq.1.8 with Eq.1.10 reduces to

$$\frac{df_j}{dt} = \tilde{\nu}_{jk} \frac{\partial}{\partial \mathbf{V}} \left(\mathbf{V} f_j + \frac{T_k}{m_k} \frac{\partial f_j}{\partial \mathbf{V}} \right) \quad (1.11)$$

with

$$\tilde{\nu}_{jk} = \frac{4\sqrt{2\pi} m_k^{1/2} \ln \Lambda (Z_j Z_k e^2)^2 n_k}{3m_j T_k^{3/2}}.$$

Eq.1.11 is called the Fokker-Planck equation [9, 12, 13]. Generally, the Fokker-Planck operator can be applied when changes in the electron velocity or energy are small [14]. Despite being linear, even in this form the equation is written in 6D phase space and thus is still computationally expensive. Further simplifications are required to reduce the dimension of the problem. One of the examples is called the *drift kinetic equation*, i.e. a kinetic equation averaged over the gyro-scale (its detailed derivation can be found in [15, 16, 17]). Indeed, in the electro-magnetic field we split the charged particle motion into the fast gyro-motion and the motion of the guiding centre. Taking L as a characteristic size of the system, we impose $\delta_j^{DK} = \rho_{cj}/L \ll 1$ and $\omega_0/\omega_{cj} \sim \delta_j^{DK} \ll 1$, where $\omega_0 = V_{Tj}/L$ is a characteristic frequency of the system we consider. Each term in the drift kinetic equation is assumed to be of order δ_j^{DK} . This approximation does not allow any fast variations and requires relatively slow $\mathbf{E} \times \mathbf{B}$ motion (compared to gyration). It reads

$$\frac{\partial f_j}{\partial t} + V_{\parallel} \nabla_{\parallel} f_j + \mathbf{V}_E \cdot \nabla f_j + \mathbf{V}_b \cdot \nabla f_j + \frac{1}{V} \left[\mu \frac{\partial B}{\partial t} + \frac{e Z_j}{m_j} (V_{\parallel} \mathbf{b} + \mathbf{V}_b) \cdot \mathbf{E} \right] \frac{\partial f_j}{\partial V} = C_j(f_j). \quad (1.12)$$

This drift kinetic approach⁷ and the kinetic equation of the form Eq.1.12 are to be applied

⁷Schematically, the initial kinetic equation can be written as $\omega_{cj} \partial f_j / \partial \phi|_{\mathbf{r}, \mathcal{K}, \mu} + \hat{\alpha} f_j = 0$ with ϕ being the gyro-angle, $\mathcal{K} = V^2/2$ and $\mu = V_{\perp}^2/2B$ for $f_j = f_j(t, \mathbf{r}, \mathbf{V}) = f_j(t, \tilde{\mathbf{r}}, \mathcal{K}, \mu, \phi)$, where $\tilde{\mathbf{r}} = \mathbf{r} + \mathbf{V} \times \mathbf{B} / B \omega_{cj}$. $\hat{\alpha}$ represents the rest of the differential/integral operators that act on f_j . The collision operator, C_j , in $\hat{\alpha}$ is assumed to be of order $\delta_j^{DK} \omega_{cj}$ or smaller. Expanding the particle distribution, $f_j = \sum_n f_j^{(n)} (\delta_j^{DK})^n$, we write $\omega_{cj} \partial f_j^{(0)} / \partial \phi|_{\mathbf{r}, \mathcal{K}, \mu} = 0$ for the leading order equation and hence we learn that $f_j^{(0)}$ is ϕ -independent. Proceeding to next order, we have $\omega_{cj} \partial f_j^{(1)} / \partial \phi|_{\mathbf{r}, \mathcal{K}, \mu} + \hat{\alpha} f_j^{(0)} = 0$. To annihilate the first term, we integrate this equation over the gyro-angle to obtain $\langle \hat{\alpha} \rangle_{\phi}^{\mathbf{r}, \mathcal{K}, \mu} f_j^{(0)} = 0$. Here $\langle \dots \rangle_{\phi}^{\mathbf{r}, \mathcal{K}, \mu}$ denotes the gyro-phase averaging operator at fixed $\mathbf{r}, \mathcal{K}, \mu$. The latter provides Eq.1.12 in the absence of plasma drifts across the field lines. To capture the guiding centre drift, we solve the $\mathcal{O}(\delta_j^{DK})$ equation for $f_j^{(1)}$ written as a function of $f_j^{(0)}$. Either perturbative or recursive techniques are allowed. The $\mathcal{O}(\delta_j^{DK})$ equation is equivalent to $\omega_{cj} \partial f_j^{(1)} / \partial \phi|_{\mathbf{r}, \mathcal{K}, \mu} = -(\hat{\alpha} - \langle \hat{\alpha} \rangle_{\phi}^{\mathbf{r}, \mathcal{K}, \mu}) f_j^{(0)}$. Integrating the latter over ϕ provides $f_j^{(1)}$ as a function of $f_j^{(0)}$. Substituting this distribution function into the solvability condition, $\langle \hat{\alpha} f_j \rangle_{\phi}^{\mathbf{r}, \mathcal{K}, \mu} = 0$, i.e.

to the neoclassical tearing mode in this work and thus this notation is to be maintained throughout the study.⁸ Here \parallel denotes a vector component along the magnetic field lines, $\nabla_{\parallel} = \mathbf{b} \cdot \nabla$, $\mathbf{b} = \mathbf{B}/B$. $\mathbf{V}_E = [\mathbf{E} \times \mathbf{B}]/B^2$ with $\mathbf{E} = -\nabla\Phi - \partial\mathbf{A}/\partial t$, where \mathbf{A} is the magnetic vector potential, and $\mathbf{V}_b = -\mathbf{V}_{\parallel} \times \nabla (V_{\parallel}/\omega_{cj})$ are the $\mathbf{E} \times \mathbf{B}$ and magnetic drift contributions, respectively. \mathbf{V}_b includes ∇B and curvature drifts. A low beta plasma approximation is employed. All spatial derivatives are taken at fixed magnetic moment, $\mu = V_{\perp}^2/2B$, and kinetic energy, $\mathcal{K} = V^2/2$, \perp denotes a vector component perpendicular to the magnetic field lines. The explicit representation of the collision integral in Eq.1.12 is to be derived by gyro-averaging the Fokker-Planck collision operator but is usually replaced with a model for a particular problem. In this study, C_j is the momentum-conserving collision operator introduced below.

Although the drift kinetic approach is widely used to describe plasma instabilities, plasma equilibrium and transport, it can also be important to include the electro-magnetic field spatial variations on the scale of Larmor radius. This is the subject of the gyro-kinetic theory. As the gyro-kinetics is not to be applied below, we leave its description beyond the scope of this work. A more detailed information can be found in [17, 18].

Before we move further, let us briefly discuss the plasma magnetohydrodynamic (MHD) description. A set of equations for moments of the particle distribution function can be obtained by multiplying the initial kinetic equation, Eq.1.8, by powers of the velocity. The plasma fluid theory typically focuses on the first three moments of the particle distribution and consists of five scalar equations. Multiplying both sides of Eq.1.8 by V_{α}^0 and integrating over velocity space yields

$$\frac{\partial n_j}{\partial t} + \nabla \cdot \mathbf{\Gamma}_j = 0 \quad (1.13)$$

in the absence of any particle sinks and sources. $\mathbf{\Gamma}_j$ is the particle flux defined as $\mathbf{\Gamma}_j = n_j \mathbf{u}_j$ with $\mathbf{u}_j = (1/n_j) \int \mathbf{V} f_j d\mathbf{V}$ being the flow velocity of species j . n_j and $\mathbf{\Gamma}_j$ represent the 0th and 1st moment of the distribution function, respectively. We note that the right hand side of Eq.1.13 is non-zero if inelastic collisions such as ionisation and recombination

the initial drift kinetic equation in the absence of plasma drifts to leading order, we obtain Eq.1.12 for $f_j^{(0)}$. $f_j^{(0)}$ here is to be replaced with f_j for simplicity unless otherwise stated.

⁸ $(d\mu/dt)\partial f_j/\partial\mu$ is omitted as a higher order correction since $d\mu/dt = \mathcal{O}(\delta_j^{DK}\beta)$, i.e. terms proportional to $\partial/\partial t$ in $d\mu/dt$ do not contribute in the island rest frame, and $\rho_{cj}\mathbf{b} \cdot \nabla \times \mathbf{b} \sim \delta_j^{DK}\beta$.

are considered. Eq.1.13 represents conservation of a total number of particles and is to be solved for n_j . However, the particle flow is unknown at this stage and is to be determined from the next moment equation. Multiplying both sides of Eq.1.8 by $m_j V_\alpha$ and integrating over \mathbf{V} , after some algebra we obtain

$$n_j m_j \left[\frac{\partial \mathbf{u}_j}{\partial t} + (\mathbf{u}_j \cdot \nabla) \mathbf{u}_j \right] = -\nabla p_j - \nabla \cdot \Pi_j + n_j e Z_j [\mathbf{E} + \mathbf{u}_j \times \mathbf{B}] + \mathbf{R}_j. \quad (1.14)$$

Eq.1.14 is a generalisation of the equation of motion, Eq.1.3, introduced above to consider plasma drifts. The plasma pressure, p_j , is defined as

$$p_j = \frac{n_j m_j}{3} \langle (\mathbf{V} - \mathbf{u}_j)^2 \rangle_{\mathbf{V}} = n_j T_j,$$

where $\langle \dots \rangle_{\mathbf{V}}$ denotes integration over \mathbf{V} with weight $f_j(t, \mathbf{r}, \mathbf{V})$. The viscosity tensor, Π_j , is given by

$$\Pi_{j\alpha\beta} = \Pi_{j\beta\alpha} = n_j m_j \left\langle (V_\alpha - u_{j\alpha})(V_\beta - u_{j\beta}) - \frac{\delta_{\alpha\beta}}{3} (\mathbf{V} - \mathbf{u}_j)^2 \right\rangle_{\mathbf{V}}.$$

The last term on the right hand side of Eq.1.14 is the friction force of species j . It originates from the collision integral being defined as

$$\mathbf{R}_{j\alpha} = \int m_j V_\alpha C_j(f_j) d\mathbf{V}.$$

Like the collision operator, the friction force is also additive, i.e. $\mathbf{R}_j = \sum_k \mathbf{R}_{jk}$ (j and k denote particle species). p_j , Π_j and \mathbf{R}_j are unknown in Eq.1.14. Thus, higher order moments of the particle distribution are required to provide the equations to determine them. However, every following moment will generate additional unknowns. So the starting kinetic equation, Eq.1.8, is equivalent to the infinite system of equations for the moments of the distribution function. Therefore, at some stage we have to introduce a *closure* relation to loop the system. For example, if we started with the Vlasov equation and worked in the absence of plasma viscosity, then the plasma pressure only would be left unknown in Eq.1.14. Imposing the adiabatic plasma behaviour, $p\mathcal{V}^\gamma = \text{const}$ (γ here denotes Poisson's constant), we close the system. Keeping the plasma viscosity and the friction force, we introduce the second moment. Integrating Eq.1.8 with weight $m_j V^2/2$,

we find the energy balance equation:

$$\begin{aligned} & \frac{\partial}{\partial t} \left(\frac{n_j m_j}{2} u_j^2 + \frac{3}{2} n_j T_j \right) + \\ & + \frac{\partial}{\partial r_\alpha} \left[\left(\frac{n_j m_j}{2} u_j^2 + \frac{5}{2} n_j T_j \right) u_{j\alpha} + \Pi_{j\alpha\beta} u_{j\beta} + q_{j\alpha} \right] = n_j e Z_j E_\alpha u_{j\alpha} + R_{j\alpha} u_{j\alpha} + Q_j. \end{aligned} \quad (1.15)$$

Here

$$\mathbf{q}_j = \frac{n_j m_j}{2} \langle (\mathbf{V} - \mathbf{u}_j)^2 (\mathbf{V} - \mathbf{u}_j) \rangle_{\mathbf{V}}$$

represents the heat flux and

$$\mathbf{Q}_j = \frac{1}{2} \int m_j (\mathbf{V} - \mathbf{u}_j)^2 C_j(f_j) d\mathbf{V}$$

is the energy gain of species j due to collisions with species k , i.e. $Q_j = \sum_k Q_{jk}$. Eq.1.15 can be combined with Eqs.1.13,1.14 to give the heat balance equation:

$$\frac{3}{2} n_j \left[\frac{\partial}{\partial t} + (\mathbf{u}_j \cdot \nabla) \right] T_j + n_j T_j \nabla \cdot \mathbf{u}_j + \Pi_{j\alpha\beta} \frac{\partial u_{j\alpha}}{\partial r_\beta} + \nabla \cdot \mathbf{q}_j = \mathbf{Q}_j. \quad (1.16)$$

Eqs.1.15,1.16 include p_j , Π_j and \mathbf{R}_j but introduce additional unknowns, \mathbf{q}_j and \mathbf{Q}_j . To close a system of Eqs.1.13,1.14,1.15/1.16, Π_j , \mathbf{R}_j , \mathbf{q}_j and \mathbf{Q}_j have to be written in terms of n_j , \mathbf{u}_j , T_j and their spatial derivatives. This procedure is provided by the hydrodynamic approximation with the sufficiently large characteristic spatial and time scales and when collisions are frequent. The criteria is as follows:

$$\lambda_{mfp,j} \ll L, \quad \rho_{cj} \ll L,$$

where L is the characteristic size of the system, $\lambda_{mfp,j}$ is the mean free path of species j . L is usually understood as the density/temperature gradient length scale, i.e. $|L_{n,T}| = |\nabla_r \ln n, T|^{-1}$. The characteristic time, τ , is assumed to be greater than the time between collisions, $\nu_{jj/jk}^{-1}$ (j and k denote the colliding particle species), or the inverse cyclotron frequency, ω_{cj}^{-1} . In a fully ionised plasma, the electric field is assumed to be weak compared to $\sim 4\pi e^3 \ln \Lambda n_j / T_e (4\pi \epsilon_0)^2$, the Dreicer field [9]. In the non-homogeneous

magnetic field the criteria has to include drifts of the Larmor orbits [9]. In regions of plasma with low density, the collisionality is low and thus the kinetic approach is required. In the hydrodynamic approach, Π_j , \mathbf{R}_j , \mathbf{q}_j , \mathbf{Q}_j and ∇T_j , $T_j - T_k$, $\mathbf{u}_j - \mathbf{u}_k$, $W_{j\alpha\beta} = \partial u_{j\alpha}/\partial x_\beta + \partial u_{j\beta}/\partial x_\alpha - (2/3)\delta_{\alpha\beta}\nabla \cdot \mathbf{u}_j$ (introduced to denote shifts of temperature and flow velocity from the equilibrium) are linearly connected. The latter, in turn, can be linearly expressed through the perturbed part of the particle distribution function (its equilibrium contribution is assumed to be Maxwellian), f_j^1 . Thus, the problem reduces to the determination of f_j^1 . Once, it is known, the transport coefficients can be calculated. A set of Eqs.1.13,1.14,1.15/1.16 with known transport coefficients is called the Braginskii fluid equations [9, 19]. One of the approaches to find f_j^1 is considered in the Chapman-Enskog theory [9, 20].

Eqs.1.13,1.14 written for the ion and electron plasma components form the so called plasma two-fluid MHD equations. The electron inertia is usually neglected as $m_e \ll m_i$. The ion/electron pressure and temperature are connected via the adiabatic law. Summing the ion and electron continuity equations, we obtain

$$\frac{\partial \rho}{\partial t} + \nabla \cdot (\rho \mathbf{u}_j) = 0,$$

where the mass density $\rho \approx n_i m_i$. Similarly, we obtain the force balance equation,

$$n_i m_i \frac{d\mathbf{u}_i}{dt} = -\nabla p + \mathbf{J} \times \mathbf{B},$$

from Eq.1.14 written for ions and electrons. \mathbf{J} is the plasma current density defined as $\mathbf{J} = eZ_i n_i \mathbf{u}_i - e n_e \mathbf{u}_e$. p is the total plasma pressure. According to Ohm's law, the current and the electric field are related via $\mathbf{E} + \mathbf{u} \times \mathbf{B} = \hat{\eta} \mathbf{J}$ ($\hat{\eta}$ is the plasma resistivity tensor). The MHD theory is then called resistive MHD. If $\hat{\eta} = 0$, it reduces to the ideal MHD.

The two fluid MHD can be rewritten in the form that excludes the explicit representation of the electric field and currents in it [9]:

$$\begin{aligned} \frac{\partial \mathbf{B}}{\partial t} &= \nabla \times [\mathbf{u} \times \mathbf{B}] - \frac{1}{\mu_0} \nabla \times (\hat{\sigma}^{-1} [\nabla \times \mathbf{B}]), \\ n_j m_i \frac{d\mathbf{u}}{dt} &= -\nabla \left(p + \frac{B^2}{2\mu_0} \right) + \frac{1}{\mu_0} (\mathbf{B} \cdot \nabla) \mathbf{B}, \end{aligned}$$

$$\frac{\partial n_j}{\partial t} + \nabla \cdot (n_j \mathbf{u}) = 0, \quad (1.17)$$

$$p = p(n_j).$$

This is referred to as a single fluid MHD. Here $\mathbf{u} = \mathbf{u}_i$, $n_j = n_e \approx n_i$, $\hat{\sigma}$ is the conductivity tensor, $\hat{\sigma} = \hat{\eta}^{-1}$. The last equation implies the adiabatic law. $B^2/2\mu_0$ is called the magnetic field pressure. The first term on the right hand side of the first equation in Eq.1.17 is called the *frozen in* contribution. If this term is dominant, the first equation of Eq.1.17 provides the *frozen in* condition. Plasma and fields evolve together to conserve the magnetic flux, i.e. the flux is frozen into the plasma, provided $\hat{\eta} = 0$ [9, 12]. The second term describes the magnetic field diffusion through the plasma. The ratio of these two terms,

$$\mathcal{S} = \frac{|\nabla \times [\mathbf{u} \times \mathbf{B}]|}{|\mu_0^{-1} \nabla \cdot (\hat{\sigma}^{-1} [\nabla \cdot \mathbf{B}])|} \approx \frac{|\nabla \times [\mathbf{u} \times \mathbf{B}]|}{|\eta \mu_0^{-1} \nabla^2 \mathbf{B}|} \approx \frac{\mu_0 L c_A}{\eta},$$

is known as the Lundquist number. $c_A = \sqrt{B^2/(\mu_0 n_j m_i)}$ is the Alfvén velocity (note: it can be estimated from the second equation in Eq.1.17). L is the characteristic length scale. $\hat{\eta}$ has been replaced with a scalar η for simplicity. When $\mathcal{S} \lesssim 1$, the resistivity plays a significant role⁹. When the current diffusion term dominates (or comparable to the frozen in term), the magnetic field topology can be reformed. This is the subject to the magnetic field line reconnection theory [25]. The event when the magnetic field lines approach and reconnect might be accompanied by the formation of magnetic islands. The magnetic reconnection can be forced in experiments and can occur spontaneously, being triggered by plasma instabilities. Such a plasma instability is called a *tearing mode* and is to be considered in the current work.

Although the kinetic plasma theory is used throughout this study, it was important to provide a brief introduction to the plasma fluid theory. Firstly, it justifies the choice of the kinetic approach to consider tearing modes in low collisionality plasmas. Secondly, it introduces the main terminology applied below. The tokamak plasma equilibrium is determined by the Grad-Shafranov equation (e.g. [9, 12]). As this is not the subject of the current study, we do not discuss it here. A pioneering work by Grad and Shafranov

⁹In some cases, even for very large \mathcal{S} , resistivity can be important.

can be found in [21, 22, 23, 24].

1.6 Tokamak concept

In MCF a magnetic field is applied to hold the plasma. Let us consider a cylinder of plasma. To avoid end-losses (e.g. they occur in magnetic mirror systems [26], pinches [9]), it is bent around on itself. This creates a closed loop system (see Fig.1.4) and can be achieved by placing a set of toroidal magnetic field coils around the plasma or by passing a current carrying rod through the centre of the torus.

The first technique is implemented in the *conventional* tokamak configuration (e.g. T10, DIII-D, JET, the ITER tokamak that is now under construction). It is shown in Fig.1.4. The second technique is applied in *spherical* tokamaks (STs, e.g. MAST, NSTX, Globus-M). STs are compact but topologically there is no difference between conventional and spherical devices. Using a single large conductor inside the torus to generate the toroidal magnetic field, B_φ , around it allows the

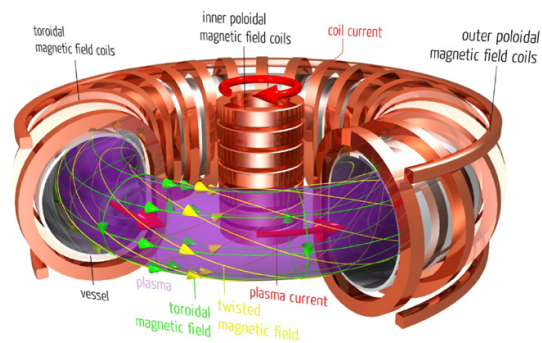


Figure 1.4: Sketch of a conventional tokamak (source: [27]). A set of the toroidal field coils, the inner/outer set of the poloidal field coils, the vacuum vessel region are indicated. The toroidal and poloidal magnetic field components form the total, helical magnetic field.

aspect ratio, A , to be reduced (note: the tokamak aspect ratio is defined as R_0/a , where R_0 is the major radius of the torus and a is its minor radius), $A \sim 1$. This reduces the total cost of the fusion reactor. Therefore, STs can in principle allow one to achieve the same triple product factor as conventional devices but with only $\sim 1/10$ of the total magnetic field. Furthermore, a different plasma shaping allows one to avoid certain types of plasma instabilities improving the plasma stability. Indeed, the plasma is more stable on the inner section of the tokamak [9]. In a large aspect ratio tokamak with circular poloidal cross section, the plasma particles spend approximately the same amount of time on the inboard and outboard sides of the torus (slightly less in the inner region due to shorter radius). In contrast, in STs plasma spends more time on the inside of the torus.

This results in a great stability improvement. However, in modern conventional tokamak devices the circular cross section has been replaced with a D-shaped poloidal cross section where the inside surface of the torus is expanded. This shaping is typically more extreme in an ST. The ST experimental results including operational limits are discussed in [28] and the features of the ST plasma in [29]. In our current work, we impose conventional tokamak geometry with circular cross section. The effects of elongation, triangularity and the Shafranov shift can be introduced in our model. However, as we shall see in the forthcoming sections, corrections of order ε^2 and higher ($\varepsilon = A^{-1}$ is the inverse aspect ratio) would contribute only to the curvature term in the modified Rutherford equation that is negligible in any conventional tokamaks and thus would not provide any significant changes to the final results.

The toroidal magnetic field component only is not sufficient to maintain the pressure in the plasma due to the consequences of the ∇B and curvature drifts. In a tokamak, the magnetic field is not homogeneous, $B_\varphi \propto 1/R$, where R is a varying major radius of a tokamak (R_0 is its value at the magnetic axis, see Fig.1.6), and thus there is a gradient of the magnetic field that points inwards (in the direction of the

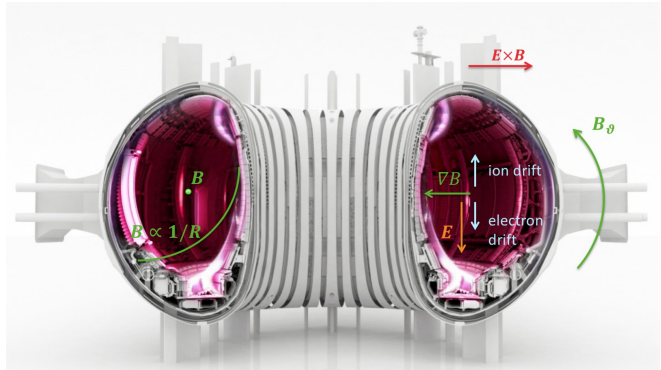


Figure 1.5: Sketch of a conventional tokamak (source: [30]). The origin of the $\mathbf{E} \times \mathbf{B}$ drift in tokamak plasmas is demonstrated.

high magnetic field side, see Fig.1.5). This, in turn, generates the ∇B plasma drift orthogonal to the main magnetic field (i.e. vertically). Being charge dependent, this drift is in opposite directions for the ions and electrons. The charge separation then forms a vertical electric field. The toroidal magnetic field and the vertical electric field generate an $\mathbf{E} \times \mathbf{B}$ drift that points outwards resulting in a loss of confinement. Therefore, the additional, poloidal magnetic field component, B_θ , is required to provide a zero average of the ∇B and curvature drifts, and thus to confine charged particles in the toroidal magnetic field configuration. The total magnetic field is helical (see Fig.1.4). Roughly, $B_\varphi : B_\theta : B_V = 100 : 10 : 1$ in the conventional device (note: B_V is the vertical magnetic field component provided by the vertical coils to shape the plasma and control its position;

a total poloidal field includes the poloidal component itself as well as the vertical magnetic field contribution), while the toroidal and poloidal components are almost comparable in STs. There are two main concepts to generate the poloidal magnetic field. In the first concept, the poloidal field component is produced by the toroidal current through the plasma (see Fig.1.4). This is a *tokamak* concept. To summarise, in a tokamak the plasma is confined by the magnetic field generated by external coils around the torus/by passing a current through the rod at the centre of the torus (toroidal magnetic field) and the magnetic field resulted from the current in the plasma itself (poloidal magnetic field). The tokamak was invented by I. Tamm and A. Sakharov in the 1950s in the Soviet Union. The second, *stellarator* concept is to hold the plasma by an external single coil set. There is no (or very little) current in the plasma itself and thus stellarators are more suitable for steady state operation, while tokamaks require auxiliary facilities to achieve steady state. The magnetic coils and hence the plasma shape are complicated in stellarators and they are not easy to build. The stellarator was invented by L. Spitzer in 1951 [31]. The tokamak and stellarator plasma are compared in [32].

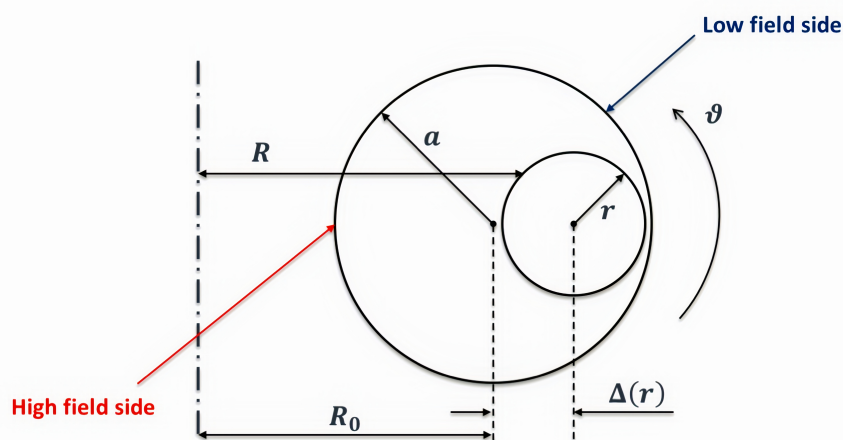


Figure 1.6: A schematic representation of the conventional tokamak circular poloidal cross section. r and R are the minor and major radii of the tokamak ($r = a$ at the plasma edge and $R = R_0$ at the magnetic axis). $\Delta = \Delta(r)$ denotes the Shafranov shift of the magnetic flux surfaces in the direction of the low magnetic field side. ϑ is the poloidal angle.

Focusing on a tokamak plasma, let us briefly discuss the heating and current drive techniques. A toroidal current used to generate the poloidal field component is induced by varying the magnetic flux through the plasma centre. This is known as *inductive*

current drive and significantly limits the plasma performance by a pulsed mode. To achieve continuous operation of a tokamak, alternative, *non-inductive* current drive schemes [33, 34] are required. Furthermore, the non-inductive methods allow the plasma current density profile to be shaped to control the plasma MHD instabilities. One of the possibilities is to drive waves at the ion/electron cyclotron frequency (i.e. ion/electron cyclotron current drive, I/ECCD) or lower hybrid resonance frequency (i.e. lower hybrid current drive, LHCD). Another option is to inject highly energetic neutral particle beams (energies \sim several 100keV – 1MeV required to penetrate the plasma of $\sim 10^{20}$ particles per cubic meter are estimated for ITER) [33]. This method is known as neutral beam injection (NBI). The bootstrap current [35] that occurs in a low collisionality regime generates itself in the plasma and hence is considered to be a crucial part of the steady state additional current drive. The wave resonances (ion cyclotron, lower hybrid and Alfvén wave heating) as well as NBI are also to be applied to heat the plasma towards fusion conditions. Indeed, the Ohmic heating (OH) is not sufficient to reach plasma temperatures required for ignition according to Lawson’s criteria. Firstly, the OH power being proportional to plasma resistivity decreases with the electron temperature as $T_e^{-3/2}$ (as the plasma conductivity is inversely proportional to the collision frequency and hence the parallel component of the conductivity tensor, $\sigma_{\parallel} \propto T_e^{3/2}$, in the fully ionised plasma). Secondly, MHD instabilities (such as neoclassical tearing modes to be addressed in the following chapters) set the current and pressure limits and can terminate the tokamak discharge in a disruption.

1.7 Overview

In this chapter we have briefly discussed the fundamental principles required to develop the novel neoclassical tearing mode theory that is discussed in the forthcoming sections. Chapter II introduces a neoclassical tearing mode (NTM) in tokamak plasmas and describes the existing approaches used for its understanding. Here we also derive the NTM drift kinetic (DK) equation for the small inverse aspect ratio tokamak low collisionality plasma that is then used to determine the NTM marginal magnetic island width (a detailed derivation is presented in Appendix D). This is already sufficient for an accurate calculation of the bootstrap current drive to the NTM magnetic island growth. However,

the polarisation current contribution also requires the knowledge of the island propagation frequency that is determined by plasma dissipation processes. Leaving the effects of error fields and plasma sheared flows beyond the scope of this study, we note that the only source of dissipation is the collisional dissipation from a thin boundary layer in the vicinity of the trapped-passing boundary in pitch angle space. Here collisions become comparable to the parallel streaming and thus we solve a 2D boundary layer problem employing the momentum-conserving collision operator. This is addressed in Chapter III. The full solution of the NTM DK problem derived in Chapter II is presented in Chapters III and IV and includes the regions inside and outside the magnetic island as well as a narrow layer in the vicinity of the island separatrix. This is crucial for an accurate determination of the polarisation current contribution. The solution technique implemented in the "RDK-NTM" (reduced drift kinetic NTM solver) code is discussed in Chapter IV (a numerical scheme is derived in Appendices D and E). The results follow. In Chapter V we use a similar approach and adopt RDK-NTM to solve a different problem - we analyse stability of secondary modes driven by an island in phase space. A summary and conclusions are given in Chapter VI.

Chapter II

2 Neoclassical tearing modes

Tokamak confinement is provided by the fact that to 0th order plasma electrons and ions follow the field lines that are located on the toroidally symmetric flux surfaces. Certain kinds of instabilities in a tokamak plasma though change their geometry, and this can significantly limit the plasma performance. The tearing mode is one of such instabilities [36].

Neoclassical tearing modes are classified as large scale resistive magnetohydrodynamic plasma instabilities [37]. They arise due to a filamentation of the plasma current density parallel to the magnetic field lines. This filamentation changes the topology of the magnetic flux surfaces, forming magnetic islands (their schematic representation is shown in Fig.2.1 and Figs.2.2,2.3, and their formation mechanism is discussed in Appendix A).

They occur when a poloidal beta¹⁰ threshold is exceeded (e.g. Fig.2.4), and are usually triggered by another MHD perturbation (e.g. sawtooth oscillations, fishbone modes, edge localised modes etc.) that creates a seed island for NTMs. According to the conventional theory [38], in the absence of heat/particle sources, the plasma pressure gradient in a region inside the island and hence the total

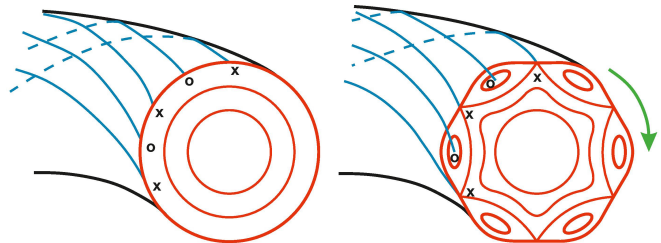


Figure 2.1: Formation of magnetic islands in large aspect ratio circular cross section tokamak geometry. Poloidal cross section in the absence of NTM activity (left); in the presence of NTM magnetic islands (right). O and X denote the magnetic island O- and X-points, respectively. Green arrow is in the poloidal direction (figure courtesy of H. Wilson).

plasma pressure in the core are reduced due to the enhanced particle and heat transport across the island (see Fig.2.5). This flattening of the pressure profile, in turn, leads to a hole in the bootstrap current near the island O-point. As the bootstrap current density rises with beta, the island width also grows with beta, resulting in a degradation of confinement [39, 40, 41]. Along with the fact that NTMs define operational limits of a

¹⁰Plasma beta is plasma pressure divided by the magnetic field pressure and hence the toroidal/poloidal

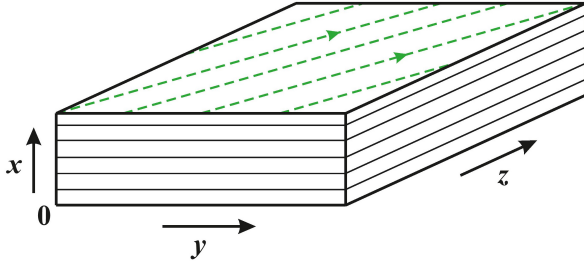


Figure 2.2: A ring of toroidal plasma in slab geometry in the absence of NTM activity. $\{x, y, z\}$ correspond to $\{r, \vartheta, \varphi\}$ with r being the radial coordinate, ϑ the poloidal angle and φ the toroidal angle, respectively (figure courtesy of H. Wilson).

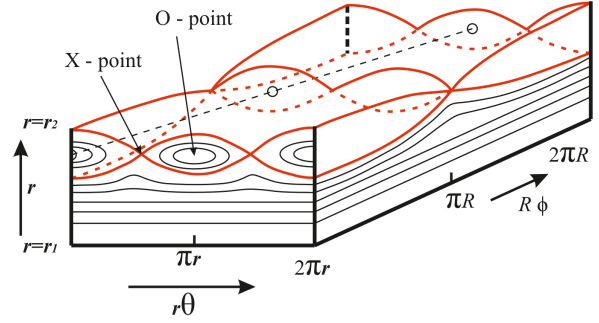


Figure 2.3: Same as Fig.2.2 but in the presence of NTM magnetic islands. The O-point at the centre of the island and the X-point at the separatrix are indicated. The red curve indicates the magnetic island separatrix, i.e. the last closed magnetic flux surface of the island (note: a similar structure can be seen in the poloidal cross section of a tokamak with double-null divertor). Here poloidal/toroidal mode numbers are $m = 2/n = 1$, respectively (figure courtesy of H. Wilson).

magnetically confined plasma system, they can also lead to plasma disruptions through mode locking, threatening the structural integrity of the first wall of a tokamak-reactor. NTMs occur in the standard ELMy H-mode as well as in advanced scenarios. Hence, understanding the physics of the NTM onset and its suppression is a key problem in achieving controlled fusion. One of the most promising NTM control techniques is to generate microwaves at the electron cyclotron frequency to drive current inside the island to replace the missing bootstrap current. This O-point electron cyclotron current drive (ECCD) has demonstrated complete NTM stabilisation on a number of machines [41] and is to be applied to drive the island width down to mitigate the confinement degradation and/or suppress the NTM in fusion devices such as ITER. However, an issue here is to determine how much of the ECCD current is required for the NTM stabilisation and how localised it must be, which leads to a necessity for a more detailed understanding of the threshold physics. Experimentally, this threshold is related to a critical beta and a critical island width. The latter is the subject of this study.

The NTM magnetic islands can either grow or shrink, depending on the current density perturbation parallel to the magnetic field, J_{\parallel} . According to the modified Rutherford

beta is $2\mu_0 p / B_{\varphi/\vartheta}^2$.

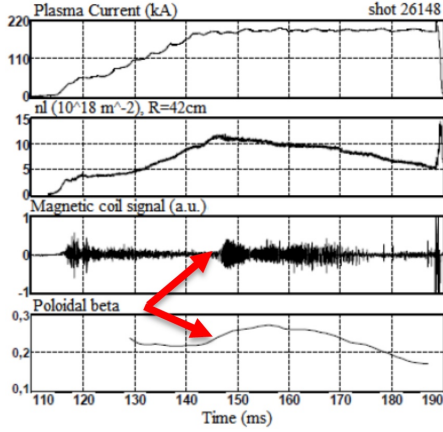


Figure 2.4: The Globus-M shot 26148 (saturated plasma current, $I_\varphi = 200\text{kA}$, $B_\varphi = 0.4\text{T}$). Time traces of the plasma current, chord-averaged density, nl , magnetic field perturbation obtained by the Mirnov coil system and poloidal beta reconstructed by EFIT. Arrows indicate the beginning of the NTM activity (at plasma beta $\beta_\theta \approx 0.25$).

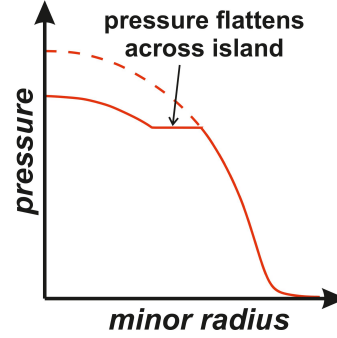


Figure 2.5: Confinement loss due to the tearing mode occurrence. Dashed curve indicates the radial plasma pressure profile in the absence of the magnetic island. Solid curve corresponds to the pressure profile in the presence of the NTM. The pressure flattening inside the island results in its reduction in a core. If plasma temperature is constant, the bootstrap current density is $\propto \varepsilon^{1/2} B_\varphi^{-1} \nabla_r p$ and hence has a hole inside the island (figure courtesy of H. Wilson).

theory [41, 42, 43], the island time evolution is described by

$$\frac{2\tau_R}{r_s^2} \frac{dw}{dt} = \Delta'(w) + \int J_\parallel dq, \quad (2.1)$$

where $\tau_R \sim \mu_0 a^2 / \eta$ is the resistive diffusion time, η is local plasma resistivity, w is the island half-width and r_s is the radius of the rational surface, i.e. denotes position of the magnetic island. Δ' is the classical tearing mode stability parameter [44, 45, 46]. It arises due to a discontinuity in the perturbed magnetic flux gradient near the rational surface¹¹ and measures the free magnetic energy in the equilibrium current density to drive instability¹². In Rutherford's original work [52], only the induced current associated with the island growth contributes to J_\parallel . Adding tokamak neoclassical effects, denoted by the second term

¹¹The reconnection event occurs when resistivity is non-zero in the first equation of Eq.1.17, otherwise the field line structure is conserved. Around the rational surface, there is a narrow boundary layer where the ideal MHD theory can no longer be applied and should be replaced with resistive MHD. Outside the layer, ideal MHD is valid. Solving Ampère's law for the poloidal flux function, ψ , we have to match solutions from inside/outside the layer. Hence, we find that $\nabla_r \psi$ has a jump across the island, which is characterised by Δ' : $\Delta' = \lim_{\delta r \rightarrow \infty} \psi^{-1} (\nabla_r \psi|_{r=\delta r} - \nabla_r \psi|_{r=-\delta r}), \forall \delta r > 0$.

¹²see Appendix A. Eq.A.7/A.8 multiplied by $r\psi$ and integrated over r provides the magnetic energy related to the destabilising effect due to the equilibrium current density gradient. See also [12] for a more detailed derivation.

on the right hand side of Eq.2.1 (\mathbf{q} here is a tuple of generalised coordinates), leads to the modified Rutherford equation (MRE). MRE's main contributions come from the bootstrap [47, 48], curvature [49] and polarisation [50, 51] currents and are denoted by Δ_{bs} , Δ_{cur} and Δ_{pol} , respectively. The perturbed bootstrap current exists in the *banana* regime in a tokamak (i.e. trapped particles execute complete orbits before experiencing a collision) and is written through a linear combination of the electron/ion density and temperature gradients [34]. In the island region, the plasma pressure (i.e. density/temperature) can be considered as a flux surface function due to the rapid parallel transport. Hence, the pressure gradient and the bootstrap current perturbation tend to be excluded from the inside of the island in the absence of any sinks and sources there. Outside the island, the bootstrap current still exists [36]. For larger w ¹³, $\Delta_{bs} \sim \varepsilon^{1/2} (L_q/L_p) (\beta_\theta/w)$ [43, 53] and hence is destabilising, except for reversed magnetic shear discharges. β_θ is poloidal beta; the safety factor and pressure length scales are $L_{q,p}^{-1} = \pm \nabla_r \ln q, p > 0$. The saturated island width, obtained by balancing Δ_{bs} with Δ' , is then found to be proportional to β_θ that sets a *soft* beta limit in a tokamak. When w becomes comparable to a (which can occur for modes with lower poloidal numbers), the plasma discharge terminates in a disruption. However, there is much additional physics must be included for smaller w . According to experimental observations [54, 55], small magnetic islands heal themselves. This fact suggests the existence of the tearing mode threshold mechanism that, as we shall see later in this study, restores the density/temperature gradient in the island, weakening the bootstrap drive, or introduces a new current density perturbation that opposes the bootstrap current. This originates from the effects of finite radial diffusion [38, 56] and finite orbit widths [50, 53, 57, 58, 59, 60, 61, 62, 63, 64]. The heat transport model provides the threshold island width, w_χ , when the radial diffusion can compete with the transport along the magnetic field (or with free streaming in a hot plasma in the absence of collisions). This threshold can be estimated through the ratio of heat conductivities perpendicular and parallel to the magnetic field lines to the quarter power [38] and thus has a strong dependence on the model used for the perpendicular conductivity.

Another source of concern comes from the finite orbit width effects. For small magnetic islands of width comparable to the ion banana orbit width, ρ_{bi} , the polarisation current plays a key role. When $w \sim \rho_{bi}$, the electrons and ions respond in a different way to

¹³Islands much bigger than the ion poloidal Larmor radius.

the magnetic perturbation: the ion response is determined by the $\mathbf{E} \times \mathbf{B}$ drift, while the electron response comes from free streaming along the field lines. Hence, an electrostatic potential needs to be generated to maintain plasma quasi-neutrality. It is localised to the island vicinity as the electrons and ions stay unaffected by the tearing mode perturbation far from the island. In toroidal geometry, trapped ions experience the potential averaged over their banana orbits. In contrast, electrons experience the local potential as their banana orbit is $\sim (m_e/m_i)^{1/2}$ narrower than those of the ions [36]. This causes a difference in their $\mathbf{E} \times \mathbf{B}$ drifts and hence generates the neoclassical polarisation current across the magnetic field lines. This current is not divergence-free. Thus, an electric field is required to drive a current along the field lines that contributes to the island time evolution. This contribution is denoted by Δ_{pol} and tends to zero for $w \gg \rho_{bi}$, because then the orbit-averaged and local electric fields are comparable. According to previous works [64, 56], the polarisation current consists of an external contribution that comes from the region outside the island and the layer part from the island separatrix vicinity. They have been found to be comparable for small ρ_{ci}/w but acting in opposite directions¹⁴. For larger ρ_{ci}/w , the layer part exceeds that from outside the boundary layer [64]. In the current work, both the inside and outside island contributions are considered. Δ_{pol} previously derived from the drift kinetic theory has been found to be $\propto 1/w^3$, provided $w \gg \rho_{bi}$ [43, 53]. In [65] a heuristic model was proposed to provide threshold behaviour at small island widths.

We define Δ_{cur} to be the stabilising curvature contribution introduced by Glasser, Greene and Johnson [49], which describes the tokamak curvature effects on the evolution of the island width [66]. In large aspect ratio tokamaks, the curvature contribution is much less than the bootstrap drive and hence is usually omitted. In spherical tokamaks though, these two contributions can be comparable [67].

With all these effects taken into account, the MRE reads as

$$\begin{aligned} \frac{2\tau_R}{r_s^2} \frac{dw}{dt} = & \Delta'(w) + a_{bs} \varepsilon^{1/2} \frac{\beta_\vartheta}{w} \frac{L_q}{L_p} \frac{w^2}{w^2 + w_\chi^2} + a_{pol} g(\varepsilon, \nu_{ii}, \omega) \beta_\vartheta \left(\frac{L_q}{L_p} \right)^2 \frac{w \rho_{bi}^2}{w^4 + \rho_{bi}^4} \\ & + a_{cur} D_R \frac{1}{(w^2 + 0.65w_\chi^2)^{1/2}} + \Delta_{ECCD}. \end{aligned} \quad (2.2)$$

¹⁴This makes the calculation of Δ_{pol} challenging. To address the layer contribution, the accurate treatment of the boundary layer around the island separatrix is required.

The terms in a_{bs} , a_{pol} and a_{cur} correspond to the bootstrap (Δ_{bs}), polarisation (Δ_{pol}) and curvature (Δ_{cur}) neoclassical contributions, respectively. Δ_{ECCD} is the impact of the ECCD current drive required for the NTM stabilisation. Here a_{bs} , a_{pol} and a_{cur} are order one numerical constants. a_{bs} and a_{pol} are assumed to be positive, while $a_{cur} < 0$, making Δ_{bs}/Δ_{cur} destabilising/stabilising, respectively. D_R is the resistive interchange parameter that is estimated as $(\varepsilon^2 \beta_\vartheta / s) (L_q / L_p) (1 - q^{-2})$ [66], where s is the magnetic shear and q is the safety factor. This ε^2 dependence makes Δ_{cur} negligible in conventional tokamaks. Whether Δ_{pol} has stabilising/destabilising effect on the island evolution depends on the sign of g . g , in turn, depends on the island propagation frequency, ω [53, 68], the ion collision frequency, ν_{ii} [60, 69], and ε . The existing theory of NTMs requires the island width to be much larger than the ion banana orbit width. There is no theory developed for the polarisation contribution for $w \lesssim \rho_{\vartheta i}$ ($\rho_{\vartheta e, i}$ is the electron/ion poloidal Larmor radius)¹⁵. The MRE form we use in Eq.2.2 is continued heuristically to a region where $w < \rho_{bi}$. However, there is no rigorous theoretical justification for it. In [71] it has been shown that the marginal island width below which the NTM is removed, i.e. $dw/dt < 0$, is about $2\rho_{bi}$ in both ECCD and beta rampdown discharges, and is about $3\rho_{bi}$ in [72]. This is exactly the region where the existing theory breaks down. Thus, a new theory is required to determine all the MRE neoclassical contributions allowing the limit of $w \sim \rho_{\vartheta i}$ (in this study, we find that it is $\rho_{\vartheta i} = \varepsilon^{-1/2} \rho_{bi}$ that is responsible for the magnetic island threshold), which is crucial in providing the NTM threshold island width scaling for ITER and other future conventional tokamak devices.

The first and the main focus of this study is on the role of finite orbit width effects on the neoclassical¹⁶ contributions to the island growth and determination of the NTM threshold width. Here we take [53] as a starting point and extend our previous results [73, 74], obtained in the island rest frame ($\omega = 0$), by treating the electrons in a way similar to ions, i.e. resolving length scales of $\sim \rho_{\vartheta e}$, and by adding the polarisation term. One can say that removing the assumption $w \gg \rho_{\vartheta e}$ is not crucial since the NTM islands below

¹⁵Although some of the previous works, e.g. [70], allow $w \lesssim \rho_{\vartheta i}$ and propose the form of g numerically, they impose a model potential. At $w \lesssim \rho_{\vartheta i}$, there is no complete theory for the MRE neoclassical contributions.

¹⁶The main focus is on the bootstrap contribution. The polarisation contribution is also to be addressed in the forthcoming chapters. However, its determination was not the purpose of this work. Regarding the curvature contribution, we have to note that concentrating on a large aspect ratio tokamak we do not keep all the terms of order ε^2 . An accurate Δ_{cur} calculation requires these higher order corrections. However, Δ_{cur} being $\sim \varepsilon^2$ does not provide any significant contribution to our final results.

the marginal width self-heal and shrink away; and the marginal island width as stated above is expected to be $\sim \rho_{bi}$. However, such a treatment ensures we capture physics associated with narrow boundary layers even for islands of width $\sim \rho_{\vartheta i} \gg \rho_{\vartheta e}$. Inclusion of the polarisation contribution is significant in the NTM threshold calculation since all the tokamak neoclassical effects that we keep in Eq.2.2 play a role in experiments and have to be taken into consideration. Earlier works have achieved a limit of $w \sim \rho_{\vartheta i}$ in solving the drift kinetic equation through a particle-in-cell computational modelling [75] and by addressing the problem analytically [76]. They both confirmed that the ion density gradient is not removed from the region inside the island. However, they focused on the ion plasma response only, omitting the electron component and hence neglecting the effects of the plasma quasi-neutrality condition. [76] omitted the effects of trapped particles as well. Our analytic approach explains the physical origin of the density gradient across the island and provides a new NTM threshold physics that arises from both, ion and electron plasma components, and the self-consistent potential required for quasi-neutrality. When $w \gg \rho_{bi}$, the electron and ion distribution functions reproduce the results of the original paper [53]. However, when $\rho_{be} \ll w \sim \rho_{bi}$, the electron and ion solutions localised to the island vicinity differ significantly, which results in a difference in the electron and ion densities, if the electrostatic potential, Φ , is neglected. Therefore, we should stress the importance of deriving Φ self-consistently from plasma quasi-neutrality, which is implemented in our model. Once the plasma responses are found, we proceed to the NTM threshold width calculation determining the total perturbed current density along the field lines. In this study, we include contributions to the localised current density that come from the inner and outer island regions, while the original paper [53] kept the outer contribution only.

The second focus of this study is on the polarisation contribution to the island time evolution and hence on the island propagation frequency. Since Δ_{pol} is expected to have a strong ω dependence, its effect on the NTM island cannot be found until ω is calculated. The earlier theory [77] approached the problem in the two-fluid MHD limit keeping plasma rotation and the parallel component of the ion viscosity tensor. In [53] the low collision frequency limit of $\nu_j < \varepsilon\omega$ (j labels particle species) has been considered using the drift-kinetic model. The NTM mode frequency in that model was found to be in the direction of the electron diamagnetic frequency, $\omega_{dia,e}$, and the corresponding polarisation current contribution stabilising. However, [53] provides the analysis valid only outside

the NTM magnetic island and requires island widths greater than $\varepsilon^{1/2}\rho_{\vartheta i}$. In this study, we allow the magnetic islands being around the threshold and include the inner island region as well as the island separatrix layer, which is crucial in determining Δ_{pol} . The island mode frequency comes from the dissipation processes in a tokamak plasma [78] and/or can be defined by error fields, i.e. non-axisymmetric component of the vacuum magnetic field. Once the mode frequency is sufficiently low, the NTM (usually with lower m/n , i.e. poloidal/toroidal mode number) can be locked, i.e. stop rotating. The Mirnov magnetic signal becomes zero, but the island still exists and grows to a large saturated level, terminating the discharge in a disruption. Here we follow [53] and neglect the effects of error fields as well as plasma sheared flows, focusing on collisional dissipation that arises in a narrow layer in pitch angle in the vicinity of the trapped-passing boundary.

The remainder of this chapter is organised as follows. Section 2.1 introduces the magnetic geometry and the mode dispersion relation. In Sections 2.2 and 2.3 we calculate the plasma response to the NTM magnetic perturbation. The drift magnetic island concept is described in Section 2.4. The self-consistent electrostatic potential is found in Section 2.5. We calculate the neoclassical contributions to the modified Rutherford equation and determine the threshold magnetic island width in the next chapters. The island propagation frequency is the subject of the following chapters as well.

2.1 Magnetic topology and NTM dispersion relation

A small inverse aspect ratio tokamak with circular poloidal cross section is considered. A 3-tuple of spatial variables $\{\psi, \varphi, \vartheta\}$ provides an orthogonal set of coordinates according $\nabla\varphi \times \nabla\psi = rB_{\vartheta}\nabla\vartheta$, where ψ is the poloidal flux function, φ and ϑ are the toroidal and poloidal angles, respectively. The equilibrium magnetic field is given by

$$\mathbf{B}_0 = I(\psi)\nabla\varphi + \nabla\varphi \times \nabla\psi, \quad (2.3)$$

where $I = RB_{\varphi}$ is the poloidal current. As $\varepsilon \ll 1$ and $B_{\vartheta}/B_0 \sim \varepsilon$, $B_0 = B_{\varphi} + \mathcal{O}(\varepsilon^2)$, where $B_0 = |\mathbf{B}_0|$. The safety factor¹⁷ and B_0 are approximated as $q \approx rB_{\varphi}/RB_{\vartheta}$ and

¹⁷A number of times the magnetic field line travels around the tokamak in the toroidal direction to wrap it around once in the poloidal direction.

$B_0(\psi, \vartheta) \approx B_0(\psi)(1 - \varepsilon \cos \vartheta)$, respectively. We employ a low beta approximation and to keep zero divergence of the total magnetic field, a magnetic field perturbation associated with the tearing mode is taken to be of the form

$$\mathbf{B}_1 = \nabla \times (A_{\parallel} \mathbf{b}) \quad (2.4)$$

with $\mathbf{b} = \mathbf{B}_0/B_0$ being a unit vector in the direction of the equilibrium magnetic field. A_{\parallel} is the parallel component of the vector potential connected to the NTM poloidal flux function perturbation, $\delta\psi$, via

$$RA_{\parallel} = -\delta\psi \quad (2.5)$$

with $\delta\psi = \tilde{\psi}f(\xi)$. ξ here is a helical angle in the island rest frame defined as

$$\xi = \varphi - q_s\vartheta, \quad (2.6)$$

where $q_s = m/n$ is the safety factor evaluated at the rational surface, $\psi = \psi_s$, around which the magnetic island is centered. f describes a form of the perturbation in ξ space and is taken as $f = \cos n\xi$ provided a single isolated NTM island is considered. $\tilde{\psi} = (w_{\psi}^2/4)(q'_s/q_s)$ is the NTM perturbation amplitude with w_{ψ} being the island half-width in ψ space related to w in r space via $w = w_{\psi}/(RB_{\vartheta})$ (note: in ψ space we work in terms of w_{ψ} , and hence the ψ index is to be omitted for simplicity in the forthcoming sections, unless otherwise stated). q'_s denotes $\partial q/\partial\psi$ evaluated at the resonant surface, $\psi = \psi_s$. For further analysis, it is convenient to switch from the coordinate system $\{\psi, \varphi, \vartheta\}$ introduced above to $\{\psi, \xi, \vartheta\}$. To describe the magnetic island geometry, we introduce a perturbed flux surface function Ω that satisfies $\mathbf{B} \cdot \nabla\Omega = 0$:

$$\Omega = \frac{2(\psi - \psi_s)^2}{w_{\psi}^2} - \cos n\xi. \quad (2.7)$$

The tearing mode introduces the radial component of the magnetic field that is required to generate the island. Hence, Eq.2.7 can be obtained by integrating a field line trajectory with Ω being a constant of the integration and q Taylor expanded about the rational surface. Here $\xi \in [-\pi, \pi]$. The surfaces of constant Ω describe the topology of the magnetic island. $\Omega = 1$ describes the separatrix and $\Omega = -1$ is at the island O-point. Eq.2.7 implies a constant ψ approximation and also requires the island to be sufficiently

small that a Taylor expansion of equilibrium quantities is valid in its vicinity. Introducing $\tilde{\psi}$ as a function of r [79] and keeping a more realistic radial q profile provide non-symmetric islands in the radial direction [80, 81].

To derive the dispersion relation for the NTM, we address the Gauss-Ampère law that reads as $\partial_\alpha F^{\alpha\beta} = \mu_0 J^\beta$, where F is the electromagnetic tensor, J is the four-current and ∂ represents the four-gradient. It is equivalent to finding the extremum of the functional $\mathcal{L} = -(1/4\mu_0) F^{\alpha\beta} F_{\alpha\beta} - A_\alpha J^\alpha$ with respect to A , the four-potential. As the magnetic perturbation is given by the parallel component of the vector potential according to Eq.2.4 with Eq.2.5, the Lagrangian density reduces to

$$\mathcal{L} = \frac{1}{2} \left(\varepsilon_0 |\partial_{\mathbf{q}} \Phi|^2 - \frac{1}{\mu_0 R^2} |\partial_{\mathbf{q}} \delta\psi|^2 \right) + J_{\parallel} A_{\parallel} - \rho \Phi^{18}. \quad (2.8)$$

ρ here is the charge density. \mathbf{q} is to be understood as $\{\psi, \xi, \vartheta\}$, which is equivalent to $\{\Omega, \xi, \vartheta; \sigma_\psi\}$ with σ_ψ being a sign of $\psi - \psi_s$. Seeking the extremum of this functional for any given A_{\parallel}/Φ , we obtain the parallel component of Ampère's law/Poisson's equation. Restricting the analysis to a single harmonic in ξ , i.e. $\propto e^{-in\xi}$, in accordance with the $\cos n\xi$ form of Ω and taking the $\cos \xi$ and $\sin \xi$ components in the parallel component of Ampère's law, we provide integration through the island area¹⁹ to obtain

$$\frac{1}{\mu_0 R} \Delta' \tilde{\psi} - \int_{\mathbb{R}} d\psi \int_{-\pi}^{\pi} d\xi \bar{J}_{\parallel} \cos \xi = 0, \quad (2.9)$$

$$\int_{\mathbb{R}} d\psi \int_{-\pi}^{\pi} d\xi \bar{J}_{\parallel} \sin \xi = 0, \quad (2.10)$$

and Poisson's equation reads

$$\varepsilon_0 \partial_{\mathbf{q}}^2 \Phi = -\rho. \quad (2.11)$$

The electrostatic potential is to be found to keep plasma quasi-neutral, i.e.

$$\sum_j e Z_j n_j = 0.$$

¹⁸In Chapter V we will use $\mathcal{L} = \frac{1}{2} \left(\varepsilon_0 |\mathbf{E}|^2 - \frac{1}{\mu_0} |\mathbf{B}|^2 \right) + \mathbf{J} \cdot \mathbf{A}^* - \rho \Phi^*$ integrated through the phase space island. Now we concentrate on the collisional dissipation, omitting any external dissipative contributions (e.g. [78]) and take the perturbation of the form, Eq.2.5, and hence a complex conjugated pair, (\mathbf{A}^*, Φ^*) , is to be replaced with (\mathbf{A}, Φ) .

¹⁹Below we restrict the analysis to the 2/1 NTM for simplicity, and hence n is to be replaced with $n = 1$.

Here summing over j represents a sum over all the species; eZ_j and n_j are charge and density of a species. \bar{J}_{\parallel} is the ϑ -average of J_{\parallel} , $\int d\mathbf{q} = \int_{-\pi}^{\pi} d\xi \int_{\mathbb{R}} d\psi = \frac{w_{\psi}}{2\sqrt{2}} \sum_{\sigma_{\psi}} \sigma_{\psi} \oint d\xi \int_{-1}^{+\infty} \frac{d\Omega}{(\Omega + \cos\xi)^{1/2}}$, which results from Eq.2.7 with $n = 1$. At fixed Ω , outside the magnetic island $\Omega \geq 1$, we simply integrate over a period in ξ , i.e. $[-\pi, \pi]$. Inside the island, i.e. $-1 \leq \Omega < 1$, we have to integrate over ξ between bounce points, given by $\xi_b^{\Omega} = \pm \arccos(-\Omega)$, and sum over the two streams, $\sigma_{\psi} = \pm 1$, to provide continuity at each bounce point.

Eqs.2.9-2.11 represent a system for the threshold magnetic island half-width, w_c , the island propagation frequency and the electrostatic potential. Δ' results from the integration through the island, as $\partial_{\mathbf{q}}\psi$ is not smooth across the island, and represents the classical tearing mode stability parameter. Deriving Eq.2.10, we neglected any external dissipation forces (the island interaction with a resistive wall is considered in [77, 82, 83, 78]). Eqs.2.9,2.10 reproduce the nonlinear tearing mode dispersion relation [84, 53, 59]. This system provides w_c and ω , once the perturbed current localised about the island, J_{\parallel} , is obtained. This is to be calculated from the ion and electron distribution functions, which we find in the following sections.

2.2 Ion response

The ion/electron response to the NTM magnetic perturbation is described by the drift kinetic equation that is given by Eq.1.12 for each particle species, j .²⁰ The $\partial/\partial t$ term vanishes in the island rest frame. A system of two particle species is addressed: plasma electrons and ions²¹. Φ is the electrostatic potential localised about the island vicinity and is associated with a difference in the electron and ion responses to the magnetic perturbation. It is to be determined below from plasma quasi-neutrality. All spatial derivatives are calculated at fixed magnetic moment, $\mu = V_{\perp}^2/2B$, and kinetic energy, $\mathcal{K} = V^2/2$. In velocity space, following [53], it is convenient to introduce a triple of velocity variables as $\{\lambda, V; \sigma\}$, where $\lambda = 2\mu/V^2$ is the pitch angle, V is the absolute value of velocity and $\sigma = V_{\parallel}/|V_{\parallel}|$ is the sign of the parallel component of velocity. Hence, the

²⁰ $\mathbf{b} = \mathbf{B}/B$. In Eq.2.4 the unit vector is introduced in the direction of the equilibrium field lines.

²¹The energetic particle/ impurity contribution will be introduced as the third particle species in the secondary mode stability analysis, Chapter V.

velocity space integral and V_{\parallel} become

$$\int d\mathbf{V} = \pi B \sum_{\sigma} \int_{\mathbb{R}^+} V^2 dV \int_0^{B^{-1}} \frac{d\lambda}{(1 - \lambda B)^{1/2}}, \quad (2.12)$$

$$V_{\parallel} = \sigma V (1 - \lambda B)^{1/2}. \quad (2.13)$$

Thus, the trapped-passing boundary in pitch angle space is at the inverse of the maximum value of the magnetic field, i.e. $\lambda_c = 1/B_0 (1 + \varepsilon)$ for the equilibrium given in Sec.2.1. $\lambda \in [0, \lambda_c]$ for passing and $\lambda \in (\lambda_c, \lambda_{fin}]$ with $\lambda_{fin} = 1/B_0 (1 - \varepsilon)$ for trapped particles.

Assuming a Maxwell-Boltzmann equilibrium plasma, we write $f_j = f_j^{MB} + g_j$ with

$$f_j^{MB}(\psi) = \frac{n_{eqm}(\psi)}{\pi^{3/2} V_{Tj}^3(\psi)} e^{-V^2/V_{Tj}^2(\psi)} \quad (2.14)$$

denoting the Maxwell-Boltzmann distribution of a species j . n_{eqm} is the equilibrium Boltzmann density, i.e. $n_{eqm} = n_0 (1 - eZ_j\Phi/T_j)$ provided $eZ_j\Phi \ll T_j$. $V_{Tj} = (2T_j/m_j)^{1/2}$ is the thermal velocity of a species. The first term in f_j is the classical Maxwell-Boltzmann contribution, while the second term describes the perturbation in the particle distribution due to the tearing mode occurrence. Seeking the solution localised to the magnetic island, we Taylor expand the Maxwellian around the rational surface, $\psi = \psi_s$, i.e.

$$f_j = \left(1 - \frac{eZ_j\Phi}{T_j(\psi_s)}\right) f_j^M(\psi_s) + g_j, \quad (2.15)$$

where $f_j^M = n_0(\psi_s) \pi^{-3/2} V_{Tj}^{-3}(\psi_s) e^{-V^2/V_{Tj}^2(\psi_s)}$ and the electrostatic potential being expanded around the rational surface, i.e. $\Phi = \Phi'_{eqm}|_{\psi=\psi_s} (\psi - \psi_s) + \delta\Phi$ (prime denotes the derivative with respect to ψ), and thus $\Phi(\psi_s) = \delta\Phi$. Φ_{eqm} is the equilibrium potential in the absence of the island, and $\delta\Phi$ is the perturbation associated with the tearing mode. The perturbed distribution, g_j , then must be linear in ψ far from the island to match to the Maxwellian equilibrium, $\partial g_j / \partial \psi|_{\psi \rightarrow \pm\infty} = \partial_{\psi} f_j^M(\psi_s)$.

To solve Eq.1.12 for g_j , we define a small parameter $\Delta = w/a \ll 1$. The following orderings are assumed: $eZ_j\Phi/T_j \sim \Delta$, $g_j/f_j^M \sim \Delta$, $\delta\Phi/\Phi \sim \Delta$. Then $B_1/B_0 \sim \varepsilon\Delta^2$, where $B_1 = |\mathbf{B}_1|$ (see Appendix B for more detail). Considering Eq.27 for electrons and Eq.39 for ions from the original paper [53], we notice that the dimension of the problem can be reduced by switching from $\{\psi, \xi, \vartheta, \lambda, V; \sigma\}$ to $\{p_{\varphi}, \xi, \vartheta, \lambda, V; \sigma\}$, where

$p_\varphi = \psi - \psi_s - IV_{\parallel}/\omega_{cj}$ is the toroidal component of the canonical angular momentum (a more detailed explanation can be found in Appendix C). $IV_{\parallel}/\omega_{cj}$ is the excursion of a particle orbit from the reference flux surface. As $w \ll a$, plasma is toroidally symmetric to leading order and thus the toroidal component of p_φ is constant on a particle orbit. Thus, to $\mathcal{O}(\Delta^1)$ Eq.1.12 for g_j becomes

$$\begin{aligned}
& \left\{ \frac{V_{\parallel}}{B_0} \frac{I}{qR^2} \left[1 - I \frac{\partial}{\partial \psi} \Big|_{\vartheta} \left(\frac{V_{\parallel}}{\omega_{cj}} \right) \right] + \frac{B_\varphi^2}{qB_0^2} \frac{\partial \Phi}{\partial \psi} \Big|_{\xi, \vartheta} \right\} \frac{\partial g_j}{\partial \vartheta} \Big|_{p_\varphi, \xi, \mu, V} + \\
& + \left\{ \frac{V_{\parallel}}{B_0} (\mathbf{B}_1 \cdot \nabla p_\varphi) + \frac{\partial \Phi}{\partial \xi} \Big|_{\psi, \vartheta} \right\} \frac{\partial g_j}{\partial p_\varphi} \Big|_{\vartheta, \xi, \mu, V} + \\
& + \left\{ \frac{V_{\parallel}}{B_0} \left[\frac{I}{qR^2} q'_s \left(p_\varphi + \frac{IV_{\parallel}}{\omega_{cj}} \right) + B_0^2 \frac{\partial}{\partial \psi} \Big|_{\vartheta} \left(\frac{V_{\parallel}}{\omega_{cj}} \right) + \vartheta' B_\vartheta^2 \frac{\partial}{\partial \vartheta} \Big|_{\psi} \left(\frac{V_{\parallel}}{\omega_{cj}} \right) \right] - \right. \\
& \left. - \frac{\partial \Phi}{\partial \psi} \Big|_{\xi, \vartheta} \right\} \frac{\partial g_j}{\partial \xi} \Big|_{p_\varphi, \vartheta, \mu, V} - \frac{eZ_j}{m_j q V} \frac{V_{\parallel}}{B_0} \frac{I}{R^2} \frac{\partial \Phi}{\partial \vartheta} \Big|_{p_\varphi, \xi} \frac{\partial g_j}{\partial V} \Big|_{p_\varphi, \vartheta, \xi, \mu} = C_j(g_j). \tag{2.16}
\end{aligned}$$

Here $m - nq$ has been Taylor expanded about the rational surface; ϑ' denotes $\partial \vartheta / \partial \psi = R^{-2} B_\vartheta^{-2} (\nabla \psi \cdot \nabla \vartheta)$. The derivatives of g_j in the Vlasov part of Eq.2.16 are taken at fixed μ . At this stage, the form of the collision operator has not been specified. $(\mathbf{B}_1 \cdot \nabla \vartheta)$ and $(\mathbf{B}_1 \cdot \nabla \xi)$ have been neglected as higher order terms in the limit of small magnetic islands. We note that $\partial / \partial \psi, p_\varphi \sim R^{-1} B_\vartheta^{-1} \partial / \partial r$ on equilibrium quantities and $\partial / \partial \psi, p_\varphi \sim R^{-1} B_\vartheta^{-1} \partial / \partial w$ on perturbed quantities ($\partial p_\varphi / \partial \psi = 1$ to leading order in $\rho_{\vartheta j} / a$). To solve Eq.2.16 for g_j , we employ an expansion in Δ :

$$g_j = \sum_{\alpha} g_j^{(\alpha)} \Delta^\alpha. \tag{2.17}$$

The $\mathcal{O}(\Delta^0)$ equation is

$$\frac{IV_{\parallel}}{qR^2 B_0} \frac{\partial g_j^{(0)}}{\partial \vartheta} \Big|_{p_\varphi, \xi} = 0. \tag{2.18}$$

The $\mathbf{V}_b \cdot \nabla g_j$ and $\mathbf{V}_E \cdot \nabla g_j$ parts of the first term of Eq.2.16 are $\sim \Delta$ and hence do not contribute²². Working in the banana collisionality regime, we assume that the collision operator on the right hand side of Eq.2.16 is order Δ smaller than the free streaming. Hence we learn that the leading order distribution function, $g_j^{(0)}$, is ϑ -independent at fixed p_φ , i.e. $g_j^{(0)}(p_\varphi, \xi, \mu, V) = g_j^{(0)}(\psi, \vartheta, \xi, \mu, V)$.

²²A step by step derivation of the final NTM drift kinetic equation is presented in Appendix D.

Proceeding to next order in Δ and multiplying both sides of Eq.2.16 by $R^2 B_0 / IV_{\parallel}$, we obtain an equation for $g_j^{(0)}$:

$$\begin{aligned}
& \frac{1}{q} \frac{\partial g_j^{(1)}}{\partial \vartheta} \Big|_{p_{\varphi}, \xi, \lambda, V; \sigma} + \\
& + \left[\frac{R^2}{I} (\mathbf{B}_1 \cdot \nabla p_{\varphi}) + \frac{R^2 B_0}{IV_{\parallel}} \frac{\partial \Phi}{\partial \xi} \Big|_{\psi, \vartheta} \right] \frac{\partial g_j^{(0)}}{\partial p_{\varphi}} \Big|_{\vartheta, \xi, \lambda, V; \sigma} + \\
& + \left[\frac{q'_s}{q} \left(p_{\varphi} + \frac{IV_{\parallel}}{\omega_{cj}} \right) + \frac{R^2 B_0^2}{I} \frac{\partial}{\partial \psi} \Big|_{\vartheta} \left(\frac{V_{\parallel}}{\omega_{cj}} \right) + \frac{R^2 B_{\vartheta}^2}{I} \vartheta' \frac{\partial}{\partial \vartheta} \Big|_{\psi} \left(\frac{V_{\parallel}}{\omega_{cj}} \right) - \right. \\
& - \left. \frac{R^2 B_0}{IV_{\parallel}} \frac{\partial \Phi}{\partial \psi} \Big|_{\xi, \vartheta} \right] \frac{\partial g_j^{(0)}}{\partial \xi} \Big|_{p_{\varphi}, \vartheta, \lambda, V; \sigma} - \frac{e Z_j}{m_j q V} \frac{\partial \Phi}{\partial \vartheta} \Big|_{p_{\varphi}, \xi} \frac{\partial g_j^{(0)}}{\partial V} \Big|_{p_{\varphi}, \xi, \vartheta, \lambda; \sigma} + \\
& + 2 \frac{e Z_j}{m_j q V^2} \frac{\partial \Phi}{\partial \vartheta} \Big|_{p_{\varphi}, \xi} \lambda \frac{\partial g_j^{(0)}}{\partial \lambda} \Big|_{p_{\varphi}, \xi, \vartheta, V; \sigma} = \frac{R^2 B_0}{IV_{\parallel}} C_j \left(g_j^{(0)} \right). \tag{2.19}
\end{aligned}$$

To employ the collision operator from [53], we have switched from $\{\mu, V\}$ to $\{\lambda, V; \sigma\}$ in the Vlasov part of Eq.2.16.

To solve Eq.2.19 for $g_j^{(0)}$, we have to eliminate a term in $g_j^{(1)}$, integrating the equation over ϑ . This is equivalent to an orbit-averaging procedure at fixed p_{φ} (see Fig.2.6). For passing particles, g_j is periodic in ϑ and thus we simply integrate over a period in ϑ assuming $g_j(-\pi) = g_j(\pi)$. Trapped particles oscillate between bounce points, $\pm \vartheta_b$, defined from $\lambda B_0(\vartheta_b) = 1$, where V_{\parallel} tends to zero. The requirement on their distribution function is that

$$g_j(\vartheta = \pm \vartheta_b, \sigma = +1) = g_j(\vartheta = \pm \vartheta_b, \sigma = -1).$$

Thus, we integrate between $\pm \vartheta_b$ and sum over σ . As continuity is required at each bounce point, this annihilates the $\partial g_j^{(1)} / \partial \vartheta \Big|_{p_{\varphi}}$ term. Thus, an orbit-averaged form of Eq.2.19 is

$$\begin{aligned}
& \left[\frac{q'_s}{q} p_{\varphi} \cdot \Theta(\lambda_c - \lambda) + \omega_D - \omega_{E, \xi} \right] \frac{\partial g_j^{(0)}}{\partial \xi} \Big|_{p_{\varphi}, \vartheta, \lambda, V; \sigma} + \left[\left\langle \frac{R^2}{I} (\mathbf{B}_1 \cdot \nabla p_{\varphi}) \right\rangle_{\vartheta}^{p_{\varphi}} + \omega_{E, r} \right] \frac{\partial g_j^{(0)}}{\partial p_{\varphi}} \Big|_{\vartheta, \xi, \lambda, V; \sigma} \\
& = \left\langle \frac{R^2 B}{IV_{\parallel}} C_j \left(g_j^{(0)} \right) \right\rangle_{\vartheta}^{p_{\varphi}}, \tag{2.20}
\end{aligned}$$

where

$$\omega_D = \frac{q'_s}{q} \left\langle \frac{IV_{\parallel}}{\omega_{cj}} \right\rangle_{\vartheta}^{p_\varphi} + \frac{1}{I} \left\langle R^2 B^2 \frac{\partial}{\partial \psi} \Big|_{\vartheta, \xi} \left(\frac{V_{\parallel}}{\omega_{cj}} \right) \right\rangle_{\vartheta}^{p_\varphi} + \frac{1}{I} \left\langle R^2 B_{\vartheta}^2 \vartheta' \frac{\partial}{\partial \vartheta} \Big|_{\psi, \xi} \left(\frac{V_{\parallel}}{\omega_{cj}} \right) \right\rangle_{\vartheta}^{p_\varphi}, \quad (2.21)$$

$$\omega_{E, \xi} = \frac{1}{I} \left\langle \frac{R^2 B}{V_{\parallel}} \frac{\partial \Phi}{\partial \psi} \Big|_{\vartheta, \xi} \right\rangle_{\vartheta}^{p_\varphi} \quad (2.22)$$

and

$$\omega_{E, r} = \frac{1}{I} \left\langle \frac{R^2 B}{V_{\parallel}} \frac{\partial \Phi}{\partial \xi} \Big|_{\psi, \vartheta} \right\rangle_{\vartheta}^{p_\varphi} \quad (2.23)$$

are the magnetic and $\mathbf{E} \times \mathbf{B}$ drift frequencies in ξ and radial directions, respectively. Θ denotes the Heaviside step function. The last term in ω_D provides $\sim \varepsilon^2$ correction for the small inverse aspect ratio, circular cross section tokamak approximation. The ϑ -averaging operator at fixed p_φ is defined as

$$\langle \dots \rangle_{\vartheta}^{p_\varphi} = \begin{cases} \frac{1}{2\pi} \int_{-\pi}^{\pi} \dots d\vartheta, & \lambda \leq \lambda_c \\ \frac{1}{4\pi} \sum_{\sigma} \sigma \int_{-\vartheta_b}^{\vartheta_b} \dots d\vartheta, & \lambda \geq \lambda_c. \end{cases} \quad (2.24)$$

In Eq.2.20 Φ has been assumed to be periodic in ϑ . Using Eq.2.4, we find $\langle R^2 (\mathbf{B}_1 \cdot \nabla p_\varphi) \rangle_{\vartheta}^{p_\varphi} = -\langle R^2 B_0 dA_{\parallel} / d\xi \rangle_{\vartheta}^{p_\varphi} + \mathcal{O}(\Delta^2)$. Due to Eq.2.5, $dA_{\parallel} / d\xi = -(\tilde{\psi} / R) df / d\xi$. For a single isolated magnetic island, this simply reads $dA_{\parallel} / d\xi = (\tilde{\psi} / R) n \sin n\xi$. Eq.2.20 is the final ϑ -averaged non-normalised equation for the ion/electron plasma component to $\mathcal{O}(\Delta^1)$ in $\{p_\varphi, \xi, \lambda, V; \sigma\}$ space.

Following [53], we close our system by taking a collision operator that conserves particles and momentum, C_i , of the form:

$$C_i(g_i) = C_{ii}(g_i) = \nu_{ii}(V) \left[2 \frac{(1 - \lambda B)^{1/2}}{B} \frac{\partial}{\partial \lambda} \Big|_{\psi} \left(\lambda (1 - \lambda B)^{1/2} \frac{\partial g_i}{\partial \lambda} \Big|_{\psi} \right) + \frac{V_{\parallel} \bar{u}_{\parallel i}(g_i)}{V_{Ti}^2} f_i^M \right] \quad (2.25)$$

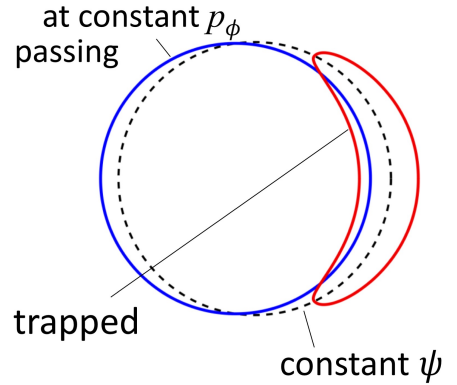


Figure 2.6: Projections of passing and trapped particle trajectories shown in a tokamak poloidal cross section (figure courtesy of K. Imada).

with $\nu_{ii}(V) = \nu_{ii}(V_{Ti})(V_{Ti}/V)^3$ and

$$\bar{u}_{\parallel j} = \frac{3\pi^{1/2}}{2n_0} V_{Tj}^3 \int d\mathbf{V} \frac{V_{\parallel} g_j}{V^3}, \quad (2.26)$$

$$u_{\parallel j} = \frac{1}{n_0} \int d\mathbf{V} V_{\parallel} g_j, \quad (2.27)$$

$j = e, i$. Ion-electron collisions are small and hence to be neglected.

2.3 Electron response

The procedure described in Sec.2.2 is also to be applied to the electrons. We arrive at Eq.2.20 for the leading order electron distribution function, $g_e^{(0)}$, with the following collision integral:

$$C_e(g_e) = C_{ee}(g_e) + C_{ei}(g_e) \quad (2.28)$$

with

$$C_{ee}(g_e) = \nu_{ee}(V) \left[2 \frac{(1-\lambda B)^{1/2}}{B} \frac{\partial}{\partial \lambda} \Big|_{\psi} \left(\lambda (1-\lambda B)^{1/2} \frac{\partial g_e}{\partial \lambda} \Big|_{\psi} \right) + \frac{V_{\parallel} \bar{u}_{\parallel e}(g_e)}{V_{Te}^2} f_e^M \right] \quad (2.29)$$

and

$$C_{ei}(g_e) = \nu_{ei}(V) \left[2 \frac{(1-\lambda B)^{1/2}}{B} \frac{\partial}{\partial \lambda} \Big|_{\psi} \left(\lambda (1-\lambda B)^{1/2} \frac{\partial g_e}{\partial \lambda} \Big|_{\psi} \right) + \frac{2}{V_{Te}^2} V_{\parallel} u_{\parallel i}(g_i) f_e^M \right]. \quad (2.30)$$

For electrons, collisions with ions and like-particle collisions must be retained. Here $\nu_{ej}(V) = \nu_{ej}(V_{Te})(V_{Te}/V)^3$, $j = e, i$. $\bar{u}_{\parallel e}$ and $u_{\parallel i}$ are introduced according to Eqs.2.26,2.27. Eq.2.20 with Eqs.2.25/2.28 for ions/electrons is to be further reduced, which is discussed in the following section.

2.4 Drift magnetic islands

To modify Eq.2.20 further, we introduce the following dimensionless system:

$$\hat{\rho}_{\partial j} = \frac{IV_{Tj}}{\omega_{cj}w}, \quad x = \frac{\psi - \psi_s}{w},$$

$$\begin{aligned}
\hat{V}_{\parallel} &= \frac{V_{\parallel}}{V_{Tj}}, & \hat{V} &= \frac{V}{V_{Tj}}, \\
\hat{L}_q^{-1} &= \frac{q'_s}{q} \psi_s, & \hat{L}_B^{-1} &= \frac{\psi_s}{B} \frac{\partial B}{\partial \psi}, & \hat{w} &= \frac{w}{\psi_s}, & \hat{\psi} &= \frac{\psi}{w} \\
\hat{\Phi} &= \frac{eZ_j \Phi}{T_j(\psi_s)}, & \hat{p}_{\varphi} &= x - \hat{\rho}_{\vartheta j} \hat{V}_{\parallel}
\end{aligned} \tag{2.31}$$

(note: λ is kept non-normalised, w normalised to ψ_s/r_s denotes the magnetic island half-width in ψ/r space, respectively). Then Eq.2.20 becomes

$$\begin{aligned}
& \left[\frac{\hat{w}}{\hat{L}_q} \hat{p}_{\varphi} \cdot \Theta(\lambda_c - \lambda) - \hat{\rho}_{\vartheta i} \hat{\omega}_D - \hat{\omega}_{E,\xi} \right] \frac{\partial g_i^{(0)}}{\partial \xi} \Big|_{p_{\varphi}, \vartheta, \lambda, V; \sigma} + \\
& + \left[\frac{1}{4} \left\langle \frac{B_0}{B_{\varphi}} \frac{\hat{w}}{\hat{L}_q} \frac{df}{d\xi} \right\rangle_{\vartheta}^{p_{\varphi}} + \hat{\omega}_{E,r} \right] \frac{\partial g_i^{(0)}}{\partial \hat{p}_{\varphi}} \Big|_{\vartheta, \xi, \lambda, V; \sigma} = \\
& = \hat{\nu}_{ii} \left[\frac{2}{\hat{V}} \left\langle \frac{\partial}{\partial \lambda} \Big|_{\psi} \left(\sigma \lambda (1 - \lambda B)^{1/2} \frac{R}{B_{\varphi}} \frac{\partial g_i^{(0)}}{\partial \lambda} \Big|_{\psi} \right) \right\rangle_{\vartheta}^{p_{\varphi}} + \right. \\
& \left. + \frac{3}{2} e^{-\hat{V}^2} \left\langle \frac{R}{B_{\varphi}} B_0^2 \sum_{\sigma} \sigma \int_{\mathbb{R}^+} d\hat{V} \int_0^{B^{-1}} g_i^{(0)} d\lambda \right\rangle_{\vartheta}^{p_{\varphi}} \right]
\end{aligned} \tag{2.32}$$

for ions (with V being normalised to V_{Ti}) and

$$\begin{aligned}
& \left[\frac{\hat{w}}{\hat{L}_q} \hat{p}_{\varphi} \cdot \Theta(\lambda_c - \lambda) - \hat{\rho}_{\vartheta e} \hat{\omega}_D - \hat{\omega}_{E,\xi} \right] \frac{\partial g_e^{(0)}}{\partial \xi} \Big|_{p_{\varphi}, \vartheta, \lambda, V; \sigma} + \\
& + \left[\frac{1}{4} \left\langle \frac{B_0}{B_{\varphi}} \frac{\hat{w}}{\hat{L}_q} \frac{df}{d\xi} \right\rangle_{\vartheta}^{p_{\varphi}} + \hat{\omega}_{E,r} \right] \frac{\partial g_e^{(0)}}{\partial \hat{p}_{\varphi}} \Big|_{\vartheta, \xi, \lambda, V; \sigma} = \\
& = (\hat{\nu}_{ee} + \hat{\nu}_{ei}) \frac{2}{\hat{V}_e} \left\langle \frac{\partial}{\partial \lambda} \Big|_{\psi} \left(\sigma \lambda (1 - \lambda B)^{1/2} \frac{R}{B_{\varphi}} \frac{\partial g_e^{(0)}}{\partial \lambda} \Big|_{\psi} \right) \right\rangle_{\vartheta}^{p_{\varphi}} + \\
& + \frac{3}{2} e^{-\hat{V}_e^2} \hat{\nu}_{ee} \left\langle \frac{R}{B_{\varphi}} B_0^2 \sum_{\sigma} \sigma \int_{\mathbb{R}^+} d\hat{V}_e \int_0^{B^{-1}} g_e^{(0)} d\lambda \right\rangle_{\vartheta}^{p_{\varphi}} + \\
& + \frac{2}{\pi^{1/2}} e^{-\hat{V}_e^2} \left(\frac{m_e}{m_i} \right)^2 \hat{\nu}_{ei} \left\langle \frac{R}{B_{\varphi}} B_0^2 \sum_{\sigma} \sigma \int_{\mathbb{R}^+} d\hat{V}_i \hat{V}_i^3 \int_0^{B^{-1}} g_i^{(0)} d\lambda \right\rangle_{\vartheta}^{p_{\varphi}}
\end{aligned} \tag{2.33}$$

for electrons (with V_e/V_i being normalised to V_{Te}/V_{Ti}). Here $\hat{\nu}_{ii} = \nu_{ii}/V_{Ti}$ and $\hat{\nu}_{ej} = \nu_{ej}/V_{Te}$, $j = e, i$. Dimensionless drift frequencies are

$$\hat{\omega}_D = - \frac{\hat{w}}{\hat{L}_q} \left\langle \hat{V}_{\parallel} \right\rangle_{\vartheta}^{p_{\varphi}} + \left\langle \frac{B^2}{B_{\varphi}^2} \frac{\hat{w}}{\hat{L}_B} \left[\hat{V}_{\parallel} + \frac{\lambda \hat{V}^2}{2 \hat{V}_{\parallel}} B \right] \right\rangle_{\vartheta}^{p_{\varphi}},$$

$$\hat{\omega}_{E,\xi} = \frac{1}{2} \left\langle \frac{B^2}{B_\varphi^2} \hat{\rho}_{\vartheta j} \frac{\partial \hat{\Phi}}{\partial \hat{\psi}} \bigg|_{\xi,\vartheta} \right\rangle_{\vartheta}^{p_\varphi}, \quad \hat{\omega}_{E,r} = \frac{1}{2} \left\langle \frac{B^2}{B_\varphi^2} \hat{\rho}_{\vartheta j} \frac{\partial \hat{\Phi}}{\partial \xi} \bigg|_{\psi,\vartheta} \right\rangle_{\vartheta}^{p_\varphi}. \quad (2.34)$$

Employing the conventional large aspect ratio, circular cross section tokamak approximation, we write $B_\varphi \approx B_0 \approx B$ as stated in Sec.2. As $\partial \hat{\Phi} / \partial \hat{\psi} \big|_{\xi,\vartheta} = (\partial \hat{\rho}_\varphi / \partial \hat{\psi}) \partial \hat{\Phi} / \partial \hat{\rho}_\varphi \big|_{\xi,\vartheta}$, and using the fact that the orbit-averaging at fixed p_φ and $\partial / \partial \hat{\rho}_\varphi$ are commutative, we have

$$\left\langle \frac{\hat{\rho}_{\vartheta j}}{\hat{V}_\parallel} \frac{\partial \hat{\Phi}}{\partial \hat{\psi}} \bigg|_{\xi,\vartheta} \right\rangle_{\vartheta}^{p_\varphi} = \frac{\partial}{\partial \hat{\rho}_\varphi} \bigg|_{\xi,\vartheta} \left\langle \frac{\hat{\rho}_{\vartheta j} \hat{\Phi}}{\hat{V}_\parallel} \right\rangle_{\vartheta}^{p_\varphi}$$

Here we have assumed that the fastest p_φ variation is in Φ and hence we note $\partial \hat{\rho}_\varphi / \partial \hat{\psi} = 1$ to leading order in $\rho_{\vartheta j} / a$. Similarly, we obtain²³

$$\left\langle \frac{\hat{\rho}_{\vartheta j}}{\hat{V}_\parallel} \frac{\partial \hat{\Phi}}{\partial \xi} \bigg|_{\psi,\vartheta} \right\rangle_{\vartheta}^{p_\varphi} = \frac{\partial}{\partial \xi} \bigg|_{p_\varphi,\vartheta} \left\langle \frac{\hat{\rho}_{\vartheta j} \hat{\Phi}}{\hat{V}_\parallel} \right\rangle_{\vartheta}^{p_\varphi}.$$

This allows Eq.2.32/Eq.2.33 to be rewritten in the form:

$$\begin{aligned} & \left[\frac{\hat{w}}{\hat{L}_q} \hat{p}_\varphi \cdot \Theta(\lambda_c - \lambda) - \hat{\rho}_{\vartheta j} \hat{\omega}_D - \frac{\partial}{\partial \hat{\rho}_\varphi} \bigg|_{\xi,\vartheta} \frac{1}{2} \left\langle \frac{\hat{\rho}_{\vartheta j} \hat{\Phi}}{\hat{V}_\parallel} \right\rangle_{\vartheta}^{p_\varphi} \right] \frac{\partial g_j^{(0)}}{\partial \xi} \bigg|_{p_\varphi,\vartheta,\lambda,V;\sigma} + \\ & + \left[\frac{\partial}{\partial \xi} \bigg|_{p_\varphi,\vartheta} \frac{1}{2} \left\langle \frac{\hat{\rho}_{\vartheta j} \hat{\Phi}}{\hat{V}_\parallel} \right\rangle_{\vartheta}^{p_\varphi} - \frac{1}{4} \frac{\hat{w}}{\hat{L}_q} \sin \xi \cdot \Theta(\lambda_c - \lambda) \right] \frac{\partial g_j^{(0)}}{\partial \hat{p}_\varphi} \bigg|_{\vartheta,\xi,\lambda,V;\sigma} = \tilde{C}_j, \end{aligned} \quad (2.35)$$

where \tilde{C}_j represents the right hand side of Eq.2.32/Eq.2.33 for ions/electrons, respectively (note: to simplify the analysis below we take $n = 1$, unless otherwise stated). Eq.2.35 is equivalent to

$$\left[\frac{\hat{w}}{\hat{L}_q} \hat{p}_\varphi \cdot \Theta(\lambda_c - \lambda) - \hat{\rho}_{\vartheta j} \hat{\omega}_D - \frac{\partial}{\partial \hat{\rho}_\varphi} \bigg|_{\xi,\vartheta} \frac{1}{2} \left\langle \frac{\hat{\rho}_{\vartheta j} \hat{\Phi}}{\hat{V}_\parallel} \right\rangle_{\vartheta}^{p_\varphi} \right] \frac{\partial g_j^{(0)}}{\partial \xi} \bigg|_{S,\vartheta,\lambda,V;\sigma} = \tilde{C}_j \quad (2.36)$$

with

$$S = \frac{\hat{w}}{4\hat{L}_q} \left[2 \left(\hat{p}_\varphi - \frac{\hat{\omega}_D \hat{\rho}_{\vartheta j} \hat{L}_q}{\hat{w}} \right)^2 - \cos \xi \right] \Theta(\lambda_c - \lambda) - \hat{\omega}_D \hat{\rho}_{\vartheta j} \hat{p}_\varphi \Theta(\lambda - \lambda_c) - \frac{1}{2} \left\langle \frac{\hat{\rho}_{\vartheta j} \hat{\Phi}}{\hat{V}_\parallel} \right\rangle_{\vartheta}^{p_\varphi}. \quad (2.37)$$

²³ p_φ is ξ -independent at any fixed ψ and hence $\partial / \partial \xi \big|_{\psi,\vartheta} = \partial / \partial \xi \big|_{p_\varphi,\vartheta}$.

We note that S is ϑ -independent and is to be treated as a new *radial* coordinate.

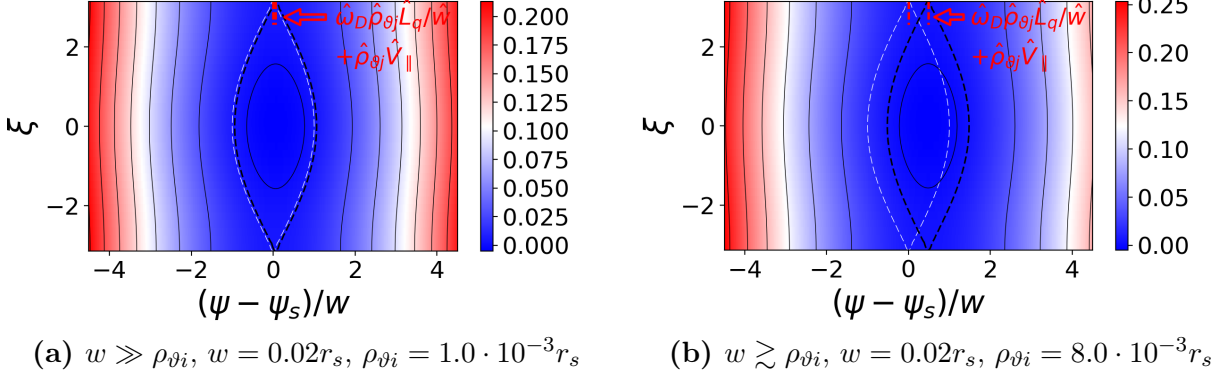


Figure 2.7: Contours of constant S in the (x, ξ) plane in the absence of the electrostatic potential, $\hat{\Phi} = 0$, for $w \gg \rho_{\vartheta i}$ (left) and $w \gtrsim \rho_{\vartheta i}$ (right). $\lambda = 0.84$, $\varepsilon = 0.1$, $V = V_{Ti}$, $\sigma = +1$, $\hat{L}_q = 1$. White dashed line indicates the position of the magnetic island separatrix, $\Omega = 1$. The S island separatrix is at $\hat{w}/4\hat{L}_q$ (black dashed line).

Eqs.2.36,2.37 complete the transition from $\{p_\varphi, \xi, \lambda, V; \sigma\}$ to $\{S, \xi, \lambda, V; \sigma\}$, and the particle distribution function is to be found as $g_j^{(0)} = g_j^{(0)}(S, \xi, \lambda, V; \sigma)$. According to its definition, S is a function of p_φ , ξ , λ and V for each σ , and depends on the form of the electrostatic potential, which is, in turn, a function of ψ , ξ and ϑ . For passing particles in the absence of the electrostatic potential, i.e. when the $\mathbf{E} \times \mathbf{B}$ drift effects are ignored, the contours of constant S reproduce the magnetic island structure given by Eq.2.7 but have a radial shift by the amount $\hat{\omega}_D \hat{\rho}_{\vartheta j} \hat{L}_q / \hat{w} + \hat{\rho}_{\vartheta j} \hat{V}_{\parallel}^{24}$, proportional to the poloidal Larmor radius (see Figs.2.7a,2.7b). This shift arises due to the ∇B and curvature tokamak drifts, and as $\hat{\omega}_D$ is σ -dependent in the passing branch, the shift is in opposite directions for $V_{\parallel} \gtrless 0$. These S island structures in the contours of constant S are to be referred to as *drift* islands. A similar drift island structure in view of plasma tokamak transport has been identified by Kadomtsev in [85], where the chains of islands much smaller than $\rho_{\vartheta i}$ but larger than $\rho_{\vartheta e}$ are considered.

In Figs.2.7a,2.7b we plot S contours in the (x, ξ) plane for passing ions at different $\rho_{\vartheta i}/w$. We also note that $\hat{\omega}_D$ being a function of λ provides the ν_{ii} dependence of the radial shift as we approach the trapped-passing boundary²⁵. For trapped particles, S is simply proportional to \hat{p}_φ when $\Phi = 0$, and is σ -independent due to the summation over σ in the orbit-averaging operator, Eq.2.24. Inclusion of Φ , in principle, might modify the

²⁴Here \hat{p}_φ has been written in terms of $\hat{\psi}$ in Eq.2.37.

²⁵This is to be explained in the next chapter.

S structure significantly. However, as we will see in the forthcoming sections, the self-consistent electrostatic potential obtained from plasma quasi-neutrality does not add any significant quantitative modifications to the form of S , keeping the surfaces of constant S closed for passing and open for trapped particles. Moving from p_φ to S as the radial coordinate leads to the perturbed passing particle distribution function being found as a superposition of two solutions: localised in the vicinity of $\sigma = +1$ and $\sigma = -1$ drift islands rather than the actual magnetic island. As we shall see later, this creates new physics for islands of width $\sim \rho_{\theta i}$.

To solve Eq.2.36 for $g_j^{(0)}$ as a function of S , we employ weak collisional dissipation. In the reference frame in which the equilibrium radial electric field is zero, this is equivalent to imposing $\delta_i \equiv \nu_{ii}/\varepsilon\omega \ll 1$ for ions and $\delta_e \equiv \nu_{ej}/\varepsilon\omega \ll 1$ for electrons. Treating the system perturbatively, similar to Eq.2.17, and applying an expansion in δ_j , we come to

$$\left. \frac{\partial g_j^{(0,0)}}{\partial \xi} \right|_{S,\vartheta,\lambda,V;\sigma} = 0 \quad (2.38)$$

to leading order. Here we learn that $g_j^{(0,0)}$ is ξ -independent at fixed S , i.e. $g_j^{(0,0)} = g_j^{(0,0)}(S, \lambda, V; \sigma) = g_j^{(0,0)}(p_\varphi, \xi, \lambda, V; \sigma)$. Proceeding to next order in δ_j and introducing collisions, we derive an equation for $g_j^{(0,0)}$:

$$\mathcal{A} \left. \frac{\partial g_j^{(0,1)}}{\partial \xi} \right|_{S,\vartheta,\lambda,V;\sigma} = \tilde{C}_j \left(g_j^{(0,0)} \right), \quad (2.39)$$

where \mathcal{A} denotes the coefficient in front of $\partial g_j^{(0,0)}/\partial \xi \Big|_{S,\vartheta,\lambda,V;\sigma}$ on the left hand side of Eq.2.36. To eliminate the term in $g_j^{(0,1)}$, we divide both sides of Eq.2.39 by \mathcal{A} and introduce the annihilation operator similar to Eq.2.24 to provide ξ -averaging at fixed S . As the particle distribution is periodic in ξ , we integrate Eq.2.39 over a period in ξ outside the S island for passing particles. Inside the drift island, i.e. $S < S_c$ (S_c denotes the S island separatrix), we integrate between the ξ -bounce points given by $\xi_{b1,2} = \xi_{b1,2}(S, p_{\varphi 0}, \lambda, V; \sigma)$, where $p_{\varphi 0}$ is the stationary point of $S = S(p_\varphi)$ for each ξ, λ, V and σ . In the absence of the electrostatic potential, $\hat{p}_{\varphi 0} = \hat{\omega}_D \hat{\rho}_{\vartheta j} \hat{L}_q / \hat{w}$ and $\xi_{b1,2} = \pm \arccos \left(-S \cdot 4\hat{L}_q / \hat{w} \right)$ but generally there is no analytic form for them. S as a function of p_φ has two branches for each λ, V and σ . Hence, inside the drift island we also sum over the two streams, $\sigma_{p_\varphi} = \pm 1$, where σ_{p_φ} is

the sign of $p_\varphi - p_{\varphi 0}$. This annihilates $\partial g_j^{(0,1)}/\partial \xi|_{S,\vartheta,\lambda,V;\sigma}$ due to the continuity requirement at both bounce points. The above procedure is also to be applied to trapped particles. In the absence of the island-like structure, we integrate over a period in ξ , imposing a periodic boundary condition (note: the self-consistent electrostatic potential does not provide closed contours of constant S in the trapped branch in ranges of parameters we consider). Thus, Eq.2.39 reduces to

$$\left\langle \frac{\tilde{C}_j}{\mathcal{A}} \right\rangle_\xi^S g_j^{(0,0)} = 0 \quad (2.40)$$

with the ξ -averaging operator at fixed S being defined as

$$\langle \dots \rangle_\xi^S = \begin{cases} \frac{1}{2\pi} \int_{-\pi}^{\pi} \dots d\xi, & S \geq S_c \\ \frac{1}{4\pi} \sum_{\sigma_{p_\varphi}} \sigma_{p_\varphi} \int_{\xi_{b,1}}^{\xi_{b,2}} \dots d\xi, & S < S_c \end{cases} \quad (2.41)$$

for passing and

$$\langle \dots \rangle_\xi^S = \frac{1}{2\pi} \int_{-\pi}^{\pi} \dots d\xi \quad (2.42)$$

for trapped particles. While collisions are neglected in Eq.2.36, the combined effect of the parallel flow, ∇B and curvature drifts would force the particle distribution to be flattened inside the drift islands. Introducing collisions at next order provides a full solution for the perturbed distribution function. However, the perturbative approach we apply breaks down in a *dissipation* layer, i.e. a narrow region in pitch angle space in the vicinity of the trapped-passing boundary, $\lambda = \lambda_c$ (see Fig.2.8). Here collisional dissipation becomes comparable to parallel streaming, $\sim \mathcal{A} \partial/\partial \xi|_S$, due to the steep gradient in λ , and thus a full solution of Eq.2.36 is required in the layer. We solve Eq.2.36 for $g_j^{(0)}$ in this collisional layer in the following chapter to calculate the island propagation frequency as this layer provides the dominant source of the collisional dissipation. This solution is then used to provide boundary conditions to match $g_j^{(0,0)}$ across the trapped-passing boundary and thus

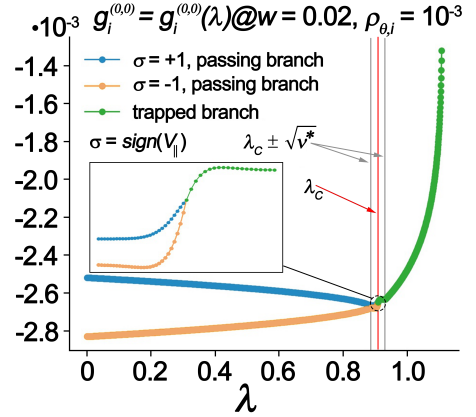
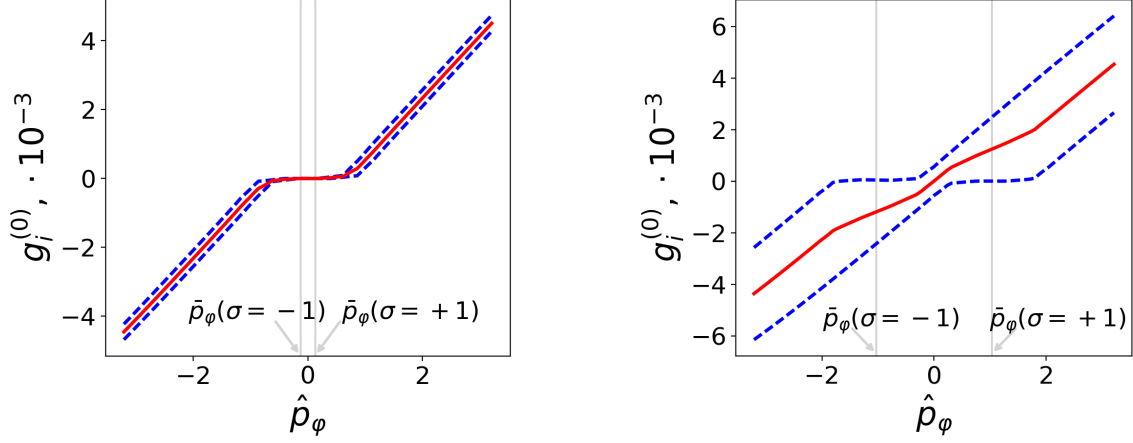


Figure 2.8: Leading order ion distribution function $g_i^{(0,0)}$ vs. pitch angle, λ , at $\hat{p}_\varphi = 1.83$, $\xi = 0$, $w = 0.02r_s$, $\rho_{\vartheta i} = 1.0 \cdot 10^{-3}r_s$, ion collisionality $\nu_i^* = 10^{-4}$ ²⁶, $\varepsilon = 0.1$, $\hat{L}_q = 1$. $g_i^{(0,0)}$ is normalised to $n_0/(\pi^{3/2}V_{Ti}^3)$. Inset: a full solution of Eq.2.36 in a collisional layer around λ_c . $\sqrt{\nu^*}$ represents the width of the layer with $\nu^* = \nu_{ii}/\varepsilon\omega$. The trapped branch solution is σ -independent due to the summation over σ in Eq.2.24.

²⁶The plasma collisionality is defined as $\nu_j^* = \nu_{jj/ei} \sqrt{m_j/T_j} \varepsilon^{-3/2} qR$, where j labels electrons and ions. For electrons, $\nu_{ei} \approx \nu_{ee}$.

to solve Eq.2.40 for $g_j^{(0,0)}$ in external regions, i.e. $\lambda \in [0, \lambda_c - \sqrt{\nu^*}] \cup [\lambda_c + \sqrt{\nu^*}, \lambda_{fin}]$. A detailed description of the solution technique can be found in Chapters III and IV.



(a) $w \gg \rho_{\vartheta i}$, $w = 0.02r_s$, $\rho_{\vartheta i} = 1.0 \cdot 10^{-3}r_s$ (b) $w \gtrsim \rho_{\vartheta i}$, $w = 0.02r_s$, $\rho_{\vartheta i} = 8.0 \cdot 10^{-3}r_s$

Figure 2.9: Sketch of the ion distribution function vs. \hat{p}_φ at $\lambda = 0.89$, $\xi = 0$ for $w \gg \rho_{\vartheta i}$ (left) and $w \gtrsim \rho_{\vartheta i}$ (right). $g_i^{(0)}$ is normalised to $n_0/(\pi^{3/2}V_{Ti}^3)$. $\varepsilon = 0.1$, $\hat{L}_q = 1$. Ion density/temperature length scales, $L_{n0}/L_{Ti} = 1$. $\bar{p}_\varphi(\sigma) = \hat{\omega}_D(\sigma)\hat{\rho}_{\vartheta i}\hat{L}_q/\hat{w}$. Dashed lines indicate the $\sigma = \pm 1$ passing ion distribution function, $g_i^{(0),\sigma}$, while solid line represents $\frac{1}{2}\sum_\sigma g_i^{(0),\sigma}$. The $\sigma = \pm 1$ drift islands are centered around $\bar{p}_\varphi(\sigma = \pm 1)$. The magnetic island is located between them; $\hat{p}_\varphi = \pm 1$ corresponds to the separatrix of the magnetic island.

In Figs.2.9a,2.9b we show how the ion distribution function varies with \hat{p}_φ at $\lambda_c - \sqrt{\nu^*}$, where the radial shift in S is maximum in the external region for given $\rho_{\vartheta i}$ and w . The radial shift, $\hat{\omega}_D(\sigma)\hat{\rho}_{\vartheta i}\hat{L}_q/\hat{w} + \hat{\rho}_{\vartheta j}\hat{V}_\parallel$, is proportional to σ and hence the $\sigma = +1$ shift is equal but opposite to the $\sigma = -1$ shift. Constructing the ion/electron density, we have to sum the passing distributions over σ according to Eq.2.12. As the areas of the distribution profile flattening are shifted in opposite directions for $\sigma = \pm 1$, summation over σ provides a substantial $\sum_\sigma g_i^{(0),\sigma}$ /density/temperature gradient inside the NTM magnetic island for $w \sim \rho_{\vartheta i}$ (see Fig.2.9b). When $\rho_{\vartheta i}/w \ll 1$, the profile flattening is maintained inside the magnetic island as the $\sigma = \pm 1$ shift is kept relatively small (see Fig.2.9a). This is to be referred to as finite orbit width effects and is explained in more detail in the forthcoming sections²⁷. As $\rho_{\vartheta e}$ is a factor $(m_e/m_i)^{1/2}$ smaller than $\rho_{\vartheta i}$, this effect is less significant for electrons in the absence of the electrostatic potential and thus would create a significant difference in the electron and ion responses for $w \sim \rho_{\vartheta i}$. However, as plasma is quasi-neutral, the electrostatic potential adjusts to provide the same density gradient

²⁷see "Contributions to the modified Rutherford equation"

for electrons as we have for the ions. This is to be discussed in the following section²⁸. In Figs.2.10a,2.10b we plot a sum of the $\sigma = \pm 1$ leading order ion distribution functions against $y = \sqrt{S - S_{\min}}$, where S_{\min} is a minimum value of S as a function of \hat{p}_φ , ξ , λ , \hat{V} for each σ and is given by $-\hat{w}/(4\hat{L}_q)$ in the absence of Φ . y is chosen as an extra variable to provide a Neumann boundary far from the island. $g_i^{(0)}$ shown in Figs.2.10a,2.10b takes into account the electrostatic potential found from the plasma quasi-neutrality condition. The $\sigma_{p_\varphi} = +1$ branch is used to reconstruct the particle distribution in a region of $p_\varphi > 0$, while $\sigma_{p_\varphi} = -1$ provides the distribution function in a region of $p_\varphi < 0$. In accordance with the drift island effects described above, $\sum_\sigma g_i^{(0),\sigma}$ (which is a measure of density due to Eq.2.12) is flattened inside the magnetic island for $w = 0.02r_s$, $\rho_{\vartheta i} = 1.0 \cdot 10^{-3}$. For $w = 0.02r_s$, $\rho_{\vartheta i} = 8.0 \cdot 10^{-3}$, the $\sum_\sigma g_i^{(0),\sigma}$ gradient is restored in the magnetic island region.

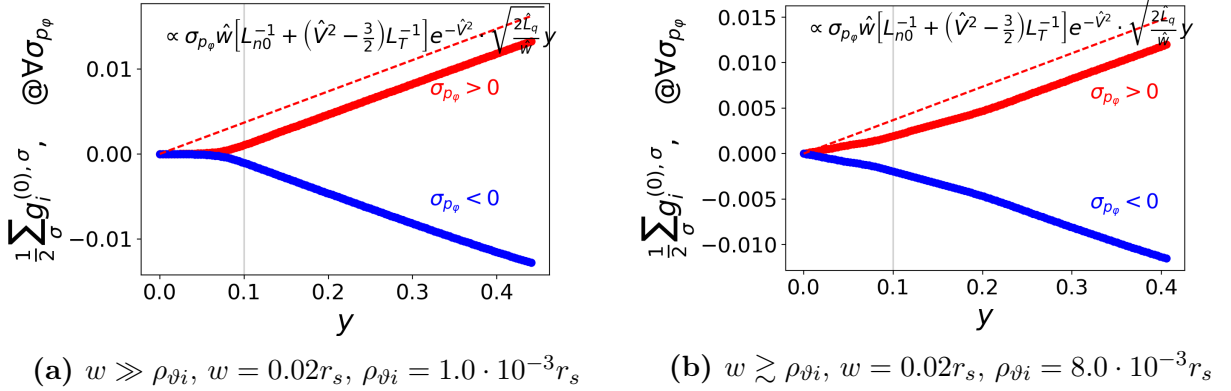


Figure 2.10: Sum of the $\sigma = \pm 1$ leading order ion distribution functions plotted against $y = \sqrt{S - S_{\min}}$ at $\lambda = 0.89$, $\xi = 0$ for $w \gg \rho_{\vartheta i}$ (left) and $w \gtrsim \rho_{\vartheta i}$ (right). $g_i^{(0)}$ is normalised to $n_0/(\pi^{3/2}V_{Ti}^3)$. $\varepsilon = 0.1$, $\hat{L}_q = 1$. $L_n \equiv L_{n0}/(1 + \hat{\omega}_E)$ with $L_{n0} = 1$ being the density gradient length scale, $\hat{\omega}_E \equiv m\Phi'_{eqm}/q_s\omega_{dia,e} = 0$. $\eta_i \equiv L_n/L_{Ti} = 1$. L_{Tj} is the ion/electron temperature gradient length scale. Dashed line represents the analytic limit far from the island in the absence of Φ .

Let us now return to the electrostatic potential localised to the island vicinity, which we consider neglecting the global plasma flows around the magnetic island. Its calculation is the subject of the following section.

²⁸see "Plasma quasi-neutrality and electrostatic potential"

2.5 Plasma quasi-neutrality and electrostatic potential

Technically speaking, the electrostatic potential is to be determined from Poisson's equation implying plasma quasi-neutrality²⁹. We adopt a Maxwell-Boltzmann equilibrium plasma and so we obtain

$$\hat{n}_i = 1 - \delta\hat{\Phi} + \delta\hat{n}_i \quad (2.43)$$

for ions and

$$\hat{n}_e = 1 + \delta\hat{\Phi} + \delta\hat{n}_e \quad (2.44)$$

for the electron density integrating Eq.2.15 over \mathbf{V} . Here $\hat{n}_j = n_j/n_0$, $\delta\hat{n}_j = \delta n_j/n_0$ and $\delta\hat{\Phi} = e\delta\Phi/T_j$ provided $Z_i = 1$ and $T_e = T_i$ (this assumption is maintained throughout the study unless otherwise stated). δn_j is the perturbed density associated with g_j and hence is given by

$$\delta n_j(\psi, \xi, \vartheta) = \pi B \sum_{\sigma} \int_{\mathbb{R}^+} V^2 dV \int_0^{B^{-1}} \frac{g_j(\psi, \xi, \vartheta, \lambda, V; \sigma) d\lambda}{(1 - \lambda B)^{1/2}}.$$

Thus, balancing the electron and ion densities, we find

$$\delta\hat{\Phi} = \frac{\delta\hat{n}_i - \delta\hat{n}_e}{2}. \quad (2.45)$$

As mentioned in the previous section, the electron and ion responses to the NTM magnetic perturbation differ in the absence of the electrostatic potential, especially for $w \sim \rho_{\vartheta i}$. Indeed, when $w/\rho_{\vartheta i} \gg 1$, both the electron and ion density profiles would be flattened inside the magnetic island and then the role of Φ is not crucial. When $w \sim \rho_{\vartheta i}$, the ion density becomes steepened in the vicinity of the magnetic island O-point, while the electron density is still flattened in the absence of Φ . So the strong electron parallel flow

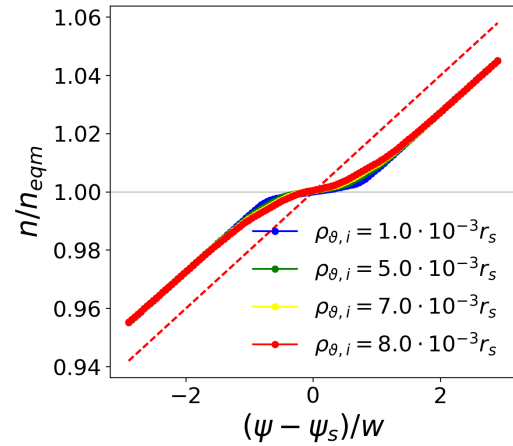


Figure 2.11: Radial density profile across the magnetic island O-point ($\xi = 0$) for different $\rho_{\vartheta i}$. $w = 0.02r_s$, $\varepsilon = 0.1$, $\hat{L}_q = 1$, ion collisionality $\nu_i^* = 10^{-3}$. Dashed line indicates the equilibrium density profile, $\propto L_n^{-1} \hat{w} \hat{\psi}$, $\hat{\omega}_E = 0$. Here n_{eqm} is the equilibrium density, i.e. in the absence of the magnetic island.

²⁹We consider length scales greater than the Debye length, and thus we can impose quasi-neutrality.

tends to keep their density flattened across the magnetic island. However, to maintain plasma quasi-neutrality, Φ is to be generated and adjusts to provide equal full ion and electron densities. Its form is more complicated than Eq.2.45 suggests as both the electron and ion responses, $\delta\hat{n}_{e,i}$, depend on Φ . We iterate over Φ until n_i and n_e become equal to a specified numerical error. So in contrast to [75], we state that the restoration of the density/temperature gradient across the magnetic island is influenced not only by ions but by the electrons as well. This goes beyond the Boltzmann plasma approximation and is valid as long as the plasma quasi-neutrality is incorporated in a model.

To illustrate the above, in Fig.2.11 we plot the full density, Eq.2.43/Eq.2.44, against ψ . The corresponding self-consistent electrostatic potential differentiated with respect to ψ in the (ψ, ξ) plane is shown in Figs.2.13a,2.13b,2.13c,2.13d and its cross-section across the magnetic island O-point in Fig.2.12. The electron/ion distribution function is normalised to $n_0/(\pi^{3/2}V_{Tj}^3)$. Thus, its limit far from the island reads $\partial\hat{f}_j/\partial x|_{x\rightarrow\pm\infty} = \hat{w} \left[L_n^{-1} + \left(\hat{V}^2 - 3/2 \right) L_{Tj}^{-1} \right] e^{-\hat{V}^2}$, where $\hat{f}_j = f_j\pi^{3/2}V_{Tj}^3/n_0$. L_n and L_{Tj} are the density and temperature length scales defined

$$\text{as } L_n^{-1} = (1/n_{eqm})(\partial n_{eqm}/\partial\psi),$$

$$L_{Tj}^{-1} = (1/T_j)(\partial T_j/\partial\psi). \quad n_{eqm} \text{ is the}$$

Boltzmann equilibrium density, i.e.

$$n_{eqm} \cong n_0(1 - eZ_j\Phi/T_j) \text{ provided}$$

$$eZ_j\Phi/T_j \ll 1. \text{ Hence, } L_n^{-1} \cong L_{n0}^{-1} - eZ_j\Phi'/T_j$$

$$\text{with } L_{n0}^{-1} = (1/n_0)(\partial n_0/\partial\psi) \text{ and}$$

$$\Phi' = \partial\Phi/\partial\psi. \text{ Normalising the second}$$

term to the electron diamagnetic frequency,

$$\omega_{dia,e} = mT_e n_0' / (-eq_s n_0), \text{ we have}$$

$$L_n^{-1} = L_{n0}^{-1}(1 + Z_j\omega_E/\omega_{dia,e}) \text{ with } \omega_E \equiv m\Phi'/q_s$$

(prime denotes the derivative with respect to ψ)³⁰. Thus according to Eq.2.45,

$$\hat{\Phi} \propto \hat{\omega}_E L_{n0}^{-1} \hat{w} \hat{\psi} \text{ far from the magnetic island,}$$

$$\hat{\omega}_E = \omega_E/\omega_{dia,e}.$$

Working in the island rest frame ($\omega = 0$), we require an equilibrium radial electric field

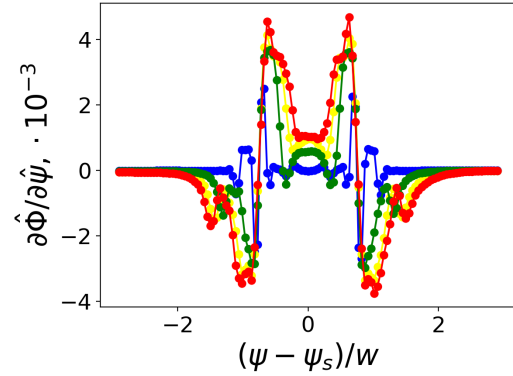


Figure 2.12: Radial derivative of the electrostatic potential, $\partial\hat{\Phi}/\partial\hat{\psi}$, across the magnetic island O-point ($\xi = 0$) for different $\rho_{\partial i}$ (notations are the same as used in Fig.2.11). $w = 0.02r_s$, $\varepsilon = 0.1$, $\hat{L}_q = 1$, ion collisionality $\nu_i^* = 10^{-3}$. The equilibrium density profile $\propto L_n^{-1}\hat{w}\hat{\psi}$, $\hat{\omega}_E = 0$. $\partial_{\hat{\psi}}\hat{\Phi}|_{\hat{\psi}\rightarrow\pm\infty} = 0$.

³⁰As the electrostatic potential is Taylor expanded about the rational surface, i.e. $\Phi = \Phi'_{eqm}|_{\psi=\psi_s}(\psi - \psi_s) + \delta\Phi$ with $\delta\Phi|_{\psi\rightarrow\infty} \rightarrow 0$, $\omega_E \equiv m\Phi'_{eqm}/q_s$.

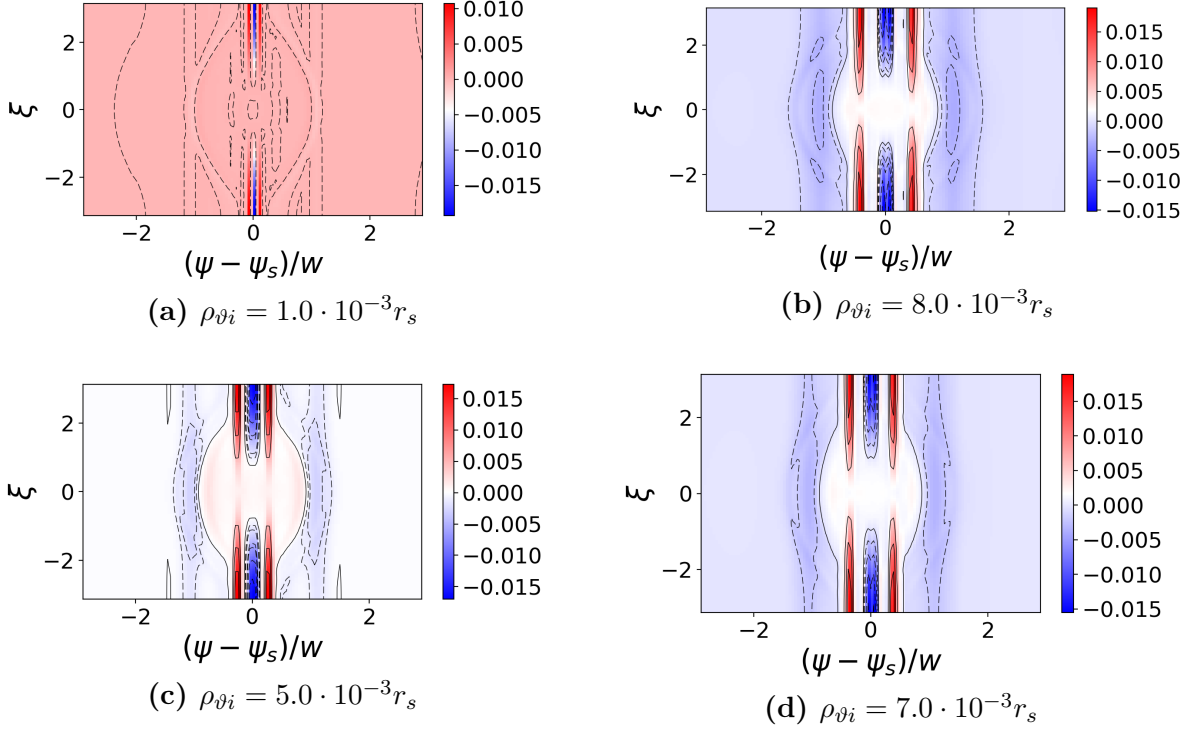


Figure 2.13: Contours of constant $\partial\hat{\Phi}/\partial\hat{\psi}$ in the (x, ξ) plane for a different ion poloidal Larmor radius value. $\varepsilon = 0.1$, $\hat{L}_q = 1$, $w = 0.02r_s$, ion collisionality $\nu_i^* = 10^{-3}$. The equilibrium density profile $\propto L_n^{-1}\hat{w}\hat{\psi}$, $\hat{\omega}_E = 0$. $\partial_\psi\hat{\Phi}|_{\hat{\psi}\rightarrow\pm\infty} = 0$.

to be retained. We can move to any other reference frame via toroidal rotation (note: the effects of centrifugal and Coriolis forces are neglected). As $\mathbf{E} + \mathbf{V} \times \mathbf{B}$ is constant, we write $\Delta\mathbf{E} = \Delta\mathbf{V} \times \mathbf{B} = -RV_\varphi\nabla\varphi \times \mathbf{B}$ for the variation of the electric field, where V_φ is the toroidal component of velocity. Due to Eq.2.3, we deduce $\Delta\mathbf{E} = (V_\varphi/R)\nabla\psi$. Setting $\Delta\mathbf{E} = -(\partial\Phi_{eqm}/\partial\psi)\nabla\psi$, we obtain $\Phi'_{eqm} = -V_\varphi/R$ for the equilibrium potential gradient far from the magnetic island (prime denotes the derivative with respect to ψ). We define ω_0 to be the island propagation frequency in the reference frame where the radial component of the electric field is zero far from the magnetic island. In any other frame rotating relative to this, we have

$$\frac{\partial}{\partial t} + \frac{V_\varphi}{R} \frac{\partial}{\partial\varphi} \Big|_{\psi, \vartheta} = - \left(\omega + \frac{mV_\varphi}{Rq_s} \right) \frac{\partial}{\partial\xi} \Big|_{\psi, \vartheta} \quad ^{31},$$

where ω is the island propagation frequency in that frame. Denoting $\omega_E = -mV_\varphi/Rq_s = m\Phi'_{eqm}/q_s$ in accordance with the above expression, we note $\omega - \omega_E$ is independent of

³¹The helical angle here is defined as in [53]. With the definition given in Sec.2.1, we have $\partial/\partial t + (V_\varphi/R)\partial/\partial\varphi|_{\psi, \vartheta} = (-\omega + V_\varphi/R)\partial/\partial\xi|_{\psi, \vartheta}$.

frame. Thus, moving to the reference frame where $\omega = 0$, we require $V_\varphi = \omega R q_s / m$, and thus $\Phi'_{eqm} = -\omega q_s / m$ or $\omega_0 = -\omega_E$. Therefore, the ω_E dependence in the island rest frame provides the ω dependence in the reference frame, in which the equilibrium electric field is zero far from the magnetic island.

In Figs.2.14-2.28 we show contours of constant S for passing and trapped particles in the (\hat{p}_φ, ξ) plane in the presence of the electrostatic potential. As can be seen from Figs.2.14-2.18, an island-like structure is maintained in the presence of Φ even at λ close to the trapped-passing boundary where the radial shift in Eq.2.37 is maximum³². For trapped particles, contours of constant S are open in a whole range of λ variation³³ for considered input parameters. This justifies a choice of Eq.2.42 for the ξ -averaging operator in the region of trapped particles.

2.6 Summary

In this chapter we have introduced the neoclassical tearing mode and magnetic islands whose formation always accompanies NTMs in tokamak plasmas. To predict the NTM behaviour, one has to know the plasma response to the NTM magnetic perturbation. This plasma response is written through the ion/electron distribution function that in this study is to be found as a solution of the drift kinetic equation in the vicinity of the magnetic island. To reduce the dimension of the problem we switched from the poloidal flux, ψ , to the toroidal canonical momentum, p_φ , and then from p_φ to S for the radial coordinate. This S island concept mathematically explains why the density gradient is not removed across the magnetic island for $w \sim \rho_{\theta i}$ as previously found in large scale PIC simulations for small magnetic islands [75]. Moreover, this introduces the ion poloidal Larmor radius rather than the ion banana orbit width as a key parameter to estimate a threshold, i.e. a marginal magnetic island width below which NTMs are suppressed.

The technique discussed in this chapter is valid while collisions can be treated perturbatively. The low collisionality plasma regime is justified as the bootstrap current exists in the

³² $\rho_{\theta i} = 5.0 \cdot 10^{-3} r_s$ is sufficient to provide partial steepening of the density profile across the magnetic island.

³³ $\lambda = 0.84$ and $\lambda = 0.97$ for given ε and ion collisionality are located at the edges of a boundary dissipation layer where collisions play a role. For $\lambda \in (0.84, 0.97)$, a layer solution is required, which is the subject of the following chapter.

banana regime. However, to match the passing and trapped distribution functions across the trapped-passing boundary, λ_c , we require consideration of the thin boundary dissipative layer around λ_c . Furthermore, as this layer provides the dominant source of dissipation in our problem, it also allows one to determine the island propagation frequency and thus the corresponding dependence of the polarisation current contribution to the island evolution. This is to be addressed in the following chapters.

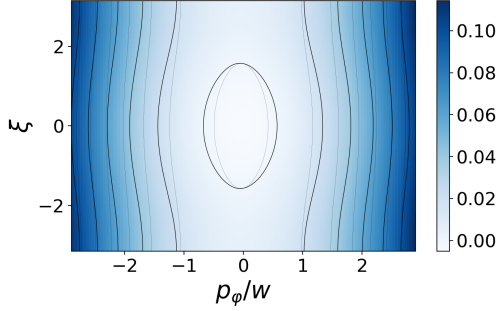


Figure 2.14: Contours of constant S in the $(\hat{\rho}_\varphi, \xi)$ plane in the presence of the self-consistent electrostatic potential. $\lambda = 0.84$ ($\lambda_c = 0.91$), $\varepsilon = 0.1$, $V = V_{Ti}$, $\sigma = -1$, $\hat{L}_q = 1$, $w = 0.02r_s$, $\rho_{\vartheta i} = 1.0 \cdot 10^{-3}r_s$, ion collisionality $\nu_i^* = 10^{-3}$. Grey contour lines represent contours of constant S in the absence of the potential for the same input parameters.

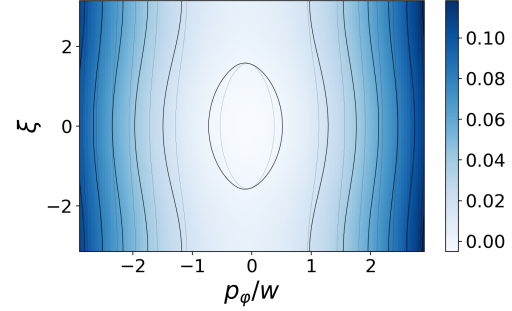


Figure 2.15: Contours of constant S in the $(\hat{\rho}_\varphi, \xi)$ plane in the presence of the self-consistent electrostatic potential. $\lambda = 0.84$ ($\lambda_c = 0.91$), $\varepsilon = 0.1$, $V = V_{Ti}$, $\sigma = -1$, $\hat{L}_q = 1$, $w = 0.02r_s$, $\rho_{\vartheta i} = 2.0 \cdot 10^{-3}r_s$, ion collisionality $\nu_i^* = 10^{-3}$. Grey contour lines represent contours of constant S in the absence of the potential for the same input parameters.

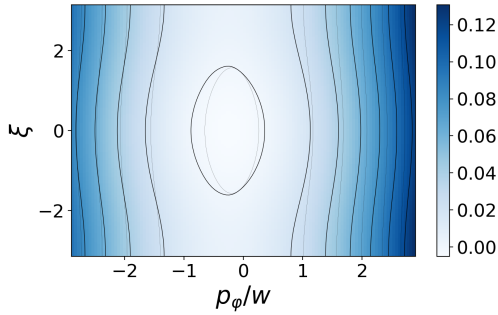


Figure 2.16: Same as Figs.2.14,2.15 except for the ion poloidal Larmor radius value, $\rho_{\vartheta i} = 5.0 \cdot 10^{-3}r_s$.

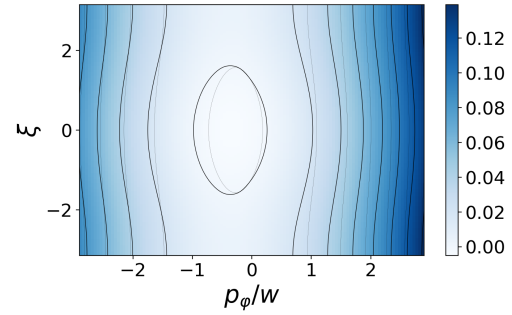


Figure 2.17: Same as Figs.2.14,2.15 except for the ion poloidal Larmor radius value, $\rho_{\vartheta i} = 7.0 \cdot 10^{-3}r_s$.

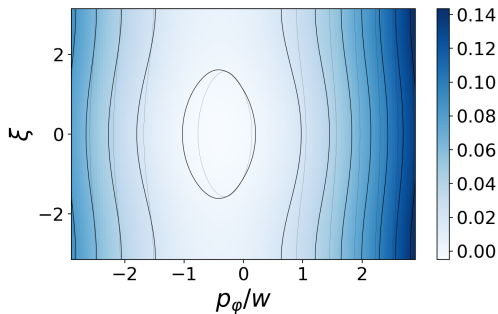


Figure 2.18: Same as Figs.2.14,2.15 except for the ion poloidal Larmor radius value, $\rho_{\vartheta i} = 8.0 \cdot 10^{-3}r_s$.

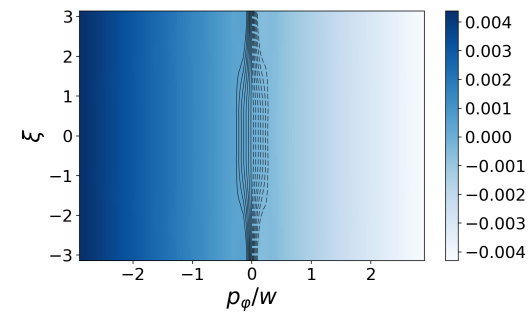


Figure 2.19: Same as Figs.2.14,2.15 except for $\lambda = 0.98$, $\sigma = \sigma_t$, $\rho_{\vartheta i} = 1.0 \cdot 10^{-3}r_s$.

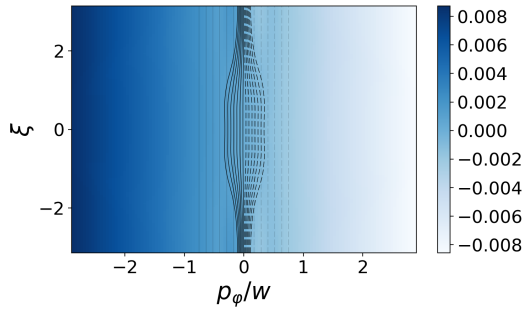


Figure 2.20: Same as Figs.2.14,2.15 except for $\lambda = 0.98$, $\sigma = \sigma_t$, $\rho_{\partial i} = 2.0 \cdot 10^{-3} r_s$.

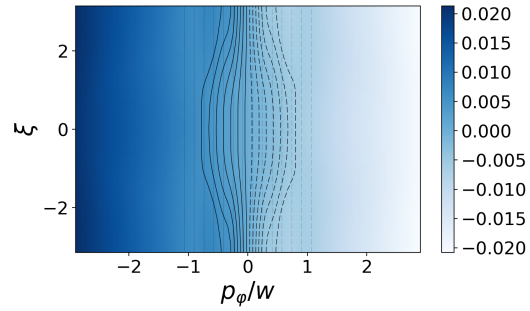


Figure 2.21: Same as Figs.2.14,2.15 except for $\lambda = 0.98$, $\sigma = \sigma_t$, $\rho_{\partial i} = 5.0 \cdot 10^{-3} r_s$.

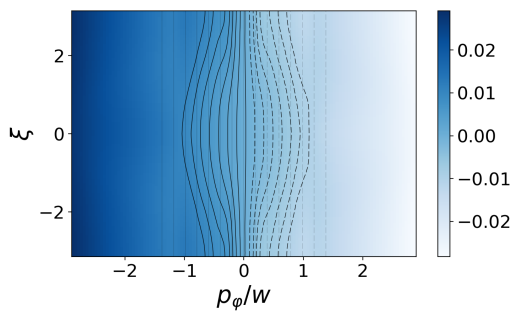


Figure 2.22: Same as Figs.2.14,2.15 except for $\lambda = 0.98$, $\sigma = \sigma_t$, $\rho_{\partial i} = 7.0 \cdot 10^{-3} r_s$.

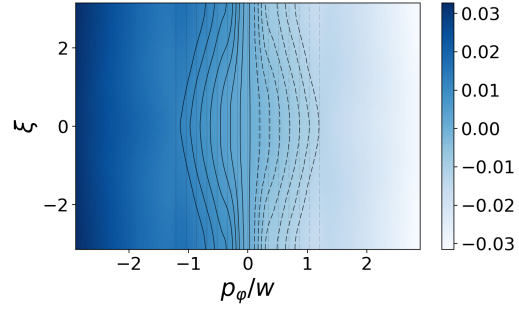


Figure 2.23: Same as Figs.2.14,2.15 except for $\lambda = 0.98$, $\sigma = \sigma_t$, $\rho_{\partial i} = 8.0 \cdot 10^{-3} r_s$.

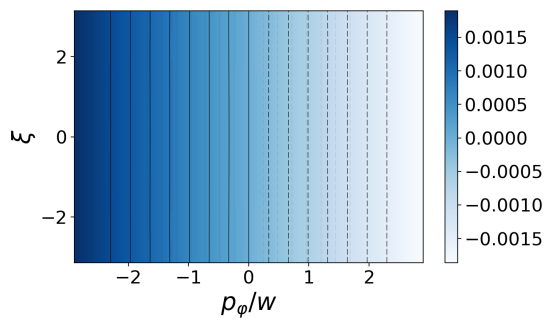


Figure 2.24: Same as Figs.2.14,2.15 except for $\lambda = \lambda_{fin}$, $\sigma = \sigma_t$, $\rho_{\partial i} = 1.0 \cdot 10^{-3} r_s$.

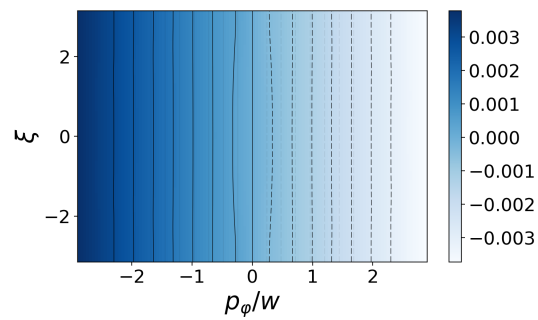


Figure 2.25: Same as Figs.2.14,2.15 except for $\lambda = \lambda_{fin}$, $\sigma = \sigma_t$, $\rho_{\partial i} = 2.0 \cdot 10^{-3} r_s$.

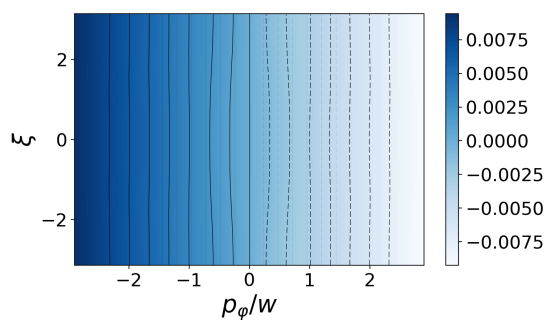


Figure 2.26: Same as Figs.2.14,2.15 except for $\lambda = \lambda_{fin}$, $\sigma = \sigma_t$, $\rho_{\partial i} = 5.0 \cdot 10^{-3} r_s$.

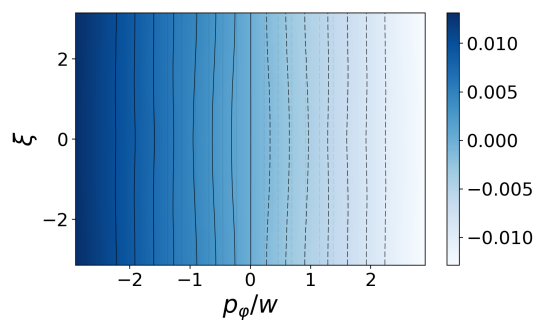


Figure 2.27: Same as Figs.2.14,2.15 except for $\lambda = \lambda_{fin}$, $\sigma = \sigma_t$, $\rho_{\partial i} = 7.0 \cdot 10^{-3} r_s$.

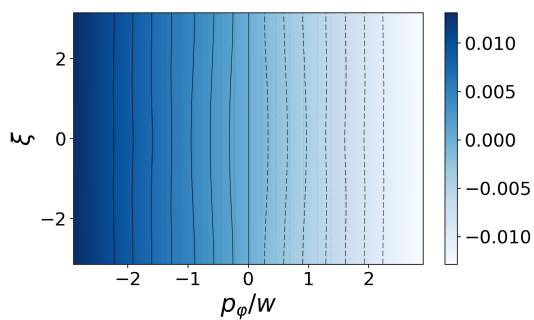


Figure 2.28: Same as Figs.2.14,2.15 except for $\lambda = \lambda_{fin}$, $\sigma = \sigma_t$, $\rho_{\partial i} = 8.0 \cdot 10^{-3} r_s$.

Chapter III

3 Boundary layer solution in the vicinity of the trapped-passing boundary

Earlier we have identified a narrow *dissipation* layer in pitch angle space around the trapped-passing boundary where collisional dissipation is no longer negligible and modifies the electron/ion distribution function (see Fig.2.8). This layer provides the dominant source of the collisional dissipation and hence is the only contribution to the island propagation frequency in this study. We have to stress here that the effects of error fields and plasma sheared flows are not considered. To calculate ω and the corresponding ω dependence of the polarisation contribution to the magnetic island time evolution, we have to address a system of Eqs.2.9-2.11. Projecting out the $\cos \xi$ and $\sin \xi$ components of J_{\parallel} in Ampère's law written along the field lines and providing the integration through the island, we obtain Eqs.2.9,2.10. Eq.2.10 is equivalent to the toroidal torque balance. This set of equations provides a system for the magnetic island threshold, w_c (Eq.2.9), ω (Eq.2.10) and Φ that has been determined from the plasma quasi-neutrality condition in the previous section³⁴.

The dominant contribution to the component of J_{\parallel} that is in phase with the magnetic perturbation, $\propto \cos \xi$, comes from external regions, i.e. outside the dissipative layer. The contribution to this from the dissipation layer is two orders less. In contrast, around 99.(9)%³⁵ of the out-of-phase current, $\propto \sin \xi$, comes from the layer around λ_c and hence determines ω . The electron layer width is a factor $\sim (\nu_{ei}/\nu_{ii})^{1/2}$ larger than the ion layer width. In a fully ionised plasma, $\nu_{ee} \sim \nu_{ei} = (4\sqrt{2\pi}/3)(n_e e^4 \ln \Lambda / m_e^{1/2} T_e^{3/2})$ and $\nu_{ii} = (4\sqrt{\pi}/3)(n_e e^4 \ln \Lambda / m_i^{1/2} T_i^{3/2})$ (from Braginskii's original derivations in cgs). Thus, the electron layer width dominates by a factor $(m_i/m_e)^{1/4}$ provided $T_e = T_i$.

In this thin boundary region collisions cannot be treated perturbatively and hence a full

³⁴The integral form of Eq.2.11, in principle, can be used to find the mode frequency if the potential is determined by a model. The latter will be applied to the secondary mode stability analysis in Chapter V.

³⁵The dissipative layer width is estimated through $\sqrt{\nu_{jj/ei}/\varepsilon\omega}$, and thus the corresponding layer contribution depends on the ratio, $\nu_{jj/ei}/\varepsilon\omega$. j labels the particle species, $j = e, i$.

solution of Eq.2.36 is required. Following [53], we impose the matching conditions

$$\begin{aligned}
\sum_{\sigma} \sigma g_j^{\sigma,p} &= 0, \\
\sum_{\sigma} g_j^{\sigma,p} &= 2g_j^{|\sigma|,t}, \\
\sum_{\sigma} \frac{\partial g_j^{\sigma,p}}{\partial \lambda} \Big|_{\psi} &= 2 \frac{\partial g_j^{|\sigma|,t}}{\partial \lambda} \Big|_{\psi}
\end{aligned} \tag{3.1}$$

at the trapped-passing boundary to provide continuity of the particle distribution function and its first λ derivative across the boundary. Here indices p and t denote the passing and trapped regions, respectively. These matching conditions can be treated as the particle conservation law as we cross the boundary. The first two conditions of Eq.3.1 are introduced to match g_j across λ_c keeping the trapped particle distribution function, $g_j^{|\sigma|,t}$, σ -independent. The third condition provides the same rate for passing/trapped particles scattered into trapped/passing orbits, respectively. We note that originally matching is imposed at fixed ψ . However, moving from ψ to S for the new radial coordinate and solving Eq.2.40 at the 0th iteration in Φ , we find $g_j^{(0,0)} = g_j^{(0,0)}(S, \lambda, V; \sigma) = g_j^{(0,0)}[S(p_{\varphi}, \xi, \lambda, V; \sigma), \lambda, V; \sigma]$ for the leading order passing and $g_j^{(0,0)} = g_j^{(0,0)}(S, \lambda, V; \sigma) = g_j^{(0,0)}[S(p_{\varphi}, \lambda, V; \sigma), \lambda, V; \sigma]$ for the leading order trapped particle distribution (here we have used the S definition for passing/trapped particles, Eq.2.37). The continuity of the particle distribution across the trapped-passing boundary at fixed p_{φ}/ψ simply cannot be provided without introducing the layer as the definition of S is different as $\lambda \rightarrow \lambda_c \pm 0$ (e.g. the trapped particle solution is ξ -independent at fixed p_{φ}/ψ in the absence of Φ , while the passing distribution function is a function of ξ). The introduction of this layer allows g_j to vary on S contours, and hence enables the matching conditions, Eq.3.1. This explains mathematically the necessity of the dissipation layer.

The calculation of the ion/electron distribution function in the layer is presented in the following section. Once a full solution of the ϑ -averaged drift kinetic equation to leading order in Δ (Eq.2.35 in the dissipative layer and Eq.2.40 outside the layer) with the electrostatic potential calculated self-consistently from plasma quasi-neutrality is found, we return to Eq.2.9,2.10 to determine w_c and ω_E , respectively. We note that J_{\parallel} is to be ϑ -averaged as integrands in Eq.2.9,2.10 have to be integrated over all spatial variables to provide w_c and ω_E .

3.1 Dissipative layer solution

We start with Eq.2.35, the ϑ -averaged drift kinetic equation for the leading order distribution function in Δ in $\{p_\varphi, \xi, \lambda, V; \sigma\}$ space and seek its general solution of the form:

$$g_j^{(0)} = G_j^{(0)} + \mathcal{C} \cdot \hat{p}_\varphi \quad (3.2)$$

with \mathcal{C} being the limit of the distribution function far from the island introduced in the previous chapter. The particle distribution is normalised to $n_0/(\pi^{3/2}V_{Tj}^3)$ as stated previously. $\partial G_j^{(0)}/\partial x|_{x \rightarrow \pm\infty} = 0$ and thus $\partial G_j^{(0)}/\partial S^p|_{S^p \rightarrow +\infty} = 0$ for passing and $\partial G_j^{(0)}/\partial S^t|_{S^t \rightarrow \pm\infty} = 0$ for trapped particles (here $S^{p/t}$ denotes S in the passing/trapped region, Eq.2.37). $\mathcal{C} \cdot \hat{p}_\varphi$ is the drive term that reads

$$\sigma_{p_\varphi} \sqrt{\frac{1}{2} \left(\frac{4\hat{L}_q}{\hat{w}} S^p + \cos \xi \right)} \cdot \mathcal{C} + \frac{\hat{\omega}_D \hat{\rho}_{\vartheta j} \hat{L}_q}{\hat{w}} \cdot \mathcal{C}$$

for passing and $-\mathcal{C} S^t / \hat{\omega}_D \hat{\rho}_{\vartheta j}$ for trapped particles in the absence of the electrostatic potential. At the end of each iteration in Φ , the transcendental equation $S^{p/t} = S^{p/t}(\hat{p}_\varphi, \xi, \lambda, \hat{V}; \sigma)$ is to be solved for $\hat{p}_\varphi = \hat{p}_\varphi(S^{p/t}, \xi, \lambda, \hat{V}; \sigma)$. Eq.2.35 for $G_j^{(0)}$ then reads

$$\begin{aligned} & \left[\frac{\hat{w}}{\hat{L}_q} \hat{p}_\varphi \cdot \Theta(\lambda_c - \lambda) - \hat{\rho}_{\vartheta j} \hat{\omega}_D |_{\lambda_{p/t}} - \frac{\partial}{\partial \hat{p}_\varphi} \Big|_{\xi, \vartheta} \frac{1}{2} \left\langle \frac{\hat{\rho}_{\vartheta j} \hat{\Phi}}{\hat{V}_\parallel} \right\rangle_{\vartheta} \Big|_{\lambda_{p/t}}^{p_\varphi} \right] \frac{\partial G_j^{(0)}}{\partial \xi} \Big|_{p_\varphi, \vartheta, \lambda, V; \sigma} + \\ & + \left[\frac{\partial}{\partial \xi} \Big|_{p_\varphi, \vartheta} \frac{1}{2} \left\langle \frac{\hat{\rho}_{\vartheta j} \hat{\Phi}}{\hat{V}_\parallel} \right\rangle_{\vartheta} \Big|_{\lambda_{p/t}}^{p_\varphi} - \frac{1}{4} \frac{\hat{w}}{\hat{L}_q} \sin \xi \cdot \Theta(\lambda_c - \lambda) \right] \frac{\partial G_j^{(0)}}{\partial \hat{p}_\varphi} \Big|_{\vartheta, \xi, \lambda, V; \sigma} + \\ & + \frac{\partial}{\partial \xi} \Big|_{p_\varphi, \vartheta} \frac{\mathcal{C}}{2} \left\langle \frac{\hat{\rho}_{\vartheta j} \hat{\Phi}}{\hat{V}_\parallel} \right\rangle_{\vartheta} \Big|_{\lambda_{p/t}}^{p_\varphi} - \frac{\mathcal{C}}{4} \frac{\hat{w}}{\hat{L}_q} \sin \xi \cdot \Theta(\lambda_c - \lambda) = \tilde{\mathcal{C}}_j \Big|_{\lambda_{p/t}}, \end{aligned} \quad (3.3)$$

where taking into account the narrowness of the dissipation layer, we have fixed all the coefficients in Eq.2.35 at $\lambda_{p/t} \equiv \lambda_c \mp \epsilon$. ϵ is the width of the layer and is to be introduced

later in this section³⁶. Eq.3.3 is equivalent to

$$\begin{aligned} & \left[\frac{\hat{w}}{\hat{L}_q} \hat{p}_\varphi \cdot \Theta(\lambda_c - \lambda) - \hat{\rho}_{\vartheta j} \hat{\omega}_D \Big|_{\lambda_{p/t}} - \frac{\partial}{\partial \hat{p}_\varphi} \Big|_{\xi, \vartheta} \frac{1}{2} \left\langle \frac{\hat{\rho}_{\vartheta j} \hat{\Phi}}{\hat{V}_\parallel} \right\rangle_{\vartheta}^{p_\varphi} \Big|_{\lambda_{p/t}} \right] \frac{\partial G_j^{(0)}}{\partial \xi} \Big|_{\hat{S}, \vartheta, \lambda, V; \sigma} = \\ & = \tilde{C}_j \Big|_{\lambda_{p/t}} - \frac{\partial}{\partial \xi} \Big|_{p_\varphi, \vartheta} \frac{\mathcal{C}}{2} \left\langle \frac{\hat{\rho}_{\vartheta j} \hat{\Phi}}{\hat{V}_\parallel} \right\rangle_{\vartheta}^{p_\varphi} \Big|_{\lambda_{p/t}} + \frac{\mathcal{C}}{4} \frac{\hat{w}}{\hat{L}_q} \sin \xi \cdot \Theta(\lambda_c - \lambda) \end{aligned} \quad (3.4)$$

with

$$\begin{aligned} \hat{S} = & \frac{\hat{w}}{4\hat{L}_q} \left[2 \left(\hat{p}_\varphi - \frac{\hat{\omega}_D \hat{\rho}_{\vartheta j} \hat{L}_q}{\hat{w}} \Big|_{\lambda_p} \right)^2 - \cos \xi \right] \Theta(\lambda_c - \lambda) - \hat{\omega}_D \hat{\rho}_{\vartheta j} \Big|_{\lambda_t} \hat{p}_\varphi \Theta(\lambda - \lambda_c) - \\ & - \frac{1}{2} \left\langle \frac{\hat{\rho}_{\vartheta j} \hat{\Phi}}{\hat{V}_\parallel} \right\rangle_{\vartheta}^{p_\varphi} \Big|_{\lambda_{p/t}}. \end{aligned} \quad (3.5)$$

\hat{S} is λ -independent, i.e. $\hat{S} = \hat{S}(\hat{p}_\varphi, \xi, V; \sigma)$ (note: Eq.2.36 reduces to Eq.3.4 with S being Taylor expanded around $\lambda_{p/t}$, $S = \hat{S} + \partial_\lambda S_{\lambda_{p/t}} (\lambda - \lambda_{p/t})$). Employing the thinness of the layer again, we write

$$\frac{\partial}{\partial \lambda} \Big|_{\psi} \simeq \frac{\partial}{\partial \lambda} \Big|_{p_\varphi} = \frac{\partial}{\partial \lambda} \Big|_{\hat{S}}$$

and thus

$$\begin{aligned} \mathcal{A} \left(\hat{S}, \xi, \lambda_{p/t}, V; \sigma \right) \frac{\partial G_j^{(0)}}{\partial \xi} \Big|_{\hat{S}, \vartheta, \lambda, V; \sigma} = & \hat{\nu}_j \frac{2}{\hat{V}} a(\lambda_{p/t}) \frac{\partial^2 G_j^{(0)}}{\partial \lambda^2} \Big|_{\hat{S}} - \\ & - \frac{\partial}{\partial \xi} \Big|_{p_\varphi, \vartheta} \frac{\mathcal{C}}{2} \left\langle \frac{\hat{\rho}_{\vartheta j} \hat{\Phi}}{\hat{V}_\parallel} \right\rangle_{\vartheta}^{p_\varphi} \Big|_{\lambda_{p/t}} + \frac{\mathcal{C}}{4} \frac{\hat{w}}{\hat{L}_q} \sin \xi \cdot \Theta(\lambda_c - \lambda) \end{aligned} \quad (3.6)$$

for the final equation to be solved in the layer. a is defined as $\left\langle \sigma \lambda (1 - \lambda B)^{1/2} R / B_\varphi \right\rangle_{\vartheta}^{p_\varphi}$. $\hat{\nu}_j$ is to be understood as $\hat{\nu}_{ii}$ for ions and $\hat{\nu}_{ee} + \hat{\nu}_{ei}$ for electrons. As $\epsilon \ll 1$, the collision operator is dominated by $\partial^2 / \partial \lambda^2 \Big|_{\psi}$ and the momentum-conservation term, $\propto \bar{u}_{\parallel j} / u_{\parallel j}$, can be dropped. Imposing

$$G_j^{(0)} = -\sqrt{S_c} \int^{\hat{S}} \frac{\mathcal{C}}{\mathcal{A}(\hat{S}', \xi, \lambda_{p/t}, V; \sigma)} d\hat{S}' + G_j^{(0),l}, \quad (3.7)$$

³⁶Earlier, ν^* has been introduced just to provide an estimation of its width.

we come to

$$\mathcal{A}\left(\hat{S}, \xi, \lambda_{p/t}, V; \sigma\right) \frac{\partial G_j^{(0),l}}{\partial \xi} \Big|_{\hat{S}, \vartheta, \lambda, V; \sigma} = \hat{v}_j \frac{2}{\hat{V}} a(\lambda_{p/t}) \frac{\partial^2 G_j^{(0),l}}{\partial \lambda^2} \Big|_{\hat{S}} \quad (3.8)$$

for $G_j^{(0),l}$. The first term on the right hand side of Eq.3.7 provides the drive in Eq.3.6. In the absence of the electrostatic potential, it equals $-\sigma_{p\varphi} \sqrt{\frac{1}{2} \left(\frac{4\hat{L}_q}{\hat{w}} S^p + \cos \xi \right)} \cdot \mathcal{C}$ for passing particles and is independent of ξ and equals $\mathcal{C} S^t / \hat{\omega}_D \hat{\rho}_{\vartheta j}$ in the trapped branch (note: $S_c = 1$ in the absence of the separatrix). Eq.3.8 can be reduced to a simple diffusion equation

$$\frac{\partial G_j^{(0),l}}{\partial x^{\pm/t}} \Big|_{\hat{S}} = D^{\pm/t} \frac{\partial^2 G_j^{(0),l}}{\partial \lambda^2} \Big|_{\hat{S}}, \quad (3.9)$$

where $D^{\pm/t} = \hat{v}_j \frac{2}{\hat{V}} a(\lambda_{p/t})$ for passing, $\sigma = \pm 1$, and trapped branches. To simplify the calculations below, we have introduced a new variable, $x^{\pm/t}$, instead of ξ :

$$x^{out(\pm)/t} = \frac{\sigma_{p\varphi}}{\int_{-\pi}^{\pi} \frac{d\xi}{2\pi|\mathcal{A}|}} \int_0^{\xi} \frac{d\xi'}{\mathcal{A}(\hat{S}, \xi', V; \sigma)} \quad (3.10)$$

for trapped particles and for passing particles outside the \hat{S} island. For passing particles inside the \hat{S} island,

$$x^{in(\pm)} = \frac{1}{\int_{-\xi_b}^{\xi_b} \frac{d\xi}{\pi|\mathcal{A}|}} \int_0^{\xi} \frac{d\xi'}{\mathcal{A}(\hat{S}, \xi', V; \sigma)}, \quad \sigma_{p\varphi} > 0 \quad (3.11)$$

and

$$x^{in(\pm)} = \pi - \frac{1}{\int_{-\xi_b}^{\xi_b} \frac{d\xi}{\pi|\mathcal{A}|}} \int_0^{\xi} \frac{d\xi'}{\mathcal{A}(\hat{S}, \xi', V; \sigma)}, \quad \sigma_{p\varphi} < 0. \quad (3.12)$$

Here we note

- $x^{\pm/t}$ increases monotonically with ξ along the passing/trapped trajectory at given \hat{S} . It varies from $-\pi/2$ to $\pi/2$ for $\xi \in [-\xi_b; \xi_b]$, and from $\pi/2$ to $3\pi/2$ on the way back, i.e. $\xi \in [\xi_b; -\xi_b]$ (ξ_b reduces to π outside the \hat{S} island as well as in the trapped branch).
- $x^{\pm/t}$ is an angle variable since it spans $[-\pi/2; 3\pi/2]$ along the closed passing trajectory.

- the choice grants that $\xi = \xi(\hat{S}, x^{\pm/t})$ is an odd function of $x^{\pm/t}$. It also satisfies $\xi(\hat{S}, x^{\pm/t}; \sigma_{p\varphi} = +1) = \xi(\hat{S}, \pi - x^{\pm/t}; \sigma_{p\varphi} = -1)$. Hence, the relation between $x^{\pm/t}$ and ξ , given above, can be inverted. Therefore, we find it convenient to express $G_j^{(0),l}$ as a function of \hat{S} and $x^{\pm/t}$ only; $x^{\pm/t}$ also contains the information on $\sigma_{p\varphi}$. According to Barrow's theorem, we have $\langle \mathcal{A}^{-1} \rangle_{\xi}^{\hat{S}} dx^{\pm/t} = d\xi / \mathcal{A}$ for both passing and trapped branches. $\langle \mathcal{A}^{-1} \rangle_{\xi}^{\hat{S}} = \sigma_{p\varphi} \int_{-\xi_b}^{\xi_b} \frac{d\xi}{\pi|\mathcal{A}|}$ inside and $\langle \mathcal{A}^{-1} \rangle_{\xi}^{\hat{S}} = \sigma_{p\varphi} \int_{-\pi}^{\pi} \frac{d\xi}{2\pi|\mathcal{A}|}$ outside the \hat{S} island.
- This procedure guarantees that if $G_j^{(0),l}$ is treated as a function of $x^{\pm/t}$ instead of ξ , it is continuous at $\xi = \xi_b$, i.e. $x^{\pm/t} = \pi/2$.

$\bar{\lambda} = \left[\langle \mathcal{A}^{-1} \rangle_{\xi}^{\hat{S}} \right]^{-1/2} (\lambda - \lambda_c)$ is a new pitch angle variable. $\bar{\lambda} = 0$ defines the trapped/passing boundary; $\bar{\lambda} \leq 0$ corresponds to the passing/trapped region, respectively. In contrast to [53], our layer solution includes both regions inside and outside the magnetic island. Eq.3.9 allows the analytic solution of the following form: $G_j^{(0),l} = \sum_{n \geq 0} C_n^{\pm/t} e^{\frac{i+1}{\sqrt{2}} \sqrt{\frac{n}{D^{\pm/t}} \bar{\lambda}}} e^{inx^{\pm/t}}$ and thus

$$G_j^{(0),\pm} = \sum_{n > 0} \left\{ a_n^{\pm} e^{\sqrt{\frac{n}{2D^{\pm}} \bar{\lambda}}} \cos \left[nx^{\pm} \pm \sqrt{\frac{n}{2D^{\pm}} \bar{\lambda}} \right] - b_n^{\pm} e^{\sqrt{\frac{n}{2D^{\pm}} \bar{\lambda}}} \sin \left[nx^{\pm} \pm \sqrt{\frac{n}{2D^{\pm}} \bar{\lambda}} \right] \right\} + H^{\pm}, \quad (3.13)$$

and

$$G_j^{(0),t} = \sum_{n > 0} \left\{ a_n^t e^{-\sqrt{\frac{n}{2D^t} \bar{\lambda}}} \cos \left[nx^t - \sqrt{\frac{n}{2D^t} \bar{\lambda}} \right] - b_n^t e^{-\sqrt{\frac{n}{2D^t} \bar{\lambda}}} \sin \left[nx^t - \sqrt{\frac{n}{2D^t} \bar{\lambda}} \right] \right\} + H^t. \quad (3.14)$$

Here $H^{\pm/t}$ represents a sum of the drive term/contribution from outside the layer (first term of Eq.3.7) and the 0th harmonic, $a_0^{\pm/t}$. The width of the dissipation layer, ϵ , is estimated as $\epsilon \sim \sqrt{D^{\pm/t}} \approx \sqrt{\hat{\nu}_j 2a(\lambda_c) / \hat{V}}$ ³⁷. Provided $\nu_{ei} \sim \nu_{ee} \approx \frac{4\sqrt{2\pi}}{3} \frac{n_e \epsilon^4 \ln \Lambda}{\sqrt{m_e T_e^{3/2}}}$, $\nu_{ii} \approx \frac{4\sqrt{\pi}}{3} \frac{n_e \epsilon^4 \ln \Lambda}{\sqrt{m_i T_i^{3/2}}}$ and $T_e \sim T_i$, $\hat{\nu}_{ii} \sim \hat{\nu}_{ee} \sim \hat{\nu}_{ei}$. However, as $\hat{V} = V/V_{Tj}$, the electron dissipation layer width dominates by a factor $\sim (m_i/m_e)^{1/4}$. In Eqs.3.13,3.14, the increasing branch of the solution has been dropped as we require $\partial_{\bar{\lambda}} G_j^{(0),l} \Big|_{\bar{\lambda} \rightarrow \pm\infty} = 0$. This implies the boundary conditions that $g_j^{(0)}$ has to match the external solutions outside the dissipation layer, i.e.

³⁷In the layer all the coefficients are considered to be localised in the vicinity of the trapped-passing boundary due to its thinness associated with the assumption of the low collisionality plasma. Thus, ω_D is to be evaluated at $\lambda_{p/t}$ in the layer for passing/trapped particles. In the layer, the radial shift of the drift \hat{S} islands being proportional to ω_D is then found to be a function of the ion/electron collision frequency through $\lambda_{p/t}$.

$\lambda \in [0, \lambda_p] \cup [\lambda_t, \lambda_{fin}]$. The Fourier coefficients, $a_n^{\pm/t}$, $b_n^{\pm/t}$ ($n \geq 0$), are unknown and to be found from matching at $\bar{\lambda} = 0$, Eq.3.1:

$$\begin{aligned}
H^+ + \sum_{n>0} \{a_n^+ \cos nx^+ - b_n^+ \sin nx^+\} &= H^- + \sum_{n>0} \{a_n^- \cos nx^- - b_n^- \sin nx^-\} = \\
&= H^t + \sum_{n>0} \{a_n^t \cos nx^t - b_n^t \sin nx^t\}, \\
\sum_{n>0} \cos nx^+ \sqrt{\frac{n}{2D^+}} [a_n^+ - b_n^+] - \sin nx^+ \sqrt{\frac{n}{2D^+}} [a_n^+ + b_n^+] &+ \\
+ \sum_{n>0} \cos nx^- \sqrt{\frac{n}{2D^+}} [a_n^- + b_n^-] + \sin nx^- \sqrt{\frac{n}{2D^+}} [a_n^- - b_n^-] &= \\
= 2 \sum_{n>0} \cos nx^t \sqrt{\frac{n}{2D^t}} [b_n^t - a_n^t] + \sin nx^t \sqrt{\frac{n}{2D^t}} [a_n^t + b_n^t]. &
\end{aligned} \tag{3.15}$$

Eq.3.15 is a set of three equations for $6N + 3$ unknowns, $n \in [0, N]$. Due to a difference in $x^{\pm/t}$, matching at fixed ψ/p_φ cannot be provided in n space in the presence of Φ . However, $x^{\pm/t}$ and n are conjugated variables, and $x^{\pm/t}$ is connected with ξ via Eqs.3.10-3.12. Thus, taking a number of points in ξ space $N_\xi = 2N + 1$ and treating $x^{\pm/t} = x^{\pm/t}(\hat{S}, \xi, V) = x^{\pm/t}[\hat{S}(\hat{p}_\varphi, \xi, V), \xi, V]$, we can solve Eq.3.15 numerically for $a_n^{\pm/t}$, $b_n^{\pm/t}$, providing matching at fixed p_φ and ξ . Here we have to stress the importance of including drive in Eq.3.15 to avoid trivial solutions for the Fourier coefficients. Substituting the obtained Fourier coefficients into Eqs.3.13,3.14 and taking into account Eq.3.2 provides the layer electron/ion distribution function, which is then to be used to calculate the external solution, $g_j^{(0,0)}$, (see Chapter IV for more detail). The distribution function in the layer, $g_j^{(0)}$ is calculated as a function of \hat{p}_φ , ξ and λ for each σ (here \hat{V} is considered as a parameter) and is then to be rewritten as a function of S , ξ and λ , i.e. $g_j^{(0)} = g_j^{(0)}(\hat{p}_\varphi, \xi, \lambda, \hat{V}; \sigma) = g_j^{(0)}[S, \xi, \lambda_{p/t}, \hat{V}; \sigma], \xi, \lambda, \hat{V}; \sigma]$, to solve Eq.2.40 for $g_j^{(0,0)}$ in the regions outside the layer. To illustrate the above solution, in Figs.3.1-3.20 we plot $g_j^{(0)}$ against λ for small and large $\rho_{\vartheta i}$ inside and outside the magnetic island separatrix.

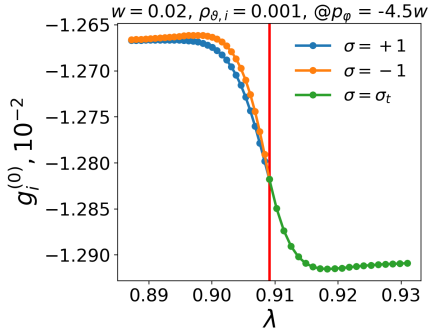


Figure 3.1: $g_j^{(0)}$ vs. λ at $\hat{p}_\varphi = -4.5$, $\xi = 0$, $V = V_{Ti}$. $w = 0.02r_s$, $\rho_{\vartheta i} = 1.0 \cdot 10^{-3}r_s$, ion collisionality $\hat{\nu}_i = 10^{-4}$, $\varepsilon = 0.1$, $\hat{L}_q = 1$. $g_i^{(0)}$ is normalised to $n_0/(\pi^{3/2}V_{Ti}^3)$. Red line indicates the trapped-passing boundary.

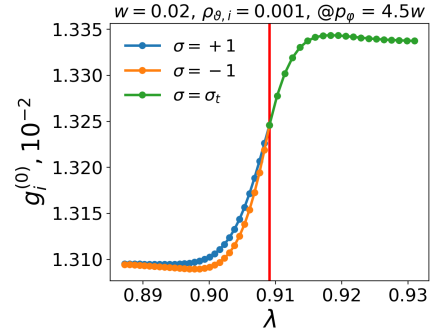


Figure 3.2: $g_j^{(0)}$ vs. λ at $\hat{p}_\varphi = 4.5$, $\xi = 0$, $V = V_{Ti}$. $w = 0.02r_s$, $\rho_{\vartheta i} = 1.0 \cdot 10^{-3}r_s$, ion collisionality $\hat{\nu}_i = 10^{-4}$, $\varepsilon = 0.1$, $\hat{L}_q = 1$. $g_i^{(0)}$ is normalised to $n_0/(\pi^{3/2}V_{Ti}^3)$. Red line indicates the trapped-passing boundary.

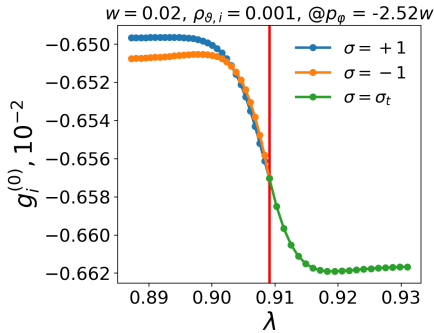


Figure 3.3: Same as Figs.3.1,3.2 except for $\hat{p}_\varphi = -2.52$.

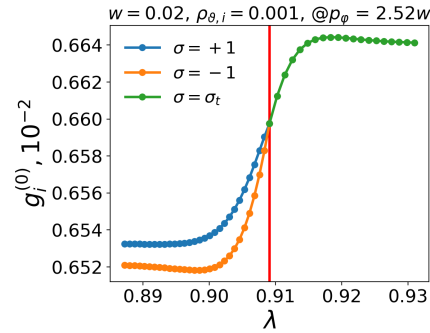


Figure 3.4: Same as Figs.3.1,3.2 except for $\hat{p}_\varphi = 2.52$.

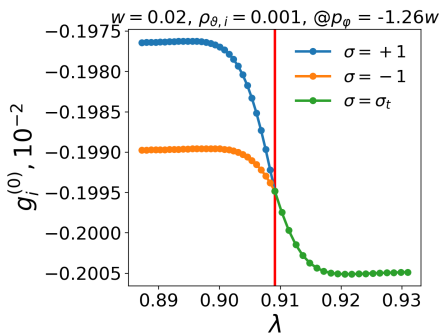


Figure 3.5: Same as Figs.3.1,3.2 except for $\hat{p}_\varphi = -1.26$.

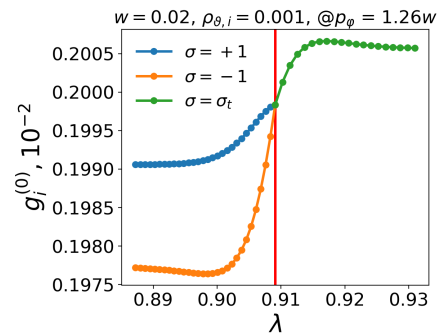


Figure 3.6: Same as Figs.3.1,3.2 except for $\hat{p}_\varphi = 1.26$.

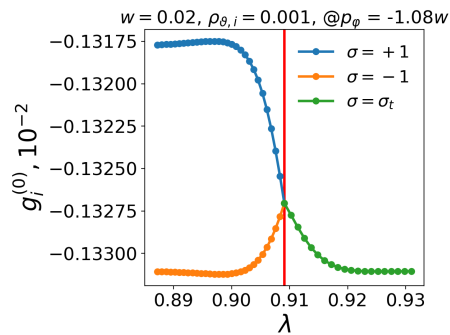


Figure 3.7: Same as Figs.3.1,3.2 except for $\hat{p}_\varphi = -1.08$.

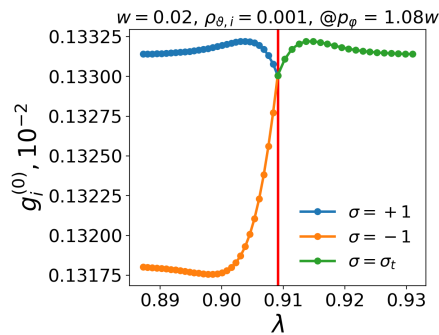


Figure 3.8: Same as Figs.3.1,3.2 except for $\hat{p}_\varphi = 1.08$.

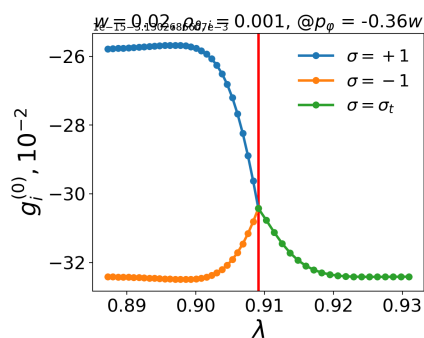


Figure 3.9: Same as Figs.3.1,3.2 except for $\hat{p}_\varphi = -0.36$.

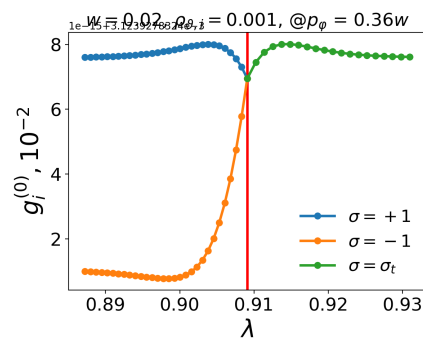


Figure 3.10: Same as Figs.3.1,3.2 except for $\hat{p}_\varphi = 0.36$.

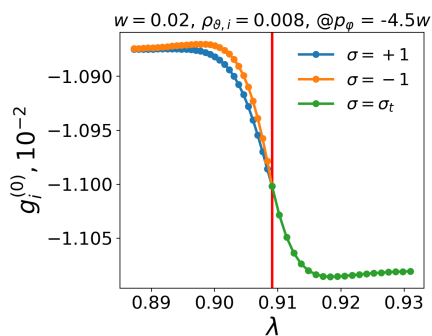


Figure 3.11: Same as Figs.3.1,3.2 except for $\rho_{\vartheta i} = 8.0 \cdot 10^{-3} r_s$.

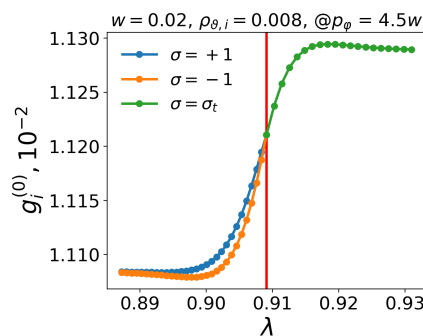


Figure 3.12: Same as Figs.3.1,3.2 except for $\rho_{\vartheta i} = 8.0 \cdot 10^{-3} r_s$.

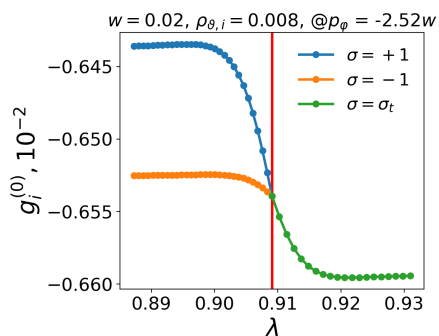


Figure 3.13: Same as Figs.3.1,3.2 except for $\hat{p}_\varphi = -2.52$, $\rho_{\vartheta i} = 8.0 \cdot 10^{-3} r_s$.

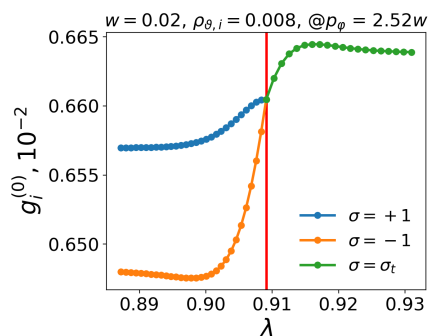


Figure 3.14: Same as Figs.3.1,3.2 except for $\hat{p}_\varphi = 2.52$, $\rho_{\vartheta i} = 8.0 \cdot 10^{-3} r_s$.

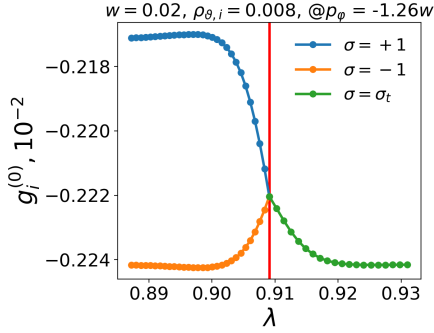


Figure 3.15: Same as Figs.3.1,3.2 except for $\hat{p}_\varphi = -1.26$, $\rho_{\vartheta i} = 8.0 \cdot 10^{-3} r_s$.

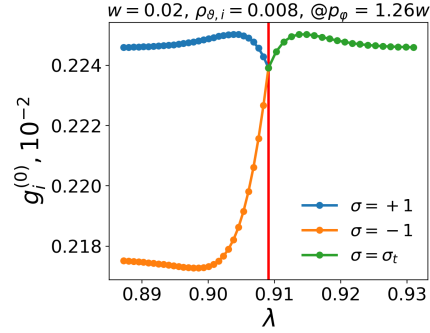


Figure 3.16: Same as Figs.3.1,3.2 except for $\hat{p}_\varphi = 1.26$, $\rho_{\vartheta i} = 8.0 \cdot 10^{-3} r_s$.

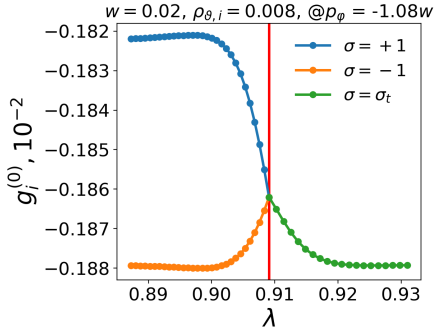


Figure 3.17: Same as Figs.3.1,3.2 except for $\hat{p}_\varphi = -1.08$, $\rho_{\vartheta i} = 8.0 \cdot 10^{-3} r_s$.

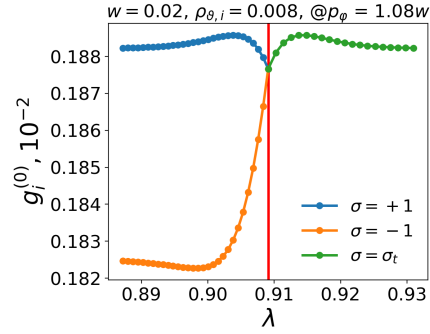


Figure 3.18: Same as Figs.3.1,3.2 except for $\hat{p}_\varphi = 1.08$, $\rho_{\vartheta i} = 8.0 \cdot 10^{-3} r_s$.

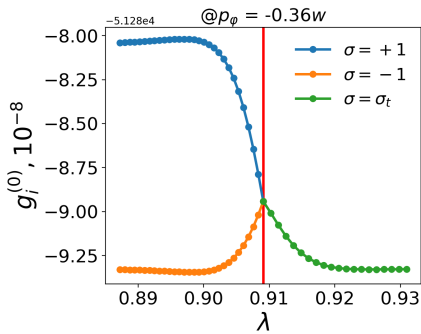


Figure 3.19: Same as Figs.3.1,3.2 except for $\hat{p}_\varphi = -0.36$, $\rho_{\vartheta i} = 8.0 \cdot 10^{-3} r_s$.

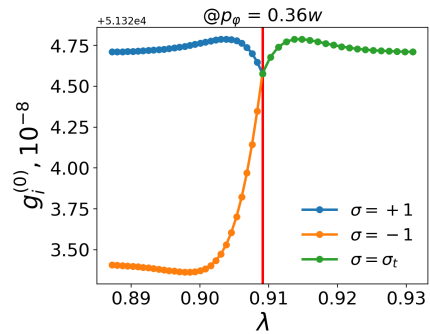


Figure 3.20: Same as Figs.3.1,3.2 except for $\hat{p}_\varphi = 0.36$, $\rho_{\vartheta i} = 8.0 \cdot 10^{-3} r_s$.

3.2 Summary

In this chapter we have determined the particle distribution function in a boundary layer in the vicinity of the trapped-passing boundary, λ_c , required to match external passing, $\lambda \leq \lambda_p$, and trapped, $\lambda \geq \lambda_t$, solutions across λ_c . Now we return to external regions where collisions can be treated perturbatively and solve Eq.2.40 for $g_j^{(0,0)}$. The solution technique is described in Chapter IV.

Chapter IV

4 Solution technique and the RDK-NTM results

The numerical solution technique for the orbit averaged drift kinetic equation, Eq.2.35 in the dissipation layer, i.e. $\lambda \in [\lambda_p, \lambda_c] \cup (\lambda_c, \lambda_t]$, and Eq.2.40 in external regions outside the layer, i.e. $\lambda \in [0, \lambda_p] \cup [\lambda_t, \lambda_{fin}]$, with matching conditions at the trapped/passing boundary, $\lambda = \lambda_c$, given by Eq.3.1, is presented in this chapter. In previous sections we have identified a narrow collisional boundary layer in pitch angle around the trapped-passing boundary of width $\propto \sqrt{\hat{\nu}_j/\hat{V}}$. In this region, collisions cannot be treated perturbatively and S no longer describes the streamlines. In Chapter III we have provided the solution to the 2D boundary layer problem, $\{x^{\pm/t}, \lambda\}$ inside and outside the drift S island, employing the momentum-conserving collision operator (its pitch angle scattering contribution dominates due to the layer thinness), allowing us to rigorously connect the trapped ($\lambda > \lambda_t$) and passing ($\lambda < \lambda_p$) regions. The layer solution, $g_j^{(0)}$ is then used as a starting point to construct the external solution, $g_j^{(0,0)}$, outside the layer. The rest of the chapter focuses on the obtained results.

4.1 Numerical algorithm

Eq.2.40 is a 3D integro-differential equation in $\{S^{\pm/t}, \lambda, \hat{V}; \sigma\}$ space. \hat{V} appears as a parameter at the 0th iteration in the momentum conservation term, $\propto \bar{u}_{\parallel j}$, in the collisional operator. $\bar{u}_{\parallel j}$ is evaluated at fixed $\hat{\psi}$, and the corresponding \hat{V} dependence appears through the S function, Eq.2.37. Writing the left hand side of Eq.2.40 explicitly, we derive the collisional constraint in S space given by Eq.D.60 for the ion and Eq.D.61 for the electron plasma component³⁸. To provide the Maxwellian behaviour far from the magnetic island, we require $\partial \hat{f}_j / \partial x \Big|_{x \rightarrow \pm\infty} = \hat{w} \left[L_n^{-1} + \left(\hat{V}^2 - 3/2 \right) L_{Tj}^{-1} \right] e^{-\hat{V}^2}$, where $\hat{f}_j = f_j \pi^{3/2} V_{Tj}^3 / n_0$. To set the Neumann boundary in the passing and trapped regions,

³⁸A detailed step by step derivation is presented in Appendix D

it is convenient to introduce an extra variable, $y^{\pm/t}$, such that $y^{\pm} = \sqrt{S^{\pm} - S_{\min}^{\pm}}$ in the passing and $y^t = S^t$ in the trapped branch³⁹. In the absence of the perturbed electrostatic potential, this translates into

$$\left. \frac{\partial \hat{f}_j}{\partial y^{\pm}} \right|_{y^{\pm} \rightarrow +\infty} = \sigma_{p\varphi} \hat{w} \left[L_n^{-1} + \left(\hat{V}^2 - \frac{3}{2} \right) L_{Tj}^{-1} \right] e^{-\hat{V}^2} \sqrt{\frac{2\hat{L}_q}{\hat{w}}} \quad (4.1)$$

for $\lambda \leq \lambda_p$ and

$$\left. \frac{\partial \hat{f}_j}{\partial y^t} \right|_{y^t \rightarrow \pm\infty} = - \frac{\hat{w}}{\hat{\omega}_D \hat{\rho}_{\vartheta j} + \frac{\hat{\rho}_{\vartheta j}}{2} \left\langle \frac{1}{\hat{V}_{\parallel}} \right\rangle_{\vartheta}^{p\varphi} L_{n0}^{-1} \hat{w} \hat{\omega}_E} \left[L_n^{-1} + \left(\hat{V}^2 - \frac{3}{2} \right) L_{Tj}^{-1} \right] e^{-\hat{V}^2} \quad (4.2)$$

for $\lambda \geq \lambda_t$, and is to be updated at each iteration in Φ , provided the inverse function, $y^{\pm/t} = y^{\pm/t}(\hat{p}_\varphi)$, exists for each ξ , λ , \hat{V} and σ . The bottom boundary condition in the passing branch in y space is

$$\left. \frac{\partial \hat{f}_j}{\partial y^{\pm}} \right|_{y^{\pm}=0} = 0 \quad (4.3)$$

due to the flattening requirement inside the S island. Due to Eq.2.15, both \hat{f}_j and $g_j^{(0,0)} \pi^{3/2} V_{Tj}^3 / n_0$ satisfy Eqs.4.1-4.3 (L_n is to be replaced by L_{n0} in the condition for $g^{(0,0)}$). In λ space we require the distribution function and its first derivative to be finite at $\lambda = 0$ and $\lambda = \lambda_{fin}$, where λ_{fin} is given by $1/B_0(1 - \varepsilon)$ in accordance with Sec.2.2. As the coefficient of the term in $\partial^2/\partial\lambda^2$ vanishes at $\lambda = 0$ and $\lambda = \lambda_{fin}$, we impose Eq.D.60/Eq.D.61 evaluated at $\lambda = 0$, i.e.

$$\begin{aligned} & \left\langle \sigma \frac{R}{B_\varphi} \right\rangle_{\vartheta}^{p\varphi} \left\langle \frac{1}{\mathcal{A}} \right\rangle_{\xi}^S \left. \frac{\partial g_j^{(0,0)}}{\partial \lambda} \right|_{\lambda=0} + \\ & + \left[\left\langle \sigma \frac{R}{B_\varphi} \right\rangle_{\vartheta}^{p\varphi} \left\langle \frac{1}{\mathcal{A}} \frac{\partial S}{\partial \lambda} \right|_{p\varphi, \xi} \right]_{\xi}^S + \left\langle \frac{\hat{\rho}_{\vartheta i}}{2} \hat{V} R \right\rangle_{\vartheta}^{\hat{p}\varphi} \left\langle \frac{1}{\mathcal{A}} \frac{\partial S}{\partial p_\varphi} \right\rangle_{\xi}^S \left. \frac{\partial g_j^{(0,0)}}{\partial S} \right|_{\lambda=0} \\ & + U(g_j^{(0,0)}) = 0, \end{aligned} \quad (4.4)$$

for the boundary condition at the deeply passing end and similarly Eq.D.60/Eq.D.61 evaluated at $\lambda = \lambda_{fin}$ for the boundary condition at the deeply trapped end. Here U

³⁹A different definition of $y^{\pm/t}$ is justified as both passing and trapped external regions, i.e. $\lambda \in [0, \lambda_p] \cup [\lambda_t, \lambda_{fin}]$, are not connected directly but via a dissipative layer where the perturbative approach becomes invalid.

represents the momentum conservation term. To solve Eq.D.60/Eq.D.61, we apply a shooting method⁴⁰ in λ direction, reducing Eq.D.60/Eq.D.61 to a matrix equation at each λ grid point. Applying the finite difference scheme in λ space (central difference to the equation and forward/backward difference at the edges of λ space), we obtain the following matrix equation:

$$\mathbf{P}_j^{\sigma,p/t} \mathbf{g}_{j+1}^{\sigma,p/t} + \mathbf{Q}_j^{\sigma,p/t} \mathbf{g}_j^{\sigma,p/t} + \mathbf{R}_j^{\sigma,p/t} \mathbf{g}_{j-1}^{\sigma,p/t} + \mathbf{A}_j^{\sigma,p/t} = 0 \quad (4.5)$$

for the vector solution, $\mathbf{g}_j^{\sigma,p/t}$, we seek at each λ grid point, j . $\sigma = \pm 1$ for the passing and $\sigma = |\sigma|$ for the trapped branches. $\mathbf{P}_j^{\sigma,p/t}$, $\mathbf{Q}_j^{\sigma,p/t}$ and $\mathbf{R}_j^{\sigma,p/t}$ are square tri-diagonal matrices of size $N_y \times N_y$, and $\mathbf{A}_j^{\sigma,p/t}$ is the right hand side vector; both, $\mathbf{g}_j^{\sigma,p/t}$ and $\mathbf{A}_j^{\sigma,p/t}$,

are of length N_y (N_y is a total number of points in y direction, i.e. inside and outside the S island/in the trapped region; note: the number of points can be different in $y^{\pm/t}$ direction as the \pm/t branches become independent once the layer solution is found).

The left boundary in its general form in λ space (i.e. for deeply passing particles at $j = 0$) reads

$$\hat{\mathbf{P}}_0^{\sigma,p} \mathbf{g}_0^{\sigma,p} + \hat{\mathbf{Q}}_0^{\sigma,p} \mathbf{g}_1^{\sigma,p} + \hat{\mathbf{R}}_0^{\sigma,p} \mathbf{g}_2^{\sigma,p} + \hat{\mathbf{A}}_0^{\sigma,p} = 0. \quad (4.6)$$

To set the $j = 0$ th element, we assume a linear relation between $\mathbf{g}_j^{\sigma,p}$ at j th and $(j + 1)$ th grid points, and hence we write

$$\mathbf{g}_j^{\sigma,p} = \boldsymbol{\alpha}_j^{\sigma,p} \mathbf{g}_{j+1}^{\sigma,p} + \boldsymbol{\beta}_j^{\sigma,p} \quad (4.7)$$

from the side of passing particles. Here $\boldsymbol{\alpha}_j^{\sigma,p}$ is the square matrix of $N_y \times N_y$ and $\boldsymbol{\beta}_j^{\sigma,p}$ is a vector of length N_y . Combining Eqs.4.5,4.7, we obtain the following recurrence relation:

$$\begin{aligned} \boldsymbol{\alpha}_j^{\sigma,p} &= -[\mathbf{Q}_j^{\sigma,p} + \mathbf{R}_j^{\sigma,p} \boldsymbol{\alpha}_{j-1}^{\sigma,p}]^{-1} \mathbf{P}_j^{\sigma,p}, \\ \boldsymbol{\beta}_j^{\sigma,p} &= -[\mathbf{Q}_j^{\sigma,p} + \mathbf{R}_j^{\sigma,p} \boldsymbol{\alpha}_{j-1}^{\sigma,p}]^{-1} [\mathbf{R}_j^{\sigma,p} \boldsymbol{\beta}_{j-1}^{\sigma,p} + \mathbf{A}_j^{\sigma,p}]. \end{aligned} \quad (4.8)$$

⁴⁰see Appendix E.

⁴¹Courtesy of A. Doroshenko for her assistance with the sketch 4.1 implementation.

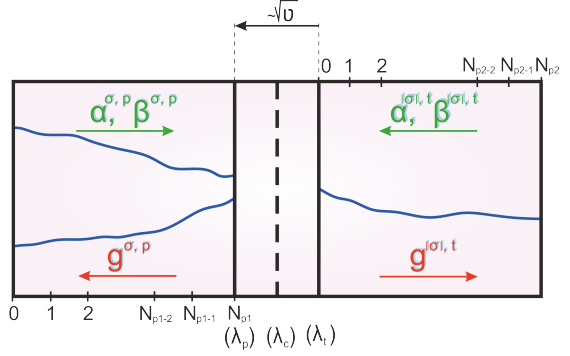


Figure 4.1: A schematic representation of the solution technique.⁴¹

Combining Eqs.4.6-4.8, we calculate $\alpha_0^{\sigma,p}$ and $\beta_0^{\sigma,p}$ at the deeply passing end. Then using Eq.4.8 we find all $\alpha_j^{\sigma,p}$ s and $\beta_j^{\sigma,p}$ s up to the point where perturbative approach described in Chapter II breaks down, $\lambda = \lambda_p$ ($j = N_{p1}$), as shown in Fig.4.1. We apply the exact same algorithm to the trapped branch. The right boundary condition, i.e. for deeply trapped particles at $j = N_{p2}$, is

$$\hat{P}_{N_{p2}}^{|\sigma|,t} g_{N_{p2}}^{|\sigma|,t} + \hat{Q}_{N_{p2}}^{|\sigma|,t} g_{N_{p2}-1}^{|\sigma|,t} + \hat{R}_{N_{p2}}^{|\sigma|,t} g_{N_{p2}-2}^{|\sigma|,t} + \hat{A}_{N_{p2}}^{|\sigma|,t} = 0. \quad (4.9)$$

Employing

$$g_j^{|\sigma|,t} = \alpha_j^{|\sigma|,t} g_{j-1}^{|\sigma|,t} + \beta_j^{|\sigma|,t}, \quad (4.10)$$

and substituting this into the initial equation, Eq.4.5, we come to

$$\begin{aligned} \alpha_j^{|\sigma|,t} &= - \left[P_j^{|\sigma|,t} \alpha_{j+1}^{|\sigma|,t} + Q_j^{|\sigma|,t} \right]^{-1} R_j^{|\sigma|,t}, \\ \beta_j^{|\sigma|,t} &= - \left[P_j^{|\sigma|,t} \alpha_{j+1}^{|\sigma|,t} + Q_j^{|\sigma|,t} \right]^{-1} \left[P_j^{|\sigma|,t} \beta_{j+1}^{|\sigma|,t} + A_j^{|\sigma|,t} \right]. \end{aligned} \quad (4.11)$$

Combining Eqs.4.9-4.11, we calculate $\alpha_{N_{p2}}^{|\sigma|,t}$ and $\beta_{N_{p2}}^{|\sigma|,t}$ at the deeply trapped end and using Eq.4.11 we find all $\alpha_j^{|\sigma|,t}$ s and $\beta_j^{|\sigma|,t}$ s back to $\lambda = \lambda_t$ ($j = 0$) from the trapped side (in accordance with Fig.4.1). Once the layer solution is calculated (see Chapter III) and all $\alpha_j^{\sigma,p/t}$ s and $\beta_j^{\sigma,p/t}$ s are obtained from the passing and the trapped sides, we reconstruct the remaining solution elements outside the layer from Eqs.4.7 and 4.10 up to the trapped/passing edges. The described solution technique is illustrated in Fig.4.1. We note that in the problem, matching at the trapped-passing boundary, Eq.3.1, is provided by the layer solution found in Chapter III.

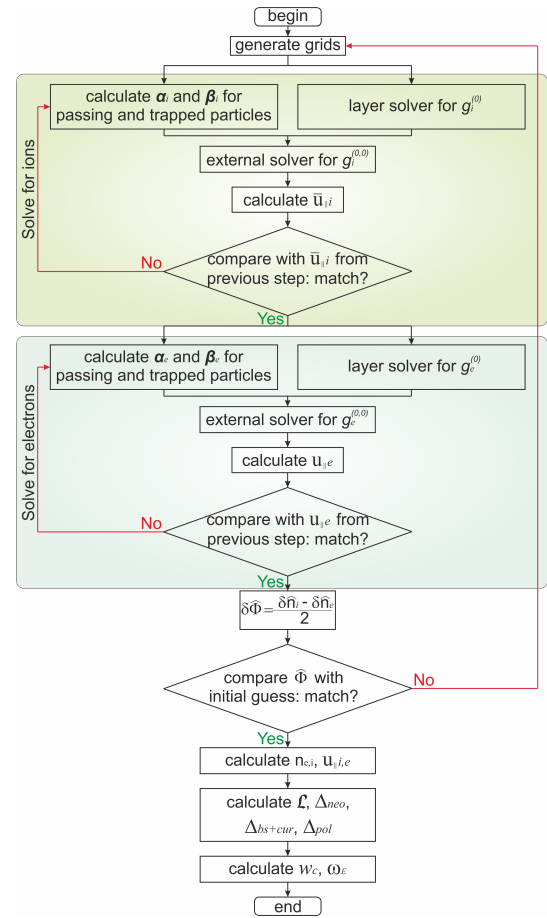


Figure 4.2: A schematic block diagram of the RDK-NTM solver.⁴²

⁴²Courtesy of A. Doroshenko for her assistance with the sketch 4.2 implementation.

To implement the algorithm described above, a new code, *RDK-NTM* (Reduced Drift Kinetic Neoclassical Tearing Mode solver) has been developed in Python ⁴³. A detailed derivation of the numerical scheme can be found in Appendix E. A schematic block diagram of the drift kinetic solver is shown in Fig.4.2 and Fig.E.1 of Appendix E.7. We have checked that the obtained solution converges and satisfies the equation and the boundary conditions.

⁴³Python 2.7.12, NumPy 1.12.0, SciPy 0.18.1, Matplotlib 2.0.0, numba 0.42.1.

4.2 The ion/electron distribution function and its density and flow moments

In previous sections we have calculated the solution of the orbit-averaged drift kinetic equation to leading order in Δ for ions and electrons that takes into account the electrostatic potential found self-consistently from the plasma quasi-neutrality condition. Before we move further and calculate the parallel current density perturbation in the vicinity of the rational surface, let us briefly discuss the distribution function behaviour.

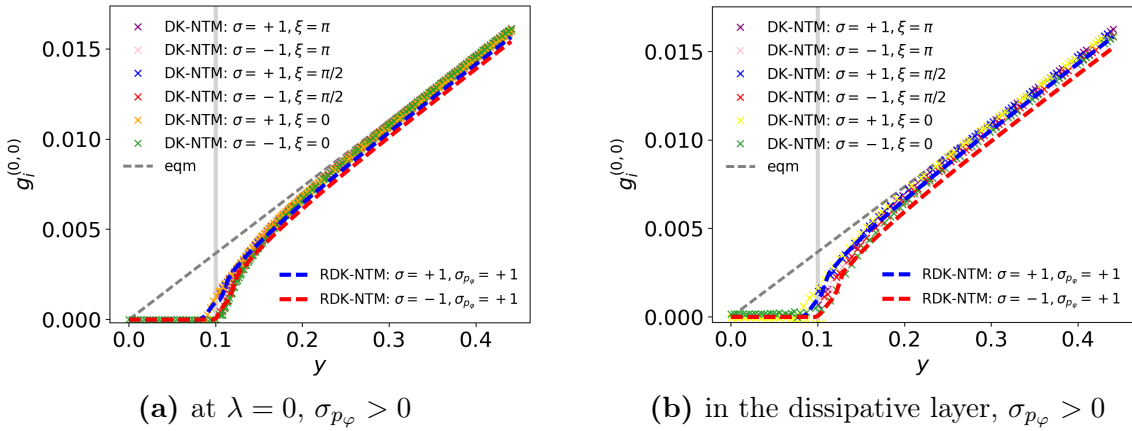


Figure 4.3: The leading order ion distribution function plotted against y . Dashed curves correspond to $g_i^{(0,0)}$, i.e. the RDK-NTM solution. Markers indicate the solution of Eq.2.35 [73, 74, 93], which is a function of p_φ , ξ and λ and keeps collisions to leading order for a full range of λ variation (to be referred to as the DK-NTM solution). $\nu_i^* = 10^{-2}$, $\rho_{\partial i}/w = 0.05$, $w/r_s = 0.02$. The distribution function is normalised to $n_0/(\pi^{3/2}V_{Ti}^3)$.⁴⁴

In Figs.4.3a,4.3b we show the ion distribution function plotted against y at the deeply passing end, $\lambda = 0$, and in the collisional dissipation layer in pitch angle space. In the RDK-NTM solver, we drop collisions to leading order at $\lambda < \lambda_p$ and $\lambda > \lambda_t$, and learn that the particle distribution is flattened across the drift or S islands but not the real magnetic island. Then proceeding to next order in δ_j and adding collisions, we reconstruct the actual form of the particle distribution function, $g_j^{(0,0)} = g_j^{(0,0)}(S, \lambda, V; \sigma)$, i.e. $g_j^{(0,0)}$ is independent of ξ at fixed S . In the vicinity of the trapped-passing boundary, though, collisions are comparable to parallel streaming, and so we predict $g_j^{(0,0)}$ will depend on ξ at fixed S . Thus, here we solve Eq.2.36 in full, exploiting the collisional layer thinness, and

⁴⁴EPS conference on Plasma Physics 2019. Benchmarking of the drift kinetic model for the NTM threshold.

provide matching at λ_c at fixed p_φ as was discussed in the previous chapter. In the layer, the particle distribution is a function of \hat{S} , i.e. S localised around λ_c in accordance with Chapter III, ξ , λ , V and σ and hence is a function of p_φ , ξ , λ , V and σ . To leading order, the \hat{S} dependence is introduced parametrically. In Figs.4.3a and 4.3b we also plot the full solution of Eq.2.35, $g_j^{(0)} = g_j^{(0)}(p_\varphi, \xi, \lambda, V; \sigma)$, for the ion component [94]. In Fig.4.4 we plot the DK-NTM solution outside and inside the collisional dissipative layer around the trapped-passing boundary. As we can see from Figs.4.3a,4.3b,4.4 the ξ dependence of $g_j^{(0)}$ in y/S space is indeed weak at the deeply passing end and becomes significant only when λ approaches λ_p , i.e. the collisional dissipation layer. Both solutions match the equilibrium gradient far from the magnetic island and demonstrate flattening in the vicinity of the S island O-point. At $\nu_i^* = 10^{-2}$, the (R)DK-NTM solutions agree well even in the vicinity of the S island separatrix. If we decrease ν_i^* , a small discrepancy near the S island separatrix appears and continues to grow with decreasing ion collisionality.

- This collisionality dependence can be explained by the fact that the pitch angle scattering outside the dissipative layer is small, and is dominated by $\mathcal{A}\partial/\partial\xi|_S$. ν_i^* is a factor in front of the pitch angle scattering operator, and $\nu_i^* \lesssim 10^{-3}$ is already difficult to resolve in a full DK-NTM solver, where all terms are treated on an equal footing. In contrast, the RDK-NTM solver requires the low collisionality, $\nu_i^* \lesssim 10^{-2}$, to implement the layer solution discussed in Chapter III.
- Another source of the discrepancy near the separatrix is a difference in the boundary conditions used in (R)DK-NTM. Indeed, the RDK-NTM solver deals with the S island directly accounting for a difference in S contours inside and outside the drift island and providing the \mathbb{R}^1 continuity⁴⁵ for the coefficients in Eq.2.40 across the S island separatrix. In contrast, the DK-NTM solution requires the Neumann boundary at $p_\varphi \rightarrow \pm\infty$ [73, 74, 93]. Potentially, the latter implies the \mathbb{R}^n ($n > 1$) continuity. On the other hand, since DK-NTM does not introduce the island explicitly, it might not capture the vicinity of the island separatrix with sufficient accuracy, and thus higher resolution would be required there.
- The discrepancy around the S island separatrix close to $\lambda = \lambda_p$ might arise due to the narrowness of the dissipative layer implemented in the layer solution. The is no

⁴⁵The coefficients of Eq.2.40 and their first derivatives have been matched at the drift island separatrix.

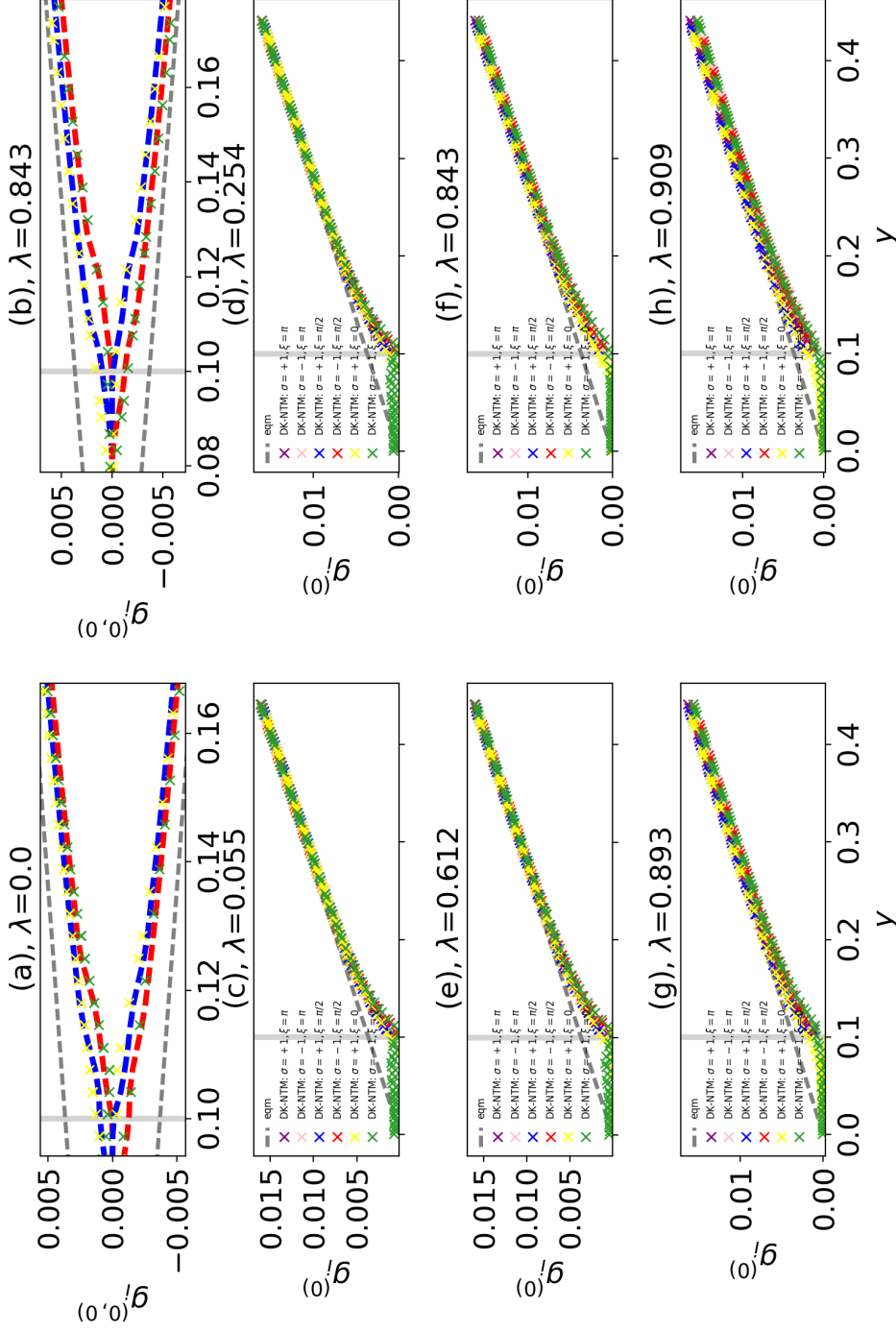


Figure 4.4: The DK-NTM leading order ion distribution function, $g_i^{(0)}$, plotted against y at different λ . (a),(b): zoom in the vicinity of the S island separatrix, $y = 0.1$, denoted by the grey vertical line. The green ($\sigma = -1$) and blue ($\sigma = +1$) dashed curves correspond to the RDK-NTM solution, $g_i^{(0,0)}$. The grey dashed line is the equilibrium in the absence of the island. (c)-(e) outside and (f)-(h) inside the dissipative layer (zoom in the vicinity of the drift island is shown in Fig.F.2). (h) is at the trapped-passing boundary. $\sigma_{p\varphi} > / < 0$ in the upper/lower half-plane. $g_i^{(0,0)}$ is normalised to $n_0/(\pi^3/2V_{Ti}^3)$. $w = 0.02r_s$, $\rho_{\theta i} = 1.0 \cdot 10^{-3}r_s$, $\nu_i^* = 10^{-2}$, $\varepsilon = 0.1$, $\hat{L}_q = 1$, $L_{n0} = 1$, $\hat{\omega}_E = 0$. (c)-(h): markers are as in Figs.4.3a,4.3b.

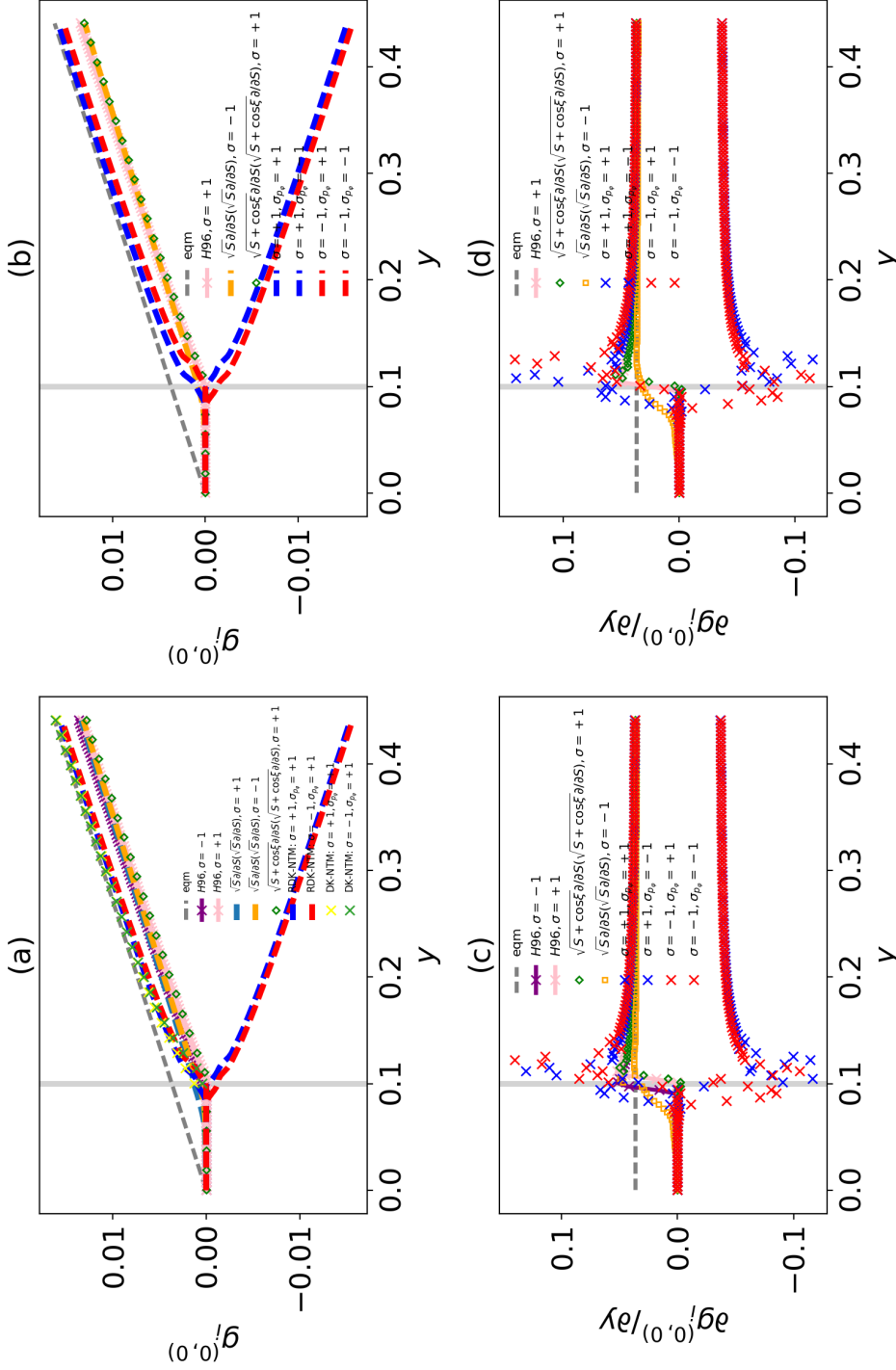


Figure 4.5: The leading order ion distribution function, $g_i^{(0,0)}$, and its y derivative, $\partial g_i^{(0,0)} / \partial y|_{\xi, \lambda}$, localised to the vicinity of the magnetic island of width $w = 0.02r_s$ at the deeply passing end, $\lambda = 0$, (a) and (c), and at $\lambda = \lambda_p$, (b) and (d) (blue and red dashed curves/x-markers, $\sigma_{p,\varphi} > / < 0$ is the upper/lower half-plane). $g_i^{(0,0)}$ is normalised to $n_0 / (\pi^{3/2} V_{Ti}^3)$. $\rho_{\theta i} = 1.0 \cdot 10^{-3} r_s$, $v_i^* = 10^{-2}$, $\varepsilon = 0.1$, $\hat{L}_q = 1$, $L_{n0} = 1$, $\hat{\omega}_E = 0$. The dashed grey line corresponds to an analytic limit far from the magnetic island, i.e. equilibrium gradient denoted by *eqm*. The solid grey line indicates the location of the S island separatrix. DK-NTM results are presented across the S island O-point. Pink and purple *H96* curves represent an analytic solution, $h(\Omega)$, [53] rewritten in terms of y (a),(b) and differentiated with respect to y (c),(d) for $\sigma = \pm 1$, respectively. $h(\Omega)$ is valid in the limit of large w and small $\rho_{\theta i}$ outside the magnetic island separatrix. The light blue and orange curves/green diamond markers indicate the RDK-NTM solution with the model S diffusion with $\sqrt{S} / \sqrt{S + \cos \xi}$ taken for the weight function for $\sigma = \pm 1$.

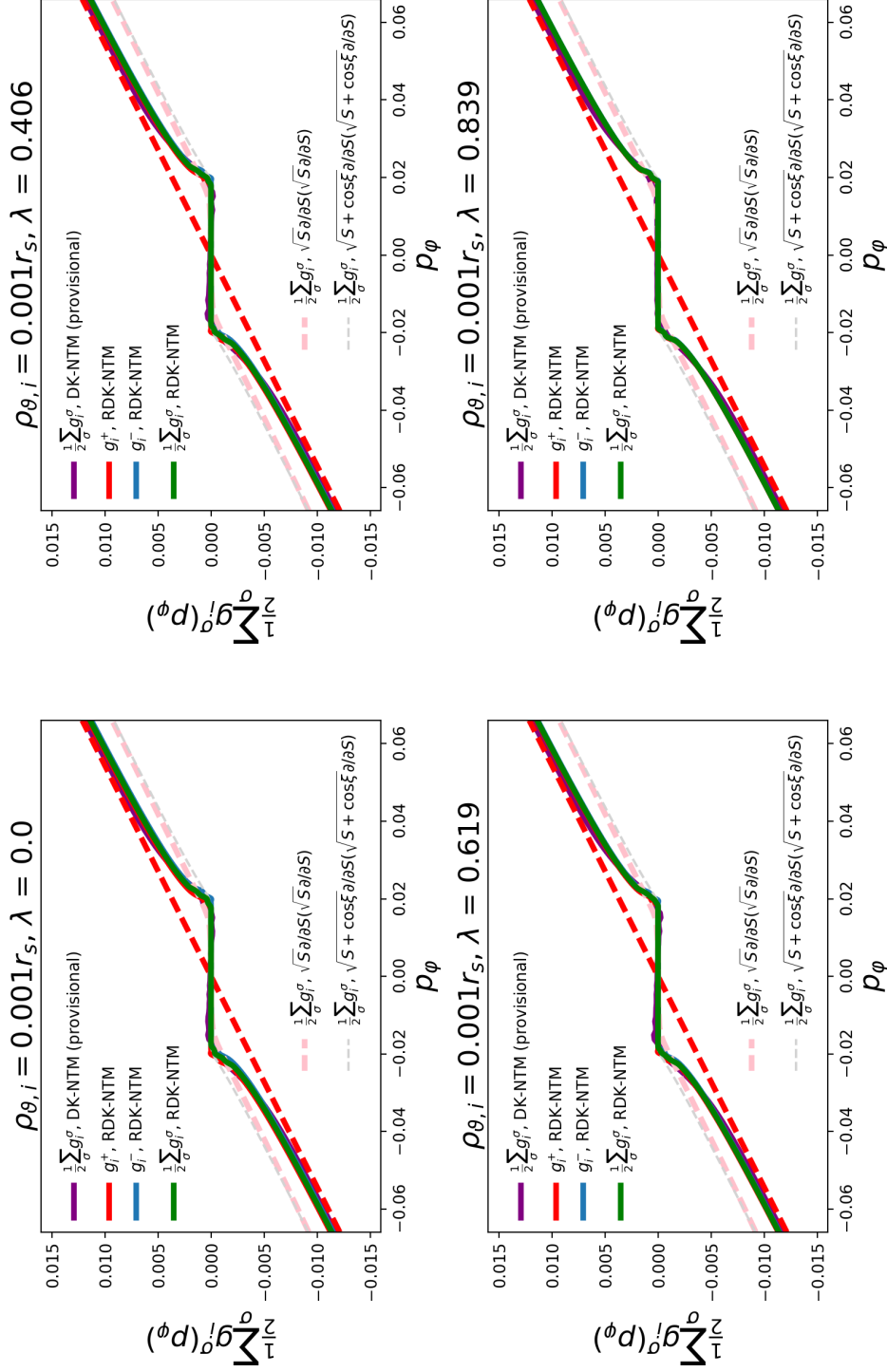
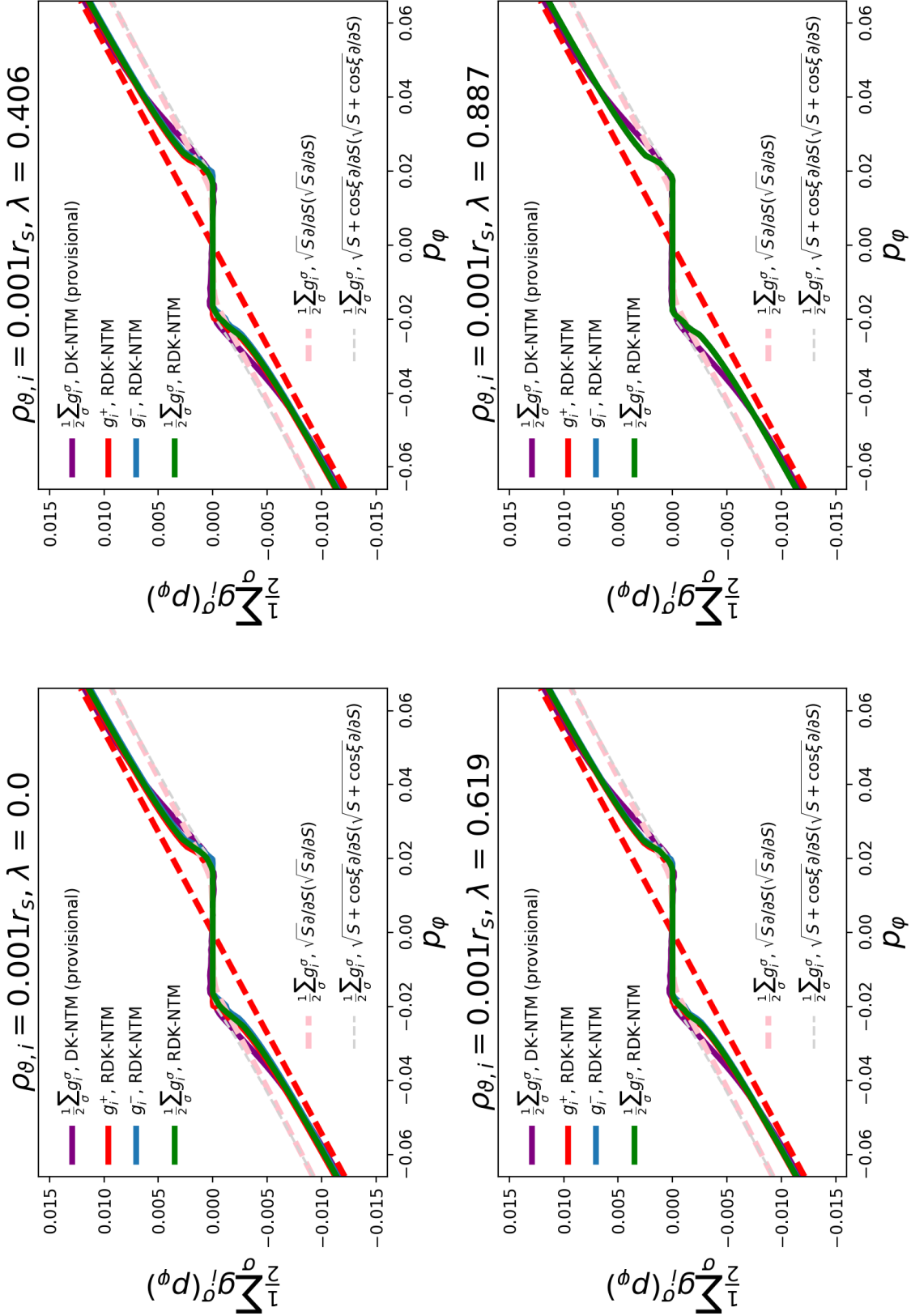


Figure 4.6: Sum of the $\sigma = \pm 1$ leading order ion distribution functions plotted against p_ϕ at fixed λ . $g_i^{(0,0)}$ is normalised to $n_0 / (\pi^{3/2} V_{Ti}^3)$. $w = 0.02r_s$, $\rho_{\theta i} = 1.0 \cdot 10^{-3} r_s$, $\nu_i^* = 10^{-2}$, $\varepsilon = 0.1$, $\hat{L}_q = 1$, $L_{r0} = 1$, $\hat{\omega}_E = 0$. The red dashed line represents the analytic limit far from the magnetic island in the absence of the electrostatic potential. DK-NTM denotes the solution of Eq.2.35 [73, 74, 93]. However, in contrast to [73, 74, 93], DK-NTM (provisional) adds numerical electrons to the model similar to the RDK-NTM solver.

Figure 4.7: Same as Fig.4.6 except for $\nu_i^* = 10^{-3}$.

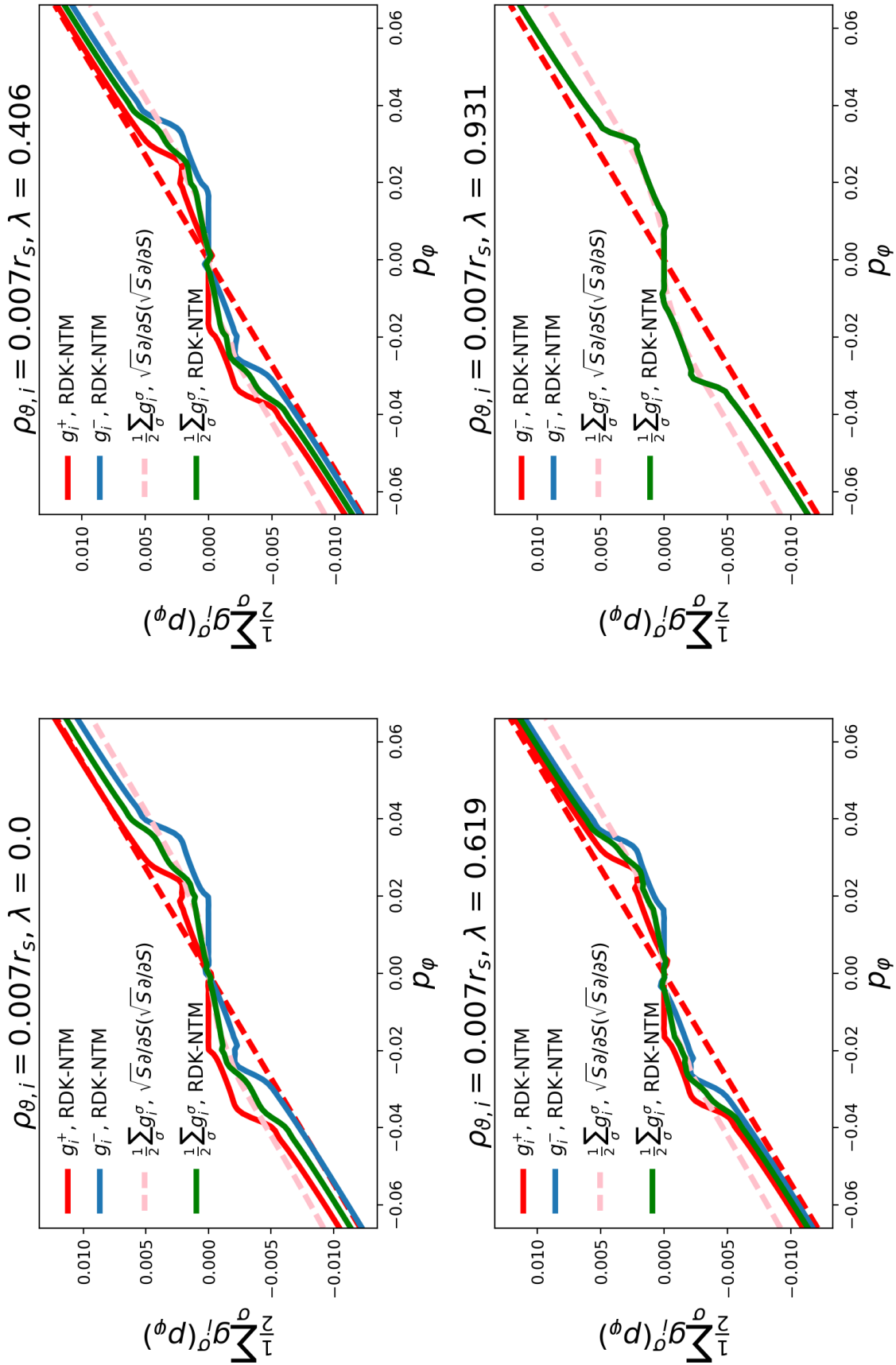


Figure 4.8: Same as Fig.4.7 except for $\rho_{\theta i} = 7.0 \cdot 10^{-3} r_s$, corresponding to $\rho_{\theta i} / w = 0.35$.

λ variation in S in the leading order solution. This does not play a significant role inside the layer but can cause a small difference when $\lambda \rightarrow \lambda_p + 0$.

- In the vicinity of the S island separatrix, there is a region where S derivatives can be comparable to parallel streaming, which would invalidate the perturbative treatment of collisions in RDK-NTM. This region then is to be treated in a way similar to the dissipative layer solution discussed in the previous chapter.

However, as we can see from Fig.4.4(a),(b), the last three points are not crucial, and the main source of difference is caused by the plasma collisionality limitations.

The curvature of the distribution function in the vicinity of the island separatrix is determined by the diffusion terms in Eq.2.40/Eq.2.35 that arise from switching from ψ to S/p_φ in the pitch angle scattering collision operator.⁴⁶ These diffusion terms are proportional to $\partial^k/\partial S^k|_{\lambda,\xi}$ or $\partial^k/\partial p_\varphi^k|_{\lambda,\xi}$ ($k = 1, 2$), respectively. In Fig.4.5 we compare the RDK-NTM solution plotted against y at $\lambda = 0$ (a) and $\lambda = \lambda_p$ (b) for plasma and tokamak parameters considered in Figs.4.3a,4.3b,4.4 and an analytic solution valid in the limit of large islands outside the magnetic island separatrix [53]. The latter is denoted by *H96*. The corresponding leading order ion distribution differentiated with respect to y and plotted against y at $\lambda = 0$ and $\lambda = \lambda_p$ is shown in Fig.4.5 (c) and (d), respectively.

H96 is derived from a model diffusion of the form $\Gamma_\psi = -D\partial n/\partial\psi$, where Γ_ψ is the particle flux in the radial direction and D is the diffusion coefficient that has been assumed to be a slowly varying function across the magnetic island O-point. The model diffusion is sufficient for the accurate determination of the bootstrap drive at large w . However, it does not provide a full polarisation current contribution to the magnetic island growth/decay. Indeed, as we shall see later in this chapter, a significant amount of the polarisation drive comes from the vicinity of the magnetic island separatrix. In Fig.4.5 we also show the solution of Eqs.D.60,D.61 where the S diffusion terms, i.e. terms proportional to $\partial^k/\partial S^k|_{\lambda,\xi}$ ($k = 1, 2$), have been replaced with a model S diffusion. The first model imposes $\partial^2/\partial y^2$ or $\sqrt{S}\partial/\partial S(\sqrt{S}\partial/\partial S)$ at fixed λ and ξ and is obtained by replacing

⁴⁶The pitch angle scattering collision operator is introduced at fixed ψ . To solve Eq.2.40/Eq.2.35 in S/p_φ space, one has to rewrite the λ differentials at fixed S/p_φ , respectively. In the dissipative layer around λ_c , the $\partial^2/\partial\lambda^2$ term is dominant and hence the S differentials have been dropped to leading order. However, we have to stress here that the leading order curvature around the \hat{S} island separatrix is still included via the drive, $H^{\pm/t}$. The \hat{S} dependence of $H^{\pm/t}$ is parameteric and is found from matching at λ_c at fixed p_φ as discussed in the previous chapter.

$p_\varphi = p_\varphi(S, \xi, \lambda, V; \sigma)$ with $\sigma_{p_\varphi} \sqrt{2\hat{L}_q S^\pm / \hat{w}}$. In the dissipation layer, the drive term then has to be replaced with $\sigma_{p_\varphi} \sqrt{2\hat{L}_q S^\pm / \hat{w}}$ as well. This \sqrt{S} diffusion model with a constant diffusion coefficient excludes the spectrum in ξ , and hence leaves the solution unperturbed outside the magnetic island separatrix (see Fig.4.5(c),(d)). The second model imposes the S diffusion weighted by $\sqrt{S + \cos \xi}$ and hence reproduces the *H96* solution at large w outside the island^{47,48}. Replacing the actual S diffusion in Eqs.D.60,D.61 with a model, either \sqrt{S} or $\sqrt{S + \cos \xi}$, removes a significant fraction of the perturbation right outside the separatrix. Keeping all the terms $\propto \partial^k / \partial S^k \big|_{\lambda, \xi}$ ($k = 1, 2$), we obtain a full solution of Eqs.D.60,D.61. As we can see from Fig.4.4(a),(b), the full RDK-NTM solution in S space and the full DK-NTM solution in p_φ space agree well in the vicinity of the S island separatrix. Therefore, we stress that the curvature of the distribution function around the separatrix is governed by the actual S diffusion in Eqs.D.60/D.61 and is necessary for the accurate calculation of the polarisation term in the MRE. In Figs.4.6,4.7 we plot the same solutions but in p_φ space. The DK-NTM (provisional⁴⁹) solution denotes the DK-NTM solution that includes the numerical electrons, i.e. treats the electron component numerically in a way similar to the RDK-NTM solver (see Fig.4.2). In Fig.4.8 we show the RDK-NTM results for larger $\rho_{\vartheta i} / w \lesssim 1$.

In Fig.4.9 we plot the ion distribution function against \hat{p}_φ and λ at certain $\rho_{\vartheta i} / w$ and

⁴⁷These model solutions have been introduced to benchmark the RDK-NTM solutions against known analytic limits and to demonstrate the importance of the S diffusion.

⁴⁸The starting equation schematically reads $V_{\parallel} \nabla_{\parallel} g_j + \hat{L} g_j = \nu_{ii} \mathcal{D}_\lambda g_j + D \partial^2 g_j / \partial \psi^2 \big|_{\xi}$, where \hat{L} represents the rest of the differential operators that act on g_j in the left hand side of the drift-kinetic equation. \mathcal{D}_λ is the pitch angle scattering operator and D is a constant diffusion coefficient. Dropping the drift effects, $\hat{L} g_j$, and replacing $\nu_{ii} \mathcal{D}_\lambda g_j$ with the Krook collisions, we obtain Eq.7 of [64]. Treating the right hand side perturbatively outside the island at $\lambda < \lambda_p$, and solving $\left[(\nu_{ii} / V_{\parallel}) D_\lambda + (D / V_{\parallel}) \partial^2 / \partial \psi^2 \big|_{\xi} \right] g_j^{(0)} = 0$, we obtain *H96* for the leading order distribution. Similarly, the dominant contribution in S space reads $\int_{\hat{w}/4\hat{L}_q}^S C_1 \left(\left\langle \sqrt{\frac{1}{2} \left(\frac{4\hat{L}_q}{\hat{w}} S' + \cos \xi \right)} \right\rangle_{\xi}^{S'} \right)^{-1} dS'$ in the absence of the electrostatic potential and the momentum conservation term. Here $\left\langle \sqrt{\frac{1}{2} \left(\frac{4\hat{L}_q}{\hat{w}} S + \cos \xi \right)} \right\rangle_{\xi}^S = \frac{\sqrt{2}}{\pi} \sqrt{\frac{4\hat{L}_q}{\hat{w}} S - 1} \cdot E \left(-\frac{2\hat{w}}{4\hat{L}_q S - 1} \right)$, where E is the complete elliptic integral of the second kind. $E \left(-\frac{2\hat{w}}{4\hat{L}_q S - 1} \right) \rightarrow \frac{\pi}{2}$, $S \rightarrow \infty$. C_1 is a constant of integration to be determined to match to the equilibrium Maxwellian gradient far from the island. In Fig.4.5 we show that the model $\sqrt{S + \cos \xi}$ RDK-NTM solution matches this analytic solution. Away from the island, S reduces to Ω and hence the latter reproduces *H96*. Dropping the ξ dependence in the diffusion term on the right hand side of this model kinetic equation, we obtain the \sqrt{S} model diffusion solution outside the island, i.e. $\sigma_{p_\varphi} \hat{w} \left[L_n^{-1} + \left(\hat{V}^2 - 3/2 \right) L_{Tj}^{-1} \right] e^{-\hat{V}^2} \sqrt{4\hat{L}_q / \hat{w}} \left[y - \sqrt{\hat{w} / 4\hat{L}_q} \right]$ in agreement with Fig.4.5.

⁴⁹To be further tested for larger $\rho_{\vartheta i}$.

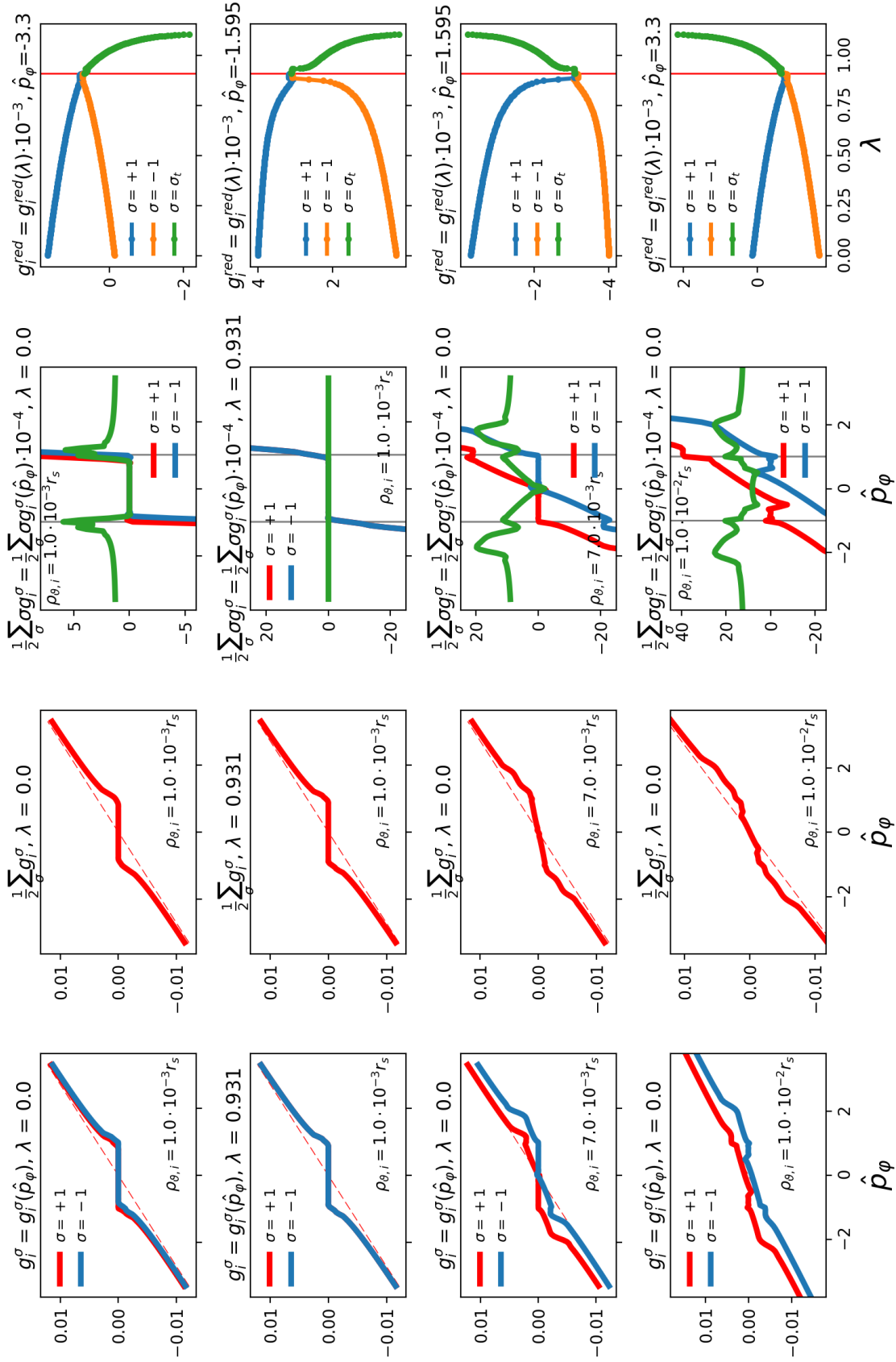
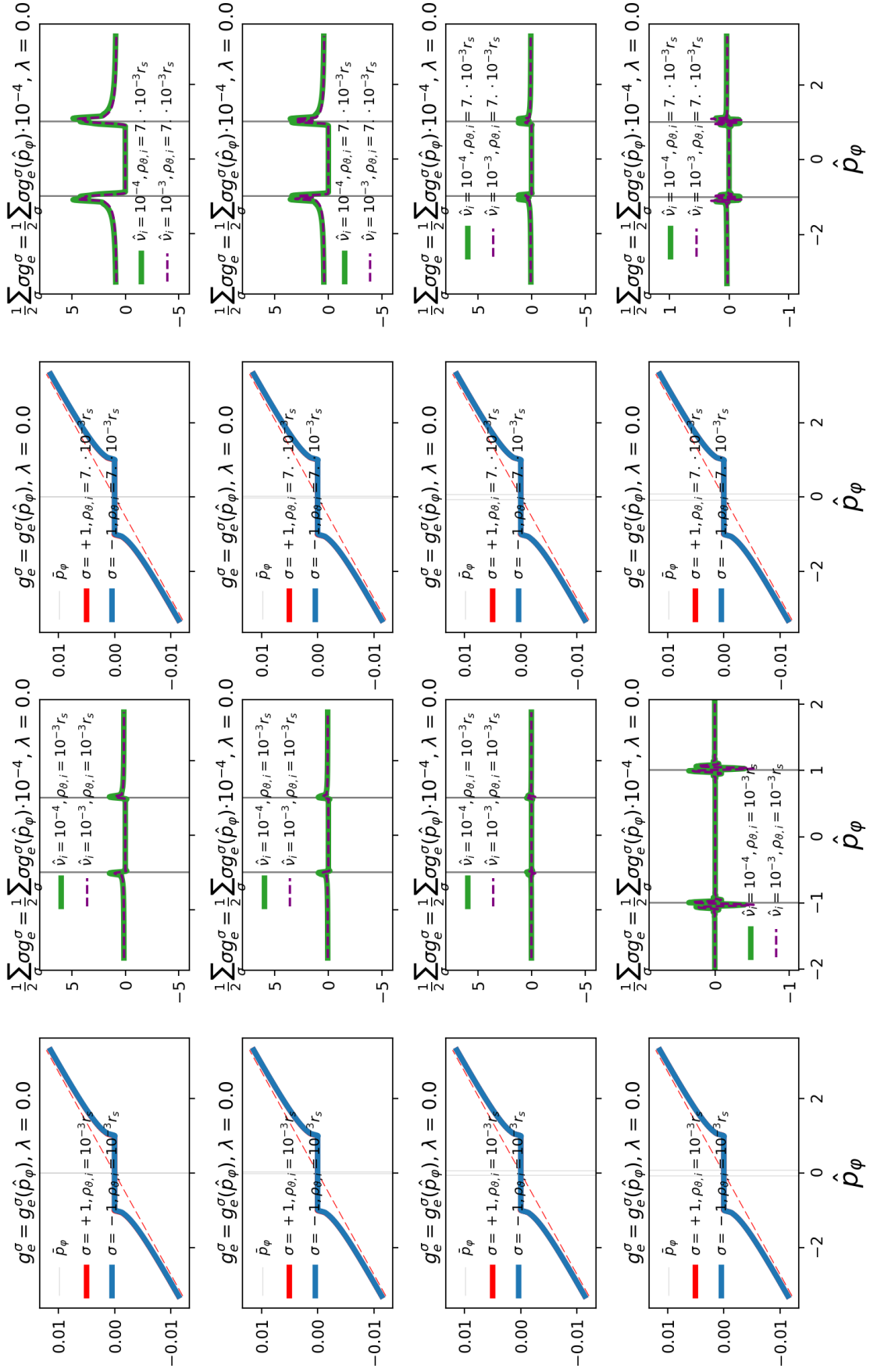


Figure 4.9: (right-to-left) The leading order ion distribution function vs. $\hat{\rho}_\phi$, $g_i^\sigma = g_i^\sigma(\hat{\rho}_\phi)$ at fixed λ at the 0th iteration in Φ . Its density moment, $(1/2) \sum_{\sigma} \sigma g_i^\sigma$, against $\hat{\rho}_\phi$. Dashed red line corresponds to equilibrium in the absence of the magnetic island. Its flow moment, $(1/2) \sum_{\sigma} \sigma g_i^\sigma$, against $\hat{\rho}_\phi$. $g_i^{\text{red}} \equiv g_i^{\text{red}} - C\hat{\rho}_\phi$ against λ at fixed $\hat{\rho}_\phi$. The λ dependence is presented at $\rho_{\theta,i} = 7.0 \cdot 10^{-3} r_s$. The vertical red line indicates the trapped-passing boundary, $\lambda_c \approx 0.909$. $w = 0.02r_s$, $\varepsilon = 0.1$, $\hat{L}_q = 1$, $\hat{L}_q = 1$, $\hat{\omega}_E = 1$, $\hat{\omega}_E = 1$, $\eta_i = 1$ and $\hat{v}_i = 10^{-4}$.

Figure 4.10: Same as Fig.4.9 but for the electron plasma component. $\hat{v}_i = 10^{-4}$ unless otherwise stated.

ion collisionality. A sum of the ion distribution functions over $\sigma = \pm 1$ is found to be flattened in the vicinity of $\hat{p}_\varphi = 0$ and thus inside the magnetic island for small $\rho_{\vartheta i}/w$. Due to Eq.1.6 and Eq.2.12, this results in flattening of the ion density profile around the magnetic island O-point for $\rho_{\vartheta i}/w \ll 1$. In contrast, when the radial shift of the drift S islands compared to the magnetic island (which is proportional to $\hat{\rho}_{\vartheta i}$) becomes significant, the flattening of $\sum_\sigma g_i^{(0,0),\sigma}$ and hence the density flattening are removed from inside the magnetic island. $\rho_{\vartheta i} = 5.0 \cdot 10^{-3} r_s$ is sufficient to partially restore the density gradient across the magnetic island of width $w = 0.02 r_s$. If $\rho_{\vartheta i}/w \gtrsim 1$, the profile will be further steepened across the O-point. This explains the density profiles we demonstrate in Fig.2.11 of Chapter II and in Fig.4.11. The gradient inside the magnetic island is a consequence of the drift island structures, and is a property of the passing (but not trapped) particles.

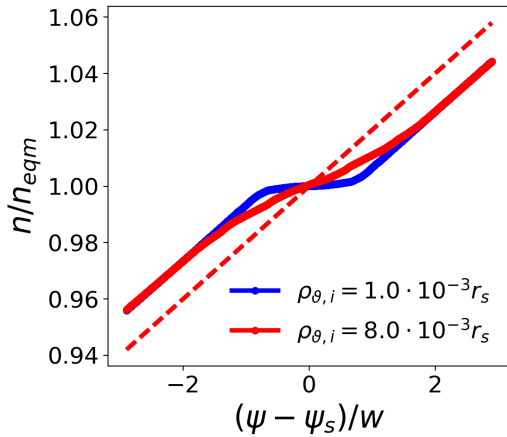


Figure 4.11: Same as Fig.2.11 except for the ion collisionality $\nu_i^* = 10^{-4}$.

For electrons, the radial shift in Eq.2.37 is small as $\rho_{\vartheta e} \ll \rho_{\vartheta i}$ (e.g. see Fig.4.10). Hence, the drift island effect is less significant for the electron distribution function. This creates a significant difference in the electron and ion density profiles especially at large $\rho_{\vartheta i}$ in the absence of the electrostatic potential. Indeed, when $\rho_{\vartheta i}/w \ll 1$, the ion and electron density gradients are both removed from inside the magnetic island. In contrast, when $\rho_{\vartheta i}$ and w are comparable, a non-zero, finite ion density gradient is sustained around the magnetic

island O-point, while the electron density gradient is still removed in the absence of any potential due to the strong electron parallel streaming and $\rho_{\vartheta e} \ll w$. However, to keep plasma quasi-neutral, the electrostatic potential is required. It adjusts to provide $n_i \approx n_e$. Hence, the ion density steepening at large $\rho_{\vartheta i}$ is explained by the radial shift in S given by Eq.2.37, while the sustainability of the electron density gradient is associated with the self-consistent electrostatic potential. $\sum_\sigma \sigma g_{i,e}^{(0,0),\sigma}$ is responsible for the parallel flow profile due to Eq.2.27 with Eqs.2.12,2.13. The main contribution to the flow is provided by passing particles due to the summation over σ in the ϑ -averaging operator introduced for trapped particles, Eq.2.24. $\sum_\sigma \sigma g_i^{(0,0),\sigma}$

is shown in Fig.4.9 and Fig.4.10 for different $\rho_{\vartheta i}/w$. However, we have to note that the trapped branch also contributes to Eq.2.27 as the integration in Eq.2.27 is imposed at fixed ψ , and $g_i^{(0,0),t} = g_i^{(0,0),t}(\hat{p}_\varphi, \xi, \lambda, \hat{V}) = g_i^{(0,0),t}(\hat{\psi}, \xi, \vartheta, \lambda, \hat{V}; \sigma)$ with $\hat{p}_\varphi = x - \hat{\rho}_{\vartheta i} \hat{V}_\parallel = x - \sigma \hat{\rho}_{\vartheta i} \hat{V} \sqrt{1 - \lambda B(\vartheta)}$.

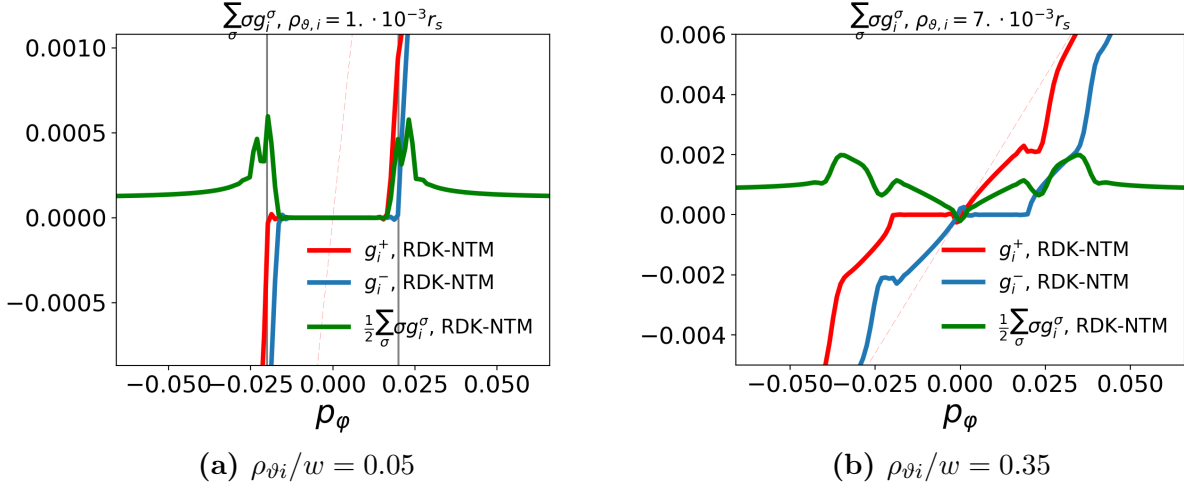


Figure 4.12: The ion flow moment, $\sum_{\sigma} \sigma g_i^{\sigma}$, plotted against p_{φ} at $\lambda = 0.0873$, $\xi = 0$ for $w = 0.02r_s$, $\rho_{\vartheta i} = 1.0 \cdot 10^{-3}r_s$ (left) and $w = 0.02r_s$, $\rho_{\vartheta i} = 7.0 \cdot 10^{-3}r_s$ (right), $\varepsilon = 0.1$, $\hat{L}_q = 1$, $L_{n0} = 1$, $\hat{\omega}_E = 0$, $\eta_i = 1$ and $\hat{v}_i = 10^{-4}$. The grey lines in Fig.4.12a correspond to $p_{\varphi} = w$, which is close to the magnetic island separatrix for small $\rho_{\vartheta i}/w$. The red dashed line in Figs.4.12a,4.12b corresponds to the equilibrium gradient, i.e. in the absence of the NTM island.

In Figs.4.12a,4.12b we compare the ion flow moments at small and large $\rho_{\vartheta i}/w$. In Fig.4.12a $\sum_{\sigma} \sigma g_i^{\sigma}$ is flattened and zero across the magnetic island O-point in accordance with the conventional picture when the bootstrap flow experiences a hole around the island O-point. In Fig.4.12b, corresponding to larger $\rho_{\vartheta i}/w$, there is a non-zero contribution to $\sum_{\sigma} \sigma g_i^{\sigma}$ in the island centre which as we shall see in the following section provides the basis for an NTM threshold.

In Sec.2.5 of Chapter II we have defined ω_E , which being proportional to Φ'_{eqm} , describes the electrostatic potential gradient away from the magnetic island, provided Φ is localised to the island vicinity. Therefore, as ω_E appears through the equilibrium electrostatic potential far from the NTM island, its effect on the radial distribution function/density profile has to be similar to that from $\rho_{\vartheta i}$. Indeed, provided the electrostatic potential is localised around the resonant surface, $S^{\pm} = (\hat{w}/4\hat{L}_q) [2(\hat{p}_{\varphi} - \bar{p}_{\varphi})^2 - \cos \xi] - (1/2) \left\langle \hat{\rho}_{\vartheta j} \delta \hat{\Phi} / \hat{V}_{\parallel} \right\rangle_{\vartheta}^{p_{\varphi}}$ with $\bar{p}_{\varphi} = \hat{\rho}_{\vartheta j} (\hat{L}_q / \hat{w}) (\hat{\omega}_D + \left\langle 1/2 \hat{V}_{\parallel} \right\rangle_{\vartheta}^{p_{\varphi}} \hat{\omega}_E L_{n0}^{-1} \hat{w})$. Thus, $\hat{\omega}_E$ and its sign also result in the radial shift along with $\rho_{\vartheta i}$.⁵⁰ However, this contribution, being also w dependent, is

⁵⁰ A similar effect has been addressed in [92] in the drift kinetic approximation for the model electrostatic

one-two orders of amplitude less than the effect of the ion poloidal Larmor radius. We also notice that the reduction in w results in more rapid changes in the radial shift of S in p_φ space, denoted by \bar{p}_φ , as $\bar{p}_\varphi \propto \hat{\rho}_{\partial i} / \hat{w} = \rho_{\partial i} \psi_s / w^2$.

4.3 Contributions to the modified Rutherford equation

We can now move to Eq.2.1 and consider the parallel current density perturbation localised around the resonant surface, J_{\parallel} , that contributes to the time evolution of the magnetic island width. The second term on the right hand side of Eq.2.1 adds tokamak neoclassical effects to the Rutherford equation, i.e. bootstrap, curvature and polarisation contributions to $w = w(t)$. We note that Eq.2.9 is equivalent to Eq.2.1 if a single isolated stationary NTM magnetic island is considered. Thus, when the island is stationary, the classical tearing mode stability parameter, Δ' , is balanced against the sum of all the neoclassical contributions, $\Delta' + \Delta_{neo} = 0$, where

$$\Delta_{neo} = -\frac{\mu_0 R}{2\tilde{\psi}} \int_{\mathbb{R}} d\psi \int_{-\pi}^{\pi} d\xi \bar{J}_{\parallel} \cos \xi. \quad (4.12)$$

Here \bar{J}_{\parallel} is the ϑ -average of J_{\parallel} .

Substituting the obtained ion/electron distribution function into Eq.2.27, yields the expression for the ion/electron parallel flow, $u_{\parallel,j}$, with $J_{\parallel} = \sum_j eZ_j u_{\parallel,j}$. Defining the polarisation current density as the part of the parallel current density perturbation that flux surface averages to zero, we write

$$\Delta_{bs} + \Delta_{cur} = -\frac{\mu_0 R}{2\tilde{\psi}} \int_{\mathbb{R}} d\psi \int_{-\pi}^{\pi} d\xi \langle \bar{J}_{\parallel} \rangle_{\xi}^{\Omega} \cos \xi \quad (4.13)$$

for the sum of the bootstrap and curvature contributions and hence

$$\Delta_{pol} = \Delta_{neo} - (\Delta_{bs} + \Delta_{cur}) \quad (4.14)$$

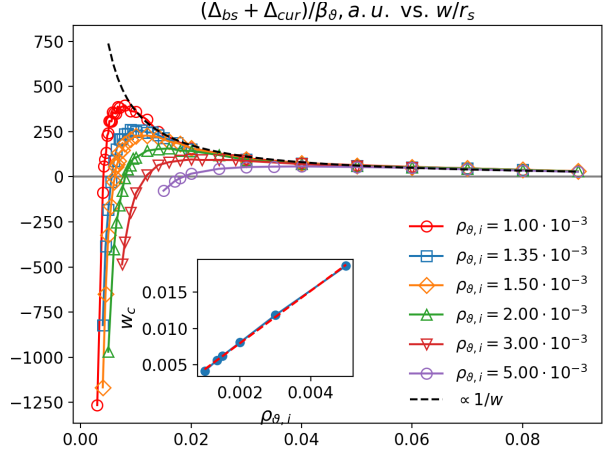


Figure 4.13: The sum of the bootstrap and curvature contributions to the modified Rutherford equation normalised to poloidal beta, $(\Delta_{bs} + \Delta_{cur})/\beta_{\vartheta}$, vs. w/r_s for different values of the ion poloidal Larmor radius, $\rho_{\vartheta,i}$. The dashed line is the analytic result for the bootstrap current contribution, valid in the limit of large magnetic island widths. Here w_c defined as a solution of $\Delta_{bs} + \Delta_{cur} = 0$ represents a magnetic island threshold, also called a critical magnetic island half-width. Inset: w_c vs. $\rho_{\vartheta,i}$. $\varepsilon = 0.1$, $\hat{L}_q = 1$, ion collisionality $\nu_i^* = 10^{-4}$. The equilibrium density and temperature gradients are $L_n^{-1} = 1$ with $\hat{\omega}_E = 0$, $L_{Tj}^{-1} = 1$.

for the polarisation term. Here the ξ -averaging operator at fixed Ω is defined as

$$\langle \dots \rangle_{\xi}^{\Omega} = \frac{\oint \dots (\Omega + \cos \xi)^{-1/2} d\xi}{\oint (\Omega + \cos \xi)^{-1/2} d\xi} \quad (4.15)$$

similar to Eq.2.41. As we mentioned earlier, we focus on a large aspect ratio, circular cross section tokamak approximation. Thus, some of the terms of order ε^2 are neglected. An accurate calculation of the curvature contribution requires these higher order corrections. However, as $\Delta_{cur} = \mathcal{O}(\varepsilon^2)$, it does not provide a significant contribution to the threshold nor to the island propagation frequency results discussed below. Thus, $\Delta_{bs} + \Delta_{cur}$ used here is just a symbolic representation of all the MRE contributions that do not flux surface average to zero. To $\mathcal{O}(\varepsilon)$, this reduces to the bootstrap current contribution for magnetic islands of large widths, $w \gg \rho_{\vartheta i}$. In Fig.4.13 we plot $(\Delta_{bs} + \Delta_{cur})/\beta_{\vartheta}$ against w/r_s . In

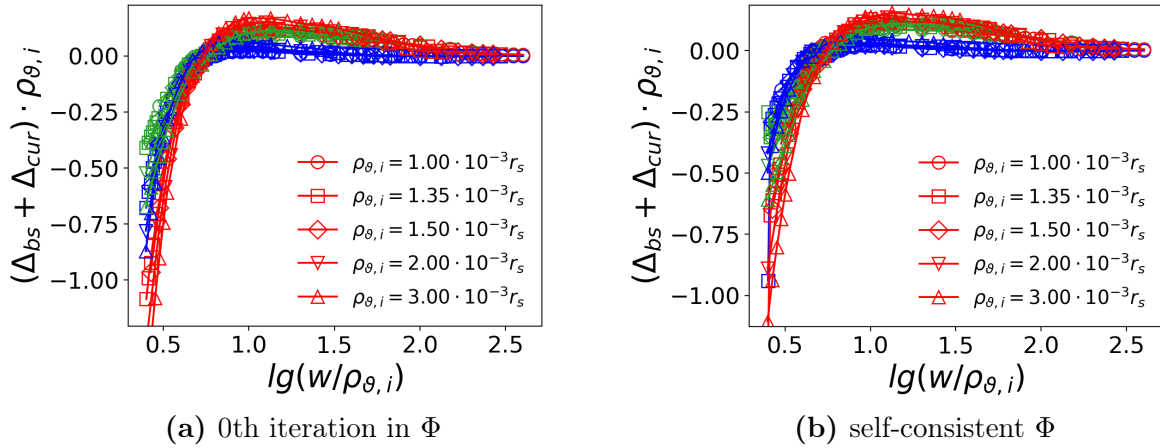


Figure 4.14: A sum of the bootstrap and curvature contributions, $\Delta_{bs} + \Delta_{cur}$, plotted against $w/\rho_{\vartheta i}$ for different $\rho_{\vartheta i}$ at the end of the 0th iteration in Φ (left) and with self-consistent electrostatic potential Φ (right) (green: electrons, blue: ions, red: total; markers denote the corresponding value of $\rho_{\vartheta i}$). $\varepsilon = 0.1$, $\hat{L}_q = 1$, $\hat{\nu}_i = 10^{-4}$. The equilibrium density and temperature gradients are $L_n^{-1} = 1$, $L_{Tj}^{-1} = 1$. The ion/electron distribution function has been calculated with the model $\propto \sqrt{S}$ diffusion.

the limit of $w \gg \rho_{\vartheta i}$, $\Delta_{bs} + \Delta_{cur}$ is inversely proportional to w , which is expected from the existing analytic theory (e.g. Eq.(85) of [53]). When w tends to zero, $\Delta_{bs} + \Delta_{cur}$ becomes negative providing a threshold for NTMs, i.e. a value of w below which the mode is stable, $\Delta_{bs} + \Delta_{cur} < 0$. This value is denoted by w_c and is to be referred to as the critical magnetic island half-width. w_c is different for each ion poloidal Larmor radius and hence can be scaled by $\rho_{\vartheta i}$. This kind of behaviour at $w \sim \rho_{\vartheta i}$ is the direct result of the inclusion of the drift islands in our model and is in qualitative agreement

with experimentally observed self-healing of small magnetic islands below the threshold (e.g. [72])⁵¹. As we learned from the previous section, the plasma density gradient is not removed across the magnetic island at small w . This, in turn, restores the bootstrap current near the island O-point.

To compare the electron and ion contributions to the drive, in Figs.4.14a,4.14b,4.15 we plot $\Delta_{bs} + \Delta_{cur}$ as a function of $\lg w/\rho_{\vartheta i}$ at the 0th iteration in the electrostatic potential⁵² and also with Φ found self-consistently from the plasma quasi-neutrality condition. In Figs.4.14a,4.14b the S diffusion terms in Eqs.D.60,D.61 have been replaced with a model, i.e. the $\propto \sqrt{S}$ diffusion addressed in the previous section. In accordance with the previous section, this solution almost reproduces the *H96* solution (see Fig.4.5) outside the island but also captures the region inside the magnetic island separatrix.

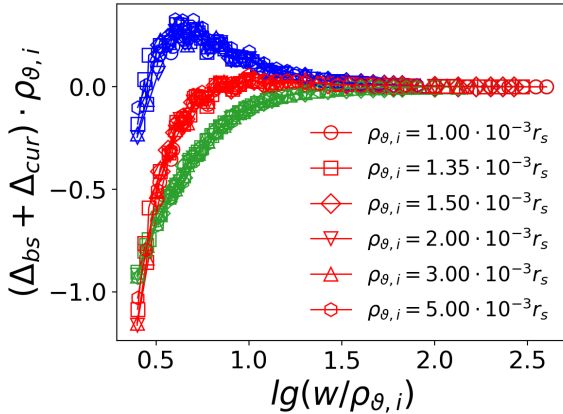


Figure 4.15: Same as Fig.4.14b but based on the full RDK-NTM solution.

In both cases, the electron and ion contributions match the analytic limit at large w in accordance with [53]. As can be seen from Figs.4.14a,4.14b both, ions and electrons, contribute to the threshold in the limit of $w \sim \rho_{\vartheta i}$ in the absence of the actual S diffusion. Keeping the actual S diffusion, i.e. solving Eqs.D.60,D.61 in full, we obtain $\Delta_{bs} + \Delta_{cur}$ shown in Fig.4.15. In contrast to Figs.4.14a,4.14b, here the electron component dominates the plasma response at small w .

Physically, this might be explained by the fact that $m_e \ll m_i$ and thus $\rho_{\vartheta i} \gg \rho_{\vartheta e}$ or $\rho_{bi} \gg \rho_{be}$. Therefore, at $w \ll \rho_{bi}$ the ion plasma component averages over the electro-magnetic field generated by the island, while electrons due to the narrowness of their banana orbits still respond to the local value of the field. This is in agreement with the DK-NTM solution presented in [73, 93, 74]⁵³. However, we highlight that the origin of the electron/ion behaviour at $w \lesssim \rho_{\vartheta i}$ is still an open question and is the subject of further

⁵¹To provide the quantitative agreement, one has to include the classical tearing mode stability parameter, Δ' .

⁵² $\hat{\Phi} = \hat{\omega}_E L_{n0}^{-1} \hat{w} \hat{\psi}$ is taken for the initial guess unless otherwise stated.

⁵³In [73, 93, 74], the electrons are treated analytically at the 0th iteration in the electrostatic potential due to $m_e \ll m_i$.

investigations. Mathematically, we stress the importance of the distribution function curvature around the magnetic island separatrix provided by the *radial* S diffusion.

To compare the NTM threshold with its experimental value, we have to keep all the neoclassical contributions, Δ_{neo} , and thus the contribution of the polarisation current is required. In Fig.4.16 we show $\Delta_{bs} + \Delta_{cur}$ and Δ_{pol} as a function of w/r_s for different $\rho_{\vartheta i}$. Δ_{pol} is calculated in accordance with Eq.4.14. Working in the island rest frame, $\omega = 0$, we determine Δ_{pol} as the residual contribution to the island evolution. The actual polarisation current contribution will require the island propagation frequency dependence. The polarisation contribution is inversely proportional to w^3 at large w in agreement with previous analytic results (e.g. [53, 43], note: Eq.(85) of [53] is obtained in the reference frame in which the equilibrium radial electric field is zero, while we work in the island reference frame)⁵⁴. For smaller w comparable to the ion poloidal Larmor radius, there is a threshold similar to one obtained for the "bootstrap" drive, $\Delta_{bs} + \Delta_{cur}$. However, as the "bootstrap" drive dominates over the polarisation term as we can see from Fig.4.16 in a range of parameters we consider, Δ_{neo} reproduces the form of the $(\Delta_{bs} + \Delta_{cur}) = (\Delta_{bs} + \Delta_{cur})(w)$ curve providing self-healing (e.g. see Fig.F.1 of Appendix F).

In Fig.4.17 we define w_c as a solution of $\Delta_{neo}(w) = 0$ to find $w_c \approx 3\rho_{\vartheta i}$ in the conventional tokamak geometry with $\varepsilon = 0.1$ in the absence of the Shafranov shift, plasma elongation and triangularity (equilibrium density and temperature gradients are $L_n^{-1} = 1$ with $\hat{\omega}_E = 0$, $L_{Tj} = 1$, $\tau \equiv T_e/T_i = 1$). We emphasise that this threshold physics is related to passing particle dynamics, and not the finite banana width effects of the trapped particles. A basis for the threshold is the result of the radial shift of drift islands described by the S function, Eq.2.37, and, in particular, the pressure gradient restoration across the magnetic island O-point at $w \sim \rho_{\vartheta i}$. As discussed in the previous section, the latter mainly arises from the behaviour of the σ -dependent part of the ion distribution function, $\sum_{\sigma} g_i^{(0,0),\sigma}$, at small w . In this sense, the relevant parameter for w_c is the ion poloidal Larmor radius, $\rho_{\vartheta i}$, and not the ion banana orbit width, ρ_{bi} .

We have to stress here that at this stage we still cannot consider the contribution of the polarisation current as being fully determined. Fig.4.16 shows the residual contribution to

⁵⁴The impact of the polarisation contribution from the vicinity of the magnetic island separatrix is addressed in Sec.4.4.

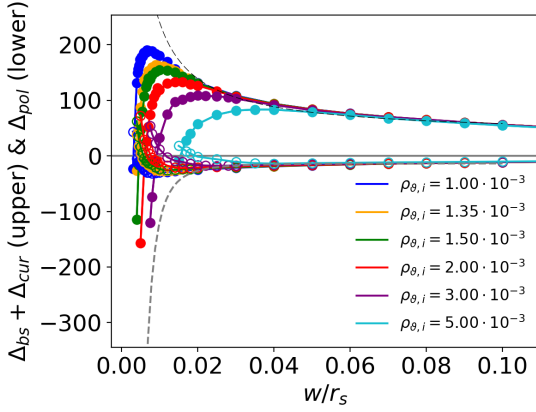


Figure 4.16: The sum of the bootstrap and curvature contributions, $\Delta_{bs} + \Delta_{cur}$, (filled markers, extremum in the upper half-plane) and the polarisation contribution, Δ_{pol} , (unfilled markers, extremum in the lower half-plane) against w/r_s for different $\rho_{\theta,i}$ with self-consistent Φ . The dashed black line $\propto 1/w$ and the dashed grey line $\propto 1/w^3$ indicate the limit of large magnetic island width. $\varepsilon = 0.1$, $\hat{L}_q = 1$, ion collisionality $\nu_i^* = 10^{-3}$. The equilibrium density and temperature gradients are $L_n^{-1} = 1$, $L_{Tj}^{-1} = 1$.

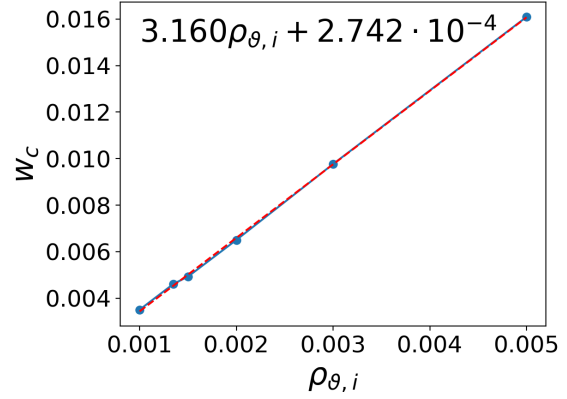


Figure 4.17: The full critical magnetic island width, w_c , defined as a solution of $\Delta_{neo}(w) = 0$ as a function of the ion poloidal Larmor radius, $\rho_{\theta,i}$. The red dashed line is the best fit line that provides the approximation. w_c and $\rho_{\theta,i}$ are normalised to the radius of the rational surface, r_s . $\varepsilon = 0.1$, $\hat{L}_q = 1$, ion collisionality $\nu_i^* = 10^{-4}$. The equilibrium density and temperature gradients are $L_n^{-1} = 1$ with $\hat{\omega}_E = 0$, $L_{Tj}^{-1} = 1$.

the island evolution, Δ_{pol} , when the island propagation frequency, ω , is zero. To conclude if the polarisation term is stabilising or destabilising, we have to find its ω dependence and its sign at the island propagation frequency which will be addressed in the following section.

4.4 Polarisation contribution and island propagation frequency

To determine the island propagation frequency, we return to the system of Eqs.2.9,2.10. Eq.2.9 provided the marginal magnetic island half-width, w_c . Eq.2.10 represents the toroidal torque balance [53] and thus makes the island propagation frequency dependent on the dissipation processes in the plasma included in a model. Following [53], we leave the effects of error fields and plasma sheared flows beyond the scope of this work. Therefore, the only source of dissipation in this study is the collisional dissipation around the trapped-passing boundary in pitch angle space, which provides a dominant contribution to the island propagation frequency.

Once a full solution of the ϑ -averaged drift kinetic equation to leading order in Δ is determined (Eq.2.35 in the dissipative layer and Eq.2.40 outside the layer) with the electrostatic potential calculated self-consistently from plasma quasi-neutrality, we calculate the current density perturbation parallel to the field lines, J_{\parallel} , and then substitute it into Eq.2.10 to determine ω_E .⁵⁵ Eq.2.10 is the integrated through the island $\sin \xi$ component of Ampère's law written along to the

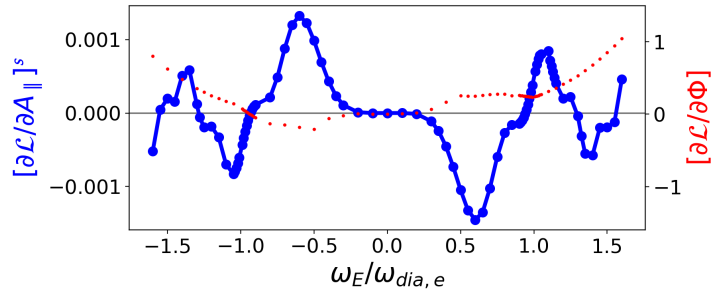


Figure 4.18: (left) The integrated through the island sine component of $\partial\mathcal{L}/\partial A_{\parallel}$ plotted against ω_E with the self-consistent electrostatic potential. (right) $\partial\mathcal{L}/\partial\Phi$, integrated through the island region, plotted against ω_E for the model potential, $\hat{\Phi} = \hat{\omega}_E L_{n0}^{-1} \hat{w} \hat{\psi}$ (circle red markers). The Lagrangian density, \mathcal{L} , is given by Eq.2.8. Solutions of $[\partial\mathcal{L}/\partial A_{\parallel}]^s(\omega) = 0$ and $[\partial\mathcal{L}/\partial\Phi](\omega) = 0$ match at $\omega_E = -0.93\omega_{dia,e}$. Ion collisionality $\nu_i^* = 10^{-4}$, $\varepsilon = 0.1$, $\hat{L}_q = 1$. The equilibrium density and temperature gradients are $L_{n0}^{-1} = 1$, $L_{Tj}^{-1} = 1$.

field lines. The left hand side of Eq.2.10 is denoted by $[\partial\mathcal{L}/\partial A_{\parallel}]^s$, i.e. the integrated through the island sine component of $\partial\mathcal{L}/\partial A_{\parallel}$. It is a function of ω_E and thus is a function of ω , and a root of $[\partial\mathcal{L}/\partial A_{\parallel}]^s(\omega) = 0$ provides the island propagation frequency, ω_0 . In Fig.4.18, we plot $[\partial\mathcal{L}/\partial A_{\parallel}]^s$ against ω_E . The Lagrangian is calculated based on the full distribution function. However, as stated above, the layer $g_j^{(0)}$ provides the dominant

⁵⁵As noted above, $\omega - \omega_E$ is independent of the reference frame. Thus, ω_E in the island rest frame provides the ω dependence in the frame, in which the radial electric field is zero far from the island.

contribution to Eq.2.10.

As we can see from Fig.4.18, there is a number of roots that satisfy the equation: $\hat{\omega}_E = \{\dots - 1.28, -0.93, 0, 0.94, 1.29, \dots\}$. We note that these values are obtained for the self-consistent electrostatic potential that provides plasma quasi-neutrality. ω_0 is one of the roots of $[\partial\mathcal{L}/\partial A_{\parallel}]^s(\omega) = 0$. Although, multiple solutions of $[\partial\mathcal{L}/\partial A_{\parallel}]^s(\omega) = 0$ provide an array of possible ω_0 values⁵⁶, this is still sufficient to analyse the stability of the polarisation current contribution, as we shall see later in this section. In [53], the island propagation frequency has been found to be in the direction of the electron diamagnetic frequency with $\omega_0 = 1.25\omega_{dia,e}$ at $L_{n0} = 1.$, $L_{Te} = 1$. In [86], the island propagation frequency is also found to be in the direction of $\omega_{dia,e}$ but scales as $(1 - \eta_e)\omega_{dia,e}$, where $\eta_e = L_{n0}/L_{Te}$. Both solutions are located within the range of possible roots for ω_E determined above. In contrast, in [87] the island propagation frequency has been found to be in the direction of the ion diamagnetic frequency, $\omega_{dia,i}$, in experiments with the co-injected NBI beam. Substituting $\varepsilon = 0.1$ and $\eta_i = 1$ into the scaling presented in [87], we obtain $\omega_0 = 1.11\omega_{dia,i}$.

Before we consider the polarisation current as a function of the island propagation frequency, let us discuss the polarisation current that arises from a narrow layer in the vicinity of the magnetic island separatrix relative to its external contribution that comes from the region outside the magnetic island. [53] provides the analysis valid outside the magnetic island separatrix and requires island scale lengths greater than $\varepsilon^{1/2}\rho_{\partial i}$. This then excludes the separatrix layer from the analysis (e.g. Fig.F.3), being though still sufficient for the accurate determination of the bootstrap drive in the limit of large islands. The polarisation current contribution has been found to be negative, i.e. stabilising at ω_0 (see Eq.85 of [53]). A thin boundary layer that surrounds the separatrix of the magnetic island has been shown to provide a significant contribution to the polarisation current [82, 68, 61]

⁵⁶The NTM is associated with the perturbation of the vector potential parallel to the magnetic field lines, A_{\parallel} , and ω_0 has to satisfy Eq.2.10, i.e. $[\partial L/\partial A_{\parallel}]^s(\omega) = 0$. In the following chapter we analyse the stability of secondary modes associated with the electrostatic perturbation and employ Eq.2.11, $\partial\mathcal{L}/\partial\Phi = 0$, integrated over space to provide the dispersion relation and to calculate the eigen frequency. In Fig.4.18 we plot $\partial\mathcal{L}/\partial\Phi$ integrated through the island as a function of ω_E , $[\partial\mathcal{L}/\partial\Phi](\omega_E)$, imposing $\hat{\Phi} = \hat{\omega}_E L_{n0}^{-1} \hat{w} \hat{\psi}$ for the electrostatic potential just as an illustration. $[\partial\mathcal{L}/\partial\Phi](\omega_E) = 0$ has two roots: $\hat{\omega}_E = \{-0.93, 0\}$. Omitting the trivial solution, we have $\omega_E = -0.93\omega_{dia,e}$ in the island rest frame. The interesting fact is that sets of solutions of $[\partial L/\partial A_{\parallel}]^s(\omega) = 0$ with the self-consistent electrostatic potential and sets of solutions of $[\partial\mathcal{L}/\partial\Phi] = 0$ with $\hat{\Phi} = \hat{\omega}_E L_{n0}^{-1} \hat{w} \hat{\psi}$ overlap.

and to invert its sign making the polarisation contribution, Δ_{pol} , destabilising [50, 88, 89]. [82, 50, 88, 89] investigate the effect of the polarisation current employing the plasma fluid description, i.e. imposing the Pfirsch-Schluter regime, while the low collisionality plasma has been assumed in this study⁵⁷. [61] employs the gyro-kinetic model to determine the island propagation frequency dependence of the MRE polarisation contribution, also covering the coupling to the electron drift waves, i.e. allowing $0 \leq \omega/\omega_{dia,e} \leq 1$. The polarisation current was also calculated in [90, 91] from the drift kinetic theory, and in [63, 64] from the gyro-kinetics and then compared to the perturbative analytic results. Although the listed works include the layer contribution to Δ_{pol} , they all impose a model potential. This is crucial, as the polarisation current is associated with a difference in the electron and ion responses to the magnetic perturbation and thus is determined by the electric field required to keep plasma quasi-neutral. In this study, the electrostatic potential is determined from plasma quasi-neutrality as discussed in Chapter II.

4.4.1 The polarisation current contribution with the model $\propto \sqrt{S}$ diffusion

As mentioned above, *H96* imposes a model radial diffusion and captures only the region outside the magnetic island separatrix, and hence excludes the separatrix layer contribution to the parallel current density from the analysis (e.g. see Fig.F.3). In [53], $\Delta_{pol} \propto -\omega [\omega - \omega_{dia,e}(1 + \eta_i)] < 0$, i.e. has been found to be stabilising in the limit of large w . [63, 64] still imposes $\Gamma_\psi = -D\partial n/\partial\psi$ but captures the region around the island separatrix. The latter makes Δ_{pol} destabilising at certain ω .

In this subsection we address the model $\propto \sqrt{S}$ diffusion introduced in Sec.4.2. In Fig.4.19, Table 4.1, Table 4.2 we compare the contributions to the cosine component of the parallel current density perturbation, i.e. the space integral on the right hand side of Eq.4.12, from inside and outside the separatrix of the magnetic island for different $\rho_{\theta i}$, w and \hat{v}_i for this case.

⁵⁷To investigate the bootstrap drive, the low collisionality plasma is required.

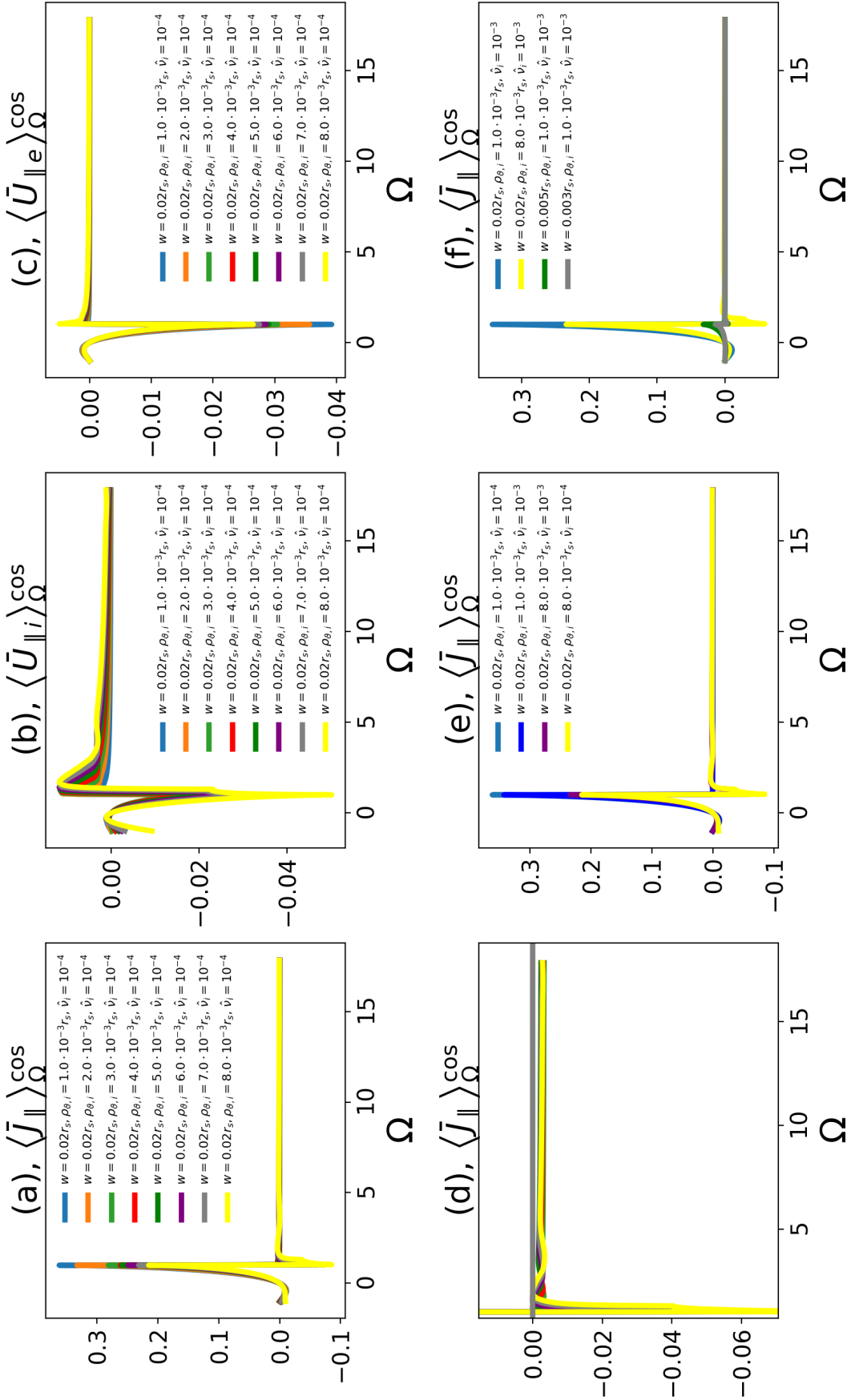


Figure 4.19: (a) The cosine component of the ϑ -averaged parallel current density perturbation integrated over ξ at fixed Ω , $\langle \bar{J}_{\parallel} \cos \xi \rangle_{\xi}^{\Omega}$, plotted against Ω for different $\rho_{\theta i}$. The in-phase component of the ion (b)/electron (c) parallel flow averaged over ϑ and over ξ at fixed Ω plotted against Ω for different $\rho_{\theta i}$. (d) Zoom of (a) outside the magnetic island separatrix, i.e. $\Omega \geq 1$. (e) $\langle \bar{J}_{\parallel} \cos \xi \rangle_{\xi}^{\Omega}$ for different \hat{v}_i . (f) $\langle \bar{J}_{\parallel} \cos \xi \rangle_{\xi}^{\Omega}$ for different w .

$\int_{-1}^1 \langle \bar{J}_{\parallel} \cos \xi \rangle_{\xi}^{\Omega} d\Omega$ vs. $\int_1^{\Omega_{fin}} \langle \bar{J}_{\parallel} \cos \xi \rangle_{\xi}^{\Omega} d\Omega$			
$\rho_{\vartheta i}$	$\int_{-1}^1 \langle \bar{J}_{\parallel} \cos \xi \rangle_{\xi}^{\Omega} d\Omega$	$\int_1^{\Omega_{fin}} \langle \bar{J}_{\parallel} \cos \xi \rangle_{\xi}^{\Omega} d\Omega,$ $max(\hat{\psi}) = 2.9,$ $w = 0.02r_s$	$\int_1^{\Omega_{fin}} \langle \bar{J}_{\parallel} \cos \xi \rangle_{\xi}^{\Omega} d\Omega,$ $max(\hat{\psi}) = 10.,$ $w = 0.02r_s$
$1.0 \cdot 10^{-3}r_s$	0.0801884964943	-0.0401392885124	-0.08379370129052
$2.0 \cdot 10^{-3}r_s$	0.0733667684839	-0.0388039440297	-0.08197527291581999
$3.0 \cdot 10^{-3}r_s$	0.0595189600977	-0.0523387088605	-0.10990103866624
$4.0 \cdot 10^{-3}r_s$	0.0550939317948	-0.0485169637716	-0.10056931082046
$5.0 \cdot 10^{-3}r_s$	0.055130353552	-0.0406898886297	-0.08276866300038
$6.0 \cdot 10^{-3}r_s$	0.0517537477945	-0.0474968529734	-0.09396710170214001
$7.0 \cdot 10^{-3}r_s$	0.0469708166399	-0.051688518276	-0.09846639999317999
$8.0 \cdot 10^{-3}r_s$	0.0395467334553	-0.0600175912761	-0.11050108250526

Table 4.1: Area under the $\langle \bar{J}_{\parallel} \cos \xi \rangle_{\xi}^{\Omega}$ curve inside, $-1 \leq \Omega \leq 1$, and outside the magnetic island, $\Omega \geq 1$ for a different right limit, i.e. maximum value of ψ/w . $\hat{\psi} = 2.9$ corresponds to 1.45 island widths, and $\hat{\psi} = 10$ corresponds to 5 island widths. $w = 0.02r_s$, $\hat{\nu}_i = 10^{-4}$, $\varepsilon = 0.1$, $\hat{L}_q = 1$, $\eta_i = 1$. The presented data corresponds to Fig.4.19, (a).

In Fig.4.19 the contribution from inside the separatrix is finite and decreases with the ion poloidal Larmor radius. In contrast, a spike outside the separatrix increases with $\rho_{\vartheta i}$, which makes both (inside and outside the separatrix) contributions comparable at large $\rho_{\vartheta i}$ even at the distance of $\approx 1 - 2$ island widths from the separatrix. In contrast, when $\rho_{\vartheta i}$ is small, the layer contribution dominates the external contribution at the distance of ≈ 2 island widths from the separatrix and is almost balanced by the external contribution at ≈ 5 island widths from the separatrix. An increase in $\hat{\nu}_i$ from 10^{-4} to 10^{-3} reduces the layer contribution inside the separatrix in this model as well as the outer contribution at small $\rho_{\vartheta i}$ (see Fig.4.19, (e) and Tables 4.1,4.2). At large $\rho_{\vartheta i}$ though, both inner and outer contributions compensate each other. Changes in $J_{\parallel} \cos \xi$ due to the reduction in w (see Fig.4.19, (f)) are more rapid as the radial shift of S in p_{φ} space is $\bar{p}_{\varphi} \propto \hat{\rho}_{\vartheta i}/\hat{w} = \rho_{\vartheta i}\psi_s/w^2$.

The results presented in Fig.4.19 and Tables 4.1,4.2 are obtained for the model diffusion. However, even this simplified case shows the significance of the separatrix layer ξ contribution. In [64] it has been concluded that the current density contribution from a thin boundary layer in the vicinity of the island separatrix and the external contribution from outside the island almost cancel out at large w . Roughly, we also can see this in Tables 4.1,4.2 for the model diffusion. At small w though, the layer contribution is found to be dominant in [64]. [64] treats diffusion perturbatively outside the magnetic island and drops collisions in the separatrix layer keeping the diffusion and parallel streaming to leading order. The

$\int_{-1}^1 \langle \bar{J}_{\parallel} \cos \xi \rangle_{\xi}^{\Omega} d\Omega$ vs. $\int_1^{\Omega_{fin}} \langle \bar{J}_{\parallel} \cos \xi \rangle_{\xi}^{\Omega} d\Omega$			
$\rho_{\vartheta i}$	$\int_{-1}^1 \langle \bar{J}_{\parallel} \cos \xi \rangle_{\xi}^{\Omega} d\Omega$	$\int_1^{\Omega_{fin}} \langle \bar{J}_{\parallel} \cos \xi \rangle_{\xi}^{\Omega} d\Omega,$ $max(\hat{\psi}) = 2.9,$ $w = 0.02r_s$	$\int_1^{\Omega_{fin}} \langle \bar{J}_{\parallel} \cos \xi \rangle_{\xi}^{\Omega} d\Omega,$ $max(\hat{\psi}) = 10.,$ $w = 0.02r_s$
$1.0 \cdot 10^{-3}r_s$	0.0772334825588	-0.027573515526	-0.0576922054224
$2.0 \cdot 10^{-3}r_s$	0.0712222449229	-0.0331705387838	-0.06993131861773999
$3.0 \cdot 10^{-3}r_s$	0.0592157718941	-0.0398634783683	-0.0839597436284
$4.0 \cdot 10^{-3}r_s$	0.0547498468307	-0.0480637058615	-0.10007060513102001
$5.0 \cdot 10^{-3}r_s$	0.0555873563479	-0.0426389885447	-0.08762728862948001
$6.0 \cdot 10^{-3}r_s$	0.0542500573304	-0.0438184246256	-0.0883043616248
$7.0 \cdot 10^{-3}r_s$	0.0507779220968	-0.050239549732	-0.09923754891568
$8.0 \cdot 10^{-3}r_s$	0.0477558648903	-0.0540243193465	-0.10368453130371999

Table 4.2: Same as Table 4.1, except for $\hat{\nu}_i = 10^{-3}$.

tokamak drift effects are excluded from the model in [64]⁵⁸. In [64] the diffusion coefficient is assumed to be constant, however, the drive term in the particle distribution function takes into account the ξ dependence at fixed Ω . The latter is crucial for the distribution function curvature right outside the separatrix. Therefore, a more accurate treatment of the region around the magnetic island separatrix is required in our analysis. In the following subsection we address the parallel current density based on the full solution of Eqs.D.60,D.61, i.e. retaining the actual S diffusion terms.

4.4.2 The polarisation current contribution based on the full RDK-NTM solution

Similar to Fig.4.19, in Fig.4.20 we plot the cosine component of the orbit averaged parallel current density perturbation against Ω but based on a full solution of Eq.2.36 localised around λ_c in the collisional dissipative layer and Eq.2.40 outside the layer in pitch angle space. As we can see from Fig.4.20, there is an additional destabilising layer contribution to J_{\parallel} right outside the magnetic island separatrix similar to that shown in Fig.2 of [63]. However, this part of the separatrix layer contribution was not allowed in the model we took in Sec.4.4.1. At small $\rho_{\vartheta i}/w$, the separatrix layer contribution now slightly dominates the plasma response. As we increase the ion poloidal Larmor radius and approach the NTM threshold, the contribution around the island separatrix grows and dominates over

⁵⁸In accordance with Chapter II, the radial shift in S is associated with the magnetic drift in a tokamak.

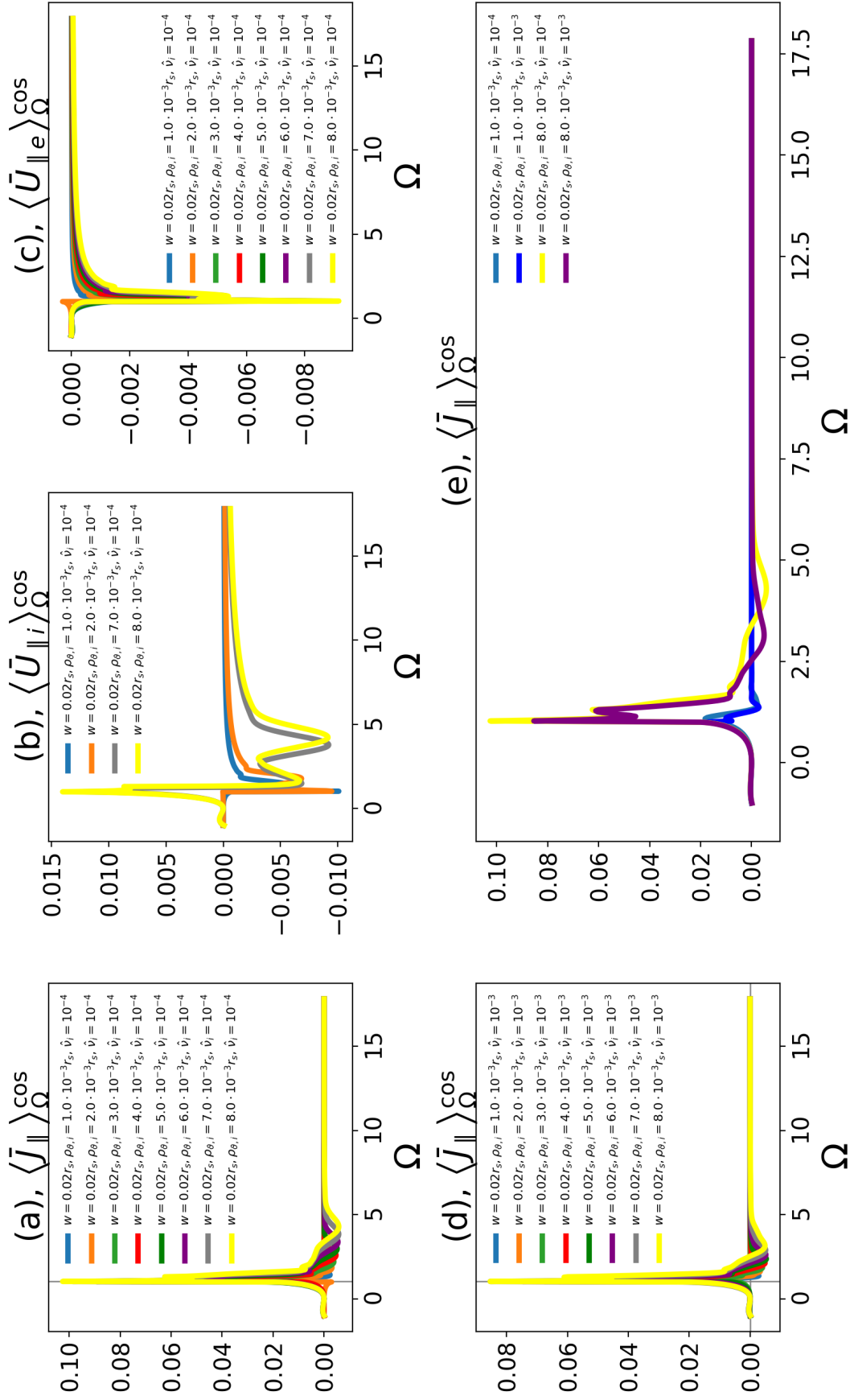


Figure 4.20: (a) The cosine component of the ϑ -averaged parallel current density perturbation integrated over ξ at fixed Ω , $\langle \bar{J}_{\parallel} \cos \xi \rangle_{\xi}^{\Omega}$, plotted against Ω for different $\rho_{\theta i}$. The in-phase component of the ion (b) / electron (c) parallel flow averaged over ϑ and over ξ at fixed Ω plotted against Ω for different $\rho_{\theta i}$. (d) Same as (a) except for $\hat{\nu}_i = 10^{-3}$. (e) $\langle \bar{J}_{\parallel} \cos \xi \rangle_{\xi}^{\Omega}$ at small and large $\rho_{\theta i}$.

the contribution outside this layer (e.g. see Fig.4.20(e)). This is in agreement with [64].

In Fig.4.21 we plot the contribution of the polarisation current against ω_E ⁵⁹. As we can see from the figure, the set of solutions of $[\partial\mathcal{L}/\partial A_{\parallel}]^s(\omega) = 0$ provides $\Delta_{pol} > 0$, i.e. destabilising polarisation term. This kind of behaviour can be explained as follows: as was mentioned above, the effect of ω_E is similar to that from $\rho_{\partial i}$, as it appears via the equilibrium electrostatic potential away from the island. The increase in $\rho_{\partial i}$ increases the separatrix layer contribution to $J_{\parallel} \cos \xi$. ω_E acts in a similar way making Δ_{pol} more destabilising. Δ_{pol} scales as ω_E^2 except for the region in the vicinity of $\omega_E = 0$. The ω_E^2 behaviour is consistent with previous works: [53] outside the magnetic island separatrix at large w , [68] without and [61] with included coupling to the electron drift wave in gyro-kinetics, [90, 91] in the drift kinetic approach at large w and [63, 64] in the slab formulation^{60,61}. However, the behaviour of Δ_{pol} around $\omega_E = 0$ is more complicated and is beyond the main purpose of the current NTM threshold study. The similar island propagation frequency dependence of Δ_{pol} has been obtained in [68, 61, 90, 91, 63, 64]. [68, 63, 64] excludes $0 \leq \omega \leq \omega_{dia,e}$. In [91] the sign change in range $-1 \lesssim \hat{\omega}_E \lesssim 1$ is explained by the competition of the toroidal precession and the island propagation frequency.

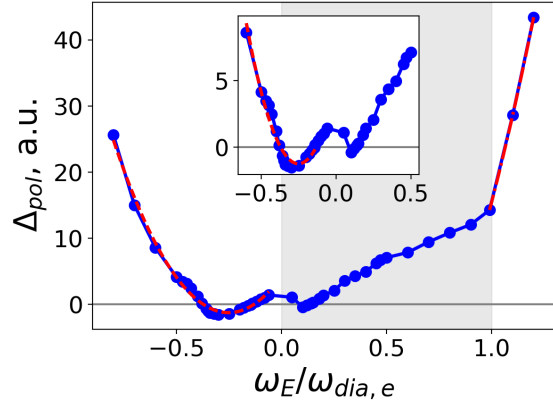


Figure 4.21: The polarisation contribution to the evolution of the magnetic island vs. ω_E (note: region of $\Delta_{pol} < 0$ is stable). The ω_E dependence in the island rest frame provides the ω_0 dependence in the reference frame, where the radial electric field is zero far from the island. Inset: zoom in a region $\Delta_{pol}(\omega_E) = 0$. Red curves indicate a parabolic approximation. The ω_E^2 behaviour is predicted in the analytic limit of large w . Ion collisionality $\nu_i^* = 10^{-4}$, $\varepsilon = 0.1$, $\hat{L}_q = 1$, $L_{n0}^{-1} = -0.1$. $0 \leq \omega_E \leq \omega_{dia,e}$ corresponds to a region of coupling to electron drift waves. For these parameters: $\omega_0/\omega_{dia,e} \in \{\dots, -1.04, -0.93, 0, 0.92, \dots\}$.

⁵⁹There is no polarisation current at the zero island propagation frequency and hence this point has been excluded from the dependence.

⁶⁰They all impose a model potential.

⁶¹Roughly, the electrostatic potential is proportional to ω_E . Dropping the pressure and viscosity gradients in the force balance and replacing the velocity with the $\mathbf{E} \times \mathbf{B}$ drift velocity, we obtain $J_{\perp,pol} \propto \omega_E^2$ for the polarisation current.

4.5 Summary

The first part of this chapter describes the solution technique used to solve the reduced drift kinetic equation for the NTM problem in the conventional tokamak approximation. The technique is based on the *shooting* method employed to solve a 3D integro-differential equation in $\{S^{\pm/t}, \lambda, \hat{V}; \sigma\}$ space. The momentum conservation term in the pitch angle scattering collision operator as well as the electrostatic potential have been introduced iteratively. The first one is required for an accurate calculation of the "bootstrap" current drive. Indeed, as has been demonstrated in [53], the momentum conservation term eliminates the island propagation frequency dependence of the bootstrap current. The electrostatic potential is determined to provide the plasma quasi-neutrality. The algorithm has been implemented in a new code, *RDK-NTM*, developed in Python. It has been checked that the solution converges and satisfies the equation, Eq.2.35 in the dissipation layer, i.e. $\lambda \in [\lambda_p, \lambda_c] \cup (\lambda_c, \lambda_t]$, and Eq.2.40 in external regions outside the layer, i.e. $\lambda \in [0, \lambda_p] \cup [\lambda_t, \lambda_{fin}]$, with matching conditions at the trapped/passing boundary, $\lambda = \lambda_c$, given by Eq.3.1, and the boundary conditions as well as the plasma quasi-neutrality requirement. The obtained numerical results for moments of the particle distribution function have been successfully benchmarked against an analytic solution provided by the conventional tokamak neoclassical theory valid in the limit of large islands (e.g. Figs.F.3 and 4.13,4.16,4.21). It has been checked that the RDK-NTM solution matches the analytic limit of large magnetic islands (compared to the ion poloidal Larmor radius) and that the island propagation frequency dependence of the polarisation current is consistent with the earlier theoretical results obtained in the presence of the layer polarisation current contribution. The latter arises in the vicinity of the magnetic island separatrix. The code has been tested⁶² and then adopted to solve the secondary mode problem that will be the subject of the following chapter⁶³.

The second part of the chapter focuses on the obtained results. Employing weak collisional

⁶²The reduced drift kinetic NTM (RDK-NTM) solver has been tested: it has been checked that the solution (its layer and external contributions) converges and provides the plasma quasi-neutrality condition. The solver module has been tested for a number of simplified problems that allow an analytic solution (homogeneous/non-homogeneous equations with constant/factorised/non-factorised coefficients).

⁶³The RDK-NTM code has been adopted to analyse the stability of secondary modes in a tokamak. The corresponding solution has been benchmarked against the conventional bump-on-tail problem and the COBBLES results in a pure diffusion case and in the presence of the dynamical friction. They are found to be in good agreement.

dissipation, we solve the drift kinetic equation. The perturbative approach we apply breaks down in a narrow region in pitch angle space in the vicinity of the trapped-passing boundary. In this region, collisional dissipation is no longer negligible and S cannot be used to describe the ion/electron streamlines. Here we employ the momentum-conserving collision operator (which is dominated by the pitch angle scattering contribution due to the dissipation layer thinness) and solve the 2D boundary layer problem to match solutions in the trapped and passing regions provided by the perturbative theory. Once the electron/ion solution of the orbit-averaged drift kinetic equation consistent with plasma quasi-neutrality is obtained, we calculate the parallel current density perturbation localised around the resonant surface, J_{\parallel} , that contributes to the time evolution of the magnetic island width. We have calculated contributions of neoclassical "bootstrap" and "polarisation" currents to the magnetic island evolution and have demonstrated that the plasma response to the NTM magnetic perturbation is stabilising in a certain range of w . For the small inverse aspect ratio circular cross section tokamak plasma, a threshold island width below which the tearing mode is stable is $w \leq w_c = 2.67\rho_{\vartheta i}$ [73, 93, 74] and $w \leq w_c = 3.16\rho_{\vartheta i}$ from full orbit-averaged (DK-NTM) and low collisionality plasma orbit-averaged (RDK-NTM) solutions, respectively. This result, $w_c = 3\rho_{\vartheta i}$, provides the experimentally observed self-healing of small magnetic islands. The island propagation frequency dependence of the polarisation contribution has been determined. The analysis includes the contribution to the polarisation current that comes from a narrow separatrix layer around the magnetic island as well as the outer contribution that arises outside the island separatrix. They act in opposite directions and depend on $\rho_{\vartheta i}$, w , ω_E and \hat{v}_i for certain equilibrium density and temperature gradients, L_{n0} and L_{Tj} . All these results are novel in tokamak geometry and include physics inside and outside the magnetic island. They provide a new understanding of how finite orbit width effects influence the island threshold and are crucial for the NTM stabilisation on ITER and future tokamak devices. The next chapter focuses on the stability analysis of secondary modes driven by an island in phase space. Despite having a different physical origin, this problem being associated with the island-like structure shares the mathematical basis with the NTM problem.

Chapter V

5 Stability analysis of secondary modes, driven by a phase space island

In this chapter⁶⁴ we discuss a new theoretical approach that is based on the Hamiltonian formalism and employed to investigate the stability of islands in phase space, generated by trapping of energetic particles (EPs) in plasma waves in a tokamak [95, 96]. Working in terms of the Hamiltonian function allows for a reduction in dimensionality from a 6D dynamics in phase space to a 2D dynamics of a phase space island. Depending on the form of the Hamiltonian, the results produced below can be applied to a reduced pure electrostatic slab problem or can be extended further to a tokamak case with the magnetic field included. We find this approach convenient to describe the stability of EP-MHD modes, i.e. MHD modes that are driven by EPs (e.g. toroidal Alfvén eigenmodes or TAEs, EP-driven geodesic acoustic modes or EGAMs, fishbones). The problem of a single isolated EP-MHD mode then reduces to a 2D Hamiltonian dynamics system around a phase space island. The latter is usually introduced to describe the conventional Langmuir wave/bump-on-tail problem.

We solve the Fokker-Planck equation in the presence of an effective velocity space drag and diffusion to calculate a *perturbed* equilibrium associated with these phase space islands. Its stability is then investigated through the Vlasov/Fokker-Planck – Poisson system. The Lagrangian of this system provides the secondary mode dispersion relation⁶⁵ and allows one to estimate the mode onset. The secondary instabilities have been found in a certain range of primary mode numbers and primary island widths. The maximum secondary mode growth rate is obtained when the associated resonant velocity is in the vicinity of the primary island separatrix. Hence, the onset of the secondary mode can be prevented if the primary mode number is the lowest available.

⁶⁴The work and results presented in this chapter have previously been published in A. V. Dudkovskaia, X. Garbet, M. Lesur, H. R. Wilson *J. Phys.: Conf. Ser.* 1125 (2018) 012009 and A. V. Dudkovskaia, X. Garbet, M. Lesur, H. R. Wilson *Nucl. Fusion* **59** (2019) 086010.

⁶⁵Here we have to address Eq.2.11 integrated through the phase space island as instabilities we consider are now associated with the perturbations of the electrostatic potential, while Eqs.2.9,2.10 provide the NTM dispersion relation.

5.1 Specification of the problem

Interactions between particles and waves play a crucial role in a number of applications. In the burning plasma of a reactor, EPs are considered for additional heating and current drive. They can be generated by NBI or resonance frequency (RF) heating, or produced by fusion reactions. These EPs can excite Alfvén eigenmodes resonating with plasma waves. This, in turn, results in EP losses degrading heating and confinement. Since the alpha particles generated by the DT reaction are expected to be the main heating source in a future tokamak reactor, the EP losses have to be predicted and suppressed/prevented in an optimal situation. In the simplest case, this problem becomes the bump-on-tail problem with the Maxwellian thermal electron background neutralised by steady ions, and the fraction of fast electrons described by a shifted Maxwellian (see Fig.5.1). The latter is localised in the vicinity of a beam velocity, V_b .

This is a 2D problem, $\{x, V\}$, where x is the spatial coordinate and V is the velocity variable. The electron distribution function experiences a positive slope around V_b making the mode unstable, provided V_b is large enough. In the original work [97], this was applied to Langmuir waves, and also allows to be extended to a tokamak case, e.g. to consider toroidal Alfvén modes [98, 99]. The drive for the bump-on-tail instability is provided by the

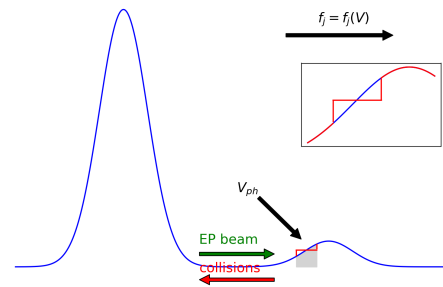


Figure 5.1: Sketch of the bump-on-tail distribution function. The local maximum is localised around V_b .

particle-wave resonance that occurs when the particle velocity matches the phase velocity of the wave, $V_{ph} = \omega_0/k_0$ with ω_0 being the mode pulsation frequency and k_0 its wave number. There is a number of scenarios of the evolution of a single mode (ω_0, k_0) [100, 101] depending on the dissipation rate. The saturation towards steady state occurs as a result of the island formation in the vicinity of the resonant velocity, $V = V_{ph}$, provided the dissipation is sufficient. The particle distribution is then found to be flattened inside the island, which decreases the drive. Around the island separatrix though, the distribution function gradient experiences steepening which is prone to instabilities. Saturation is also allowed in the collisionless plasma via the plateau formation in velocity space inside the

island, and the onset of O’Neil-Mazitov oscillations [102, 103, 104]. Here the analysis is restricted to the case of finite dissipation. The primary mode here is to be understood as an unstable wave (ω_0, k_0) that evolves towards the phase space island formation [96]. Within the island, a plateau forms surrounded by the separatrix. Secondary modes are then expected to arise at the edges of this plateau, i.e. near the island separatrix. Their onset in the vicinity of the phase space island is the subject of the current chapter, where we exploit some mathematical similarities with our study of NTMs in earlier chapters.

Seeking secondary instabilities, we address the conventional Vlasov/Fokker-Planck – Poisson system, i.e. a system of Vlasov/Fokker-Planck equations for each particle species, j , coupled to Poisson’s equation

$$\varepsilon_0 \nabla^2 \Phi = - \sum_j e Z_j \int_{\mathbb{R}} f_j d\mathbf{V}. \quad (5.1)$$

Here we assume a system of three particle species: j labels thermal background of electrons and ions, as well as a fraction of EPs, i.e. energetic electrons/ions that trigger the bump-on-tail instability [96]. In toroidal coordinates, the particle distribution, f_j , is to be treated as $f_j = f_j(t, \psi, \vartheta, \zeta, \mathbf{V})$, where ψ is the poloidal flux, ϑ and ζ are the poloidal and helical angles, respectively. ζ is defined according to $m_0 \vartheta - n_0 \varphi - \omega_0 t$, where m_0/n_0 is the poloidal/toroidal primary mode number, φ is the toroidal angle, and ω_0 is the primary mode frequency.

The starting Vlasov/Fokker-Planck equation allows to be rewritten through Hamilton’s equations for a pair of angular and action variables, $\{\boldsymbol{\alpha}, \mathbf{J}\}$ [105, 96]. In the plasma of a tokamak, the components of \mathbf{J} are represented by three adiabatic invariants of motion of charged particles. Imposing a single perturbation, associated with the phase space island, we write $\mathcal{H}_0(\mathbf{J}, \boldsymbol{\alpha}, t) = \mathcal{H}_{00}(\mathbf{J}) + h \cos(\mathbf{n}\boldsymbol{\alpha} - \omega_0 t)$ for the full primary Hamiltonian. Here \mathcal{H}_{00} is the unperturbed Hamiltonian, i.e. in the absence of the island, and $\mathbf{n} = (n_1, n_2, n_3)$ is a triplet of integers. We set $\xi = \mathbf{n}\boldsymbol{\alpha} - \omega_0 t$ to define a resonant surface by $\sum_{i=1}^3 n_i \Omega_i(\mathbf{J}) = \omega_0$ with $d\boldsymbol{\alpha}/dt = \boldsymbol{\Omega}(\mathbf{J})$. The action vector then reads $\mathbf{J} = \mathbf{J}_{res} + \mathbf{n}I$ near the resonant surface, where \mathbf{J}_{res} spans the resonant surface and I measures the distance to it (see Fig.5.2). Then one can verify that $\mathcal{H}_0(\mathbf{J}, \boldsymbol{\alpha}, t) = \mathcal{H}_{00}(\mathbf{J}_{res}) + CI^2/2 + h \cos \xi$, where C is the Hessian of the Hamiltonian on the resonant surface. To simplify the algebra below, we assume that

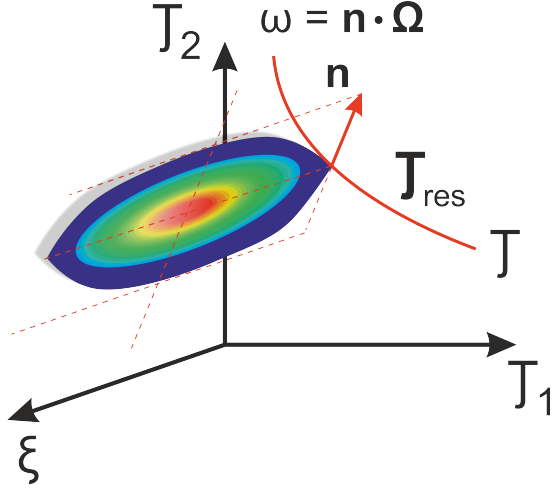


Figure 5.2: A phase space island near the resonant surface, $\mathbf{n} \cdot \boldsymbol{\Omega}(\mathbf{J}) = 0$ [96].

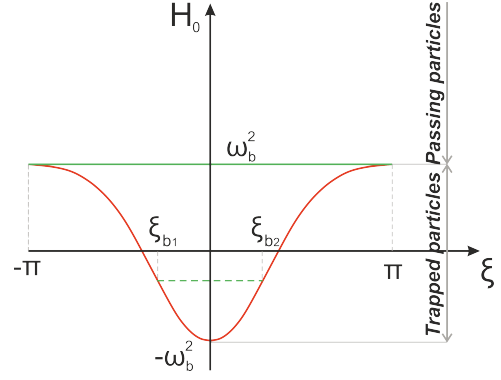


Figure 5.3: Sketch of H_0 against ξ at $p = 0$ [96]. ξ varies from $-\pi$ to π outside the phase space island and between the bounce points, $\xi_{b1,2}$, given by $H_0 = -\omega_b^2 \cos \xi_{b1,2}$, inside the island region.

h varies slowly over the island width. Setting $p = CI$, we find

$$H_0 = p^2/2 - \omega_b^2 \cos \xi \quad (5.2)$$

for a new full primary Hamiltonian. ω_b is the bounce frequency of deeply trapped particles (i.e. particles trapped in phase space, see Fig.5.3) defined as $\omega_b^2 = -Ch$. Here we highlight that a 6D dynamics in phase space can be reduced to a 2D dynamics of a phase space island, if two invariants of motion are located on the resonant surface.

In slab geometry in the absence of tokamak drifts, the starting equation simply reads

$$\frac{\partial f_j}{\partial t} + V \frac{\partial f_j}{\partial x} - \frac{eZ_j}{m_j} \frac{\partial \Phi}{\partial x} \frac{\partial f_j}{\partial V} = C_j(f_j) + \mathcal{S}, \quad (5.3)$$

where a combination of the collision operator, C_j , and the source, \mathcal{S} , is to be introduced below. The kinetic equation is to be solved for f_j , a time dependent particle distribution function, treated as a function of position, $\{\psi, \vartheta, \zeta\}/x$, and velocity, \mathbf{V}/V in the toroidal/slab formulation, respectively. The electrostatic potential, Φ , is to be considered as a function of position and time. For simplicity, we reduce the analysis to the (t, x) plane. Assuming that a primary wave has been developed and saturated towards an island-like structure, we impose $\Phi(x, t) = \Phi_0 \cos(k_0 x - \omega_0 t)$ for the potential. Then we find it convenient to work in the wave reference frame and define a new spatial coordinate $\xi = k_0 x - \omega_0 t$ conjugated to a momentum, $p = \partial \xi / \partial t = k_0 V - \omega_0$. Hence, we obtain

$H_0(x, V) = (k_0 V - \omega_0)^2/2 - k_0^2 (eZ_j/m_j) \Phi_0 \cos(k_0 x - \omega_0 t)$ for the Hamiltonian. It is equivalent to p as a velocity space variable, if the sign of p , denoted by σ_p , is kept as an extra variable. Defining the bounce frequency in the limit of deeply trapped particles as $\omega_b^2 = k_0^2 eZ_j \Phi_0/m_j$, we obtain Eq.5.2 for the full primary Hamiltonian in the (p, ξ) plane. Replacing $H_0(x, V)$ with $H_0(\psi, \varphi, \vartheta, \mathbf{V}) = V_{\parallel}^2/2 + \mu B + eZ_j \Phi(\psi, \varphi, \vartheta)$ [105], where $\mu = V_{\perp}^2/2B$ is the magnetic moment and B is the total magnetic field, we provide a generalisation of the problem to a magnetic configuration with toroidal geometry. Here $\Phi = \Phi_0 \cos \zeta$ (the ψ dependence of Φ_0 has been omitted for simplicity). We highlight that the guiding centre equations of motion that fully account for the magnetic drifts as well as their reduced formulation in slab geometry allow the Hamiltonian formulation. Thus, from a mathematical point of view EP-MHD problems, Langmuir wave and the TAE problems, become identical in the toroidal and slab cases, provided they are written through the Hamiltonian function.

Contours of constant H_0 plotted in the (p, ξ) plane describe an island-like structure and thus are to be referred to as an island in phase space. A new equilibrium, described by $f_{0,j}$, is to be determined from the Fokker-Planck equation, which now reads

$$\frac{\partial f_{0,j}}{\partial t} - \{H_0, f_{0,j}\} = C_j(f_{0,j}) + \mathcal{S}. \quad (5.4)$$

Here curly brackets denote the conventional Poisson bracket, i.e. $\{f, g\} = \frac{\partial f}{\partial \xi} \frac{\partial g}{\partial p} - \frac{\partial f}{\partial p} \frac{\partial g}{\partial \xi}$. Once $f_{0,j}$ is found, we analyse the stability of this new *perturbed* equilibrium, i.e. the stability of secondary waves, taken of the form $\Phi_{k\omega} e^{ikx - i\omega t} + c.c.$, where k and ω are their wave number and frequency, respectively. In the frame of the primary wave, these waves are $\Phi_{k\omega} e^{il\xi - i\delta\omega t} + c.c.$ with $l = k/k_0$ and $\delta\omega = \omega - l\omega_0$. We note that l is not necessarily integer. If the electrostatic potential has a form $\Phi(x, t) = \Phi_{\omega} e^{-i\omega t} + c.c.$, then the full Hamiltonian and the full EP distribution read $H(\xi, p) = H_0(\xi, p) + \delta H$ and $f_j(\xi, p) = f_{0,j}(\xi, p) + \delta f_j$ with $\delta H = h_{\omega}(\xi, p) e^{-i\delta\omega t} + c.c.$ and $\delta f_j = f_{j\omega}(\xi, p) e^{-i\delta\omega t} + c.c.$, respectively. Here $H_0(\xi, p)$ and $f_{0,j}(\xi, p)$ represent the new primary equilibrium, while δH and δf_j are perturbations associated with the secondary modes. $h_{\omega} = k_0^2 eZ_j \Phi_{\omega}/m_j$ is

$h_\omega(\xi, p) = h_{k\omega} e^{il\xi}$ ⁶⁶. Following Sec.2.1 of Chapter II, we introduce the Lagrangian⁶⁷:

$$\mathcal{L}(\omega) = \frac{\varepsilon_0}{2} \int_0^L dx |\nabla \Phi_\omega|^2 - \sum_j eZ_j \int_0^L dx \int_{\mathbb{R}} f_{j\omega}(\xi, p) \Phi_\omega^*(\xi, p) dV. \quad (5.5)$$

Here L is the characteristic length, chosen as a multiple of the primary period, $k_0 L = 2\pi j_0$, where j_0 is an integer. Poisson's equation is equivalent to the condition, where the Lagrangian density of the electro-magnetic field is extremum for any Φ_ω^* variation. $\mathcal{L}(\omega)$ of the form given by Eq.5.5 will provide the secondary mode dispersion relation.

Rewriting Eq.5.5 in terms of $\{p, \xi\}$, we have

$$\mathcal{L}(\omega, l) = -l^2 |h_{k\omega}|^2 + \sum_j \mathcal{L}_j(\omega) \quad (5.6)$$

with

$$\mathcal{L}_j(\omega) = \omega_{pj}^2 \int_{-\pi}^{\pi} \frac{d\xi}{2\pi} \int_{\mathbb{R}} f_j h_\omega^* dp \quad (5.7)$$

being the Lagrangian of a given particle species, and ω_{pj} is the plasma frequency of a species, $\omega_{pj}^2 = n_j (eZ_j)^2 / \varepsilon_0 m_j$. The first term on the right hand side of Eq.5.6 represents the field contribution. The distribution function is normalised to density of a considered species, n_j , in p coordinates, and hence $\int_{\mathbb{R}} f_j dp = 1$. $h_{k\omega} = k_0^2 eZ_j \Phi_{k\omega} / m_j$ is the perturbed Hamiltonian⁶⁸. The perturbed distribution, $f_{j\omega}$, is then a solution of the linearised Fokker-Planck equation that reads

$$-i\delta\omega f_{j\omega} - \{H_0, f_{j\omega}\} = \{h_\omega, f_{0,j}\}. \quad (5.8)$$

$f_{0,j}$ is a non-trivial function of $H_0(p, \xi)$, and hence the Poisson brackets $\{H_0, f_{j\omega}\}$ and $\{h_\omega, f_{0,j}\}$ generate multiples of the basic harmonic, $l\xi - \delta\omega t$. Away from the island though, $H_0 \simeq p^2/2$, and the corresponding solution becomes trivial. The system then behaves as if there is no interaction between primary and secondary waves. This illustrates the thermal background, provided thermal resonances occur far from the EP resonances. The second

⁶⁶ kx has to be replaced with $m\vartheta - n\varphi$ for the toroidal formulation, where m/n is the poloidal/toroidal secondary wave number.

⁶⁷The Lagrangian is the Lagrangian density integrated over space, i.e. $\mathcal{L} = \int \mathcal{L} d\mathbf{q}$. Note: in this chapter the notation \mathcal{L} will be used to denote the Lagrangian.

⁶⁸A constant normalisation factor has been omitted here for convenience. In our set of variables, $\{x, k_0 V - \omega_0\}$ instead of conventional $\{x, m_j V\}$, the scaling factor is $\varepsilon_0 k_0^2 L / A^2$, where $A = eZ_j k_0^2 / m_j$.

approach, which is to be run numerically, is to maintain the basic harmonics only, i.e.

$$-i\delta\omega f_{j\omega} - \{H_0, f_{j\omega}\} = \left\{ h_\omega, \langle f_{0,j} \rangle_\xi \right\}. \quad (5.9)$$

An angular bracket here indicates an averaging operator over ξ to be defined below. Finally, a full nonlinear solution can be calculated by switching from $\{\xi, p\}$ to $\{\xi, H_0; \sigma_p\}$ and will be discussed at the end of this chapter.

5.2 Primary equilibrium

We start with a calculation of a new primary equilibrium, described by $f_{0,j}$. $f_{0,j}$ is a solution of Eq.5.4 and represents the plasma response to an isolated phase space island, associated with the bump-on-tail instability. Imposing the Maxwellian behaviour for the background plasma, we solve Eq.5.4 for the EP fraction only, i.e. fast electrons/ions, whose population is small compared to the bulk plasma.

The right hand side of Eq.5.4 is represented by the Fokker-Planck collision operator that includes collisions on fast particles by the thermal, Maxwellian background. The initial form of this collision operator that acts on the EP distribution is

$$\begin{aligned} C_j + \mathcal{S} &= \\ &= 2\nu_j \frac{(1-\lambda B)^{1/2}}{B} \frac{\partial}{\partial \lambda} \Big|_\psi \left[\lambda(1-\lambda B)^{1/2} \frac{\partial}{\partial \lambda} \Big|_\psi \right] + \frac{1}{V^2} \frac{\partial}{\partial V} \left[V^3 \left(\nu_{slow} + \frac{\nu_{\parallel}}{2} V \frac{\partial}{\partial V} \right) \right], \end{aligned} \quad (5.10)$$

where ν_j , ν_{slow} and ν_{\parallel} are the pitch angle scattering, slowing down and parallel velocity diffusion rates, respectively. Following [106, 107], we project Eq.5.10 on the rational phase space surface to replace it with a combination of operators in p space. This reduces the dimension of the collision operator from 2D to 1D in velocity space. The Jacobian of the corresponding coordinate transformation can be found in [106]. After this procedure, we obtain

$$C_j(f_{0,j}) + \mathcal{S} = D_p \frac{\partial^2}{\partial p^2} \Big|_\xi (f_{0,j} - f_{eqm,j}) + \nu_{f,p} \frac{\partial}{\partial p} \Big|_\xi (f_{0,j} - f_{eqm,j}). \quad (5.11)$$

Here D_p and $\nu_{f,p}$ are the diffusion and dynamical friction coefficients in p space, related to the diffusion $\nu_{d,V}$ and friction $\nu_{f,V}$ rates in velocity space through $D_p = \nu_{d,V}^3(k_0/k)^2$ and $\nu_{f,p} = \nu_{f,V}^2(k_0/k)$, respectively [95, 96]. $f_{eqm,j}$ is the unperturbed distribution being introduced in the absence of the island in phase space, and appears as a dotted line in Fig.5.4. The Vlasov part of the Fokker-Planck equation [111] is

$$\frac{df_{0,j}}{dt} \equiv \frac{\partial f_{0,j}}{\partial t} - \tau \left[\partial_t H_0 - \langle \partial_t H_0 \rangle_\xi \right] \frac{\partial f_{0,j}}{\partial J} + p \frac{\partial f_{0,j}}{\partial \xi} \quad (5.12)$$

with J denoting the action variable, defined as

$$J(H_0, t) = \oint \frac{d\xi}{2\pi} p(t, \xi, H_0; \sigma_p),$$

and τ being the bounce period,

$$\tau = \oint \frac{d\xi}{2\pi} p^{-1}(t, \xi, H_0; \sigma_p)$$

(an angular bracket denotes the average over ξ and is to be introduced later in this section). Working in the wave reference frame and seeking the time-independent solution, we rewrite a system of Eqs.5.4,5.11,5.12 as

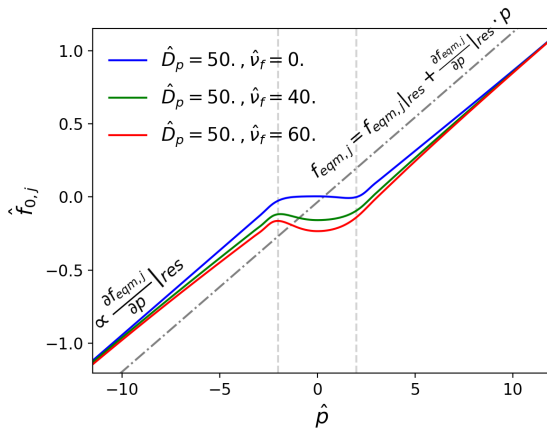


Figure 5.4: The EP distribution function $\hat{f}_{0,j}$ plotted against \hat{p} across the island O-point, i.e. $\xi = 0$, for arbitrary \hat{D}_p and $\hat{\nu}_{f,p}$. The solution, $\hat{f}_{0,j}$, is localised to the island vicinity, which allows the initial equilibrium distribution function to be Taylor expanded around the resonant surface. The dashed lines indicate the position of the phase space island separatrix, $\hat{H}_0 = \hat{\omega}_b^2$. Hats indicate the normalisation that has been chosen as in [95].⁶⁹

$$p(\xi, H_0; \sigma_p) \left. \frac{\partial f_{0,j}}{\partial \xi} \right|_{H_0} = D_p p^2(\xi, H_0; \sigma_p) \left. \frac{\partial^2}{\partial H_0^2} \right|_\xi (f_{0,j} - f_{eqm,j}) + [D_p + \nu_{f,p} p(\xi, H_0; \sigma_p)] \left. \frac{\partial}{\partial H_0} \right|_\xi (f_{0,j} - f_{eqm,j}), \quad (5.13)$$

where p has been replaced with a pair $\{H_0; \sigma_p\}$ and is considered as a function of ξ and H_0 for each σ_p . We find it convenient to define $g_{0,j} = f_{0,j} - f_{eqm,j}$ to measure a shift from the equilibrium state. $g_{0,j}$ represents a full solution of Eq.5.13. To solve Eq.5.13, we introduce a small parameter δ that characterises the ratio of time scales and comes from Eq.5.12,

⁶⁹ $\hat{f}_{0,j} = f_{0,j} \cdot (\partial f_{eqm}/\partial p|_{res})^{-1}$, $\hat{p} = p/(\gamma_L - \gamma_d)$, $\hat{H}_0 = H_0/(\gamma_L - \gamma_d)^2$, $\hat{D}_p = D_p/(\gamma_L - \gamma_d)^3$, $\hat{\nu}_{f,p} = \nu_{f,p}/(\gamma_L - \gamma_d)^2$ and $\hat{\omega}_b = \omega_b/(\gamma_L - \gamma_d)$. Here γ_L is the EP contribution to the growth rate of the wave, while γ_d is the wave damping rate due to dissipation processes.

provided the right hand side of the equation is given by Eq.5.11. Using $\partial_J \sim 1/\omega_b$ and implying weak collisional dissipation, we obtain $\delta = \max(D_p/\omega_b^3, \nu_{f,p}/\omega_b^2) \ll 1$. We solve Eq.5.13 by an expansion in δ ,

$$g_{0,j} = \sum_{\alpha} g_{0,j}^{(\alpha)} \delta^{\alpha},$$

to find $g_{0,j}^{(0)}$, i.e. the leading order EP distribution function. The leading order equation reads

$$\left. \frac{\partial g_{0,j}^{(0)}}{\partial \xi} \right|_{H_0} = 0. \quad (5.14)$$

Thus, we learn that $g_{0,j}^{(0)}$ is independent of ξ at any fixed H_0 , i.e. $g_{0,j}^{(0)} = g_{0,j}^{(0)}(H_0; \sigma_p)$. Introducing collisions at next order, we determine an exact form of $g_{0,j}^{(0)}$ from the collisional constraint. The $\mathcal{O}(\delta^1)$ equation is

$$p(\xi, H_0; \sigma_p) \left. \frac{\partial g_{0,j}^{(1)}}{\partial \xi} \right|_{H_0} = D_p p^2(\xi, H_0; \sigma_p) \left. \frac{\partial^2 g_{0,j}^{(0)}}{\partial H_0^2} \right|_{\xi} + [D_p + \nu_{f,p} p(\xi, H_0; \sigma_p)] \left. \frac{\partial g_{0,j}^{(0)}}{\partial H_0} \right|_{\xi}. \quad (5.15)$$

To annihilate the term in $g_{0,j}^{(1)}$, we divide both sides of Eq.5.15 by p and integrate over ξ at fixed H_0 . To consider particles outside the phase space island⁷⁰, i.e. $H_0 \geq \omega_b^2$ (see Fig.5.3), we integrate over a period in ξ , imposing $g_{0,j}(-\pi) = g_{0,j}(\pi)$. For particles trapped within the island, $-\omega_b^2 \leq H_0 < \omega_b^2$, we have to integrate between bounce points, given by $\xi_b = \pm \arccos(-H_0/\omega_b^2)$, and, in general, sum over the two streams, $\sigma_p = \pm 1$, to ensure continuity at both bounce points. Therefore, we introduce

$$\langle \dots \rangle_{\xi} = \begin{cases} \frac{1}{2\pi} \int_{-\pi}^{\pi} \dots d\xi, & H_0 \geq \omega_b^2 \\ \frac{1}{4\pi} \sum_{\sigma_p} \sigma_p \int_{-\xi_b}^{\xi_b} \dots d\xi, & -\omega_b^2 \leq H_0 < \omega_b^2 \end{cases} \quad (5.16)$$

$H_0 = \omega_b^2$ is the separatrix of the phase space island. Applying Eq.5.16 to Eq.5.15, we obtain

$$\langle D_p p(\xi, H_0; \sigma_p) \rangle_{\xi} \left. \frac{\partial^2 g_{0,j}^{(0)}}{\partial H_0^2} \right|_{\xi} + \left\langle \frac{D_p}{p(\xi, H_0; \sigma_p)} + \nu_{f,p} \right\rangle_{\xi} \left. \frac{\partial g_{0,j}^{(0)}}{\partial H_0} \right|_{\xi} = 0, \quad (5.17)$$

to be solved for $g_{0,j}^{(0)}$. To provide matching across the trapped-passing boundary, $H_0^c = \omega_b^2$, we impose $\sum_{\sigma_p} \sigma_p g^p = 0$, $\sum_{\sigma_p} g^p = 2g^t$ and $\sum_{\sigma_p} \partial g^p / \partial H_0 = 2\partial g^t / \partial H_0$ similar to Eq.3.1

⁷⁰They are also to be referred to as passing particles in phase space.

of Chapter III for our NTM analysis. Here indices p and t denote passing and trapped particles, respectively.

Away from the island, $f_{0,j}$ matches the Maxwellian equilibrium and thus is linear in p . Since $f_{0,j} = f_{eqm,j} + g_{0,j}$, $g_{0,j}$ must satisfy $\partial_p g_{0,j}|_{p \rightarrow \pm\infty} = 0$. We solve this numerically for $g_{0,j}^{(0)}$ as a function of H_0 at each σ_p . D_p , $\nu_{f,p}$ and ω_b are arbitrary parameters. $f_{0,j}^{(0)}$ vs. H_0 is shown in Fig.5.5 for passing and trapped particles⁷¹. The trapped particle solution is

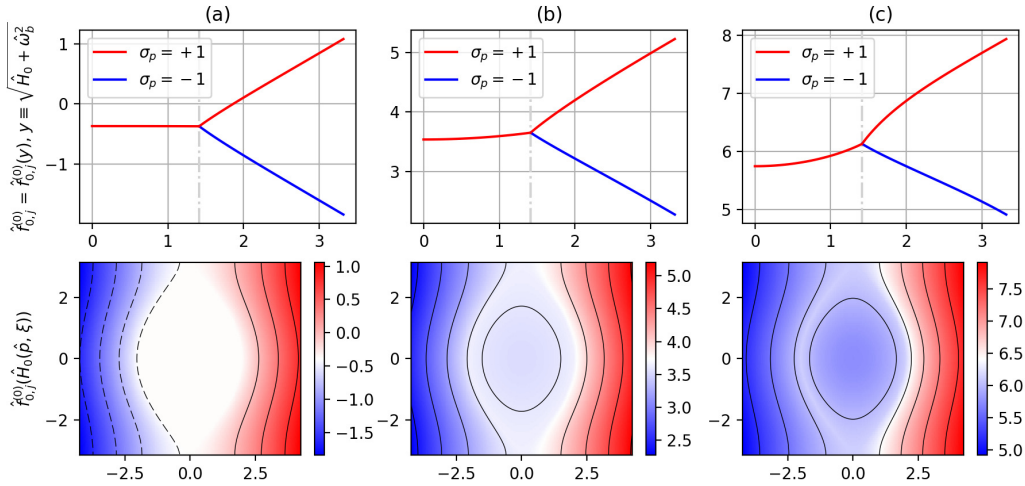


Figure 5.5: (top) The leading order EP distribution function vs. $y = \sqrt{\hat{H}_0 + \hat{\omega}_b^2}$ for two branches of the stream, $\sigma_p = \pm 1$ for (a) a case of pure diffusion, (b) when velocity diffusion and drag are comparable and (c) when the drag term is dominant. The dotted line represents the trapped-passing boundary, $y_b = \sqrt{2}\hat{\omega}_b$. $y \geq y_b$ and $0 \leq y < y_b$ correspond to the passing and trapped regions, respectively. The trapped particle solution is σ_p -independent and hence both σ_p branches match in the trapped region. (bottom) Contours of constant $\hat{f}_{0,j}^{(0)}$ in the (\hat{p}, ξ) plane, which reproduce the phase space island structure; $\hat{\omega}_b = 1$. Hats indicate the normalisation that has been chosen as in [95].⁶⁹

σ_p -independent due to Eq.5.16. Once $f_{0,j}^{(0)} = f_{0,j}^{(0)}(H_0; \sigma_p)$ is calculated, we immediately find $f_{0,j}^{(0)}$ in p space, i.e. $f_{0,j}^{(0)}(H_0(\xi, p); \sigma_p)$.

Similar to the NTM problem, we have to identify the dissipation layer, where δ is no longer small. Eq.5.17 becomes invalid in a thin region of phase space in the vicinity of the phase space island separatrix. Here collisional dissipation is not negligible to leading order in δ but comparable to $\sim p\partial/\partial\xi$, and thus we must find a full solution of Eq.5.13. Solving Eq.5.13 with the boundary conditions in H_0 space given above and applying

⁷¹The numerical scheme can be found in the appendix and in [96].

$f_{0,j}(-\xi_b) = f_{0,j}(\xi_b)$ ⁷² in ξ , we obtain $f_{0,j} = f_{0,j}(\xi, H_0(\xi, p); \sigma_p)$. $f_{0,j}$ vs. p is illustrated in Fig.5.4 for arbitrary \hat{D}_p and $\hat{\nu}_{f,p}$. As can be seen from Fig.5.4, the EP distribution function remains flattened across the island O-point in a pure diffusion case.

$f_{0,j}$ approaches the solution provided by Zakharov and Karpman [97], but includes a more detailed treatment of the separatrix vicinity. Adding drag creates a hole around the island O-point, which grows with growing $\nu_{f,p}$. The destabilising effect of dynamical friction has been demonstrated by Lilley [107] in slab geometry. In [107] it was shown that the slowing down effect might be dominant over the collisional diffusion near the resonance.

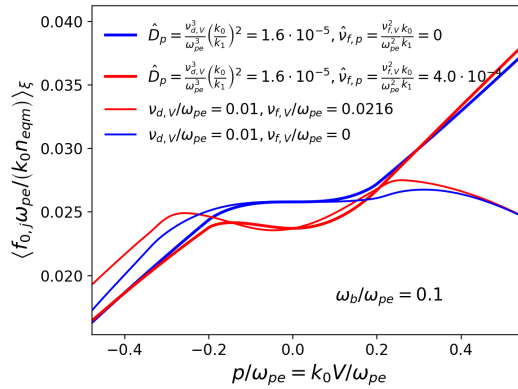


Figure 5.6: The ξ -averaged EP distribution function, $\langle f_{0,j} \rangle_{\xi}$, vs. p for arbitrary D_p and $\nu_{f,p}$, $\omega_b = 0.1\omega_{pe}$. $f_{0,j}$ is normalised to $n_{eqm}k_0/\omega_{pe}$, n_{eqm} is the equilibrium density. Thick lines indicate the solution of Eq.(14), which is localised to the island vicinity. Thin lines indicate the COBBLES distribution function. Diffusion and friction rates in velocity space are $\nu_{d,V} = 0.01\omega_{pe}$ and $\nu_{f,V} = 0$ (blue curves), $\nu_{d,V} = 0.01\omega_{pe}$ and $\nu_{f,V} = 0.0216\omega_{pe}$ (red curves). In p space, these correspond to diffusion $\hat{D}_p = \nu_{d,V}^2(k_0/k_1)^2 = 1.6 \cdot 10^{-5}\omega_{pe}^3$ and drag $\nu_{f,p} = \nu_{f,V}^2(k_0/k_1) = 0/4.0 \cdot 10^{-4}\omega_{pe}^2$, respectively. $\nu_{f,V}/\nu_{d,V} = 2.16$.

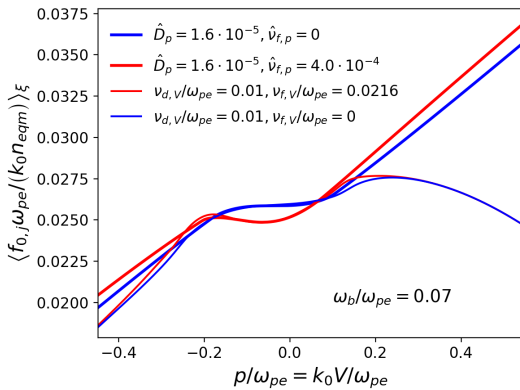


Figure 5.7: Same as Fig.5.6 except for the bounce frequency value, $\omega_b = 0.07\omega_{pe}$.

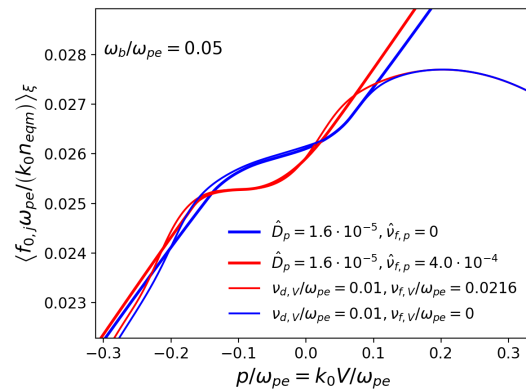


Figure 5.8: Same as Fig.5.6 except for the bounce frequency value, $\omega_b = 0.05\omega_{pe}$.

⁷² ξ_b reduces to π for passing particles

In Figs.5.6-5.8 we benchmark $f_{0,j}$ against the full- f approach, provided by COBBLES [96, 99, 108, 109, 110]. Two scenarios are considered: (1) pure diffusion and (2) $\nu_{f,V} \gtrsim \nu_{d,V}$. The friction/diffusion ratio $\nu_{f,V}/\nu_{d,V} \lesssim 1$ in a typical NBI discharge and $\nu_{f,V}/\nu_{d,V} \gtrsim 1$ in the vicinity of the TAE resonance ($\nu_{f,V}/\nu_{d,V} = 2.16$ chosen in our model). The behaviour in the island vicinity is found to be in good agreement with the COBBLES simulation results. The discrepancy away from the island was expected due to the difference in the boundary conditions we apply.

5.2.1 Self-consistency

The perturbed Hamiltonian has to be consistent with a system of Maxwell's equations. In accordance with the $\cos \xi$ dependence of the perturbed Hamiltonian, we keep the first harmonic only in ξ in the particle distribution function. Thus, we define:

$$g_{0,j}^\omega(J, t) = \oint \frac{d\xi}{2\pi} g_{0,j}(\xi, J, t) e^{-i\xi} \quad (5.18)$$

in ω space. A set of Ampère's law and Poisson's equation is equivalent to finding an extremum of the Lagrangian density of the electro-magnetic field with respect to the vector potential \mathbf{A}_ω^* and electrostatic potential Φ_ω^* . We split the electro-magnetic field Lagrangian into $\mathcal{L}(\omega) = \mathcal{L}^{(field)}(\omega) + \mathcal{L}^{(part)}(\omega)$ with $\mathcal{L}^{(field)}$ and $\mathcal{L}^{(part)}$ being defined as

$$\mathcal{L}^{(field)}(\omega) = \int d\mathbf{x} \left(\frac{\varepsilon_0}{2} \mathbf{E}_\omega \cdot \mathbf{E}_\omega^* - \frac{1}{2\mu_0} \mathbf{B}_\omega \cdot \mathbf{B}_\omega^* \right) \quad (5.19)$$

and

$$\mathcal{L}^{(part)}(\omega) = \int d\mathbf{x} (\mathbf{j}_\omega \cdot \mathbf{A}_\omega^* - \rho_\omega \cdot \Phi_\omega^*), \quad (5.20)$$

where \mathbf{E}_ω is the electric field, \mathbf{B}_ω is the magnetic field, \mathbf{j}_ω and ρ_ω are the current and charge densities, respectively. Solving the bump-on-tail problem, we omit the contribution of the magnetic field and thus

$$\mathcal{L}^{(part)}(\omega) = - \sum_j \int d\mathbf{x} d\mathbf{p} g_{0,j}^\omega h_\omega^* \quad (5.21)$$

with $h_\omega = eZ_j\Phi_\omega$ being the perturbed Hamiltonian⁷³, and $\mathbf{V} = \mathbf{p}/m_j$ the unperturbed velocity. j denotes the particle species. Eqs.5.19,5.21 reduce to Eqs.5.6,5.7. When $\delta\omega \ll \omega_0$, the Lagrangian allows the form $\mathcal{L}(\omega) = \mathcal{L}_0(\omega) + \mathcal{L}_1(\omega)$ [96] (and references therein), where \mathcal{L}_0 is related to the MHD energy, while \mathcal{L}_1 corresponds to weak resonant interactions between the perturbed electro-magnetic field and plasma.

$$\mathcal{L}_1 = \int d\mathbf{x} d\mathbf{p} g_{0,j}^\omega h_\omega^*,$$

provided one resonant species is considered. To leading order, we find a dispersion relation that reads $\mathcal{L}_0(\omega_0) = 0$. The next order provides

$$2\omega_0 \left. \frac{\partial \mathcal{L}_0}{\partial \omega} \right|_{\omega=\omega_0} [\delta\omega + i(\gamma + \gamma_d)] = -2\omega_0 \mathcal{L}_1. \quad (5.22)$$

Defining $\Lambda_\omega = \omega_0 \partial \mathcal{L}_0 / \partial \omega|_{\omega=\omega_0}$, we obtain the following constraint

$$\begin{aligned} \delta\omega &= -\frac{\omega_0}{\Lambda_\omega} \Re \mathcal{L}_1, \\ \gamma &= -\frac{\omega_0}{\Lambda_\omega} \Im \mathcal{L}_1 - \gamma_d. \end{aligned} \quad (5.23)$$

The first equation of Eq.5.23 is responsible for the frequency shift, $\delta\omega$, while the second one is used for the mode growth/decay rate, γ . An ad-hoc damping rate, γ_d , has been introduced in Eq.5.23. If there was a second stabilising species in the problem, this would correspond to an energy sink associated with the Landau damping. Switching to $\{\xi, p\}$, we have⁷⁴

$$\mathcal{L}_1 = \frac{|h_\omega|^2}{\omega_b^2} \int_{-\pi}^{\pi} \frac{d\xi}{2\pi} \int dp g_{0,j}(\xi, p, t) e^{-i\xi},$$

where

$$\frac{d\xi}{2\pi} dp = \sum_{\sigma_p} \frac{d\xi}{2\pi} \frac{dH_0}{p} = \sum_{\sigma_p} \frac{d\xi}{2\pi} \frac{dJ}{\tau p}. \quad (5.24)$$

⁷³Keeping the \mathbf{A}_ω component, we write $h_\omega = eZ_j(\Phi_\omega - \mathbf{V} \cdot \mathbf{A}_\omega)$ for the perturbed Hamiltonian.

⁷⁴note: $dId\xi = dpd\xi/C = -hdpd\xi/\omega_b^2$, $h = -h_\omega$ in relation to the present notations.

Then Eq.5.23 reduces to

$$\begin{aligned}\delta\omega &= -\frac{\omega_0}{\omega_b^2} \frac{|h_\omega|^2}{\Lambda_\omega} \sum_{\sigma_p} \int_0^{J_{\max}} dJ \langle g_{0,j} \cos \xi \rangle_\xi, \\ \gamma &= \frac{\omega_0}{\omega_b^2} \frac{|h_\omega|^2}{\Lambda_\omega} \sum_{\sigma_p} \int_0^{J_{\max}} dJ \langle g_{0,j} \sin \xi \rangle_\xi - \gamma_d,\end{aligned}\tag{5.25}$$

where J_{\max} has been chosen to provide the integration over the entire phase space, inside and outside the island, i.e. $J_{\max} = \infty$. $\langle \dots \rangle_\xi$ represents the ξ average operator with the corresponding weight functions taken in accordance with Eq.5.24. This is also valid for the Zakharov and Karpman solution [97]. Defining $\gamma_L = \pi\omega_0 \left. \frac{\partial f_{eqm,j}}{\partial p} \right|_{res} \frac{|h_\omega|^2}{\Lambda_\omega}$ as in [112, 113], we obtain the main result of [112, 113]:

$$\begin{pmatrix} -\delta\omega \\ \gamma_d \end{pmatrix} = \frac{1}{\pi} \frac{\gamma_L}{\omega_b^2} \left(\left. \frac{\partial f_{eqm,j}}{\partial p} \right|_{res} \right)^{-1} \sum_{\sigma_p} \int_0^{J_{\max}} dJ \begin{pmatrix} \langle g_{0,j} \cos \xi \rangle_\xi \\ \langle g_{0,j} \sin \xi \rangle_\xi \end{pmatrix},\tag{5.26}$$

where J_{\max} corresponds to the separatrix of a hole/clump, and $g_{0,j}$ has to be understood as $f_{0,j} - f_{eqm,j}|_{res} - (\partial f_{eqm,j}/\partial p)|_{res} p$ ⁷⁵. γ has been assumed to be zero provided there is no exponential growth/decay. γ_L has no amplitude dependence since the mode energy density Λ_ω is proportional to $|h_\omega|^2$ ⁷⁶.

5.3 Stability analysis. Secondary modes

5.3.1 Filtered solution

Let us consider the situation when $f_{0,j}$ is independent of ξ . This is valid for the thermal background since $p \gg \omega_b$, or for $f_{0,j}$ being averaged over ξ space. The latter corresponds

⁷⁵Here *res* indicates the position of the resonant surface.

⁷⁶It can be demonstrated that γ_L is the linear growth rate in the absence of any dissipation, i.e. $\gamma_d = 0$. Indeed, the linear solution of the Vlasov equation is $g_{0,j} = -\frac{1}{2} \left. \frac{\partial f_{eqm,j}}{\partial p} \right|_{res} \frac{\omega_b^2}{p - i0^+}$, and thus $\Im \mathcal{L}_1 = \frac{|h_\omega|^2}{\omega_b^2} \int_{\mathbb{R}} dp \Im g_{0,j} = -\frac{\pi}{2} |h_\omega|^2 \left. \frac{\partial f_{eqm,j}}{\partial p} \right|_{res}$. Substituting this into Eq.5.23 provides the growth rate $\gamma = \gamma_L - \gamma_d$, where γ_L is defined above. $\gamma = \gamma_L$ when $\gamma_d = 0$, so that γ_L might be understood as the linear growth rate in the absence of dissipation processes.

to the *filtered* solution. Then the solution of Eq.5.8 reads

$$f_{j,k\omega} = -\frac{l}{\delta\omega - lp + i0^+} \left\langle \frac{\partial f_{0,j}}{\partial p} \right\rangle_{\xi} h_{k\omega}. \quad (5.27)$$

Substituting this into Eq.5.6 with Eq.5.7 yields

$$\mathcal{L}(\delta\omega, l) = \left[-l^2 - \sum_j \omega_{pj}^2 \int_{\mathbb{R}} \frac{l}{\delta\omega - lp + i0^+} \left\langle \frac{\partial f_{0,j}}{\partial p} \right\rangle_{\xi} dp \right] |h_{k\omega}|^2. \quad (5.28)$$

For the background plasma, we impose $f_{0,j} = (2\pi)^{-1/2} V_{Tj}^{-1} e^{-V^2/2V_{Tj}^2}$, where $V_{Tj} = \sqrt{T_j/m_j}$ is the thermal velocity. Therefore, we derive the following dispersion relation

$$1 - \sum_{j=e,i} \frac{\omega_{pj}^2}{\omega_{tj}^2} \int_{\mathbb{R}} \frac{d\zeta}{(2\pi)^{1/2}} e^{-\zeta^2/2} \frac{\omega_{tj}\zeta}{\omega - \omega_{tj}\zeta + i0^+} = 0$$

from $\mathcal{L}(\delta\omega, l) = 0$ for thermal electrons and ions. Here $\omega_{tj} = kV_{Tj}$ is the transit frequency.

If the mode is close to marginality $\gamma = \Im\omega \ll \omega_r = \Re\omega$, and in the limit of large frequency $\omega \sim \omega_{pj} \gg \omega_{tj}$, one can employ the Sokhotski-Plemelj formula to find

$$\frac{1}{\omega - \omega_{tj}\zeta + i0^+} \simeq \frac{1}{\omega} \left(1 + \frac{\omega_{tj}\zeta}{\omega} \right) - i\pi\delta(\omega - \omega_{tj}\zeta),$$

where δ is the Dirac delta function. Thus, the dispersion relation for the Maxwellian background reduces to

$$1 - \sum_{j=e,i} \left[\frac{\omega_{pj}^2}{\omega^2} - i \left(\frac{\pi}{2} \right)^{1/2} \frac{\omega\omega_{pj}^2}{\omega_{tj}^3} e^{-\omega_{pj}^2/2\omega_{tj}^2} \right] = 0.$$

This can be further expanded with respect to $\gamma/\omega_r \ll 1$ to deduce that $\omega_r \simeq \omega_{pe}$ and $\gamma = -\gamma_e$ with $\gamma_e = \frac{1}{2} \left(\frac{\pi}{2} \right)^{1/2} \omega_{pe} \frac{\omega_{pe}^3}{\omega_{te}^3} e^{-\omega_{pe}^2/2\omega_{te}^2}$ ⁷⁷. This is known as the conventional expression for the Landau damping rate of the Langmuir wave. Thus, the thermal particle contribution to the total Lagrangian is

$$\mathcal{L}_j(\delta\omega, l) = l^2 \left(\frac{\omega_{pj}^2}{\omega^2} + 2i \frac{\omega\gamma_j}{\omega_{pj}^2} \right) |h_{k\omega}|^2. \quad (5.29)$$

⁷⁷Here $\omega_{pe} \gg \omega_{pi}$ has been implied.

$j = e, i$ here denotes main electrons/ions. The EP contribution is then

$$\mathcal{L}_{EP,j}(\delta\omega, l) = -\omega_{pj}^2 \left[\int_{\mathbb{R}} \frac{l}{\delta\omega - lp + i0^+} \left\langle \frac{\partial f_{0,j}}{\partial p} \right\rangle_{\xi} dp \right] |h_{k\omega}|^2. \quad (5.30)$$

In Eq.5.30 $j = fe, fi$ corresponds to the fast electrons/ions that provide the drive for the bump-on-tail instability. The total Lagrangian, Eq.5.6, is of the form $\mathcal{L}(\delta\omega, l) = D(\delta\omega, l) |h_{k\omega}|^2$, where D is the dispersion function. Therefore, the dispersion relation is

$$-1 + \sum_{j=e,i} \left(\frac{\omega_{pj}^2}{\omega^2} + 2i \frac{\omega\gamma_j}{\omega_{pj}^2} \right) - \sum_{j=fe,fi} \frac{\omega_{pj}^2}{l^2} \int_{\mathbb{R}} \frac{l}{\delta\omega - lp + i0^+} \left\langle \frac{\partial f_{0,j}}{\partial p} \right\rangle_{\xi} dp = 0. \quad (5.31)$$

5.3.2 Full solution of the Vlasov/Fokker-Planck – Poisson system

Formal solution of the Vlasov/Fokker-Planck equation

Let us rewrite Eq.5.8 for the perturbed distribution function as

$$-i\delta\omega f_{j\omega} + p \frac{\partial f_{j\omega}}{\partial \xi} = ilp \frac{\partial f_{0,j}}{\partial H_0} h_{k\omega} e^{il\xi}, \quad (5.32)$$

where $f_{j\omega}$ and p are considered as functions of ξ and H_0 for each σ_p , while $h_{k\omega}$ is taken to be constant. $f_{0,j}$ describes the primary equilibrium calculated in the previous section. To simplify the analysis below, let us split the perturbed distribution into the adiabatic response and the resonant contribution:

$$f_{j\omega} = \frac{\partial f_{0,j}}{\partial H_0} h_{k\omega} e^{il\xi} + g_{j\omega}. \quad (5.33)$$

Solving Eq.5.32 for $g_{j\omega}$, we obtain

$$g_{j\omega} = i\delta\omega \frac{\partial f_{0,j}}{\partial H_0} h_{k\omega} e^{i\delta\omega Q} \left[\int_{-\xi_b}^{\xi} \frac{d\xi'}{p'} e^{il\xi' - i\delta\omega Q'} + C(\sigma_p) \right], \quad (5.34)$$

where p' and Q' denote $p(\xi', H_0; \sigma_p)$ and $Q(\xi', H_0; \sigma_p)$, respectively⁷⁸. We have defined Q as

$$Q(\xi, H_0; \sigma_p) = \int_0^{\xi} \frac{d\xi'}{p(\xi', H_0; \sigma_p)}, \quad (5.35)$$

⁷⁸ ξ_b is to be replaced with π in the passing branch.

which can also be written through the incomplete elliptic integral of the first kind,

$$\sqrt{2}\sigma_p(H_0 + \omega_b^2)^{-1/2} F\left(\frac{\xi}{2}, \frac{2\omega_b^2}{H_0 + \omega_b^2}\right).$$

$C(\sigma_p)$ is a constant of integration and is different on each branch of σ_p . Its calculation will be the subject of the next section. Applying

$$\int_{\mathbb{R}} dp \int_{-\pi}^{\pi} \frac{d\xi}{2\pi} = \sum_{\sigma_p} \int_{-\omega_b^2}^{+\infty} dH_0 \oint \frac{d\xi}{2\pi} \frac{1}{p},$$

we rewrite the EP Lagrangian as

$$\mathcal{L}_{EP,j}(\delta\omega, l) = \omega_{pj}^2 \sum_{\sigma_p} \int_{-\omega_b^2}^{+\infty} dH_0 \oint \frac{d\xi}{2\pi} \frac{1}{p} f_{j\omega} h_{k\omega}^* e^{-il\xi}. \quad (5.36)$$

Substituting Eq.5.33 into Eq.5.36, we split the Lagrangian into the adiabatic and resonant contributions, $\mathcal{L}_{EP,j}(\delta\omega, l) = \mathcal{L}_{ad,j}(\delta\omega, l) + \mathcal{L}_{res,j}(\delta\omega, l)$. At this stage, $C(\sigma_p)$ still remains to be calculated.

Matching conditions

We have found the perturbed EP distribution, $g_{j\omega}$, in terms of the arbitrary constant, $C(\sigma_p)$, whose calculation is addressed in this subsection.

Let us define $-\xi_0$ as a starting point in ξ space. The passing particle distribution must have the same value at $\xi = -\xi_0$ and $\xi = \xi_0$ for each σ_p . However, for trapped particles the matching condition is less convenient if written in terms of ξ . Indeed, their distribution must match at both $\xi = \xi_0$ after half a bounce on the interval $[-\xi_0; \xi_0]$ and again at $\xi = -\xi_0$ at the end of the way back to the starting bounce angle. We note that $\sigma_p > 0$ when a particle moves from $-\xi_0$ to ξ_0 , and $\sigma_p < 0$ on the return branch, from ξ_0 to $-\xi_0$. Thus, both branches, $\sigma_p = \pm 1$, have to be connected at fixed H_0 . To avoid the cumbersome calculations in the trapped branch, we find it convenient to replace ξ with the following variable α ⁷⁹ for trapped particles:

$$\alpha = \Omega_b \int_0^{\xi} \frac{d\xi'}{p'}, \quad p > 0 \quad (5.37)$$

⁷⁹This is similar to the matching provided in Chapter III.

and

$$\alpha = \pi - \Omega_b \int_0^\xi \frac{d\xi'}{p'}, \quad p < 0, \quad (5.38)$$

where $\Omega_b(H_0) = \left(\int_{-\xi_0}^{\xi_0} \frac{d\xi}{\pi|p|} \right)^{-1}$ is the bounce frequency⁸⁰. α has the same features as $x^{in(\pm)}$ introduced in Sec.3.1.

The perturbed distribution function, $g_{j\omega}$, then becomes:

$$g_{j\omega} = i\delta\omega \frac{\partial f_{0,j}}{\partial H_0} h_{k\omega} e^{i\frac{\delta\omega}{\Omega_b}\alpha} \left[\int_{-\pi/2}^\alpha \frac{d\alpha'}{\Omega_b} e^{i(l\xi' - \frac{\delta\omega}{\Omega_b}\alpha')} + C(\sigma_p) \right], \quad (5.39)$$

which is valid in range $-\pi/2 \leq \alpha < 3\pi/2$. Providing continuity at $\xi = -\xi_0$ after one bounce, i.e. $g_{j\omega}(H_0, \alpha = -\pi/2) = g_{j\omega}(H_0, \alpha = 3\pi/2)$, we immediately obtain

$$C = \frac{\int_{-\pi}^\pi \frac{d\alpha}{\Omega_b} e^{i(l\xi - \frac{\delta\omega}{\Omega_b}\alpha)}}{e^{-2\pi i \frac{\delta\omega}{\Omega_b}} - 1}. \quad (5.40)$$

Here we have implied that the limits of integration can be shifted for a periodic function, integrated over its period⁸¹. Eq.5.40 allows an equivalent representation via

$$\sum_{k=1}^{+\infty} e^{2\pi k i \frac{\delta\omega}{\Omega_b}} = \frac{1}{e^{-2\pi i \frac{\delta\omega}{\Omega_b}} - 1}. \quad (5.41)$$

(see [96] for more detail). Rewriting the resonant part of the EP Lagrangian in α space, we have

$$\begin{aligned} \mathcal{L}_{res,j}(\delta\omega, l) = \\ 2\pi i \delta\omega \cdot \omega_{pj}^2 |h_{k\omega}|^2 \int_{-\omega_b^2}^{+\infty} \frac{dH_0}{\Omega_b^2} \int_{-\pi}^\pi \frac{d\alpha}{2\pi} \frac{\partial f_{0,j}}{\partial H_0} e^{-i(l\xi - \frac{\delta\omega}{\Omega_b}\alpha)} \left[\int_{-\pi/2}^\alpha \frac{d\alpha'}{2\pi} e^{i(l\xi' - \frac{\delta\omega}{\Omega_b}\alpha')} + C(\sigma_p) \right] \end{aligned} \quad (5.42)$$

for trapped particles with $C(\sigma_p)$ given by Eq.5.40. Here both, α and α' , have been shifted by $\pi/2$ for convenience. We stress that α' can be redefined as an extended angle in the domain $(-\infty; \pi]$, and hence an integral over $\alpha' \in [-\pi/2, \alpha]$ can be replaced with $\alpha' \in (-\infty; \alpha]$.

For passing particles, the $\sigma_p = \pm 1$ branches are not connected. Nevertheless, we can still

⁸⁰ ω_b is its value in the limit of deeply trapped particles, i.e. $H_0 \rightarrow -\omega_b^2$.

⁸¹Periodicity in α space is provided by our choice of α , while periodicity in ξ space is not required.

define:

$$\alpha = \Omega_b \int_0^\xi \frac{d\xi'}{p'}, \quad (5.43)$$

where $\Omega_b(H_0) = \sigma_p \left(\int_{-\pi}^\pi \frac{d\xi}{2\pi|p|} \right)^{-1}$ is the transit frequency. The properties of $\alpha(\xi, H_0; \sigma_p)$ for passing and trapped particles are the same. The bounce frequency $\Omega_b < 0$ when $\sigma_p = -1$, and hence ξ and α rotate in opposite directions. Thus, the final expression for the resonant Lagrangian reads:

$$\begin{aligned} \mathcal{L}_{res,j}(\delta\omega, l) &= 2\pi i \omega_{pj}^2 |h_{k\omega}|^2 \\ &\sum_{\sigma_p} \int_{-\omega_b^2}^{+\infty} \frac{dH_0}{\Omega_b} \frac{\delta\omega}{|\Omega_b|} \int_{-\pi}^\pi \frac{d\alpha}{2\pi} \frac{\partial f_{0,j}}{\partial H_0} e^{-i(l\xi - \frac{\delta\omega}{\Omega_b}\alpha)} \left[\int_{-\infty}^{+\infty} \frac{d\alpha'}{2\pi} e^{i(l\xi' - \frac{\delta\omega}{\Omega_b}\alpha')} \cdot \Theta[\sigma_p(\alpha - \alpha')] + C(\sigma_p) \right]. \end{aligned} \quad (5.44)$$

The sum over σ_p applies only to the passing branch with σ_p being the sign of Ω_b . This convention will be used throughout the study, unless otherwise stated. To ensure the validity of Eq.5.44, we can consider the limit when the contribution of trapped particles is negligible, and ξ becomes a linear function of α , i.e. the limit of deeply passing particles. In this case, Eq.5.44 in its resonant⁸² and non-resonant forms reduces to Eq.5.28 at the deeply passing end, $H_0 \gg \omega_b^2$. Eq.5.28, in turn, provides the conventional expression for the Landau damping rate of the Langmuir wave as well as the bump-on-tail dispersion relation.

Explicit form of the resonance Eq.5.44 allows the representation where resonances are introduced explicitly. As secondary modes are expected when the gradient of $f_{0,j}(H_0)$ is the largest, a new form of Eq.5.44 should be valid in entire phase space. Technically speaking, we have to rewrite Eq.5.34/Eq.5.39 and hence the functional given by Eq.5.44 in a resonant form. This transition is not obvious but becomes straightforward if we note that α is an angle for both trapped and passing branches and thus we can search for $g_{j\omega}$ as a Fourier series in α :

$$g_{j\omega}(\alpha, H_0; \sigma_p) = \sum_n g_{j,n\omega}(H_0; \sigma_p) e^{in\alpha}, \quad (5.45)$$

where the σ_p dependence is to be applied to passing branch. As noted above, the perturbed

⁸²Its resonant formulation is addressed in the following subsection.

Hamiltonian is an exponential function of ξ with only one harmonic in ξ space and hence it is an exponential function of α but with an infinite number of harmonics, i.e.

$$h_\omega = h_{k\omega} e^{i l \xi} = \sum_{n=-\infty}^{+\infty} h_{n\omega}(H_0; \sigma_p) e^{i n \alpha}. \quad (5.46)$$

Applying $d\alpha/\Omega_b = d\xi/p$ according to Barrow's theorem, we obtain

$$g_{j,n\omega} = -\frac{\delta\omega}{\delta\omega - n\Omega_b + i0^+} \frac{\partial f_{0,j}}{\partial H_0} h_{n\omega} \quad (5.47)$$

and the corresponding resonant Lagrangian:

$$\mathcal{L}_{res,j}(\delta\omega, l) = -\omega_{pj}^2 \sum_{n=-\infty}^{+\infty} \sum_{\sigma_p} \int_{-\omega_b^2}^{+\infty} \frac{dH_0}{\Omega_b} \frac{\delta\omega}{\delta\omega - n\Omega_b + i0^+} \frac{\partial f_{0,j}}{\partial H_0} |h_{n\omega}|^2, \quad (5.48)$$

where the perturbed Hamiltonian Fourier components, $h_{n\omega}$, are given by

$$h_{n\omega} = h_{k\omega} \int_{-\pi}^{\pi} \frac{d\alpha}{2\pi} e^{i(l\xi - n\alpha)}. \quad (5.49)$$

Here ξ is to be treated as a function of α and H_0 at each σ_p . n matches l at the deeply passing end, $H_0 \rightarrow +\infty$, where $\alpha = \xi$. In the appendix and in [96], we prove that both representations, Eq.5.44 and Eqs.5.48,5.49 are equivalent. Including the adiabatic contribution, we obtain

$$\mathcal{L}_{EP,j}(\delta\omega, l) = -\omega_{pj}^2 \sum_{n=-\infty}^{+\infty} \sum_{\sigma_p} \int_{-\omega_b^2}^{+\infty} \frac{dH_0}{\Omega_b} \frac{n\Omega_b}{\delta\omega - n\Omega_b + i0^+} \frac{\partial f_{0,j}}{\partial H_0} |h_{n\omega}|^2. \quad (5.50)$$

for the full EP Lagrangian. Eq.5.50 has a form similar to Eq.5.30 still being the exact solution of the problem.

Full secondary mode dispersion relation

To summarise, the final form of the dispersion function that takes into account the island

formation in phase space is

$$\begin{aligned}
D(\delta\omega, l) = & -l^2 + l^2 \sum_{j=e,i} \left(\frac{\omega_{pj}^2}{\omega^2} + 2i \frac{\omega\gamma_j}{\omega_{pj}^2} \right) \\
& - \sum_{j=f_e, f_i} \omega_{pj}^2 \sum_{n=-\infty}^{+\infty} \sum_{\sigma_p} \int_{-\omega_b^2}^{+\infty} \frac{dH_0}{\Omega_b} \frac{n\Omega_b}{\delta\omega - n\Omega_b + i0^+} \frac{\partial f_{0,j}}{\partial H_0} \left| \bar{h}_{n\omega} \right|^2
\end{aligned} \tag{5.51}$$

with the coefficients $\bar{h}_{n\omega}$ given by

$$\bar{h}_{n\omega} = \int_{-\pi}^{\pi} \frac{d\alpha}{2\pi} e^{i(l\xi - n\alpha)} \tag{5.52}$$

in its resonant formulation. Its equivalent non-resonant representation is

$$\begin{aligned}
D(\delta\omega, l) = & -l^2 + l^2 \sum_{j=e,i} \left(\frac{\omega_{pj}^2}{\omega^2} + 2i \frac{\omega\gamma_j}{\omega_{pj}^2} \right) + \sum_{j=f_e, f_i} \omega_{pj}^2 \sum_{\sigma_p} \int_{-\omega_b^2}^{+\infty} \frac{dH_0}{\Omega_b} \frac{\partial f_{0,j}}{\partial H_0} + \\
& 2\pi i \sum_{j=f_e, f_i} \omega_{pj}^2 \sum_{\sigma_p} \int_{-\omega_b^2}^{+\infty} \frac{dH_0}{\Omega_b} \frac{\delta\omega}{|\Omega_b|} \frac{\partial f_{0,j}}{\partial H_0} \int_{-\pi}^{\pi} \frac{d\alpha}{2\pi} e^{-i(l\xi - \frac{\delta\omega}{\Omega_b}\alpha)} \times \\
& \times \left\{ \int_{-\infty}^{+\infty} \frac{d\alpha'}{2\pi} e^{i(l\xi' - \frac{\delta\omega}{\Omega_b}\alpha')} \cdot \Theta[\sigma_p(\alpha - \alpha')] + C(\sigma_p) \right\}.
\end{aligned} \tag{5.53}$$

Here we highlight that Eqs.5.51,5.52/Eq.5.53 reduce to Eq.5.31 in the limit of deeply passing particles, i.e. when $H_0 \gg \omega_b^2$. $\delta\omega$ is complex, i.e. can be written as $\delta\omega + i\gamma$, where γ is the secondary mode growth/decay rate. D here is the dispersion function defined according to $\mathcal{L}(\delta\omega, l) = D(\delta\omega, l) |h_{k\omega}|^2$. $D(\delta\omega, \gamma) = 0$ provides the dispersion relation of a secondary mode. To analyse its stability, we have to address contours of constant $|D(\delta\omega, \gamma)|$ in the $(\delta\omega, \gamma)$ plane [95, 96]. Any root of $|D(\delta\omega, \gamma)|$ appears as a pole of $|D(\delta\omega, \gamma)|^{-1}$. If it is located in the upper/lower half-plane, it provides the secondary mode growth/decay rate, γ , respectively. For simplicity, we keep the energetic electron component only, dropping the background ion contribution in Eqs.5.51,5.52/Eq.5.53, as $\omega_{pi} \ll \omega_{pe}$, provided the plasma quasi-neutrality requirement is met. The EP fraction is kept small by default.

In Fig.5.9 we plot γ as a function of $l = k/k_0$, based on the full secondary mode dispersion relation, Eqs.5.51,5.52/Eq.5.53, with $f_{0,j}$ being the solution of Eq.5.13 and shown in Fig.5.6. According to Fig.5.9, secondary modes are stable for $l < l_c$ and $l \geq l_s$, where l_c and l_s are defined as roots of $\gamma = \gamma(l)$ and hence they determine the secondary mode

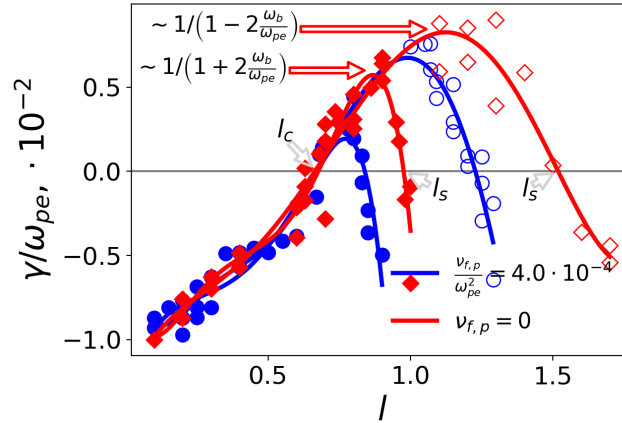


Figure 5.9: The normalised secondary mode growth/decay rate as a function of l in a pure diffusion case (diamond markers) and in the presence of drag (circle markers). Solid lines represent the best fit line for each case. The bounce frequency at the deeply trapped end is $\omega_b/\omega_{p,e} = 0.1$. The D_p and $\nu_{f,p}$ values and normalisation correspond to Figs.5.6-5.8, i.e. $D_p = 1.6 \cdot 10^{-5} \omega_{pe}^3$, $\nu_{f,p} = 4.0 \cdot 10^{-4} \omega_{pe}^2/0$. The regions of negative γ are stable.

stability region(s).

Due to a larger number of poles of $|D|^{-1}$ in the decreasing region of γ as a function of l , we define two decreasing branches. This provides two maximum values of γ as a function of l . Indeed, if ω_0/k_0 and ω/k are the primary island and the secondary mode resonant velocities, we can estimate the l value that corresponds to the maximum growth rate of the secondary wave from $\omega/k \approx \omega_0/k_0 \pm 2\omega_b/k_0$. We would expect to see the maximum of the growth rate when the secondary wave resonant velocity is close to the boundary of the primary island, $\pm 2\omega_b/k_0$, i.e. where the gradient of the primary equilibrium distribution function is the largest. This is associated with the steepening of the electron (ion) distribution near the primary island separatrix, which, in turn, results from its flattening across the island O-point in the absence of drag (blue curves in Figs.5.6-5.8). When drag is included, this would be associated with a hole in the particle distribution in the vicinity of the O-point (red curves in Figs.5.6-5.8).

As $\omega \approx \omega_0 \approx \omega_{pe}$ to 0th order, the latter condition roughly becomes $1 \pm 2\omega_b/\omega_{pe} \approx k_0/k = 1/l$, which provides an estimation for l at a given island half-width, ω_b (0.83 and 1.25 for $\omega_b = 0.1$, respectively). Fig.5.9 shows that γ is a non-monotonic function of l with maxima being in accordance with these estimates. Inclusion of dynamical friction results in a hole at the island O-point and thus shifts the largest gradient of the particle distribution function closer to the island centre, decreasing the stationary point of $\gamma = \gamma(l)$.

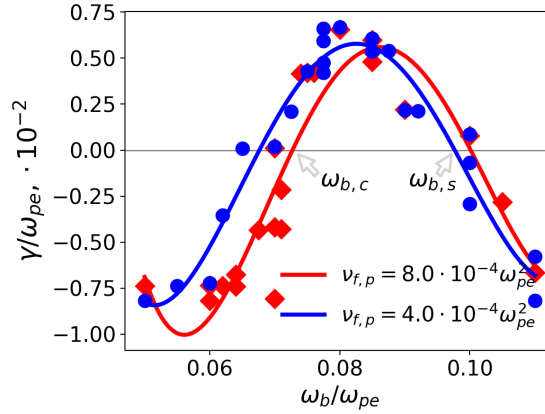


Figure 5.10: The normalised secondary mode growth/decay rate as a function of the bounce frequency of the deeply trapped particles, ω_b , in the presence of slowing down, $\nu_{f,p}$ (solid lines represent the best fit line for each case). The p space diffusion is kept fixed, $D_p = 1.6 \cdot 10^{-5} \omega_{pe}^3$. The primary/secondary wave number ratio, $l = 1.25$. The D_p and $\nu_{f,p}$ normalisation correspond to Figs.5.6-5.8. In each case arrows indicate roots of $\gamma = \gamma(\omega_b)$. The first root, $\omega_{b,c}$, denotes a critical island half-width, below which the secondary mode stability is achieved. The second root, $\omega_{b,s}$ corresponds to the saturation level, above which the secondary mode is stable. The regions of negative γ are stable.

Varying the bounce frequency at the deeply trapped end, ω_b , we determine γ as a function of ω_b for different slowing down rates (see Fig.5.10) and in the absence of drag at different densities of bulk plasma (see Fig.5.11). $\gamma = \gamma(\omega_b)$ is found to be non-monotonic. This allows one to define a region of the secondary mode marginal stability. γ grows monotonically with ω_b , crossing $\gamma = 0$; reaches a maximum and then decreases, crossing $\gamma = 0$ for the second time.

The above solution has been benchmarked against the full- f approach. In Fig.5.11 we plot γ against ω_b for different equilibrium plasma density, n_e , and the ad-hoc damping rate, $\gamma_{d,0}$. An analytic solution is provided by Eqs.5.51,5.52/Eq.5.53, while the full- f version of the COBBLES code (see [96] and the references therein for more detail) has been adopted for the numerical simulations. Both solutions are found to be in good agreement. The benchmarking details are presented in [96].⁸³

⁸³ $\omega_b \approx 0.15\omega_{pe}$ for given plasma parameters is approximately the point above which the comparison is no longer allowed. This corresponds to longer times, when the effects beyond the secondary mode stability analysis become crucial such as the mode non-linear saturation and the mode-mode coupling.

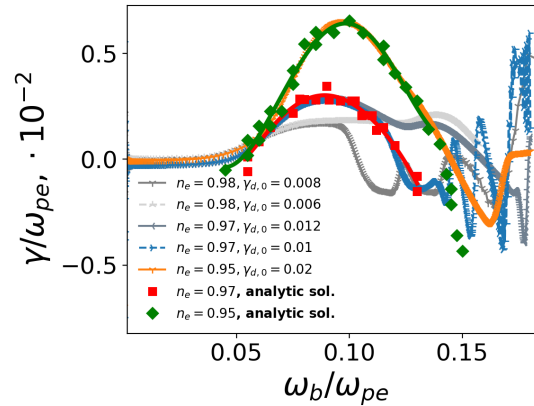


Figure 5.11: The secondary mode growth/decay rate vs. ω_b in a pure diffusion case, $D_p = 1.6 \cdot 10^{-5} \omega_{pe}^3$ (D_p value and normalisation correspond to Figs.5.6-5.8). The primary/secondary mode number ratio, $k_0/k = 4/5$. An analytic solution (square and diamond markers) is calculated based on Eqs.5.51,5.52/Eq.5.53. Solid lines indicate the COBBLES growth/decay rates. The regions of negative γ are stable.

5.4 Summary

To conclude, the purpose of the work described in this chapter is to identify the conditions under which a phase space island, generated by trapping of EPs in a plasma wave, is subject to secondary instabilities in the presence of collisions. The initial equilibrium distribution function, i.e. in the absence of the island, is described by a Maxwellian. Being localised to the island vicinity, the latter appears as a straight line near the beam velocity, V_b . The EP fraction forms a phase space island. The shape of the total particle distribution is then governed by the competition of the effective velocity diffusion and slowing down rates in p space. The diffusion is responsible for the distribution function steepening in the separatrix boundary layer ⁸⁴, while drag results in its hole across the island O-point. The numerical solution of Eq.5.13/Eq.5.17 ⁸⁵ with the boundary conditions described in Sec.5.2 has been successfully benchmarked against the COBBLES simulations [96] (and the references therein). The stability of this new, *perturbed*, equilibrium is then addressed through the Vlasov/Fokker-Planck – Poisson system. Secondary modes have been found to be unstable in a certain range of plasma and wave parameters.

The obtained results are relevant to plasma MHD instabilities that are excited by

⁸⁴This is due to the distribution function flattening inside the phase space island.

⁸⁵In contrast to the NTM problem, a full equation, Eq.5.13, has been solved in the entire range of H_0 to add the collisional dissipation to the model.

EPs in a tokamak. However, we stress that the impact of this work goes beyond a conventional problem of Alfvén modes in tokamak plasmas. The particle dynamics in toroidal magnetised plasmas can be described by a set of action-angle variables in 6D phase space. An isolated perturbation of the Hamiltonian forms an island in the vicinity of the rational surface. The dynamics close to the phase space island allows to be reduced to 2D provided two invariants of motion are located on the rational surface. Therefore, a problem of an isolated EP-MHD mode can be treated as a reduced 2D Hamiltonian dynamics in the vicinity of the phase space island. This can be applied to the fishbone modes, EGAMs or TAEs.

Here we have investigated the stability of the dissipative primary equilibrium, associated with a single island in phase space, with no restrictions on the island width. Generally, there can be a number of resonant harmonics. They can be resonant on same resonant surface, and hence the island configuration will be maintained but deformed at the separatrix. On the other hand, when they are resonant on different rational surfaces, a number of islands is formed and can overlap in accordance with the Chirikov criteria. This, in principle, can prevent the occurrence of secondary modes in the stochastic layer. This case is beyond the scope of this work and is left for future investigation.

Chapter VI

6 Summary and Conclusions

The presence of neoclassical tearing mode magnetic islands is anticipated for the ITER baseline scenario as well as advanced tokamak scenarios. They limit the plasma performance causing a loss of core pressure and hence reducing the fusion power output, and sometimes result in plasma disruptions through mode locking. At large island widths and in the absence of local sources, the pressure profile is flattened across the island leading to a hole in the bootstrap current in the vicinity of the island O-point. This local reduction in the bootstrap current density provides the main drive for NTMs. Based on the conventional modified Rutherford equation (e.g. [114]), the saturated island width is proportional to $(\beta_{\vartheta}/2m)r_s$. Thus, increasing plasma beta, we also increase the island width, resulting in a soft beta limit. As has been demonstrated in a number of devices, this beta limit is well below the Troyon ideal MHD beta limit. This argument also explains why NTMs with lower poloidal mode number are most dangerous and can lead to a discharge termination in a disruption. Alongside seed island control, two main control techniques have been proposed and successfully implemented. One is NTM stabilisation, which uses local O-point electron cyclotron current drive to compensate the missing bootstrap current and appears to be more preferable due to its high radial localisation. Another possibility is to modify Δ' , making it more negative, i.e. stabilising, by altering the global current density profile. The latter has been implemented by LHCD on COMPASS-D successfully providing complete NTM stabilisation [115]. A key parameter for the NTM stabilisation is the magnetic island threshold width denoted above by w_c , below which magnetic islands self-heal. The calculation of w_c has been a main aim of the work of this dissertation.

The original paper [53] determined the NTM threshold island width by balancing the destabilising bootstrap drive and stabilising polarisation current contribution. w_c was then found to be proportional to $\varepsilon^{1/2}\rho_{\vartheta i}$ and dependent on the equilibrium density and temperature gradients. However, [53] is subject to some significant limitations:

- A model radial diffusion is imposed, i.e. $\Gamma_{\psi} = -D\partial n/\partial\psi$. As we saw in Chapter IV, this provides the correct gradient of the particle distribution function away from the

island and thus is sufficient to determine the conventional bootstrap drive. However, it excludes a significant amount of the parallel current density right outside the magnetic island separatrix.

- It captures only the region away from the magnetic island separatrix and hence does not consider the above-mentioned separatrix layer contribution (its inner and outer parts) to the current density parallel to the magnetic field lines. This boundary layer contribution and the contribution outside the layer act in opposite directions and are of comparable size. Their relative size influences the island rotation frequency dependence of the polarisation contribution found in [53], which is especially important when $\rho_{\vartheta i} \lesssim w$ ⁸⁶.
- [53] imposes a model form for the electrostatic potential, which nevertheless satisfies quasi-neutrality at large w . However, as we saw in Chapter II, the drift island effect will make the electrostatic potential, required to ensure plasma quasi-neutrality, dependent on $\rho_{\vartheta i}$.
- [53] provides the NTM dispersion relation, Eq.85 of [53], valid at large w . To solve the drift kinetic equation for the ion plasma component, [53] introduces two small parameters: w/a ⁸⁷ and $\varepsilon^{1/2}\rho_{\vartheta i}/w = \rho_{bi}/w$. The latter condition excludes self-healing of small magnetic islands observed in experiments.

Following [53], we have employed the drift kinetic approach to determine the ion/electron plasma response to the NTM magnetic perturbation, assuming small magnetic islands relative to the tokamak minor radius but accurately treating the limit $w \sim \rho_{bi}$ to keep the effects of finite orbit widths. To reduce the dimension of the problem, we have derived the streamlines, described by the S function, which is to be treated as a new radial coordinate. Treating collisions perturbatively, we learn that the particle distribution function is constant along these streamlines in the absence of collisions. Proceeding to next order and introducing collisions, we reconstruct the actual form of the ion/electron distribution, i.e. its S and pitch angle, λ , dependence. In the absence of the electrostatic potential, S reproduces the shape of the magnetic island in $\{\psi, \xi\}$ space but has a radial

⁸⁶The inclusion of the separatrix layer contribution inverts the island rotation frequency dependence of the polarisation term.

⁸⁷Small magnetic islands compared to the tokamak minor radius are also considered in the current study.

shift by an amount proportional to $\rho_{\vartheta i/e}/w$. The electrostatic potential, which is calculated iteratively to ensure plasma quasi-neutrality, only slightly modifies the contours of constant S in the (ψ, ξ) plane. The radial shift in S is introduced for the passing particle branch only and plays a key role in the NTM threshold physics. This shift is in opposite directions for $V_{\parallel} \lesseqgtr 0$ (corresponding to S^{\pm}). The particle distribution function being flattened across these S^{\pm} islands but not the actual magnetic island provides a gradient in the pressure profile across magnetic islands of width $w \gtrsim \rho_{\vartheta i}$ and keeps pressure flattened across larger islands of width $w \gg \rho_{\vartheta i}$ in agreement with the conventional theory. As $\rho_{\vartheta e} \ll \rho_{\vartheta i}$, this effect is less significant for the electron distribution function, although the electron density is influenced by the ion physics via their response to the potential which arises from the plasma quasi-neutrality requirement. The fact that the pressure gradient is not removed across the magnetic island O-point at $w \gtrsim \rho_{\vartheta i}$ provides the physics that influences the NTM threshold.

The perturbative treatment of collisions becomes invalid in a thin boundary layer in pitch angle that surrounds the trapped-passing boundary. Here we have employed the pitch angle scattering collision operator with the momentum conservation term and solved the 2D boundary layer problem to rigorously match the passing and trapped solutions from outside this layer. This collisional layer being the dominant source of dissipation in our problem is responsible for the island rotation frequency and hence the polarisation current contribution to the island evolution. From our calculations, the plasma response to an NTM magnetic perturbation has been found to be stabilising at $w \leq 3\rho_{\vartheta i}$ for a small inverse aspect ratio, circular cross section tokamak approximation with $\varepsilon = 0.1$, $L_n/L_{Tj} = 1$ and $\omega_E = 0$.

To summarise

- A new drift kinetic theory of magnetic islands, valid for $w \sim \rho_{\vartheta i}$, has been developed in a low collisionality plasma.
- The electron/ion distribution function is flattened across drift islands, which are radially shifted by a value $\propto \rho_{\vartheta e,i}/w$ compared to the magnetic island.
- As a result, the pressure (density/temperature) gradient is sustained across the magnetic island of $w \lesssim \rho_{\vartheta i}$.

- At $w \lesssim \rho_{\vartheta i}$, the finite ion density gradient is sustained around the magnetic island O-point due to the drift island effect, i.e. the radial shift in S ,
 - the electron density gradient is also not removed across the island O-point due to the plasma quasi-neutrality requirement and the electron response to the electrostatic potential.
- This suppresses the NTM drive when w is small providing the NTM threshold.
 - We highlight that this threshold physics arises from the passing particle dynamics, and not the finite banana width of trapped particles.
 - Therefore, the relevant parameter for w_c is the ion poloidal Larmor radius, and not the ion banana orbit width: we find $w_c = 3\rho_{\vartheta i}$ for large aspect ratio.
 - This NTM threshold result is mostly governed by the electron component⁸⁸ in the presence of the S diffusion. Roughly, this can be explained by the fact that $m_e \ll m_i$, and hence at $w \rightarrow 0$ the ions average over the electro-magnetic field associated with the island, while electrons still respond to the field as their banana orbits are narrow.⁸⁹
 - The island propagation frequency dependence of the polarisation current contribution⁹⁰ has been determined at certain ν_i^* , $\rho_{\vartheta i}$, w , L_{n0} and L_{Tj} . There are two main contributions to the parallel current density that act in opposite directions: one is in a layer in the vicinity of the island separatrix, and the one is outside this layer.
 - At $w \gg \rho_{\vartheta i}$, the contribution to the parallel current density around the magnetic island separatrix only slightly dominates over that outside the island.
 - At $w \gtrsim \rho_{\vartheta i}$, the separatrix layer contribution is dominant and exceeds the contribution outside the layer.
 - The island propagation frequency is determined by the dissipation processes in

⁸⁸This is in agreement with the DK-NTM solution with analytic electrons [73, 93, 74].

⁸⁹We stress that the origin of this behaviour at small w is still an open question and is to be further investigated.

⁹⁰At large frequencies, $\Delta_{pol} \propto \omega^2$, i.e. is parabolic, which is consistent with previous analytic/numerical works. The behaviour of Δ_{pol} near $\omega = 0$ including the region of coupling to the drift waves is more complicated and its explanation is to be a part of future investigations. In [90, 91] the sign change in this area has been explained by the competition of the island rotation and the toroidal precession.

a tokamak plasma and/or might be influenced by error fields or coupling to a resistive wall⁹¹. Neglecting any external torques, we find that the dominant source of dissipation is the collisional dissipation arising from a layer near the trapped-passing boundary in pitch angle. Employing the component of Ampère's law which is out-of-phase with the magnetic island provides an equation for the island propagation frequency. A set of solutions has been found. Δ_{pol} evaluated at these values of ω provides $\Delta_{pol} > 0$, i.e. destabilising, at given ν_i^* , $\rho_{\partial i}$, w , L_{n0} and L_{Tj} .

Chapter V of this dissertation addresses a different problem: here we investigate the stability of an island in phase space, generated by trapping of energetic particles in plasma waves. The Hamiltonian formalism has been employed to provide the dimensionality reduction to a 2D dynamics of a phase space island. This problem shares the mathematical basis with the NTM problem to reveal the dynamics of an island-like structure.

- Solving the Fokker-Planck equation in the presence of the effective velocity space diffusion and drag, we find a *perturbed* equilibrium associated with these phase space islands.
- To investigate its stability, we then address the Vlasov/Fokker-Planck – Poisson system. The Lagrangian of this system provides the secondary mode dispersion relation.
- Considering contours of constant $|D(\delta\omega, \gamma)|^{-1}$ in the $(\delta\omega, \gamma)$ plane, where D is the secondary mode dispersion function, $\delta\omega$ and γ are the real and imaginary parts of the mode frequency, we search for poles of $|D(\delta\omega, \gamma)|^{-1}$. Being located in the upper/lower half-plane, they provide the secondary mode growth/decay rate.
- Secondary instabilities have been found in a certain range of mode numbers and primary island widths.
- γ becomes positive above some marginal island width, grows to a maximum value, as the island width increases, and then decays crossing the zero level for the second time. This dependence is in agreement with the time dependent numerical simulation provided by COBBLES.
- The maximum growth rate of secondary modes is obtained when the accessible

⁹¹These effects have been previously investigated, e.g. [77, 78].

resonant phase velocity is near the separatrix of the primary island. This result is anticipated as the instability is driven by a positive slope of the distribution function, and its gradient is the steepest at the edge of the island in a pure diffusion case.

We note that the impact of the work presented in Chapter V and in [95, 96] goes beyond a conventional problem of Alfvén modes in tokamak plasmas. It can be applied to EP-MHD modes such as TAEs, fishbones or EGAMs.⁹²

6.1 Future work

Although the limitations of [53] have been eliminated in the presented work, it still can be further improved. Alongside^{89,90}, the effects of plasma shaping can be added to the model (see Appendix E.7). These effects on NTMs are generally weak in conventional tokamaks. Since the curvature term $\Delta_{cur} \propto \varepsilon^2$, it can provide a significant contribution only in spherical tokamaks [67, 116]. However, plasma shaping affects the global confinement properties and hence the pressure and current density profiles [41], which results in changes in Δ' , Δ_{bs} and Δ_{pol} . Furthermore, plasma shaping can influence MHD instabilities that create a seed for NTMs. The latter is not to be considered as a part of the future NTM work, but is subject to possible NTM trigger mechanisms⁹³.

The RDK-NTM solution presented in this dissertation as well as the DK-NTM solution with model analytic electrons discussed in [73, 93, 74] give $w_c = 3\rho_{\theta i}$ for the NTM magnetic island threshold. This result is obtained for the small inverse aspect ratio circular cross section tokamak approximation at certain ε , L_n , L_{Tj} , L_q and plasma collisionality in the magnetic island rest frame. It is based on the neoclassical contributions to the island evolution only⁹⁴ and does not account for the Rutherford term, Δ' . The equilibrium density and temperature gradients as well as the safety factor profile have been assumed to be localised (constant)⁹⁵ near the rational surface. Although, the RDK-NTM generally

⁹²Possible asides are discussed in "Stability of an island in phase space", Festival de Théorie, Aix-en-Provence, France, 2019 (presentation).

⁹³ECCD has shown a complete NTM stabilisation on a number of machines even with the sawtooth oscillations or fishbone modes in a discharge [41]. However, with ECCD being turned off, triggers generate the NTM again.

⁹⁴Some of the terms of $\mathcal{O}(\varepsilon^2)$ have been dropped as higher order contributions.

⁹⁵The actual density, temperature, q profiles/equilibrium profiles reconstructed by equilibrium codes, e.g. EFIT, can be added to the primary equilibrium model. However, this is an order w/a affect, and hence the terms of $\mathcal{O}(w/a)$ would also have to be introduced.

allows the poloidal magnetic field variation, it has not been included in the current result. Therefore, along with ^{89,90} we consider

- Plasma shaping with the poloidal magnetic field variation are to be accounted for. The accurate determination of the curvature contribution will require corrections of order ε^2 and higher added to Eqs.2.35,2.36.
- RDK-NTM treats both, electrons and ions, numerically. The DK-NTM solution presented in [73, 93, 74] includes numerical ions and analytic electrons due to the fact that $\rho_{\vartheta e} \ll \rho_{\vartheta i}$. A new version of the DK-NTM code that adds the drift island effects to the electron component and solves Eq.2.35 for electrons as well is under development. Its initial results for the ion component⁹⁶ benchmarked against the RDK-NTM ion distribution function are presented in Sec.4.2. The comparison of both solutions is to be further updated when a new version of DK-NTM is available.
- At $\nu_i^* \sim 10^{-2}$, the (R)DK-NTM solutions are in agreement in the vicinity of the S island separatrix in the entire range of λ variation even with the following limitations of the reduced drift kinetic approach:
 - In the RDK-NTM solver, we introduce a thin boundary layer around the trapped-passing boundary to match passing and trapped solutions outside the layer. Employing the layer thinness, we exclude any λ variations from S to leading order.
 - At any λ in the passing branch, S diffusion and free streaming can be of the same order near the S island separatrix (this situation was modelled in [64]). Perturbative treatment implemented in the RDK-NTM approach would not be valid, and one would require a full solution of the drift kinetic equation near the separatrix. However, it will not influence our magnetic island threshold result associated with the bootstrap contribution. Furthermore, even with this possible limitation, the RDK-NTM and DK-NTM solutions are in agreement close to the S separatrix⁹⁷.

as a part of further improvements.

⁹⁶The electrostatic potential is found from the plasma quasi-neutrality requirement with the electron density being calculated from the electron solution of Eq.2.35.

⁹⁷Note that both, RDK-NTM and DK-NTM, treat collisions perturbatively compared to $(V_{\parallel}/Rq)\partial/\partial\vartheta$, but allow $k_{\parallel}V_{\parallel} \sim \nu_j\partial^2/\partial\lambda^2$ in the collisional dissipation layer/for the full range of λ , respectively.

Appendix

A Formation of magnetic islands

In this appendix we describe the formation of magnetic islands. For simplicity, we focus on the slab non-tokamak formulation similar to that addressed in Figs.2.2,2.3.

Let us assume that the main unperturbed magnetic field, $B_y^0(x)$, is in y direction ⁹⁸ (see Fig.A.1) and changes with x with $B_y^0(0) = 0$, which corresponds to the neutral layer. This magnetic field is generated by

$$J_z^0 = \frac{1}{\mu_0} \frac{\partial B_y^0}{\partial x}.$$

The equilibrium state is described by

$$\frac{\partial p^0}{\partial x} + B_y^0 J_z^0 = 0.$$

Introducing the magnetic field perturbation in x direction, $B_x^1 \propto \exp(-i\omega t +iky)$, we write

$$\frac{\partial B_x^1}{\partial x} + ikB_y^1 = 0$$

due to $\text{div}\mathbf{B} = 0$. The time varying B_x^1 generates the electric field in z direction:

$$\frac{\partial B_x^1}{\partial t} = -\frac{\partial E_z^1}{\partial y}.$$

This electric field, in turn, leads to the plasma $\mathbf{E} \times \mathbf{B}$ drift with

$$u_x^1 = -\frac{E_z^1}{B_y^0} \quad (\text{A.1})$$

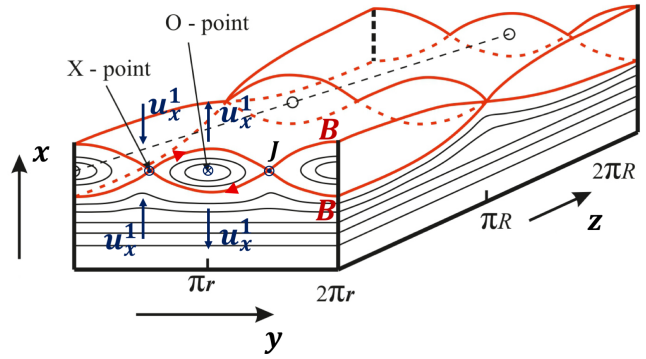


Figure A.1: A ring of toroidal plasma in the presence of the NTM magnetic islands.

⁹⁸To address a conventional tokamak case, we have to keep the dominant toroidal magnetic field component, i.e. B_z^0 . In spherical tokamaks, $B_z^0 \sim B_y^0$ roughly.

in x direction as shown in Fig.A.1. In the vicinity of the neutral layer, $u_x^1 \rightarrow \infty$ as the unperturbed magnetic field $B_y^0 \rightarrow 0$ when $x \rightarrow 0$. In this region, the finite plasma conductivity has to be taken into account, and hence we replace the above expression for u_x^1 with

$$u_x^1 = -\frac{E_z^1}{B_y^0} + \frac{\eta J_z^1}{B_y^0}. \quad (\text{A.2})$$

The latter is Ohm's law in resistive MHD. Here $\eta = \sigma_{\parallel}^{-1} = 0.51 m_e \nu_{ei} / n_e e^2$ for a hydrogen plasma. B_x^1 being positive in the vicinity of the neutral layer, where $B_y^0 = 0$, leads the magnetic field line away from $x = 0$ into the region of positive x . Away from the neutral layer, B_y^0 becomes non-zero leading the field line in y direction. When the phase of the perturbed field, B_x^1 , changes, the field line approaches $x = 0$ and then passes into the region of negative x . Here B_y^0 is non-zero, and thus the field line progresses in the $-y$ direction, closing the loop to form an island as shown in Fig.A.1.

This simple example illustrates the mechanism of magnetic island formation provided the B_y^0 component is dominant. In a tokamak though, there is a strong magnetic field in z direction that has to be accounted for. Everywhere in a plasma, except for the resistive layer in the vicinity of the rational surface, we write

$$\mathbf{J} \times \mathbf{B} = \nabla p$$

and hence $\text{rot}[\mathbf{J} \times \mathbf{B}] = 0$. The latter reads

$$\mathbf{J} \cdot \nabla \mathbf{B} - \mathbf{B} \cdot \nabla \mathbf{J} = 0 \quad (\text{A.3})$$

since $\text{div} \mathbf{B} = 0$ and $\text{div} \mathbf{J} = 0$. Imposing the small inverse aspect ratio circular cross section tokamak approximation, we write $B_{\vartheta}^0 \sim \varepsilon B_{\varphi}^0$ for equilibrium magnetic fields and $J_{\vartheta}^0 \sim \varepsilon J_{\varphi}^0$ for equilibrium currents. For perturbations, we impose $B_{\varphi}^1 \sim \varepsilon B_r^1 \sim \varepsilon B_{\vartheta}^1$ and $\varepsilon J_{\varphi}^1 \sim J_{\vartheta}^1 \sim J_r^1$ (similar to the above example). Therefore, Eq.A.3 reduces to

$$\mathbf{B}^0 \cdot \nabla J_{\varphi}^1 + \mathbf{B}^1 \cdot \nabla J_{\varphi}^0 = 0 \quad (\text{A.4})$$

provided $\mathbf{J}^0 \cdot \nabla B_\varphi^0 \ll \mathbf{B}^0 \cdot \nabla J_\varphi^0$. $\text{div} \mathbf{B} = 0$ now reads

$$\frac{\partial}{\partial r} (r B_r^1) + \frac{\partial}{\partial \vartheta} B_\vartheta^1 = 0.$$

Defining ψ as

$$\begin{cases} B_r^1 = -\frac{1}{r} \frac{\partial \psi}{\partial \vartheta} \\ B_\vartheta^1 = \frac{\partial \psi}{\partial r} \end{cases}, \quad (\text{A.5})$$

we obtain

$$\mu_0 J_\varphi^1 = \frac{1}{r^2} \frac{\partial}{\partial r} r \frac{\partial \psi}{\partial r} + \frac{1}{r^2} \frac{\partial^2 \psi}{\partial \vartheta^2} \quad (\text{A.6})$$

from Ampère's law. Replacing the form of the perturbation $\propto \exp(-i\omega t + ik y)$ with $\propto \exp(im\vartheta - in\varphi)$ and combining Eqs.A.4,A.5,A.6, we write

$$\frac{1}{\mu_0} \left[\frac{m B_\vartheta^0}{r} - \frac{n B_\varphi^0}{R} \right] \Delta \psi - \frac{m}{r} \frac{dJ_\varphi^0}{dr} \psi = 0, \quad (\text{A.7})$$

where Δ is the Laplacian given by the right hand side operator of Eq.A.6. Eq.A.7 can be further reduced using the expression for the safety factor in the cylindrical approximation:

$$\Delta \psi = \frac{\mu_0}{B_\vartheta^0} \frac{m}{m - nq} \frac{dJ_\varphi^0}{dr} \psi. \quad (\text{A.8})$$

Eq.A.7/A.8 for ψ is valid in the entire plasma volume in the limit of large aspect ratio circular cross section tokamak, except for the layer in the vicinity of the rational surface, where plasma conductivity has to be treated as being finite. Indeed, a singularity appears in Eq.A.8 at $r = r_s$ (or $\psi = \psi_s$ if ψ is taken for the radial coordinate), i.e. $q(\psi_s) = m/n$ similar to Eq.A.1 in the slab formulation. In the resistive layer, imposing $\mathbf{E} + \mathbf{V} \times \mathbf{B} = \eta \mathbf{J}$ and taking its rotor return

$$-\frac{\partial B_r}{\partial t} + \mathbf{B} \cdot \nabla V_r = -\frac{\eta}{\mu_0} \Delta B_r,$$

where V_r is the radial component of velocity. Taking $\propto \exp(\gamma t + im\vartheta - in\varphi)$ for the perturbation and using Eq.A.5 to obtain $B_r = -im\psi/r$, we come to

$$\Delta \psi = \frac{\mu_0}{\eta} \gamma \psi + \frac{\mu_0 B_\vartheta^0}{\eta} \frac{m - nq}{m} V_r. \quad (\text{A.9})$$

Here $\Delta\psi \approx d^2\psi/dr^2$ due to layer thinness. As we can see from Eq.A.9, the singularity at $q = m/n$ is now removed. Eq.A.9 has to be coupled to the equation of motion to determine V_r .

Eq.A.9 is to be solved for ψ in the layer, while Eq.A.7/A.8 is to be applied in the region outside the layer, i.e. $r > r_s$ and $r < r_s$. Solutions at $r > r_s$ and $r < r_s$ provide a jump of $\nabla_r\psi$ across the magnetic island. This jump is referred to as the classical tearing mode stability parameter. The matching is provided by the resistive layer, i.e. solutions of Eq.A.7/A.8 at $r \gtrsim r_s$ and Eq.A.9 in the layer and their derivatives have then to be matched. The solution for ψ in the layer is close to a constant [12], and the constant ψ approximation is imposed in the majority of problems. Here we have briefly discussed the tokamak case and the calculation of Δ' . As the focus of the current study is on the neoclassical bootstrap and polarisation contributions to the island time evolution, we omit further details regarding Δ' . A more detailed derivation can be found in [12].

B Magnetic island perturbation

We decompose Eq.2.4 to write

$$\mathbf{B}_1 = (\nabla A_{\parallel}) \times \mathbf{b} + A_{\parallel} \nabla \times \mathbf{b},$$

where

$$\nabla A_{\parallel} = \frac{n\tilde{\psi}}{R} \sin n\xi \left(\nabla\varphi - \frac{m}{n} \nabla\vartheta \right),$$

and hence

$$\begin{aligned} (\nabla A_{\parallel}) \times \mathbf{b} &= \frac{n\tilde{\psi}}{RB_0} \sin n\xi \left(\nabla\varphi - \frac{m}{n} \nabla\vartheta \right) \times (I\nabla\varphi + \nabla\varphi \times \nabla\psi) = \\ &= -\frac{m\tilde{\psi}}{rR^2B_{\vartheta}} \frac{B_{\varphi}}{B_0} \left(1 + \frac{n}{m} \frac{rB_{\vartheta}}{RB_{\varphi}} \right) \sin n\xi \nabla\psi = \\ &= -\frac{m\tilde{\psi}}{rR^2B_{\vartheta}} \sin n\xi \nabla\psi + \mathcal{O}(\varepsilon^2); \end{aligned}$$

$$\begin{aligned} A_{\parallel} \nabla \times \mathbf{b} &= -\frac{\tilde{\psi}}{R} \cos n\xi \left(\frac{1}{B_0} \nabla \times \mathbf{B}_0 - \frac{1}{B_0^2} \nabla B_0 \times \mathbf{B}_0 \right) = \\ &= -\frac{\tilde{\psi}}{R} \cos n\xi \left[\frac{\mu_0}{B_0} \mathbf{J}_0 - \frac{1}{B_0^2} \nabla B_0 \times (I\nabla\varphi + \nabla\varphi \times \nabla\psi) \right] = \\ &= -\frac{\tilde{\psi}}{R} \cos n\xi \left[\frac{\mu_0}{B_0} \mathbf{J}_0 - \frac{1}{B_0^2} \left(\frac{\partial B_0}{\partial \psi} I\nabla\psi \times \nabla\varphi + \frac{\partial B_0}{\partial \psi} |\nabla\psi|^2 \nabla\varphi + \frac{\partial B_0}{\partial \vartheta} I\nabla\vartheta \times \nabla\varphi \right) \right] = \\ &= -\frac{\tilde{\psi}}{R} \cos n\xi \left[\frac{\mu_0}{B_0} \mathbf{J}_0 - \frac{1}{B_0^2} \left(\frac{B_{\varphi}}{rRB_{\vartheta}} \frac{\partial B_0}{\partial \vartheta} \nabla\psi - \frac{\partial B_0}{\partial \psi} IrB_{\vartheta} \nabla\vartheta + R^2B_{\vartheta}^2 \frac{\partial B_0}{\partial \psi} \nabla\varphi \right) \right]. \end{aligned}$$

Estimating each term, we obtain

$$|(\nabla A_{\parallel}) \times \mathbf{b}| \sim \frac{m\tilde{\psi}}{rR^2B_{\vartheta}} |\nabla\psi| \sim \frac{\tilde{\psi}}{rR};$$

combination of the term that contains the poloidal component of \mathbf{J}_0 and the second term in round brackets of $A_{\parallel} \nabla \times \mathbf{b}$ is of order

$$\frac{\tilde{\psi}}{R} rB_{\vartheta} \frac{\partial}{\partial \psi} \left(\frac{I}{B_0} \right) |\nabla\vartheta| \sim \frac{\tilde{\psi}}{rR} rB_{\vartheta} \frac{\partial R}{\partial \psi} \sim \frac{\tilde{\psi}}{rR};$$

the term that contains the toroidal component of \mathbf{J}_0 is of order

$$\begin{aligned} \frac{\tilde{\psi}}{R} \frac{1}{B_0} \frac{\partial}{\partial \psi} (r B_\vartheta) |\nabla \psi \times \nabla \vartheta| &\sim \frac{\tilde{\psi}}{R} \frac{1}{B_0} \frac{\partial}{\partial \psi} (r B_\vartheta) \frac{R^2 B_\vartheta}{r} |\nabla \varphi| \sim \\ \frac{\tilde{\psi}}{r R} \frac{B_\vartheta}{B_0} &\sim \varepsilon \frac{\tilde{\psi}}{r R}; \end{aligned}$$

the first and the last terms in round brackets of $A_{\parallel} \nabla \times \mathbf{b}$ are of order

$$\frac{\tilde{\psi}}{R} \frac{1}{B_0^2} \frac{B_\varphi}{r R B_\vartheta} \frac{\partial B_0}{\partial \vartheta} |\nabla \psi| \sim \frac{\tilde{\psi}}{r R} \frac{1}{B_0^2} \frac{B_\varphi}{R B_\vartheta} \varepsilon B_0 R B_\vartheta \sim \varepsilon \frac{\tilde{\psi}}{r R}$$

and

$$\frac{\tilde{\psi}}{R} \frac{1}{B_0^2} R^2 B_\vartheta^2 \frac{\partial B_0}{\partial \psi} |\nabla \varphi| \sim \frac{\tilde{\psi}}{r R} \frac{B_\vartheta}{B_0} R |\nabla \varphi| \sim \varepsilon \frac{\tilde{\psi}}{r R},$$

respectively. Therefore,

$$\frac{B_1}{B_0} \sim \frac{\tilde{\psi}}{r R B_0} \sim \frac{w^2 R B_\vartheta^2 q'_s}{r B_0 q_s} \sim \frac{w^2 R B_\vartheta^2}{r B_0} \frac{1}{r R B_\vartheta} \sim \frac{w^2}{r^2} \frac{B_\vartheta}{B_0} \sim \varepsilon \Delta^2.$$

Thus, the total magnetic field becomes

$$\begin{aligned} \mathbf{B} &= I(\psi) \nabla \varphi + \nabla \varphi \times \nabla \psi - \\ &- m \tilde{\psi} \sin n \xi \nabla \vartheta \times \nabla \varphi + \frac{\tilde{\psi}}{R} \frac{\partial}{\partial \psi} \left(\frac{I}{B_0} \right) \cos n \xi \nabla \varphi \times \nabla \psi + \mathcal{O}(\varepsilon^2 \Delta^2 B_0). \end{aligned}$$

Aside: in the limit of circular poloidal cross section in the absence of the Shafranov shift keeping terms up to $\mathcal{O}(\varepsilon \Delta^2 B_0)$ in \mathbf{B} , we write

$$\begin{aligned} \mathbf{B} \cdot \nabla \psi &= -m \tilde{\psi} \frac{B_\vartheta}{r} \sin n \xi, \\ \mathbf{B} \cdot \nabla \vartheta &= \frac{B_\vartheta}{r} \left[1 + \frac{\tilde{\psi}}{R} \frac{\partial}{\partial \psi} \left(\frac{I}{B_0} \right) \cos n \xi \right], \\ \mathbf{B} \cdot \nabla \varphi &= \frac{B_\varphi}{R}, \\ \mathbf{B} \cdot \nabla \xi &= \frac{B_\vartheta}{r} \left[q - \frac{m}{n} - \frac{m \tilde{\psi}}{n R} \frac{\partial}{\partial \psi} \left(\frac{I}{B_0} \right) \cos n \xi \right] \end{aligned}$$

provided $q = (\mathbf{B}_0 \cdot \nabla \varphi) / (\mathbf{B}_0 \cdot \nabla \vartheta) = IJ/R^2$ and $|\nabla \vartheta| = 1/r$. J is defined as in Sec.D.1.

C Switching from poloidal flux function, ψ , to toroidal canonical momentum, p_φ

In the above derivations, Eq.1.12 for the perturbed distribution function has been rewritten in $\{p_\varphi, \xi, \vartheta, \lambda, V; \sigma\}$ space directly. In this appendix we explain why it is convenient to switch from the poloidal flux, ψ , to the toroidal canonical momentum, p_φ , and consider p_φ as the new radial coordinate.

To solve Eq.1.12, we expand the particle distribution function, g_j , in Δ and obtain Eq.2.18 for the leading order distribution, $g_j^{(0)}$, at fixed p_φ . If we worked in $\{\psi, \xi, \vartheta, \lambda, V; \sigma\}$ space, we would obtain

$$\frac{IV_{\parallel}}{R^2qB_0} \left[\left. \frac{\partial g_j^{(0)}}{\partial \vartheta} \right|_{\psi, \xi, \lambda, V} + I \frac{\partial}{\partial \vartheta} \left(\frac{V_{\parallel}}{\omega_{cj}} \right) \frac{\partial g_j^{(0)}}{\partial \psi} \right] = 0 \quad (\text{C.1})$$

for the leading order equation. This is equivalent to Eq.2.18 with

$$p_\varphi = \psi - \psi_s - \frac{IV_{\parallel}}{\omega_{cj}}.$$

Introducing p_φ allows one to reduce the dimension of the problem by stating that the leading order particle distribution is ϑ -independent provided p_φ is fixed. Eq.2.18 represents the combination of free streaming along unperturbed magnetic field lines and the leading contribution of the magnetic drift. It describes how the particles follow orbits to preserve p_φ .

D Derivation of the drift magnetic island kinetic equation

D.1 Some useful identities

The Grad-Shafranov notations are

$$\nabla R = \mathbf{e}_R, \quad \nabla \varphi = \frac{\mathbf{e}_\varphi}{R}, \quad \nabla Z = \mathbf{e}_Z. \quad (\text{D.1})$$

$\{\psi, \varphi, \chi\}$ provides the orthogonal toroidal coordinate system, i.e.

$$\nabla \psi \cdot \nabla \varphi = \nabla \psi \cdot \nabla \chi = \nabla \varphi \cdot \nabla \chi = 0.$$

Here χ corresponds to the poloidal direction. The corresponding Jacobian, \mathcal{J} , is

$$\nabla \varphi \times \nabla \psi = \mathcal{J} B_\vartheta^2 \nabla \chi, \quad \mathcal{J}^{-1} = [\nabla \varphi \times \nabla \psi] \cdot \nabla \chi. \quad (\text{D.2})$$

In conventional toroidal coordinates, $\{\psi, \varphi, \vartheta\}$,

$$\nabla \psi \cdot \nabla \varphi = \nabla \varphi \cdot \nabla \vartheta = 0, \quad (\text{D.3})$$

$\nabla \psi \cdot \nabla \vartheta \neq 0$, i.e. the basis is non-orthogonal. ϑ here is the poloidal angle. The Jacobian of this system, J , is

$$J^{-1} = \nabla \psi \cdot [\nabla \vartheta \times \nabla \varphi].$$

Thus, the following useful identities are

$$\begin{aligned} |\nabla \psi| &= R B_\vartheta, & |\nabla \varphi| &= \frac{1}{R}, & |\nabla \vartheta| &= \frac{1}{J B_\vartheta}, & |\nabla \chi| &= \frac{1}{\mathcal{J} B_\vartheta} \\ [\nabla \varphi \times \nabla \psi] \times \nabla \varphi &= \frac{\nabla \psi}{R^2}, \end{aligned} \quad (\text{D.4})$$

ϑ and χ are connected via

$$\vartheta = \frac{1}{q} \int^{\chi} \nu d\chi' \quad (\text{D.5})$$

with $\nu = (\mathbf{B}_0 \cdot \nabla \varphi) / (\mathbf{B}_0 \cdot \nabla \chi) = I\mathcal{J}/R^2$. From Eq.D.5,

$$\nabla \vartheta = \vartheta'_\chi \nabla \chi + \vartheta'_\psi \nabla \psi, \quad (\text{D.6})$$

according to Barrow's theorem, $\vartheta'_\chi \equiv \partial \vartheta / \partial \chi = \nu(\chi)/q = I\mathcal{J}/qR^2$. $\vartheta'_\psi \equiv \partial \vartheta / \partial \psi = R^{-2} B_\vartheta^{-2} (\nabla \psi \cdot \nabla \vartheta)$.

The vector cross product

$$\begin{aligned} \text{div} [\mathbf{A} \times \mathbf{B}] &\equiv \nabla \cdot [\mathbf{A} \times \mathbf{B}] = \varepsilon_{ijk} \partial_i A_j B_k = [\nabla \times \mathbf{A}] \cdot \mathbf{B} - \mathbf{A} \cdot [\nabla \times \mathbf{B}], \\ \text{rot} [\mathbf{A} \times \mathbf{B}] &\equiv \nabla \times [\mathbf{A} \times \mathbf{B}] = \mathbf{A} (\nabla \cdot \mathbf{B}) - \mathbf{B} (\nabla \cdot \mathbf{A}) + (\mathbf{B} \cdot \nabla) \mathbf{A} - (\mathbf{A} \cdot \nabla) \mathbf{B} = \\ &= (\nabla \cdot \mathbf{B} + \mathbf{B} \cdot \nabla) \mathbf{A} - (\nabla \cdot \mathbf{A} + \mathbf{A} \cdot \nabla) \mathbf{B}, \end{aligned} \quad (\text{D.7})$$

ε_{ijk} is the three dimensional Levi-Civita symbol.

Addition and multiplication

$$\begin{aligned} (\mathbf{A} \cdot \mathbf{B}) &= (\mathbf{B} \cdot \mathbf{A}) \\ [\mathbf{A} \times \mathbf{B}] &= -[\mathbf{B} \times \mathbf{A}] \\ \mathbf{A} \cdot [\mathbf{B} \times \mathbf{C}] &= \mathbf{B} \cdot [\mathbf{C} \times \mathbf{A}] = \mathbf{C} \cdot [\mathbf{A} \times \mathbf{B}] \\ \mathbf{A} \times [\mathbf{B} \times \mathbf{C}] &= \mathbf{B} (\mathbf{A} \cdot \mathbf{C}) - \mathbf{C} (\mathbf{A} \cdot \mathbf{B}), \end{aligned} \quad (\text{D.8})$$

where \mathbf{A} , \mathbf{B} and \mathbf{C} are vectors.

D.2 Derivation of the NTM orbit averaged drift kinetic equation

We solve Eq.1.12 in the island rest frame for the ion/electron response to the NTM perturbation of the magnetic field. j denotes main electrons and ions. As discussed in the main part, we assume the Maxwell-Boltzmann plasma and thus impose

$$f_j = \left(1 - \frac{eZ_j \Phi}{T_j} \right) f_j^M + g_j, \quad (\text{D.9})$$

provided $eZ_j\Phi \ll T_j$ and $f_j^M(\psi) = n_0(\psi) \pi^{-3/2} V_{T_j}^{-3}(\psi) e^{-V^2/V_{T_j}^2(\psi)}$ being the Maxwellian of a species j . n_0 is the equilibrium density, i.e. $n_{eqm} \cong n_0(1 - eZ_j\Phi/T_j)$ with n_{eqm} being the Boltzmann density, and $V_{T_j} = (2T_j/m_j)^{1/2}$ is the thermal velocity of a species. g_j is the perturbed distribution function associated with the tearing mode and is to be determined to provide the NTM threshold physics and the island propagation frequency. As we seek the solution localised to the vicinity of the magnetic island, we Taylor expand the Maxwell-Boltzmann term and the electrostatic potential about the resonant surface. Hence, $f_j^M(\psi_s)$ has no spatial dependence, only the velocity dependence. This provides the Neumann boundary as $\psi \rightarrow \infty$.

Substituting Eq.D.9 Taylor expanded around the rational surface into Eq.1.12 gives

$$\begin{aligned} & V_{\parallel} \nabla_{\parallel} g_j + \mathbf{V}_E \cdot \nabla g_j + \mathbf{V}_b \cdot \nabla g_j - \frac{eZ_j}{m_j V} [V_{\parallel} \nabla_{\parallel} \Phi + \mathbf{V}_b \cdot \nabla \Phi] \frac{\partial g_j}{\partial V} = C_j(g_j) + \\ & + \frac{eZ_j}{T_j(\psi_s)} f_j^M(\psi_s) [V_{\parallel} \nabla_{\parallel} \Phi + \mathbf{V}_E \cdot \nabla \Phi + \mathbf{V}_b \cdot \nabla \Phi] + \\ & + \frac{eZ_j}{m_j V} [V_{\parallel} \nabla_{\parallel} \Phi + \mathbf{V}_b \cdot \nabla \Phi] \left(1 - \frac{eZ_j \Phi(\psi_s)}{T_j(\psi_s)}\right) \frac{\partial f_j^M(\psi_s)}{\partial V} + C_j \left[\left(1 - \frac{eZ_j \Phi(\psi_s)}{T_j(\psi_s)}\right) f_j^M(\psi_s) \right] \end{aligned}$$

Since the $\mathbf{E} \times \mathbf{B}$ drift is perpendicular to $\mathbf{E} = -\nabla\Phi$ and \mathbf{B} ,

$$\mathbf{V}_E \cdot \nabla \Phi = \frac{\mathbf{E} \times \mathbf{B}}{B^2} \cdot \nabla \Phi = \frac{\mathbf{B} \times \nabla \Phi}{B^2} \cdot \nabla \Phi = 0.$$

$$C_j \left[\left(1 - \frac{eZ_j \Phi}{T_j(\psi_s)}\right) f_j^M(\psi_s) \right] = \left(1 - \frac{eZ_j \Phi}{T_j(\psi_s)}\right) C_j [f_j^M(\psi_s)] = 0,$$

as the collision operator acts in velocity space, and the Maxwellian is *collisionless* by its definition, i.e. the Maxwellian eliminates Eq.1.9 in its general form. In particular, the pitch angle scattering collision operator employed in Sec.2.2 acts in λ space at fixed ψ and thus eliminates the Maxwellian (the momentum conservation term is eliminated due to the summation over σ at fixed ψ).

$$\begin{aligned} & V_{\parallel} \nabla_{\parallel} g_j + \mathbf{V}_E \cdot \nabla g_j + \mathbf{V}_b \cdot \nabla g_j - \frac{eZ_j}{m_j V} [V_{\parallel} \nabla_{\parallel} \Phi + \mathbf{V}_b \cdot \nabla \Phi] \frac{\partial g_j}{\partial V} = \\ & = C_j(g_j) + \frac{eZ_j}{T_j(\psi_s)} f_j^M(\psi_s) [V_{\parallel} \nabla_{\parallel} \Phi + \mathbf{V}_b \cdot \nabla \Phi] + \end{aligned}$$

$$+ \frac{eZ_j}{m_j V} [V_{\parallel} \nabla_{\parallel} \Phi + \mathbf{V}_b \cdot \nabla \Phi] \left(1 - \frac{eZ_j \Phi(\psi_s)}{T_j(\psi_s)} \right) f_j^M(\psi_s) \left(-\frac{m_j V}{T_j(\psi_s)} \right).$$

Since the highlighted terms cancel out, we obtain

$$\begin{aligned} & V_{\parallel} \nabla_{\parallel} g_j + \mathbf{V}_E \cdot \nabla g_j + \mathbf{V}_b \cdot \nabla g_j - \frac{eZ_j}{m_j V} [V_{\parallel} \nabla_{\parallel} \Phi + \mathbf{V}_b \cdot \nabla \Phi] \frac{\partial g_j}{\partial V} = \\ & = C_j(g_j) + \left(\frac{eZ_j}{T_j(\psi_s)} \right)^2 f_j^M(\psi_s) [V_{\parallel} \nabla_{\parallel} \Phi + \mathbf{V}_b \cdot \nabla \Phi] \Phi(\psi_s). \end{aligned} \quad (\text{D.10})$$

Note: later we introduce the orderings: $eZ_j \Phi / T_j \sim \Delta$, $g_j / f_j^M \sim \Delta$, $\delta \Phi / \Phi \sim \Delta$, and thus Eq.D.10 will reduce to

$$V_{\parallel} \nabla_{\parallel} g_j + \mathbf{V}_E \cdot \nabla g_j + \mathbf{V}_b \cdot \nabla g_j - \frac{eZ_j}{m_j V} [V_{\parallel} \nabla_{\parallel} \Phi + \mathbf{V}_b \cdot \nabla \Phi] \frac{\partial g_j}{\partial V} = C_j(g_j) \quad (\text{D.11})$$

to be solved for g_j . Eq.1.12/D.10/D.11 is the drift kinetic equation in 5D phase space, $\{\mathbf{r}, \mu, \mathcal{K}\} / \{\mathbf{r}, \lambda, V; \sigma\}$. Here \mathbf{r} is a 3-tuple of spatial coordinates. The gyro-angle dependence is averaged out at fixed \mathbf{r} . The time dependence is omitted as we work in the island rest frame, i.e. $\omega = 0$. Working in a tokamak geometry, we seek $g_j(\mathbf{r}, \lambda, V; \sigma) = g_j(\psi, \xi, \vartheta, \lambda, V; \sigma)$. Furthermore, as we mentioned in the main part, it is convenient to switch from the poloidal flux function, ψ , to the toroidal canonical momentum, p_{φ} , given by $\psi - \psi_s - IV_{\parallel} / \omega_{cj}$, to reduce the dimension of the problem. Thus, g_j is to be considered as $g_j = g_j(p_{\varphi}, \xi, \vartheta, \lambda, V; \sigma)$. To rewrite Eq.D.10/D.11 in $\{p_{\varphi}, \xi, \vartheta, \lambda, V; \sigma\}$ space, let us consider the following identities: $\mathbf{B}_0 \cdot \nabla \vartheta$, $\mathbf{B}_0 \cdot \nabla p_{\varphi}$, $\mathbf{B}_0 \cdot \nabla \xi$.

Using the expression for the equilibrium magnetic field, Eq.2.3,

$$\mathbf{B}_0 \cdot \nabla \vartheta = [I \nabla \varphi + \nabla \varphi \times \nabla \psi] \cdot \nabla \vartheta = [\nabla \varphi \times \nabla \psi] \cdot \nabla \vartheta =$$

and substituting Eq.D.6 and then Eq.D.2, we obtain

$$= [\nabla \varphi \times \nabla \psi] \cdot \frac{I \mathcal{J}}{q R^2} \nabla \chi = \boxed{\frac{I}{q R^2} = \mathbf{B}_0 \cdot \nabla \vartheta}. \quad (\text{D.12})$$

Using the definition of p_{φ} , we write

$$\mathbf{B}_0 \cdot \nabla p_{\varphi} = \mathbf{B}_0 \cdot \nabla \left[\psi - \psi_s - I \frac{V_{\parallel}}{\omega_{cj}} \right] = \mathbf{B}_0 \cdot \nabla \psi - \mathbf{B}_0 \cdot \nabla \left(\frac{IV_{\parallel}}{\omega_{cj}} \right) =$$

as the equilibrium magnetic field is given by Eq.2.3, $\mathbf{B}_0 \cdot \nabla \psi = 0$, and hence

$$\begin{aligned} &= -I \mathbf{B}_0 \cdot \nabla \left(\frac{V_{\parallel}}{\omega_{cj}} \right) = -I \mathbf{B}_0 \cdot \nabla \vartheta \left. \frac{\partial}{\partial \vartheta} \right|_{\psi} \left(\frac{V_{\parallel}}{\omega_{cj}} \right) - \mathbf{B}_0 \cdot \nabla \psi \left. \frac{\partial}{\partial \psi} \right|_{\vartheta} \left(\frac{IV_{\parallel}}{\omega_{cj}} \right) \\ &= \boxed{-\frac{I^2}{qR^2} \left. \frac{\partial}{\partial \vartheta} \right|_{\psi} \left(\frac{V_{\parallel}}{\omega_{cj}} \right) = \mathbf{B}_0 \cdot \nabla p_{\varphi}} \end{aligned} \quad (\text{D.13})$$

(note: Eq.D.12 has been applied).

$$\mathbf{B}_0 \cdot \nabla \xi = \mathbf{B}_0 \cdot \nabla \varphi - q_s \mathbf{B}_0 \cdot \nabla \vartheta = \frac{I}{R^2} \left[1 - \frac{q_s}{q} \right] = \boxed{\frac{I}{qR^2} \left[q - \frac{m}{n} \right] = \mathbf{B}_0 \cdot \nabla \xi}, \quad (\text{D.14})$$

where $\mathbf{B}_0 \cdot \nabla \varphi = I/R^2$.

Now let us consider $\mathbf{B}_1 \cdot \nabla \vartheta$, $\mathbf{B}_1 \cdot \nabla p_{\varphi}$, $\mathbf{B}_1 \cdot \nabla \xi$. Using the expression for the magnetic field perturbation, Eq.2.4, and the second relation in Eq.D.7, we write

$$\begin{aligned} \mathbf{B}_1 \cdot \nabla \vartheta &= [\nabla \times (A_{\parallel} \mathbf{b})] \cdot \nabla \vartheta = \nabla \cdot [A_{\parallel} \mathbf{b} \times \nabla \vartheta] + A_{\parallel} \mathbf{b} \cdot [\nabla \times \nabla \vartheta] = \\ &= \nabla \cdot [A_{\parallel} \mathbf{b} \times \nabla \vartheta], \end{aligned}$$

$$\mathbf{B}_1 \cdot \nabla \vartheta = \nabla \cdot \left[A_{\parallel} \frac{\mathbf{B}_0}{B_0} \times \nabla \vartheta \right]. \quad (\text{D.15})$$

Similar to Eq.D.15, we write

$$\mathbf{B}_1 \cdot \nabla p_{\varphi} = \nabla \cdot \left[A_{\parallel} \frac{\mathbf{B}_0}{B_0} \times \nabla p_{\varphi} \right]. \quad (\text{D.16})$$

and

$$\mathbf{B}_1 \cdot \nabla \xi = \nabla \cdot \left[A_{\parallel} \frac{\mathbf{B}_0}{B_0} \times \nabla \xi \right]. \quad (\text{D.17})$$

From Appendix B, we learn

$$\frac{\mathbf{B}_1 \cdot \nabla \vartheta}{\mathbf{B}_0 \cdot \nabla \vartheta} \sim \frac{\mathbf{B}_1 \cdot \nabla p_{\varphi}}{\mathbf{B}_0 \cdot \nabla p_{\varphi}} \sim \frac{\mathbf{B}_1 \cdot \nabla \xi}{\mathbf{B}_0 \cdot \nabla \xi} \sim \Delta^2.$$

We have introduced scalar products between \mathbf{B} and the basis vectors. Now let us consider

the corresponding cross products:

$$\mathbf{B}_0 \times \nabla \vartheta = I \nabla \varphi \times \nabla \vartheta + [\nabla \varphi \times \nabla \psi] \times \nabla \vartheta. \quad (\text{D.18})$$

As $d\vartheta = \vartheta'_\psi d\psi + \vartheta'_\chi d\chi$, the first term of Eq.D.18 can be written as

$$I \nabla \varphi \times \nabla \vartheta = I \vartheta'_\psi \mathcal{J} B_\vartheta^2 \nabla \chi + I \vartheta'_\chi \nabla \varphi \times \nabla \chi.$$

To obtain an expression for $\nabla \varphi \times \nabla \chi$, let us cross both sides of the first relation in Eq.D.2 with $\nabla \varphi$:

$$\begin{aligned} \mathcal{J} B_\vartheta^2 \nabla \varphi \times \nabla \chi &= \nabla \varphi \times [\nabla \varphi \times \nabla \psi] = \\ &= \nabla \varphi (\nabla \varphi \cdot \nabla \psi) - \nabla \psi |\nabla \varphi|^2 = -\frac{\nabla \psi}{R^2} \end{aligned}$$

and thus

$$\nabla \varphi \times \nabla \chi = -\frac{\nabla \psi}{\mathcal{J} R^2 B_\vartheta^2}.$$

The second term of Eq.D.18 is

$$\begin{aligned} -\nabla \vartheta \times [\nabla \varphi \times \nabla \psi] &= -\nabla \varphi (\nabla \vartheta \cdot \nabla \psi) + \nabla \psi (\nabla \vartheta \cdot \nabla \varphi) = \\ &= -\nabla \varphi \vartheta'_\psi |\nabla \psi|^2 = -\vartheta'_\psi R^2 B_\vartheta^2 \nabla \varphi. \end{aligned}$$

Therefore, Eq.D.18 becomes

$$\begin{aligned} I \vartheta'_\psi \mathcal{J} B_\vartheta^2 \nabla \chi - I \vartheta'_\chi \frac{\nabla \psi}{\mathcal{J} R^2 B_\vartheta^2} - \vartheta'_\psi R^2 B_\vartheta^2 \nabla \varphi &= \\ = I \vartheta' \underbrace{[\mathbf{B}_0 - I \nabla \varphi]}_{\mathcal{J} B_\vartheta^2 \nabla \chi = \nabla \varphi \times \nabla \psi} - \frac{I^2 \mathcal{J}}{q R^2} \frac{\nabla \psi}{\mathcal{J} R^2 B_\vartheta^2} - \vartheta' R^2 B_\vartheta^2 \nabla \varphi &= \\ = I \vartheta' \mathbf{B}_0 - \vartheta' R^2 [B_\vartheta^2 + B_\varphi^2] \nabla \varphi - \frac{B_\varphi^2}{q R^2 B_\vartheta^2} \nabla \psi, \end{aligned}$$

$$\boxed{I \vartheta' \mathbf{B}_0 - \vartheta' R^2 B_\vartheta^2 \nabla \varphi - \frac{B_\varphi^2}{q R^2 B_\vartheta^2} \nabla \psi = \mathbf{B}_0 \times \nabla \vartheta}. \quad (\text{D.19})$$

The toroidal field function is $I = R B_\varphi$ by its definition. Prime denotes the derivative with

respect to ψ . Using the expression for the equilibrium magnetic field, we derive

$$\mathbf{B}_0 \times \nabla \psi = I \underbrace{[\nabla \varphi \times \nabla \psi]}_{\mathbf{B}_0 - I \nabla \varphi} - \underbrace{\nabla \psi \times [\nabla \varphi \times \nabla \psi]}_{\nabla \varphi |\nabla \psi|^2 - \nabla \psi (\nabla \psi \cdot \nabla \varphi)} = I \mathbf{B}_0 - R^2 B_0^2 \nabla \varphi \quad (\text{D.20})$$

Therefore,

$$\begin{aligned} \mathbf{B}_0 \times \nabla p_\varphi &= \mathbf{B}_0 \times \nabla \psi - \mathbf{B}_0 \times \nabla \left(\frac{IV_{\parallel}}{\omega_{cj}} \right) = \\ &= \mathbf{B}_0 \times \nabla \psi - \mathbf{B}_0 \times \left[\frac{\partial}{\partial \psi} \Big|_{\vartheta} \left(\frac{IV_{\parallel}}{\omega_{cj}} \right) \nabla \psi + \frac{\partial}{\partial \vartheta} \Big|_{\psi} \left(\frac{IV_{\parallel}}{\omega_{cj}} \right) \nabla \vartheta \right] = \\ &= \left[1 - \frac{\partial}{\partial \psi} \Big|_{\vartheta} \left(\frac{IV_{\parallel}}{\omega_{cj}} \right) \right] [\mathbf{B}_0 \times \nabla \psi] - \frac{\partial}{\partial \vartheta} \Big|_{\psi} \left(\frac{IV_{\parallel}}{\omega_{cj}} \right) [\mathbf{B}_0 \times \nabla \vartheta]. \end{aligned}$$

and substituting Eqs.D.19,D.20, we obtain

$$\begin{aligned} \mathbf{B}_0 \times \nabla p_\varphi &= \left[1 - \frac{\partial}{\partial \psi} \Big|_{\vartheta} \left(\frac{IV_{\parallel}}{\omega_{cj}} \right) \right] [I \mathbf{B}_0 - R^2 B_0^2 \nabla \varphi] - \\ &- \frac{\partial}{\partial \vartheta} \Big|_{\psi} \left(\frac{IV_{\parallel}}{\omega_{cj}} \right) \left[I \vartheta' \mathbf{B}_0 - \vartheta' R^2 B_0^2 \nabla \varphi - \frac{B_\varphi^2}{q R^2 B_\vartheta^2} \nabla \psi \right]. \end{aligned} \quad (\text{D.21})$$

Therefore, we deduce

$$\begin{aligned} V_{\parallel} \nabla_{\parallel} g_j &= \frac{V_{\parallel}}{B} \left[(\mathbf{B} \cdot \nabla \vartheta) \frac{\partial}{\partial \vartheta} \Big|_{p_\varphi, \xi} + (\mathbf{B} \cdot \nabla p_\varphi) \frac{\partial}{\partial p_\varphi} \Big|_{\vartheta, \xi} + (\mathbf{B} \cdot \nabla \xi) \frac{\partial}{\partial \xi} \Big|_{p_\varphi, \vartheta} \right] g_j = \\ &= \frac{V_{\parallel}}{B_0} \left[(\mathbf{B}_0 \cdot \nabla \vartheta) \frac{\partial g_j}{\partial \vartheta} \Big|_{p_\varphi, \xi} + (\mathbf{B}_0 \cdot \nabla p_\varphi) \frac{\partial g_j}{\partial p_\varphi} \Big|_{\vartheta, \xi} + (\mathbf{B}_0 \cdot \nabla \xi) \frac{\partial g_j}{\partial \xi} \Big|_{p_\varphi, \vartheta} + \right. \\ &+ \left. (\mathbf{B}_1 \cdot \nabla p_\varphi) \frac{\partial g_j}{\partial p_\varphi} \Big|_{\vartheta, \xi} \right] + \mathcal{O}(\Delta^2) = \\ &= \frac{V_{\parallel}}{B_0} \left[\frac{I}{q R^2} \frac{\partial g_j}{\partial \vartheta} \Big|_{p_\varphi, \xi} - \frac{I^2}{q R^2} \frac{\partial}{\partial \vartheta} \Big|_{\psi} \left(\frac{V_{\parallel}}{\omega_{cj}} \right) \frac{\partial g_j}{\partial p_\varphi} \Big|_{\vartheta, \xi} - \frac{I}{n q R^2} (m - n q) \frac{\partial g_j}{\partial \xi} \Big|_{p_\varphi, \vartheta} + \right. \\ &+ \left. (\mathbf{B}_1 \cdot \nabla p_\varphi) \frac{\partial g_j}{\partial p_\varphi} \Big|_{\vartheta, \xi} \right] + \mathcal{O}(\Delta^2). \end{aligned} \quad (\text{D.22})$$

The $\mathbf{B}_1 \cdot \nabla p_\varphi$ contribution is maintained as $\partial/\partial \psi \sim (1/RB_\vartheta)\partial/\partial w$ on perturbed quantities.

To rewrite the $\mathbf{E} \times \mathbf{B}$ and magnetic drift contributions in Eq.1.12, let us consider

$$\mathbf{V}_b \cdot \nabla p_\varphi = - \left[\mathbf{V}_{\parallel} \times \nabla \left(\frac{V_{\parallel}}{\omega_{cj}} \right) \right] \cdot \nabla p_\varphi \equiv - \frac{V_{\parallel}}{B_0} \left[\mathbf{B}_0 \times \nabla \left(\frac{V_{\parallel}}{\omega_{cj}} \right) \right] \cdot \nabla p_\varphi =$$

$$= \frac{V_{\parallel}}{B_0} [\mathbf{B}_0 \times \nabla p_{\varphi}] \cdot \nabla \left(\frac{V_{\parallel}}{\omega_{cj}} \right) =$$

Here the third identity of Eq.D.8 has been applied. Now we substitute the expression for $\mathbf{B}_0 \times \nabla p_{\varphi}$ given by Eq.D.21 to write:

$$\begin{aligned} &= \frac{V_{\parallel}}{B_0} \left\{ \left[1 - \frac{\partial}{\partial \psi} \Big|_{\vartheta} \left(\frac{IV_{\parallel}}{\omega_{cj}} \right) \right] [I\mathbf{B}_0 - R^2 B_0^2 \nabla \varphi] \cdot \nabla \left(\frac{V_{\parallel}}{\omega_{cj}} \right) - \right. \\ &- I\vartheta' \frac{\partial}{\partial \vartheta} \Big|_{\psi} \left(\frac{IV_{\parallel}}{\omega_{cj}} \right) \mathbf{B}_0 \cdot \nabla \left(\frac{V_{\parallel}}{\omega_{cj}} \right) + \vartheta' R^2 B_0^2 \frac{\partial}{\partial \vartheta} \Big|_{\psi} \left(\frac{IV_{\parallel}}{\omega_{cj}} \right) \nabla \varphi \cdot \nabla \left(\frac{V_{\parallel}}{\omega_{cj}} \right) + \\ &\left. + \frac{B_{\varphi}^2}{qR^2 B_{\vartheta}^2} \frac{\partial}{\partial \vartheta} \Big|_{\psi} \left(\frac{IV_{\parallel}}{\omega_{cj}} \right) \nabla \psi \cdot \nabla \left(\frac{V_{\parallel}}{\omega_{cj}} \right) \right\} = \end{aligned}$$

As

$$\nabla \left(\frac{V_{\parallel}}{\omega_{cj}} \right) = \frac{\partial}{\partial \vartheta} \Big|_{\psi} \left(\frac{V_{\parallel}}{\omega_{cj}} \right) \nabla \vartheta + \frac{\partial}{\partial \psi} \Big|_{\vartheta} \left(\frac{V_{\parallel}}{\omega_{cj}} \right) \nabla \psi,$$

the highlighted terms vanish and thus

$$\begin{aligned} &= \frac{V_{\parallel}}{B_0} \left\{ \left[1 - \frac{\partial}{\partial \psi} \Big|_{\vartheta} \left(\frac{IV_{\parallel}}{\omega_{cj}} \right) \right] \left[I \frac{\partial}{\partial \vartheta} \Big|_{\psi} \left(\frac{V_{\parallel}}{\omega_{cj}} \right) \underbrace{\mathbf{B}_0 \cdot \nabla \vartheta}_{I/qR^2} + I \frac{\partial}{\partial \psi} \Big|_{\vartheta} \left(\frac{V_{\parallel}}{\omega_{cj}} \right) \mathbf{B}_0 \cdot \nabla \psi \right] - \right. \\ &- I\vartheta' \frac{\partial}{\partial \vartheta} \Big|_{\psi} \left(\frac{IV_{\parallel}}{\omega_{cj}} \right) \underbrace{\mathbf{B}_0 \cdot \nabla \left(\frac{V_{\parallel}}{\omega_{cj}} \right)}_{\frac{I}{qR^2} \frac{\partial}{\partial \vartheta} \Big|_{\psi} \left(\frac{V_{\parallel}}{\omega_{cj}} \right)} + \frac{I^2}{qR^4 B_{\vartheta}^2} \frac{\partial}{\partial \vartheta} \Big|_{\psi} \left(\frac{IV_{\parallel}}{\omega_{cj}} \right) \nabla \psi \cdot \nabla \left(\frac{V_{\parallel}}{\omega_{cj}} \right) \left. \right\} = \end{aligned}$$

Also, we use

$$\begin{aligned} \nabla \psi \cdot \nabla \left(\frac{V_{\parallel}}{\omega_{cj}} \right) &= \frac{\partial}{\partial \vartheta} \Big|_{\psi} \left(\frac{V_{\parallel}}{\omega_{cj}} \right) \underbrace{\nabla \psi \cdot \nabla \vartheta}_{\frac{\partial \vartheta}{\partial \psi} \nabla \psi \cdot \nabla \psi + \frac{\partial \vartheta}{\partial \chi} \nabla \psi \cdot \nabla \chi} + \frac{\partial}{\partial \psi} \Big|_{\vartheta} \left(\frac{V_{\parallel}}{\omega_{cj}} \right) |\nabla \psi|^2 = \\ &= \vartheta' \frac{\partial}{\partial \vartheta} \Big|_{\psi} \left(\frac{V_{\parallel}}{\omega_{cj}} \right) R^2 B_{\vartheta}^2 + \frac{\partial}{\partial \psi} \Big|_{\vartheta} \left(\frac{V_{\parallel}}{\omega_{cj}} \right) R^2 B_{\vartheta}^2, \end{aligned}$$

and substituting this into the previous expression, we obtain

$$\begin{aligned} &= \frac{V_{\parallel}}{B_0} \left\{ \left[1 - I \frac{\partial}{\partial \psi} \Big|_{\vartheta} \left(\frac{V_{\parallel}}{\omega_{cj}} \right) - \frac{IV_{\parallel}}{\omega_{cj}} \right] \frac{I^2}{qR^2} \frac{\partial}{\partial \vartheta} \Big|_{\psi} \left(\frac{V_{\parallel}}{\omega_{cj}} \right) + \right. \\ &\left. + \frac{I^2}{qR^2} \frac{\partial}{\partial \vartheta} \Big|_{\psi} \left(\frac{IV_{\parallel}}{\omega_{cj}} \right) \frac{\partial}{\partial \psi} \Big|_{\vartheta} \left(\frac{V_{\parallel}}{\omega_{cj}} \right) \right\} = \end{aligned}$$

Here we have taken into account that $I = RB_\varphi$ is ϑ -independent but is a function of ψ . Highlighted terms cancel out. By definition, $I' = \partial I / \partial \psi$. Therefore,

$$= \boxed{\frac{I^2}{qR^2} \frac{V_{\parallel}}{B_0} \left[\frac{\partial}{\partial \vartheta} \Big|_{\psi} \left(\frac{V_{\parallel}}{\omega_{cj}} \right) - \frac{I'}{2} \frac{\partial}{\partial \vartheta} \Big|_{\psi} \left(\frac{V_{\parallel}}{\omega_{cj}} \right)^2 \right]} = \mathbf{V}_b \cdot \nabla p_\varphi. \quad (\text{D.23})$$

The second term in Eq.D.23 is to be neglected in a low beta approximation. Similarly, we consider

$$\mathbf{V}_b \cdot \nabla \vartheta = \frac{V_{\parallel}}{B_0} [\mathbf{B}_0 \times \nabla \vartheta] \cdot \nabla \left(\frac{V_{\parallel}}{\omega_{cj}} \right) =$$

in accordance with Eq.D.19

$$= \frac{V_{\parallel}}{B_0} \left[I \vartheta' \frac{\partial}{\partial \vartheta} \Big|_{\psi} \left(\frac{V_{\parallel}}{\omega_{cj}} \right) \frac{I}{qR^2} - \frac{B_\varphi^2}{qR^2 B_\vartheta^2} \frac{\partial}{\partial \vartheta} \Big|_{\psi} \left(\frac{V_{\parallel}}{\omega_{cj}} \right) \vartheta' R^2 B_\vartheta^2 - \frac{B_\varphi^2}{qR^2 B_\vartheta^2} \frac{\partial}{\partial \psi} \Big|_{\vartheta} \left(\frac{V_{\parallel}}{\omega_{cj}} \right) R^2 B_\vartheta^2 \right],$$

$$\boxed{\mathbf{V}_b \cdot \nabla \vartheta} = - \frac{I^2}{qR^2} \frac{V_{\parallel}}{B_0} \frac{\partial}{\partial \psi} \Big|_{\vartheta} \left(\frac{V_{\parallel}}{\omega_{cj}} \right). \quad (\text{D.24})$$

For $\mathbf{V}_b \cdot \nabla \xi$, we have

$$\mathbf{V}_b \cdot \nabla \xi = \frac{V_{\parallel}}{B_0} [\mathbf{B}_0 \times \nabla \xi] \cdot \nabla \left(\frac{V_{\parallel}}{\omega_{cj}} \right). \quad (\text{D.25})$$

Let us now consider

$$\begin{aligned} \mathbf{B}_0 \times \nabla \xi &= \mathbf{B}_0 \times \nabla \varphi - \frac{m}{n} \mathbf{B}_0 \times \nabla \vartheta = \\ &= \underbrace{[I \nabla \varphi + \nabla \varphi \times \nabla \psi] \times \nabla \varphi}_{= -\nabla \varphi (\nabla \varphi \cdot \nabla \psi) + \nabla \psi |\nabla \varphi|^2 = \nabla \psi / R^2} - \frac{m}{n} \mathbf{B}_0 \times \nabla \vartheta = \end{aligned}$$

Substituting Eq.D.19 into the previous line yields

$$= \boxed{\frac{1}{R^2} \left(1 + \frac{m}{n} \frac{B_\varphi^2}{q B_\vartheta^2} \right) \nabla \psi - \frac{m}{n} I \vartheta' \mathbf{B}_0 + \frac{m}{n} \vartheta' R^2 B_0^2 \nabla \varphi = \mathbf{B}_0 \times \nabla \xi}. \quad (\text{D.26})$$

Then Eq.D.25 becomes

$$= \frac{V_{\parallel}}{B_0} \left\{ \frac{1}{R^2} \left(\frac{B_0^2}{B_\vartheta^2} + \frac{m - nq}{nq} \frac{B_\varphi^2}{B_\vartheta^2} \right) \left[\vartheta' \frac{\partial}{\partial \vartheta} \Big|_{\psi} \left(\frac{V_{\parallel}}{\omega_{cj}} \right) + \frac{\partial}{\partial \psi} \Big|_{\vartheta} \left(\frac{V_{\parallel}}{\omega_{cj}} \right) \right] R^2 B_\vartheta^2 - \right.$$

$$\begin{aligned}
& -\frac{m}{n} I \vartheta' \frac{\partial}{\partial \psi} \Big|_{\vartheta} \left(\frac{V_{\parallel}}{\omega_{cj}} \right) \underbrace{\mathbf{B}_0 \cdot \nabla \psi}_0 - \frac{m}{n} I \vartheta' \frac{\partial}{\partial \vartheta} \Big|_{\psi} \left(\frac{V_{\parallel}}{\omega_{cj}} \right) \frac{I}{qR^2} + \\
& + \frac{m}{n} \vartheta' R^2 B_0^2 \frac{\partial}{\partial \vartheta} \Big|_{\psi} \left(\frac{V_{\parallel}}{\omega_{cj}} \right) \underbrace{\nabla \varphi \cdot \nabla \vartheta}_0 + \frac{m}{n} \vartheta' R^2 B_0^2 \frac{\partial}{\partial \psi} \Big|_{\vartheta} \left(\frac{V_{\parallel}}{\omega_{cj}} \right) \underbrace{\nabla \varphi \cdot \nabla \psi}_0 \Big\} = \\
& = \frac{V_{\parallel}}{B_0} \left[\left(B_0^2 + \frac{m-nq}{nq} B_{\varphi}^2 \right) \frac{\partial}{\partial \psi} \Big|_{\vartheta} \left(\frac{V_{\parallel}}{\omega_{cj}} \right) + \left(B_0^2 + \frac{m-nq}{nq} B_{\varphi}^2 \right) \vartheta' \frac{\partial}{\partial \vartheta} \Big|_{\psi} \left(\frac{V_{\parallel}}{\omega_{cj}} \right) - \right. \\
& \left. - \frac{m}{n} \vartheta' \frac{B_{\varphi}^2}{q} \frac{\partial}{\partial \vartheta} \Big|_{\psi} \left(\frac{V_{\parallel}}{\omega_{cj}} \right) \right] =
\end{aligned}$$

since highlighted terms cancel out,

$$= \boxed{\frac{V_{\parallel}}{B_0} \left[\left(B_0^2 + \frac{m-nq}{nq} B_{\varphi}^2 \right) \frac{\partial}{\partial \psi} \Big|_{\vartheta} \left(\frac{V_{\parallel}}{\omega_{cj}} \right) + \vartheta' B_{\vartheta}^2 \frac{\partial}{\partial \vartheta} \Big|_{\psi} \left(\frac{V_{\parallel}}{\omega_{cj}} \right) \right]} = \mathbf{V}_b \cdot \nabla \xi. \quad (\text{D.27})$$

Since

$$\mathbf{V}_b \cdot \nabla g_j = \left[(\mathbf{V}_b \cdot \nabla p_{\varphi}) \frac{\partial}{\partial p_{\varphi}} \Big|_{\vartheta, \xi} + (\mathbf{V}_b \cdot \nabla \vartheta) \frac{\partial}{\partial \vartheta} \Big|_{p_{\varphi}, \xi} + (\mathbf{V}_b \cdot \nabla \xi) \frac{\partial}{\partial \xi} \Big|_{p_{\varphi}, \vartheta} \right] g_j, \quad (\text{D.28})$$

we combine Eqs.D.22,D.28 with Eqs.D.23,D.24,D.27 to write

$$\begin{aligned}
V_{\parallel} \nabla_{\parallel} g_j + \mathbf{V}_b \cdot \nabla g_j &= \frac{V_{\parallel}}{B_0} \left[\left(\underbrace{\frac{I}{qR^2}}_{\mathcal{O}(1)} - \underbrace{\frac{I^2}{qR^2} \frac{\partial}{\partial \psi} \Big|_{\vartheta} \left(\frac{V_{\parallel}}{\omega_{cj}} \right)}_{\mathcal{O}(\Delta)} + \underbrace{\mathbf{B}_1 \cdot \nabla \vartheta}_{\mathcal{O}(\Delta^2)} \right) \frac{\partial g_j}{\partial \vartheta} \Big|_{p_{\varphi}, \xi} + \right. \\
& + \left(\underbrace{\mathbf{B}_1 \cdot \nabla p_{\varphi}}_{\mathcal{O}(\Delta)} - \underbrace{\frac{I^2}{qR^2} \frac{I'}{2} \frac{\partial}{\partial \vartheta} \Big|_{\psi} \left(\frac{V_{\parallel}}{\omega_{cj}} \right)}_{\mathcal{O}(\Delta)} \right) \frac{\partial g_j}{\partial p_{\varphi}} \Big|_{\vartheta, \xi} + \\
& \left(-\frac{I}{nqR^2} (m-nq) + \left(\underbrace{B_0^2}_{\mathcal{O}(\Delta)} + \underbrace{\frac{m-nq}{nq} B_{\varphi}^2}_{\mathcal{O}(\Delta^2)} \right) \frac{\partial}{\partial \psi} \Big|_{\vartheta} \left(\frac{V_{\parallel}}{\omega_{cj}} \right) + \underbrace{\vartheta' B_{\vartheta}^2 \frac{\partial}{\partial \vartheta} \Big|_{\psi} \left(\frac{V_{\parallel}}{\omega_{cj}} \right)}_{\mathcal{O}(\Delta)} + \right. \\
& \left. \left. + \underbrace{\mathbf{B}_1 \cdot \nabla \xi}_{\mathcal{O}(\Delta^2)} \right) \frac{\partial g_j}{\partial \xi} \Big|_{p_{\varphi}, \vartheta} \right].
\end{aligned}$$

The ordering of terms is $1 : \Delta : \Delta^2 : \Delta : \Delta : \Delta : \Delta : \Delta^2 : \Delta : \Delta^2$.⁹⁹

As an example, in a large aspect ratio tokamak with circular poloidal cross section, $\Delta(r) = 0$, we estimate each term in the above expression as follows

$$\begin{aligned} \frac{V_{\parallel}}{B_0} \frac{I}{qR^2} \frac{\partial g_j}{\partial \vartheta} &\sim \frac{V_{Tj}}{B_0} \frac{B_{\varphi}}{qR} g_j \sim \varepsilon \frac{V_{Tj}}{r} g_j \sim \frac{V_{Tj}}{R} \Delta f_j^M, \\ \frac{V_{\parallel}}{B_0} \frac{I^2}{qR^2} \frac{\partial}{\partial \psi} \left(\frac{V_{\parallel}}{\omega_{cj}} \right) \frac{\partial g_j}{\partial \vartheta} &\sim \frac{V_{Tj}}{B_0} \frac{I}{qR^2} (\varepsilon^{1/2}) \Delta g_j \sim \varepsilon (\varepsilon^{1/2}) \frac{V_{Tj}}{r} \Delta g_j \sim (\varepsilon^{1/2}) \frac{V_{Tj}}{R} \Delta^2 f_j^M, \end{aligned}$$

where $\varepsilon^{1/2}$ is a fraction of trapped particles.

$$\begin{aligned} (\mathbf{B}_1 \cdot \nabla p_{\varphi}) \frac{\partial g_j}{\partial p_{\varphi}} \Big|_{\vartheta, \xi} &= \mathbf{B}_1 \cdot \left[\nabla \psi - \nabla \left(\frac{IV_{\parallel}}{\omega_{cj}} \right) \right] \frac{\partial \psi}{\partial p_{\varphi}} \frac{\partial g_j}{\partial \psi} \Big|_{\vartheta, \xi} \cong \\ &\cong \left[\mathbf{B}_1 \cdot \nabla \psi - I \frac{\partial}{\partial \psi} \left(\frac{V_{\parallel}}{\omega_{cj}} \right) \mathbf{B}_1 \cdot \nabla \psi - I \frac{\partial}{\partial \vartheta} \left(\frac{V_{\parallel}}{\omega_{cj}} \right) \mathbf{B}_1 \cdot \nabla \vartheta \right] \frac{\partial g_j}{\partial \psi} \Big|_{\vartheta, \xi}, \end{aligned}$$

$\partial p_{\varphi} / \partial \psi = 1$ to leading order in $\rho_{\vartheta j} / a$. Here

$$\begin{aligned} \frac{V_{\parallel}}{B_0} (\mathbf{B}_1 \cdot \nabla \psi) \frac{\partial g_j}{\partial \psi} \Big|_{\vartheta, \xi} &\sim \frac{V_{Tj}}{B_0} m \tilde{\psi} \frac{B_{\vartheta}}{r} \frac{g_j}{RB_{\vartheta} w} \sim \varepsilon \Delta^2 \frac{V_{Tj}}{w} g_j \sim \varepsilon \frac{V_{Tj}}{r} \Delta g_j \sim \frac{V_{Tj}}{R} \Delta^2 f_j^M, \\ \frac{IV_{\parallel}}{B_0} \frac{\partial}{\partial \psi} \left(\frac{V_{\parallel}}{\omega_{cj}} \right) (\mathbf{B}_1 \cdot \nabla \psi) \frac{\partial g_j}{\partial \psi} \Big|_{\vartheta, \xi} &\sim \varepsilon (\varepsilon^{1/2}) \frac{V_{Tj}}{r} \Delta^2 g_j \sim (\varepsilon^{1/2}) \frac{V_{Tj}}{R} \Delta^3 f_j^M, \\ \frac{IV_{\parallel}}{B_0} \frac{\partial}{\partial \vartheta} \left(\frac{V_{\parallel}}{\omega_{cj}} \right) (\mathbf{B}_1 \cdot \nabla \vartheta) \frac{\partial g_j}{\partial \psi} \Big|_{\vartheta, \xi} &\sim \frac{V_{Tj}}{B_0} RB_{\varphi} \frac{\partial}{\partial \vartheta} \left(\frac{V \sqrt{1 - \lambda B}}{\omega_{cj}} \right) \frac{B_{\vartheta}}{r} \frac{\tilde{\psi}}{R} \frac{\partial}{\partial \psi} \left(\frac{RB_{\varphi}}{B_0} \right) \frac{g_j}{RB_{\vartheta} w} \\ &\sim \Delta^2 \frac{\partial \rho_{\vartheta j}}{\partial \vartheta} \frac{V_{Tj}}{r} \frac{g_j}{w} \sim \varepsilon (\varepsilon^{3/2}) \Delta^3 V_{Tj} \frac{g_j}{w} \sim \varepsilon (\varepsilon^{3/2}) \frac{V_{Tj}}{r} \Delta^2 g_j \sim \varepsilon (\varepsilon^{3/2}) \frac{V_{Tj}}{R} \Delta^3 f_j^M, \end{aligned}$$

and thus only the $\mathbf{B}_1 \cdot \nabla \psi$ contribution is to be maintained. Since

$$1 - \frac{q}{q_s} \cong 1 - \frac{q_s + w_{\psi} q'_s}{q_s} \sim \frac{w}{r}, \quad (\text{D.29})$$

we have

$$\begin{aligned} \frac{V_{\parallel}}{B_0} \frac{I}{nqR^2} (m - nq) \frac{\partial g_j}{\partial \xi} &\sim \frac{V_{Tj}}{R} \Delta g_j \sim \varepsilon \frac{V_{Tj}}{r} \Delta g_j \sim \frac{V_{Tj}}{R} \Delta^2 f_j^M, \\ \frac{V_{\parallel}}{B_0} B_0^2 \frac{\partial}{\partial \psi} \left(\frac{V_{\parallel}}{\omega_{cj}} \right) \frac{\partial g_j}{\partial \xi} &\sim \frac{V_{Tj}}{I} B_0 (\varepsilon^{1/2}) \Delta g_j \sim (\varepsilon^{1/2}) \frac{V_{Tj}}{R} \Delta g_j \sim (\varepsilon^{1/2}) \frac{V_{Tj}}{R} \Delta^2 f_j^M, \\ \frac{V_{\parallel}}{B_0} \frac{m - nq}{nq} B_{\varphi}^2 \frac{\partial}{\partial \psi} \left(\frac{V_{\parallel}}{\omega_{cj}} \right) \frac{\partial g_j}{\partial \xi} &\sim (\varepsilon^{1/2}) \frac{V_{Tj}}{R} \Delta^2 g_j \sim (\varepsilon^{1/2}) \frac{V_{Tj}}{R} \Delta^3 f_j^M, \\ \frac{V_{\parallel}}{B_0} \vartheta' B_{\vartheta}^2 \frac{\partial}{\partial \vartheta} \left(\frac{V_{\parallel}}{\omega_{cj}} \right) \frac{\partial g_j}{\partial \xi} &\sim \frac{V_{Tj}}{B_0} \frac{\vartheta}{RB_{\vartheta} r} B_{\vartheta}^2 \frac{\partial \rho_{\vartheta j}}{\partial \vartheta} g_j \sim \varepsilon (\varepsilon^{3/2}) \Delta \frac{V_{Tj}}{R} \frac{B_{\vartheta}}{B_0} g_j \\ &\sim \varepsilon^2 (\varepsilon^{5/2}) \frac{V_{Tj}}{R} \Delta g_j \sim \varepsilon^2 (\varepsilon^{5/2}) \frac{V_{Tj}}{R} \Delta^2 f_j^M. \end{aligned}$$

⁹⁹With no restrictions on beta, the second term in $\partial g_j / \partial p_{\varphi} |_{\vartheta, \xi}$ averages out over ϑ at fixed p_{φ} .

As we seek the solution localised to the island vicinity, we Taylor expand $m - nq$ around the rational surface, $q = q_s \equiv m/n$,

$$m - nq \cong m - n [q_s + q'_s (\psi - \psi_s)] = -nq'_s (\psi - \psi_s) = -nq'_s \left(p_\varphi + \frac{IV_{\parallel}}{\omega_{cj}} \right).$$

Thus,

$$\begin{aligned} V_{\parallel} \nabla_{\parallel} g_j + \mathbf{V}_b \cdot \nabla g_j &= \frac{V_{\parallel}}{B_0} \left\{ \left[\frac{I}{qR^2} - \frac{I^2}{qR^2} \frac{\partial}{\partial \psi} \Big|_{\vartheta} \left(\frac{V_{\parallel}}{\omega_{cj}} \right) \right] \frac{\partial g_j}{\partial \vartheta} \Big|_{p_\varphi, \xi} + \right. \\ &+ (\mathbf{B}_1 \cdot \nabla p_\varphi) \frac{\partial g_j}{\partial p_\varphi} \Big|_{\vartheta, \xi} + \\ &\left. + \left[\frac{I}{qR^2} q'_s \left(p_\varphi + \frac{IV_{\parallel}}{\omega_{cj}} \right) + B_0^2 \frac{\partial}{\partial \psi} \Big|_{\vartheta} \left(\frac{V_{\parallel}}{\omega_{cj}} \right) + \vartheta' B_\vartheta^2 \frac{\partial}{\partial \vartheta} \Big|_{\psi} \left(\frac{V_{\parallel}}{\omega_{cj}} \right) \right] \frac{\partial g_j}{\partial \xi} \Big|_{p_\varphi, \vartheta} \right\} + \mathcal{O}(\Delta^2). \end{aligned} \quad (\text{D.30})$$

To rewrite the $\mathbf{E} \times \mathbf{B}$ drift contribution to Eq.1.12, we consider

$$\mathbf{V}_E \cdot \nabla \vartheta = \frac{\mathbf{E} \times \mathbf{B}}{B^2} \cdot \nabla \vartheta =$$

provided $\mathbf{E} = -\text{grad}\Phi$,

$$= -\frac{1}{B^2} [\mathbf{B} \times \nabla \vartheta] \cdot \nabla \Phi \cong -\frac{1}{B_0^2} [\mathbf{B}_0 \times \nabla \vartheta] \cdot \nabla \Phi =$$

Substituting the expression for $\mathbf{B}_0 \times \nabla \vartheta$ given by Eq.D.19, we have

$$\begin{aligned} &= -\frac{1}{B_0^2} \left\{ \left[\left[I \vartheta' \underbrace{\mathbf{B}_0 \cdot \nabla \vartheta}_{I/qR^2} - \vartheta' R^2 B_0^2 \underbrace{\nabla \varphi \cdot \nabla \vartheta}_0 - \frac{B_\varphi^2}{qR^2 B_\vartheta^2} \underbrace{\nabla \psi \cdot \nabla \vartheta}_{\vartheta'_{\psi} |\nabla \psi|^2 + \vartheta'_{\chi} \nabla \psi \cdot \nabla \chi = -\vartheta' R^2 B_\vartheta^2} \right] \frac{\partial \Phi}{\partial \vartheta} \Big|_{\psi, \xi} + \right. \\ &+ \left[I \vartheta' \underbrace{\mathbf{B}_0 \cdot \nabla \psi}_0 - \vartheta' R^2 B_0^2 \underbrace{\nabla \varphi \cdot \nabla \psi}_0 - \frac{B_\varphi^2}{qR^2 B_\vartheta^2} |\nabla \psi|^2 \right] \frac{\partial \Phi}{\partial \psi} \Big|_{\vartheta, \xi} + \\ &\left. + \left[I \vartheta' \underbrace{\mathbf{B}_0 \cdot \nabla \xi}_{\frac{I}{qR^2} (q - q_s)} - \vartheta' R^2 B_0^2 \underbrace{\nabla \varphi \cdot \nabla \xi}_{\nabla \varphi \cdot \nabla (\varphi - \frac{m}{n} \vartheta) = |\nabla \varphi|^2 = 1/R^2} - \frac{B_\varphi^2}{qR^2 B_\vartheta^2} \underbrace{\nabla \psi \cdot \nabla \xi}_{\nabla \psi \cdot \nabla (\varphi - \frac{m}{n} \vartheta) = -\frac{m}{n} \vartheta' R^2 B_\vartheta^2} \right] \frac{\partial \Phi}{\partial \xi} \Big|_{\psi, \vartheta} \right\} = \end{aligned}$$

as $\Phi = \Phi(\psi, \vartheta, \xi)$ and hence

$$= -\frac{1}{B_0^2} \left(-\frac{B_\varphi^2}{q} \frac{\partial \Phi}{\partial \psi} \Big|_{\vartheta, \xi} - \vartheta' B_\vartheta^2 \frac{\partial \Phi}{\partial \xi} \Big|_{\psi, \vartheta} \right)$$

Thus, we obtain

$$\boxed{\mathbf{V}_E \cdot \nabla \vartheta = \frac{B_\varphi^2}{q B_0^2} \frac{\partial \Phi}{\partial \psi} \Big|_{\xi, \vartheta} + \frac{\vartheta' B_\vartheta^2}{B_0^2} \frac{\partial \Phi}{\partial \xi} \Big|_{\psi, \vartheta}}. \quad (\text{D.31})$$

Similarly,

$$\mathbf{V}_E \cdot \nabla \psi = -\frac{1}{B^2} [\mathbf{B} \times \nabla \psi] \cdot \nabla \Phi \cong -\frac{1}{B_0^2} [\mathbf{B}_0 \times \nabla \psi] \cdot \nabla \Phi =$$

Substituting the expression for $\mathbf{B}_0 \times \nabla \psi$, Eq.D.20, we write

$$\begin{aligned} &= -\frac{1}{B_0^2} \left\{ [I \mathbf{B}_0 \cdot \nabla \vartheta - R^2 B_0^2 \nabla \varphi \cdot \nabla \vartheta] \frac{\partial \Phi}{\partial \vartheta} \Big|_{\psi, \xi} + [I \mathbf{B}_0 \cdot \nabla \psi - R^2 B_0^2 \nabla \varphi \cdot \nabla \psi] \frac{\partial \Phi}{\partial \psi} \Big|_{\vartheta, \xi} \right. \\ &+ \left. [I \mathbf{B}_0 \cdot \nabla \xi - R^2 B_0^2 \nabla \varphi \cdot \nabla \xi] \frac{\partial \Phi}{\partial \xi} \Big|_{\psi, \vartheta} \right\} = \\ &= -\frac{1}{B_0^2} \left\{ \frac{I^2}{q R^2} \frac{\partial \Phi}{\partial \vartheta} \Big|_{\psi, \xi} + \left[\frac{I^2}{q R^2} \left(q - \frac{m}{n} \right) - B_0^2 \right] \frac{\partial \Phi}{\partial \xi} \Big|_{\psi, \vartheta} \right\}, \end{aligned}$$

$$\boxed{\mathbf{V}_E \cdot \nabla \psi = -\frac{B_\varphi^2}{q B_0^2} \frac{\partial \Phi}{\partial \vartheta} \Big|_{\psi, \xi} + \left[1 - \frac{B_\varphi^2}{B_0^2} \frac{nq - m}{nq} \right] \frac{\partial \Phi}{\partial \xi} \Big|_{\psi, \vartheta}}. \quad (\text{D.32})$$

In a similar way we consider

$$\mathbf{V}_E \cdot \nabla \xi \cong -\frac{1}{B_0^2} [\mathbf{B}_0 \times \nabla \xi] \cdot \nabla \Phi =$$

Substituting the expression for $\mathbf{B}_0 \times \nabla \xi$ from Eq.D.26, we have

$$\begin{aligned} &= -\frac{1}{B_0^2} \left[-\frac{m}{n} I \vartheta' \mathbf{B}_0 + \frac{m}{n} \vartheta' R^2 B_0^2 \nabla \varphi + \left(\frac{B^2}{R^2 B_\vartheta^2} + \frac{m - nq}{nq} \frac{B_\varphi^2}{R^2 B_\vartheta^2} \right) \nabla \psi \right] \cdot \nabla \Phi = \\ &= -\frac{1}{B_0^2} \left\{ \left[-\frac{m}{n} I \vartheta' \underbrace{\mathbf{B}_0 \cdot \nabla \vartheta}_{I/qR^2} + \frac{m}{n} \vartheta' R^2 B_0^2 \underbrace{\nabla \varphi \cdot \nabla \vartheta}_0 + \left(\frac{B^2}{R^2 B_\vartheta^2} + \frac{m - nq}{nq} \frac{B_\varphi^2}{R^2 B_\vartheta^2} \right) \underbrace{\nabla \psi \cdot \nabla \vartheta}_{\vartheta' R^2 B_\vartheta^2} \right] \frac{\partial \Phi}{\partial \vartheta} \Big|_{\psi, \xi} + \right. \end{aligned}$$

$$\begin{aligned}
& + \left[-\frac{m}{n} I \vartheta' \underbrace{\mathbf{B}_0 \cdot \nabla \psi}_0 + \frac{m}{n} \vartheta' R^2 B_0^2 \underbrace{\nabla \varphi \cdot \nabla \psi}_0 + \left(\frac{B^2}{R^2 B_\vartheta^2} + \frac{m-nq}{nq} \frac{B_\varphi^2}{R^2 B_\vartheta^2} \right) \frac{|\nabla \psi|^2}{R^2 B_\vartheta^2} \right] \frac{\partial \Phi}{\partial \psi} \Big|_{\vartheta, \xi} + \\
& + \left[-\frac{m}{n} I \vartheta' \underbrace{\mathbf{B}_0 \cdot \nabla \xi}_{\frac{1}{qR^2}(q-\frac{m}{n})} + \frac{m}{n} \vartheta' R^2 B_0^2 \underbrace{\nabla \varphi \cdot \nabla \xi}_{1/R^2} + \left(\frac{B^2}{R^2 B_\vartheta^2} + \frac{m-nq}{nq} \frac{B_\varphi^2}{R^2 B_\vartheta^2} \right) \frac{\nabla \psi \cdot \nabla \xi}{-\frac{m}{n} \vartheta' R^2 B_\vartheta^2} \right] \frac{\partial \Phi}{\partial \xi} \Big|_{\psi, \vartheta} \Bigg\} = \\
& = \boxed{-\vartheta' \frac{B_\vartheta^2}{B_0^2} \frac{\partial \Phi}{\partial \vartheta} \Big|_{\psi, \xi} - \left[1 + \frac{m-nq}{nq} \frac{B_\varphi^2}{B_0^2} \right] \frac{\partial \Phi}{\partial \psi} \Big|_{\xi, \vartheta} = \mathbf{V}_E \cdot \nabla \xi}. \tag{D.33}
\end{aligned}$$

Combining Eqs.D.31,D.32, we obtain

$$\begin{aligned}
\mathbf{V}_E \cdot \nabla p_\varphi & = \mathbf{V}_E \cdot \nabla \left(\psi - \psi_s - \frac{IV_{\parallel}}{\omega_{cj}} \right) = \\
& = \left[1 - \frac{\partial}{\partial \psi} \Big|_{\vartheta} \left(\frac{IV_{\parallel}}{\omega_{cj}} \right) \right] \mathbf{V}_E \cdot \nabla \psi - \frac{\partial}{\partial \vartheta} \Big|_{\psi} \left(\frac{IV_{\parallel}}{\omega_{cj}} \right) \mathbf{V}_E \cdot \nabla \vartheta. \tag{D.34}
\end{aligned}$$

Combining Eqs.D.31,D.32,D.33 and Eq.D.34, we write

$$\begin{aligned}
\mathbf{V}_E \cdot \nabla g_j & = \left[(\mathbf{V}_E \cdot \nabla p_\varphi) \frac{\partial}{\partial p_\varphi} \Big|_{\vartheta, \xi} + (\mathbf{V}_E \cdot \nabla \vartheta) \frac{\partial}{\partial \vartheta} \Big|_{p_\varphi, \xi} + (\mathbf{V}_E \cdot \nabla \xi) \frac{\partial}{\partial \xi} \Big|_{p_\varphi, \vartheta} \right] g_j = \\
& = \left\{ \left[1 - \frac{\partial}{\partial \psi} \Big|_{\vartheta} \left(\frac{IV_{\parallel}}{\omega_{cj}} \right) \right] \left[-\frac{B_\varphi^2}{qB_0^2} \frac{\partial \Phi}{\partial \vartheta} \Big|_{\psi, \xi} + \underbrace{\left(1 - \frac{B_\varphi^2}{B_0^2} \frac{nq-m}{nq} \right)}_{\mathcal{O}(\Delta^2)} \frac{\partial \Phi}{\partial \xi} \Big|_{\psi, \vartheta} \right] - \right. \\
& \quad \left. - \frac{\partial}{\partial \vartheta} \Big|_{\psi} \left(\frac{IV_{\parallel}}{\omega_{cj}} \right) \left[\frac{B_\varphi^2}{qB_0^2} \frac{\partial \Phi}{\partial \psi} \Big|_{\xi, \vartheta} + \underbrace{\frac{\vartheta' B_\vartheta^2}{B_0^2} \frac{\partial \Phi}{\partial \xi} \Big|_{\psi, \vartheta}}_{\mathcal{O}(\Delta^2)} \right] \right\} \frac{\partial g_j}{\partial p_\varphi} \Big|_{\vartheta, \xi} + \\
& + \left[\frac{B_\varphi^2}{qB_0^2} \frac{\partial \Phi}{\partial \psi} \Big|_{\xi, \vartheta} + \underbrace{\frac{\vartheta' B_\vartheta^2}{B_0^2} \frac{\partial \Phi}{\partial \xi} \Big|_{\psi, \vartheta}}_{\mathcal{O}(\Delta^2)} \right] \frac{\partial g_j}{\partial \vartheta} \Big|_{p_\varphi, \xi} + \\
& + \left[\underbrace{-\vartheta' \frac{B_\vartheta^2}{B_0^2} \frac{\partial \Phi}{\partial \vartheta} \Big|_{\psi, \xi}}_{\mathcal{O}(\Delta^2)} - \underbrace{\left(1 + \frac{m-nq}{nq} \frac{B_\varphi^2}{B_0^2} \right)}_{\mathcal{O}(\Delta^2)} \frac{\partial \Phi}{\partial \psi} \Big|_{\xi, \vartheta} \right] \frac{\partial g_j}{\partial \xi} \Big|_{p_\varphi, \vartheta}.
\end{aligned}$$

As an example, in a large aspect ratio tokamak with circular poloidal cross section, $\Delta(r) = 0$, we

estimate each term in the above expression as follows

$$\begin{aligned} \frac{B_\varphi^2}{qB_0^2} \frac{\partial \Phi}{\partial \vartheta} \frac{\partial g_j}{\partial p_\varphi} &\sim \frac{1}{wrB_\varphi} \frac{T}{e} \Delta g_j \sim \frac{V_{Tj}}{w\omega_{cj}} \frac{V_{Tj}}{r} \Delta g_j \sim \frac{\rho_{\vartheta j}}{w} \frac{B_\vartheta}{B_\varphi} \frac{V_{Tj}}{r} \Delta g_j \sim \varepsilon \frac{V_{Tj}}{r} \Delta g_j, \\ \frac{B_\varphi^2}{qB_0^2} I \frac{\partial}{\partial \psi} \left(\frac{V_{\parallel}}{\omega_{cj}} \right) \frac{\partial \Phi}{\partial \vartheta} \frac{\partial g_j}{\partial p_\varphi} &\sim \varepsilon (\varepsilon^{3/2}) \frac{V_{Tj}}{r} \Delta^2 g_j, \end{aligned}$$

where $\varepsilon^{1/2}$ corresponds to a fraction of trapped particles, $T_i \sim T_e \sim T$.

$$\begin{aligned} \frac{\partial \Phi}{\partial \xi} \frac{\partial g_j}{\partial p_\varphi} &\sim \frac{1}{RB_\vartheta w} \frac{T}{e} \Delta g_j \sim \frac{1}{rB_\varphi w} \frac{T}{e} \Delta g_j \sim \varepsilon \frac{V_{Tj}}{r} \Delta g_j, \\ I \frac{\partial}{\partial \psi} \left(\frac{V_{\parallel}}{\omega_{cj}} \right) \frac{\partial \Phi}{\partial \xi} \frac{\partial g_j}{\partial p_\varphi} &\sim \varepsilon (\varepsilon^{3/2}) \frac{V_{Tj}}{r} \Delta^2 g_j, \\ \frac{nq - m}{nq} \frac{B_\varphi^2}{B_0^2} \frac{\partial \Phi}{\partial \xi} \frac{\partial g_j}{\partial p_\varphi} &\sim \varepsilon \frac{V_{Tj}}{r} \frac{m}{nq} \left(\frac{nq}{m} - 1 \right) \Delta g_j \sim \varepsilon \frac{V_{Tj}}{r} \Delta^2 g_j, \\ \frac{nq - m}{nq} \frac{B_\varphi^2}{B_0^2} I \frac{\partial}{\partial \psi} \left(\frac{V_{\parallel}}{\omega_{cj}} \right) \frac{\partial \Phi}{\partial \xi} \frac{\partial g_j}{\partial p_\varphi} &\sim \varepsilon (\varepsilon^{3/2}) \frac{V_{Tj}}{r} \Delta^3 g_j, \end{aligned}$$

$$\frac{B_\varphi^2}{qB_0^2} I \frac{\partial}{\partial \vartheta} \left(\frac{V_{\parallel}}{\omega_{cj}} \right) \frac{\partial \Phi}{\partial \psi} \frac{\partial g_j}{\partial p_\varphi} \sim \varepsilon (\varepsilon^{3/2}) \frac{RB_\varphi}{qR^2 B_\vartheta^2 w^2} \rho_{\vartheta j} \frac{T}{e} \Delta g_j \sim (\varepsilon^{1/2}) \frac{1}{rB_\varphi w} \frac{T}{e} \Delta g_j \sim \varepsilon (\varepsilon^{3/2}) \frac{V_{Tj}}{r} \Delta g_j,$$

$$\begin{aligned} \vartheta' \frac{B_\vartheta^2}{B_0^2} I \frac{\partial}{\partial \vartheta} \left(\frac{V_{\parallel}}{\omega_{cj}} \right) \frac{\partial \Phi}{\partial \xi} \frac{\partial g_j}{\partial p_\varphi} &\sim \varepsilon^3 (\varepsilon^{7/2}) \frac{V_{Tj}}{r} \Delta^2 g_j, \\ \frac{B_\varphi^2}{qB_0^2} \frac{\partial \Phi}{\partial \psi} \frac{\partial g_j}{\partial \vartheta} &\sim \varepsilon \frac{V_{Tj}}{r} \Delta g_j, \\ \vartheta' \frac{B_\vartheta^2}{B_0^2} \frac{\partial \Phi}{\partial \xi} \frac{\partial g_j}{\partial \vartheta} &\sim \varepsilon^3 \frac{V_{Tj}}{r} \Delta^2 g_j, \\ \vartheta' \frac{B_\vartheta^2}{B_0^2} \frac{\partial \Phi}{\partial \vartheta} \frac{\partial g_j}{\partial \xi} &\sim \varepsilon^3 \frac{V_{Tj}}{r} \Delta^2 g_j, \\ \frac{\partial \Phi}{\partial \psi} \frac{\partial g_j}{\partial \xi} &\sim \varepsilon \frac{V_{Tj}}{r} \Delta g_j, \\ \frac{m - nq}{nq} \frac{B_\varphi^2}{B_0^2} \frac{\partial \Phi}{\partial \psi} \frac{\partial g_j}{\partial \xi} &\sim \varepsilon \frac{V_{Tj}}{r} \Delta^2 g_j. \end{aligned}$$

Keeping the $\mathcal{O}(\Delta^0)$ and $\mathcal{O}(\Delta^1)$ terms only, we have

$$\begin{aligned} \mathbf{V}_E \cdot \nabla g_j &= \frac{\partial g_j}{\partial p_\varphi} \Big|_{\vartheta, \xi} \left(-\frac{B_\varphi^2}{qB_0^2} \frac{\partial \Phi}{\partial \vartheta} \Big|_{\psi, \xi} + \frac{\partial \Phi}{\partial \xi} \Big|_{\psi, \vartheta} - \frac{B_\varphi^2}{qB_0^2} \frac{\partial}{\partial \vartheta} \Big|_{\psi} \left(\frac{IV_{\parallel}}{\omega_{cj}} \right) \frac{\partial \Phi}{\partial \psi} \Big|_{\xi, \vartheta} \right) + \\ &+ \frac{B_\varphi^2}{qB_0^2} \frac{\partial \Phi}{\partial \psi} \Big|_{\xi, \vartheta} \frac{\partial g_j}{\partial \vartheta} \Big|_{p_\varphi, \xi} - \frac{\partial \Phi}{\partial \psi} \Big|_{\xi, \vartheta} \frac{\partial g_j}{\partial \xi} \Big|_{p_\varphi, \vartheta} + \mathcal{O}(\Delta^2). \end{aligned} \quad (\text{D.35})$$

Substituting Eqs.D.30,D.35 into Eq.D.11 yields

$$\begin{aligned}
& \left\{ \frac{V_{\parallel}}{B_0} \frac{I}{qR^2} \left[1 - I \frac{\partial}{\partial \vartheta} \Big|_{\vartheta} \left(\frac{V_{\parallel}}{\omega_{cj}} \right) \right] + \frac{B_{\varphi}^2}{qB_0^2} \frac{\partial \Phi}{\partial \psi} \Big|_{\xi, \vartheta} \right\} \frac{\partial g_j}{\partial \vartheta} \Big|_{p_{\varphi}, \xi} + \\
& \left\{ \frac{V_{\parallel}}{B_0} \mathbf{B}_1 \cdot \nabla p_{\varphi} - \frac{B_{\varphi}^2}{qB_0^2} \frac{\partial \Phi}{\partial \vartheta} \Big|_{\psi, \xi} + \frac{\partial \Phi}{\partial \xi} \Big|_{\psi, \vartheta} - \frac{B_{\varphi}^2}{qB_0^2} \frac{\partial}{\partial \vartheta} \Big|_{\psi} \left(\frac{IV_{\parallel}}{\omega_{cj}} \right) \frac{\partial \Phi}{\partial \psi} \Big|_{\xi, \vartheta} \right\} \frac{\partial g_j}{\partial p_{\varphi}} \Big|_{\vartheta, \xi} + \\
& + \left\{ \frac{V_{\parallel}}{B_0} \left[\frac{I}{qR^2} q'_s \left(p_{\varphi} + \frac{IV_{\parallel}}{\omega_{cj}} \right) + B_0^2 \frac{\partial}{\partial \psi} \Big|_{\vartheta} \left(\frac{V_{\parallel}}{\omega_{cj}} \right) + \vartheta' B_{\vartheta}^2 \frac{\partial}{\partial \vartheta} \Big|_{\psi} \left(\frac{V_{\parallel}}{\omega_{cj}} \right) \right] - \right. \\
& \left. - \frac{\partial \Phi}{\partial \psi} \Big|_{\xi, \vartheta} \right\} \frac{\partial g_j}{\partial \xi} \Big|_{p_{\varphi}, \vartheta} - \frac{eZ_j}{m_j V} [V_{\parallel} \nabla_{\parallel} \Phi + \mathbf{V}_b \cdot \nabla \Phi] \frac{\partial g_j}{\partial V} \Big|_{\psi} = C_j(g_j). \tag{D.36}
\end{aligned}$$

The term

$$\left(\frac{eZ_j}{T_j(\psi_s)} \right)^2 f_j^M(\psi_s) [V_{\parallel} \nabla_{\parallel} \Phi + \mathbf{V}_b \cdot \nabla \Phi] \Phi(\psi_s) \sim \frac{V_{Tj}}{r} \frac{\delta \Phi}{\Phi} \Delta g_j \sim \frac{V_{Tj}}{r} \Delta^2 g_j$$

in Eq.D.10, and hence is to be omitted.

Let us consider a combination of terms in velocity space,

$$V_{\parallel} \nabla_{\parallel} \Phi + \mathbf{V}_b \cdot \nabla \Phi = V_{\parallel} \nabla_{\parallel} \Phi - \frac{V_{\parallel}}{B_0} \left[\mathbf{B}_0 \times \nabla \left(\frac{V_{\parallel}}{\omega_{cj}} \right) \right] \cdot \nabla \Phi \tag{D.37}$$

with

$$V_{\parallel} \nabla_{\parallel} \Phi = \frac{V_{\parallel}}{B_0} \mathbf{B}_0 \cdot \nabla \Phi = \frac{V_{\parallel}}{B_0} \left[\frac{I}{qR^2} \frac{\partial \Phi}{\partial \vartheta} \Big|_{\psi, \xi} + \frac{I}{qR^2} (q - q_s) \frac{\partial \Phi}{\partial \xi} \Big|_{\psi, \vartheta} \right]$$

and

$$\begin{aligned}
& \left[\mathbf{B}_0 \times \nabla \left(\frac{V_{\parallel}}{\omega_{cj}} \right) \right] \cdot \nabla \Phi = \frac{\partial}{\partial \vartheta} \Big|_{\psi} \left(\frac{V_{\parallel}}{\omega_{cj}} \right) [\mathbf{B}_0 \times \nabla \vartheta] \cdot \nabla \Phi + \frac{\partial}{\partial \psi} \Big|_{\vartheta} \left(\frac{V_{\parallel}}{\omega_{cj}} \right) [\mathbf{B}_0 \times \nabla \psi] \cdot \nabla \Phi = \\
& = - \frac{\partial}{\partial \vartheta} \Big|_{\psi} \left(\frac{V_{\parallel}}{\omega_{cj}} \right) \left[\frac{I^2}{qR^2} \frac{\partial \Phi}{\partial \psi} \Big|_{\vartheta, \xi} + \vartheta' B_{\vartheta}^2 \frac{\partial \Phi}{\partial \xi} \Big|_{\psi, \vartheta} \right] + \\
& + \frac{\partial}{\partial \psi} \Big|_{\vartheta} \left(\frac{V_{\parallel}}{\omega_{cj}} \right) \left[\frac{I^2}{qR^2} \frac{\partial \Phi}{\partial \vartheta} \Big|_{\psi, \xi} + \frac{I^2}{qR^2} \frac{\partial \Phi}{\partial \xi} \Big|_{\psi, \vartheta} \left(q - \frac{m}{n} \right) - B_0^2 \frac{\partial \Phi}{\partial \xi} \Big|_{\psi, \vartheta} \right],
\end{aligned}$$

where we have applied Eqs.D.12-D.14 and Eqs.D.19,D.20. Substituting these into Eq.D.37

and then into Eq.D.36, we obtain

$$\begin{aligned} & - \frac{eZ_j}{m_j V} \frac{V_{\parallel}}{B_0} \frac{\partial g_j}{\partial V} \Big|_{\psi} \left\{ \frac{I}{qR^2} \frac{\partial \Phi}{\partial \vartheta} \Big|_{\psi, \xi} + \frac{I}{qR^2} (q - q_s) \frac{\partial \Phi}{\partial \xi} \Big|_{\psi, \vartheta} + \right. \\ & + \left. \frac{\partial}{\partial \vartheta} \Big|_{\psi} \left(\frac{V_{\parallel}}{\omega_{cj}} \right) \left[\frac{I^2}{qR^2} \frac{\partial \Phi}{\partial \psi} \Big|_{\vartheta, \xi} + \vartheta' B_{\vartheta}^2 \frac{\partial \Phi}{\partial \xi} \Big|_{\psi, \vartheta} \right] - \right. \\ & \left. - \frac{\partial}{\partial \psi} \Big|_{\vartheta} \left(\frac{V_{\parallel}}{\omega_{cj}} \right) \left[\frac{I^2}{qR^2} \frac{\partial \Phi}{\partial \vartheta} \Big|_{\psi, \xi} + \frac{I^2}{qR^2} \frac{\partial \Phi}{\partial \xi} \Big|_{\psi, \vartheta} \left(q - \frac{m}{n} \right) - B_0^2 \frac{\partial \Phi}{\partial \xi} \Big|_{\psi, \vartheta} \right] \right\} \end{aligned}$$

for the last term on the left hand side of Eq.D.36. The ordering of terms here is as follows $\Delta : \Delta^2 : \Delta : \Delta^2 : \Delta^2 : \Delta^3 : \Delta^2$.

As an example, in a large aspect ratio tokamak with circular poloidal cross section, $\Delta(r) = 0$, we estimate each term in the above expression as follows

$$\begin{aligned} \frac{eZ_j}{m_j V} \frac{V_{\parallel}}{B_0} \frac{I}{qR^2} \frac{\partial \Phi}{\partial \vartheta} \frac{\partial g_j}{\partial V} & \sim \frac{e}{m_j V_{Tj}^2} \frac{V_{Tj}}{B_0} \frac{B_{\varphi} R T}{qR^2} \Delta g_j \sim \varepsilon \frac{V_{Tj}}{r} \Delta g_j, \\ \frac{eZ_j}{m_j V} \frac{V_{\parallel}}{B_0} \frac{I}{qR^2} (q - q_s) \frac{\partial \Phi}{\partial \xi} \frac{\partial g_j}{\partial V} & \sim \frac{V_{Tj}}{R} \Delta^2 g_j \sim \varepsilon \frac{V_{Tj}}{r} \Delta^2 g_j, \end{aligned}$$

$$\begin{aligned} \frac{eZ_j}{m_j V} \frac{V_{\parallel}}{B_0} \frac{I^2}{qR^2} \frac{\partial}{\partial \vartheta} \Big|_{\psi} \left(\frac{V_{\parallel}}{\omega_{cj}} \right) \frac{\partial \Phi}{\partial \psi} \frac{\partial g_j}{\partial V} & \sim \varepsilon (\varepsilon^{3/2}) \frac{V_{Tj}}{B_0} \frac{I^2}{qR^2} \frac{\rho_{\vartheta j}}{R B_{\vartheta} w} \Delta g_j \\ & \sim (\varepsilon^{1/2}) \frac{V_{Tj}}{R} \Delta g_j \sim \varepsilon (\varepsilon^{3/2}) \frac{V_{Tj}}{r} \Delta g_j, \end{aligned}$$

$$\begin{aligned} \frac{eZ_j}{m_j V} \frac{V_{\parallel}}{B_0} \vartheta' B_{\vartheta}^2 \frac{\partial}{\partial \vartheta} \Big|_{\psi} \left(\frac{V_{\parallel}}{\omega_{cj}} \right) \frac{\partial \Phi}{\partial \xi} \frac{\partial g_j}{\partial V} & \sim \varepsilon^3 (\varepsilon^{7/2}) \frac{V_{Tj}}{r} \Delta^2 g_j, \\ \frac{eZ_j}{m_j V} \frac{V_{\parallel}}{B_0} \frac{I^2}{qR^2} \frac{\partial}{\partial \psi} \Big|_{\vartheta} \left(\frac{V_{\parallel}}{\omega_{cj}} \right) \frac{\partial \Phi}{\partial \vartheta} \frac{\partial g_j}{\partial V} & \sim \varepsilon (\varepsilon^{3/2}) \frac{V_{Tj}}{r} \Delta^2 g_j, \end{aligned}$$

$$\begin{aligned} \frac{eZ_j}{m_j V} \frac{V_{\parallel}}{B_0} \frac{I^2}{qR^2} \left(q - \frac{m}{n} \right) \frac{\partial}{\partial \psi} \Big|_{\vartheta} \left(\frac{V_{\parallel}}{\omega_{cj}} \right) \frac{\partial \Phi}{\partial \xi} \frac{\partial g_j}{\partial V} & \sim (\varepsilon^{1/2}) \frac{V_{Tj}}{R} \Delta^3 g_j \sim \varepsilon (\varepsilon^{3/2}) \frac{V_{Tj}}{r} \Delta^3 g_j, \\ \frac{eZ_j}{m_j V} \frac{V_{\parallel}}{B_0} B_0^2 \frac{\partial}{\partial \psi} \Big|_{\vartheta} \left(\frac{V_{\parallel}}{\omega_{cj}} \right) \frac{\partial \Phi}{\partial \xi} \frac{\partial g_j}{\partial V} & \sim (\varepsilon^{1/2}) \frac{V_{Tj}}{R} \Delta^2 g_j \sim \varepsilon (\varepsilon^{3/2}) \frac{V_{Tj}}{r} \Delta^2 g_j. \end{aligned}$$

Therefore, the velocity contribution becomes

$$- \frac{eZ_j}{m_j V} \frac{V_{\parallel}}{B_0} \frac{I}{qR^2} \left[\frac{\partial \Phi}{\partial \vartheta} \Big|_{\psi, \xi} + I \frac{\partial}{\partial \vartheta} \Big|_{\psi} \left(\frac{V_{\parallel}}{\omega_{cj}} \right) \frac{\partial \Phi}{\partial \psi} \Big|_{\vartheta, \xi} \right] \frac{\partial g_j}{\partial V} \Big|_{\psi} + \mathcal{O}(\Delta^2) =$$

$$= -\frac{eZ_j}{m_j V} \frac{V_{\parallel}}{B_0} \frac{I}{qR^2} \frac{\partial \Phi}{\partial \vartheta} \Big|_{p_{\varphi}, \xi} \frac{\partial g_j}{\partial V} \Big|_{\psi} + \mathcal{O}(\Delta^2), \quad (\text{D.38})$$

where

$$\frac{\partial \Phi}{\partial \vartheta} \Big|_{p_{\varphi}} = \frac{\partial \Phi}{\partial \vartheta} \Big|_{\psi} + \frac{\partial \psi}{\partial \vartheta} \Big|_{p_{\varphi}} \frac{\partial \Phi}{\partial \psi} \Big|_{\vartheta} \quad (\text{D.39})$$

with

$$\begin{aligned} \frac{\partial \psi}{\partial \vartheta} \Big|_{p_{\varphi}} &= \frac{\partial}{\partial \vartheta} \Big|_{p_{\varphi}} \left(\frac{IV_{\parallel}}{\omega_{cj}} \right) = \frac{\partial}{\partial \vartheta} \Big|_{\psi} \left(\frac{IV_{\parallel}}{\omega_{cj}} \right) + \frac{\partial \psi}{\partial \vartheta} \Big|_{p_{\varphi}} \frac{\partial}{\partial \psi} \Big|_{\vartheta} \left(\frac{IV_{\parallel}}{\omega_{cj}} \right) = \\ &= \frac{\partial}{\partial \vartheta} \Big|_{\psi} \left(\frac{IV_{\parallel}}{\omega_{cj}} \right) + \frac{\partial}{\partial \vartheta} \Big|_{p_{\varphi}} \left(\frac{IV_{\parallel}}{\omega_{cj}} \right) \frac{\partial}{\partial \psi} \Big|_{\vartheta} \left(\frac{IV_{\parallel}}{\omega_{cj}} \right) \end{aligned}$$

in accordance with the definition of p_{φ} . The last term in $\partial \psi / \partial \vartheta \Big|_{p_{\varphi}}$ does not contribute to $\mathcal{O}(\Delta^1)$. Indeed,

$$\begin{aligned} &\frac{eZ_j}{m_j V} \frac{V_{\parallel}}{B_0} \frac{I}{qR^2} \frac{\partial}{\partial \vartheta} \Big|_{p_{\varphi}} \left(\frac{IV_{\parallel}}{\omega_{cj}} \right) \frac{\partial}{\partial \psi} \Big|_{\vartheta} \left(\frac{IV_{\parallel}}{\omega_{cj}} \right) \frac{\partial \Phi}{\partial \psi} \frac{\partial g_j}{\partial V} \\ &\sim \frac{V_{Tj}}{B_0} \frac{1}{Rwr} \frac{\partial}{\partial \vartheta} \Big|_{\psi} \left(\frac{IV_{\parallel}}{\omega_{cj}} \right) \frac{\partial}{\partial \psi} \Big|_{\vartheta} \left(\frac{IV_{\parallel}}{\omega_{cj}} \right) \Delta g_j \sim \varepsilon(\varepsilon^{3/2}) \frac{V_{Tj}}{r} \frac{\partial}{\partial \psi} \Big|_{\vartheta} \left(\frac{IV_{\parallel}}{\omega_{cj}} \right) \Delta g_j \\ &\sim \varepsilon(\varepsilon^2) \frac{V_{Tj}}{r} \Delta^2 g_j \end{aligned}$$

to leading order (terms of order $\mathcal{O}(\Delta^3)$ and higher order corrections are neglected).

Therefore, Eq.D.36 reads

$$\begin{aligned} &\left\{ \frac{V_{\parallel}}{B_0} \frac{I}{qR^2} \left[1 - I \frac{\partial}{\partial \psi} \Big|_{\vartheta} \left(\frac{V_{\parallel}}{\omega_{cj}} \right) \right] + \frac{B_{\varphi}^2}{qB_0^2} \frac{\partial \Phi}{\partial \psi} \Big|_{\xi, \vartheta} \right\} \frac{\partial g_j}{\partial \vartheta} \Big|_{p_{\varphi}, \xi} + \\ &+ \left\{ \frac{V_{\parallel}}{B_0} \mathbf{B}_1 \cdot \nabla p_{\varphi} + \frac{\partial \Phi}{\partial \xi} \Big|_{\psi, \vartheta} \right\} \frac{\partial g_j}{\partial p_{\varphi}} \Big|_{\vartheta, \xi} + \\ &+ \left\{ \frac{V_{\parallel}}{B_0} \left[\frac{I}{qR^2} q'_s \left(p_{\varphi} + \frac{IV_{\parallel}}{\omega_{cj}} \right) + B_0^2 \frac{\partial}{\partial \psi} \Big|_{\vartheta} \left(\frac{V_{\parallel}}{\omega_{cj}} \right) + \vartheta' B_{\vartheta}^2 \frac{\partial}{\partial \vartheta} \Big|_{\psi} \left(\frac{V_{\parallel}}{\omega_{cj}} \right) \right] - \right. \\ &\left. - \frac{\partial \Phi}{\partial \psi} \Big|_{\xi, \vartheta} \right\} \frac{\partial g_j}{\partial \xi} \Big|_{p_{\varphi}, \vartheta} - \frac{eZ_j}{m_j qV} \frac{V_{\parallel}}{B_0} \frac{I}{R^2} \frac{\partial \Phi}{\partial \vartheta} \Big|_{p_{\varphi}, \xi} \frac{\partial g_j}{\partial V} \Big|_{p_{\varphi}} = C_j(g_j), \quad (\text{D.40}) \end{aligned}$$

where the term in $\partial g_j / \partial p_{\varphi}$ has been rearranged using Eq.D.39, and the velocity contribution has been rewritten as

$$\frac{\partial}{\partial V} \Big|_{\psi} = \frac{\partial}{\partial V} \Big|_{p_{\varphi}} + \frac{\partial p_{\varphi}}{\partial V} \Big|_{\psi} \frac{\partial}{\partial p_{\varphi}} \Big|_V$$

with $\partial p_\varphi / \partial V|_\psi = -(I/\omega_{cj}) \partial V_\parallel / \partial V|_{\psi, \vartheta, \mu} = -(I/\omega_{cj})(V/V_\parallel)$ (note: here we have used the definition of p_φ , Eq.2.13 and $V^2 = V_\parallel^2 + V_\perp^2 = V_\parallel^2 + 2\mu B$, and thus $2V \partial V|_{\psi, \vartheta, \mu} = 2V_\parallel \partial V_\parallel|_{\psi, \vartheta, \mu}$).

Eq.D.40 is a full drift kinetic equation in toroidal geometry to $\mathcal{O}(\Delta^1)$ in a low beta limit, written in $\{p_\varphi, \xi, \vartheta, \mu, V\}$ space.¹⁰⁰ At this stage we have not specified a form of the collision operator. To employ the collision operator from [53], we switch from $\{\mu, V\}$ to $\{\lambda, V; \sigma\}$ in velocity space, where $\lambda = 2\mu/V^2$ is the pitch angle and $\sigma = V_\parallel/|V_\parallel|$. To rewrite Eq.D.40 in $\{p_\varphi, \xi, \vartheta, \lambda, V; \sigma\}$ space, we use

$$\frac{\partial}{\partial V}\bigg|_\mu = \frac{\partial}{\partial V}\bigg|_\lambda + \frac{\partial \lambda}{\partial V}\bigg|_\mu \frac{\partial}{\partial \lambda}\bigg|_V$$

with $\partial \lambda / \partial V|_\mu = -4\mu/V^3$ and thus Eq.D.40 becomes

$$\begin{aligned} & \left\{ \frac{V_\parallel}{B_0} \frac{I}{qR^2} \left[1 - I \frac{\partial}{\partial \psi}\bigg|_\vartheta \left(\frac{V_\parallel}{\omega_{cj}} \right) \right] + \frac{B_\varphi^2}{qB_0^2} \frac{\partial \Phi}{\partial \psi}\bigg|_{\xi, \vartheta} \right\} \frac{\partial g_j}{\partial \vartheta}\bigg|_{p_\varphi, \xi, \lambda, V; \sigma} + \\ & + \left\{ \frac{V_\parallel}{B_0} \mathbf{B}_1 \cdot \nabla p_\varphi + \frac{\partial \Phi}{\partial \xi}\bigg|_{\psi, \vartheta} \right\} \frac{\partial g_j}{\partial p_\varphi}\bigg|_{\vartheta, \xi, \lambda, V; \sigma} + \\ & + \left\{ \frac{V_\parallel}{B_0} \left[\frac{I}{qR^2} q'_s \left(p_\varphi + \frac{IV_\parallel}{\omega_{cj}} \right) + B_0^2 \frac{\partial}{\partial \psi}\bigg|_\vartheta \left(\frac{V_\parallel}{\omega_{cj}} \right) + \vartheta' B_\vartheta^2 \frac{\partial}{\partial \vartheta}\bigg|_\psi \left(\frac{V_\parallel}{\omega_{cj}} \right) \right] - \right. \\ & - \left. \frac{\partial \Phi}{\partial \psi}\bigg|_{\xi, \vartheta} \right\} \frac{\partial g_j}{\partial \xi}\bigg|_{p_\varphi, \vartheta, \lambda, V; \sigma} - \frac{eZ_j}{m_j q V} \frac{V_\parallel}{B_0} \frac{I}{R^2} \frac{\partial \Phi}{\partial \vartheta}\bigg|_{p_\varphi, \xi} \frac{\partial g_j}{\partial V}\bigg|_{p_\varphi, \xi, \vartheta, \lambda; \sigma} + \\ & + 2 \frac{eZ_j}{m_j q V^2} \frac{V_\parallel}{B_0} \frac{I}{R^2} \frac{\partial \Phi}{\partial \vartheta}\bigg|_{p_\varphi, \xi} \lambda \frac{\partial g_j}{\partial \lambda}\bigg|_{p_\varphi, \xi, \vartheta, V; \sigma} = C_j(g_j). \end{aligned} \quad (\text{D.41})$$

Eq.D.41 is the final drift kinetic equation in toroidal geometry to $\mathcal{O}(\Delta^1)$ in a low beta approximation with completed transition from $\{\psi, \xi, \vartheta, \mu, V\}$ to $\{p_\varphi, \xi, \vartheta, \lambda, V; \sigma\}$ space.

D.3 Perturbative treatment

As we noted in the main part, to solve Eq.D.41 for g_j , we define a small parameter $\Delta = w/a \ll 1$ with the following orderings: $eZ_j \Phi / T_j \sim \Delta$, $g_j / f_j^M \sim \Delta$, $\delta \Phi / \Phi \sim \Delta$. Employing an expansion in Δ , we write $g_j = \sum_\alpha g_j^{(\alpha)} \Delta^\alpha$. To $\mathcal{O}(\Delta^0)$ we have Eq.2.18. Thus, we deduce that the leading order distribution function in Δ , $g_j^{(0)}$, is ϑ -independent

¹⁰⁰The derivatives in the Vlasov part of Eq.D.40 are taken at fixed μ .

at fixed p_φ . Multiplying both sides of Eq.D.40 by $R^2 B_0 / IV_\parallel$ and proceeding to $\mathcal{O}(\Delta^1)$, we come to an equation for $g_j^{(0)}$:

$$\begin{aligned}
& \frac{1}{q} \frac{\partial g_j^{(1)}}{\partial \vartheta} \Big|_{p_\varphi, \xi, \lambda, V; \sigma} + \left[\frac{I}{V_\parallel q B_0} \frac{\partial \Phi}{\partial \psi} \Big|_{\xi, \vartheta} - \frac{I}{q} \frac{\partial}{\partial \psi} \Big|_{\vartheta} \left(\frac{V_\parallel}{\omega_{cj}} \right) \right] \frac{\partial g_j^{(0)}}{\partial \vartheta} \Big|_{p_\varphi, \xi, \lambda, V; \sigma} + \\
& + \left[\frac{R^2}{I} \mathbf{B}_1 \cdot \nabla p_\varphi + \frac{R^2 B_0}{IV_\parallel} \frac{\partial \Phi}{\partial \xi} \Big|_{\psi, \vartheta} \right] \frac{\partial g_j^{(0)}}{\partial p_\varphi} \Big|_{\vartheta, \xi, \lambda, V; \sigma} + \\
& + \left[\frac{q'_s}{q} \left(p_\varphi + \frac{IV_\parallel}{\omega_{cj}} \right) + \frac{R^2 B_0^2}{I} \frac{\partial}{\partial \psi} \Big|_{\vartheta} \left(\frac{V_\parallel}{\omega_{cj}} \right) + \frac{R^2 B_\vartheta^2}{I} \vartheta' \frac{\partial}{\partial \vartheta} \Big|_{\psi} \left(\frac{V_\parallel}{\omega_{cj}} \right) - \right. \\
& \left. - \frac{R^2 B_0}{IV_\parallel} \frac{\partial \Phi}{\partial \psi} \Big|_{\xi, \vartheta} \right] \frac{\partial g_j^{(0)}}{\partial \xi} \Big|_{p_\varphi, \vartheta, \lambda, V; \sigma} - \frac{e Z_j}{m_j q V} \frac{\partial \Phi}{\partial \vartheta} \Big|_{p_\varphi, \xi} \frac{\partial g_j^{(0)}}{\partial V} \Big|_{p_\varphi, \xi, \vartheta, \lambda; \sigma} + \\
& + 2 \frac{e Z_j}{m_j q V^2} \frac{\partial \Phi}{\partial \vartheta} \Big|_{p_\varphi, \xi} \lambda \frac{\partial g_j^{(0)}}{\partial \lambda} \Big|_{p_\varphi, \xi, \vartheta, V; \sigma} = \frac{R^2 B_0}{IV_\parallel} C_j \left(g_j^{(0)} \right). \tag{D.42}
\end{aligned}$$

The highlighted term equals zero due to Eq.2.18, and thus Eq.D.42 reduces to Eq.2.19.

D.4 Orbit averaging

To eliminate a term in $g_j^{(1)}$ in Eq.2.19, we have to integrate the equation over ϑ , which is equivalent to orbit-averaging at fixed p_φ . The annihilation operator is introduced as follows:

$$\langle \dots \rangle_{\vartheta}^{p_\varphi} = \begin{cases} \frac{1}{2\pi} \int_{-\pi}^{\pi} \dots d\vartheta, & \lambda \leq \lambda_c \\ \frac{1}{2} \sum_{\sigma} \frac{\sigma}{\vartheta_{b_2} - \vartheta_{b_1}} \int_{\vartheta_{b_1}}^{\vartheta_{b_2}} \dots d\vartheta, & \lambda \geq \lambda_c. \end{cases} \tag{D.43}$$

The second condition approximately can be rewritten as $\frac{1}{4\pi} \sum_{\sigma} \sigma \int_{-\vartheta_b}^{\vartheta_b} \dots d\vartheta$. Here we have applied symmetry of the bounce points provided by the form of the equilibrium magnetic field we impose (see Sec.2.1 of Chapter II) and the fact that the λ dependence of $\vartheta_{b_{1,2}}$ is weak for this equilibrium magnetic field.¹⁰¹ Thus, Eq.D.43 reduces to Eq.2.24. As the particle distribution function, g_j , is required to be periodic in ϑ , we have

$$\left\langle \frac{1}{q} \frac{\partial g_j^{(1)}}{\partial \vartheta} \Big|_{p_\varphi, \xi, \lambda, V; \sigma} \right\rangle_{\vartheta}^{p_\varphi} = 0.$$

¹⁰¹The λ dependence of $\vartheta_{b_{1,2}}$ is assumed to be faster than of $\vartheta_{b_2} - \vartheta_{b_1}$.

Note: $1/q$ and $\langle \dots \rangle_{\vartheta}^{p_{\varphi}}$ are not necessarily commutative. However, as we seek the solution localised to the island vicinity, we can pull $1/q$ through the averaging operator. Thus, the orbit-averaged form of Eq.2.19 for $g_j^{(0)}$ reads

$$\begin{aligned}
& \left[\left\langle \frac{R^2}{I} \mathbf{B}_1 \cdot \nabla p_{\varphi} \right\rangle_{\vartheta}^{p_{\varphi}} + \left\langle \frac{R^2 B_0}{IV_{\parallel}} \frac{\partial \Phi}{\partial \xi} \Big|_{\psi, \vartheta} \right\rangle_{\vartheta}^{p_{\varphi}} \right] \frac{\partial g_j^{(0)}}{\partial p_{\varphi}} \Big|_{\vartheta, \xi, \lambda, V; \sigma} + \\
& + \left[\frac{q'_s}{q} \left\langle p_{\varphi} + \frac{IV_{\parallel}}{\omega_{cj}} \right\rangle_{\vartheta}^{p_{\varphi}} + \left\langle \frac{R^2 B_0^2}{I} \frac{\partial}{\partial \psi} \Big|_{\vartheta} \left(\frac{V_{\parallel}}{\omega_{cj}} \right) \right\rangle_{\vartheta}^{p_{\varphi}} + \left\langle \frac{R^2 B_{\vartheta}^2}{I} \vartheta' \frac{\partial}{\partial \vartheta} \Big|_{\psi} \left(\frac{V_{\parallel}}{\omega_{cj}} \right) \right\rangle_{\vartheta}^{p_{\varphi}} - \\
& - \left\langle \frac{R^2 B_0}{IV_{\parallel}} \frac{\partial \Phi}{\partial \psi} \Big|_{\xi, \vartheta} \right\rangle_{\vartheta}^{p_{\varphi}} \right] \frac{\partial g_j^{(0)}}{\partial \xi} \Big|_{p_{\varphi}, \vartheta, \lambda, V; \sigma} - \frac{eZ_j}{m_j q V} \left\langle \frac{\partial \Phi}{\partial \vartheta} \Big|_{p_{\varphi}, \xi} \right\rangle_{\vartheta}^{p_{\varphi}} \frac{\partial g_j^{(0)}}{\partial V} \Big|_{p_{\varphi}, \xi, \vartheta, \lambda; \sigma} + \\
& + 2 \frac{eZ_j}{m_j q V^2} \left\langle \frac{\partial \Phi}{\partial \vartheta} \Big|_{p_{\varphi}, \xi} \right\rangle_{\vartheta}^{p_{\varphi}} \lambda \frac{\partial g_j^{(0)}}{\partial \lambda} \Big|_{p_{\varphi}, \xi, \vartheta, V; \sigma} = \left\langle \frac{R^2 B_0}{IV_{\parallel}} C_j \left(g_j^{(0)} \right) \right\rangle_{\vartheta}^{p_{\varphi}}.
\end{aligned}$$

The electrostatic potential is periodic in ϑ as the distribution function requires periodicity. Therefore,

$$\left\langle \frac{\partial \Phi}{\partial \vartheta} \Big|_{p_{\varphi}, \xi} \right\rangle_{\vartheta}^{p_{\varphi}} = 0.$$

Then the ϑ -averaged equation to $\mathcal{O}(\Delta^1)$ becomes Eq.2.20 with drift frequencies defined as Eqs.2.21,2.22,2.23. Since in $\{p_{\varphi}, \xi, \vartheta, \lambda, V; \sigma\}$ space the orbit averaging procedure eliminates the term in $\partial g_j^{(0)}/\partial V \Big|_{p_{\varphi}}$, the only V dependence comes from the collision operator and is parametric. Eq.2.20 is to be solved for $g_j^{(0)} = g_j^{(0)}(p_{\varphi}, \xi, \lambda; V)$ at each σ ($\sigma = \pm 1$ for passing particles and $\sigma = \sigma_t$ for trapped particles). Before we proceed further and introduce the normalised quantities, let us rearrange $\langle R^2 (\mathbf{B}_1 \cdot \nabla p_{\varphi}) \rangle_{\vartheta}^{p_{\varphi}}$.

We highlight that Eq.2.20 with Eqs.2.21,2.22,2.23 is obtained to $\mathcal{O}(\Delta^1)$ in the drift kinetic approximation in the low beta plasma limit. It contains terms of order ε^2 . However, as we choose the equilibrium magnetic field from Sec.2.1 (e.g. to calculate bounce points for trapped particles), i.e. we exploit a large aspect ratio circular poloidal cross section tokamak approximation, terms of order ε^2 provide higher order corrections and hence can be omitted.

D.5 The $\langle R^2 (\mathbf{B}_1 \cdot \nabla p_\varphi) \rangle_\vartheta^{p_\varphi}$ term

Since $\partial/\partial\psi$ is estimated via $(1/RB_\vartheta\partial/\partial w)$ on perturbed quantities, the leading order $\mathbf{B}_1 \cdot \nabla\psi$ term from $\mathbf{B}_1 \cdot \nabla p_\varphi$ does contribute to the Vlasov part of the drift kinetic equation. As shown above, $I\partial(V_{\parallel}/\omega_{cj})/\partial\psi(\mathbf{B}_1 \cdot \nabla\psi)$ and $I\partial(V_{\parallel}/\omega_{cj})/\partial\vartheta(\mathbf{B}_1 \cdot \nabla\vartheta)$ provide corrections of order Δ^2 and hence are to be omitted. In accordance with Eq.2.4, we write

$$\langle R^2 (\mathbf{B}_1 \cdot \nabla p_\varphi) \rangle_\vartheta^{p_\varphi} = \left\langle R^2 \left[\nabla \times A_{\parallel} \frac{\mathbf{B}_0}{B_0} \right] \cdot \nabla p_\varphi \right\rangle_\vartheta^{p_\varphi} = \left\langle R^2 \nabla \cdot \left[A_{\parallel} \frac{\mathbf{B}_0 \times \nabla p_\varphi}{B_0} \right] \right\rangle_\vartheta^{p_\varphi}$$

In a large aspect ratio tokamak with circular poloidal cross section, we estimate each term of Eq.D.21 as follows

$$\begin{aligned} |\mathbf{IB}_0| &\sim |R^2 B_0^2 \nabla \varphi| \sim B_0^2 R, \\ \frac{\partial}{\partial \psi} \Big|_{\vartheta} \left(\frac{IV_{\parallel}}{\omega_{cj}} \right) |\mathbf{IB}_0| &\sim \frac{\partial}{\partial \psi} \Big|_{\vartheta} \left(\frac{IV_{\parallel}}{\omega_{cj}} \right) |R^2 B_0^2 \nabla \varphi| \sim (\varepsilon^{1/2}) \Delta B_0^2 R, \\ \frac{\partial}{\partial \vartheta} \Big|_{\psi} \left(\frac{IV_{\parallel}}{\omega_{cj}} \right) I\vartheta' |\mathbf{B}_0| &\sim \varepsilon(\varepsilon^{3/2}) \rho_{\vartheta j} B_\varphi^2 R^2 \frac{B_0}{RB_\vartheta r} \sim (\varepsilon^{1/2}) \Delta B_0^2 R, \\ \frac{\partial}{\partial \vartheta} \Big|_{\psi} \left(\frac{IV_{\parallel}}{\omega_{cj}} \right) \vartheta' R^2 B_0^2 |\nabla \varphi| &\sim (\varepsilon^{1/2}) \Delta B_0^2 R, \\ \frac{\partial}{\partial \vartheta} \Big|_{\psi} \left(\frac{IV_{\parallel}}{\omega_{cj}} \right) \frac{B_\varphi^2}{qR^2 B_\vartheta^2} \nabla \psi &\sim \varepsilon(\varepsilon^{3/2}) \Delta B_0^2 R. \end{aligned}$$

Then we have

$$\begin{aligned} \langle R^2 (\mathbf{B}_1 \cdot \nabla p_\varphi) \rangle_\vartheta^{p_\varphi} &= \left\langle R^2 \nabla \cdot \left\{ [I\mathbf{B}_0 - R^2 B^2 \nabla \varphi] \frac{A_{\parallel}}{B_0} \right\} \right\rangle_\vartheta^{p_\varphi} + \mathcal{O}(\Delta^2) = \\ &= \left\langle R^2 \frac{A_{\parallel}}{B_0} \nabla \cdot [I\mathbf{B}_0 - R^2 B^2 \nabla \varphi] \right\rangle_\vartheta^{p_\varphi} + \left\langle R^2 [I\mathbf{B}_0 - R^2 B^2 \nabla \varphi] \cdot \nabla \left(\frac{A_{\parallel}}{B_0} \right) \right\rangle_\vartheta^{p_\varphi} + \mathcal{O}(\Delta^2) = \\ &= \left\langle R^2 [I\mathbf{B}_0 - R^2 B^2 \nabla \varphi] \cdot \nabla \left(\frac{A_{\parallel}}{B_0} \right) \right\rangle_\vartheta^{p_\varphi} + \mathcal{O}(\Delta^2) = \end{aligned}$$

as the magnetic field is divergence free.

$$= \left\langle \frac{R^2}{B_0} [I\mathbf{B}_0 - R^2 B^2 \nabla \varphi] \cdot \nabla A_{\parallel} \right\rangle_\vartheta^{p_\varphi} + \left\langle R^2 A_{\parallel} [I\mathbf{B}_0 - R^2 B^2 \nabla \varphi] \cdot \nabla \left(\frac{1}{B_0} \right) \right\rangle_\vartheta^{p_\varphi} + \mathcal{O}(\Delta^2) =$$

since the NTM perturbation is introduced through ψ or A_{\parallel} connected via Eq.2.5 with Eq.2.6

$$\begin{aligned}
&= \left\langle \frac{R^2}{B_0} [IB_0 - R^2 B^2 \nabla \varphi] \cdot \frac{dA_{\parallel}}{d\xi} \nabla \xi \right\rangle_{\vartheta}^{p_{\varphi}} + \\
&+ \left\langle IA_{\parallel} R^2 \mathbf{B}_0 \cdot \nabla \left(\frac{1}{B_0} \right) \right\rangle_{\vartheta}^{p_{\varphi}} - \left\langle \underbrace{B^2 R^4 A_{\parallel} \nabla \varphi \cdot \nabla \left(\frac{1}{B_0} \right)}_{-B_0^{-2} \nabla \varphi \cdot \nabla B_0 = 0} \right\rangle_{\vartheta}^{p_{\varphi}} + \mathcal{O}(\Delta^2) =
\end{aligned}$$

The third term vanishes due to Eq.D.3 and toroidal symmetry.

$$\begin{aligned}
&= - \left\langle \frac{R^2}{B_0} R^2 B^2 \frac{dA_{\parallel}}{d\xi} \underbrace{\nabla \varphi \cdot \nabla \xi}_{|\nabla \varphi|^2} \right\rangle_{\vartheta}^{p_{\varphi}} + \\
&+ \left\langle IA_{\parallel} R^2 \left[\frac{\partial}{\partial \vartheta} \Big|_{\psi} \left(\frac{1}{B_0} \right) \mathbf{B}_0 \cdot \nabla \vartheta + \frac{\partial}{\partial \psi} \Big|_{\vartheta} \left(\frac{1}{B_0} \right) \mathbf{B}_0 \cdot \nabla \psi \right] \right\rangle_{\vartheta}^{p_{\varphi}} + \mathcal{O}(\Delta^2) = \\
&\quad \underbrace{\left\langle \mathbf{B}_0 \cdot \nabla (1/B_0) \right\rangle_{\vartheta}}_{\vartheta}^{p_{\varphi}} + \mathcal{O}(\Delta^2) =
\end{aligned}$$

$\mathbf{B}_0 \cdot \nabla \xi$ provides the higher order correction in Δ due to Eq.D.29. Substituting Eq.D.12, we obtain

$$= - \left\langle R^2 B_0 \frac{dA_{\parallel}}{d\xi} \right\rangle_{\vartheta}^{p_{\varphi}} + \left\langle \frac{I^2}{q} A_{\parallel} \frac{\partial}{\partial \vartheta} \Big|_{\psi, \xi} \left(\frac{1}{B_0} \right) \right\rangle_{\vartheta}^{p_{\varphi}} + \mathcal{O}(\Delta^2) =$$

As $1/B_0 \propto 1 + \varepsilon \cos \vartheta$, $\partial B_0^{-1} / \partial \vartheta \Big|_{\psi, \xi} \propto \sin \vartheta$ and hence the second term does not contribute.

Thus, we deduce

$$\left\langle R^2 (\mathbf{B}_1 \cdot \nabla p_{\varphi}) \right\rangle_{\vartheta}^{p_{\varphi}} = - \left\langle R^2 B_0 \frac{dA_{\parallel}}{d\xi} \right\rangle_{\vartheta}^{p_{\varphi}} + \mathcal{O}(\Delta^2). \quad (\text{D.44})$$

Due to Eq.2.5, $dA_{\parallel}/d\xi = -(\tilde{\psi}/R)f'$, $f' \equiv df/d\xi$. For a single isolated magnetic island, this reduces to $dA_{\parallel}/d\xi = (\tilde{\psi}/R)n \sin n\xi$.

D.6 Normalisation

The normalised quantities are given by Eq.2.31. λ is non-normalised; w^2 is defined as $4\tilde{\psi}q_s/q'_s$. Let us multiply both sides of Eq.2.20 by ψ_s/w . For the first term of Eq.2.20 we

have

$$\frac{q'_s}{q} p_\varphi \frac{\psi_s}{w} = \hat{L}_q^{-1} \left[\frac{\psi - \psi_s}{w} - \frac{IV_{\parallel} V_{Tj}}{\omega_{cj} w V_{Tj}} \right] = \hat{L}_q^{-1} \left[x - \hat{\rho}_{\vartheta j} \hat{V}_{\parallel} \right] = \hat{p}_\varphi \hat{L}_q^{-1}.$$

To normalise ω_D we consider

$$\frac{q'_s}{q} \left\langle \frac{IV_{\parallel}}{\omega_{cj}} \right\rangle_{\vartheta}^{p_\varphi} \frac{\psi_s}{w} = \hat{L}_q^{-1} \left\langle \frac{IV_{\parallel} V_{Tj}}{\omega_{cj} w V_{Tj}} \right\rangle_{\vartheta}^{p_\varphi} = \hat{L}_q^{-1} \left\langle \hat{\rho}_{\vartheta j} \hat{V}_{\parallel} \right\rangle_{\vartheta}^{p_\varphi}.$$

To rewrite the second term in ω_D , we rearrange

$$\begin{aligned} \frac{\partial}{\partial \psi} \Big|_{\vartheta, \xi} \left(\frac{V_{\parallel}}{B} \right) &= \frac{\partial}{\partial \psi} \Big|_{\vartheta, \xi} \left(\frac{\sigma V \sqrt{1 - \lambda B}}{B} \right) = \sigma V \frac{\partial B}{\partial \psi} \frac{\partial}{\partial B} \left(\frac{\sqrt{1 - \lambda B}}{B} \right) = \\ &= -\frac{1}{B} \frac{\partial B}{\partial \psi} \left(\frac{\lambda V^2}{2V_{\parallel}} + \frac{V_{\parallel}}{B} \right) \end{aligned}$$

and hence

$$\begin{aligned} &\left\langle \frac{R^2 B_0^2}{I} \frac{\partial}{\partial \psi} \Big|_{\vartheta, \xi} \left(\frac{V_{\parallel}}{\omega_{cj}} \right) \right\rangle_{\vartheta}^{p_\varphi} \frac{\psi_s}{w} = -\left\langle \frac{R^2 B_0^2}{I} \frac{m_j}{e Z_j} \frac{1}{B} \frac{\partial B}{\partial \psi} \left(\frac{\lambda V^2}{2V_{\parallel}} + \frac{V_{\parallel}}{B} \right) \right\rangle_{\vartheta}^{p_\varphi} \frac{\psi_s}{w} = \\ &= -\left\langle \frac{R^2 B_0^2}{I} \frac{m_j}{e Z_j} \frac{V_{Tj}}{w \hat{L}_B} \left(\frac{\lambda V^2}{2V_{\parallel} V_{Tj}} + \frac{\hat{V}_{\parallel}}{B} \right) \right\rangle_{\vartheta}^{p_\varphi} = \\ &= -\left\langle \frac{R^2 B_0^2}{I} \frac{m_j}{e Z_j} \frac{V_{Tj}}{w \hat{L}_B} \left(\frac{\hat{V}_{\parallel}}{B} + \frac{\lambda V^2 V_{Tj}^2}{2V_{\parallel} V_{Tj} V_{Tj}^2} \right) \right\rangle_{\vartheta}^{p_\varphi} = \\ &= -\left\langle \frac{R^2 B_0^2}{I} \frac{m_j}{e Z_j} \frac{V_{Tj}}{w \hat{L}_B} \left(\frac{\hat{V}_{\parallel}}{B} + \frac{\lambda \hat{V}^2}{2\hat{V}_{\parallel}} \right) \right\rangle_{\vartheta}^{p_\varphi} = \\ &= -\left\langle \frac{R^2 B_0^2}{B_0} \frac{I m_j V_{Tj}}{I^2} \frac{1}{e Z_j B_0 w \hat{L}_B} \left(\frac{\hat{V}_{\parallel}}{B} + \frac{\lambda \hat{V}^2}{2\hat{V}_{\parallel}} \right) \right\rangle_{\vartheta}^{p_\varphi} = -\left\langle \frac{B_0^2}{B_\varphi^2} \frac{\hat{\rho}_{\vartheta j}}{\hat{L}_B} \left(\hat{V}_{\parallel} + \frac{\lambda B \hat{V}^2}{2\hat{V}_{\parallel}} \right) \right\rangle_{\vartheta}^{p_\varphi}. \end{aligned}$$

The last term in ω_D is a higher order term in the small inverse aspect ratio circular poloidal cross section tokamak approximation and hence is to be omitted.

$$\begin{aligned} &\left\langle \frac{R^2}{I} (\mathbf{B}_1 \cdot \nabla p_\varphi) \right\rangle_{\vartheta}^{p_\varphi} \frac{\psi_s}{w} = -\left\langle \frac{R^2 B_0}{I} \frac{dA_{\parallel}}{d\xi} \right\rangle_{\vartheta}^{p_\varphi} \frac{\psi_s}{w} = \left\langle \frac{R B_0}{I} \tilde{\psi} f' \right\rangle_{\vartheta}^{p_\varphi} \frac{\psi_s}{w} = \\ &= \left\langle \frac{R B_0}{I} f' \frac{w^2 q'_s}{4q_s} \frac{\psi_s}{w} \right\rangle_{\vartheta}^{p_\varphi} = \left\langle \frac{R B_0}{I} f' w \frac{1}{4\hat{L}_q} \frac{\psi_s}{\psi_s} \right\rangle_{\vartheta}^{p_\varphi} = \left\langle \frac{1}{4} \frac{R B_0}{I} \frac{\hat{w}}{\hat{L}_q} f' \right\rangle_{\vartheta}^{p_\varphi} \psi_s \end{aligned}$$

as $dA_{\parallel}/d\xi = -(\tilde{\psi}/R)df/d\xi$. Here $f' = df/d\xi$. Now let us consider the $\mathbf{E} \times \mathbf{B}$ drift frequencies:

$$\begin{aligned} \omega_{E,\xi} \frac{\psi_s}{w} &= \frac{1}{I} \left\langle \frac{R^2 B_0}{V_{\parallel}} \frac{\partial \Phi}{\partial \psi} \Big|_{\xi,\vartheta} \right\rangle_{\vartheta}^{p_{\varphi}} \frac{\psi_s e Z_j T_j}{w T_j e Z_j} = \left\langle \frac{R^2 B_0}{I \hat{V}_{\parallel}} \frac{\psi_s}{w} \frac{\partial \hat{\Phi}}{\partial \hat{\psi}} \Big|_{\xi,\vartheta} \right\rangle_{\vartheta}^{p_{\varphi}} \frac{T_j}{e Z_j V_{Tj}} = \\ &= \frac{1}{2} \left\langle \frac{R^2 B_0^2}{I \hat{V}_{\parallel}} \frac{\psi_s}{w^2} \frac{\partial \hat{\Phi}}{\partial \hat{\psi}} \Big|_{\xi,\vartheta} \frac{2 T_j m_j}{e Z_j B_0 V_{Tj}} \frac{1}{m_j} \right\rangle_{\vartheta}^{p_{\varphi}} = \frac{1}{2} \left\langle \frac{R^2 B_0^2}{I^2 \hat{V}_{\parallel}} \frac{\hat{\rho}_{\vartheta j}}{\hat{w}} \frac{\partial \hat{\Phi}}{\partial \hat{\psi}} \Big|_{\xi,\vartheta} \right\rangle_{\vartheta}^{p_{\varphi}} = \\ &= \frac{1}{2} \left\langle \frac{B_0^2}{B_{\varphi}^2} \frac{\hat{\rho}_{\vartheta j}}{\hat{V}_{\parallel} \hat{w}} \frac{\partial \hat{\Phi}}{\partial \hat{\psi}} \Big|_{\xi,\vartheta} \right\rangle_{\vartheta}^{p_{\varphi}} \end{aligned}$$

and

$$\begin{aligned} \omega_{E,r} \frac{\psi_s}{w} &= \frac{1}{I} \left\langle \frac{R^2 B_0}{V_{\parallel}} \frac{\partial \Phi}{\partial \xi} \Big|_{\psi,\vartheta} \right\rangle_{\vartheta}^{p_{\varphi}} \frac{\psi_s}{w} = \frac{1}{2} \left\langle \frac{R^2 B_0^2}{I \hat{V}_{\parallel}} \frac{\psi_s}{w} \frac{\partial \hat{\Phi}}{\partial \xi} \Big|_{\psi,\vartheta} \right\rangle_{\vartheta}^{p_{\varphi}} \frac{2 T_j}{e Z_j B_0 V_{Tj}} \frac{1}{m_j} = \\ &= \frac{1}{2} \left\langle \frac{R^2 B_0^2}{I^2 \hat{V}_{\parallel}} \frac{\hat{\rho}_{\vartheta j}}{\hat{w}} \frac{\partial \hat{\Phi}}{\partial \xi} \Big|_{\psi,\vartheta} \right\rangle_{\vartheta}^{p_{\varphi}} \psi_s = \frac{1}{2} \left\langle \frac{B_0^2}{B_{\varphi}^2} \frac{\hat{\rho}_{\vartheta j}}{\hat{V}_{\parallel}} \frac{\partial \hat{\Phi}}{\partial \xi} \Big|_{\psi,\vartheta} \right\rangle_{\vartheta}^{p_{\varphi}} \psi_s \end{aligned}$$

Now we have to rewrite the right hand side of Eq.2.20.

D.6.1 Ion-ion and electron-electron/ion collision operator

Employing Eq.2.25, we write

$$\begin{aligned} \frac{\psi_s}{w} \left\langle C_{ii}(g_i) \frac{R^2 B_0}{I V_{\parallel}} \right\rangle_{\vartheta}^{p_{\varphi}} &= \\ &= \left\langle \nu_{ii}(V) \left[2 \frac{(1-\lambda B)^{1/2}}{B} \frac{\partial}{\partial \lambda} \Big|_{\psi} \left(\lambda (1-\lambda B)^{1/2} \frac{\partial g_i}{\partial \lambda} \Big|_{\psi} \right) + \frac{V_{\parallel} \bar{u}_{\parallel i}(g_i) f_i^M}{V_{Ti}^2} \right] \frac{R^2 B_0}{I V_{\parallel}} \right\rangle_{\vartheta}^{p_{\varphi}} \frac{1}{\hat{w}} = \end{aligned}$$

$\bar{u}_{\parallel i}$ is given by Eq.2.26.

$$\begin{aligned} &= \frac{\nu_{ii}}{\hat{w}} \left\langle \left[\frac{2}{\sigma V B} \frac{\partial}{\partial \lambda} \Big|_{\psi} \left(\lambda (1-\lambda B)^{1/2} \frac{\partial g_i}{\partial \lambda} \Big|_{\psi} \right) + \frac{\bar{u}_{\parallel i}(g_i) f_i^M}{V_{Ti}^2} \right] \frac{R^2 B_0}{I} \right\rangle_{\vartheta}^{p_{\varphi}} = \\ &= \frac{\nu_{ii}}{\hat{w}} \left\langle \left[\frac{2}{\sigma V B} \frac{\partial}{\partial \lambda} \Big|_{\psi} \left(\lambda (1-\lambda B)^{1/2} \frac{\partial g_i}{\partial \lambda} \Big|_{\psi} \right) \frac{V_{Ti}}{V_{Ti}} + \frac{f_i^M}{V_{Ti}^2} \frac{3\pi^{1/2}}{2n_0} V_{Ti}^3 \int d\mathbf{V} \frac{V_{\parallel} g_i}{V^3} \right] \frac{R^2 B_0}{I} \right\rangle_{\vartheta}^{p_{\varphi}}. \end{aligned}$$

Before we move further, let us consider the integral term:

$$\bar{u}_{\parallel i}(g_i) = \frac{3\pi^{1/2}}{2n_0} \int d\mathbf{V} \frac{V_{\parallel} g_i}{\hat{V}^3} = \frac{3\pi^{3/2}}{2n_0} B \sum_{\sigma} \int_{\mathbb{R}^+} \hat{V}^2 d\hat{V} \int_0^{B^{-1}} \frac{d\lambda}{(1-\lambda B)^{1/2}} \frac{\hat{V}_{\parallel} g_i}{\hat{V}^3} \cdot V_{Ti}^4.$$

Here we have used the expression for the velocity space integral, Eq.2.12. The Maxwellian is to be evaluated at the rational surface, $\psi = \psi_s$, i.e. $f_i^M = n_0 (\psi_s) \pi^{-3/2} V_{Ti}^{-3} (\psi_s) e^{-V^2/V_{Ti}^2(\psi_s)}$ and hence

$$\frac{f_i^M}{V_{Ti}^2} \bar{u}_{\parallel i} = \frac{3}{2} \frac{1}{V_{Ti}} e^{-\hat{V}^2} \cdot B \sum_{\sigma} \int_{\mathbb{R}^+} \hat{V}^2 d\hat{V} \int_0^{B^{-1}} \frac{d\lambda}{(1-\lambda B)^{1/2}} \frac{\hat{V}_{\parallel} g_i}{\hat{V}^3}.$$

Substituting this into $\langle C_{ii}(g_i) R^2 B_0 / IV_{\parallel} \rangle_{\vartheta}^{p_{\varphi}}$ gives

$$\begin{aligned} \left\langle C_{jj}(g_j) \frac{R^2 B_0}{IV_{\parallel}} \right\rangle_{\vartheta}^{p_{\varphi}} \frac{\psi_s}{w} &= \frac{\hat{\nu}_{jj}}{\hat{w}} \left\langle \left[\frac{2}{\sigma \hat{V} B} \frac{\partial}{\partial \lambda} \Big|_{\psi} \left(\lambda (1-\lambda B)^{1/2} \frac{\partial g_j}{\partial \lambda} \Big|_{\psi} \right) + \right. \\ &+ \left. \frac{3}{2} e^{-\hat{V}^2} \cdot B \sum_{\sigma} \int_{\mathbb{R}^+} \hat{V}^2 d\hat{V} \int_0^{B^{-1}} \frac{d\lambda}{(1-\lambda B)^{1/2}} \frac{\hat{V}_{\parallel} g_j}{\hat{V}^3} \right] \frac{R^2 B_0}{I} \right\rangle_{\vartheta}^{p_{\varphi}} \end{aligned} \quad (\text{D.45})$$

with $\hat{\nu}_{jj} = \nu_{jj}/V_{Tj}$ and $\hat{V}_{\parallel} = \sigma \hat{V} (1-\lambda B)^{1/2}$. $j = i$ for ions; V and V_{\parallel} are normalised to the ion thermal velocity, V_{Ti} . $\langle C_{ee}(g_e) R^2 B_0 / IV_{\parallel} \rangle_{\vartheta}^{p_{\varphi}}$ repeats Eq.D.45 with $j = e$. Ion-electron collisions are small and hence to be neglected. Electron-electron and electron-ion collisions are comparable and thus we consider:

$$\begin{aligned} \frac{\psi_s}{w} \left\langle C_{ei}(g_e) \frac{R^2 B_0}{IV_{\parallel}} \right\rangle_{\vartheta}^{p_{\varphi}} &= \\ &= \left\langle \nu_{ei}(V) \left[2 \frac{(1-\lambda B)^{1/2}}{B} \frac{\partial}{\partial \lambda} \Big|_{\psi} \left(\lambda (1-\lambda B)^{1/2} \frac{\partial g_e}{\partial \lambda} \Big|_{\psi} \right) + \frac{2}{V_{Te}^2} V_{\parallel} u_{\parallel i}(g_i) f_e^M \right] \frac{R^2 B_0}{IV_{\parallel}} \right\rangle_{\vartheta}^{p_{\varphi}} \frac{1}{\hat{w}} \end{aligned}$$

with C_{ei} and $u_{\parallel i}$ given by Eq.2.30 and Eq.2.27, respectively. Let us consider $(2/V_{Te}^2) u_{\parallel i}(g_i) f_e^M$ with f_e^M being the Maxwellian localised around the rational surface.

$$\begin{aligned} \frac{2}{V_{Te}^2} f_e^M u_{\parallel i}(g_i) &= \frac{2}{V_{Te}^2} f_e^M \frac{1}{n_0} \int dV V_{\parallel} g_i = \\ &= \frac{2}{V_{Te}^2} f_e^M \frac{1}{n_0} \pi B \sum_{\sigma} \int_{\mathbb{R}^+} \hat{V}_i^2 d\hat{V}_i \int_0^{B^{-1}} \frac{d\lambda}{(1-\lambda B)^{1/2}} \hat{V}_{\parallel i} g_i \cdot V_{Ti}^4 = \\ &= \frac{2}{\pi^{1/2}} e^{-\hat{V}_i^2} B \sum_{\sigma} \int_{\mathbb{R}^+} \hat{V}_i^2 d\hat{V}_i \int_0^{B^{-1}} \frac{d\lambda}{(1-\lambda B)^{1/2}} \hat{V}_{\parallel i} g_i \cdot \frac{V_{Ti}^4}{V_{Te}^4} \frac{1}{V_{Te}} \end{aligned}$$

with $\hat{V}_j = V_j/V_{Tj}$ and $\hat{V}_{\parallel j} = V_{\parallel j}/V_{Tj}$. Substituting this into $\langle C_{ei}(g_e) R^2 B_0 / IV_{\parallel} \rangle_{\vartheta}^{p_{\varphi}}$ provides

$$\begin{aligned} & \frac{\psi_s}{w} \left\langle C_{ei}(g_e) \frac{R^2 B_0}{IV_{\parallel}} \right\rangle_{\vartheta}^{p_{\varphi}} = \\ & = \frac{\hat{\nu}_{ei}}{\hat{w}} \left\langle \left[\frac{2}{\sigma \hat{V}_e B} \frac{\partial}{\partial \lambda} \right]_{\psi} \left(\lambda (1 - \lambda B)^{1/2} \frac{\partial g_e}{\partial \lambda} \right)_{\psi} \right\rangle_{\vartheta} + \\ & + \frac{2}{\pi^{1/2}} e^{-\hat{V}_e^2} B \sum_{\sigma} \int_{\mathbb{R}^+} \hat{V}_i^2 d\hat{V}_i \int_0^{B^{-1}} \frac{d\lambda}{(1 - \lambda B)^{1/2}} \hat{V}_{\parallel i} g_i \cdot \left(\frac{m_e}{m_i} \right)^2 \left[\frac{R^2 B_0}{I} \right]_{\vartheta}^{p_{\varphi}} \end{aligned} \quad (\text{D.46})$$

with $\hat{\nu}_{ei} = \nu_{ei}/V_{Te}$. We have to note that the momentum-conservation term does not contribute to the trapped particle solution to leading order in $\rho_{\vartheta j}/a$ ¹⁰² due to the summation over σ in the ϑ -averaging operator.

D.6.2 Orbit averaged drift kinetic equation in normalised form

Substituting the normalised terms derived above into Eq.2.20 and multiplying both sides by $\hat{w} = w/\psi_s$, we obtain Eq.2.32 for ions and Eq.2.33 for electrons with normalised drift frequencies defined in accordance with Eq.2.34. Here $dp_{\varphi} = w d\hat{p}_{\varphi}$. We note that the $\partial/\partial \lambda|_{\psi}$ and $\langle \dots \rangle_{\vartheta}^{p_{\varphi}}$ are not commutative. Employing the conventional tokamak approximation and noting that the fastest \hat{p}_{φ} variation is in the electrostatic potential, we come to Eq.2.35, provided a single isolated magnetic island is considered.

D.7 \mathcal{S} island formalism.

Drift kinetic equation in \mathcal{S} space

In the main part we noted that Eq.2.35 in $\{p_{\varphi}, \xi, \lambda, V; \sigma\}$ space is equivalent to Eq.2.36 written in $\{S, \xi, \lambda, V; \sigma\}$ space, where S is given by Eq.2.37. In this appendix we prove that both representations are equivalent. We use Eq.2.37 and

$$\frac{\partial}{\partial \xi} \Big|_S = \frac{\partial}{\partial \xi} \Big|_{\hat{p}_{\varphi}} + \frac{\partial \hat{p}_{\varphi}}{\partial \xi} \Big|_S \frac{\partial}{\partial \hat{p}_{\varphi}} \Big|_{\xi} \quad (\text{D.47})$$

¹⁰²The trapped particle solution is independent of σ at fixed p_{φ} . However, Eq.2.26 and Eq.2.27 are to be calculated at fixed ψ .

to write

$$\begin{aligned} \frac{\partial S}{\partial \xi} \Big|_S = 0 &= \frac{\hat{w}}{4\hat{L}_q} \left[4 \left(\hat{p}_\varphi - \frac{\hat{\omega}_D \hat{\rho}_{\vartheta j} \hat{L}_q}{\hat{w}} \right) \frac{\partial \hat{p}_\varphi}{\partial \xi} \Big|_S + \sin \xi \right] \Theta(\lambda_c - \lambda) - \\ &- \hat{\omega}_D \hat{\rho}_{\vartheta j} \frac{\partial \hat{p}_\varphi}{\partial \xi} \Big|_S \Theta(\lambda - \lambda_c) - \\ &- \frac{\partial}{\partial \xi} \Big|_{\hat{p}_\varphi} \frac{1}{2} \left\langle \frac{\hat{\rho}_{\vartheta j} \hat{\Phi}}{\hat{V}_\parallel} \right\rangle_{\vartheta}^{p_\varphi} - \frac{\partial \hat{p}_\varphi}{\partial \xi} \Big|_S \frac{\partial}{\partial \hat{p}_\varphi} \Big|_\xi \frac{1}{2} \left\langle \frac{\hat{\rho}_{\vartheta j} \hat{\Phi}}{\hat{V}_\parallel} \right\rangle_{\vartheta}^{p_\varphi}. \end{aligned}$$

This, in turn, reads

$$\begin{aligned} &\left\{ \frac{\hat{w}}{\hat{L}_q} \hat{p}_\varphi \Theta(\lambda_c - \lambda) - \hat{\omega}_D \hat{\rho}_{\vartheta j} [\Theta(\lambda_c - \lambda) + \Theta(\lambda - \lambda_c)] - \frac{\partial}{\partial \hat{p}_\varphi} \Big|_\xi \frac{1}{2} \left\langle \frac{\hat{\rho}_{\vartheta j} \hat{\Phi}}{\hat{V}_\parallel} \right\rangle_{\vartheta}^{p_\varphi} \right\} \frac{\partial \hat{p}_\varphi}{\partial \xi} \Big|_S = \\ &= -\frac{\hat{w}}{4\hat{L}_q} \sin \xi \cdot \Theta(\lambda_c - \lambda) + \frac{\partial}{\partial \xi} \Big|_{p_\varphi} \frac{1}{2} \left\langle \frac{\hat{\rho}_{\vartheta j} \hat{\Phi}}{\hat{V}_\parallel} \right\rangle_{\vartheta}^{p_\varphi} \end{aligned}$$

and hence we obtain the following expression for $\partial \hat{p}_\varphi / \partial \xi|_S$:

$$\frac{\partial \hat{p}_\varphi}{\partial \xi} \Big|_S = \frac{-\frac{\hat{w}}{4\hat{L}_q} \sin \xi \cdot \Theta(\lambda_c - \lambda) + \frac{\partial}{\partial \xi} \Big|_{\hat{p}_\varphi} \frac{1}{2} \left\langle \frac{\hat{\rho}_{\vartheta j} \hat{\Phi}}{\hat{V}_\parallel} \right\rangle_{\vartheta}^{p_\varphi}}{\frac{\hat{w}}{\hat{L}_q} \hat{p}_\varphi \Theta(\lambda_c - \lambda) - \hat{\omega}_D \hat{\rho}_{\vartheta j} - \frac{\partial}{\partial \hat{p}_\varphi} \Big|_\xi \frac{1}{2} \left\langle \frac{\hat{\rho}_{\vartheta j} \hat{\Phi}}{\hat{V}_\parallel} \right\rangle_{\vartheta}^{p_\varphi}} \quad (\text{D.48})$$

Substituting Eqs.D.47,D.48 into Eq.2.36, we obtain Eq.2.35.

Employing weak collision dissipation, we solve Eq.2.36 by an expansion in δ_j . From the $\mathcal{O}(\Delta^1 \delta_j^0)$ equation we learn that the leading order ion/electron distribution function, $g_j^{(0,0)}$, is independent of ξ at fixed S . Proceeding to $\mathcal{O}(\Delta^1 \delta_j^1)$ provides an equation to be solved for $g_j^{(0,0)}$, Eq.2.39. To eliminate the term in $g_j^{(0,1)}$, we introduce an annihilation operator, Eq.2.41/Eq.2.42, similar to Eq.2.24. Due to the periodicity requirement in ξ , $\partial g_j^{(0,1)} / \partial \xi \Big|_{S, \vartheta, \lambda, V; \sigma}$ averages to zero, and we write

$$\left\langle \frac{\partial g_j^{(0,1)}}{\partial \xi} \Big|_{S, \vartheta, \lambda, V; \sigma} \right\rangle_\xi = 0 = \left\langle \frac{\tilde{C}_j(g_j^{(0,0)})}{\mathcal{A}} \right\rangle_\xi = \left\langle \frac{\tilde{C}_j}{\mathcal{A}} \right\rangle_\xi g_j^{(0,0)}.$$

This provides Eq.2.40. Here we have used the fact that $g_j^{(0,0)}$ is not a function of ξ at any fixed S . Now let us derive an explicit representation for Eq.2.40. Note: Eq.2.36 is to be solved for $g_j^{(0)} = g_j^{(0)}(\xi, S, \lambda)$ at each V and σ , while Eq.2.40 is to be solved

for $g_j^{(0,0)} = g_j^{(0,0)}(S, \lambda)$ at each V and σ . As we noted above, $\partial/\partial\lambda|_\psi$ and $\langle \dots \rangle_\vartheta^{p_\varphi}$ are not commutative and thus we have to rewrite \tilde{C}_j , the right hand side of Eq.2.32/Eq.2.33 for ions/electrons, using

$$\frac{\partial}{\partial\lambda}\Big|_\psi = \frac{\partial}{\partial\lambda}\Big|_{\hat{p}_\varphi} + \frac{\partial\hat{p}_\varphi}{\partial\lambda}\Big|_\psi \frac{\partial}{\partial\hat{p}_\varphi}\Big|_\lambda \quad (\text{D.49})$$

and

$$\frac{\partial}{\partial\lambda}\Big|_{\hat{p}_\varphi} = \frac{\partial}{\partial\lambda}\Big|_S + \frac{\partial S}{\partial\lambda}\Big|_{\hat{p}_\varphi} \frac{\partial}{\partial S}\Big|_\lambda \quad (\text{D.50})$$

with

$$\frac{\partial\hat{p}_\varphi}{\partial\lambda}\Big|_\psi = \hat{p}_{\vartheta j} \frac{\sigma\hat{V}B}{2(1-\lambda B)^{1/2}} \equiv p_\lambda(\vartheta, \lambda, V; \sigma)$$

(note: the direct transition from ψ to S is also allowed. However, the factorisation of the ϑ and ξ averages is not straightforward in this case). Let us consider

$$\frac{\partial}{\partial\lambda}\Big|_{\psi, \xi, \vartheta, V; \sigma} \left(\sigma\lambda\sqrt{1-\lambda B} \frac{R}{B_\varphi} \frac{\partial g}{\partial\lambda}\Big|_{\psi, \xi, \vartheta, V; \sigma} \right) =$$

Substituting Eq.D.49, we obtain

$$\begin{aligned} &= \left[\frac{\partial}{\partial\lambda}\Big|_{\hat{p}_\varphi} + p_\lambda \frac{\partial}{\partial\hat{p}_\varphi}\Big|_\lambda \right] \left(\sigma\lambda\sqrt{1-\lambda B} \frac{R}{B_\varphi} \left[\frac{\partial}{\partial\lambda}\Big|_{\hat{p}_\varphi} + p_\lambda \frac{\partial}{\partial\hat{p}_\varphi}\Big|_\lambda \right] g \right) = \\ &= \frac{\partial}{\partial\lambda}\Big|_{\hat{p}_\varphi} \left(\sigma\lambda\sqrt{1-\lambda B} \frac{R}{B_\varphi} \frac{\partial g}{\partial\lambda}\Big|_{\hat{p}_\varphi} \right) + \frac{\partial}{\partial\lambda}\Big|_{\hat{p}_\varphi} \left(\sigma\lambda\sqrt{1-\lambda B} \frac{R}{B_\varphi} p_\lambda \frac{\partial g}{\partial\hat{p}_\varphi}\Big|_\lambda \right) + \\ &+ p_\lambda \frac{\partial}{\partial\hat{p}_\varphi}\Big|_\lambda \left(\sigma\lambda\sqrt{1-\lambda B} \frac{R}{B_\varphi} \frac{\partial g}{\partial\lambda}\Big|_{\hat{p}_\varphi} \right) + p_\lambda \frac{\partial}{\partial\hat{p}_\varphi}\Big|_\lambda \left(\sigma\lambda\sqrt{1-\lambda B} \frac{R}{B_\varphi} p_\lambda \frac{\partial g}{\partial\hat{p}_\varphi}\Big|_\lambda \right) = \end{aligned}$$

(note: ξ , ϑ , \hat{V} and σ are kept fixed). Expanding the brackets, we write

$$\begin{aligned} &= \sigma\lambda\sqrt{1-\lambda B} \frac{R}{B_\varphi} \frac{\partial^2 g}{\partial\lambda^2}\Big|_{\hat{p}_\varphi} + \sigma \frac{2-3\lambda B}{2\sqrt{1-\lambda B}} \frac{R}{B_\varphi} \frac{\partial g}{\partial\lambda}\Big|_{\hat{p}_\varphi} + \\ &+ \frac{\partial}{\partial\lambda}\Big|_{\hat{p}_\varphi} \left(\sigma\lambda\sqrt{1-\lambda B} \frac{R}{B_\varphi} p_\lambda \right) \frac{\partial g}{\partial\hat{p}_\varphi}\Big|_\lambda + \sigma\lambda\sqrt{1-\lambda B} \frac{R}{B_\varphi} p_\lambda \frac{\partial}{\partial\lambda}\Big|_{\hat{p}_\varphi} \left(\frac{\partial g}{\partial\hat{p}_\varphi}\Big|_\lambda \right) + \\ &+ \sigma\lambda\sqrt{1-\lambda B} \frac{R}{B_\varphi} p_\lambda \frac{\partial}{\partial\hat{p}_\varphi}\Big|_\lambda \left(\frac{\partial g}{\partial\lambda}\Big|_{\hat{p}_\varphi} \right) + \sigma\lambda\sqrt{1-\lambda B} \frac{R}{B_\varphi} p_\lambda^2 \frac{\partial^2 g}{\partial\hat{p}_\varphi^2}\Big|_\lambda = \end{aligned}$$

Inserting the expression for p_λ ,

$$\begin{aligned}
&= \sigma \lambda \sqrt{1 - \lambda B} \frac{R}{B_\varphi} \frac{\partial^2 g}{\partial \lambda^2} \Big|_{\hat{p}_\varphi} + \sigma \frac{2 - 3\lambda B}{2\sqrt{1 - \lambda B}} \frac{R}{B_\varphi} \frac{\partial g}{\partial \lambda} \Big|_{\hat{p}_\varphi} + \\
&+ \frac{\hat{\rho}_{\vartheta j}}{2} \hat{V} B \frac{R}{B_\varphi} \frac{\partial g}{\partial \hat{p}_\varphi} \Big|_\lambda + \frac{\hat{\rho}_{\vartheta j}}{2} \lambda \hat{V} B \frac{R}{B_\varphi} \frac{\partial}{\partial \lambda} \Big|_{\hat{p}_\varphi} \left(\frac{\partial g}{\partial \hat{p}_\varphi} \Big|_\lambda \right) + \\
&+ \frac{\hat{\rho}_{\vartheta j}}{2} \lambda \hat{V} B \frac{R}{B_\varphi} \frac{\partial}{\partial \hat{p}_\varphi} \Big|_\lambda \left(\frac{\partial g}{\partial \lambda} \Big|_{\hat{p}_\varphi} \right) + \sigma \frac{\hat{\rho}_{\vartheta j}^2}{4} \frac{\hat{V}^2 B^2 \lambda}{\sqrt{1 - \lambda B}} \frac{R}{B_\varphi} \frac{\partial^2 g}{\partial \hat{p}_\varphi^2} \Big|_\lambda =
\end{aligned}$$

$\partial/\partial \lambda|_{\hat{p}_\varphi}$ and $\partial/\partial \hat{p}_\varphi|_\lambda$ are commutative

$$\frac{\partial}{\partial \lambda} \Big|_{\hat{p}_\varphi} \frac{\partial}{\partial \hat{p}_\varphi} \Big|_\lambda = \frac{\partial}{\partial \hat{p}_\varphi} \Big|_\lambda \frac{\partial}{\partial \lambda} \Big|_{\hat{p}_\varphi}$$

in accordance with Schwartz's theorem (note: it is not necessarily valid for \hat{p}_φ written as a function of S , and thus these two terms are to be considered separately to provide transition from \hat{p}_φ to S space) and thus we come to

$$\begin{aligned}
&= \sigma \lambda \sqrt{1 - \lambda B} \frac{R}{B_\varphi} \frac{\partial^2 g}{\partial \lambda^2} \Big|_{\hat{p}_\varphi} + \sigma \frac{2 - 3\lambda B}{2\sqrt{1 - \lambda B}} \frac{R}{B_\varphi} \frac{\partial g}{\partial \lambda} \Big|_{\hat{p}_\varphi} + \\
&+ \sigma \frac{\hat{\rho}_{\vartheta j}^2}{4} \frac{\hat{V}^2 B^2 \lambda}{\sqrt{1 - \lambda B}} \frac{R}{B_\varphi} \frac{\partial^2 g}{\partial \hat{p}_\varphi^2} \Big|_\lambda + \frac{\hat{\rho}_{\vartheta j}}{2} \hat{V} B \frac{R}{B_\varphi} \frac{\partial g}{\partial \hat{p}_\varphi} \Big|_\lambda + \hat{\rho}_{\vartheta j} \lambda \hat{V} B \frac{R}{B_\varphi} \frac{\partial}{\partial \lambda} \Big|_{\hat{p}_\varphi} \left(\frac{\partial g}{\partial \hat{p}_\varphi} \Big|_\lambda \right).
\end{aligned}$$

The annihilation operator, $\langle \dots \rangle_\vartheta^{p_\varphi}$, and $\partial/\partial \lambda|_{\hat{p}_\varphi, \xi, \vartheta, V; \sigma}$, $\partial/\partial \hat{p}_\varphi|_{\lambda, \xi, \vartheta, V; \sigma}$ are commutative and hence we can write

$$\begin{aligned}
&\left\langle \frac{\partial}{\partial \lambda} \Big|_\psi \left(\sigma \lambda (1 - \lambda B)^{1/2} \frac{R}{B_\varphi} \frac{\partial g_j^{(0)}}{\partial \lambda} \Big|_\psi \right) \right\rangle_\vartheta^{p_\varphi} = \\
&= \left\langle \sigma \lambda \sqrt{1 - \lambda B} \frac{R}{B_\varphi} \right\rangle_\vartheta^{p_\varphi} \frac{\partial^2 g_j^{(0)}}{\partial \lambda^2} \Big|_{\hat{p}_\varphi} + \left\langle \sigma \frac{2 - 3\lambda B}{2\sqrt{1 - \lambda B}} \frac{R}{B_\varphi} \right\rangle_\vartheta^{p_\varphi} \frac{\partial g_j^{(0)}}{\partial \lambda} \Big|_{\hat{p}_\varphi} + \\
&+ \left\langle \sigma \frac{\hat{\rho}_{\vartheta j}^2}{4} \frac{\hat{V}^2 B^2 \lambda}{\sqrt{1 - \lambda B}} \frac{R}{B_\varphi} \right\rangle_\vartheta^{p_\varphi} \frac{\partial^2 g_j^{(0)}}{\partial \hat{p}_\varphi^2} \Big|_\lambda + \left\langle \frac{\hat{\rho}_{\vartheta j}}{2} \hat{V} R \right\rangle_\vartheta^{p_\varphi} \frac{\partial g_j^{(0)}}{\partial \hat{p}_\varphi} \Big|_\lambda + \\
&+ \left\langle \hat{\rho}_{\vartheta j} \hat{V} R \lambda \right\rangle_\vartheta^{p_\varphi} \frac{\partial}{\partial \lambda} \Big|_{\hat{p}_\varphi} \left(\frac{\partial g_j^{(0)}}{\partial \hat{p}_\varphi} \Big|_\lambda \right),
\end{aligned} \tag{D.51}$$

$j = e, i$. Here the large aspect ratio circular cross section tokamak approximation has been applied, $B \approx B_\varphi$. Eq.D.51 allows Eqs.2.32,2.33 to be written in p_φ space. Now we have to move from p_φ to S space to reduce the dimension of the problem replacing

$\partial/\partial\xi|_{\hat{p}_\varphi}$ with $\partial/\partial\xi|_{\mathcal{S}}$. Applying Eq.D.50, we write

$$\begin{aligned}
& \left\langle \sigma \lambda \sqrt{1 - \lambda B} \frac{R}{B_\varphi} \right\rangle_{\vartheta}^{p_\varphi} \frac{\partial^2 g}{\partial \lambda^2} \Big|_{\hat{p}_\varphi, \xi} = \\
& = \left\langle \sigma \lambda \sqrt{1 - \lambda B} \frac{R}{B_\varphi} \right\rangle_{\vartheta}^{p_\varphi} \frac{\partial^2 g}{\partial \lambda^2} \Big|_{\mathcal{S}, \xi} + \left\langle \sigma \lambda \sqrt{1 - \lambda B} \frac{R}{B_\varphi} \right\rangle_{\vartheta}^{p_\varphi} \left(\frac{\partial S}{\partial \lambda} \Big|_{\hat{p}_\varphi} \right)^2 \frac{\partial^2 g}{\partial S^2} \Big|_{\lambda, \xi} + \\
& + \left\langle \sigma \lambda \sqrt{1 - \lambda B} \frac{R}{B_\varphi} \right\rangle_{\vartheta}^{p_\varphi} \left[\frac{\partial}{\partial \lambda} \Big|_{\mathcal{S}} \left(\frac{\partial S}{\partial \lambda} \Big|_{\hat{p}_\varphi} \right) + \frac{\partial S}{\partial \lambda} \Big|_{\hat{p}_\varphi} \frac{\partial}{\partial S} \Big|_{\lambda} \left(\frac{\partial S}{\partial \lambda} \Big|_{\hat{p}_\varphi} \right) \right] \frac{\partial g}{\partial S} \Big|_{\lambda, \xi} + \\
& + 2 \left\langle \sigma \lambda \sqrt{1 - \lambda B} \frac{R}{B_\varphi} \right\rangle_{\vartheta}^{p_\varphi} \frac{\partial S}{\partial \lambda} \Big|_{\hat{p}_\varphi} \frac{\partial^2 g}{\partial \lambda \partial S} \Big|_{\xi}
\end{aligned} \tag{D.52}$$

for the first term of Eq.D.51. Here we have used the fact that the following operators are commutative:

$$\frac{\partial}{\partial \lambda} \Big|_{\mathcal{S}} \frac{\partial}{\partial S} \Big|_{\lambda} = \frac{\partial}{\partial S} \Big|_{\lambda} \frac{\partial}{\partial \lambda} \Big|_{\mathcal{S}}.$$

The second term of Eq.D.51 gives

$$\left\langle \sigma \frac{2 - 3\lambda B}{2\sqrt{1 - \lambda B}} \frac{R}{B_\varphi} \right\rangle_{\vartheta}^{p_\varphi} \frac{\partial g}{\partial \lambda} \Big|_{\hat{p}_\varphi, \xi} = \left\langle \sigma \frac{2 - 3\lambda B}{2\sqrt{1 - \lambda B}} \frac{R}{B_\varphi} \right\rangle_{\vartheta}^{p_\varphi} \left(\frac{\partial}{\partial \lambda} \Big|_{\mathcal{S}, \xi} + \frac{\partial S}{\partial \lambda} \Big|_{\hat{p}_\varphi} \frac{\partial}{\partial S} \Big|_{\lambda, \xi} \right) g. \tag{D.53}$$

To rewrite the third term we use

$$\frac{\partial g}{\partial \hat{p}_\varphi} \Big|_{\xi, \vartheta, \lambda, V; \sigma} = \left(\frac{\partial S}{\partial \hat{p}_\varphi} \right)_{\xi, \lambda, V; \sigma} \frac{\partial g}{\partial S} \Big|_{\xi, \vartheta, \lambda, V; \sigma}. \tag{D.54}$$

Note:

$$d\hat{p}_\varphi = \frac{\partial \hat{p}_\varphi}{\partial S} dS + \frac{\partial \hat{p}_\varphi}{\partial \xi} d\xi + \frac{\partial \hat{p}_\varphi}{\partial \lambda} d\lambda + \frac{\partial \hat{p}_\varphi}{\partial \hat{V}} d\hat{V}$$

for each σ . Therefore, we obtain

$$\begin{aligned}
& \left\langle \sigma \frac{\hat{\rho}_{\vartheta j}^2}{4} \frac{\hat{V}^2 B^2 \lambda}{\sqrt{1 - \lambda B}} \frac{R}{B_\varphi} \right\rangle_{\vartheta}^{p_\varphi} \frac{\partial^2 g}{\partial \hat{p}_\varphi^2} \Big|_{\lambda} = \\
& = \left\langle \sigma \frac{\hat{\rho}_{\vartheta j}^2}{4} \frac{\hat{V}^2 B^2 \lambda}{\sqrt{1 - \lambda B}} \frac{R}{B_\varphi} \right\rangle_{\vartheta}^{p_\varphi} \left(\frac{\partial S}{\partial \hat{p}_\varphi} \right)_{\xi, \lambda, V; \sigma} \frac{\partial}{\partial S} \Big|_{\lambda, \xi} \left(\frac{\partial S}{\partial \hat{p}_\varphi} \right)_{\xi, \lambda, V; \sigma} \frac{\partial g}{\partial S} \Big|_{\lambda, \xi} + \\
& + \left\langle \sigma \frac{\hat{\rho}_{\vartheta j}^2}{4} \frac{\hat{V}^2 B^2 \lambda}{\sqrt{1 - \lambda B}} \frac{R}{B_\varphi} \right\rangle_{\vartheta}^{p_\varphi} \left(\frac{\partial S}{\partial \hat{p}_\varphi} \right)_{\xi, \lambda, V; \sigma}^2 \frac{\partial^2 g}{\partial S^2} \Big|_{\lambda, \xi}
\end{aligned} \tag{D.55}$$

for the third term, and hence for the fourth term:

$$\left\langle \frac{\hat{\rho}_{\vartheta j} \hat{V} R}{2} \right\rangle_{\vartheta}^{p_{\varphi}} \frac{\partial g}{\partial \hat{p}_{\varphi}} \Big|_{\lambda} = \left\langle \frac{\hat{\rho}_{\vartheta j} \hat{V} R}{2} \right\rangle_{\vartheta}^{p_{\varphi}} \left(\frac{\partial S}{\partial \hat{p}_{\varphi}} \right)_{\xi, \lambda, V; \sigma} \frac{\partial g}{\partial S} \Big|_{\lambda, \xi}. \quad (\text{D.56})$$

The mixed derivative contribution becomes

$$\begin{aligned} & \frac{1}{2} \left\langle \hat{\rho}_{\vartheta j} \hat{V} R \lambda \right\rangle_{\vartheta}^{p_{\varphi}} \frac{\partial}{\partial \lambda} \Big|_{\hat{p}_{\varphi}, \xi} \left(\frac{\partial g}{\partial \hat{p}_{\varphi}} \Big|_{\lambda, \xi} \right) = \\ & = \frac{1}{2} \left\langle \hat{\rho}_{\vartheta j} \hat{V} R \lambda \right\rangle_{\vartheta}^{p_{\varphi}} \left[\frac{\partial}{\partial \lambda} \Big|_{S, \xi} + \frac{\partial S}{\partial \lambda} \Big|_{\hat{p}_{\varphi}} \frac{\partial}{\partial S} \Big|_{\lambda, \xi} \right] \left(\frac{\partial S}{\partial \hat{p}_{\varphi}} \Big|_{\xi, \lambda} \frac{\partial g}{\partial S} \Big|_{\lambda, \xi} \right) = \\ & = \frac{1}{2} \left\langle \hat{\rho}_{\vartheta j} \hat{V} R \lambda \right\rangle_{\vartheta}^{p_{\varphi}} \frac{\partial}{\partial \lambda} \Big|_{S, \xi} \left(\frac{\partial S}{\partial \hat{p}_{\varphi}} \Big|_{\xi, \lambda} \right) \frac{\partial g}{\partial S} \Big|_{\lambda, \xi} + \frac{1}{2} \left\langle \hat{\rho}_{\vartheta j} \hat{V} R \lambda \right\rangle_{\vartheta}^{p_{\varphi}} \frac{\partial S}{\partial \hat{p}_{\varphi}} \Big|_{\xi, \lambda} \frac{\partial^2 g}{\partial \lambda \partial S} \Big|_{\xi} + \\ & + \frac{1}{2} \left\langle \hat{\rho}_{\vartheta j} \hat{V} R \lambda \right\rangle_{\vartheta}^{p_{\varphi}} \frac{\partial S}{\partial \lambda} \Big|_{\hat{p}_{\varphi}} \frac{\partial}{\partial S} \Big|_{\lambda, \xi} \left(\frac{\partial S}{\partial \hat{p}_{\varphi}} \Big|_{\xi, \lambda} \right) \frac{\partial g}{\partial S} \Big|_{\lambda, \xi} + \frac{1}{2} \left\langle \hat{\rho}_{\vartheta j} \hat{V} R \lambda \right\rangle_{\vartheta}^{p_{\varphi}} \frac{\partial S}{\partial \lambda} \Big|_{\hat{p}_{\varphi}} \frac{\partial S}{\partial \hat{p}_{\varphi}} \Big|_{\xi, \lambda} \frac{\partial^2 g}{\partial S^2} \Big|_{\lambda, \xi}. \end{aligned} \quad (\text{D.57})$$

and

$$\begin{aligned} & \frac{1}{2} \left\langle \hat{\rho}_{\vartheta j} \hat{V} R \lambda \right\rangle_{\vartheta}^{p_{\varphi}} \frac{\partial}{\partial \hat{p}_{\varphi}} \Big|_{\lambda, \xi} \left(\frac{\partial g}{\partial \lambda} \Big|_{\hat{p}_{\varphi}, \xi} \right) = \\ & = \frac{1}{2} \left\langle \hat{\rho}_{\vartheta j} \hat{V} R \lambda \right\rangle_{\vartheta}^{p_{\varphi}} \frac{\partial S}{\partial \hat{p}_{\varphi}} \Big|_{\xi, \lambda} \frac{\partial}{\partial S} \Big|_{\lambda, \xi} \left[\frac{\partial}{\partial \lambda} \Big|_{S, \xi} + \frac{\partial S}{\partial \lambda} \Big|_{\hat{p}_{\varphi}} \frac{\partial}{\partial S} \Big|_{\lambda, \xi} \right] g = \\ & = \frac{1}{2} \left\langle \hat{\rho}_{\vartheta j} \hat{V} R \lambda \right\rangle_{\vartheta}^{p_{\varphi}} \frac{\partial S}{\partial \hat{p}_{\varphi}} \Big|_{\xi, \lambda} \frac{\partial^2 g}{\partial S \partial \lambda} \Big|_{\xi} + \\ & + \frac{1}{2} \left\langle \hat{\rho}_{\vartheta j} \hat{V} R \lambda \right\rangle_{\vartheta}^{p_{\varphi}} \frac{\partial S}{\partial \hat{p}_{\varphi}} \Big|_{\xi, \lambda} \frac{\partial}{\partial S} \Big|_{\lambda, \xi} \left(\frac{\partial S}{\partial \lambda} \Big|_{\hat{p}_{\varphi}} \right) \frac{\partial g}{\partial S} \Big|_{\lambda, \xi} + \\ & + \frac{1}{2} \left\langle \hat{\rho}_{\vartheta j} \hat{V} R \lambda \right\rangle_{\vartheta}^{p_{\varphi}} \frac{\partial S}{\partial \hat{p}_{\varphi}} \Big|_{\xi, \lambda} \frac{\partial S}{\partial \lambda} \Big|_{\hat{p}_{\varphi}} \frac{\partial^2 g}{\partial S^2} \Big|_{\lambda, \xi}. \end{aligned} \quad (\text{D.58})$$

Thus, writing all the above contributions, Eq.D.52-D.58, together we come to

$$\begin{aligned}
& \left\langle \frac{\partial}{\partial \lambda} \Big|_{\psi} \left(\sigma \lambda (1 - \lambda B)^{1/2} \frac{R}{B_{\varphi}} \frac{\partial g_j^{(0)}}{\partial \lambda} \Big|_{\psi} \right) \right\rangle_{\vartheta}^{p_{\varphi}} = \\
& = \left\langle \sigma \lambda \sqrt{1 - \lambda B} \frac{R}{B_{\varphi}} \right\rangle_{\vartheta}^{p_{\varphi}} \frac{\partial^2 g_j^{(0)}}{\partial \lambda^2} \Big|_{S, \xi} + \left\langle \sigma \frac{2 - 3\lambda B}{2\sqrt{1 - \lambda B}} \frac{R}{B_{\varphi}} \right\rangle_{\vartheta}^{p_{\varphi}} \frac{\partial g_j^{(0)}}{\partial \lambda} \Big|_{S, \xi} + \\
& + \left[\left\langle \sigma \lambda \sqrt{1 - \lambda B} \frac{R}{B_{\varphi}} \right\rangle_{\vartheta}^{p_{\varphi}} \left(\frac{\partial S}{\partial \lambda} \Big|_{\hat{p}_{\varphi}, \xi} \right)^2 + \left\langle \hat{\rho}_{\vartheta j} \hat{V} R \lambda \right\rangle_{\vartheta}^{p_{\varphi}} \frac{\partial S}{\partial \lambda} \Big|_{\hat{p}_{\varphi}, \xi} \frac{\partial S}{\partial \hat{p}_{\varphi}} \Big|_{\xi, \lambda} + \right. \\
& + \left. \left\langle \sigma \frac{\hat{\rho}_{\vartheta j}^2}{4} \frac{\hat{V}^2 B^2 \lambda}{\sqrt{1 - \lambda B}} \frac{R}{B_{\varphi}} \right\rangle_{\vartheta}^{p_{\varphi}} \left(\frac{\partial S}{\partial \hat{p}_{\varphi}} \Big|_{\xi, \lambda} \right)^2 \right] \frac{\partial^2 g_j^{(0)}}{\partial S^2} \Big|_{\lambda, \xi} + \\
& + \left[\left\langle \sigma \lambda \sqrt{1 - \lambda B} \frac{R}{B_{\varphi}} \right\rangle_{\vartheta}^{p_{\varphi}} \left(\frac{\partial}{\partial \lambda} \Big|_{S, \xi} \left(\frac{\partial S}{\partial \lambda} \Big|_{\hat{p}_{\varphi}, \xi} \right) + \frac{\partial S}{\partial \lambda} \Big|_{\hat{p}_{\varphi}, \xi} \frac{\partial}{\partial S} \Big|_{\lambda, \xi} \left(\frac{\partial S}{\partial \lambda} \Big|_{\hat{p}_{\varphi}, \xi} \right) \right) + \right. \\
& + \left. \left\langle \sigma \frac{2 - 3\lambda B}{2\sqrt{1 - \lambda B}} \frac{R}{B_{\varphi}} \right\rangle_{\vartheta}^{p_{\varphi}} \frac{\partial S}{\partial \lambda} \Big|_{\hat{p}_{\varphi}, \xi} + \left\langle \sigma \frac{\hat{\rho}_{\vartheta j}^2}{4} \frac{\hat{V}^2 B^2 \lambda}{\sqrt{1 - \lambda B}} \frac{R}{B_{\varphi}} \right\rangle_{\vartheta}^{p_{\varphi}} \frac{\partial S}{\partial \hat{p}_{\varphi}} \Big|_{\xi, \lambda} \frac{\partial}{\partial S} \Big|_{\lambda, \xi} \left(\frac{\partial S}{\partial \hat{p}_{\varphi}} \Big|_{\xi, \lambda} \right) + \right. \\
& + \left. \frac{1}{2} \left\langle \hat{\rho}_{\vartheta j} \hat{V} R \lambda \right\rangle_{\vartheta}^{p_{\varphi}} \frac{\partial}{\partial \lambda} \Big|_{S, \xi} \left(\frac{\partial S}{\partial \hat{p}_{\varphi}} \Big|_{\xi, \lambda} \right) + \frac{1}{2} \left\langle \hat{\rho}_{\vartheta j} \hat{V} R \lambda \right\rangle_{\vartheta}^{p_{\varphi}} \frac{\partial S}{\partial \lambda} \Big|_{\hat{p}_{\varphi}} \frac{\partial}{\partial S} \Big|_{\lambda, \xi} \left(\frac{\partial S}{\partial \hat{p}_{\varphi}} \Big|_{\xi, \lambda} \right) + \right. \\
& + \left. \frac{1}{2} \left\langle \hat{\rho}_{\vartheta j} \hat{V} R \lambda \right\rangle_{\vartheta}^{p_{\varphi}} \frac{\partial S}{\partial \hat{p}_{\varphi}} \Big|_{\xi, \lambda} \frac{\partial}{\partial S} \Big|_{\lambda, \xi} \left(\frac{\partial S}{\partial \lambda} \Big|_{\hat{p}_{\varphi}} \right) + \left\langle \frac{\hat{\rho}_{\vartheta j}}{2} \hat{V} R \right\rangle_{\vartheta}^{p_{\varphi}} \frac{\partial S}{\partial \hat{p}_{\varphi}} \Big|_{\xi, \lambda} \right] \frac{\partial g_j^{(0)}}{\partial S} \Big|_{\lambda, \xi} + \\
& + \left[2 \left\langle \sigma \lambda \sqrt{1 - \lambda B} \frac{R}{B_{\varphi}} \right\rangle_{\vartheta}^{p_{\varphi}} \frac{\partial S}{\partial \lambda} \Big|_{\hat{p}_{\varphi}, \xi} + \left\langle \hat{\rho}_{\vartheta j} \hat{V} R \lambda \right\rangle_{\vartheta}^{p_{\varphi}} \frac{\partial S}{\partial \hat{p}_{\varphi}} \Big|_{\xi, \lambda} \right] \frac{\partial^2 g_j^{(0)}}{\partial \lambda \partial S} \Big|_{\xi},
\end{aligned} \tag{D.59}$$

$j = e, i$. Here the validity of Schwartz's theorem has been assumed. Substituting Eq.D.59 into Eqs.2.36 gives the orbit-averaged equation written in terms of S . Substituting Eq.D.59 into Eq.2.40 and multiplying both sides of Eq.2.40 by $\hat{V}/2\hat{\nu}_{ii}$ provides the

collisional constraint in \mathcal{S} space:

$$\begin{aligned}
& \left\langle \sigma \lambda \sqrt{1 - \lambda B} \frac{R}{B_\varphi} \right\rangle_{\vartheta}^{p_\varphi} \left\langle \frac{1}{\mathcal{A}} \right\rangle_{\xi}^S \frac{\partial^2 g_i^{(0,0)}}{\partial \lambda^2} \Big|_{S, \xi} + \left\langle \sigma \frac{2 - 3\lambda B}{2\sqrt{1 - \lambda B}} \frac{R}{B_\varphi} \right\rangle_{\vartheta}^{p_\varphi} \left\langle \frac{1}{\mathcal{A}} \right\rangle_{\xi}^S \frac{\partial g_i^{(0,0)}}{\partial \lambda} \Big|_{S, \xi} + \\
& + \left[\left\langle \sigma \lambda \sqrt{1 - \lambda B} \frac{R}{B_\varphi} \right\rangle_{\vartheta}^{p_\varphi} \left\langle \frac{1}{\mathcal{A}} \left(\frac{\partial S}{\partial \lambda} \Big|_{\hat{p}_\varphi, \xi} \right)^2 \right\rangle_{\xi}^S + \left\langle \hat{\rho}_{\vartheta j} \hat{V} R \lambda \right\rangle_{\vartheta}^{p_\varphi} \left\langle \frac{1}{\mathcal{A}} \frac{\partial S}{\partial \lambda} \Big|_{\hat{p}_\varphi, \xi} \frac{\partial S}{\partial \hat{p}_\varphi} \Big|_{\xi, \lambda} \right\rangle_{\xi}^S + \\
& + \left\langle \sigma \frac{\hat{\rho}_{\vartheta j}^2}{4} \frac{\hat{V}^2 B^2 \lambda}{\sqrt{1 - \lambda B}} \frac{R}{B_\varphi} \right\rangle_{\vartheta}^{p_\varphi} \left\langle \frac{1}{\mathcal{A}} \left(\frac{\partial S}{\partial \hat{p}_\varphi} \Big|_{\xi, \lambda} \right)^2 \right\rangle_{\xi}^S \frac{\partial^2 g_i^{(0,0)}}{\partial S^2} \Big|_{\lambda, \xi} + \\
& + \left[\left\langle \sigma \lambda \sqrt{1 - \lambda B} \frac{R}{B_\varphi} \right\rangle_{\vartheta}^{p_\varphi} \left(\left\langle \frac{1}{\mathcal{A}} \frac{\partial}{\partial \lambda} \Big|_{S, \xi} \left(\frac{\partial S}{\partial \lambda} \Big|_{\hat{p}_\varphi, \xi} \right) \right\rangle_{\xi}^S + \left\langle \frac{1}{\mathcal{A}} \frac{\partial S}{\partial \lambda} \Big|_{\hat{p}_\varphi, \xi} \frac{\partial}{\partial S} \Big|_{\lambda, \xi} \left(\frac{\partial S}{\partial \lambda} \Big|_{\hat{p}_\varphi, \xi} \right) \right\rangle_{\xi}^S \right] + \\
& + \left\langle \sigma \frac{2 - 3\lambda B}{2\sqrt{1 - \lambda B}} \frac{R}{B_\varphi} \right\rangle_{\vartheta}^{p_\varphi} \left\langle \frac{1}{\mathcal{A}} \frac{\partial S}{\partial \lambda} \Big|_{\hat{p}_\varphi, \xi} \right\rangle_{\xi}^S + \\
& + \left\langle \sigma \frac{\hat{\rho}_{\vartheta j}^2}{4} \frac{\hat{V}^2 B^2 \lambda}{\sqrt{1 - \lambda B}} \frac{R}{B_\varphi} \right\rangle_{\vartheta}^{p_\varphi} \left\langle \frac{1}{\mathcal{A}} \frac{\partial S}{\partial \hat{p}_\varphi} \Big|_{\xi, \lambda} \frac{\partial}{\partial S} \Big|_{\lambda, \xi} \left(\frac{\partial S}{\partial \hat{p}_\varphi} \Big|_{\xi, \lambda} \right) \right\rangle_{\xi}^S + \\
& + \frac{1}{2} \left\langle \hat{\rho}_{\vartheta j} \hat{V} R \lambda \right\rangle_{\vartheta}^{p_\varphi} \left\langle \frac{1}{\mathcal{A}} \frac{\partial}{\partial \lambda} \Big|_{S, \xi} \left(\frac{\partial S}{\partial \hat{p}_\varphi} \Big|_{\xi, \lambda} \right) \right\rangle_{\xi}^S + \frac{1}{2} \left\langle \hat{\rho}_{\vartheta j} \hat{V} R \lambda \right\rangle_{\vartheta}^{p_\varphi} \left\langle \frac{1}{\mathcal{A}} \frac{\partial S}{\partial \lambda} \Big|_{\hat{p}_\varphi} \frac{\partial}{\partial S} \Big|_{\lambda, \xi} \left(\frac{\partial S}{\partial \hat{p}_\varphi} \Big|_{\xi, \lambda} \right) \right\rangle_{\xi}^S + \\
& + \frac{1}{2} \left\langle \hat{\rho}_{\vartheta j} \hat{V} R \lambda \right\rangle_{\vartheta}^{p_\varphi} \left\langle \frac{1}{\mathcal{A}} \frac{\partial S}{\partial \hat{p}_\varphi} \Big|_{\xi, \lambda} \frac{\partial}{\partial S} \Big|_{\lambda, \xi} \left(\frac{\partial S}{\partial \lambda} \Big|_{\hat{p}_\varphi} \right) \right\rangle_{\xi}^S + \left\langle \frac{\hat{\rho}_{\vartheta j}}{2} \hat{V} R \right\rangle_{\vartheta}^{p_\varphi} \left\langle \frac{1}{\mathcal{A}} \frac{\partial S}{\partial \hat{p}_\varphi} \Big|_{\xi, \lambda} \right\rangle_{\xi}^S \frac{\partial g_i^{(0)}}{\partial S} \Big|_{\lambda, \xi} + \\
& + \left[2 \left\langle \sigma \lambda \sqrt{1 - \lambda B} \frac{R}{B_\varphi} \right\rangle_{\vartheta}^{p_\varphi} \left\langle \frac{1}{\mathcal{A}} \frac{\partial S}{\partial \lambda} \Big|_{\hat{p}_\varphi, \xi} \right\rangle_{\xi}^S + \left\langle \hat{\rho}_{\vartheta j} \hat{V} R \lambda \right\rangle_{\vartheta}^{p_\varphi} \left\langle \frac{1}{\mathcal{A}} \frac{\partial S}{\partial \hat{p}_\varphi} \Big|_{\xi, \lambda} \right\rangle_{\xi}^S \right] \frac{\partial^2 g_i^{(0,0)}}{\partial \lambda \partial S} \Big|_{\xi} + \\
& + \frac{\hat{V}}{2} \left\langle \frac{1}{\mathcal{A}} \bar{U}_{\parallel i}(g_i^{(0,0)}) \right\rangle_{\xi}^S = 0
\end{aligned} \tag{D.60}$$

with $\bar{U}_{\parallel i}(g_i^{(0,0)}) = \frac{3}{2} e^{-\hat{V}^2} \left\langle R B_0 \sum_{\sigma} \sigma \int_{\mathbb{R}^+} d\hat{V} \int_0^{B^{-1}} g_i^{(0,0)} d\lambda \right\rangle_{\vartheta}^{p_\varphi}$ for ions. Here we have taken into account that the following operators are commutative: $\partial^k / \partial \lambda^k \Big|_{S, \xi}$ and $\partial^k / \partial S^k \Big|_{\lambda, \xi}$ ($k = 1, 2$) with $\langle \dots \rangle_{\xi}^S$, and the fact that the leading order distribution function, $g_i^{(0,0)}$ is ξ -independent at fixed S . As \hat{v}_{ii} is a function of V only, it has been pulled through the ξ average. Eq.D.60 is the final equation to be solved for the ion plasma component in the external regions where collisions are small, i.e. $\lambda \leq \lambda_p$ and $\lambda \geq \lambda_t$. We note that Eq.D.60 does not contain the collision frequency dependence. Instead it is to be provided by a thin boundary layer in the vicinity of λ_c where collisions play a role. Similarly, multiplying

both sides of Eq.2.40 by $\hat{V}_e/2$ and dividing by $\hat{v}_{ee} + \hat{v}_{ei}$ we obtain the following equation for electrons:

$$\begin{aligned}
& \left\langle \sigma \lambda \sqrt{1 - \lambda B} \frac{R}{B_\varphi} \right\rangle_{\vartheta}^{p_\varphi} \left\langle \frac{1}{\mathcal{A}} \right\rangle_{\xi}^S \frac{\partial^2 g_e^{(0,0)}}{\partial \lambda^2} \Big|_{S,\xi} + \left\langle \sigma \frac{2 - 3\lambda B}{2\sqrt{1 - \lambda B}} \frac{R}{B_\varphi} \right\rangle_{\vartheta}^{p_\varphi} \left\langle \frac{1}{\mathcal{A}} \right\rangle_{\xi}^S \frac{\partial g_e^{(0,0)}}{\partial \lambda} \Big|_{S,\xi} + \\
& + \left[\left\langle \sigma \lambda \sqrt{1 - \lambda B} \frac{R}{B_\varphi} \right\rangle_{\vartheta}^{p_\varphi} \left\langle \frac{1}{\mathcal{A}} \left(\frac{\partial S}{\partial \lambda} \Big|_{\hat{p}_\varphi, \xi} \right)^2 \right\rangle_{\xi}^S + \left\langle \hat{\rho}_{\vartheta j} \hat{V} R \lambda \right\rangle_{\vartheta}^{p_\varphi} \left\langle \frac{1}{\mathcal{A}} \frac{\partial S}{\partial \lambda} \Big|_{\hat{p}_\varphi, \xi} \frac{\partial S}{\partial \hat{p}_\varphi} \Big|_{\xi, \lambda} \right\rangle_{\xi}^S + \\
& + \left\langle \sigma \frac{\hat{\rho}_{\vartheta j}^2}{4} \frac{\hat{V}^2 B^2 \lambda}{\sqrt{1 - \lambda B}} \frac{R}{B_\varphi} \right\rangle_{\vartheta}^{p_\varphi} \left\langle \frac{1}{\mathcal{A}} \left(\frac{\partial S}{\partial \hat{p}_\varphi} \Big|_{\xi, \lambda} \right)^2 \right\rangle_{\xi}^S \frac{\partial^2 g_e^{(0,0)}}{\partial S^2} \Big|_{\lambda, \xi} + \\
& + \left[\left\langle \sigma \lambda \sqrt{1 - \lambda B} \frac{R}{B_\varphi} \right\rangle_{\vartheta}^{p_\varphi} \left(\left\langle \frac{1}{\mathcal{A}} \frac{\partial}{\partial \lambda} \Big|_{S, \xi} \left(\frac{\partial S}{\partial \lambda} \Big|_{\hat{p}_\varphi, \xi} \right) \right\rangle_{\xi}^S + \left\langle \frac{1}{\mathcal{A}} \frac{\partial S}{\partial \lambda} \Big|_{\hat{p}_\varphi, \xi} \frac{\partial}{\partial S} \Big|_{\lambda, \xi} \left(\frac{\partial S}{\partial \lambda} \Big|_{\hat{p}_\varphi, \xi} \right) \right\rangle_{\xi}^S \right) + \\
& + \left\langle \sigma \frac{2 - 3\lambda B}{2\sqrt{1 - \lambda B}} \frac{R}{B_\varphi} \right\rangle_{\vartheta}^{p_\varphi} \left\langle \frac{1}{\mathcal{A}} \frac{\partial S}{\partial \lambda} \Big|_{\hat{p}_\varphi, \xi} \right\rangle_{\xi}^S + \\
& + \left\langle \sigma \frac{\hat{\rho}_{\vartheta j}^2}{4} \frac{\hat{V}^2 B^2 \lambda}{\sqrt{1 - \lambda B}} \frac{R}{B_\varphi} \right\rangle_{\vartheta}^{p_\varphi} \left\langle \frac{1}{\mathcal{A}} \frac{\partial S}{\partial \hat{p}_\varphi} \Big|_{\xi, \lambda} \frac{\partial}{\partial S} \Big|_{\lambda, \xi} \left(\frac{\partial S}{\partial \hat{p}_\varphi} \Big|_{\xi, \lambda} \right) \right\rangle_{\xi}^S + \\
& + \frac{1}{2} \left\langle \hat{\rho}_{\vartheta j} \hat{V} R \lambda \right\rangle_{\vartheta}^{p_\varphi} \left\langle \frac{1}{\mathcal{A}} \frac{\partial}{\partial \lambda} \Big|_{S, \xi} \left(\frac{\partial S}{\partial \hat{p}_\varphi} \Big|_{\xi, \lambda} \right) \right\rangle_{\xi}^S + \frac{1}{2} \left\langle \hat{\rho}_{\vartheta j} \hat{V} R \lambda \right\rangle_{\vartheta}^{p_\varphi} \left\langle \frac{1}{\mathcal{A}} \frac{\partial S}{\partial \lambda} \Big|_{\hat{p}_\varphi} \frac{\partial}{\partial S} \Big|_{\lambda, \xi} \left(\frac{\partial S}{\partial \hat{p}_\varphi} \Big|_{\xi, \lambda} \right) \right\rangle_{\xi}^S + \\
& + \frac{1}{2} \left\langle \hat{\rho}_{\vartheta j} \hat{V} R \lambda \right\rangle_{\vartheta}^{p_\varphi} \left\langle \frac{1}{\mathcal{A}} \frac{\partial S}{\partial \hat{p}_\varphi} \Big|_{\xi, \lambda} \frac{\partial}{\partial S} \Big|_{\lambda, \xi} \left(\frac{\partial S}{\partial \lambda} \Big|_{\hat{p}_\varphi} \right) \right\rangle_{\xi}^S + \left\langle \frac{\hat{\rho}_{\vartheta j}}{2} \hat{V} R \right\rangle_{\vartheta}^{p_\varphi} \left\langle \frac{1}{\mathcal{A}} \frac{\partial S}{\partial \hat{p}_\varphi} \Big|_{\xi, \lambda} \right\rangle_{\xi}^S \frac{\partial g_e^{(0,0)}}{\partial S} \Big|_{\lambda, \xi} + \\
& + \left[2 \left\langle \sigma \lambda \sqrt{1 - \lambda B} \frac{R}{B_\varphi} \right\rangle_{\vartheta}^{p_\varphi} \left\langle \frac{1}{\mathcal{A}} \frac{\partial S}{\partial \lambda} \Big|_{\hat{p}_\varphi, \xi} \right\rangle_{\xi}^S + \left\langle \hat{\rho}_{\vartheta j} \hat{V} R \lambda \right\rangle_{\vartheta}^{p_\varphi} \left\langle \frac{1}{\mathcal{A}} \frac{\partial S}{\partial \hat{p}_\varphi} \Big|_{\xi, \lambda} \right\rangle_{\xi}^S \right] \frac{\partial^2 g_e^{(0,0)}}{\partial \lambda \partial S} \Big|_{\xi} + \\
& + \frac{\hat{V}_e}{2} \left\langle \frac{1}{\mathcal{A}} \bar{U}_{\parallel e}(g_e^{(0,0)}) \right\rangle_{\xi}^S + \frac{\hat{V}_e}{2} \left\langle \frac{1}{\mathcal{A}} U_{\parallel ei}(g_i^{(0,0)}) \right\rangle_{\xi}^S = 0
\end{aligned} \tag{D.61}$$

with $\bar{U}_{\parallel e}(g_e^{(0,0)}) = \frac{3}{2} e^{-\hat{V}_e^2} \frac{\hat{v}_{ee}}{\hat{v}_{ee} + \hat{v}_{ei}} \left\langle B_0^2 \frac{R}{B_\varphi} \sum_{\sigma} \sigma \int_{\mathbb{R}^+} d\hat{V}_e \int_0^{B^{-1}} g_e^{(0,0)} d\lambda \right\rangle_{\vartheta}^{p_\varphi}$ and $U_{\parallel ei}(g_i^{(0,0)}) = \frac{2}{\pi^{1/2}} e^{-\hat{V}_e^2} \left(\frac{m_e}{m_i} \right)^2 \frac{\hat{v}_{ei}}{\hat{v}_{ee} + \hat{v}_{ei}} \left\langle \frac{R}{B_\varphi} B_0^2 \sum_{\sigma} \sigma \int_{\mathbb{R}^+} d\hat{V}_i \hat{V}_i^3 \int_0^{B^{-1}} g_i^{(0,0)} d\lambda \right\rangle_{\vartheta}^{p_\varphi}$. Here we have taken into account that $g_e^{(0,0)}$ does not have the helical angle dependence. As \hat{v}_{ee} and \hat{v}_{ei} have the velocity dependence only, they have been pulled through the ξ -averaging operator at fixed S . Eq.D.61 is the final equation to be solved for the electrons in the external regions where collisions can be treated perturbatively. We have to note that the integral terms in Eqs.D.60,D.61 average to zero over ϑ at fixed p_φ (but not ψ) for trapped particles due

to the summation over σ in the orbit averaging operator. Eqs.D.60,D.61 are final ϑ -, ξ -averaged equations for ions/electrons to $\mathcal{O}(\Delta^1 \delta_j^1)$ in a large aspect ratio circular cross section tokamak. The solution technique is the subject of Chapter IV and the following sections of this appendix.

D.7.1 Direct switch from ψ to \mathcal{S}

The explicit representation of the final reduced drift kinetic equation equivalent to Eqs.D.60,D.61 can be obtained by switching directly from ψ to \mathcal{S} in the collision operator. Since \mathcal{S} is not a function of ϑ at fixed \hat{p}_φ , $\partial^k/\partial\lambda^k|_{\mathcal{S},\xi,\vartheta}$ and $\partial^k/\partial\mathcal{S}^k|_{\lambda,\xi,\vartheta}$ ($k = 1, 2$) are commutative with $\langle \dots \rangle_{\vartheta}^{p_\varphi}$, and hence

$$\begin{aligned}
& \left\langle \sigma \lambda \sqrt{1 - \lambda B} \frac{R}{B_\varphi} \right\rangle_{\vartheta}^{p_\varphi} \left\langle \frac{1}{\mathcal{A}} \right\rangle_{\xi}^{\mathcal{S}} \frac{\partial^2 g_i^{(0,0)}}{\partial \lambda^2} \Big|_{\mathcal{S},\xi,\vartheta,\hat{V};\sigma} + \left\langle \sigma \frac{2 - 3\lambda B}{2\sqrt{1 - \lambda B}} \frac{R}{B_\varphi} \right\rangle_{\vartheta}^{p_\varphi} \left\langle \frac{1}{\mathcal{A}} \right\rangle_{\xi}^{\mathcal{S}} \frac{\partial g_i^{(0,0)}}{\partial \lambda} \Big|_{\mathcal{S},\xi,\vartheta,\hat{V};\sigma} + \\
& + \left\langle \left\langle \sigma \lambda \sqrt{1 - \lambda B} \frac{R}{B_\varphi} \left(\frac{\partial \mathcal{S}}{\partial \lambda} \Big|_{\psi} \right)^2 \right\rangle_{\vartheta}^{p_\varphi} \frac{1}{\mathcal{A}} \right\rangle_{\xi}^{\mathcal{S}} \frac{\partial^2 g_i^{(0,0)}}{\partial \mathcal{S}^2} \Big|_{\lambda,\xi,\vartheta,\hat{V};\sigma} + \\
& + \left\langle \left\langle \sigma \frac{2 - 3\lambda B}{2\sqrt{1 - \lambda B}} \frac{R}{B_\varphi} \frac{\partial \mathcal{S}}{\partial \lambda} \Big|_{\psi} + \sigma \lambda \sqrt{1 - \lambda B} \frac{R}{B_\varphi} \frac{\partial}{\partial \lambda} \Big|_{\mathcal{S}} \left(\frac{\partial \mathcal{S}}{\partial \lambda} \Big|_{\psi} \right) \right\rangle_{\vartheta} \right. \\
& + \left. \sigma \lambda \sqrt{1 - \lambda B} \frac{R}{B_\varphi} \frac{\partial \mathcal{S}}{\partial \lambda} \Big|_{\psi} \frac{\partial}{\partial \mathcal{S}} \Big|_{\lambda} \left(\frac{\partial \mathcal{S}}{\partial \lambda} \Big|_{\psi} \right) \right\rangle_{\vartheta}^{p_\varphi} \frac{1}{\mathcal{A}} \right\rangle_{\xi}^{\mathcal{S}} \frac{\partial g_i^{(0,0)}}{\partial \mathcal{S}} \Big|_{\lambda,\xi,\vartheta,\hat{V};\sigma} + \\
& + \left\langle \left\langle 2\sigma \lambda \sqrt{1 - \lambda B} \frac{R}{B_\varphi} \frac{\partial \mathcal{S}}{\partial \lambda} \Big|_{\psi} \right\rangle_{\vartheta}^{p_\varphi} \frac{1}{\mathcal{A}} \right\rangle_{\xi}^{\mathcal{S}} \frac{\partial^2 g_i^{(0,0)}}{\partial \lambda \partial \mathcal{S}} \Big|_{\xi,\vartheta,\hat{V};\sigma} + \frac{\hat{V}}{2} \left\langle \frac{1}{\mathcal{A}} \bar{U}_{\parallel i} \left(g_i^{(0,0)} \right) \right\rangle_{\xi}^{\mathcal{S}} = 0
\end{aligned} \tag{D.62}$$

for ions. For electrons, the last term is to be replaced with

$$\frac{\hat{V}_e}{2} \left\langle \frac{1}{\mathcal{A}} \bar{U}_{\parallel e} \left(g_e^{(0,0)} \right) \right\rangle_{\xi}^{\mathcal{S}} + \frac{\hat{V}_e}{2} \left\langle \frac{1}{\mathcal{A}} U_{\parallel ei} \left(g_i^{(0,0)} \right) \right\rangle_{\xi}^{\mathcal{S}}.$$

$\bar{U}_{\parallel i}$, $\bar{U}_{\parallel e}$ and $U_{\parallel ei}$ are defined as in Eqs.D.60,D.61. As $\partial/\partial\lambda|_{\psi}$ and $\langle \dots \rangle_{\vartheta}^{p_\varphi}$ are not commutative,¹⁰³ to solve the drift kinetic equation in a form Eq.D.62 is computationally more expensive than Eqs.D.60,D.61, where ϑ - and ξ -averages are factorised. Thus, the representation Eqs.D.60,D.61 is considered below. It can be proved mathematically

¹⁰³Here a function of $\hat{p}_\varphi, \vartheta, \xi, \lambda$ has to be averaged over ϑ , while in Eqs.D.60,D.61 a function of ϑ, λ only is to be averaged over ϑ holding \hat{p}_φ fixed.

that coefficients in Eq.D.62 can be rewritten in a form given in Eqs.D.60,D.61. These derivations are routine and left beyond the scope of this work. The numerical scheme described in Chapter IV and in Appendix E could also be applied to solve Eq.D.62.

E Numerical scheme

E.1 B coefficients

The following functions are defined:

$$\begin{aligned}
 a(\lambda) &= \left\langle \sigma \lambda \sqrt{1 - \lambda B} \frac{R}{B_\varphi} \right\rangle_{\vartheta}^{p_\varphi}, \\
 b(\lambda) &= \left\langle \sigma \frac{2 - 3\lambda B}{2\sqrt{1 - \lambda B}} \frac{R}{B_\varphi} \right\rangle_{\vartheta}^{p_\varphi}, \\
 f(\lambda) &= \left\langle \sigma \frac{\hat{\rho}_{\vartheta j}^2}{4} \frac{\hat{V}^2 B^2 \lambda}{\sqrt{1 - \lambda B}} \frac{R}{B_\varphi} \right\rangle_{\vartheta}^{p_\varphi}, \\
 g(\lambda) &= \left\langle \hat{\rho}_{\vartheta j} \hat{V} R \lambda \right\rangle_{\vartheta}^{p_\varphi}, \quad h = \left\langle \frac{\hat{\rho}_{\vartheta j}}{2} \hat{V} R \right\rangle_{\vartheta}^{p_\varphi}, \quad \mathcal{A}^{-1} = \bar{\mathcal{A}}.
 \end{aligned}$$

$\{i, j, k, m, n\}$ ($\forall i, j, k, m, n \in \mathbb{Z}$) are used to enumerate $\{S, \lambda, \sigma, \xi, \vartheta\}$, respectively. The following B coefficients are introduced:

$$\begin{aligned}
 {}^{ijk}B_1 &= \left\langle \sigma \lambda \sqrt{1 - \lambda B} \frac{R}{B_\varphi} \right\rangle_{\vartheta}^{p_\varphi} \left\langle \frac{1}{\mathcal{A}} \right\rangle_{\xi}^S = a(\lambda) \left\langle \frac{1}{\mathcal{A}} \right\rangle_{\xi}^S, \\
 {}^{ijk}B_2 &= \left\langle \sigma \frac{2 - 3\lambda B}{2\sqrt{1 - \lambda B}} \frac{R}{B_\varphi} \right\rangle_{\vartheta}^{p_\varphi} \left\langle \frac{1}{\mathcal{A}} \right\rangle_{\xi}^S = b(\lambda) \left\langle \frac{1}{\mathcal{A}} \right\rangle_{\xi}^S, \\
 {}^{ijk}B_3 &= \left\langle \sigma \lambda \sqrt{1 - \lambda B} \frac{R}{B_\varphi} \right\rangle_{\vartheta}^{p_\varphi} \left\langle \frac{1}{\mathcal{A}} \left(\frac{\partial S}{\partial \lambda} \Big|_{\hat{p}_\varphi, \xi} \right)^2 \right\rangle_{\xi}^S + \left\langle \hat{\rho}_{\vartheta j} \hat{V} R \lambda \right\rangle_{\vartheta}^{p_\varphi} \left\langle \frac{1}{\mathcal{A}} \frac{\partial S}{\partial \lambda} \Big|_{\hat{p}_\varphi, \xi} \frac{\partial S}{\partial \hat{p}_\varphi} \Big|_{\xi, \lambda} \right\rangle_{\xi}^S + \\
 &+ \left\langle \sigma \frac{\hat{\rho}_{\vartheta j}^2}{4} \frac{\hat{V}^2 B^2 \lambda}{\sqrt{1 - \lambda B}} \frac{R}{B_\varphi} \right\rangle_{\vartheta}^{p_\varphi} \left\langle \frac{1}{\mathcal{A}} \left(\frac{\partial S}{\partial \hat{p}_\varphi} \Big|_{\xi, \lambda} \right)^2 \right\rangle_{\xi}^S = \\
 &= a(\lambda) \left\langle \frac{1}{\mathcal{A}} \left(\frac{\partial S}{\partial \lambda} \Big|_{\hat{p}_\varphi, \xi} \right)^2 \right\rangle_{\xi}^S + g(\lambda) \left\langle \frac{1}{\mathcal{A}} \frac{\partial S}{\partial \lambda} \Big|_{\hat{p}_\varphi, \xi} \frac{\partial S}{\partial \hat{p}_\varphi} \Big|_{\xi, \lambda} \right\rangle_{\xi}^S + f(\lambda) \left\langle \frac{1}{\mathcal{A}} \left(\frac{\partial S}{\partial \hat{p}_\varphi} \Big|_{\xi, \lambda} \right)^2 \right\rangle_{\xi}^S, \\
 {}^{ijk}B_4 &= \left\langle \sigma \lambda \sqrt{1 - \lambda B} \frac{R}{B_\varphi} \right\rangle_{\vartheta}^{p_\varphi} \left\langle \frac{1}{\mathcal{A}} \frac{\partial}{\partial \lambda} \Big|_{S, \xi} \left(\frac{\partial S}{\partial \lambda} \Big|_{\hat{p}_\varphi, \xi} \right) \right\rangle_{\xi}^S = a(\lambda) \left\langle \frac{1}{\mathcal{A}} \frac{\partial}{\partial \lambda} \Big|_{S, \xi} \left(\frac{\partial S}{\partial \lambda} \Big|_{\hat{p}_\varphi, \xi} \right) \right\rangle_{\xi}^S, \\
 {}^{ijk}B_5 &= \left\langle \sigma \lambda \sqrt{1 - \lambda B} \frac{R}{B_\varphi} \right\rangle_{\vartheta}^{p_\varphi} \left\langle \frac{1}{\mathcal{A}} \frac{\partial S}{\partial \lambda} \Big|_{\hat{p}_\varphi, \xi} \frac{\partial}{\partial S} \Big|_{\lambda, \xi} \left(\frac{\partial S}{\partial \lambda} \Big|_{\hat{p}_\varphi, \xi} \right) \right\rangle_{\xi}^S = \\
 &= a(\lambda) \left\langle \frac{1}{\mathcal{A}} \frac{\partial S}{\partial \lambda} \Big|_{\hat{p}_\varphi, \xi} \frac{\partial}{\partial S} \Big|_{\lambda, \xi} \left(\frac{\partial S}{\partial \lambda} \Big|_{\hat{p}_\varphi, \xi} \right) \right\rangle_{\xi}^S,
 \end{aligned}$$

$$\begin{aligned}
{}^{ijk}B_6 &= \left\langle \sigma \frac{2-3\lambda B}{2\sqrt{1-\lambda B}} \frac{R}{B_\varphi} \right\rangle_\vartheta^{p_\varphi} \left\langle \frac{1}{\mathcal{A}} \frac{\partial S}{\partial \lambda} \Big|_{\hat{p}_\varphi, \xi} \right\rangle_\xi^S = b(\lambda) \left\langle \frac{1}{\mathcal{A}} \frac{\partial S}{\partial \lambda} \Big|_{\hat{p}_\varphi, \xi} \right\rangle_\xi^S, \\
{}^{ijk}B_7 &= \left\langle \sigma \frac{\hat{\rho}_{\vartheta j}^2}{4} \frac{\hat{V}^2 B^2 \lambda}{\sqrt{1-\lambda B}} \frac{R}{B_\varphi} \right\rangle_\vartheta^{p_\varphi} \left\langle \frac{1}{\mathcal{A}} \frac{\partial S}{\partial \hat{p}_\varphi} \Big|_{\xi, \lambda} \frac{\partial}{\partial S} \Big|_{\lambda, \xi} \left(\frac{\partial S}{\partial \hat{p}_\varphi} \Big|_{\xi, \lambda} \right) \right\rangle_\xi^S = \\
&= f(\lambda) \left\langle \frac{1}{\mathcal{A}} \frac{\partial S}{\partial \hat{p}_\varphi} \Big|_{\xi, \lambda} \frac{\partial}{\partial S} \Big|_{\lambda, \xi} \left(\frac{\partial S}{\partial \hat{p}_\varphi} \Big|_{\xi, \lambda} \right) \right\rangle_\xi^S, \\
{}^{ijk}B_8 &= \left\langle \frac{\hat{\rho}_{\vartheta j} \hat{V} R}{2} \right\rangle_\vartheta^{p_\varphi} \left\langle \frac{1}{\mathcal{A}} \frac{\partial S}{\partial \hat{p}_\varphi} \Big|_{\xi, \lambda} \right\rangle_\xi^S = h \left\langle \frac{1}{\mathcal{A}} \frac{\partial S}{\partial \hat{p}_\varphi} \Big|_{\xi, \lambda} \right\rangle_\xi^S, \\
{}^{ijk}B_9 &= \frac{1}{2} \left\langle \hat{\rho}_{\vartheta j} \hat{V} R \lambda \right\rangle_\vartheta^{p_\varphi} \left\langle \frac{1}{\mathcal{A}} \frac{\partial}{\partial \lambda} \Big|_{S, \xi} \left(\frac{\partial S}{\partial \hat{p}_\varphi} \Big|_{\xi, \lambda} \right) \right\rangle_\xi^S = \frac{1}{2} g(\lambda) \left\langle \frac{1}{\mathcal{A}} \frac{\partial}{\partial \lambda} \Big|_{S, \xi} \left(\frac{\partial S}{\partial \hat{p}_\varphi} \Big|_{\xi, \lambda} \right) \right\rangle_\xi^S, \\
{}^{ijk}B_{10} &= \frac{1}{2} \left\langle \hat{\rho}_{\vartheta j} \hat{V} R \lambda \right\rangle_\vartheta^{p_\varphi} \left\langle \frac{1}{\mathcal{A}} \frac{\partial S}{\partial \lambda} \Big|_{\hat{p}_\varphi} \frac{\partial}{\partial S} \Big|_{\lambda, \xi} \left(\frac{\partial S}{\partial \hat{p}_\varphi} \Big|_{\xi, \lambda} \right) \right\rangle_\xi^S = \\
&= \frac{1}{2} g(\lambda) \left\langle \frac{1}{\mathcal{A}} \frac{\partial S}{\partial \lambda} \Big|_{\hat{p}_\varphi} \frac{\partial}{\partial S} \Big|_{\lambda, \xi} \left(\frac{\partial S}{\partial \hat{p}_\varphi} \Big|_{\xi, \lambda} \right) \right\rangle_\xi^S, \\
{}^{ijk}B_{11} &= \frac{1}{2} \left\langle \hat{\rho}_{\vartheta j} \hat{V} R \lambda \right\rangle_\vartheta^{p_\varphi} \left\langle \frac{1}{\mathcal{A}} \frac{\partial S}{\partial \hat{p}_\varphi} \Big|_{\xi, \lambda} \frac{\partial}{\partial S} \Big|_{\lambda, \xi} \left(\frac{\partial S}{\partial \lambda} \Big|_{\hat{p}_\varphi} \right) \right\rangle_\xi^S = \\
&= \frac{1}{2} g(\lambda) \left\langle \frac{1}{\mathcal{A}} \frac{\partial S}{\partial \hat{p}_\varphi} \Big|_{\xi, \lambda} \frac{\partial}{\partial S} \Big|_{\lambda, \xi} \left(\frac{\partial S}{\partial \lambda} \Big|_{\hat{p}_\varphi} \right) \right\rangle_\xi^S, \\
{}^{ijk}B_{12} &= 2 \left\langle \sigma \lambda \sqrt{1-\lambda B} \frac{R}{B_\varphi} \right\rangle_\vartheta^{p_\varphi} \left\langle \frac{1}{\mathcal{A}} \frac{\partial S}{\partial \lambda} \Big|_{\hat{p}_\varphi, \xi} \right\rangle_\xi^S + \left\langle \hat{\rho}_{\vartheta j} \hat{V} R \lambda \right\rangle_\vartheta^{p_\varphi} \left\langle \frac{1}{\mathcal{A}} \frac{\partial S}{\partial \hat{p}_\varphi} \Big|_{\xi, \lambda} \right\rangle_\xi^S = \\
&= 2a(\lambda) \left\langle \frac{1}{\mathcal{A}} \frac{\partial S}{\partial \lambda} \Big|_{\hat{p}_\varphi, \xi} \right\rangle_\xi^S + g(\lambda) \left\langle \frac{1}{\mathcal{A}} \frac{\partial S}{\partial \hat{p}_\varphi} \Big|_{\xi, \lambda} \right\rangle_\xi^S, \\
{}^{ijk}B_{13} &= U,
\end{aligned}$$

where

$$U = \frac{\hat{V}}{2} \left\langle \frac{1}{\mathcal{A}} \bar{U}_{||i}(g_i^{(0,0)}) \right\rangle_\xi^S$$

for ions and

$$U = \frac{\hat{V}_e}{2} \left\langle \frac{1}{\mathcal{A}} \bar{U}_{\parallel e}(g_e^{(0,0)}) \right\rangle_{\xi}^S + \frac{\hat{V}_e}{2} \left\langle \frac{1}{\mathcal{A}} U_{\parallel ei}(g_i^{(0,0)}) \right\rangle_{\xi}^S$$

for electrons. Then Eqs.D.60,D.61 read

$$\begin{aligned} & B_1 \frac{\partial^2 g}{\partial \lambda^2} \Big|_{S,\xi} + B_2 \frac{\partial g}{\partial \lambda} \Big|_{S,\xi} + B_3 \frac{\partial^2 g}{\partial S^2} \Big|_{\lambda,\xi} + \\ & + \sum_{i=4}^{11} B_i \frac{\partial g}{\partial S} \Big|_{\lambda,\xi} + B_{12} \frac{\partial^2 g}{\partial \lambda \partial S} \Big|_{\xi} + U = 0 \end{aligned} \quad (\text{E.1})$$

with $g = g_{i,c}^{(0,0)}$. Let us consider the passing branch first. Taking into account Eq.2.37 (note: S is ϑ -independent at any fixed \hat{p}_φ), we write

$$\begin{aligned} \frac{\partial S^p}{\partial \lambda} \Big|_{\hat{p}_\varphi,\xi} &= -\hat{\rho}_{\vartheta j} \left(\hat{p}_\varphi - \frac{\hat{\omega}_D \hat{\rho}_{\vartheta j} \hat{L}_q}{\hat{w}} \right) \frac{\partial \hat{\omega}_D}{\partial \lambda} \Big|_{\hat{p}_\varphi,\xi} - \frac{1}{2} \frac{\partial}{\partial \lambda} \Big|_{\hat{p}_\varphi,\xi} \left\langle \frac{\hat{\rho}_{\vartheta j} \hat{\Phi}}{\hat{V}_{\parallel}} \right\rangle_{\vartheta}^{p_\varphi} = \\ &= -\hat{\rho}_{\vartheta j} \left(\hat{p}_\varphi - \frac{\hat{\omega}_D \hat{\rho}_{\vartheta j} \hat{L}_q}{\hat{w}} \right) \frac{\partial \hat{\omega}_D}{\partial \lambda} \Big|_{\hat{p}_\varphi,\xi} - \\ &- \frac{1}{2} \frac{\partial}{\partial \lambda} \Big|_{\hat{p}_\varphi,\xi} \left\langle \frac{\hat{\rho}_{\vartheta j} \hat{\Phi}}{\hat{V}_{\parallel}} \left(\hat{p}_\varphi + \hat{\rho}_{\vartheta j} \hat{V}_{\parallel}, \xi, \vartheta \right) \right\rangle_{\vartheta}^{p_\varphi} \left[\hat{p}_\varphi \left(S, \xi, \lambda, \hat{V}; \sigma \right), \xi, \lambda, \hat{V}; \sigma \right]. \end{aligned}$$

Here we have taken into account that the electrostatic potential is a function of spatial variables only, i.e. $\{\psi, \xi, \vartheta\}$ or $\hat{\Phi} = \hat{\Phi}(x, \xi, \vartheta)$.

$$\begin{aligned} \frac{\partial S^p}{\partial \hat{p}_\varphi} \Big|_{\lambda,\xi,\vartheta} &= \frac{\hat{w}}{\hat{L}_q} \left(\hat{p}_\varphi - \frac{\hat{\omega}_D \hat{\rho}_{\vartheta j} \hat{L}_q}{\hat{w}} \right) - \frac{1}{2} \frac{\partial}{\partial \hat{p}_\varphi} \Big|_{\lambda,\xi,\vartheta} \left\langle \frac{\hat{\rho}_{\vartheta j} \hat{\Phi}}{\hat{V}_{\parallel}} \right\rangle_{\vartheta}^{p_\varphi} = \\ &= \frac{\hat{w}}{\hat{L}_q} \left(\hat{p}_\varphi - \frac{\hat{\omega}_D \hat{\rho}_{\vartheta j} \hat{L}_q}{\hat{w}} \right) - \frac{1}{2} \left\langle \frac{\hat{\rho}_{\vartheta j}}{\hat{V}_{\parallel}} \frac{\partial \hat{\Phi} \left(\hat{p}_\varphi + \hat{\rho}_{\vartheta j} \hat{V}_{\parallel}, \xi, \vartheta \right)}{\partial \hat{p}_\varphi} \right\rangle_{\lambda,\xi,\vartheta}^{p_\varphi}. \end{aligned}$$

Thus, we have

$$\begin{aligned} \frac{\partial}{\partial \lambda} \Big|_{S,\xi} \left(\frac{\partial S^p}{\partial \lambda} \Big|_{\hat{p}_\varphi,\xi} \right) &= \frac{\partial}{\partial \lambda} \Big|_{S,\xi} \left[-\hat{\rho}_{\vartheta j} \left(\hat{p}_\varphi - \frac{\hat{\omega}_D \hat{\rho}_{\vartheta j} \hat{L}_q}{\hat{w}} \right) \frac{\partial \hat{\omega}_D}{\partial \lambda} \Big|_{\hat{p}_\varphi,\xi} - \frac{1}{2} \frac{\partial}{\partial \lambda} \Big|_{\hat{p}_\varphi,\xi} \left\langle \frac{\hat{\rho}_{\vartheta j} \hat{\Phi}}{\hat{V}_{\parallel}} \right\rangle_{\vartheta}^{p_\varphi} \right] = \\ &= -\hat{\rho}_{\vartheta j} \left(\frac{\partial \hat{p}_\varphi}{\partial \lambda} \Big|_{S,\xi} - \frac{\partial \hat{\omega}_D}{\partial \lambda} \Big|_{S,\xi} \frac{\hat{\rho}_{\vartheta j} \hat{L}_q}{\hat{w}} \right) \frac{\partial \hat{\omega}_D}{\partial \lambda} \Big|_{\hat{p}_\varphi,\xi} - \hat{\rho}_{\vartheta j} \left(\hat{p}_\varphi - \frac{\hat{\omega}_D \hat{\rho}_{\vartheta j} \hat{L}_q}{\hat{w}} \right) \frac{\partial}{\partial \lambda} \Big|_{S,\xi} \frac{\partial \hat{\omega}_D}{\partial \lambda} \Big|_{\hat{p}_\varphi,\xi} - \\ &- \frac{1}{2} \frac{\partial}{\partial \lambda} \Big|_{S,\xi} \left\{ \frac{\partial}{\partial \lambda} \Big|_{\hat{p}_\varphi,\xi} \left\langle \frac{\hat{\rho}_{\vartheta j} \hat{\Phi}}{\hat{V}_{\parallel}} \left(\hat{p}_\varphi + \hat{\rho}_{\vartheta j} \hat{V}_{\parallel}, \xi, \vartheta \right) \right\rangle_{\vartheta}^{p_\varphi} \left[\hat{p}_\varphi \left(S, \xi, \lambda, \hat{V}; \sigma \right), \xi, \lambda, \hat{V}; \sigma \right] \right\} = \end{aligned}$$

$$\begin{aligned}
&= -\hat{\rho}_{\vartheta j} \left(\frac{\partial \hat{p}_\varphi}{\partial \lambda} \Big|_{S, \xi} - \frac{\partial \hat{\omega}_D}{\partial \lambda} \Big|_{\psi, \xi} \frac{\hat{\rho}_{\vartheta j} \hat{L}_q}{\hat{w}} \right) \frac{\partial \hat{\omega}_D}{\partial \lambda} \Big|_{\psi, \xi} - \hat{\rho}_{\vartheta j} \left(\hat{p}_\varphi - \frac{\hat{\omega}_D \hat{\rho}_{\vartheta j} \hat{L}_q}{\hat{w}} \right) \frac{\partial^2 \hat{\omega}_D}{\partial \lambda^2} \Big|_{\psi, \xi} - \\
&- \frac{1}{2} \frac{\partial}{\partial \lambda} \Big|_{S, \xi} \frac{\partial}{\partial \lambda} \Big|_{\hat{p}_\varphi, \xi} \left\langle \frac{\hat{\rho}_{\vartheta j} \hat{\Phi}}{\hat{V}_\parallel} \right\rangle_{\vartheta}^{p_\varphi},
\end{aligned}$$

where we have taken into account that \hat{p}_φ is a function of λ if written in terms of S and the fact that $\hat{\omega}_D$ has the velocity dependence only, i.e. is a function of λ at each \hat{V} and σ .

$$\begin{aligned}
\frac{\partial}{\partial S} \Big|_{\lambda, \xi} \left(\frac{\partial S^p}{\partial \lambda} \Big|_{\hat{p}_\varphi, \xi} \right) &= \frac{\partial}{\partial S} \Big|_{\lambda, \xi} \left[-\hat{\rho}_{\vartheta j} \left(\hat{p}_\varphi - \frac{\hat{\omega}_D \hat{\rho}_{\vartheta j} \hat{L}_q}{\hat{w}} \right) \frac{\partial \hat{\omega}_D}{\partial \lambda} \Big|_{\hat{p}_\varphi, \xi} - \frac{1}{2} \frac{\partial}{\partial \lambda} \Big|_{\hat{p}_\varphi, \xi} \left\langle \frac{\hat{\rho}_{\vartheta j} \hat{\Phi}}{\hat{V}_\parallel} \right\rangle_{\vartheta}^{p_\varphi} \right] = \\
&= -\hat{\rho}_{\vartheta j} \frac{\partial \hat{p}_\varphi}{\partial S} \Big|_{\lambda, \xi} \frac{\partial \hat{\omega}_D}{\partial \lambda} \Big|_{\hat{p}_\varphi, \xi} - \\
&- \frac{1}{2} \frac{\partial}{\partial S} \Big|_{\lambda, \xi} \left\{ \frac{\partial}{\partial \lambda} \Big|_{\hat{p}_\varphi, \xi} \left\langle \frac{\hat{\rho}_{\vartheta j} \hat{\Phi}}{\hat{V}_\parallel} \left(\hat{p}_\varphi + \hat{\rho}_{\vartheta j} \hat{V}_\parallel, \xi, \vartheta \right) \right\rangle_{\vartheta}^{p_\varphi} \left[\hat{p}_\varphi \left(S, \xi, \lambda, \hat{V}; \sigma \right), \xi, \lambda, \hat{V}; \sigma \right] \right\} = \\
&= -\hat{\rho}_{\vartheta j} \frac{\partial \hat{p}_\varphi}{\partial S} \Big|_{\lambda, \xi} \frac{\partial \hat{\omega}_D}{\partial \lambda} \Big|_{\hat{p}_\varphi, \xi} - \frac{1}{2} \frac{\partial}{\partial S} \Big|_{\lambda, \xi} \frac{\partial}{\partial \lambda} \Big|_{\hat{p}_\varphi, \xi} \left\langle \frac{\hat{\rho}_{\vartheta j} \hat{\Phi}}{\hat{V}_\parallel} \right\rangle_{\vartheta}^{p_\varphi}
\end{aligned}$$

Here \hat{p}_φ is to be understood as $\hat{p}_\varphi = \hat{p}_\varphi \left(S, \xi, \lambda, \hat{V}; \sigma \right)$.

$$\begin{aligned}
\frac{\partial}{\partial S} \Big|_{\lambda, \xi} \left(\frac{\partial S^p}{\partial \hat{p}_\varphi} \Big|_{\lambda, \xi, \vartheta} \right) &= \\
&= \frac{\partial}{\partial S} \Big|_{\lambda, \xi} \left[\frac{\hat{w}}{\hat{L}_q} \left(\hat{p}_\varphi - \frac{\hat{\omega}_D \hat{\rho}_{\vartheta j} \hat{L}_q}{\hat{w}} \right) - \frac{1}{2} \left\langle \frac{\hat{\rho}_{\vartheta j}}{\hat{V}_\parallel} \frac{\partial \hat{\Phi} \left(\hat{p}_\varphi + \hat{\rho}_{\vartheta j} \hat{V}_\parallel, \xi, \vartheta \right)}{\partial \hat{p}_\varphi} \Big|_{\lambda, \xi, \vartheta} \right\rangle_{\vartheta}^{p_\varphi} \right] = \\
&= \frac{\hat{w}}{\hat{L}_q} \frac{\partial \hat{p}_\varphi}{\partial S} \Big|_{\lambda, \xi} - \\
&- \frac{1}{2} \frac{\partial}{\partial S} \Big|_{\lambda, \xi} \left\{ \left\langle \frac{\hat{\rho}_{\vartheta j}}{\hat{V}_\parallel} \frac{\partial \hat{\Phi} \left(\hat{p}_\varphi + \hat{\rho}_{\vartheta j} \hat{V}_\parallel, \xi, \vartheta \right)}{\partial \hat{p}_\varphi} \Big|_{\lambda, \xi, \vartheta} \right\rangle_{\vartheta}^{p_\varphi} \left[\hat{p}_\varphi \left(S, \xi, \lambda, \hat{V}; \sigma \right), \xi, \lambda, \hat{V}; \sigma \right] \right\} = \\
&= \frac{\hat{w}}{\hat{L}_q} \frac{\partial \hat{p}_\varphi}{\partial S} \Big|_{\lambda, \xi} - \frac{1}{2} \frac{\partial}{\partial S} \Big|_{\lambda, \xi} \left\langle \frac{\hat{\rho}_{\vartheta j}}{\hat{V}_\parallel} \frac{\partial \hat{\Phi}}{\partial \hat{p}_\varphi} \Big|_{\lambda, \xi, \vartheta} \right\rangle_{\vartheta}^{p_\varphi}
\end{aligned}$$

and

$$\frac{\partial}{\partial \lambda} \Big|_{S, \xi} \left(\frac{\partial S^p}{\partial \hat{p}_\varphi} \Big|_{\lambda, \xi, \vartheta} \right) =$$

$$\begin{aligned}
&= \frac{\partial}{\partial \lambda} \Big|_{S, \xi} \left[\frac{\hat{w}}{\hat{L}_q} \left(\hat{p}_\varphi - \frac{\hat{\omega}_D \hat{\rho}_{\vartheta j} \hat{L}_q}{\hat{w}} \right) - \frac{1}{2} \left\langle \frac{\hat{\rho}_{\vartheta j}}{\hat{V}_\parallel} \frac{\partial \hat{\Phi}(\hat{p}_\varphi + \hat{\rho}_{\vartheta j} \hat{V}_\parallel, \xi, \vartheta)}{\partial \hat{p}_\varphi} \Big|_{\lambda, \xi, \vartheta} \right\rangle_{\vartheta}^{p_\varphi} \right] = \\
&= \frac{\hat{w}}{\hat{L}_q} \left(\frac{\partial \hat{p}_\varphi}{\partial \lambda} \Big|_{S, \xi} - \frac{\partial \hat{\omega}_D}{\partial \lambda} \Big|_{S, \xi} \frac{\hat{\rho}_{\vartheta j} \hat{L}_q}{\hat{w}} \right) - \\
&- \frac{1}{2} \frac{\partial}{\partial \lambda} \Big|_{S, \xi} \left\{ \left\langle \frac{\hat{\rho}_{\vartheta j}}{\hat{V}_\parallel} \frac{\partial \hat{\Phi}(\hat{p}_\varphi + \hat{\rho}_{\vartheta j} \hat{V}_\parallel, \xi, \vartheta)}{\partial \hat{p}_\varphi} \Big|_{\lambda, \xi, \vartheta} \right\rangle_{\vartheta}^{p_\varphi} \left[\hat{p}_\varphi(S, \xi, \lambda, \hat{V}; \sigma), \xi, \lambda, \hat{V}; \sigma \right] \right\} = \\
&= \frac{\hat{w}}{\hat{L}_q} \frac{\partial \hat{p}_\varphi}{\partial \lambda} \Big|_{S, \xi} - \hat{\rho}_{\vartheta j} \frac{\partial \hat{\omega}_D}{\partial \lambda} \Big|_{\psi, \xi} - \frac{1}{2} \frac{\partial}{\partial \lambda} \Big|_{S, \xi} \left\langle \frac{\hat{\rho}_{\vartheta j}}{\hat{V}_\parallel} \frac{\partial \hat{\Phi}}{\partial \hat{p}_\varphi} \Big|_{\lambda, \xi, \vartheta} \right\rangle_{\vartheta}^{p_\varphi}.
\end{aligned}$$

For trapped branch, we write

$$\begin{aligned}
\frac{\partial S^t}{\partial \lambda} \Big|_{\hat{p}_\varphi, \xi} &= \frac{\partial}{\partial \lambda} \Big|_{\hat{p}_\varphi, \xi} \left[-\hat{\omega}_D \hat{\rho}_{\vartheta j} \hat{p}_\varphi - \frac{1}{2} \left\langle \frac{\hat{\rho}_{\vartheta j}}{\hat{V}_\parallel} \hat{\Phi} \right\rangle_{\vartheta}^{p_\varphi} \right] = \\
&= -\hat{p}_\varphi \hat{\rho}_{\vartheta j} \frac{\partial \hat{\omega}_D}{\partial \lambda} \Big|_{\hat{p}_\varphi, \xi} - \frac{1}{2} \frac{\partial}{\partial \lambda} \Big|_{\hat{p}_\varphi, \xi} \left\langle \frac{\hat{\rho}_{\vartheta j}}{\hat{V}_\parallel} \hat{\Phi}(\hat{p}_\varphi + \hat{\rho}_{\vartheta j} \hat{V}_\parallel, \xi, \vartheta) \right\rangle_{\vartheta}^{p_\varphi},
\end{aligned}$$

$$\begin{aligned}
\frac{\partial S^t}{\partial \hat{p}_\varphi} \Big|_{\lambda, \xi, \vartheta} &= \frac{\partial}{\partial \hat{p}_\varphi} \Big|_{\lambda, \xi, \vartheta} \left[-\hat{\omega}_D \hat{\rho}_{\vartheta j} \hat{p}_\varphi - \frac{1}{2} \left\langle \frac{\hat{\rho}_{\vartheta j}}{\hat{V}_\parallel} \hat{\Phi} \right\rangle_{\vartheta}^{p_\varphi} \right] = \\
&= -\hat{\omega}_D \hat{\rho}_{\vartheta j} - \frac{1}{2} \left\langle \frac{\hat{\rho}_{\vartheta j}}{\hat{V}_\parallel} \frac{\partial}{\partial \hat{p}_\varphi} \Big|_{\lambda, \xi, \vartheta} \hat{\Phi}(\hat{p}_\varphi + \hat{\rho}_{\vartheta j} \hat{V}_\parallel, \xi, \vartheta) \right\rangle_{\vartheta}^{p_\varphi}.
\end{aligned}$$

The last term here is to be understood as a function of $(\hat{p}_\varphi(S, \xi, \lambda, \hat{V}; \sigma), \xi, \lambda, \hat{V}; \sigma)$.

$$\begin{aligned}
\frac{\partial}{\partial \lambda} \Big|_{S, \xi} \left(\frac{\partial S^t}{\partial \lambda} \Big|_{\hat{p}_\varphi, \xi} \right) &= \frac{\partial}{\partial \lambda} \Big|_{S, \xi} \left[-\hat{p}_\varphi \hat{\rho}_{\vartheta j} \frac{\partial \hat{\omega}_D}{\partial \lambda} \Big|_{\hat{p}_\varphi, \xi} - \frac{1}{2} \frac{\partial}{\partial \lambda} \Big|_{\hat{p}_\varphi, \xi} \left\langle \frac{\hat{\rho}_{\vartheta j}}{\hat{V}_\parallel} \hat{\Phi} \right\rangle_{\vartheta}^{p_\varphi} \right] = \\
&= -\hat{\rho}_{\vartheta j} \frac{\partial \hat{\omega}_D}{\partial \lambda} \Big|_{\hat{p}_\varphi, \xi} \frac{\partial \hat{p}_\varphi}{\partial \lambda} \Big|_{S, \xi} - \hat{\rho}_{\vartheta j} \frac{\partial^2 \hat{\omega}_D}{\partial \lambda^2} \Big|_{\psi, \xi} \hat{p}_\varphi - \\
&- \frac{1}{2} \frac{\partial}{\partial \lambda} \Big|_{S, \xi} \left\{ \frac{\partial}{\partial \lambda} \Big|_{\hat{p}_\varphi, \xi} \left\langle \frac{\hat{\rho}_{\vartheta j}}{\hat{V}_\parallel} \hat{\Phi}(\hat{p}_\varphi + \hat{\rho}_{\vartheta j} \hat{V}_\parallel, \xi, \vartheta) \right\rangle_{\vartheta}^{p_\varphi} \left[\hat{p}_\varphi(S, \xi, \lambda, \hat{V}; \sigma), \xi, \lambda, \hat{V}; \sigma \right] \right\} = \\
&= -\hat{\rho}_{\vartheta j} \frac{\partial \hat{\omega}_D}{\partial \lambda} \Big|_{\hat{p}_\varphi, \xi} \frac{\partial \hat{p}_\varphi}{\partial \lambda} \Big|_{S, \xi} - \hat{\rho}_{\vartheta j} \frac{\partial^2 \hat{\omega}_D}{\partial \lambda^2} \Big|_{\psi, \xi} \hat{p}_\varphi - \frac{1}{2} \frac{\partial}{\partial \lambda} \Big|_{S, \xi} \frac{\partial}{\partial \lambda} \Big|_{\hat{p}_\varphi, \xi} \left\langle \frac{\hat{\rho}_{\vartheta j}}{\hat{V}_\parallel} \hat{\Phi} \right\rangle_{\vartheta}^{p_\varphi},
\end{aligned}$$

$$\begin{aligned}
\frac{\partial}{\partial S} \Big|_{\lambda, \xi} \left(\frac{\partial S^t}{\partial \lambda} \Big|_{\hat{p}_\varphi, \xi} \right) &= \frac{\partial}{\partial S} \Big|_{\lambda, \xi} \left[-\hat{p}_\varphi \hat{\rho}_{\vartheta j} \frac{\partial \hat{\omega}_D}{\partial \lambda} \Big|_{\hat{p}_\varphi, \xi} - \frac{1}{2} \frac{\partial}{\partial \lambda} \Big|_{\hat{p}_\varphi, \xi} \left\langle \frac{\hat{\rho}_{\vartheta j}}{\hat{V}_\parallel} \hat{\Phi} \right\rangle_{\vartheta}^{p_\varphi} \right] = \\
&= -\hat{\rho}_{\vartheta j} \frac{\partial \hat{\omega}_D}{\partial \lambda} \Big|_{\hat{p}_\varphi, \xi} - \frac{\partial \hat{p}_\varphi}{\partial S} \Big|_{\lambda, \xi} - \\
&- \frac{1}{2} \frac{\partial}{\partial S} \Big|_{\lambda, \xi} \left\{ \frac{\partial}{\partial \lambda} \Big|_{\hat{p}_\varphi, \xi} \left\langle \frac{\hat{\rho}_{\vartheta j}}{\hat{V}_\parallel} \hat{\Phi} \left(\hat{p}_\varphi + \hat{\rho}_{\vartheta j} \hat{V}_\parallel, \xi, \vartheta \right) \right\rangle_{\vartheta}^{p_\varphi} \left[\hat{p}_\varphi \left(S, \xi, \lambda, \hat{V}; \sigma \right), \xi, \lambda, \hat{V}; \sigma \right] \right\} = \\
&= -\hat{\rho}_{\vartheta j} \frac{\partial \hat{\omega}_D}{\partial \lambda} \Big|_{\hat{p}_\varphi, \xi} - \frac{\partial \hat{p}_\varphi}{\partial S} \Big|_{\lambda, \xi} - \frac{1}{2} \frac{\partial}{\partial S} \Big|_{\lambda, \xi} \frac{\partial}{\partial \lambda} \Big|_{\hat{p}_\varphi, \xi} \left\langle \frac{\hat{\rho}_{\vartheta j}}{\hat{V}_\parallel} \hat{\Phi} \right\rangle_{\vartheta}^{p_\varphi}.
\end{aligned}$$

$$\begin{aligned}
\frac{\partial}{\partial S} \Big|_{\lambda, \xi} \left(\frac{\partial S^t}{\partial \hat{p}_\varphi} \Big|_{\lambda, \xi, \vartheta} \right) &= \frac{\partial}{\partial S} \Big|_{\lambda, \xi} \left[-\hat{\omega}_D \hat{\rho}_{\vartheta j} - \frac{1}{2} \left\langle \frac{\hat{\rho}_{\vartheta j}}{\hat{V}_\parallel} \frac{\partial}{\partial \hat{p}_\varphi} \Big|_{\lambda, \xi, \vartheta} \hat{\Phi} \left(\hat{p}_\varphi + \hat{\rho}_{\vartheta j} \hat{V}_\parallel, \xi, \vartheta \right) \right\rangle_{\vartheta}^{p_\varphi} \right] = \\
&= -\frac{1}{2} \frac{\partial}{\partial S} \Big|_{\lambda, \xi} \left\{ \left\langle \frac{\hat{\rho}_{\vartheta j}}{\hat{V}_\parallel} \frac{\partial}{\partial \hat{p}_\varphi} \Big|_{\lambda, \xi, \vartheta} \hat{\Phi} \left(\hat{p}_\varphi + \hat{\rho}_{\vartheta j} \hat{V}_\parallel, \xi, \vartheta \right) \right\rangle_{\vartheta}^{p_\varphi} \left[\hat{p}_\varphi \left(S, \xi, \lambda, \hat{V}; \sigma \right), \xi, \lambda, \hat{V}; \sigma \right] \right\} = \\
&= -\frac{1}{2} \frac{\partial}{\partial S} \Big|_{\lambda, \xi} \left\langle \frac{\hat{\rho}_{\vartheta j}}{\hat{V}_\parallel} \frac{\partial}{\partial \hat{p}_\varphi} \Big|_{\lambda, \xi, \vartheta} \hat{\Phi} \right\rangle_{\vartheta}^{p_\varphi}
\end{aligned}$$

and

$$\begin{aligned}
\frac{\partial}{\partial \lambda} \Big|_{S, \xi} \left(\frac{\partial S^t}{\partial \hat{p}_\varphi} \Big|_{\lambda, \xi, \vartheta} \right) &= \frac{\partial}{\partial \lambda} \Big|_{S, \xi} \left[-\hat{\omega}_D \hat{\rho}_{\vartheta j} - \frac{1}{2} \left\langle \frac{\hat{\rho}_{\vartheta j}}{\hat{V}_\parallel} \frac{\partial}{\partial \hat{p}_\varphi} \Big|_{\lambda, \xi, \vartheta} \hat{\Phi} \left(\hat{p}_\varphi + \hat{\rho}_{\vartheta j} \hat{V}_\parallel, \xi, \vartheta \right) \right\rangle_{\vartheta}^{p_\varphi} \right] = \\
&= -\hat{\rho}_{\vartheta j} \frac{\partial \hat{\omega}_D}{\partial \lambda} \Big|_{S, \xi} - \\
&- \frac{1}{2} \frac{\partial}{\partial \lambda} \Big|_{S, \xi} \left\{ \left\langle \frac{\hat{\rho}_{\vartheta j}}{\hat{V}_\parallel} \frac{\partial}{\partial \hat{p}_\varphi} \Big|_{\lambda, \xi, \vartheta} \hat{\Phi} \left(\hat{p}_\varphi + \hat{\rho}_{\vartheta j} \hat{V}_\parallel, \xi, \vartheta \right) \right\rangle_{\vartheta}^{p_\varphi} \left[\hat{p}_\varphi \left(S, \xi, \lambda, \hat{V}; \sigma \right), \xi, \lambda, \hat{V}; \sigma \right] \right\} = \\
&= -\hat{\rho}_{\vartheta j} \frac{\partial \hat{\omega}_D}{\partial \lambda} \Big|_{\psi, \xi} - \frac{1}{2} \frac{\partial}{\partial \lambda} \Big|_{S, \xi} \left\langle \frac{\hat{\rho}_{\vartheta j}}{\hat{V}_\parallel} \frac{\partial}{\partial \hat{p}_\varphi} \Big|_{\lambda, \xi, \vartheta} \hat{\Phi} \left(\hat{p}_\varphi + \hat{\rho}_{\vartheta j} \hat{V}_\parallel, \xi, \vartheta \right) \right\rangle_{\vartheta}^{p_\varphi}.
\end{aligned}$$

The electrostatic potential term, $-\frac{1}{2} \left\langle \frac{\hat{\rho}_{\vartheta j}}{\hat{V}_\parallel} \hat{\Phi} \right\rangle_{\vartheta}^{p_\varphi}$, is considered as a function of \hat{p}_φ , ξ , λ , \hat{V} and σ and thus $\left(\hat{p}_\varphi \left(S, \xi, \lambda, \hat{V}; \sigma \right), \xi, \lambda, \hat{V}; \sigma \right)$. $\hat{\omega}_D$ is a function of $\mathbf{V} = (\lambda, V, \sigma)$ only and hence $\partial \hat{\omega}_D / \partial \lambda|_{\psi} = \partial \hat{\omega}_D / \partial \lambda|_{p_\varphi} = \partial \hat{\omega}_D / \partial \lambda|_S$.

Now we have calculated all the auxiliary coefficients required to find B_{1-13} in Eq.E.1. The next step is to introduce the boundary conditions in λ and S space and implement them in the numerical scheme.

E.2 Boundary conditions in λ and S space

To provide the Maxwellian behaviour far from the magnetic island, we require $\partial \hat{f}_j / \partial x \Big|_{x \rightarrow \pm\infty} = \hat{w} \left[L_n^{-1} + (\hat{V}^2 - 3/2) L_{Tj}^{-1} \right] e^{-\hat{V}^2}$, where $\hat{f}_j = f_j \pi^{3/2} V_{Tj}^3 / n_0$. To solve Eq.E.1, this condition has to be rewritten in S space for both passing and trapped particles. As we noted in the main part, the electrostatic potential does not provide an island-like structure in the trapped region and thus we find it convenient to introduce an extra variable $y^{\pm/t}$, such that $y^\pm = \sqrt{S^\pm - S_{\min}^\pm}$, $2y^\pm dy^\pm = dS^\pm$ for passing and $y^t = S^t$, $dy_t = dS_t$ for trapped particles. A different definition of $y^{\pm/t}$ is justified as both passing and trapped external regions, i.e. $\lambda \in [0, \lambda_p] \cup [\lambda_t, \lambda_{fin}]$, are not connected directly but via a dissipation layer where the perturbative approach becomes invalid. In the absence of the electrostatic potential, this Neumann boundary condition translates into Eq.4.1 for $\lambda \leq \lambda_p$ and Eq.4.2 for $\lambda \geq \lambda_t$, and is to be updated at each iteration in Φ , provided the inverse function, $y^{\pm/t} = y^{\pm/t}(\hat{p}_\varphi)$, exists at each ξ , λ , \hat{V} and σ .

As there are no closed flux surfaces in S space for trapped particles (in range of plasma and tokamak parameters we consider), we simply require the Neumann boundary at $y^t \rightarrow \pm\infty$ updated at each iteration in Φ . For passing particles, we require the Neumann boundary at $y^\pm \rightarrow +\infty$ for $\sigma_{p_\varphi} = \pm 1$. However, an additional condition is required at $y^\pm = 0$. We introduce Eq.4.3 due to the flattening requirement inside the S island. Here we have to note that flattening inside the S island is not obvious from $\mathcal{O}(\delta_j^1)$. It comes from $\mathcal{O}(\delta_j^0)$, but $\mathcal{O}(\delta_j^1)$ might provide an additional dependence, which is weak compared to flattening from $\mathcal{O}(\delta_j^0)$. However, a zero gradient inside the S island can be justified in a different way. In the layer, where the radial shift is maximum, i.e. at $\lambda = \lambda_{p,t}$, at each $\rho_{\vartheta j}$, we work in terms of p_φ with the Neumann boundary at $p_\varphi \rightarrow \pm\infty$ with no flattening requirement inside the \hat{S} island. However, we still find the distribution function to be partially flattened even for large $\rho_{\vartheta j}$. Moving from $\lambda = \lambda_p$ to $\lambda = 0$, we move in the direction of reduction in the radial shift (i.e. S approaches the real magnetic island) and thus there still should be partial flattening. Thus, we set a zero gradient at the S island O-point. In addition, Eq.4.3 ensures continuity of $\partial \hat{f}_j / \partial y^\pm$ across the S island O-point at each σ_{p_φ} .

In λ space we require the distribution function and its first derivative to be finite at $\lambda = 0$

and $\lambda = \lambda_{fin}$. As the term in $\partial^2/\partial\lambda^2$ vanishes at $\lambda = 0$ and $\lambda = \lambda_{fin}$, we impose Eq.E.1 evaluated at $\lambda = 0$ for the boundary condition at the deeply passing end and similarly Eq.E.1 evaluated at $\lambda = \lambda_{fin}$ for the boundary condition at the deeply trapped end. This results in a mixed boundary at $\lambda = 0$ and $\lambda = \lambda_{fin}$.

Note: if Φ provided the island-like structure for trapped particles, they had to be considered such as passing particles. The subroutine is added that checks if the solution of $y^t = y^t(\hat{p}_\varphi)$ is unique at each ξ, λ, \hat{V} .

E.3 First and second order derivatives

We use the following approximations:

Central difference for passing branch

$$\begin{aligned} \left. \frac{\partial g_{j=e,i}^{(0,0),p}}{\partial \lambda} \right|_{S,\xi} &\equiv \left. \frac{\partial g^{\sigma,p}}{\partial \lambda} \right|_{S,\xi} = \frac{g_{i,j+1}^{\sigma,p} - g_{i,j-1}^{\sigma,p}}{2\Delta\lambda_p} + \mathcal{O}(\Delta\lambda_p^2), \\ \left. \frac{\partial^2 g_{j=e,i}^{(0,0),p}}{\partial \lambda^2} \right|_{S,\xi} &\equiv \left. \frac{\partial^2 g^{\sigma,p}}{\partial \lambda^2} \right|_{S,\xi} = \frac{g_{i,j+1}^{\sigma,p} - 2g_{i,j}^{\sigma,p} + g_{i,j-1}^{\sigma,p}}{\Delta\lambda_p^2} + \mathcal{O}(\Delta\lambda_p^2) \end{aligned}$$

Central difference for trapped branch

$$\begin{aligned} \left. \frac{\partial g_{j=e,i}^{(0,0),t}}{\partial \lambda} \right|_{S,\xi} &\equiv \left. \frac{\partial g^{|\sigma|,t}}{\partial \lambda} \right|_{S,\xi} = \frac{g_{i,j+1}^{|\sigma|,t} - g_{i,j-1}^{|\sigma|,t}}{2\Delta\lambda_t} + \mathcal{O}(\Delta\lambda_t^2), \\ \left. \frac{\partial^2 g_{j=e,i}^{(0,0),t}}{\partial \lambda^2} \right|_{S,\xi} &\equiv \left. \frac{\partial^2 g^{|\sigma|,t}}{\partial \lambda^2} \right|_{S,\xi} = \frac{g_{i,j+1}^{|\sigma|,t} - 2g_{i,j}^{|\sigma|,t} + g_{i,j-1}^{|\sigma|,t}}{\Delta\lambda_t^2} + \mathcal{O}(\Delta\lambda_t^2). \end{aligned}$$

$\Delta\lambda_{p/t}$ is a step in the passing/trapped region.

Central difference in S (main regions)

$$\begin{aligned} \left. \frac{\partial g_{j=e,i}^{(0,0),p}}{\partial S} \right|_{\lambda,\xi} &\equiv \left. \frac{\partial g^{\sigma,p}}{\partial S} \right|_{\lambda,\xi} = \frac{g_{i+1,j}^{\sigma,p} - g_{i-1,j}^{\sigma,p}}{2\Delta S_{in/out}} + \mathcal{O}(\Delta S_{in/out}^2), \\ \left. \frac{\partial^2 g_{j=e,i}^{(0,0),p}}{\partial S^2} \right|_{\lambda,\xi} &\equiv \left. \frac{\partial^2 g^{\sigma,p}}{\partial S^2} \right|_{\lambda,\xi} = \frac{g_{i+1,j}^{\sigma,p} - 2g_{i,j}^{\sigma,p} + g_{i-1,j}^{\sigma,p}}{\Delta S_{in/out}^2} + \mathcal{O}(\Delta S_{in/out}^2), \\ \left. \frac{\partial g_{j=e,i}^{(0,0),t}}{\partial S} \right|_{\lambda,\xi} &\equiv \left. \frac{\partial g^{|\sigma|,t}}{\partial S} \right|_{\lambda,\xi} = \frac{g_{i+1,j}^{|\sigma|,t} - g_{i-1,j}^{|\sigma|,t}}{2\Delta S_{in/out}} + \mathcal{O}(\Delta S_{in/out}^2), \end{aligned}$$

$$\left. \frac{\partial^2 g_{j=e,i}^{(0,0),t}}{\partial S^2} \right|_{\lambda,\xi} \equiv \left. \frac{\partial^2 g^{|\sigma|,t}}{\partial S^2} \right|_{\lambda,\xi} = \frac{g_{i+1,j}^{|\sigma|,t} - 2g_{i,j}^{|\sigma|,t} + g_{i-1,j}^{|\sigma|,t}}{\Delta S_{in/out}^2} + \mathcal{O}(\Delta S_{in/out}^2).$$

$\Delta S_{in/out}$ is a step inside/outside the S island. In a code, $\Delta S_{in} = \Delta S_{out}$.

Backward in S (top boundary)

$$\begin{aligned} \left. \frac{\partial g_{j=e,i}^{(0,0),p/t}}{\partial S} \right|_{\lambda,\xi} &\equiv \left. \frac{\partial g^{p/t}}{\partial S} \right|_{\lambda,\xi} = \begin{cases} \frac{g_{i,j}^{p/t} - g_{i-1,j}^{p/t}}{\Delta S_{in/out}} + \mathcal{O}(\Delta S_{in/out}), \\ \frac{3g_{i,j}^{p/t} - 4g_{i-1,j}^{p/t} + g_{i-2,j}^{p/t}}{2\Delta S_{in/out}} + \mathcal{O}(\Delta S_{in/out}^2) \end{cases} \\ \left. \frac{\partial^2 g_{j=e,i}^{(0,0),p/t}}{\partial S^2} \right|_{\lambda,\xi} &\equiv \left. \frac{\partial^2 g^{p/t}}{\partial S^2} \right|_{\lambda,\xi} = \begin{cases} \frac{1}{\Delta S_{in/out}} \left[\left. \frac{\partial g^{p/t}}{\partial S} \right|_{i,j} - \left. \frac{\partial g^{p/t}}{\partial S} \right|_{i-1,j} \right] + \mathcal{O}(\Delta S_{in/out}) \\ \frac{2g_{i,j}^{p/t} - 5g_{i-1,j}^{p/t} + 4g_{i-2,j}^{p/t} - g_{i-3,j}^{p/t}}{(\Delta S_{in/out})^2} + \mathcal{O}(\Delta S_{in/out}^2) \end{cases} = \\ &= \begin{cases} \frac{g_{i,j}^{p/t} - 2g_{i-1,j}^{p/t} + g_{i-2,j}^{p/t}}{\Delta S_{in/out}^2} + \mathcal{O}(\Delta S_{in/out}) \\ \frac{2g_{i,j}^{p/t} - 5g_{i-1,j}^{p/t} + 4g_{i-2,j}^{p/t} - g_{i-3,j}^{p/t}}{(\Delta S_{in/out})^2} + \mathcal{O}(\Delta S_{in/out}^2) \end{cases} \end{aligned}$$

Backward for passing branch (trapped/passing boundary)

note: also to be applied to the trapped branch at the deeply trapped end

$$\begin{aligned} \left. \frac{\partial g_{j=e,i}^{(0,0),p/t}}{\partial \lambda} \right|_{S,\xi} &\equiv \left. \frac{\partial g^{p/t}}{\partial \lambda} \right|_{S,\xi} = \begin{cases} \frac{g_{i,j}^{p/t} - g_{i,j-1}^{p/t}}{\Delta \lambda_{p/t}} + \mathcal{O}(\Delta \lambda_{p/t}), \\ \frac{3g_{i,j}^{p/t} - 4g_{i,j-1}^{p/t} + g_{i,j-2}^{p/t}}{2\Delta \lambda_{p/t}} + \mathcal{O}(\Delta \lambda_{p/t}^2) \end{cases} \\ \left. \frac{\partial^2 g_{j=e,i}^{(0,0),p/t}}{\partial \lambda^2} \right|_{S,\xi} &\equiv \left. \frac{\partial^2 g^{p/t}}{\partial \lambda^2} \right|_{S,\xi} = \begin{cases} \frac{1}{\Delta \lambda_{p/t}} \left[\left. \frac{\partial g^{p/t}}{\partial \lambda} \right|_{i,j} - \left. \frac{\partial g^{p/t}}{\partial \lambda} \right|_{i,j-1} \right] + \mathcal{O}(\Delta \lambda_{p/t}) \\ \frac{2g_{i,j}^{p/t} - 5g_{i,j-1}^{p/t} + 4g_{i,j-2}^{p/t} - g_{i,j-3}^{p/t}}{(\Delta \lambda_{p/t})^2} + \mathcal{O}(\Delta \lambda_{p/t}^2) \end{cases} = \\ &= \begin{cases} \frac{g_{i,j}^{p/t} - 2g_{i,j-1}^{p/t} + g_{i,j-2}^{p/t}}{\Delta \lambda_{p/t}^2} + \mathcal{O}(\Delta \lambda_{p/t}) \\ \frac{2g_{i,j}^{p/t} - 5g_{i,j-1}^{p/t} + 4g_{i,j-2}^{p/t} - g_{i,j-3}^{p/t}}{(\Delta \lambda_{p/t})^2} + \mathcal{O}(\Delta \lambda_{p/t}^2) \end{cases} \end{aligned}$$

Forward for trapped branch (trapped/passing boundary)

note: also to be applied to the passing branch at the deeply passing end

$$\left. \frac{\partial g_{j=e,i}^{(0,0),p/t}}{\partial \lambda} \right|_{S,\xi} \equiv \left. \frac{\partial g^{p/t}}{\partial \lambda} \right|_{S,\xi} = \begin{cases} \frac{g_{i,j+1}^{p/t} - g_{i,j}^{p/t}}{\Delta \lambda_{p/t}} + \mathcal{O}(\Delta \lambda_{p/t}), \\ \frac{-g_{i,j+2}^{p/t} + 4g_{i,j+1}^{p/t} - 3g_{i,j}^{p/t}}{2\Delta \lambda_{p/t}} + \mathcal{O}(\Delta \lambda_{p/t}^2) \end{cases}$$

$$\begin{aligned} \left. \frac{\partial^2 g_{j=e,i}^{(0,0),p/t}}{\partial \lambda^2} \right|_{S,\xi} &\equiv \left. \frac{\partial^2 g^{p/t}}{\partial \lambda^2} \right|_{S,\xi} = \left\{ \frac{1}{\Delta \lambda_{p/t}} \left[\left. \frac{\partial g^{p/t}}{\partial \lambda} \right|_{i,j+1} - \left. \frac{\partial g^{p/t}}{\partial \lambda} \right|_{i,j} \right] + O(\Delta \lambda_{p/t}) \right. \\ &= \left. \frac{-g_{i,j+3}^{p/t} + 4g_{i,j+2}^{p/t} - 5g_{i,j+1}^{p/t} + 2g_{i,j}^{p/t}}{(\Delta \lambda_{p/t})^2} + O(\Delta \lambda_{p/t}^2) \right\} = \\ &= \left\{ \frac{g_{i,j+2}^{p/t} - 2g_{i,j+1}^{p/t} + g_{i,j}^{p/t}}{\Delta \lambda_{p/t}^2} + O(\Delta \lambda_{p/t}) \right. \\ &= \left. \frac{-g_{i,j+3}^{p/t} + 4g_{i,j+2}^{p/t} - 5g_{i,j+1}^{p/t} + 2g_{i,j}^{p/t}}{(\Delta \lambda_{p/t})^2} + O(\Delta \lambda_{p/t}^2) \right\} \end{aligned}$$

Mixed derivatives are

$$\begin{aligned} \frac{\partial^2 g_{j=e,i}^{(0,0),p/t}}{\partial \lambda|_{S,\xi} \partial S|_{\lambda,\xi}} &= \frac{\partial^2 g_{j=e,i}^{(0,0),p/t}}{\partial S|_{\lambda,\xi} \partial \lambda|_{S,\xi}} = \\ &= \frac{g_{i+1,j+1}^{p/t} - g_{i+1,j-1}^{p/t} - g_{i-1,j+1}^{p/t} + g_{i-1,j-1}^{p/t}}{4\Delta \lambda_{p/t} \Delta S_{in/out}} + O(\Delta S_{in/out}^2, \Delta \lambda_{p/t}^2). \end{aligned}$$

for passing and trapped particles.

E.4 C coefficients

To provide the Maxwellian behaviour far from the island, we have introduced y instead of S :

$$y = \sqrt{S^\pm - S_{\min}} \cdot \Theta(\lambda_c - \lambda) + S^t \cdot \Theta(\lambda - \lambda_c)$$

for $\sigma = \pm 1/\sigma_t$ as a new radial variable. Hence, Eq.E.1 becomes

$$\begin{aligned} B_1 \left. \frac{\partial^2 g}{\partial \lambda^2} \right|_{y,\xi} + B_2 \left. \frac{\partial g}{\partial \lambda} \right|_{y,\xi} + \frac{B_3}{4y^2} \left. \frac{\partial^2 g}{\partial y^2} \right|_{\lambda,\xi} + \\ + \left(\sum_{i=4}^{11} \frac{B_i}{2y} - \frac{B_3}{4y^3} \right) \left. \frac{\partial g}{\partial y} \right|_{\lambda,\xi} + \frac{B_{12}}{2y} \left. \frac{\partial^2 g}{\partial \lambda \partial y} \right|_{\xi} + U = 0 \end{aligned} \quad (\text{E.2})$$

for passing and

$$\begin{aligned} B_1 \left. \frac{\partial^2 g}{\partial \lambda^2} \right|_{y,\xi} + B_2 \left. \frac{\partial g}{\partial \lambda} \right|_{y,\xi} + B_3 \left. \frac{\partial^2 g}{\partial y^2} \right|_{\lambda,\xi} + \\ + \sum_{i=4}^{11} B_i \left. \frac{\partial g}{\partial y} \right|_{\lambda,\xi} + B_{12} \left. \frac{\partial^2 g}{\partial \lambda \partial y} \right|_{\xi} + U = 0 \end{aligned} \quad (\text{E.3})$$

for trapped particles. Thus, we find it convenient to introduce C coefficients as follows:

$$\begin{aligned} C_1 &= B_1, \\ C_2 &= B_2, \\ C_3 &= \frac{B_3}{4y^2}, \\ C_4 &= -\frac{B_3}{4y^3} + \sum_{i=4}^{11} \frac{B_i}{2y}, \\ C_5 &= \frac{B_{12}}{2y} \end{aligned}$$

for passing and

$$\begin{aligned} C_1 &= B_1, \\ C_2 &= B_2, \\ C_3 &= B_3, \\ C_4 &= \sum_{i=4}^{11} B_i, \\ C_5 &= B_{12} \end{aligned}$$

for trapped particles. Note: both B and C coefficients are to be defined inside and outside the S island in the passing region.

E.5 A coefficients

Employing a second order central difference approximation in λ and y direction, we rewrite Eqs.E.2,E.3 in the following form:

$$\begin{aligned} & \left[\frac{ijkC_5}{4\Delta\lambda_p\Delta y_{in/out}} \right] g_{i+1,j+1}^{\sigma,p} + \left[\frac{ijkC_5}{4\Delta\lambda_p\Delta y_{in/out}} \right] g_{i-1,j-1}^{\sigma,p} + \left[\frac{-ijkC_5}{4\Delta\lambda_p\Delta y_{in/out}} \right] g_{i-1,j+1}^{\sigma,p} \\ & + \left[\frac{-ijkC_5}{4\Delta\lambda_p\Delta y_{in/out}} \right] g_{i+1,j-1}^{\sigma,p} + \\ & + \left[\frac{ijkC_3}{\Delta y_{in/out}^2} + \frac{ijkC_4}{2\Delta y_{in/out}} \right] g_{i+1,j}^{\sigma,p} + \left[\frac{ijkC_3}{\Delta y_{in/out}^2} - \frac{ijkC_4}{2\Delta y_{in/out}} \right] g_{i-1,j}^{\sigma,p} + \\ & + \left[\frac{ijkC_1}{\Delta\lambda_p^2} + \frac{ijkC_2}{2\Delta\lambda_p} \right] g_{i,j+1}^{\sigma,p} + \left[\frac{ijkC_1}{\Delta\lambda_p^2} - \frac{ijkC_2}{2\Delta\lambda_p} \right] g_{i,j-1}^{\sigma,p} + \left[-\frac{2ijkC_1}{\Delta\lambda_p^2} - \frac{2ijkC_3}{\Delta y_{in/out}^2} \right] g_{i,j}^{\sigma,p} + [U]_{ij}^{\sigma,p} = 0, \end{aligned}$$

which is equivalent to

$$\begin{aligned} & A_{1ij}^{\sigma,p} g_{i+1,j+1} + A_{1ij}^{\sigma,p} g_{i-1,j-1} + A_{3ij}^{\sigma,p} g_{i-1,j+1} + A_{3ij}^{\sigma,p} g_{i+1,j-1} + \\ & + A_{5ij}^{\sigma,p} g_{i+1,j} + A_{6ij}^{\sigma,p} g_{i-1,j} + A_{7ij}^{\sigma,p} g_{i,j+1} + A_{8ij}^{\sigma,p} g_{i,j-1} + A_{9ij}^{\sigma,p} g_{i,j} + A_{10ij}^{\sigma,p} (g_{i,j}^{\sigma,p}) = 0, \end{aligned} \quad (\text{E.4})$$

$A_{10ij}^{\sigma,p} (g_{i,j}^{\sigma,p}) = [U]_{ij}^{\sigma,p}$, $\sigma = \pm 1$, $A_{1ij}^{\sigma,p} = A_{2ij}^{\sigma,p} = -A_{3ij}^{\sigma,p} = -A_{4ij}^{\sigma,p}$ for passing particles. Similarly, we obtain for trapped branch:

$$\begin{aligned} & \left[\frac{ijk C_5}{4\Delta\lambda_t \Delta y} \right] g_{i+1,j+1}^{|\sigma|,t} + \left[\frac{ijk C_5}{4\Delta\lambda_t \Delta y} \right] g_{i-1,j-1}^{|\sigma|,t} + \left[\frac{-ijk C_5}{4\Delta\lambda_t \Delta y} \right] g_{i-1,j+1}^{|\sigma|,t} + \left[\frac{-ijk C_5}{4\Delta\lambda_t \Delta y} \right] g_{i+1,j-1}^{|\sigma|,t} \\ & + \left[\frac{ijk C_3}{\Delta y^2} + \frac{ijk C_4}{2\Delta y} \right] g_{i+1,j}^{|\sigma|,t} + \left[\frac{ijk C_3}{\Delta y^2} - \frac{ijk C_4}{2\Delta y} \right] g_{i-1,j}^{|\sigma|,t} \\ & + \left[\frac{ijk C_1}{\Delta\lambda_t^2} + \frac{ijk C_2}{2\Delta\lambda_t} \right] g_{i,j+1}^{|\sigma|,t} + \left[\frac{ijk C_1}{\Delta\lambda_t^2} - \frac{ijk C_2}{2\Delta\lambda_t} \right] g_{i,j-1}^{|\sigma|,t} + \left[-\frac{2ijk C_1}{\Delta\lambda_t^2} - \frac{2ijk C_3}{\Delta y^2} \right] g_{i,j}^{|\sigma|,t} + [U]_{ij}^{|\sigma|,t} = 0, \end{aligned}$$

which is equivalent to

$$\begin{aligned} & A_{1ij}^{|\sigma|,t} g_{i+1,j+1}^{|\sigma|,t} + A_{1ij}^{|\sigma|,t} g_{i-1,j-1}^{|\sigma|,t} + A_{3ij}^{|\sigma|,t} g_{i-1,j+1}^{|\sigma|,t} + A_{3ij}^{|\sigma|,t} g_{i+1,j-1}^{|\sigma|,t} \\ & + A_{5ij}^{|\sigma|,t} g_{i+1,j}^{|\sigma|,t} + A_{6ij}^{|\sigma|,t} g_{i-1,j}^{|\sigma|,t} + A_{7ij}^{|\sigma|,t} g_{i,j+1}^{|\sigma|,t} + A_{8ij}^{|\sigma|,t} g_{i,j-1}^{|\sigma|,t} + A_{9ij}^{|\sigma|,t} g_{i,j}^{|\sigma|,t} + A_{10ij}^{|\sigma|,t} (g_{i,j}^{|\sigma|,t}) = 0 \end{aligned} \quad (\text{E.5})$$

with $\sigma_t = |\sigma| = +1$, and $A_{1ij}^{|\sigma|,t} = A_{2ij}^{|\sigma|,t} = -A_{3ij}^{|\sigma|,t} = -A_{4ij}^{|\sigma|,t}$. We note, $A_{10ij}^{|\sigma|,t} (g_{i,j}^{|\sigma|,t}) = [U]_{ij}^{|\sigma|,t} = 0$ due to the summation over σ in the orbit-averaging operator only to leading order in $\rho_{\vartheta j}/a$. $[U]_{ij}^{|\sigma|,t} \neq 0$ in a code, since the integration in Eqs.2.26,2.27 is provided at fixed ψ . Here $\{i, j, k\}$ are used to enumerate $\{y, \lambda, \sigma\}$. y is to be understood as y^\pm for passing and $y = y^t$ for trapped particles. $\Delta y_{in/out}$ and $\Delta y \equiv \Delta y^t$ are steps in y direction inside/outside the S island for passing particles and for trapped particles, respectively.

E.6 In terms of P, Q and R

Eqs.E.4,E.5 for the passing/trapped branch can be rewritten in the matrix form as

$$\mathbf{P}_j^{\sigma,p} \mathbf{g}_{j+1}^{\sigma,p} + \mathbf{Q}_j^{\sigma,p} \mathbf{g}_j^{\sigma,p} + \mathbf{R}_j^{\sigma,p} \mathbf{g}_{j-1}^{\sigma,p} + \mathbf{A}_j^{\sigma,p} (\mathbf{g}_j^{\sigma,p}) = 0 \quad (\text{E.6})$$

and

$$\mathbf{P}_j^{|\sigma|,t} \mathbf{g}_{j+1}^{|\sigma|,t} + \mathbf{Q}_j^{|\sigma|,t} \mathbf{g}_j^{|\sigma|,t} + \mathbf{R}_j^{|\sigma|,t} \mathbf{g}_{j-1}^{|\sigma|,t} + \mathbf{A}_j^{|\sigma|,t} \left(\mathbf{g}_j^{|\sigma|,t} \right) = 0, \quad (\text{E.7})$$

respectively. As we mentioned earlier, the momentum conservation term does not contribute only to leading order in the trapped region. However, to provide a general solution we keep the free term in Eq.E.7. Here $\mathbf{g}_j^{\sigma,p}/\mathbf{g}_j^{|\sigma|,t}$ is a vector solution of length N_y in the passing/trapped region at each λ grid point, j . $\mathbf{P}_j^{\sigma,p/|\sigma|,t}$, $\mathbf{Q}_j^{\sigma,p/|\sigma|,t}$ and $\mathbf{R}_j^{\sigma,p/|\sigma|,t}$ are square tri-diagonal matrices of size $N_y \times N_y$, and $\mathbf{A}_j^{\sigma,p/|\sigma|,t}$ is the right hand side vector of length N_y . N_y is a total number of points in y direction, i.e. inside and outside the S island. We note that a number of points can be different in $y^{\pm/t}$ direction as the $\sigma = \pm 1/\sigma_t$ branches become independent once the layer solution is found. $\mathbf{P}_j^{\sigma,p}$, $\mathbf{Q}_j^{\sigma,p}$, $\mathbf{R}_j^{\sigma,p}$ and $\mathbf{A}_j^{\sigma,p}$ are constructed as

$$P_{i,i}^{\sigma,p} = A_{7,i,j}^{\sigma,p}, \quad P_{i,i+1}^{\sigma,p} = A_{1,i,j}^{\sigma,p}, \quad P_{i,i-1}^{\sigma,p} = A_{3,i,j}^{\sigma,p}, \quad i \in [1, N_y - 1)$$

$$P_{0,0}^{\sigma,p} = A_{7,0,j}^{\sigma,p}, \quad i = 0$$

$$P_{N_y-1,N_y-1}^{\sigma,p} = A_{7,N_y-1,j}^{\sigma,p}, \quad i = N_y - 1;$$

$$Q_{i,i}^{\sigma,p} = A_{9,i,j}^{\sigma,p}, \quad Q_{i,i+1}^{\sigma,p} = A_{5,i,j}^{\sigma,p}, \quad Q_{i,i-1}^{\sigma,p} = A_{6,i,j}^{\sigma,p}, \quad i \in [1, N_y - 1)$$

$$Q_{0,0}^{\sigma,p} = A_{9,0,j}^{\sigma,p}, \quad Q_{0,1}^{\sigma,p} = A_{5,0,j}^{\sigma,p} + A_{6,0,j}^{\sigma,p}, \quad i = 0$$

$$Q_{N_y-1,N_y-1}^{\sigma,p} = A_{9,N_y-1,j}^{\sigma,p}, \quad Q_{N_y-1,N_y-2}^{\sigma,p} = A_{5,N_y-1,j}^{\sigma,p} + A_{6,N_y-1,j}^{\sigma,p}, \quad i = N_y - 1;$$

$$R_{i,i}^{\sigma,p} = A_{8,i,j}^{\sigma,p}, \quad R_{i,i+1}^{\sigma,p} = A_{3,i,j}^{\sigma,p}, \quad R_{i,i-1}^{\sigma,p} = A_{1,i,j}^{\sigma,p}, \quad i \in [1, N_y - 1)$$

$$R_{0,0}^{\sigma,p} = A_{8,0,j}^{\sigma,p}, \quad i = 0$$

$$R_{N_y-1,N_y-1}^{\sigma,p} = A_{8,N_y-1,j}^{\sigma,p}, \quad i = N_y - 1$$

and

$$A_i^{\sigma,p} (g_{i,j}^{\sigma,p}) = A_{10,i,j}^{\sigma,p} (g_{i,j}^{\sigma,p}), \quad i \in [1, N_y - 1)$$

$$A_0^{\sigma,p} (g_{0,j}^{\sigma,p}) = A_{10,0,j}^{\sigma,p} (g_{0,j}^{\sigma,p}) - 2\Delta y \cdot C_1^p \cdot A_{6,0,j}^{\sigma,p}, \quad i = 0$$

$$A_{N_y-1}^{\sigma,p} (g_{N_y-1,j}^{\sigma,p}) = A_{10,N_y-1,j}^{\sigma,p} (g_{N_y-1,j}^{\sigma,p}) + 2\Delta y \cdot C_2^p \cdot A_{5,N_y-1,j}^{\sigma,p}, \quad i = N_y - 1$$

at each j for each k . Here $\Delta y_{in} = \Delta y_{out} \equiv \Delta y$. $C_1^p = 0$ sets a zero gradient inside the S island. C_2^p provides the gradient of the distribution function far from the magnetic island, i.e. Eq.4.1 for the full distribution function and

$$C_2^p = \frac{\partial \hat{g}_j^{(0,0)}}{\partial y^\pm} \Big|_{y^\pm \rightarrow +\infty} = \sigma_{p\varphi} \hat{w} \left[L_{n0}^{-1} + \left(\hat{V}^2 - \frac{3}{2} \right) L_{Tj}^{-1} \right] e^{-\hat{V}^2} \sqrt{\frac{2\hat{L}_q}{\hat{w}}} \quad (\text{E.8})$$

for the perturbation in the absence of the electrostatic potential. $\hat{g}_j^{(0,0)}$ is normalised, i.e. $g_j^{(0,0)} \pi^{3/2} V_{Tj}^3 / n_0$. This condition is to be updated at each iteration in Φ . For trapped particles, we write

$$\begin{aligned} P_{i,i}^{|\sigma|,t} &= A_{7,i,j}^{|\sigma|,t}, & P_{i,i+1}^{|\sigma|,t} &= A_{1,i,j}^{|\sigma|,t}, & P_{i,i-1}^{|\sigma|,t} &= A_{3,i,j}^{|\sigma|,t}, & i &\in [1, N_y - 1) \\ P_{0,0}^{|\sigma|,t} &= A_{7,0,j}^{|\sigma|,t}, & i &= 0 \\ P_{N_y-1, N_y-1}^{|\sigma|,t} &= A_{7, N_y-1, j}^{|\sigma|,t}, & i &= N_y - 1; \end{aligned}$$

$$\begin{aligned} Q_{i,i}^{|\sigma|,t} &= A_{9,i,j}^{|\sigma|,t}, & Q_{i,i+1}^{|\sigma|,t} &= A_{5,i,j}^{|\sigma|,t}, & Q_{i,i-1}^{|\sigma|,t} &= A_{6,i,j}^{|\sigma|,t}, & i &\in [1, N_y - 1) \\ Q_{0,0}^{|\sigma|,t} &= A_{9,0,j}^{|\sigma|,t}, & Q_{0,1}^{|\sigma|,t} &= A_{5,0,j}^{|\sigma|,t} + A_{6,0,j}^{|\sigma|,t}, & i &= 0 \\ Q_{N_y-1, N_y-1}^{|\sigma|,t} &= A_{9, N_y-1, j}^{|\sigma|,t}, & Q_{N_y-1, N_y-2}^{|\sigma|,t} &= A_{5, N_y-1, j}^{|\sigma|,t} + A_{6, N_y-1, j}^{|\sigma|,t}, & i &= N_y - 1; \end{aligned}$$

$$\begin{aligned} R_{i,i}^{|\sigma|,t} &= A_{8,i,j}^{|\sigma|,t}, & R_{i,i+1}^{|\sigma|,t} &= A_{3,i,j}^{|\sigma|,t}, & R_{i,i-1}^{|\sigma|,t} &= A_{1,i,j}^{|\sigma|,t}, & i &\in [1, N_y - 1) \\ R_{0,0}^{|\sigma|,t} &= A_{8,0,j}^{|\sigma|,t}, & i &= 0 \\ R_{N_y-1, N_y-1}^{|\sigma|,t} &= A_{8, N_y-1, j}^{|\sigma|,t}, & i &= N_y - 1 \end{aligned}$$

and

$$\begin{aligned} A_i^{|\sigma|,t} \left(g_{i,j}^{|\sigma|,t} \right) &= A_{10,i,j}^{|\sigma|,t} \left(g_{i,j}^{|\sigma|,t} \right), & i &\in [1, N_y - 1) \\ A_0^{|\sigma|,t} \left(g_{0,j}^{|\sigma|,t} \right) &= A_{10,0,j}^{|\sigma|,t} \left(g_{0,j}^{|\sigma|,t} \right) - 2\Delta y^t \cdot C_1^t(\lambda[j]) \cdot A_{6,0,j}^{\sigma,p}, & i &= 0 \\ A_{N_y-1}^{|\sigma|,t} \left(g_{N_y-1,j}^{|\sigma|,t} \right) &= A_{10, N_y-1, j}^{|\sigma|,t} \left(g_{N_y-1,j}^{|\sigma|,t} \right) + 2\Delta y^t \cdot C_2^t(\lambda[j]) \cdot A_{5, N_y-1, j}^{|\sigma|,t}, & i &= N_y - 1. \end{aligned}$$

Here Δy^t is a step in y^t direction not necessarily equal to $\Delta y_{in/out}$. N_y is a total number of points in y^t direction. As both external branches (passing and trapped) are connected through the layer solution, N_y is allowed to be different in the passing and trapped regions.

However, we note that N_y has to be the same for passing and trapped particles in phase space in the secondary mode problem [95, 96], Chapter V, as there is no layer solution in this case and both external branches are connected directly. C_1^t and C_2^t provide the gradient of the trapped particle distribution function far from the magnetic island, i.e. at $\pm\infty$. In the absence of the electrostatic potential, this is provided by Eq.4.2 for the full distribution function and

$$C_1^t = C_2^t = \left. \frac{\partial \hat{f}_j}{\partial y^t} \right|_{y^t \rightarrow \pm\infty} = - \frac{\hat{w}}{\hat{\omega}_D \hat{\rho}_{\theta j} + \frac{\hat{\rho}_{\theta j}}{2} \left\langle \frac{1}{\hat{V}_{\parallel}} \right\rangle_{\vartheta}^{p_{\varphi}} L_{n0}^{-1} \hat{w} \hat{\omega}_E} \left[L_{n0}^{-1} + \left(\hat{V}^2 - \frac{3}{2} \right) L_{Tj}^{-1} \right] e^{-\hat{V}^2} \quad (\text{E.9})$$

for its perturbed part. C_1^t and C_2^t are different at each step in λ , i.e. at each j . This condition is to be updated at each iteration in Φ .

E.6.1 Left boundary (passing branch)

The solution and its first derivative have to be finite at the deeply passing end, $\lambda = 0$, i.e. $j = 0$. Since the term in $\partial^2/\partial\lambda^2$ vanishes at $\lambda = 0$, we impose Eq.D.60,D.61/Eq.E.2 evaluated at $\lambda = 0$ for the boundary condition at the deeply passing end, i.e. Eq.4.4. Let us introduce

$$h_1^{\sigma,p} = \left\langle \sigma \frac{R}{B_{\varphi}} \right\rangle_{\vartheta}^{p_{\varphi}} \left\langle \frac{1}{A} \right\rangle_{\xi}^S,$$

$$h_2^{\sigma,p} = \left\langle \sigma \frac{R}{B_{\varphi}} \right\rangle_{\vartheta}^{p_{\varphi}} \left\langle \frac{1}{A} \frac{\partial S}{\partial \lambda} \right\rangle_{p_{\varphi}, \xi}^S + \left\langle \frac{\hat{\rho}_{\theta i}}{2} \hat{V} R \right\rangle_{\vartheta}^{\hat{p}_{\varphi}} \left\langle \frac{1}{A} \frac{\partial S}{\partial p_{\varphi}} \right\rangle_{\xi}^S.$$

Thus, Eq.4.4 reads

$$\hat{P}_0^{\sigma,p} \mathbf{g}_0^{\sigma,p} + \hat{Q}_0^{\sigma,p} \mathbf{g}_1^{\sigma,p} + \hat{R}_0^{\sigma,p} \mathbf{g}_2^{\sigma,p} + \mathbf{h}_0^{\sigma,p} (\mathbf{g}_0^{\sigma,p}) = 0 \quad (\text{E.10})$$

Here we have applied a central difference scheme in S/y direction and one-sided difference in λ direction. $\hat{P}_0^{\sigma,p}$, $\hat{Q}_0^{\sigma,p}$, $\hat{R}_0^{\sigma,p}$ and $\mathbf{h}_0^{\sigma,p}$ are introduced in a way similar to matrices that represent the equation and also contain the information about the limit far from the

magnetic island:

$$\begin{aligned}\hat{P}_{i,i}^{\sigma,p} &= \frac{-3h_{1,i,0}^{\sigma,p}}{2\Delta\lambda_p}, & \hat{P}_{i,i+1}^{\sigma,p} &= \frac{h_{2,i,0}^{\sigma,p}}{2\Delta y}, & \hat{P}_{i,i-1}^{\sigma,p} &= -\frac{h_{2,i,0}^{\sigma,p}}{2\Delta y}, & i \in [1, N_y - 1) \\ \hat{P}_{0,0}^{\sigma,p} &= \frac{-3h_{1,0,0}^{\sigma,p}}{2\Delta\lambda_p}, & i &= 0 \\ \hat{P}_{N_y-1, N_y-1}^{\sigma,p} &= \frac{-3h_{1, N_y-1, 0}^{\sigma,p}}{2\Delta\lambda_p}, & i &= N_y - 1;\end{aligned}$$

$$\hat{Q}_{i,i}^{\sigma,p} = \frac{4h_{1,i,0}^{\sigma,p}}{2\Delta\lambda_p}, \quad i \in [0, N_y);$$

$$\hat{R}_{i,i}^{\sigma,p} = \frac{-h_{1,i,0}^{\sigma,p}}{2\Delta\lambda_p}, \quad i \in [0, N_y)$$

and

$$\begin{aligned}h_i^{\sigma,p} &= U(g_{i,0}^{\sigma,p}), \quad i \in [1, N_y - 1) \\ h_0^{\sigma,p} &= U(g_{i,0}^{\sigma,p}) + C_1^p \cdot h_{2,0,0}^{\sigma,p}, \quad i = 0 \\ h_{N_y-1}^{\sigma,p} &= U(g_{i,0}^{\sigma,p}) + C_2^p \cdot h_{2, N_y-1, 0}^{\sigma,p}, \quad i = N_y - 1.\end{aligned}$$

To set a $j = 0$ th element, we impose the following linear approximation:

$$\mathbf{g}_j^{\sigma,p} = \boldsymbol{\alpha}_j^{\sigma,p} \mathbf{g}_{j+1}^{\sigma,p} + \boldsymbol{\beta}_j^{\sigma,p} \quad (\text{E.11})$$

and thus

$$\mathbf{g}_{j-1}^{\sigma,p} = \boldsymbol{\alpha}_{j-1}^{\sigma,p} \mathbf{g}_j^{\sigma,p} + \boldsymbol{\beta}_{j-1}^{\sigma,p}, \quad (\text{E.12})$$

where $\boldsymbol{\alpha}_j^{\sigma,p}$ is the square matrix of $N_y \times N_y$ and $\boldsymbol{\beta}_j^{\sigma,p}$ is a vector of length N_y at each j .

Substituting Eq.E.12 into Eq.E.6, we have

$$\mathbf{P}_j^{\sigma,p} \mathbf{g}_{j+1}^{\sigma,p} + [\mathbf{Q}_j^{\sigma,p} + \mathbf{R}_j^{\sigma,p} \boldsymbol{\alpha}_{j-1}^{\sigma,p}] \mathbf{g}_j^{\sigma,p} + \mathbf{R}_j^{\sigma,p} \boldsymbol{\beta}_{j-1}^{\sigma,p} + \mathbf{A}_j^{\sigma,p} (\mathbf{g}_j^{\sigma,p}) = 0.$$

We define $\mathbf{M}_j^{\sigma,p} = \mathbf{Q}_j^{\sigma,p} + \mathbf{R}_j^{\sigma,p} \boldsymbol{\alpha}_{j-1}^{\sigma,p}$ and hence we can write

$$\begin{aligned} \mathbf{M}_j^{\sigma,p} \mathbf{g}_j^{\sigma,p} &= -\mathbf{P}_j^{\sigma,p} \mathbf{g}_{j+1}^{\sigma,p} - \mathbf{R}_j^{\sigma,p} \boldsymbol{\beta}_{j-1}^{\sigma,p} - \mathbf{A}_j^{\sigma,p} (\mathbf{g}_j^{\sigma,p}), \\ \mathbf{g}_j^{\sigma,p} &= -(\mathbf{M}_j^{\sigma,p})^{-1} \mathbf{P}_j^{\sigma,p} \mathbf{g}_{j+1}^{\sigma,p} - (\mathbf{M}_j^{\sigma,p})^{-1} [\mathbf{R}_j^{\sigma,p} \boldsymbol{\beta}_{j-1}^{\sigma,p} + \mathbf{A}_j^{\sigma,p} (\mathbf{g}_j^{\sigma,p})] \end{aligned}$$

Comparing the latter expression with Eq.E.11, we obtain the following recurrence relation:

$$\begin{aligned} \boldsymbol{\alpha}_j^{\sigma,p} &= -(\mathbf{M}_j^{\sigma,p})^{-1} \mathbf{P}_j^{\sigma,p}, \\ \boldsymbol{\beta}_j^{\sigma,p} &= -(\mathbf{M}_j^{\sigma,p})^{-1} [\mathbf{R}_j^{\sigma,p} \boldsymbol{\beta}_{j-1}^{\sigma,p} + \mathbf{A}_j^{\sigma,p} (\mathbf{g}_j^{\sigma,p})]. \end{aligned} \tag{E.13}$$

Once $\boldsymbol{\alpha}_j^{\sigma,p}$ and $\boldsymbol{\beta}_j^{\sigma,p}$ are determined at certain j , they will be automatically determined at each j by Eq.E.13. Going back to the left boundary, we write

$$\begin{aligned} \mathbf{g}_0^{\sigma,p} &= \boldsymbol{\alpha}_0^{\sigma,p} \mathbf{g}_1^{\sigma,p} + \boldsymbol{\beta}_0^{\sigma,p}, \\ \mathbf{g}_1^{\sigma,p} &= \boldsymbol{\alpha}_1^{\sigma,p} \mathbf{g}_2^{\sigma,p} + \boldsymbol{\beta}_1^{\sigma,p} \end{aligned} \tag{E.14}$$

and hence

$$\mathbf{g}_2^{\sigma,p} = (\boldsymbol{\alpha}_1^{\sigma,p})^{-1} [\mathbf{g}_1^{\sigma,p} - \boldsymbol{\beta}_1^{\sigma,p}]. \tag{E.15}$$

Substituting Eq.E.15 into Eq.E.10 gives

$$\hat{\mathbf{P}}_0^{\sigma,p} \mathbf{g}_0^{\sigma,p} + \left[\hat{\mathbf{Q}}_0^{\sigma,p} + \hat{\mathbf{R}}_0^{\sigma,p} (\boldsymbol{\alpha}_1^{\sigma,p})^{-1} \right] \mathbf{g}_1^{\sigma,p} - \hat{\mathbf{R}}_0^{\sigma,p} (\boldsymbol{\alpha}_1^{\sigma,p})^{-1} \boldsymbol{\beta}_1^{\sigma,p} + \mathbf{h}_0^{\sigma,p} (\mathbf{g}_0^{\sigma,p}) = 0$$

and thus

$$\mathbf{g}_0^{\sigma,p} = \underbrace{-\left(\hat{\mathbf{P}}_0^{\sigma,p}\right)^{-1} \left[\hat{\mathbf{Q}}_0^{\sigma,p} + \hat{\mathbf{R}}_0^{\sigma,p} (\boldsymbol{\alpha}_1^{\sigma,p})^{-1}\right] \mathbf{g}_1^{\sigma,p}}_{\boldsymbol{\alpha}_0^{\sigma,p}} + \underbrace{\left(\hat{\mathbf{P}}_0^{\sigma,p}\right)^{-1} \hat{\mathbf{R}}_0^{\sigma,p} (\boldsymbol{\alpha}_1^{\sigma,p})^{-1} \boldsymbol{\beta}_1^{\sigma,p} - \left(\hat{\mathbf{P}}_0^{\sigma,p}\right)^{-1} \mathbf{h}_0^{\sigma,p} (\mathbf{g}_0^{\sigma,p})}_{\boldsymbol{\beta}_0^{\sigma,p}}.$$

Comparing this expression for $\mathbf{g}_0^{\sigma,p}$ with Eq.E.14, we obtain $\boldsymbol{\alpha}_0^{\sigma,p}$ in terms of $\boldsymbol{\alpha}_1^{\sigma,p}$:

$$\boldsymbol{\alpha}_0^{\sigma,p} = -\left(\hat{\mathbf{P}}_0^{\sigma,p}\right)^{-1} \left[\hat{\mathbf{Q}}_0^{\sigma,p} + \hat{\mathbf{R}}_0^{\sigma,p} (\boldsymbol{\alpha}_1^{\sigma,p})^{-1}\right]. \tag{E.16}$$

On the other hand, from the recurrence relation, Eq.E.13, we have

$$\begin{aligned}\alpha_1^{\sigma,p} &= -[\mathbf{Q}_1^{\sigma,p} + \mathbf{R}_1^{\sigma,p}\alpha_0^{\sigma,p}]^{-1}\mathbf{P}_1^{\sigma,p}, \\ \alpha_1^{\sigma,p}(\mathbf{P}_1^{\sigma,p})^{-1} &= -[\mathbf{Q}_1^{\sigma,p} + \mathbf{R}_1^{\sigma,p}\alpha_0^{\sigma,p}]^{-1}, \\ \alpha_1^{\sigma,p}(\mathbf{P}_1^{\sigma,p})^{-1}[\mathbf{Q}_1^{\sigma,p} + \mathbf{R}_1^{\sigma,p}\alpha_0^{\sigma,p}] &= -\boldsymbol{\mathcal{E}}, \\ (\mathbf{P}_1^{\sigma,p})^{-1}[\mathbf{Q}_1^{\sigma,p} + \mathbf{R}_1^{\sigma,p}\alpha_0^{\sigma,p}] &= -(\alpha_1^{\sigma,p})^{-1},\end{aligned}$$

where $\boldsymbol{\mathcal{E}}$ is a 2D array with ones on the main diagonal and zeros elsewhere. Substituting this expression for $(\alpha_1^{\sigma,p})^{-1}$ into Eq.E.16, we derive

$$\begin{aligned}\alpha_0^{\sigma,p} &= -\left(\hat{\mathbf{P}}_0^{\sigma,p}\right)^{-1}\hat{\mathbf{Q}}_0^{\sigma,p} + \left(\hat{\mathbf{P}}_0^{\sigma,p}\right)^{-1}\hat{\mathbf{R}}_0^{\sigma,p}(\mathbf{P}_1^{\sigma,p})^{-1}[\mathbf{Q}_1^{\sigma,p} + \mathbf{R}_1^{\sigma,p}\alpha_0^{\sigma,p}], \\ \alpha_0^{\sigma,p} &= \alpha_0^{\sigma,p}\boldsymbol{\mathcal{E}} = \boldsymbol{\mathcal{E}}\alpha_0^{\sigma,p} = \\ &= -\left(\hat{\mathbf{P}}_0^{\sigma,p}\right)^{-1}\hat{\mathbf{Q}}_0^{\sigma,p} + \left(\hat{\mathbf{P}}_0^{\sigma,p}\right)^{-1}\hat{\mathbf{R}}_0^{\sigma,p}(\mathbf{P}_1^{\sigma,p})^{-1}\mathbf{Q}_1^{\sigma,p} + \left(\hat{\mathbf{P}}_0^{\sigma,p}\right)^{-1}\hat{\mathbf{R}}_0^{\sigma,p}(\mathbf{P}_1^{\sigma,p})^{-1}\mathbf{R}_1^{\sigma,p}\alpha_0^{\sigma,p}, \\ \left[\boldsymbol{\mathcal{E}} - \left(\hat{\mathbf{P}}_0^{\sigma,p}\right)^{-1}\hat{\mathbf{R}}_0^{\sigma,p}(\mathbf{P}_1^{\sigma,p})^{-1}\mathbf{R}_1^{\sigma,p}\right]\alpha_0^{\sigma,p} &= -\left(\hat{\mathbf{P}}_0^{\sigma,p}\right)^{-1}\hat{\mathbf{Q}}_0^{\sigma,p} + \left(\hat{\mathbf{P}}_0^{\sigma,p}\right)^{-1}\hat{\mathbf{R}}_0^{\sigma,p}(\mathbf{P}_1^{\sigma,p})^{-1}\mathbf{Q}_1^{\sigma,p}\end{aligned}$$

the following expression for $\alpha_0^{\sigma,p}$:

$$\alpha_0^{\sigma,p} = \left[\boldsymbol{\mathcal{E}} - \left(\hat{\mathbf{P}}_0^{\sigma,p}\right)^{-1}\hat{\mathbf{R}}_0^{\sigma,p}(\mathbf{P}_1^{\sigma,p})^{-1}\mathbf{R}_1^{\sigma,p}\right]^{-1} \left[-\left(\hat{\mathbf{P}}_0^{\sigma,p}\right)^{-1}\hat{\mathbf{Q}}_0^{\sigma,p} + \left(\hat{\mathbf{P}}_0^{\sigma,p}\right)^{-1}\hat{\mathbf{R}}_0^{\sigma,p}(\mathbf{P}_1^{\sigma,p})^{-1}\mathbf{Q}_1^{\sigma,p}\right]. \quad (\text{E.17})$$

Now we use the relation for $\beta_0^{\sigma,p}$ that comes from the above expression for $g_0^{\sigma,p}$:

$$\beta_0^{\sigma,p} = \left(\hat{\mathbf{P}}_0^{\sigma,p}\right)^{-1}\hat{\mathbf{R}}_0^{\sigma,p}(\alpha_1^{\sigma,p})^{-1}\beta_1^{\sigma,p} - \left(\hat{\mathbf{P}}_0^{\sigma,p}\right)^{-1}\mathbf{h}_0^{\sigma,p}(g_0^{\sigma,p}). \quad (\text{E.18})$$

From Eq.E.16 we derive

$$-\left(\hat{\mathbf{R}}_0^{\sigma,p}\right)^{-1}\left[\hat{\mathbf{P}}_0^{\sigma,p}\alpha_0^{\sigma,p} + \hat{\mathbf{Q}}_0^{\sigma,p}\right] = (\alpha_1^{\sigma,p})^{-1}.$$

From the recurrence relation, Eq.E.13, we obtain

$$\beta_1^{\sigma,p} = -[\mathbf{Q}_1^{\sigma,p} + \mathbf{R}_1^{\sigma,p}\alpha_0^{\sigma,p}]^{-1}[\mathbf{R}_1^{\sigma,p}\beta_0^{\sigma,p} + \mathbf{A}_1^{\sigma,p}(g_1^{\sigma,p})].$$

Substituting the latter expression for $(\alpha_1^{\sigma,p})^{-1}$ into Eq.E.18:

$$\beta_0^{\sigma,p} = -\left(\hat{P}_0^{\sigma,p}\right)^{-1} \underbrace{\hat{R}_0^{\sigma,p} \left(\hat{R}_0^{\sigma,p}\right)^{-1}}_{\mathcal{E}} \left[\hat{P}_0^{\sigma,p} \alpha_0^{\sigma,p} + \hat{Q}_0^{\sigma,p}\right] \beta_1^{\sigma,p} - \left(\hat{P}_0^{\sigma,p}\right)^{-1} h_0^{\sigma,p} (g_0^{\sigma,p})$$

and then the latter expression for $\beta_1^{\sigma,p}$, we find

$$\begin{aligned} \beta_0^{\sigma,p} &= \left(\hat{P}_0^{\sigma,p}\right)^{-1} \left[\hat{P}_0^{\sigma,p} \alpha_0^{\sigma,p} + \hat{Q}_0^{\sigma,p}\right] \left[Q_1^{\sigma,p} + R_1^{\sigma,p} \alpha_0^{\sigma,p}\right]^{-1} \left[R_1^{\sigma,p} \beta_0^{\sigma,p} + A_1^{\sigma,p} (g_1^{\sigma,p})\right] - \\ &\quad - \left(\hat{P}_0^{\sigma,p}\right)^{-1} h_0^{\sigma,p} (g_0^{\sigma,p}), \\ &\left[\left(\hat{P}_0^{\sigma,p}\right)^{-1} \left[\hat{P}_0^{\sigma,p} \alpha_0^{\sigma,p} + \hat{Q}_0^{\sigma,p}\right] \left[Q_1^{\sigma,p} + R_1^{\sigma,p} \alpha_0^{\sigma,p}\right]^{-1} R_1^{\sigma,p} - \mathcal{E}\right] \beta_0^{\sigma,p} = \\ &= \left(\hat{P}_0^{\sigma,p}\right)^{-1} h_0^{\sigma,p} (g_0^{\sigma,p}) - \left(\hat{P}_0^{\sigma,p}\right)^{-1} \left[\hat{P}_0^{\sigma,p} \alpha_0^{\sigma,p} + \hat{Q}_0^{\sigma,p}\right] \left[Q_1^{\sigma,p} + R_1^{\sigma,p} \alpha_0^{\sigma,p}\right]^{-1} A_1^{\sigma,p} (g_1^{\sigma,p}) \end{aligned}$$

and hence the final expression for $\beta_0^{\sigma,p}$:

$$\begin{aligned} \beta_0^{\sigma,p} &= \left[\left(\hat{P}_0^{\sigma,p}\right)^{-1} \left[\hat{P}_0^{\sigma,p} \alpha_0^{\sigma,p} + \hat{Q}_0^{\sigma,p}\right] \left[Q_1^{\sigma,p} + R_1^{\sigma,p} \alpha_0^{\sigma,p}\right]^{-1} R_1^{\sigma,p} - \mathcal{E}\right]^{-1} \cdot \\ &\cdot \left[\left(\hat{P}_0^{\sigma,p}\right)^{-1} h_0^{\sigma,p} (g_0^{\sigma,p}) - \left(\hat{P}_0^{\sigma,p}\right)^{-1} \left[\hat{P}_0^{\sigma,p} \alpha_0^{\sigma,p} + \hat{Q}_0^{\sigma,p}\right] \left[Q_1^{\sigma,p} + R_1^{\sigma,p} \alpha_0^{\sigma,p}\right]^{-1} A_1^{\sigma,p} (g_1^{\sigma,p})\right]. \end{aligned} \tag{E.19}$$

Now we have found $\alpha_0^{\sigma,p}$ and $\beta_0^{\sigma,p}$, Eqs.E.17,E.19, at the deeply passing end, $j = 0$. Then employing the recurrence relation, Eq.E.13, we calculate all $\alpha_j^{\sigma,p}$ s and $\beta_j^{\sigma,p}$ s at each j up to the point where the perturbative approach breaks down and collisions cannot be considered perturbatively. Note: in the secondary mode problem [95, 96] we calculate all alphas and betas up to the trapped-passing boundary. In addition, $\alpha_0^{\sigma,p}$ and $\beta_0^{\sigma,p}$ let us determine $g_0^{\sigma,p}$. Indeed, we immediately calculate

$$\alpha_1^{\sigma,p} = -\left[Q_1^{\sigma,p} + R_1^{\sigma,p} \alpha_0^{\sigma,p}\right]^{-1} P_1^{\sigma,p}$$

and

$$\beta_1^{\sigma,p} = -\left[Q_1^{\sigma,p} + R_1^{\sigma,p} \alpha_0^{\sigma,p}\right]^{-1} \left[R_1^{\sigma,p} \beta_0^{\sigma,p} + A_1^{\sigma,p} (g_1^{\sigma,p})\right]$$

from $\alpha_0^{\sigma,p}$ and $\beta_0^{\sigma,p}$. Eq.E.14 provides

$$\mathbf{g}_1^{\sigma,p} = (\alpha_0^{\sigma,p})^{-1} [\mathbf{g}_0^{\sigma,p} - \beta_0^{\sigma,p}]$$

and Eq.E.15. Also, we have to employ Eq.E.6 evaluated at $j = 1$:

$$\mathbf{P}_1^{\sigma,p} \mathbf{g}_2^{\sigma,p} + \mathbf{Q}_1^{\sigma,p} \mathbf{g}_1^{\sigma,p} + \mathbf{R}_1^{\sigma,p} \mathbf{g}_0^{\sigma,p} + \mathbf{A}_1^{\sigma,p} (\mathbf{g}_1^{\sigma,p}) = 0$$

Substituting the above expression for $\mathbf{g}_2^{\sigma,p}$, Eq.E.15, into Eq.E.6 at $j = 1$

$$\left[\mathbf{P}_1^{\sigma,p} (\alpha_1^{\sigma,p})^{-1} + \mathbf{Q}_1^{\sigma,p} \right] \mathbf{g}_1^{\sigma,p} - \mathbf{P}_1^{\sigma,p} (\alpha_1^{\sigma,p})^{-1} \beta_1^{\sigma,p} + \mathbf{R}_1^{\sigma,p} \mathbf{g}_0^{\sigma,p} + \mathbf{A}_1^{\sigma,p} (\mathbf{g}_1^{\sigma,p}) = 0$$

and then inserting the latter expression for $\mathbf{g}_1^{\sigma,p}$, we obtain the final expression for $\mathbf{g}_0^{\sigma,p}$:

$$\begin{aligned} \mathbf{g}_0^{\sigma,p} = & \left[\left[\mathbf{P}_1^{\sigma,p} (\alpha_1^{\sigma,p})^{-1} + \mathbf{Q}_1^{\sigma,p} \right] (\alpha_0^{\sigma,p})^{-1} + \mathbf{R}_1^{\sigma,p} \right]^{-1} \cdot \\ & \cdot \left[\left[\mathbf{P}_1^{\sigma,p} (\alpha_1^{\sigma,p})^{-1} + \mathbf{Q}_1^{\sigma,p} \right] (\alpha_0^{\sigma,p})^{-1} \beta_0^{\sigma,p} + \mathbf{P}_1^{\sigma,p} (\alpha_1^{\sigma,p})^{-1} \beta_1^{\sigma,p} - \mathbf{A}_1^{\sigma,p} (\mathbf{g}_1^{\sigma,p}) \right]. \end{aligned}$$

Note: $\mathbf{A}_1^{\sigma,p} (\mathbf{g}_1^{\sigma,p})$ is the integral term and does not contribute at the 0th iteration in the parallel flow. This expression for $\mathbf{g}_0^{\sigma,p}$ can be used as an additional test of the validity of the total solution, $\mathbf{g}_j^{\sigma,p}$ reconstructed at each j based on the linear approximation, Eq.E.11, in the absence of U .

The similar procedure is to be applied to the trapped region.

E.6.2 Right boundary (trapped branch)

The solution and its first derivative also have to be finite at the deeply trapped end, $\lambda = \lambda_{fin}$, i.e. $j = N_{p2}$. Since the term in $\partial^2/\partial\lambda^2$ also vanishes at $\lambda = \lambda_{fin}$, we impose Eq.D.60,D.61/Eq.E.3 evaluated at $\lambda = \lambda_{fin}$ for the boundary condition at the deeply trapped end:

$$\hat{\mathbf{P}}_{N_{p2}}^{|\sigma|,t} \mathbf{g}_{N_{p2}}^{|\sigma|,t} + \hat{\mathbf{Q}}_{N_{p2}}^{|\sigma|,t} \mathbf{g}_{N_{p2}-1}^{|\sigma|,t} + \hat{\mathbf{R}}_{N_{p2}}^{|\sigma|,t} \mathbf{g}_{N_{p2}-2}^{|\sigma|,t} + \mathbf{h}_{N_{p2}}^{|\sigma|,t} \left(\mathbf{g}_{N_{p2}}^{|\sigma|,t} \right) = 0. \quad (\text{E.20})$$

Here we have applied a central difference scheme in S/y space and one-sided difference in λ space. $\hat{\mathbf{P}}_{N_{p2}}^{|\sigma|,t}$, $\hat{\mathbf{Q}}_{N_{p2}}^{|\sigma|,t}$, $\hat{\mathbf{R}}_{N_{p2}}^{|\sigma|,t}$ and $\mathbf{h}_{N_{p2}}^{|\sigma|,t}$ are defined in a way similar to $\hat{\mathbf{P}}_0^{\sigma,p}$, $\hat{\mathbf{Q}}_0^{\sigma,p}$, $\hat{\mathbf{R}}_0^{\sigma,p}$ and

$\mathbf{h}_0^{\sigma,p}$ and contain the information about the distribution function gradient far from the magnetic island. Here we assume

$$\mathbf{g}_j^{|\sigma|,t} = \boldsymbol{\alpha}_j^{|\sigma|,t} \mathbf{g}_{j-1}^{|\sigma|,t} + \boldsymbol{\beta}_j^{|\sigma|,t} \quad (\text{E.21})$$

and thus

$$\mathbf{g}_{j+1}^{|\sigma|,t} = \boldsymbol{\alpha}_{j+1}^{|\sigma|,t} \mathbf{g}_j^{|\sigma|,t} + \boldsymbol{\beta}_{j+1}^{|\sigma|,t}, \quad (\text{E.22})$$

where $\boldsymbol{\alpha}_j^{|\sigma|,t}$ is the square matrix of $N_y \times N_y$ and $\boldsymbol{\beta}_j^{|\sigma|,t}$ is a vector of length N_y at each j (N_y is allowed to be different in the passing and trapped regions when the dissipative layer solution is introduced to provide matching. In [95, 96], N_y has to be the same for passing and trapped particles in phase space). Substituting Eq.E.22 into Eq.E.7, we obtain

$$\left[\mathbf{P}_j^{|\sigma|,t} \boldsymbol{\alpha}_{j+1}^{|\sigma|,t} + \mathbf{Q}_j^{|\sigma|,t} \right] \mathbf{g}_j^{|\sigma|,t} + \mathbf{P}_j^{|\sigma|,t} \boldsymbol{\beta}_{j+1}^{|\sigma|,t} + \mathbf{R}_j^{|\sigma|,t} \mathbf{g}_{j-1}^{|\sigma|,t} + \mathbf{A}_j^{|\sigma|,t} \left(\mathbf{g}_j^{|\sigma|,t} \right) = 0.$$

We define $\mathbf{M}_j^{|\sigma|,t} = \mathbf{P}_j^{|\sigma|,t} \boldsymbol{\alpha}_{j+1}^{|\sigma|,t} + \mathbf{Q}_j^{|\sigma|,t}$ and hence derive

$$\begin{aligned} \mathbf{M}_j^{|\sigma|,t} \mathbf{g}_j^{|\sigma|,t} &= -\mathbf{P}_j^{|\sigma|,t} \boldsymbol{\beta}_{j+1}^{|\sigma|,t} - \mathbf{R}_j^{|\sigma|,t} \mathbf{g}_{j-1}^{|\sigma|,t} - \mathbf{A}_j^{|\sigma|,t} \left(\mathbf{g}_j^{|\sigma|,t} \right), \\ \mathbf{g}_j^{|\sigma|,t} &= -\left(\mathbf{M}_j^{|\sigma|,t} \right)^{-1} \mathbf{R}_j^{|\sigma|,t} \mathbf{g}_{j-1}^{|\sigma|,t} - \left(\mathbf{M}_j^{|\sigma|,t} \right)^{-1} \left[\mathbf{P}_j^{|\sigma|,t} \boldsymbol{\beta}_{j+1}^{|\sigma|,t} + \mathbf{A}_j^{|\sigma|,t} \left(\mathbf{g}_j^{|\sigma|,t} \right) \right]. \end{aligned}$$

Comparing this expression for $\mathbf{g}_j^{|\sigma|,t}$ with Eq.E.21, we derive the following recurrence relation:

$$\begin{aligned} \boldsymbol{\alpha}_j^{|\sigma|,t} &= -\left(\mathbf{M}_j^{|\sigma|,t} \right)^{-1} \mathbf{R}_j^{|\sigma|,t}, \\ \boldsymbol{\beta}_j^{|\sigma|,t} &= -\left(\mathbf{M}_j^{|\sigma|,t} \right)^{-1} \left[\mathbf{P}_j^{|\sigma|,t} \boldsymbol{\beta}_{j+1}^{|\sigma|,t} + \mathbf{A}_j^{|\sigma|,t} \left(\mathbf{g}_j^{|\sigma|,t} \right) \right]. \end{aligned} \quad (\text{E.23})$$

Once $\boldsymbol{\alpha}_j^{|\sigma|,t}$ and $\boldsymbol{\beta}_j^{|\sigma|,t}$ are found at certain j , they will be determined automatically at each j by Eq.E.23. At $j = N_{p2}$ and $j = N_{p2} - 1$ Eq.E.21 reads

$$\begin{aligned} \mathbf{g}_{N_{p2}}^{|\sigma|,t} &= \boldsymbol{\alpha}_{N_{p2}}^{|\sigma|,t} \mathbf{g}_{N_{p2}-1}^{|\sigma|,t} + \boldsymbol{\beta}_{N_{p2}}^{|\sigma|,t}, \\ \mathbf{g}_{N_{p2}-1}^{|\sigma|,t} &= \boldsymbol{\alpha}_{N_{p2}-1}^{|\sigma|,t} \mathbf{g}_{N_{p2}-2}^{|\sigma|,t} + \boldsymbol{\beta}_{N_{p2}-1}^{|\sigma|,t} \end{aligned} \quad (\text{E.24})$$

and hence

$$\mathbf{g}_{N_{p2}-2}^{|\sigma|,t} = \left(\boldsymbol{\alpha}_{N_{p2}-1}^{|\sigma|,t} \right)^{-1} \left[\mathbf{g}_{N_{p2}-1}^{|\sigma|,t} - \boldsymbol{\beta}_{N_{p2}-1}^{|\sigma|,t} \right]. \quad (\text{E.25})$$

Substituting Eq.E.25 into Eq.E.20, we have

$$\hat{\mathbf{P}}_{N_{p2}}^{|\sigma|,t} \mathbf{g}_{N_{p2}}^{|\sigma|,t} + \left[\hat{\mathbf{Q}}_{N_{p2}}^{|\sigma|,t} + \hat{\mathbf{R}}_{N_{p2}}^{|\sigma|,t} \left(\boldsymbol{\alpha}_{N_{p2-1}}^{|\sigma|,t} \right)^{-1} \right] \mathbf{g}_{N_{p2-1}}^{|\sigma|,t} - \hat{\mathbf{R}}_{N_{p2}}^{|\sigma|,t} \left(\boldsymbol{\alpha}_{N_{p2-1}}^{|\sigma|,t} \right)^{-1} \boldsymbol{\beta}_{N_{p2-1}}^{|\sigma|,t} + \mathbf{h}_{N_{p2}}^{|\sigma|,t} \left(\mathbf{g}_{N_{p2}}^{|\sigma|,t} \right) = 0$$

and thus

$$\begin{aligned} \mathbf{g}_{N_{p2}}^{|\sigma|,t} = & \underbrace{- \left(\hat{\mathbf{P}}_{N_{p2}}^{|\sigma|,t} \right)^{-1} \left[\hat{\mathbf{Q}}_{N_{p2}}^{|\sigma|,t} + \hat{\mathbf{R}}_{N_{p2}}^{|\sigma|,t} \left(\boldsymbol{\alpha}_{N_{p2-1}}^{|\sigma|,t} \right)^{-1} \right]}_{\boldsymbol{\alpha}_{N_{p2}}^{|\sigma|,t}} \mathbf{g}_{N_{p2-1}}^{|\sigma|,t} + \\ & + \underbrace{\left(\hat{\mathbf{P}}_{N_{p2}}^{|\sigma|,t} \right)^{-1} \hat{\mathbf{R}}_{N_{p2}}^{|\sigma|,t} \left(\boldsymbol{\alpha}_{N_{p2-1}}^{|\sigma|,t} \right)^{-1} \boldsymbol{\beta}_{N_{p2-1}}^{|\sigma|,t} - \left(\hat{\mathbf{P}}_{N_{p2}}^{|\sigma|,t} \right)^{-1} \mathbf{h}_{N_{p2}}^{|\sigma|,t} \left(\mathbf{g}_{N_{p2}}^{|\sigma|,t} \right)}_{\boldsymbol{\beta}_{N_{p2}}^{|\sigma|,t}}. \end{aligned}$$

Comparing this expression for $\mathbf{g}_{N_{p2}}^{|\sigma|,t}$ with the first expression in Eq.E.24, we obtain $\boldsymbol{\alpha}_{N_{p2}}^{|\sigma|,t}$ in terms of $\boldsymbol{\alpha}_{N_{p2}}^{|\sigma|,t}$:

$$\boldsymbol{\alpha}_{N_{p2}}^{|\sigma|,t} = - \left(\hat{\mathbf{P}}_{N_{p2}}^{|\sigma|,t} \right)^{-1} \left[\hat{\mathbf{Q}}_{N_{p2}}^{|\sigma|,t} + \hat{\mathbf{R}}_{N_{p2}}^{|\sigma|,t} \left(\boldsymbol{\alpha}_{N_{p2-1}}^{|\sigma|,t} \right)^{-1} \right]. \quad (\text{E.26})$$

On the other hand, from the recurrence relation, Eq.E.23, we write

$$\begin{aligned} \boldsymbol{\alpha}_{N_{p2-1}}^{|\sigma|,t} &= - \left[\mathbf{P}_{N_{p2-1}}^{|\sigma|,t} \boldsymbol{\alpha}_{N_{p2}}^{|\sigma|,t} + \mathbf{Q}_{N_{p2-1}}^{|\sigma|,t} \right]^{-1} \mathbf{R}_{N_{p2-1}}^{|\sigma|,t}, \\ \boldsymbol{\alpha}_{N_{p2-1}}^{|\sigma|,t} \left(\mathbf{R}_{N_{p2-1}}^{|\sigma|,t} \right)^{-1} &= - \left[\mathbf{P}_{N_{p2-1}}^{|\sigma|,t} \boldsymbol{\alpha}_{N_{p2}}^{|\sigma|,t} + \mathbf{Q}_{N_{p2-1}}^{|\sigma|,t} \right]^{-1}, \\ \boldsymbol{\alpha}_{N_{p2-1}}^{|\sigma|,t} \left(\mathbf{R}_{N_{p2-1}}^{|\sigma|,t} \right)^{-1} \left[\mathbf{P}_{N_{p2-1}}^{|\sigma|,t} \boldsymbol{\alpha}_{N_{p2}}^{|\sigma|,t} + \mathbf{Q}_{N_{p2-1}}^{|\sigma|,t} \right] &= -\boldsymbol{\varepsilon}, \\ \left(\mathbf{R}_{N_{p2-1}}^{|\sigma|,t} \right)^{-1} \left[\mathbf{P}_{N_{p2-1}}^{|\sigma|,t} \boldsymbol{\alpha}_{N_{p2}}^{|\sigma|,t} + \mathbf{Q}_{N_{p2-1}}^{|\sigma|,t} \right] &= - \left(\boldsymbol{\alpha}_{N_{p2-1}}^{|\sigma|,t} \right)^{-1}. \end{aligned}$$

Substituting this expression for $\left(\boldsymbol{\alpha}_{N_{p2-1}}^{|\sigma|,t} \right)^{-1}$ into Eq.E.26 provides

$$\boldsymbol{\alpha}_{N_{p2}}^{|\sigma|,t} = - \left(\hat{\mathbf{P}}_{N_{p2}}^{|\sigma|,t} \right)^{-1} \hat{\mathbf{Q}}_{N_{p2}}^{|\sigma|,t} + \left(\hat{\mathbf{P}}_{N_{p2}}^{|\sigma|,t} \right)^{-1} \hat{\mathbf{R}}_{N_{p2}}^{|\sigma|,t} \left(\mathbf{R}_{N_{p2-1}}^{|\sigma|,t} \right)^{-1} \left[\mathbf{P}_{N_{p2-1}}^{|\sigma|,t} \boldsymbol{\alpha}_{N_{p2}}^{|\sigma|,t} + \mathbf{Q}_{N_{p2-1}}^{|\sigma|,t} \right],$$

and thus we derive the following expression for $\boldsymbol{\alpha}_{N_{p2}}^{|\sigma|,t}$:

$$\begin{aligned} \boldsymbol{\alpha}_{N_{p2}}^{|\sigma|,t} &= \left[\boldsymbol{\varepsilon} - \left(\hat{\mathbf{P}}_{N_{p2}}^{|\sigma|,t} \right)^{-1} \hat{\mathbf{R}}_{N_{p2}}^{|\sigma|,t} \left(\mathbf{R}_{N_{p2-1}}^{|\sigma|,t} \right)^{-1} \mathbf{P}_{N_{p2-1}}^{|\sigma|,t} \right]^{-1} \\ &\cdot \left[- \left(\hat{\mathbf{P}}_{N_{p2}}^{|\sigma|,t} \right)^{-1} \hat{\mathbf{Q}}_{N_{p2}}^{|\sigma|,t} + \left(\hat{\mathbf{P}}_{N_{p2}}^{|\sigma|,t} \right)^{-1} \hat{\mathbf{R}}_{N_{p2}}^{|\sigma|,t} \left(\mathbf{R}_{N_{p2-1}}^{|\sigma|,t} \right)^{-1} \mathbf{Q}_{N_{p2-1}}^{|\sigma|,t} \right] \end{aligned} \quad (\text{E.27})$$

Now we use the relation for $\beta_{N_{p2}}^{|\sigma|,t}$ that comes from the above expression for $g_{N_{p2}}^{|\sigma|,t}$:

$$\beta_{N_{p2}}^{|\sigma|,t} = \left(\hat{P}_{N_{p2}}^{|\sigma|,t} \right)^{-1} \hat{R}_{N_{p2}}^{|\sigma|,t} \left(\alpha_{N_{p2-1}}^{|\sigma|,t} \right)^{-1} \beta_{N_{p2-1}}^{|\sigma|,t} - \left(\hat{P}_{N_{p2}}^{|\sigma|,t} \right)^{-1} h_{N_{p2}}^{|\sigma|,t} \left(g_{N_{p2}}^{|\sigma|,t} \right). \quad (\text{E.28})$$

From Eq.E.26 we derive

$$-\left(\hat{R}_{N_{p2}}^{|\sigma|,t} \right)^{-1} \left[\hat{P}_{N_{p2}}^{|\sigma|,t} \alpha_{N_{p2}}^{|\sigma|,t} + \hat{Q}_{N_{p2}}^{|\sigma|,t} \right] = \left(\alpha_{N_{p2-1}}^{|\sigma|,t} \right)^{-1}.$$

From the recurrence relation for trapped particles, Eq.E.23, we obtain

$$\beta_{N_{p2-1}}^{|\sigma|,t} = - \left[P_{N_{p2-1}}^{|\sigma|,t} \alpha_{N_{p2}}^{|\sigma|,t} + Q_{N_{p2-1}}^{|\sigma|,t} \right]^{-1} \left[P_{N_{p2-1}}^{|\sigma|,t} \beta_{N_{p2}}^{|\sigma|,t} + A_{N_{p2-1}}^{|\sigma|,t} \left(g_{N_{p2-1}}^{|\sigma|,t} \right) \right].$$

at $j = N_{p2} - 1$. Substituting the latter expression for $\left(\alpha_{N_{p2-1}}^{|\sigma|,t} \right)^{-1}$ into Eq.E.28:

$$\beta_{N_{p2}}^{|\sigma|,t} = - \left(\hat{P}_{N_{p2}}^{|\sigma|,t} \right)^{-1} \underbrace{\hat{R}_{N_{p2}}^{|\sigma|,t} \left(\hat{R}_{N_{p2}}^{|\sigma|,t} \right)^{-1}}_{\varepsilon} \left[\hat{P}_{N_{p2}}^{|\sigma|,t} \alpha_{N_{p2}}^{|\sigma|,t} + \hat{Q}_{N_{p2}}^{|\sigma|,t} \right] \beta_{N_{p2-1}}^{|\sigma|,t} - \left(\hat{P}_{N_{p2}}^{|\sigma|,t} \right)^{-1} h_{N_{p2}}^{|\sigma|,t} \left(g_{N_{p2}}^{|\sigma|,t} \right)$$

and then the latter expression for $\beta_{N_{p2-1}}^{|\sigma|,t}$, we find

$$\begin{aligned} \beta_{N_{p2}}^{|\sigma|,t} &= \left(\hat{P}_{N_{p2}}^{|\sigma|,t} \right)^{-1} \left[\hat{P}_{N_{p2}}^{|\sigma|,t} \alpha_{N_{p2}}^{|\sigma|,t} + \hat{Q}_{N_{p2}}^{|\sigma|,t} \right] \left[P_{N_{p2-1}}^{|\sigma|,t} \alpha_{N_{p2}}^{|\sigma|,t} + Q_{N_{p2-1}}^{|\sigma|,t} \right]^{-1} \\ &\cdot \left[P_{N_{p2-1}}^{|\sigma|,t} \beta_{N_{p2}}^{|\sigma|,t} + A_{N_{p2-1}}^{|\sigma|,t} \left(g_{N_{p2-1}}^{|\sigma|,t} \right) \right] - \left(\hat{P}_{N_{p2}}^{|\sigma|,t} \right)^{-1} h_{N_{p2}}^{|\sigma|,t} \left(g_{N_{p2}}^{|\sigma|,t} \right) \end{aligned}$$

and hence the final expression for $\beta_{N_{p2}}^{|\sigma|,t}$:

$$\begin{aligned} \beta_{N_{p2}}^{|\sigma|,t} &= \left[\varepsilon - \left(\hat{P}_{N_{p2}}^{|\sigma|,t} \right)^{-1} \left[\hat{P}_{N_{p2}}^{|\sigma|,t} \alpha_{N_{p2}}^{|\sigma|,t} + \hat{Q}_{N_{p2}}^{|\sigma|,t} \right] \left[P_{N_{p2-1}}^{|\sigma|,t} \alpha_{N_{p2}}^{|\sigma|,t} + Q_{N_{p2-1}}^{|\sigma|,t} \right]^{-1} P_{N_{p2-1}}^{|\sigma|,t} \right]^{-1} \\ &\cdot \left[\left(\hat{P}_{N_{p2}}^{|\sigma|,t} \right)^{-1} \left[\hat{P}_{N_{p2}}^{|\sigma|,t} \alpha_{N_{p2}}^{|\sigma|,t} + \hat{Q}_{N_{p2}}^{|\sigma|,t} \right] \left[P_{N_{p2-1}}^{|\sigma|,t} \alpha_{N_{p2}}^{|\sigma|,t} + Q_{N_{p2-1}}^{|\sigma|,t} \right]^{-1} A_{N_{p2-1}}^{|\sigma|,t} \left(g_{N_{p2-1}}^{|\sigma|,t} \right) - \right. \\ &\left. - \left(\hat{P}_{N_{p2}}^{|\sigma|,t} \right)^{-1} h_{N_{p2}}^{|\sigma|,t} \left(g_{N_{p2}}^{|\sigma|,t} \right) \right]. \end{aligned} \quad (\text{E.29})$$

Now we have determined $\alpha_{N_{p2}}^{|\sigma|,t}$ and $\beta_{N_{p2}}^{|\sigma|,t}$, Eqs.E.27,E.29, at the deeply trapped end, $j = N_{p2}$. Then applying the recurrence relation, Eq.E.23, we find all $\alpha_j^{|\sigma|,t}$ s and $\beta_j^{|\sigma|,t}$ s up to $\lambda = \lambda_t$ ($j = 0$) from the trapped side (see Fig.4.1). Note: in the secondary mode problem [95, 96] we determine all alphas and betas in the trapped and passing regions up

to the trapped-passing boundary (the values of the coefficients in the equation evaluated exactly at the trapped-passing boundary are excluded from the derivations). In addition, $\alpha_{N_{p2}}^{|\sigma|,t}$ and $\beta_{N_{p2}}^{|\sigma|,t}$ allows $\mathbf{g}_{N_{p2}}^{|\sigma|,t}$ to be determined. Indeed, we find

$$\alpha_{N_{p2-1}}^{|\sigma|,t} = - \left[\mathbf{P}_{N_{p2-1}}^{|\sigma|,t} \alpha_{N_{p2}}^{|\sigma|,t} + \mathbf{Q}_{N_{p2-1}}^{|\sigma|,t} \right]^{-1} \mathbf{R}_{N_{p2-1}}^{|\sigma|,t}$$

and

$$\beta_{N_{p2-1}}^{|\sigma|,t} = - \left[\mathbf{P}_{N_{p2-1}}^{|\sigma|,t} \alpha_{N_{p2}}^{|\sigma|,t} + \mathbf{Q}_{N_{p2-1}}^{|\sigma|,t} \right]^{-1} \left[\mathbf{P}_{N_{p2-1}}^{|\sigma|,t} \beta_{N_{p2}}^{|\sigma|,t} + \mathbf{A}_{N_{p2-1}}^{|\sigma|,t} \left(\mathbf{g}_{N_{p2-1}}^{|\sigma|,t} \right) \right]$$

immediately from $\alpha_{N_{p2}}^{|\sigma|,t}$ and $\beta_{N_{p2}}^{|\sigma|,t}$. For the distribution function we write

$$\mathbf{g}_{N_{p2-1}}^{|\sigma|,t} = \left(\alpha_{N_{p2}}^{|\sigma|,t} \right)^{-1} \left[\mathbf{g}_{N_{p2}}^{|\sigma|,t} - \beta_{N_{p2}}^{|\sigma|,t} \right]$$

at $j = N_{p2} - 1$ from the first expression in Eq.E.24 and Eq.E.25 at $j = N_{p2} - 2$. Also, we employ the equation, Eq.E.7, evaluated at $j = N_{p2} - 1$:

$$\mathbf{P}_{N_{p2-1}}^{|\sigma|,t} \mathbf{g}_{N_{p2}}^{|\sigma|,t} + \mathbf{Q}_{N_{p2-1}}^{|\sigma|,t} \mathbf{g}_{N_{p2-1}}^{|\sigma|,t} + \mathbf{R}_{N_{p2-1}}^{|\sigma|,t} \mathbf{g}_{N_{p2-2}}^{|\sigma|,t} + \mathbf{A}_{N_{p2-1}}^{|\sigma|,t} \left(\mathbf{g}_{N_{p2-1}}^{|\sigma|,t} \right) = 0.$$

Substituting the above expression for $\mathbf{g}_{N_{p2-2}}^{|\sigma|,t}$, Eq.E.25, into Eq.E.7 at $j = N_{p2} - 1$

$$\begin{aligned} & \mathbf{P}_{N_{p2-1}}^{|\sigma|,t} \mathbf{g}_{N_{p2}}^{|\sigma|,t} + \left[\mathbf{Q}_{N_{p2-1}}^{|\sigma|,t} + \mathbf{R}_{N_{p2-1}}^{|\sigma|,t} \left(\alpha_{N_{p2-1}}^{|\sigma|,t} \right)^{-1} \right] \mathbf{g}_{N_{p2-1}}^{|\sigma|,t} - \\ & \mathbf{R}_{N_{p2-1}}^{|\sigma|,t} \left(\alpha_{N_{p2-1}}^{|\sigma|,t} \right)^{-1} \beta_{N_{p2-1}}^{|\sigma|,t} + \mathbf{A}_{N_{p2-1}}^{|\sigma|,t} \left(\mathbf{g}_{N_{p2-1}}^{|\sigma|,t} \right) = 0 \end{aligned}$$

and then inserting the latter expression for $\mathbf{g}_{N_{p2-1}}^{|\sigma|,t}$, we find the final expression for $\mathbf{g}_{N_{p2}}^{|\sigma|,t}$:

$$\begin{aligned} \mathbf{g}_{N_{p2}}^{|\sigma|,t} &= \left[\mathbf{P}_{N_{p2-1}}^{|\sigma|,t} + \left[\mathbf{Q}_{N_{p2-1}}^{|\sigma|,t} + \mathbf{R}_{N_{p2-1}}^{|\sigma|,t} \left(\alpha_{N_{p2-1}}^{|\sigma|,t} \right)^{-1} \right] \left(\alpha_{N_{p2}}^{|\sigma|,t} \right)^{-1} \right]^{-1} \cdot \\ & \cdot \left[\left[\mathbf{Q}_{N_{p2-1}}^{|\sigma|,t} + \mathbf{R}_{N_{p2-1}}^{|\sigma|,t} \left(\alpha_{N_{p2-1}}^{|\sigma|,t} \right)^{-1} \right] \left(\alpha_{N_{p2}}^{|\sigma|,t} \right)^{-1} \beta_{N_{p2}}^{|\sigma|,t} + \mathbf{R}_{N_{p2-1}}^{|\sigma|,t} \left(\alpha_{N_{p2-1}}^{|\sigma|,t} \right)^{-1} \beta_{N_{p2-1}}^{|\sigma|,t} \right. \\ & \left. - \mathbf{A}_{N_{p2-1}}^{|\sigma|,t} \left(\mathbf{g}_{N_{p2-1}}^{|\sigma|,t} \right) \right]. \end{aligned}$$

This expression for $\mathbf{g}_{N_{p2}}^{|\sigma|,t}$ can be used to test the solution in the trapped region, $\mathbf{g}_j^{|\sigma|,t}$ at each point in λ, j , reconstructed from the linear approximation, Eq.E.21.

Once the layer solution is found and all $\alpha_j^{\sigma,p/|\sigma|,t}$ s and $\beta_j^{\sigma,p/|\sigma|,t}$ s are obtained from the passing and the trapped sides, we reconstruct the rest solution elements from Eqs.E.11,E.21 up to the passing/trapped external edges, i.e. $\lambda = \lambda_p(j = N_{p1})$ / $\lambda = \lambda_t(j = 0)$, respectively. The described solution technique is illustrated in Fig.4.1 of Chapter IV. Note: in the NTM problem, matching at the trapped-passing boundary, Eq.3.1, is provided by the layer solution found in Chapter III.

E.6.3 Matching at the trapped-passing boundary

In the vicinity of λ_c collisional dissipation becomes important, and the perturbative approach becomes invalid. Thus, we introduce the collisional dissipation layer to provide matching between $\mathbf{g}_j^{\sigma,p}$ and $\mathbf{g}_j^{|\sigma|,t}$ in external regions. The layer solution calculated at λ_p ($j = N_{p1}$) is used as a starting point to reconstruct $\mathbf{g}_j^{\sigma,p}$ from Eq.E.11 up to the deeply passing end, $\mathbf{g}_0^{\sigma,p}$. The trapped part of the layer solution at $\lambda = \lambda_t$ ($j = 0$) is a starting point to determine $\mathbf{g}_j^{|\sigma|,t}$ from Eq.E.21 up to the deeply trapped end, $\mathbf{g}_{N_{p2}}^{|\sigma|,t}$.

The technique described above is also to be applied to the secondary mode problem. Here matching is provided exactly at the trapped-passing boundary. To make the above derivations of the numerical grid consistent, we keep the already introduced notations in this subsection. However, we have to highlight that the passing region in the NTM problem, i.e. $\lambda < \lambda_c$, corresponds in this derivations to the region of particles trapped in phase space in the secondary mode problem, i.e. $H_0 < H_0^c$ and vice versa.

The function and its first derivative are required to be continuous across the trapped-passing boundary, i.e. g_j and f_j should be of class \mathbf{C}^1 . Matching is given by Eq.3.1, which reads

$$\begin{aligned} \mathbf{g}_{N_{p1}}^{+1,p} &= \mathbf{g}_{N_{p1}}^{-1,p}, \\ \mathbf{g}_{N_{p1}}^{+1,p} + \mathbf{g}_{N_{p1}}^{-1,p} &= 2\mathbf{g}_0^{|\sigma|,t}, \\ \frac{3\mathbf{g}_{N_{p1}}^{+1,p} - 4\mathbf{g}_{N_{p1}-1}^{+1,p} + \mathbf{g}_{N_{p1}-2}^{+1,p} + 3\mathbf{g}_{N_{p1}}^{-1,p} - 4\mathbf{g}_{N_{p1}-1}^{-1,p} + \mathbf{g}_{N_{p1}-2}^{-1,p}}{2\Delta\lambda_p} &= 2\frac{-\mathbf{g}_2^{|\sigma|,t} + 4\mathbf{g}_1^{|\sigma|,t} - 3\mathbf{g}_0^{|\sigma|,t}}{2\Delta\lambda_t}. \end{aligned} \tag{E.30}$$

Here $j = N_{p1}$ / $j = 0$ corresponds to the trapped-passing boundary as shown in Fig.A1 of

[96] (note: in the NTM problem $j = N_{p1}$ corresponds to $\lambda = \lambda_p$). The first two conditions provide

$$\mathbf{g}_{N_{p1}}^{+1,p} = \mathbf{g}_{N_{p1}}^{-1,p} = \mathbf{g}_0^{|\sigma|,t} \equiv \mathbf{g}_c. \quad (\text{E.31})$$

Inserting Eq.E.31 into Eq.E.30, we obtain

$$6 \left[1 + \frac{\Delta\lambda_p}{\Delta\lambda_t} \right] \mathbf{g}_c = -\frac{2\Delta\lambda_p}{\Delta\lambda_t} \mathbf{g}_2^{|\sigma|,t} + \frac{8\Delta\lambda_p}{\Delta\lambda_t} \mathbf{g}_1^{|\sigma|,t} + 4\mathbf{g}_{N_{p1}-1}^{+1,p} - \mathbf{g}_{N_{p1}-2}^{+1,p} + 4\mathbf{g}_{N_{p1}-1}^{-1,p} - \mathbf{g}_{N_{p1}-2}^{-1,p}. \quad (\text{E.32})$$

Now we apply the linear approximation, Eq.E.11, at $j = N_{p1} - 1$ and $j = N_{p1} - 2$ in the passing region and Eq.E.21, at $j = 1$ and $j = 2$ from the side of trapped particles to write

$$\begin{aligned} \mathbf{g}_{N_{p1}-1}^{\sigma,p} &= \alpha_{N_{p1}-1}^{\sigma,p} \mathbf{g}_{N_{p1}}^{\sigma,p} + \beta_{N_{p1}-1}^{\sigma,p} = \alpha_{N_{p1}-1}^{\sigma,p} \mathbf{g}_c + \beta_{N_{p1}-1}^{\sigma,p}, \\ \mathbf{g}_{N_{p1}-2}^{\sigma,p} &= \alpha_{N_{p1}-2}^{\sigma,p} \mathbf{g}_{N_{p1}-1}^{\sigma,p} + \beta_{N_{p1}-2}^{\sigma,p} \end{aligned}$$

with $\sigma = \pm 1$ and

$$\begin{aligned} \mathbf{g}_1^{|\sigma|,t} &= \alpha_1^{|\sigma|,t} \mathbf{g}_0^{|\sigma|,t} + \beta_1^{|\sigma|,t} = \alpha_1^{|\sigma|,t} \mathbf{g}_c + \beta_1^{|\sigma|,t}, \\ \mathbf{g}_2^{|\sigma|,t} &= \alpha_2^{|\sigma|,t} \mathbf{g}_1^{|\sigma|,t} + \beta_2^{|\sigma|,t}. \end{aligned}$$

First, substituting $\mathbf{g}_{N_{p1}-2}^{\sigma,p}$ and $\mathbf{g}_2^{|\sigma|,t}$ into Eq.E.32, we write

$$\begin{aligned} 6 \left[1 + \frac{\Delta\lambda_p}{\Delta\lambda_t} \right] \mathbf{g}_c &= \left[-\frac{2\Delta\lambda_p}{\Delta\lambda_t} \alpha_2^{|\sigma|,t} + \frac{8\Delta\lambda_p}{\Delta\lambda_t} \right] \mathbf{g}_1^{|\sigma|,t} + \\ &+ \left[4\mathcal{E} - \alpha_{N_{p1}-2}^{+1,p} \right] \mathbf{g}_{N_{p1}-1}^{+1,p} + \left[4\mathcal{E} - \alpha_{N_{p1}-2}^{-1,p} \right] \mathbf{g}_{N_{p1}-1}^{-1,p} - \frac{2\Delta\lambda_p}{\Delta\lambda_t} \beta_2^{|\sigma|,t} - \beta_{N_{p1}-2}^{+1,p} - \beta_{N_{p1}-2}^{-1,p}. \end{aligned} \quad (\text{E.33})$$

Then we substitute $\mathbf{g}_{N_{p1}-1}^{\sigma,p}$ and $\mathbf{g}_1^{|\sigma|,t}$ into Eq.E.33 to obtain the trapped-passing boundary element of the solution:

$$\begin{aligned} \mathbf{g}_c &= \left[6 \left(1 + \frac{\Delta\lambda_p}{\Delta\lambda_t} \right) - \left(\frac{8\Delta\lambda_p}{\Delta\lambda_t} - \frac{2\Delta\lambda_p}{\Delta\lambda_t} \alpha_2^{|\sigma|,t} \right) \alpha_1^{|\sigma|,t} \right. \\ &- \left. \left(4\mathcal{E} - \alpha_{N_{p1}-2}^{+1,p} \right) \alpha_{N_{p1}-1}^{+1,p} - \left(4\mathcal{E} - \alpha_{N_{p1}-2}^{-1,p} \right) \alpha_{N_{p1}-1}^{-1,p} \right]^{-1} \\ &\cdot \left[\left(-\frac{2\Delta\lambda_p}{\Delta\lambda_t} \alpha_2^{|\sigma|,t} + \frac{8\Delta\lambda_p}{\Delta\lambda_t} \right) \beta_1^{|\sigma|,t} + \left(4\mathcal{E} - \alpha_{N_{p1}-2}^{+1,p} \right) \beta_{N_{p1}-1}^{+1,p} + \left(4\mathcal{E} - \alpha_{N_{p1}-2}^{-1,p} \right) \beta_{N_{p1}-1}^{-1,p} \right. \\ &- \left. \frac{2\Delta\lambda_p}{\Delta\lambda_t} \beta_2^{|\sigma|,t} - \beta_{N_{p1}-2}^{+1,p} - \beta_{N_{p1}-2}^{-1,p} \right]. \end{aligned} \quad (\text{E.34})$$

This expression can be simplified provided $\Delta\lambda_p = \Delta\lambda_t$. In the secondary mode problem Eq.E.34 is used to provide matching across the trapped-passing boundary. \mathbf{g}_c is a starting point to construct $\mathbf{g}_j^{\sigma,p}/\mathbf{g}_j^{|\sigma|,t}$ up to the deeply passing/trapped end from Eq.E.11/Eq.E.21, respectively.

To solve the reduced equation, Eq.18, in [96], Eq.E.34 is to be applied in its scalar form. $\mathbf{g}_j^{\sigma,p}$ and $\mathbf{g}_j^{|\sigma|,t}$ become scalars at each point in H_0 , j . To solve Eq.14 in [96], we have to keep both σ branches in the trapped region in H_0 space and thus Eq.E.30 is to be replaced by Eq.A.8 of [96]. Note: in the secondary mode problem, σ, p is to be replaced by $|\sigma|, t$ in Eq.E.34 and vice versa.

E.7 Block diagram

A detailed block diagram is presented in Fig.E.1.

- Step 1: generate grids in phase space and enter input parameters. INPUTS:

SPLINE SETTINGS for RectBivariateSpline

MAGNETIC FIELD: B_0 , toroidal and poloidal field components. The poloidal field component is to be introduced in a large aspect ratio, shifted circular model/finite aspect ratio non-circular model for the poloidal cross section ¹⁰⁴ (included in a code but left beyond the scope of the presented study) [117].

TOKAMAK PARAMETERS: ε , R_0 , a in a small inverse aspect ratio circular cross section conventional tokamak approximation; Shafranov shift $\Delta(r)$, elongation κ , triangularity δ , $\partial_r\psi$, S_κ , S_δ from Miller's model (included in a code but left beyond the scope of the presented study) [117].

ADDITIONAL EQUILIBRIUM SETTINGS: internal inductance l_i and tokamak poloidal beta β_ϑ required for $\partial_r R_0$ from Miller's model

CHARACTERISTIC LENGTH SCALES and VELOCITY: L_q , L_{n0} , L_{Tj} , L_B ,
 $\eta_j = L_{n0}/L_{Tj}$, \hat{V}_j

¹⁰⁴A large aspect ratio, shifted circular model is fully implemented in a code, while the finite aspect ratio non-circular model requires a more detailed treatment of corrections of order ε^2 and higher. Terms of order ε^2 do not provide a significant impact on our current results but are important to study the curvature effects.

FREQUENCIES: $\hat{\nu}_i, \omega_E$, mass ratio m_i/m_e

POLOIDAL LARMOR RADIUS AND MAGNETIC ISLAND WIDTH: $\rho_{\vartheta i}, w, \psi_s$

- Step 2: introduce a model form of the electrostatic potential that is to be used at the 0th iteration in Φ . $\Phi \propto \omega_E \psi$ corresponds to its equilibrium distribution, i.e. in the absence of the magnetic island. Calculate the electrostatic potential term, $(-1/2) \left\langle \rho_{\vartheta j} \hat{\Phi} / V_{\parallel} \right\rangle_{\vartheta}^{p_{\varphi}}$, for passing and trapped particles.
- Step 3: (re)define the S grid. S depends on the form of the electrostatic potential and thus is to be updated at each iteration in Φ . For passing particles, the location of the S island separatrix is updated. For trapped particles, we check if there is an island-like structure for certain Φ . If the answer is positive, we apply the same technique we use for passing particles to trapped particles. If the answer is negative, we repeat the procedure we use at the 0th iteration in Φ when S is proportional to p_{φ} ¹⁰⁵.
- Step 4: replace $S^{\pm/t}$ with $y^{\pm/t}$ to provide Neumann boundary at infinity, far from the magnetic island.
- Step 5: calculate the inverse function, $p_{\varphi} = p_{\varphi}(y^{\pm/t})$, i.e. solve the transcendental equation $y^{\pm/t} = y^{\pm/t}(p_{\varphi})$ for p_{φ} at each ξ, λ and V ¹⁰⁶. The $y^{\pm/t}$ grid is to be updated at each iteration in the electrostatic potential.
- Step 6: calculate the \mathcal{A} coefficient for $\sigma = \pm/t$.
- Step 7: find layer solution (including moments of the particle distribution function and the electro-magnetic field Lagrangian in the layer).
- Step 8: The LAYER_SOLVER provides matching at fixed p_{φ} and thus determines the ion/electron distribution function as a function of p_{φ}, ξ and λ . To move further and use the layer solution as a starting point to find the external solution in $\{S, \lambda, V; \sigma\}$ space, we have to switch from p_{φ} to S in the layer solution. $g_j = g_j(p_{\varphi})$ is equivalent to two branches of $g_j = g_j(S)$, i.e. for $\sigma_{p_{\varphi}} \gtrless 0$.

¹⁰⁵There is no island structure in the trapped branch for plasma and tokamak parameters we consider.

¹⁰⁶The existence of this function is not generally guaranteed. The INVERSE_FUNCTION subroutine has been tested: in the absence of the electrostatic potential and for certain model forms of Φ , the numerical solution of $y^{\pm/t} = y^{\pm/t}(p_{\varphi})$ for p_{φ} matches known analytic expressions.

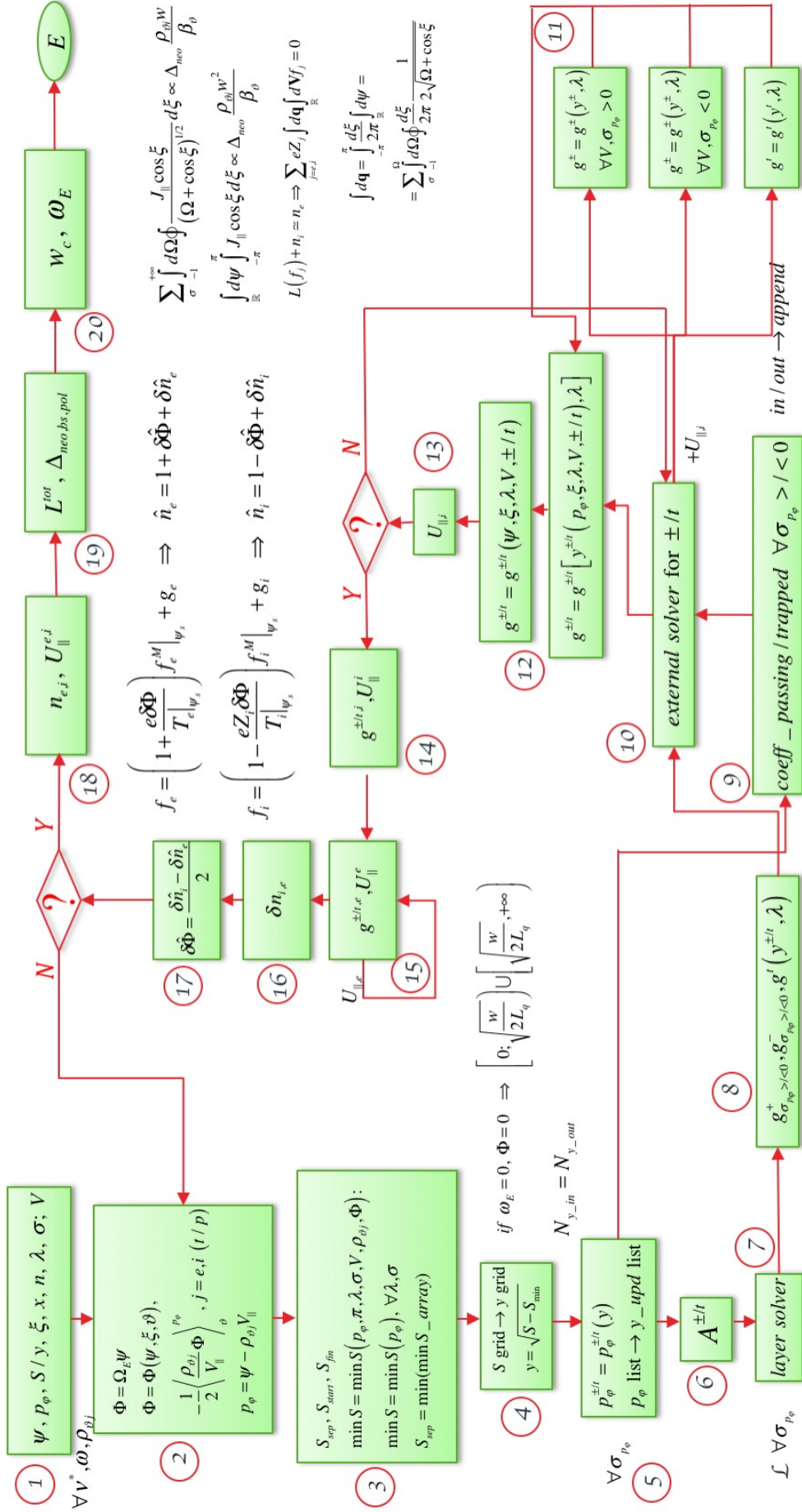


Figure E.1: Block diagram

- Step 9: find coefficients of Eqs.D.60,D.61 ¹⁰⁷.
- Step 10: Use the procedure described above in Appendix E to reconstruct the external solution in passing and trapped regions up to the deeply passing/trapped ends.
- Step 11: find solution as a function of y and λ for each σ_{p_φ} , σ and V inside and outside the drift island.
- Step 12: switch from $y^{\pm/t}$ to p_φ and then from p_φ to ψ to reconstruct the flows.
- Step 13: calculate the momentum conservation term in the collision operator. We iterate over it until it converges.
- Step 14: save results for the ion plasma component.
- Step 15: repeat the above procedure (steps 2-14) for electrons. The electron solution depends on the ion distribution function since the electron-electron collisions are comparable to the electron-ion collisions.
- Step 16: calculate density perturbations.
- Step 17: calculate the electrostatic potential from the plasma quasi-neutrality condition. We have to iterate over it until it converges. A total number of iterations depends on $\rho_{\partial i}/w$ and ω_E as both provide steepening of the particle distribution inside the magnetic island.
- Step 18: calculate total density and flows. $J_{\parallel} = eZ_i u_{\parallel i} - e u_{\parallel e}$.
- Step 19: calculate the total Lagrangian and the MRE contributions.
- Step 20: determine the critical magnetic island width and the island propagation frequency. Check if the polarisation current contribution is stabilising/destabilising at given ω .

¹⁰⁷Steps 7 and 9 are simultaneous.

F Figures not included in the main part

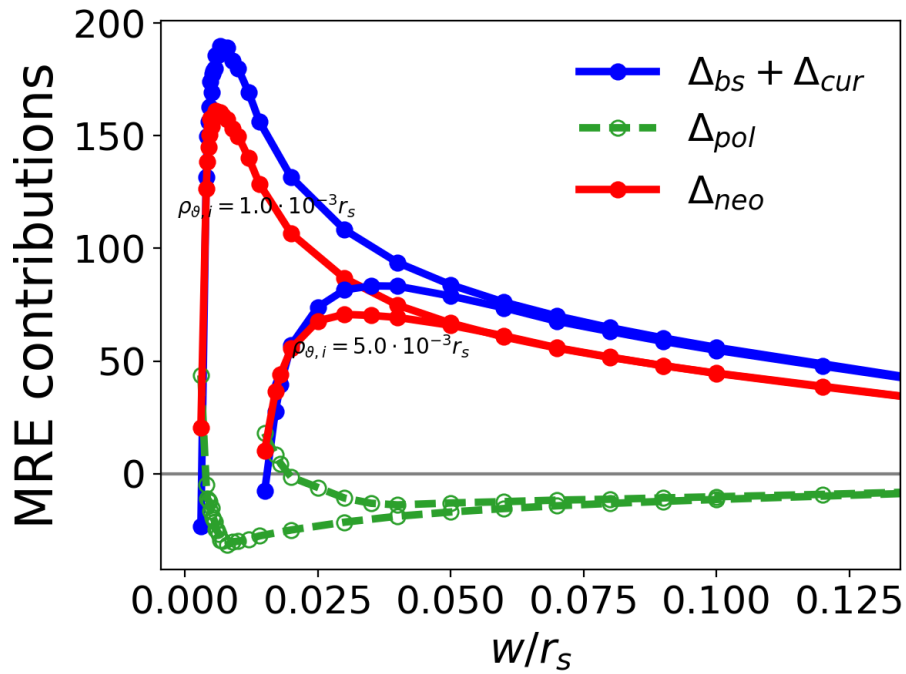


Figure F.1: The neoclassical MRE contributions to the island time evolution for different $\rho_{\theta,i}$.

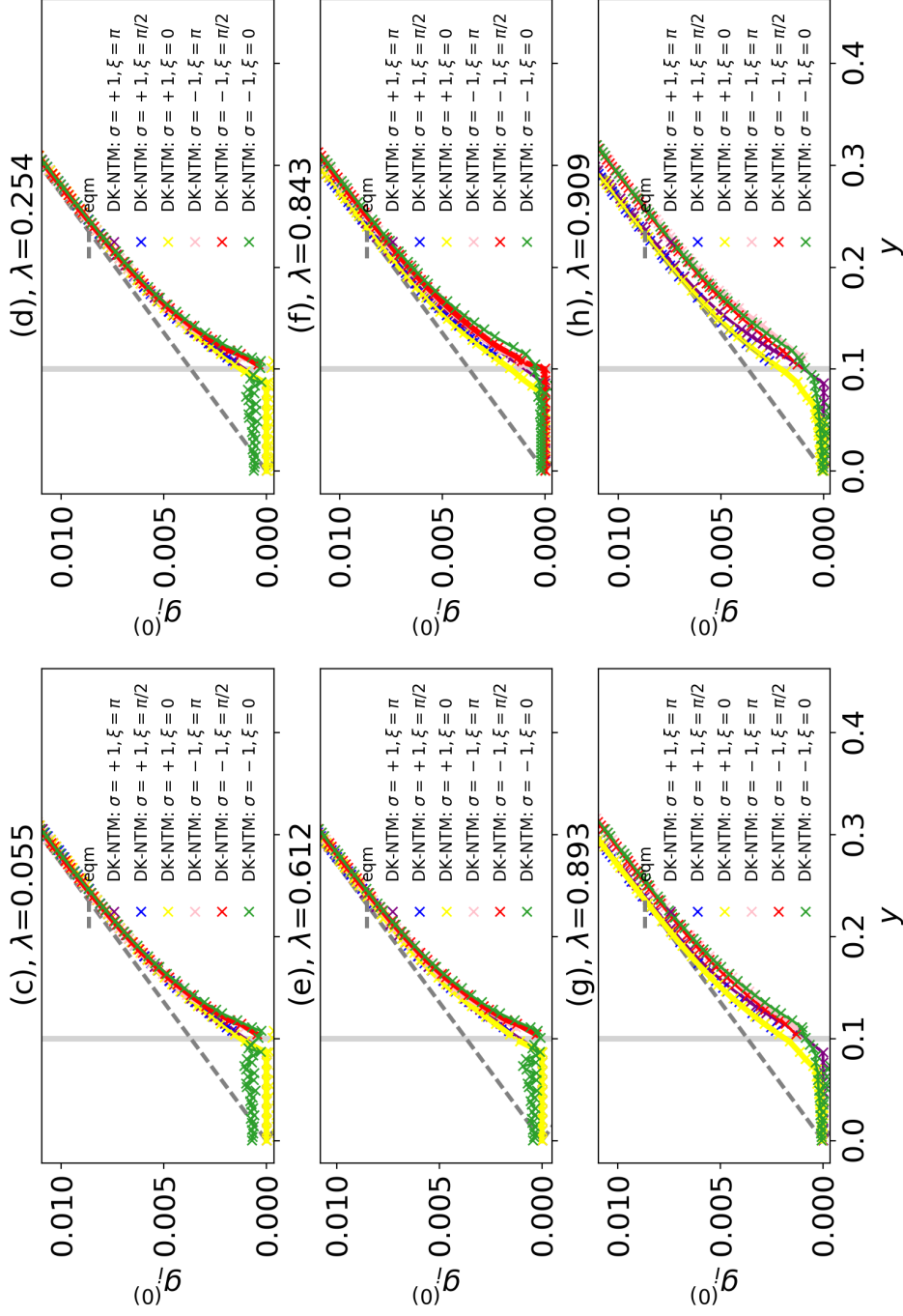


Figure F.2: Zoom of Fig.4.4(c)-(h) in the vicinity of the S island, $\sigma = \pm 1, \sigma_{p\varphi} = +1$. The ξ dependence of $g_i^{(0)}$ for each σ is weak outside the dissipative layer, (c)-(e), and becomes significant close to the trapped-passing boundary, (f)-(h).

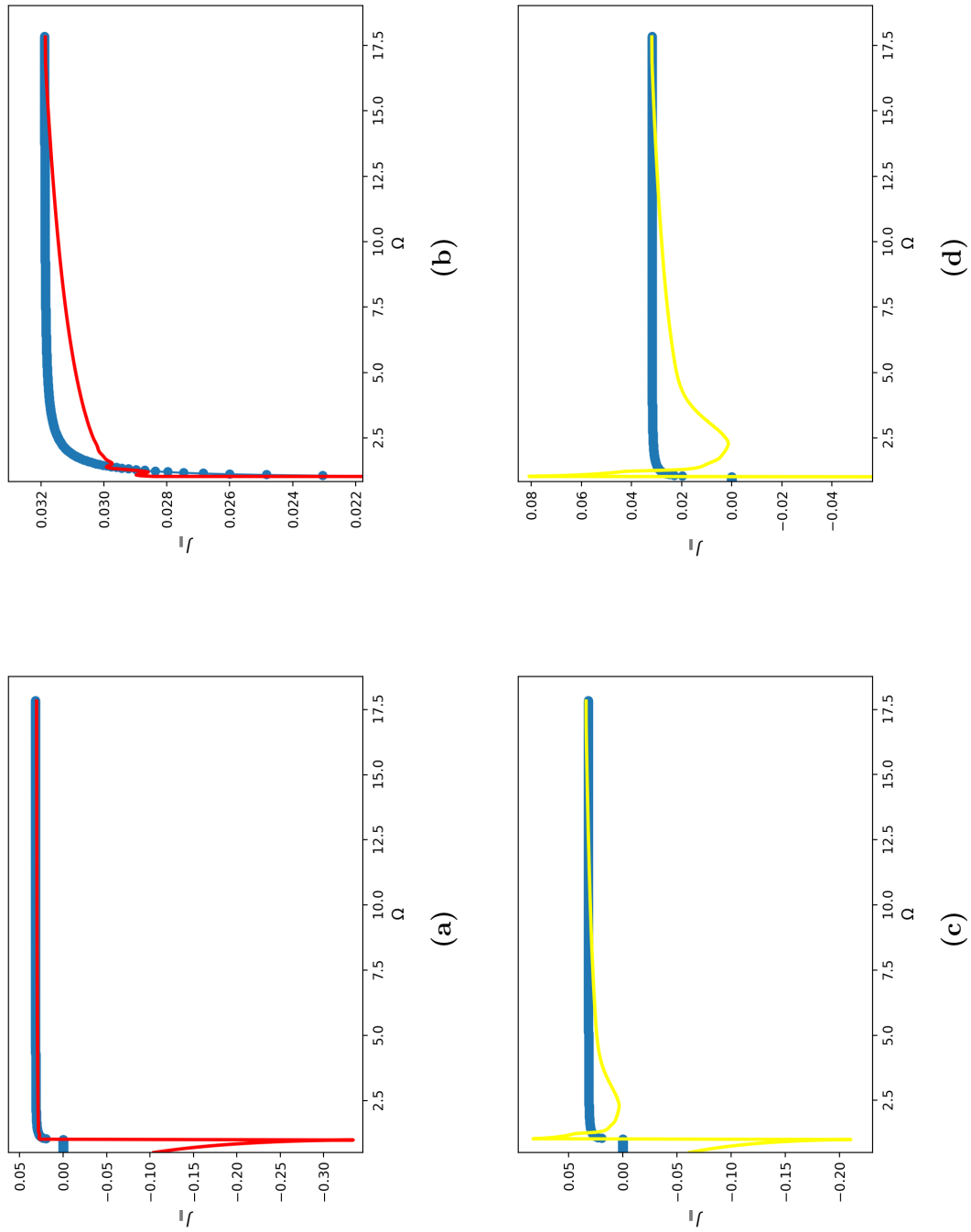


Figure F.3: Orbit-averaged parallel current density perturbation plotted against Ω in the vicinity of the magnetic island separatrix for small $\rho_{0i}/w = 0.05$ (a) and large $\rho_{0i}/w = 0.33$ (c). (b)/(d) Zoom of (a)/(c) far from the magnetic island, respectively. Blue curves indicate an analytic limit far from the magnetic island obtained in [53]. Here the maximum value of ψ is $2.9w$, i.e. 1.45 island widths.

G Stability analysis of secondary modes, driven by a phase space island: appendix

G.1 Resonant and non-resonant forms of the secondary mode dispersion relation

In this appendix we demonstrate that Eqs.5.51,5.52 and Eq.5.53 are equivalent. The most convenient way is to compare resonant contributions with the perturbed EP distribution function, $g_{j\omega}$, given by Eqs.5.34/5.39 with Eq.5.40 and Eqs.5.45,5.47. Substituting Eqs.5.47,5.49 into Eq.5.45 yields

$$g_{j\omega}(\alpha, H_0; \sigma_p) = - \sum_{n \in \mathbb{Z}} \frac{\delta\omega}{\delta\omega - n\Omega_b + i0^+} \frac{\partial f_{0,j}}{\partial H_0} h_{k\omega} e^{in\alpha} \int_{-\pi}^{\pi} \frac{d\alpha'}{2\pi} e^{i(l\xi' - n\alpha')}. \quad (\text{G.1})$$

Applying the Landau relation, which reads

$$\frac{1}{\delta\omega - n\Omega_b + i0^+} = -i \int_{\mathbb{R}^+} e^{i(\delta\omega - n\Omega_b)\sigma} d\sigma, \quad (\text{G.2})$$

and then employing the following expression for the Shah function:

$$\sum_{n \in \mathbb{Z}} e^{in(\alpha - \alpha' - \Omega_b\sigma)} = 2\pi \sum_{k \in \mathbb{Z}} \delta(\alpha - \alpha' - \Omega_b\sigma - 2\pi k) \quad (\text{G.3})$$

we rewrite the above formula to obtain

$$g_{j\omega}(\alpha, H_0; \sigma_p) = 2\pi i \delta\omega \frac{\partial f_{0,j}}{\partial H_0} h_{k\omega} \sum_{n \in \mathbb{Z}} \int_{\mathbb{R}^+} d\sigma \int_{-\pi}^{\pi} \frac{d\alpha'}{2\pi} e^{i(l\xi' + \delta\omega\sigma)} \delta(\alpha - \alpha' - \Omega_b\sigma - 2\pi n), \quad (\text{G.4})$$

which, in turn, can be written as

$$g_{j\omega}(\alpha, H_0; \sigma_p) = 2\pi i \frac{\delta\omega}{\Omega_b} \frac{\partial f_{0,j}}{\partial H_0} h_{k\omega} \sum_{n \in \mathbb{Z}} \int_{-\pi/2}^{3\pi/2} \frac{d\alpha'}{2\pi} \exp \left[i \left(l\xi' + \delta\omega \frac{\alpha - \alpha' + 2\pi n}{\Omega_b} \right) \right] \cdot \Theta \left(\frac{\alpha - \alpha' + 2\pi n}{\Omega_b} \right). \quad (\text{G.5})$$

Here we have shifted the limits of integration in accordance with the limit operation for a periodic function, and replaced n with $-n$ due to periodicity. Let us take $\Omega_b > 0$ ¹⁰⁸. As $\alpha, \alpha' \in [-\pi/2; 3\pi/2]$, $\alpha - \alpha' \in [-2\pi; 2\pi]$. For $n \leq -1$ the Heaviside function returns zero. If $n = 0$, then $\alpha' \in [-\pi/2; \alpha]$. If $n = 1$, the Heaviside function returns one. Thus,

$$g_{j\omega}(\alpha, H_0; \sigma_p) = 2\pi i \frac{\delta\omega}{\Omega_b} \frac{\partial f_{0,j}}{\partial H_0} h_{k\omega} \int_{-\pi/2}^{\alpha} \frac{d\alpha'}{2\pi} \exp \left[i \left(l\xi' + \delta\omega \frac{\alpha - \alpha'}{\Omega_b} \right) \right] + 2\pi i \frac{\delta\omega}{\Omega_b} \frac{\partial f_{0,j}}{\partial H_0} h_{k\omega} \sum_{n=1}^{+\infty} \int_{-\pi}^{\pi} \frac{d\alpha'}{2\pi} \exp \left[i \left(l\xi' + \delta\omega \frac{\alpha - \alpha' + 2\pi n}{\Omega_b} \right) \right]. \quad (\text{G.6})$$

Employing Eq.5.41, we finally obtain

$$g_{j\omega}(\alpha, H_0; \sigma_p) = 2\pi i \frac{\delta\omega}{\Omega_b} \frac{\partial f_{0,j}}{\partial H_0} h_{k\omega} \left\{ \int_{-\pi/2}^{\alpha} \frac{d\alpha'}{2\pi} \exp \left[i \left(l\xi' + \delta\omega \frac{\alpha - \alpha'}{\Omega_b} \right) \right] + \frac{\int_{-\pi}^{\pi} \frac{d\alpha'}{2\pi} \exp \left[i \left(l\xi' + \delta\omega \frac{\alpha - \alpha'}{\Omega_b} \right) \right]}{\exp \left(-2\pi i \frac{\delta\omega}{\Omega_b} \right) - 1} \right\}, \quad (\text{G.7})$$

which is exactly Eqs.5.39,5.40.

¹⁰⁸The same analysis can be produced when $\Omega_b < 0$.

Abbreviations

DK-NTM Drift kinetic NTM solver: finds a solution of the orbit-averaged drift kinetic equation to leading order in Δ , i.e. Eq.2.35 for a full range of the pitch angle variation. The electrostatic potential is calculated self-consistently from the plasma quasi-neutrality condition. DK-NTM with model analytic electrons has been developed in [73, 93, 74]. Its numerical scheme and numerical algorithm can be found in [74]. DK-NTM that treats electrons similar to RDK-NTM is under development by K. Imada.

ECCD Electron cyclotron current drive

ECRH Electron cyclotron resonance heating

EP Energetic particle

H96 An analytic drift kinetic solution valid in the limit of large islands outside the magnetic island separatrix. It implies a model radial diffusion. It has been found in [53].

ICCD Ion cyclotron current drive

ICF Inertial confinement fusion

ICRH Ion cyclotron resonance heating

LHCD Lower hybrid current drive

MCF Magnetic confinement fusion

MHD Magnetohydrodynamics

NBI Neutral beam injection

NTM Neoclassical tearing mode

OH Ohmic heating

RDK-NTM Reduced drift kinetic NTM solver: finds a solution of the reduced orbit-averaged drift kinetic equation to leading order in Δ , i.e. Eq.2.35 in the dissipative layer and Eq.2.40 outside the layer. The electrostatic potential is calculated self-consistently from the plasma quasi-neutrality condition. RDK-NTM has been developed in this dissertation. Its numerical scheme and numerical algorithm can be found in Sec.4 and Appendix E.

References

- [1] United Nations, DESA, Population division, 2019. URL <https://population.un.org/wpp/Download/Standard/Population/>
- [2] International Energy Agency, 2018. URL <https://webstore.iea.org/world-energy-balances-2018>
- [3] Atmospheric CO_2 data, URL http://scrippsco2.ucsd.edu/data/atmospheric_co2/icecore_merged_products
- [4] Carbon Dioxide Information Analysis Center, 2019. URL https://cdiac.ess-dive.lbl.gov/CO2_Emission/
- [5] Corinne Le Quéré, Robbie M. Andrew, Pierre Friedlingstein et al. *Earth Syst. Sci. Data* **10** (2018) 2141-2194. URL <https://doi.org/10.5194/essd-10-2141-2018>
- [6] URL ftp://aftp.cmdl.noaa.gov/products/trends/co2/co2_mm_mlo.txt
- [7] ITER official web site, URL <https://www.iter.org/mach/Blanket>
- [8] J. D. Lawson *Proc. Phys. Soc. B* **70** (1957) 6.
- [9] V. A. Rozhansky *Teoria Plasmi Lan'* (2012) 320.
- [10] R. J. DiPerna and P. L. Lions *Annals of Mathematics* **130** (1989) 321-366.
- [11] R. Fitzpatrick *Plasma Physics: An Introduction* CRC Press, Taylor and Francis Group (2014) ISBN: 978-1-4665-9426-5.
- [12] J. Wesson *Tokamaks* Clarendon Press, third edition (2004) ISBN: 0-19-8509227.
- [13] P. Helander and D. J. Sigmar *Collisional Transport in Magnetized Plasmas* Cambridge University Press (2002) 292.
- [14] N. G. Lehtinen *Elementary Plasma Physics* Lecture 23: Kinetics of driven plasmas I: Fokker-Planck equation (FPE) (2010) URL <http://nlpc.stanford.edu/nleht/Science/reference/kinetics.pdf> and references therein.
- [15] R. D. Hazeltine *Plasma Physics* **15** (1973) 77.

- [16] F. I. Parra *Drift kinetics* research notes, Rudolf Peierls Centre for Theoretical Physics, University of Oxford (2019) URL http://www-thphys.physics.ox.ac.uk/people/FelixParra/CollisionlessPlasmaPhysics/notes/lecII_driftkinetics.pdf
- [17] R. D. Hazeltine and J. D. Meiss *Plasma Confinement* Addison-Wesley, New York (1992) 113.
- [18] S. Cowley *Gyro-Kinetics Lectures. From ITER Time-scales to Gyro-Kinetics* lecture notes URL https://www-thphys.physics.ox.ac.uk/people/AlexanderSchekochihin/wpi/workshop3_pdfs/cowley.pdf and references therein.
- [19] F. I. Parra *Braginskii fluid equations* research notes, Rudolf Peierls Centre for Theoretical Physics, University of Oxford (2019) URL http://www-thphys.physics.ox.ac.uk/people/FelixParra/CollisionalPlasmaPhysics/notes/lecIV_braginskii.pdf
- [20] S. Chapman, T. G. Cowling *The Mathematical Theory of Non-Uniform Gases* Cambridge University Press, third edition (1970).
- [21] V. D. Shafranov *Zhurnal Experimentalnoi i Teoreticheskoi Fiziki* **33** (1957) 710 and *Sov. Phys. J.E.T.P.* **6** (1958) 545.
- [22] H. Grad and H. Rubin *Hydromagnetic equilibria and force-free fields* in *Proceedings of the Second United Nations International Conference on the Peaceful Uses of Atomic Energy* United Nations, Geneva, Vol. 32 (1958) p. 42.
- [23] V. D. Shafranov *J. Nucl. Energy, Part C Plasma Phys.* **5** (1963) 251.
- [24] V. D. Shafranov *Plasma equilibrium in a magnetic field* in *Reviews of Plasma Physics* (edited by M. A. Leontovich) Consultants Bureau, New York, Vol. 2 (1966) p. 103.
- [25] B. B. Kadomtsev *Rep. Prog. Phys.* **50** (1987) 115.
- [26] R. F. Post *Nucl. Fusion* **27** (1987) 1579.
- [27] The figure is taken from: URL <https://physics.stackexchange.com/questions/333151/how-many-times-does-plasma-do-a-full-loop-tokamak-before-fusion> and URL <https://steemit.com/science/@billthecipher/will-tokamak-fusion-power-bring-limitless-clean-energy>
- [28] A. Sykes *Nucl. Fusion* **39** (1999) 1271.

- [29] Y-K. M. Peng and D. J. Strickler *Nucl. Fusion* **26** (1986) 769.
- [30] The figure is taken from: URL <https://www.euro-fusion.org/2012/10/new-jet-results-tick-all-the-boxes-for-iter/>
- [31] L. Jr. Spitzer *Project Matterhorn Report* PM-S-1 NYO-993, Princeton University (1951).
- [32] P. Helander, C. D. Beidler, T. M. Bird et al. *Plasma Phys. Control. Fusion* **54** (2012) 124009.
- [33] C. Gormezano, A. C. C. Sips, T. C. Luce et al. Progression in the ITER Physics Basis. Chapter 6: Steady state operation. *Nucl. Fusion* **47** (2007) S128-S202, and references therein.
- [34] E. Westerhof *Non-inductive current drive* lecture notes in the proceedings of the 12th Carolus Magnus Summer School (2012) and references therein.
- [35] C. E. Kessel *Nucl. Fusion* **34** (1994) 1221.
- [36] H.R. Wilson *Noeclassical tearing modes* lecture notes in the proceedings of the 12th Carolus Magnus Summer School (2012) and references therein.
- [37] H.P. Furth, J.Killeen and M.N. Rosenbluth *Phys. Fluids* **6** (1963) 459.
- [38] R. Fitzpatrick *Phys. Plasmas* **2** (3) (1995) 825.
- [39] R.R. Dominguez and R.E. Waltz *Nucl. Fusion* **27** (1987) 65.
- [40] J.A. Snipes, D.J. Campbell, T.C. Hender et al. *Nucl. Fusion* **30** (1990) 205.
- [41] T.C. Hender, J.C Wesley, J. Bialek et al. Progression in the ITER Physics Basis. Chapter 3: MHD stability, operational limits and disruptions. *Nucl. Fusion* **47** (2007) S128-S202, and references therein.
- [42] O. Sauter, R.J. La Haye, Z. Chang et al. *Phys. Plasmas* **4** (5) (1997) 1654.
- [43] R.J. Buttery, S. Gunter, G. Giruzzi et al. *Plasma Phys. Control. Fusion* **42** (2000) B61-B73.
- [44] H.R. Strauss *Phys. Fluids* **24** (1981) 2004.
- [45] C.C. Hegna and J.D. Callen *Phys. Plasmas* **1** (1994) 2308.

- [46] Z. Chang, E.D. Fredrickson, S.H. Batha *Phys. Plasmas* **5** (4) (1998) 1076.
- [47] W.X. Qu and J.D. Callen University of Wisconsin report UWPR 85-5 (1985).
- [48] R. Carrera, R.D. Hazeltine and M. Kotschenreuther *Phys. Fluids* **29** (1986) 899.
- [49] A.H. Glasser, J.M. Greene, and J.L. Johnson *Phys. Fluids* **18** (1975) 875.
- [50] J.W. Connor, F.L. Waelbroeck, H.R. Wilson *Phys. Plasmas* **8** (2001) 2835.
- [51] R. Fitzpatrick, F.L. Waelbroeck, and F. Militello *Phys. Plasmas* **13** (2006) 122507.
- [52] P.H. Rutherford *Phys. Fluids* **16** (11) (1973) 1903-1908.
- [53] H.R. Wilson, J.W. Connor, R.J. Hastie, and C.C. Hegna *Phys. Plasmas* **3** (1) (1996) 248.
- [54] Z. Chang, J.D. Callen, E.D. Fredrickson et al. *Phys. Rev. Lett.* **74** (23) (1995) 4663-4666.
- [55] K.J. Gibson, N. Barratt, I. Chapman et al. *Plasma Phys. Control. Fusion* **52** (2010) 124041.
- [56] R.D. Hazeltine, P. Helander and P.J. Catto *Phys. Plasmas* **4** (1997) 2920.
- [57] A.I. Smolyakov *Plasma Phys. Control. Fusion* **35** (1993) 657.
- [58] H.R. Wilson, M. Alexander, J.W. Connor et al. *Plasma Phys. Control. Fusion* **38** (1996) A149.
- [59] B.N. Kuvshinov and A.B. Mikhailovskii *Plasma Physics Reports* Vol.24 No.4 (1998) 245-268. Translated from *Fizika Plasmy* Vol.4 No.4 (1998) 275-292.
- [60] A.B. Mikhailovskii, V.D. Pustovitov and A.I. Smolyakov *Plasma Phys. Control. Fusion* **42** (2000) 309.
- [61] F.L. Waelbroeck, J.W. Connor and H.R. Wilson *Phys. Rev. Lett.* **87** (2001) 215003-1.
- [62] A. Bergman, E. Poli and A.G. Peeters *Phys. Plasmas* **12** (2005) 072501.
- [63] M. James and H.R. Wilson *Plasma Phys. Control. Fusion* **48** (2006) 1647-1659.
- [64] M. James, H.R. Wilson and J.W. Connor *Plasma Phys. Control. Fusion* **52** (2010) 075008.

- [65] H. Reimerdes, O. Sauter, T. Goodman, and A. Pochelon *Phys. Rev. Lett.* **88** (10) (2002) 105005-1.
- [66] H. Lutzjens, J.-F. Luciani and X. Garbet *Phys. Plasmas Letters* **8** (10) (2001) 4267-4270.
- [67] R.J. Buttery, O. Sauter, R. Akers et al. *Phys. Rev. Lett.* **88** (12) (2002) 125005-1.
- [68] H.R. Wilson, J.W. Connor, C.G. Gimblett et al. *Theoretical understanding of tokamak pressure limits* report IAEA-CSP-8/C (2001).
- [69] K. Imada and H.R. Wilson *Phys. Plasmas* **19** (2012) 032120.
- [70] A. Bergmann, E. Poli and A. G. Peeters *Phys. Plasmas* **12** (2005) 072501.
- [71] R.J. La Haye, R. Prater, R. J. Buttery et al. *Nucl. Fusion* **46** (2006) 451-461.
- [72] R.J. La Haye, R.J. Buttery, S.P. Gerhardt et al. *Phys. Plasmas* **19** (2012) 062506.
- [73] K. Imada, H.R. Wilson, J.W. Connor, A.V. Dudkovskaia and P. Hill *Phys. Rev. Lett.* **121** (2018) 175001.
- [74] K. Imada, H.R. Wilson, J.W. Connor, A.V. Dudkovskaia and P. Hill *Nucl. Fusion* **59** (2019) 046016.
- [75] E. Poli, A.G. Peeters, A. Bergmann et al. *Phys. Rev. Lett.* **88** (7) (2002) 075001.
- [76] H. Cai, D. Li and J. Cao *Phys. Plasmas* **22** (2015) 02512.
- [77] A.I. Smolyakov, A. Hirose, E. Lazzaro et al. *Phys. Plasmas* **2** (5) (1995) 1581.
- [78] R. McAdams, H.R. Wilson and I.T. Chapman *Nucl. Fusion* **53** (2013) 083005.
- [79] D. De Lazzari and E. Westerhof *Plasma Phys. Control. Fusion* **53** (2011) 035020.
- [80] J.P. Meskat, H. Zohm, G. Gantenbein et al. *Plasma Phys. Control. Fusion* **43** (2001) 1325.
- [81] J. A. Snape, K. J. Gibson, T. O’Gorman et al. *Plasma Phys. Control. Fusion* **54** (2012) 085001.
- [82] F.L. Waelbroeck and R. Fitzpatrick *Phys. Rev. Lett.* **78** (9) (1997) 1703.

- [83] A.B. Mikhailovskii, S.V. Konovalov, and V.D. Pustovitov *Phys. Plasmas* **7** (6) (2000) 2530-2538.
- [84] B.D. Scott and A.B. Hassam *Phys. Fluids* **30** (1987) 90.
- [85] B.B. Kadomtsev *Nucl. Fusion* **31** (1991) 1301.
- [86] J.W. Connor and H.R. Wilson *Phys. Plasmas* **2** (1995) 4575.
- [87] R.J. La Haye, C. C. Petty, E. J. Strait, F. L. Waelbroeck and H. R. Wilson *Phys. Plasmas* **10** (2003) 3644.
- [88] A. B. Mikhailovskii, V. D. Pustovitov, A. I. Smolyakov and V. S. Tsypin *Phys. Plasmas* **7** (2000) 1214.
- [89] R. Fitzpatrick and F. L. Waelbroeck *Phys. Plasmas* **7** (2000) 4983.
- [90] E. Poli, A. Bergmann and A. G. Peeters *Phys. Rev. Lett.* **94** (2005) 205001.
- [91] E. Poli, A. Bergmann, A. G. Peeters et al. *Nucl. Fusion* **45** (2005) 384-390.
- [92] A. Bergmann, E. Poli and A. G. Peeters *Phys. Plasmas* **16** (2009) 092507.
- [93] K. Imada, H. R. Wilson, J. W. Connor, A. V. Dudkovskaia and P. Hill *J. Phys.: Conf. Ser.* 1125 (2018) 012013.
- [94] K. Imada, J. W. Connor, A. V. Dudkovskaia, P. Hill and H. R. Wilson *Benchmarking of the drift kinetic model for the NTM threshold* 46th EPS conference on Plasma Physics, Milan (2019).
- [95] A. V. Dudkovskaia, X. Garbet, M. Lesur, H. R. Wilson *J. Phys.: Conf. Ser.* 1125 (2018) 012009.
- [96] A. V. Dudkovskaia, X. Garbet, M. Lesur, H. R. Wilson *Nucl. Fusion* **59** (2019) 086010.
- [97] V. E. Zakharov and V. I. Karpman, *Zh. Eksp. Teor Fiz.* **43** (1962) 490 and *Sov. Phys. JETP* **16** (1963) 351.
- [98] H. L. Berk and B. N. Breizman *Phys. Fluids B* **2** 2226 (1990). H. L. Berk and B. N. Breizman *Phys. Fluids B* **2** (1990) 2235. H. L. Berk and B. N. Breizman *Phys. Fluids B* **2** (1990) 2246.

- [99] M. Lesur et al *Phys. Plasmas* **17** (2010) 122311.
- [100] R. G. L. Vann, R. O. Dendy, G. Rowlands, T. D. Arber, and N. d'Ambrumenil *Phys. Plasmas* **10** (2003) 623.
- [101] M. Lesur, Y. Idomura, and X. Garbet *Phys. Plasmas* **16** (2009) 092305.
- [102] T. O'Neil *Phys Fluids* **8** (1965) 2255.
- [103] R. K. Mazitov *Zhurnal prikladnoi mekhaniki i tekhnicheskoi fiziki* **1** (1965) 27.
- [104] A. A. Galeev and R. S. Sagdeev (1973) in Review of Plasma Physics vol.7, p.1 "Nonlinear Plasma Theory" [english version: 1979 Consultant Bureau, New York]
- [105] R. B. White, G. Spizzo and M. Gobbin *Plasma Phys. Control. Fusion*, **55** (2013) 115002.
- [106] H. L. Berk, B. N. Breizman and M. S. Pekker *Plasma Phys. Rep.* **23** (1997) 778–788.
- [107] M. K. Lilley, B. N. Breizman and S. E. Sharapov *Phys. Rev Lett.* 102(19):195003 (2009).
- [108] M. Lesur, Y. Idomura, and S. Tokuda *Kinetic simulations of electrostatic plasma waves using cubic-interpolated propagation scheme* report 2006-089 (Japan Atomic Energy Agency) (2007) 1.
- [109] M. Lesur and Y. Idomura *Nucl. Fusion* **52** (2012) 094004.
- [110] M. Lesur, P. H. Diamond, and Y. Kosuga *Plasma Phys. Control. Fusion* **56** (2014) 075005.
- [111] H. L. Berk et al. *Phys. Plasmas* **6** (1999) 3102.
- [112] H. L. Berk, B. N. Breizman, and M. Pekker *Phys. Rev. Letters* **76** (1996) 1256.
- [113] H. L. Berk, B. N. Breizman, and N. V. Petviashvili *Phys. Lett. A* **234** (1997) 213.
- [114] O. Sauter, R. J. Buttery, R. Felton et al. *Plasma Phys. Control. Fusion* **44** (2002) 1999-2019.
- [115] C. D. Warrick, R. J. Buttery, G. Cunningham et al. *Phys. Rev. Lett.* **85** (2000) 574.
- [116] S.E. Kruger, C.C. Hegna and J.D. Callen *Phys. Plasmas* **5** (1998) 455.

- [117] R. L. Miller, M. S. Chu, J. M. Greene et al. *Phys. Plasmas* **5** (1998) 4.